UNDERSTANDING ALTERED MUSCLE ACTIVATION AFTER CENTRAL OR PERIPHERAL NEUROMUSCULAR INJURIES

EDITED BY: Xiaogang Hu, Francesco Negro and Jun Yao
PUBLISHED IN: Frontiers in Neurology

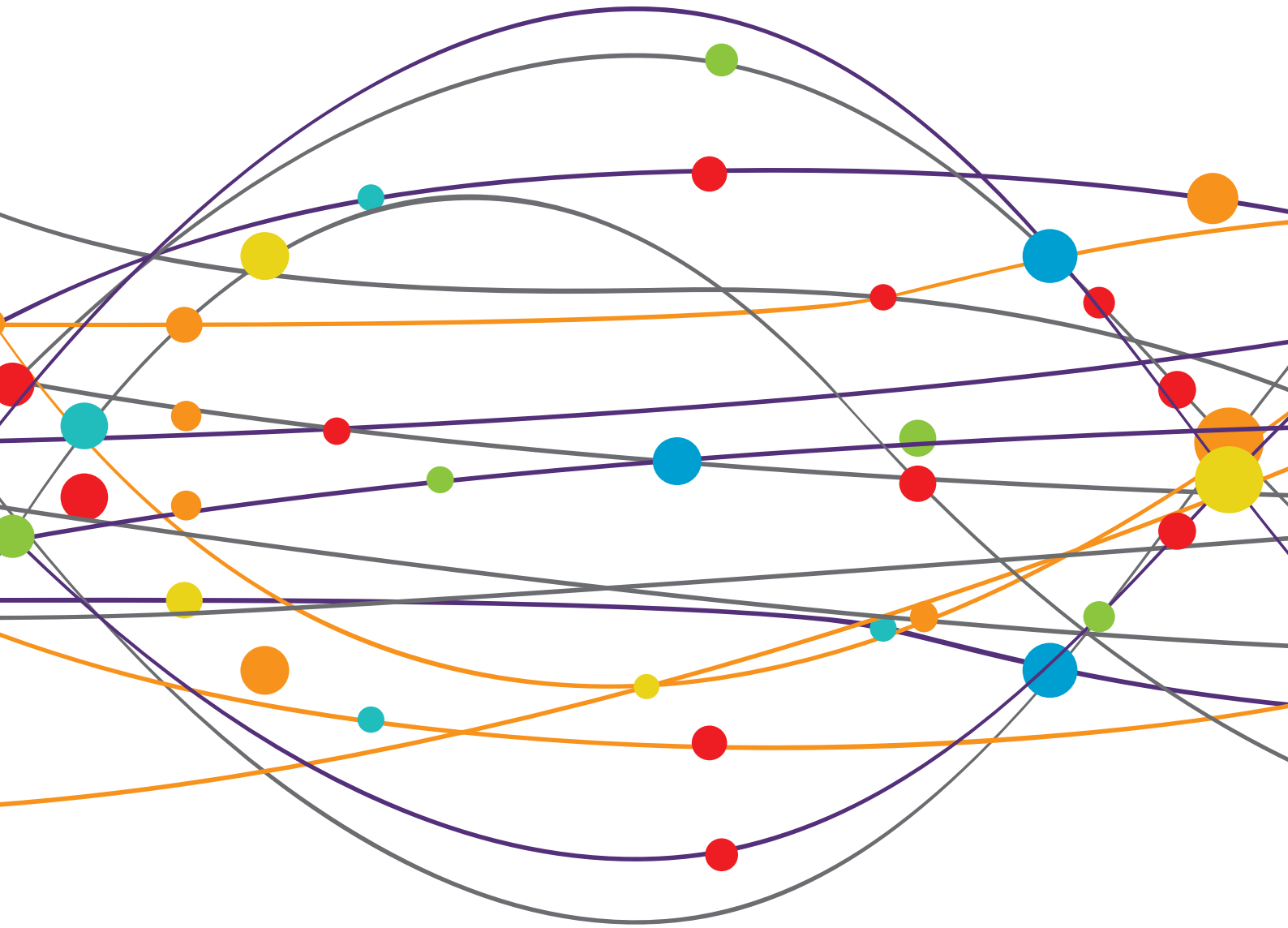

frontiers Research Topics

frontiers

ISSN 1664-8714
ISBN 978-2-88971-398-1
DOI 10.3389/978-2-88971-398-1

About Frontiers

Frontiers is more than just an open-access publisher of scholarly articles: it is a pioneering approach to the world of academia, radically improving the way scholarly research is managed. The grand vision of Frontiers is a world where all people have an equal opportunity to seek, share and generate knowledge. Frontiers provides immediate and permanent online open access to all its publications, but this alone is not enough to realize our grand goals.

Frontiers Journal Series

The Frontiers Journal Series is a multi-tier and interdisciplinary set of open-access, online journals, promising a paradigm shift from the current review, selection and dissemination processes in academic publishing. All Frontiers journals are driven by researchers for researchers; therefore, they constitute a service to the scholarly community. At the same time, the Frontiers Journal Series operates on a revolutionary invention, the tiered publishing system, initially addressing specific communities of scholars, and gradually climbing up to broader public understanding, thus serving the interests of the lay society, too.

Dedication to Quality

Each Frontiers article is a landmark of the highest quality, thanks to genuinely collaborative interactions between authors and review editors, who include some of the world's best academicians. Research must be certified by peers before entering a stream of knowledge that may eventually reach the public - and shape society; therefore, Frontiers only applies the most rigorous and unbiased reviews.
Frontiers revolutionizes research publishing by freely delivering the most outstanding research, evaluated with no bias from both the academic and social point of view. By applying the most advanced information technologies, Frontiers is catapulting scholarly publishing into a new generation.

What are Frontiers Research Topics?

Frontiers Research Topics are very popular trademarks of the Frontiers Journals Series: they are collections of at least ten articles, all centered on a particular subject. With their unique mix of varied contributions from Original Research to Review Articles, Frontiers Research Topics unify the most influential researchers, the latest key findings and historical advances in a hot research area! Find out more on how to host your own Frontiers Research Topic or contribute to one as an author by contacting the Frontiers Editorial Office: frontiersin.org/about/contact

UNDERSTANDING ALTERED MUSCLE ACTIVATION AFTER CENTRAL OR PERIPHERAL NEUROMUSCULAR INJURIES

Topic Editors:
Xiaogang Hu, University of Cagliari, Italy
Francesco Negro, University of Brescia, Italy
Jun Yao, Northwestern University, United States

Citation: Hu, X., Negro, F., Yao, J., eds. (2021). Understanding Altered Muscle Activation After Central or Peripheral Neuromuscular Injuries. Lausanne: Frontiers Media SA. doi: 10.3389/978-2-88971-398-1

Table of Contents

frontiers in Neurology

EDITORIAL
published: 29 July 2021
doi: 10.3389/fneur.2021.642207

Editorial: Understanding Altered Muscle Activation After Central or Peripheral Neuromuscular Injuries

Francesco Negro[1†], *Xiaogang Hu*[2*†] *and Jun Yao*[3,4,5†]

[1] Department of Clinical and Experimental Sciences, Research Centre for Neuromuscular Function and Adapted Physical Activity "Teresa Camplani", Università degli Studi di Brescia, Brescia, Italy, [2] Joint Department of Biomedical Engineering, University of North Carolina at Chapel Hill, North Carolina State University, Chapel Hill, NC, United States, [3] Department of Physical Therapy and Human Movement Sciences, Northwestern University, Chicago, IL, United States, [4] Northwestern University Interdepartmental Neuroscience, Northwestern University, Chicago, IL, United States, [5] Department of Biomedical Engineering, Northwestern University, Evanston, IL, United States

Keywords: motor impairment, pathophysiology, motor unit, rehabilitation, electromyogram

OPEN ACCESS

Edited and reviewed by:
Sheng Li,
University of Texas Health Science Center at Houston, United States

***Correspondence:**
Xiaogang Hu
xiaogang@unc.edu

†These authors have contributed equally to this work

Specialty section:
This article was submitted to Neurorehabilitation, a section of the journal Frontiers in Neurology

Received: *15 December 2020*
Accepted: *04 June 2021*
Published: *29 July 2021*

Citation:
Negro F, Hu X and Yao J (2021) Editorial: Understanding Altered Muscle Activation After Central or Peripheral Neuromuscular Injuries. Front. Neurol. 12:642207. doi: 10.3389/fneur.2021.642207

Editorial on the Research Topic

Understanding Altered Muscle Activation After Central or Peripheral Neuromuscular Injuries

Appropriate muscle activation plays a critical role in our daily motor activities. Therefore, quantification of muscle activation becomes an important way for diagnosing or assessing neuromuscular conditions, interfacing with machines, and assessing the efficacy of rehabilitation or assistive strategies. Recent developments in quantifying the neural control of muscles have provided an unprecedented possibility to probe into the nervous system for understanding motor impairment in pathological conditions. This Research Topic collected 15 articles that cover a wide range of novel methods or findings of muscle activation in various basic-scientific or clinical research following central or peripheral neuromuscular injuries.

In individuals with a neurological or neuromuscular condition such as a stroke or multiple sclerosis, commonly-reported movement deficits include muscle weakness, spasticity, and discoordination. Electromyography (EMG) is a non-invasive and easy-to-use probe for investigating the central nervous system's control of movements and peripheral muscular properties. It has been widely used in pathologic and rehabilitation studies. To access the stroke-induced weakness, Son and Rymer quantified the EMG-torque slops during isometric plantarflexion contractions with different ankle angles. They also used ultrasound to measure the muscle thickness and tissue stiffness. Their results reflect the reduced efficiency in muscular contraction following a stroke, which may be linked to the increased tissue stiffness. To understand the mechanisms underlying post-stroke spasticity and investigate its new treatment, Lu et al. measured the intramuscular needle EMGs before and immediately after dry needling to the flexor digitorum superficialis in stroke individuals with spasticity in finger flexors. Their preliminary results showed that dry needling leads to immediate spasticity reduction, suggesting that latent trigger points possibly exist in spastic muscles. To explore neural mechanisms underlying post-stroke discoordination,

Guo et al. quantified corticomuscular coherence based on EEG and EMG recordings. Based on results from 14 stroke participants and 10 age-matched controls, they concluded that the post-stroke proximal muscular compensations from the elbow to finger movements were cortically originated. Also using the coherence method, Laine and Valero-Cuevas reported amplified intermuscular coherence in the alpha-band in individuals with Parkinson's disease compared with healthy control participants, suggesting that intermuscular coherence in the alpha-band can be an efficient biomarker for detecting the presence of Parkinson disease. Volitional control of the ankle dorsiflexors is commonly impaired after a spinal cord injury (SCI). Hope et al. reviewed the potential association between neurophysiological changes at the corticospinal and spinal levels with impaired volitional ankle control and spasticity after SCI. This review evaluated how changes in corticospinal transmission and spinal reflex excitability contribute to volitional ankle control and spasticity. Patients with multiple sclerosis can markedly reduce push-off and toe-clearance during gait compared to healthy individuals. Jonsdottir et al. evaluated whether altered neuromotor control, as represented by muscle synergies, improves with rehabilitation. This study investigated changes in ankle motor control and associated biomechanical parameters after a 20-session intensive treadmill training. The results showed a reorganization of distal leg muscle synergy related to neurophysiological changes induced by rehabilitation, which was associated with improved ankle performance and gait speed.

In recent years, the use of multichannel intramuscular and surface electromyographic recordings offers the potential to separate central and peripheral contributions of muscle activation, and therefore unravel unique features of neuromuscular diseases. Wilson et al. used intramuscular EMG decomposition to quantify discharge rate statistics of individual motor units in patients suffering from mild-to-moderate Parkinson's disease. Interestingly, the results showed that variability in motor unit discharge and elbow flexion/extension forces were the main factors that may contribute to motor dysfunction in this patient population. Other neuromuscular diseases can also exhibit distinctive modifications in the central and peripheral properties of individual motor units. Negro et al. employed motor unit decomposition and tracking from high-density surface EMG recordings to show disease-related central changes in a cohort of chronic stroke individuals after a fatigue task. The study demonstrated that fatigability in the affected side of stroke individuals is associated with impaired rate coding and recruitment of motor units. Similarly, Vieira et al. demonstrated that neural plasticity in stroke survivors could modify the peripheral properties of motor units in the medial gastrocnemius muscles. Specifically, the motor unit action potentials in the paretic muscles showed a more extensive distribution than the non-paretic side not explained by variations in anatomical factors (subcutaneous thickness), leading to a new generation of markers of neuromuscular plasticity in stroke individuals. Motor Unit Number Index (MUNIX) has been accepted as a neurological tool for indexing the number of functioning motor unit (MU) of the target muscle, which provides a susceptive biomarker for innervation conditions in patients with neurodegenerative diseases. Gao et al. examined the effect of channel number and channel location on the repeatability of MUNIX. High-density surface electromyogram (EMG) signals were recorded from the biceps brachii muscles. The study found a significantly improved repeatability (quantified by the coefficient of variation across trials) with the proposed multi-channel MUNIX approach. Higher variability of single-channel MUNIX was observed when the recording channel is positioned away from the innervation zone. This study identified potential sources of MUNIX variations, and provided novel perspectives to improve the repeatability.

Interestingly, EMG-based electrophysiological tools may also be used to assess the neural changes in motor disorders after neural stimulation interventions. Gogeascoechea et al. assessed modifications in the common synaptic oscillations in the neural drive to muscles after the applications of trans-spinal direct current stimulation in a cohort of spinal cord injury patients. Impressively, the estimated common synaptic input decreased after administering the stimulation protocol, and the effect persisted for tens of minutes. Repetitive peripheralmagnetic nerve stimulation (rPMS) is a putative adjuvant therapy that improves the mobility of patients with spasticity, Zschorlich et al. investigated the underlying mechanisms of rPMS in spasticity reduction. The study found that, after a 5-min rPMS, there is a significant reduction of tendon-reflex activity of the targeted muscle. The findings indicate that rPMS could be used as an adjuvant therapy to reduce spasticity during motor rehabilitation of locomotion or postural control. Amyotrophic lateral sclerosis (ALS) is a type of motor neuron disease that leads to progressive muscle atrophy and weakness. Shang et al. identified the characteristics of repetitive nerve stimulation (RNS) in patients with ALS, and further verified the electrophysiological exclusion criteria of ALS. The study compared the amplitudes of the compound muscle action potential (CMAP) between the trapezius muscle and the abductor digiti minimi in low-frequency RNS. CMAP decremental responses in RNS were common in ALS patients, suggesting abnormalities of neuromuscular junctions. The study also suggested the possibility to consider a decrement $>20\%$ in CMAP from RNS as a diagnostic exclusion criterion for ALS.

Lastly, EMGs are also widely used to interface with machines for rehabilitation purposes. Kadone et al. reported a case result in a patient with Thoracic Myelopathy due to ossification of the posterior longitudinal ligament. An EMG controlled Hybrid Assistive Limb was used to improve this patient's walking ability. Both kinematic and Kinetic data before and after a 10-session intervention were reported to demonstrate the post-intervention gate improvement and the altered central nervous system control for relative muscles, suggesting that an EMG-control rehabilitation tool can effectively result in functional regain. The combination of neural decoding and the application of therapeutic interventions may open up new opportunities to design real-time closed-loop control systems for rehabilitative applications. Accordingly, Nizamis et

al. demonstrated the use of high-density surface (HD-sEMG) recordings to estimate the spatial distribution of HD-sEMG patterns in the forearm of patients suffering Duchenne muscular dystrophy for the future control of robotic exoskeletons. The results of this study showed unequivocally that patients, even with clear progressive alterations in hand/wrist motor control, can produce repeatable spatial muscle activation patterns, and they can be used for the myocontrol of wearable exoskeletons.

AUTHOR CONTRIBUTIONS

All authors listed have made a substantial, direct and intellectual contribution to the work, and approved it for publication.

Conflict of Interest: The authors declare that the research was conducted in the absence of any commercial or financial relationships that could be construed as a potential conflict of interest.

frontiers in Neurology

ORIGINAL RESEARCH
published: 26 June 2019
doi: 10.3389/fneur.2019.00686

Postural Muscle Unit Plasticity in Stroke Survivors: Altered Distribution of Gastrocnemius' Action Potentials

*Taian M. Vieira[1], Thiago Lemos[2], Laura A. S. Oliveira[2,3], Carlos H. R. Horsczaruk[2], Gabriel R. Freitas[4], Fernanda Tovar-Moll[4,5] and Erika C. Rodrigues[2,4]**

[1] Laboratorio di Ingegneria del Sistema Neuromuscolare (LISiN), Dipartimento di Elettronica e Telecomunicazioni, and PoliTo[BIO]Med Lab, Politecnico di Torino, Turin, Italy, [2] Programa de Pós-Graduação em Ciências da Reabilitação, Centro Universitário Augusto Motta – UNISUAM, Rio de Janeiro, Brazil, [3] Graduação em Fisioterapia, Instituto Federal de Educação, Ciência e Tecnologia – IFRJ, Rio de Janeiro, Brazil, [4] Unidade de Conectividade Cerebral, Instituto D'Or de Pesquisa e Ensino – IDOR, Rio de Janeiro, Brazil, [5] Programa de Pós-Graduação em Ciências Mofológicas, Instituto de Ciências Biomédicas, Universidade Federal do Rio de Janeiro – UFRJ, Rio de Janeiro, Brazil

Neuromuscular adaptations are well-reported in stroke survivors. The death of motor neurons and the reinnervation of residual muscle fibers by surviving motor neurons, for example, seem to explain the increased density of muscle units after stroke. It is, however, unknown whether reinnervation takes place locally or extensively within the muscle. Here we combine intramuscular and surface electromyograms (EMGs) to address this issue for medial gastrocnemius (MG); a key postural muscle. While seven stroke survivors stood upright, two intramuscular and 15 surface EMGs were recorded from the paretic and non-paretic gastrocnemius. Surface EMGs were triggered with the firing instants of motor units identified through the decomposition of both intramuscular and surface EMGs. The standard deviation of Gaussian curves fitting the root mean square amplitude distribution of surface potentials was considered to assess differences in the spatial distribution of motor unit action potentials and, thus, in the distribution of muscle units between limbs. The median number of motor units identified per subject in the paretic and non-paretic sides was, respectively, 2 (range: 1–3) and 3 (1–4). Action potentials in the paretic gastrocnemius were represented at a 33% wider skin region when compared to the non-paretic muscle (Mann-Whitney; $P = 0.014$). Side differences in the representation of motor unit were not associated with differences in subcutaneous thickness (skipped-Spearman $r = -0.53$; confidence interval for r: −1.00 to 0.63). Current results suggest stroke may lead to the enlargement of the gastrocnemius muscle units recruited during standing. The enlargement of muscle units, as assessed from the skin surface, may constitute a new marker of neuromuscular plasticity following stroke.

Keywords: motor unit, electromyogram, stroke, gastrocnemius, standing

OPEN ACCESS

Edited by:
Xiaogang Hu,
University of North Carolina at Chapel Hill, United States

Reviewed by:
Jakob Dideriksen,
Aalborg University, Denmark
Cristiano De Marchis,
Roma Tre University, Italy

***Correspondence:**
Erika C. Rodrigues
erikacrodrigues@gmail.com

Specialty section:
This article was submitted to Neurorehabilitation, a section of the journal Frontiers in Neurology

Received: *19 March 2019*
Accepted: *12 June 2019*
Published: *26 June 2019*

Citation:
Vieira TM, Lemos T, Oliveira LAS, Horsczaruk CHR, Freitas GR, Tovar-Moll F and Rodrigues EC (2019) Postural Muscle Unit Plasticity in Stroke Survivors: Altered Distribution of Gastrocnemius' Action Potentials. Front. Neurol. 10:686. doi: 10.3389/fneur.2019.00686

INTRODUCTION

Motor impairment is a widely recognized consequence of stroke (1). Structural changes in the spinal motor neuron and its muscle fibers have been advocated a contributing factor for the loss of motor control in stroke survivors (2, 3). Indeed, loss of motor neurons, muscle atrophy and fiber-type grouping have been reported within 2–5 months after stroke (2–5). It is the loss of motor neurons

that seems to lead to major, structural changes within the paretic muscle. More specifically, muscle fibers belonging to dead motor neurons seem to be re-innervated by surviving ones. This structural change is substantiated by increases in the size of motor unit action potentials and, more directly, by collateral sprouting and greater fiber density at chronic, stroke stages (6–8). In virtue of the increased number of fibers per motor unit, it seems therefore reasonable to ask whether these fibers span a larger region within the paretic muscle.

Different methodologies have been designed to assess the location of individual muscle units; i.e., fibers of single motor units. Muscle units may be assessed directly by staining and then locating glycogen-depleted fibers. Although this procedure was applied successfully to study the topography of cat muscle units (9), applying it in human muscles is currently unviable. Tracking action potentials of single motor units with a needle electrode moving along a corridor transverse to the fibers' direction constitutes an alternative method for assessing muscle units in humans (10). For muscles with large, physiological cross-sectional areas, however, this technique would provide a limited view of muscle units, as different corridors would have to be scanned. Recently, we have shown the surface representation of action potentials of medial gastrocnemius (MG) motor units, identified with intramuscular electrodes during standing, reflects well the distribution of muscle units (11). Notwithstanding these different, existing means, none, however, seems to have been considered to quantify the localization of muscle units following stroke.

Here we, therefore, investigate whether stroke affects the structure of MG muscle units recruited during standing. We specifically ask: how diffusely does the amplitude of action potentials of single, MG motor units distribute on the skin of paretic and non-paretic limbs? Upright stance approach was chosen because postural instability is one of the leading motor impairment observed after stroke (12, 13). Moreover, we selected MG because it seems to be greatly affected by stroke (7, 14) and because of its functional relevance to balance control (11, 15, 16). If reorganization of muscle units takes place extensively along MG, then, we would expect to detect surface potentials along a larger skin region in the paretic limb.

METHODS

Participants

Eight, ischemic stroke survivors were recruited (four females; range values; age: 47–64 years; height: 147–172 cm; body mass: 51–102 kg; months from stroke: 42–120). The presence of aphasia, cognitive impairment, other neurological diseases or lesions, rheumatologic or metabolic diseases, pregnancy, or any musculoskeletal disorders affecting the standing posture were exclusion criteria. All participants could stand upright without external support for 60 s. The experimental procedures were approved by the local Institutional Ethic Committee (reference number: 13611913.8.0000.5249). All participants gave written informed consent in accordance with the Declaration of Helsinki.

Experimental Protocol

Participants were asked to stand upright over a force-plate (AccuSwayPLUS, AMTI, Massachusetts, USA; **Figure 1A**), with their feet at a comfortable position. They were instructed to hang their arms loose alongside the body and to stand comfortably, without gross movements and without moving their feet. Two experimenters stood close to subjects at all times, to assist them in case of balance loss. Recordings started once subjects got acquainted with the standing tasks. At least two trials were applied, lasting 60 s each and with 5 min intervals. Given action potentials were occasionally not observed in both surface and intramuscular EMGs from the paretic limb in two subjects, additional trials were applied. Specifically, we provided these participants with visual feedback of their center of pressure (CoP) position and asked them to move it toward the paretic limb. After roughly 5 min of familiarization, participants could successfully load the paretic limb with at least 50% of their body weight (**Figures 2A–C**), according to the linear relationship between CoP lateral position and weight distribution between limbs (17). One trial per participant was retained for analysis; that providing the greatest number of clearly visible action potentials in surface EMGs detected from both sides. One participant did not show any motor unit action potential even when loading the paretic limb; signals recorded for this subject were disregarded.

EMG Recordings

Intramuscular EMGs were detected with two pairs of Teflon-coated, stainless-steel wire electrodes (0.2 mm diameter; A-M Systems, Carlsborg, WA). Each pair was inserted in the paretic and non-paretic MG with a 25-gauge hypodermic needle. Two arrays of 16 silver bar electrodes each (1 × 10 mm; 10 mm inter-electrode distance; Spes-Medica, Battipaglia, Italy) were used to record 15 differential surface EMGs from each MG. Arrays were fixed to the skin with bi-adhesive pads filled with conductive paste (TEN 20 Conductive Paste, Weaver).

Wire and surface electrodes were positioned at specific MG locations (**Figure 1**). Initially, the location of the distal extremity of MG superficial aponeurosis [dashed line in **Figure 1B** (11)] was identified with ultrasound imaging (see "Muscle architecture" section). After that, the distance between this location and the popliteal crease was measured and marked on the skin. Wires were inserted halfway this distance. To ensure the tip of the wires would be located roughly beneath the surface array, needles were inserted obliquely to the skin. Finally, after shaving and cleaning the skin with abrasive paste, surface electrodes were aligned parallel to the muscle longitudinal axis. Amplification factor for both intramuscular and surface recordings ranged from 1,000 to 10,000 between participants (10–4,400 Hz bandwidth amplifier, EMG-USB2, OT-Bioelettronica, Turin, Italy). EMGs and ground reaction forces were digitized synchronously at 10,240 Hz (12 bits A/D converter; EMG-USB2, OT-Bioelettronica, Turin, Italy).

Estimating the Surface Representation of Motor Units

First, EMGs were band-pass filtered with a fourth order Butterworth filter (cut-off frequencies; intramuscular: 500–3,000 Hz; surface: 20–400 Hz). Instants of motor unit firing

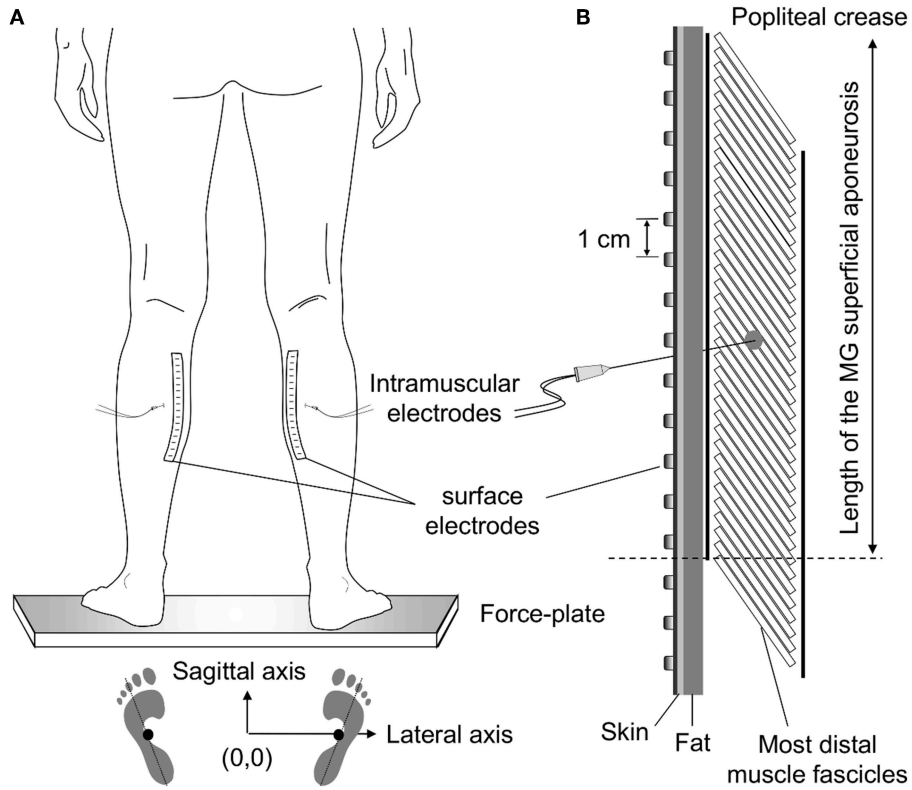

FIGURE 1 | Standing posture and electrode positioning. While individuals stood at a comfortable stance **(A)** the feet position was marked on the force plate. These drawings were considered to quantify the approximate center of pressure (CoP) position corresponding to a symmetric weight distribution between limbs (see Methods, section Experimental Protocol). **(B)** shows the relative position between medial gastrocnemius (MG) and surface and intramuscular electrodes. Wire electrodes were inserted at the MG region corresponding to the central location between the most proximal, surface electrode, and the distal extremity of the superficial aponeurosis (see dashed line); for the example illustrated in panel **(B)**, this region roughly corresponds to the position of the sixth electrode from top to bottom. The length of MG superficial aponeurosis was estimated as the distance between its distal extremity and the popliteal crease.

were then automatically identified through decomposition of intramuscular EMGs (17). Often, a greater number of motor units could be observed in surface than intramuscular recordings (**Figure 2D**). To obtain the greatest number of motor units per subject, the firing pattern of additional motor units was identified through decomposition of surface EMGs with a validated procedure (18). It should be noted this decomposition algorithm does not rely on the shape but on the finite duration of motor unit action potentials. Even though its potential to reconstruct pulse trains decreases in highly underdetermined mixtures [i.e., when few electrodes are used (19)], here we assess the surface representation and not the firing pattern of single motor units. In virtue of the gastrocnemius pennate architecture, action potentials of different motor units appear in different locations and with different shapes on the skin (11, 20), making it possible to distinguish different motor units in the surface EMGs (e.g., **Figure 3**). Given the degree of gastrocnemius activity fluctuates during standing (11), the quality of decomposition results should be not assessed with conventional metrics as e.g., the coefficient of variation of the inter-spike intervals. For this reason, we used the pulse-to-noise ratio to assess decomposition accuracy (21); this metric does not depend on how regularly motor units discharged.

Decomposed EMGs were considered to assess side differences in the distribution of muscle units following stroke. Muscle units' distribution was estimated based on the surface amplitude of action potentials, using a slightly modified approach to that described in our previous study (11). Briefly, we first averaged EMGs over 40 ms epochs, centered on the firing instants of each motor unit. The root mean square (RMS) amplitude was then calculated for each of the 15 averaged EMGs, providing the surface distribution of RMS amplitude values for individual motor units. As shown previously (11), the distribution of RMS values scales with the distribution of fibers within individual, MG muscle units; the more distributed the muscle unit is, the more diffusely the RMS values distribute on the skin. After that, we computed Gaussian curves that numerically minimized the mean square error (MSE) with respect to the RMS values obtained for EMGs detected over MG superficial aponeurosis:

$$MSE\left(\mu,\sigma,A\right)=\sum_{i=1}^{15}\left(RMS_i-\left[e^{-\frac{(i-\mu)^2}{2\sigma^2}}+A\right]\right)^2$$

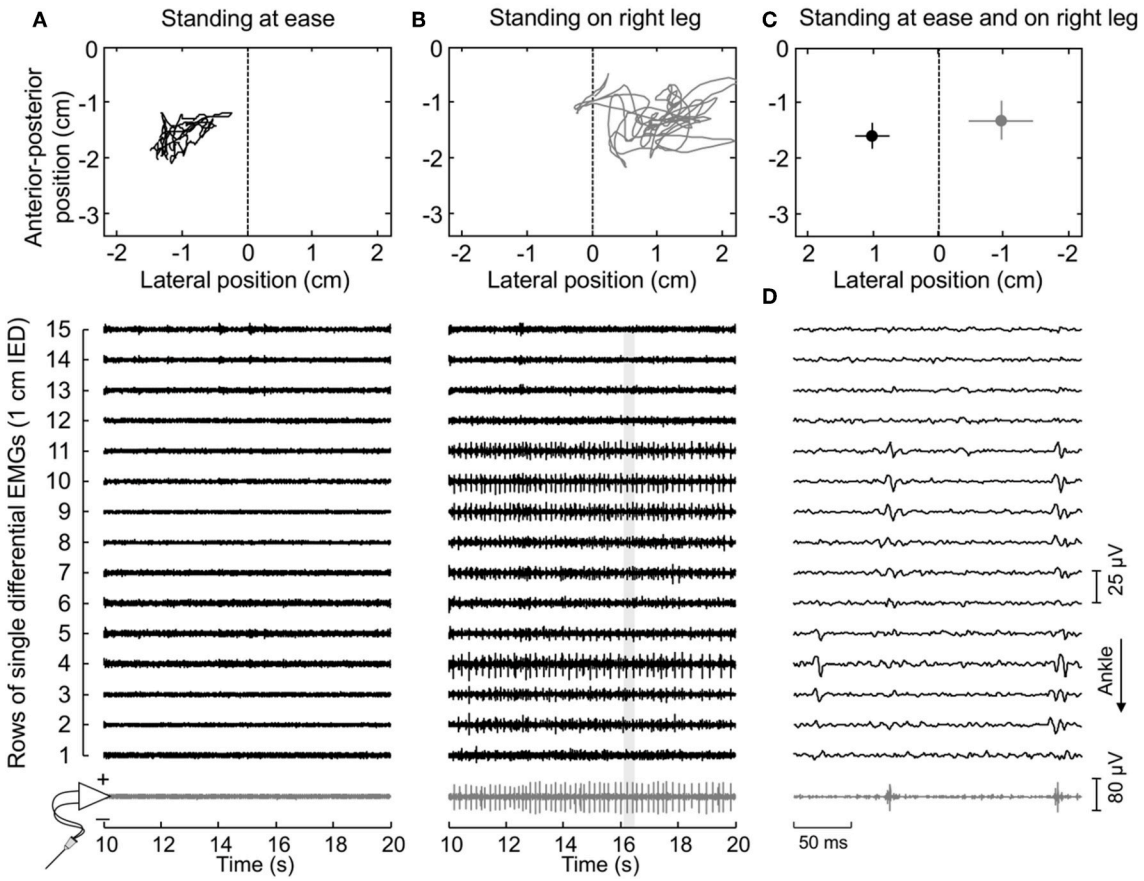

FIGURE 2 | Muscle activity and standing posture. **(A)** illustrates the CoP position along the lateral and anterior-posterior axes (top panel) and the surface (black traces) and intramuscular (gray traces) electromyograms (EMGs) detected during 10 s for a representative subject. EMGs are shown exclusively for the paretic (right) MG. The dashed line in the top panel denotes the CoP location where body weight distributes roughly symmetrically between limbs (**Figure 1A**). Note that action potentials are not present both in the surface and intramuscular recordings. When this subject shifted his CoP toward the paretic limb **(B)**, action potentials could be clearly appreciated. An expanded view of EMGs (light gray rectangle) is shown in **(D)**. Note there is a correspondence in the instants when action potentials were detected by the intramuscular electrodes and by the central though not by the distal nor proximal electrodes in the surface array. **(C)** shows the mean CoP position, calculated over the entire recording (60 s), while the subject stood at ease (black circle) and on his right leg (gray circle). Horizontal and vertical traces correspond to the standard deviation along the lateral and sagittal directions, respectively.

where RMSi corresponds to the RMS amplitude obtained from the i-th channel, normalized with respect to the maximal RMS value across the array, whereas A was allowed to vary from 0 to 0.5 at 0.01 steps. The mean value (μ) of the Gaussian fitting spanned the RMS peak position ± 2 cm and the theoretical standard deviation (σ), henceforth referred to as sigma, varied from 0.1 to 8 cm, both at 0.1 cm steps. *Sigma* values were then considered to assess how diffusely RMS values distributed on the skin [cf. **Figure 3** in (11)]. Finally, *sigma* values were normalized with respect to the length of MG superficial aponeurosis (**Figure 1B**) to control for both side differences in muscle length (due e.g., to atrophy) and inter-individual differences. The normalized *sigma* values provide, therefore, a relative indication of how largely the amplitude of motor unit action potentials distributes along the MG physiological cross-sectional area [cf. **Figure 1** in (22)].

The procedure considered above for the computation of *MSE* values is slightly different from that used in our previous study (11), where *A* was fixed at 0. This modified Gaussian curve allows for the compensation of baseline values different from 0, due both to noise and to the background activity not suppressed by averaging (**Figures 3**, **4**). To assess potential differences in the quality of the Gaussian fitting between limbs, the coefficient of determination R^2 was computed and then adjusted for the degree of freedom of the RMS variance $\left(dof_{RMS} = 15 - 1 = 14\right)$ and of the estimated error variance:

$$R^2_{adj} = 1 - \left(1 - R^2\right) \frac{dof_{RMS}}{dof_e}$$

Muscle Architecture

Ultrasound images were acquired longitudinally from MG, with the US probe roughly centered where wire electrodes were

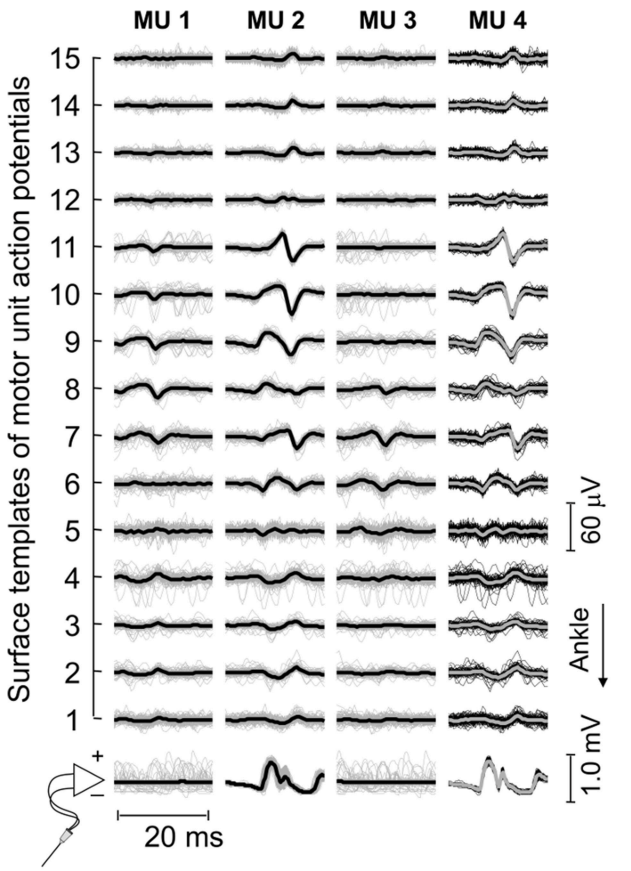

FIGURE 3 | Motor unit action potentials in surface and intramuscular recordings. Short epochs (20 ms) of EMGs detected by wire and surface electrodes are shown. These epochs (thin traces) were obtained by triggering EMGs with the firing pattern of individual motor units, separately for each surface and intramuscular recordings. Thick traces were obtained by averaging the triggered EMGs. For this participant, three motor units were identified through decomposition of surface EMGs (cf. the first three columns from left to right). Note the similarity between waveforms obtained for the motor unit (MU 2) identified from decomposition of surface recordings and those obtained for the motor unit (MU 4) identified from decomposition of intramuscular EMGs.

inserted (7 MHz, 59 mm linear probe, Echoblaster 64, Telemed, Vilnius, Lithuania). Subcutaneous and MG thicknesses were quantified for the paretic and non-paretic limbs. The first was defined as the distance between the superficial aponeurosis and the skin-fat interface, whereas MG thickness was quantified as the distance between the superficial and deep aponeuroses.

Statistics

Given data distribution was not Gaussian (Shapiro-Wilk test, $P < 0.03$ in all cases), the Mann-Whitney test was applied to quantify the significance of side differences in *sigma* values, in the adjusted coefficient of determination and pulse-to-noise ratio. Differences in the thickness of subcutaneous and MG tissues between limbs were quantified with the paired, Wilcoxon test. Skipped-Spearman correlation analysis (23) was used to assess whether there was a monotonic, positive relationship between the ratio values (paretic/non-paretic) for *sigma* and subcutaneous thickness.

RESULTS

Gastrocnemius Motor Units Identified During Standing

Thirty-four motor units (13 in the paretic MG) were identified from EMGs collected from both limbs for the seven participants analyzed. The median number of motor units identified per subject in the paretic and non-paretic sides was, respectively, 2 (range: 1–3) and 3 (1–4). As shown in **Figure 2**, more units were decomposed from surface than intramuscular EMGs; close inspection of **Figure 2B** reveals that action potentials detected distally (from channel 3 to 5 at the first 50 ms) and proximally (from channel 9 to 11) belonged to different motor units, with the proximal though not distal potentials being detected by intramuscular electrodes as well (**Figure 2D**). When considering all participants, 16 and 20 motor units were decomposed from intramuscular and surface EMGs, respectively (two common units; **Figure 3**). Pulse-to-noise-ratio values were remarkably high for all units decomposed, varying from 25.3 to 36.5 dB (median value: 32.7 dB) for the non-paretic muscle and from 23.4 to 33.4 dB (30.4 dB) for the paretic muscle. No side differences in the pulse-to-noise ratio were observed (Mann-Whitney; $P = 0.49$).

Median values (interquartile intervals) for the adjusted coefficient of determination were 0.72 (0.60–0.89; $N = 13$ units) for the paretic and 0.81 (0.68–0.90; $N = 21$ units) for the non-paretic limb. No significant side differences were observed in the adjusted coefficient of determination (Mann-Whitney; $P = 0.39$), indicating the quality of Gaussian fitting in both sides was comparable.

Side Differences in the Spatial Distribution of Muscle Units

Action potentials in the paretic and non-paretic MG were represented locally in the surface EMGs. As shown for a representative participant in **Figure 4**, action potentials with high amplitude were detected by few consecutive channels, centered at different skin regions. This local representation resulted in RMS values distributed narrowly on the skin, leading to Gaussian curves with relatively small *sigma* values in both non-paretic (0.79 and 0.88 cm) and paretic (1.05 cm) muscles. Due to a shorter aponeurosis in the paretic MG (cf. shaded area in **Figure 4**), relative side differences were emphasized by normalizing *sigma* with respect to the length of MG superficial aponeurosis (normalized *sigma*; paretic MG: 6.3%, non-paretic MG: 3.8 and 4.2%).

Group analysis confirmed that action potentials of motor units in the paretic MG were represented over a significantly larger skin region than those from the non-paretic MG. The median *sigma* value in the paretic limb was significantly greater than that obtained for motor units in the non-paretic muscle (**Figure 5A**; Mann-Whitney; $P = 0.037$; $N = 34$ motor units). Side differences increased when normalizing *sigma* with respect to the length of

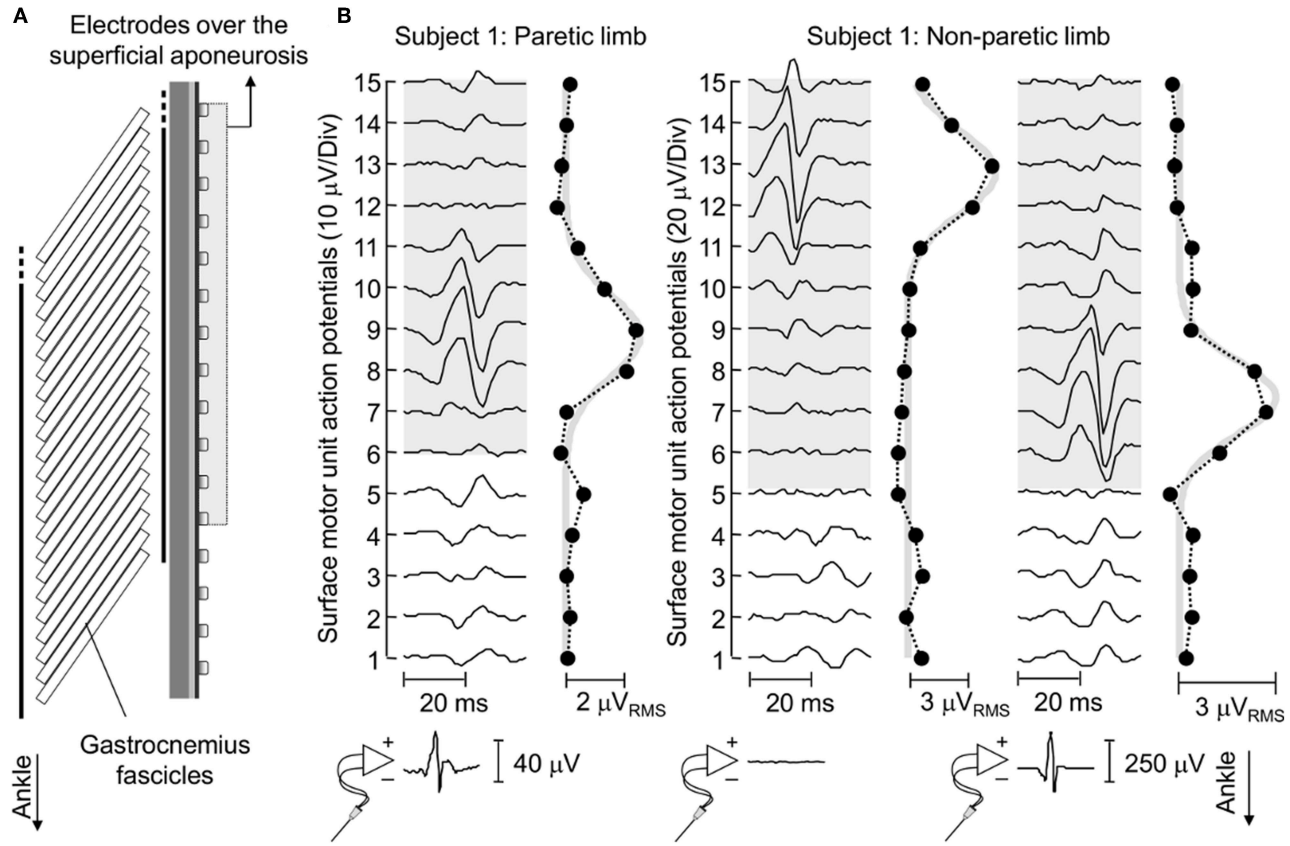

FIGURE 4 | Surface representation of motor unit action potentials. **(A)** schematically illustrates the relative position between surface electrodes and MG fascicles for a representative subject. **(B)** shows the spike triggered average potentials of motor units identified for EMGs detected from the paretic and non-paretic MG muscle, both from the skin surface and intramuscularly. The absence of an action potential in the bottom trace of the central panel indicates this motor unit was identified through decomposition of surface EMGs. Circles denote the root mean square (RMS) amplitude of each surface EMG. Note the greatest RMS values appear in correspondence of EMGs conveying the biggest potentials. Thick gray traces correspond to Gaussian curves fitted to the distribution of RMS values (11). These curves were estimated by considering the RMS values of surface EMGs detected by electrodes over the superficial aponeurosis (shaded area).

MG superficial aponeurosis (**Figure 1**), measured separately for the paretic (range: 15–21 cm) and non-paretic limbs (16–22 cm). After normalization, the difference between median values in relation to the median *sigma* value in the paretic limb increased from ∼11% (**Figure 5A**) to ∼33% (**Figure 5B**; $P = 0.014$).

Gastrocnemius and Subcutaneous Thickness

Different participants showed different degrees of structural muscle adaptations following stroke. For example, MG and subcutaneous thicknesses were similar in both limbs for subject 1 though not for participant 5, who showed thicker subcutaneous and muscle tissues for the paretic and non-paretic MG, respectively (**Figure 6A**). Notwithstanding these inter-individual differences, significantly thicker subcutaneous (Wilcoxon test; $P = 0.046$; $N = 7$ subjects) and thinner MG ($P = 0.020$, **Figure 6B**) tissues were observed in the paretic limb. No significant correlation was observed, however, for the paretic/non-paretic ratio values between *sigma* and subcutaneous thickness (**Figure 5C**; skipped-Spearman $r = -0.53$; confidence interval for r ranging from −1.00 to 0.63).

DISCUSSION

In this study, we combined intramuscular and surface EMGs to investigate structural changes in MG muscle units with stroke. Our results show action potentials of individual, postural muscle units were represented in relatively larger skin regions in the paretic than non-paretic MG (**Figures 4**, **5**). Below we discuss the possible interpretations and potential implications of our findings.

The Surface Representation of Motor Unit Action Potentials Changes With Stroke

Enlarged distribution of muscle units after stroke seems the most plausible explanation to our current findings. As evidenced by electrophysiological studies, structural changes within the neuromuscular system may be characterized by two distinct processes, occurring at different time periods after stroke.

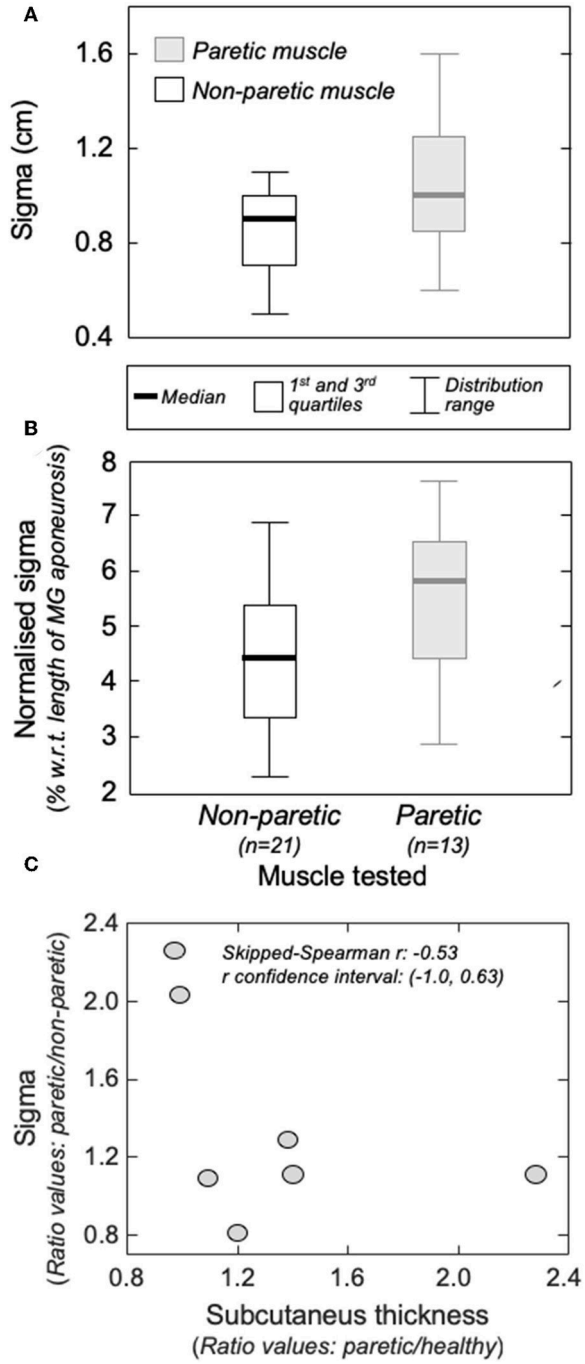

FIGURE 5 | The amplitude distribution of surface, action potentials. **(A)** shows the standard deviation (*sigma*) of the Gaussian curves fitted to the RMS distribution of motor unit action potentials identified from the non-paretic (white boxes) and from the paretic (gray boxes) MG muscles. *Sigma* values normalized with respect to the length of the MG superficial aponeurosis (see **Figure 1B**) are shown in **(B)**. Thick horizontal lines denote the median values. Boxes and whiskers correspond, respectively, to the interquartile interval and the range values. Ratios between *sigma* values obtained from the paretic and non-paretic MG (ordinate) and ratios between subcutaneous thickness values computed for the paretic and non-paretic limb (abscissa) are shown in **(C)**. The skipped-Spearman correlation coefficient and its confidence interval (23) are shown within **(C)**.

For example, a few weeks after stroke, Lukács (8) elicited smaller compound action potentials from hand muscles in the hemiparetic than non-paretic side. Similarly, the number of motor neurons estimated by Arasaki et al. (5) in the hypothenar muscles of the affected side started to decrease within the first 30 h following infarction. These findings suggest a reduction in the number of motor neurons in the acute phase post-stroke. A restoration process seems to commence though at chronic stages, whereby surviving motor neurons innervate the residual muscle fibers (6, 7), increasing the number of fibers per motor unit in the paretic side (14). The open question is whether reinnervated fibers distribute locally or diffusely within, and possibly beyond the confines of, the territory of restructured units. Based on results reported in **Figures 4**, **5**, surface potentials of single MG units are represented in a significantly larger proximo-distal region in the affected than non-affected side.

The amplitude distribution of MG surface potentials is mainly affected by two factors: the distribution of fibers within the motor units' territory and the subcutaneous thickness. Because of the MG in-depth pinnation, the superficial extremity of different MG fibers is located beneath different, proximo-distal skin sites (e.g., **Figure 4**). Surface electrodes positioned closer to the distal extremity of active fibers detect therefore greater potentials. For this reason, the standard deviation (*sigma*) of Gaussian curves fitting the amplitude distribution of surface potentials was observed to scale with the number and location of fibers of MG muscle units [cf. **Figure 4** in (11)]. Specifically, muscle units distributed locally were observed to provide surface potentials with high amplitude values distributed narrowly along MG (i.e., small *sigma* values). While the possibility of quantifying the perimeter of the territory of MG motor units with this technique could be questionable (24), it seems to provide a clear indication on the distribution of muscle units (25). Side difference in subcutaneous thickness is a potential, competing cause for obtaining greater *sigma* values in the paretic limb (**Figures 4**, **5**). Because of the tissue filtering effect, the amplitude of surface potentials decreases with the distance between intracellular action potentials and the skin (26); i.e., the subcutaneous thickness. Although we observed thicker subcutaneous layer in the paretic limb (**Figure 6**), corroborating previous evidence on thigh muscles (27), it unlikely explains the side differences in sigma values between limbs (**Figure 5**). If this were the case, in opposition to results shown in **Figure 5C**, we would expect to observe greater sigma values for subjects with thicker subcutaneous tissue. It seems, therefore, the wider representation of motor unit action potentials in the paretic gastrocnemius is more likely due to redistribution of muscle units rather than subcutaneous thickness.

A note here is important on whether sources other than the redistribution of muscle units could have affected their representation in the surface EMGs. In non-paretic muscles, larger motor units are expected to convey a greater number of muscle fibers, spanning a presumably larger region of the muscle physiological cross-sectional area (9). Nevertheless, there is neurophysiological evidence of selective degeneration of the large (high threshold) motor units chronically after a stroke (28). Here, we could not control for side-differences in the size of

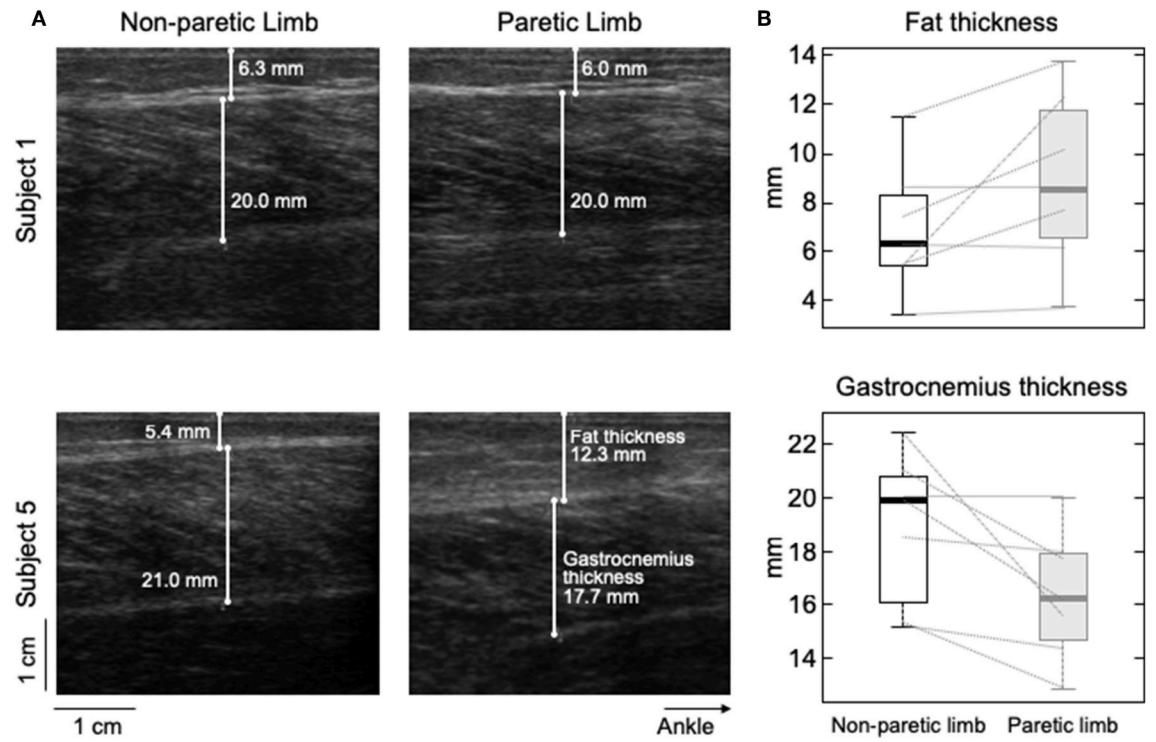

FIGURE 6 | Differences in subcutaneous thickness between limbs. Ultrasound images recorded from the calf of two participants are shown in **(A)**. Images in the right and left were, respectively, taken from the paretic and non-paretic limb. The white lines superimposed on each image indicate the thickness of fat and MG tissues. **(B)** shows the distribution of subcutaneous (top) and gastrocnemius (bottom) thicknesses estimated for the seven participants. Thick horizontal lines denote the median values. Boxes and whiskers correspond, respectively, to the interquartile interval and the range values.

motor units, even because we hypothesized the size, that is the innervation ratio, of motor units in the paretic limb had increased after stroke (6, 8). However, motor unit action potentials were often not observed in the paretic limb. Only after subjects were provided with CoP feedback and asked to voluntarily transfer their weight a few units could be appreciated in the surface EMGs (**Figure 2**). Visual inspection of surface EMGs detected from both limbs further revealed a smaller number of units in signals detected from the paretic than non-paretic limb.

Notwithstanding the small number of units decomposed from both limbs, two reasons suggest these units belonged likely exclusively to the gastrocnemius. First, the representation of motor units from soleus muscles is expectedly negligible in differential surface EMGs collected with inter-electrode distances as small as that used here [1 cm; (29)]. Second, false positives resulting from the decomposition algorithm should be <5% (21), considering the average pulse-to-noise ratio values obtained for both limbs. Therefore, it seems reasonable to state the motor units recruited in both limbs were the first recruitable or most excitable units in the gastrocnemius, suggesting like-with-like comparisons are assessed in results presented in **Figure 5**.

As discussed above, the enlarged representation of surface potentials suggests that MG muscle units span a relatively larger region in the paretic side. Advancing any mechanisms potentially accounting for such spatial enlargement with stroke would be currently speculative and is beyond the scope of the present study. It is, however, worth noting that, during the reinnervation process, the region occupied by single muscle units in the cat MG was reported to depend on how proximally the regenerating axon branches within the nerve (30); if branching occurs before the main nerve trunks, the regenerating axon may establish large territories. Despite the mechanisms accounting for the enlargement of muscle units, here we show the action potentials of single MG motor units are represented in larger proximo-distal regions in the affected (**Figure 5B**) than the non-affected side.

Potential Implications of Enlarged, Muscle Units

Impaired control of standing has been reported for stroke survivors, as evidenced by large CoP displacements and asymmetric weight distribution (31, 32). While the etiology of stroke-induced, balance disorders is debatable (13), alterations of motor unit firing properties have been reported during standing. In stroke survivors exposed to postural disturbances, for instance, motor units show delayed activation (15), reduced synchronization within- and between-muscles (33) and prolonged inter-spike intervals (16). Our results seem to reveal a new marker of neuromuscular plasticity following stroke, the enlargement of MG muscle units. Considering MG contributes both to ankle plantar flexion and inversion (34, 35),

enlarged muscle units may result in impaired regulation of force direction, possibly affecting the control of forward-backward and lateral body sways (36). Similarly, enlarged muscle units may result in a more uniform distribution of intramuscular pressure, compromising blood flow within MG (37). While further investigation is necessary to assess how changes in muscle unit distribution affect MG function, current results suggest muscle units may occupy a greater proportion of MG volume in the paretic limb of stroke survivors.

Future Perspectives and Limitations

An open question arising from this study concerns the generalization of current findings to different populations of muscle units and to different muscles. With the possibility of assessing motor units from surface EMGs collected with grids of electrodes (18), the generalization of current results to a broader population of MG units could be tested in more demanding and controlled conditions (e.g., isometric contractions). We, nevertheless, specifically focused the analysis on motor units recruited during standing, which are presumably the smallest within MG (11). Moreover, even though the median number of units identified here was roughly half of that reported in previous studies on healthy subjects (11, 24), multiple surface EMGs collected along MG were all of markedly low amplitude. Whenever a motor unit fired during standing, its action potentials were clearly appreciated in the surface EMGs (cf. **Figure 2**). The relatively low number of motor units identified in the present study may be a consequence of the active loading of muscles other than MG during standing in stroke survivors. Results presented here seem therefore to be representative of MG motor units in stroke survivors, at least of those recruited during standing.

One limiting issue we did not address here is whether side differences in the surface representation of MG potentials exist in healthy subjects. Stroke has been shown, for example, to affect the firing rate of motor units even in the non-paretic limb, possibly because of differences in corticospinal excitability between limbs in stroke survivors (38). It should be noted, however, the metric we used here is not sensitive to side differences in the synaptic drive; the spatial representation of motor units in the surface EMG depends on the number and location of their action potentials and not on how frequently action potentials are discharged. Moreover, it should be emphasized that, irrespective of any potential (mal)adaptation that the non-paretic limb could suffer because of e.g., long-term excessive usage, properties such as peak torque, rate of force development, and voluntary activation (via twitch interpolation techniques) have been shown to differ from those observed in the paretic limb (39, 40). Our results, therefore, adds by showing one potential mechanism for the uneven state of the paretic related to the non-paretic limb.

DATA AVAILABILITY

The raw data supporting the conclusions of this manuscript will be made available by the authors, without undue reservation, to any qualified researcher.

ETHICS STATEMENT

This study was carried out in accordance with the recommendations of IDOR Institutional Ethic Committee with written informed consent from all subjects. All subjects gave written informed consent in accordance with the Declaration of Helsinki. The protocol was approved by the IDOR Institutional Ethic Committee (reference number 13611913.8.0000.5249).

AUTHOR CONTRIBUTIONS

TV, LO, and ER: conception and design of the experiments. TV, TL, LO, CH, and ER: collection, analysis, and interpretation of data. TV, TL, LO, GF, FT-M, and ER: drafting the article or revising it critically for important intellectual content.

ACKNOWLEDGMENTS

This study was partially supported by Fundação Carlos Chagas Filho de Amparo à Pesquisa do Estado do Rio de Janeiro (FAPERJ), Conselho Nacional de Desenvolvimento Científico e Tecnológico (CNPq), Coordenação de Aperfeiçoamento de Pessoal de Nível Superior (CAPES, finance code 001), intramural grants from the D'Or Institute for Research and Education (IDOR), and the Italian Bank Foundation, Compagnia di San Paolo. CH was recipient of a CAPES fellowship. The funding agencies had no role in study design, data collection, and analysis, decision to publish, or preparation of the manuscript.

REFERENCES

1. Adamson J, Beswick A, Ebrahim S. Is stroke the most common cause of disability? *J Stroke Cerebrovasc Dis*. (2004) 13:171–7. doi: 10.1016/j.jstrokecerebrovasdis.2004.06.003
2. McComas AJ, Sica RE, Upton AR, Aguilera N. Functional changes in motoneurones of hemiparetic patients. *J Neurol Neurosurg Psychiatry*. (1973) 36:183–93. doi: 10.1136/jnnp.36.2.183
3. Segura RP, Sahgal V. Hemiplegic atrophy: electrophysiological and morphological studies. *Muscle Nerve*. (1981) 4:246–8.
4. Scelsi R, Marchetti C, Poggi P, Lotta S, Lommi G. Muscle fiber type morphology and distribution in paraplegic patients with traumatic cord lesion. *Acta Neuropathol*. (1982) 57:243–8. doi: 10.1007/BF00692178
5. Arasaki K, Igarashi O, Ichikawa Y, Machida T, Shirozu I, Hyodo A, et al. Reduction in the motor unit number estimate. (MUNE) after cerebral infarction. *J Neurol Sci*. (2006) 250:27–32. doi: 10.1016/j.jns.2006.06.024
6. Cruz Martinez A, del Campo F, Mingo MR, Perez Conde MC. Altered motor unit architecture in hemiparetic patients. A single fibre EMG study. *J Neurol Neurosurg Psychiatry*. (1982) 45:756–7. doi: 10.1136/jnnp.45.8.756
7. Benecke R, Berthold A, Conrad B. Denervation activity in the EMG of patients with upper motor neuron lesions: time course, local distribution and pathogenetic aspects. *J Neurol*. (1983) 230:143–51.
8. Lukács M. Electrophysiological signs of changes in motor units after ischaemic stroke. *Clin Neurophysiol*. (2005) 116:1566–70. doi: 10.1016/j.clinph.2005.04.005

9. Burke RE, Tsairis P. Anatomy and innervation ratios in motor units of cat gastrocnemius. *J Physiol*. (1973) 234:749–65. doi: 10.1113/jphysiol.1973.sp010370
10. Stålberg E, Dioszeghy P. Scanning EMG in normal muscle and in neuromuscular disorders. *Electroencephalogr Clin Neurophysiol Potentials Sect*. (1991) 81:403–16. doi: 10.1016/0168-5597(91)90048-3
11. Vieira TMM, Loram ID, Muceli S, Merletti R, Farina D. Postural activation of the human medial gastrocnemius muscle: are the muscle units spatially localised? *J Physiol*. (2011) 589:431–43. doi: 10.1113/jphysiol.2010.201806
12. Geurts ACH, de Haart M, van Nes IJW, Duysens J. A review of standing balance recovery from stroke. *Gait Posture*. (2005) 22:267–81. doi: 10.1016/j.gaitpost.2004.10.002
13. Tasseel-Ponche S, Yelnik AP, Bonan IV. Motor strategies of postural control after hemispheric stroke. *Neurophysiol Clin*. (2015) 45:327–33. doi: 10.1016/j.neucli.2015.09.003
14. Lukács M, Vécsei L, Beniczky S. Fiber density of the motor units recruited at high and low force output. *Muscle Nerve*. (2009) 40:112–14. doi: 10.1002/mus.21241
15. Marigold DS, Eng JJ. Altered timing of postural reflexes contributes to falling in persons with chronic stroke. *Exp Brain Res*. (2006) 171:459–68. doi: 10.1007/s00221-005-0293-6
16. Pollock CL, Ivanova TD, Hunt MA, Garland SJ. Behavior of medial gastrocnemius motor units during postural reactions to external perturbations after stroke. *Clin Neurophysiol*. (2015) 126:1951–8. doi: 10.1016/j.clinph.2014.12.015
17. McGill KC, Lateva ZC, Marateb HR. EMGLAB: an interactive EMG decomposition program. *J Neurosci Methods*. (2005) 149:121–33. doi: 10.1016/j.jneumeth.2005.05.015
18. Holobar A, Minetto MA, Botter A, Negro F, Farina D. Experimental analysis of accuracy in the identification of motor unit spike trains from high-density surface EMG. *IEEE Trans Neural Syst Rehabil Eng*. (2010) 18:221–9. doi: 10.1109/TNSRE.2010.2041593
19. Holobar A, Zazula D. Multichannel blind source separation using convolution kernel compensation. *IEEE Trans Signal Process*. (2007) 55:4487–96. doi: 10.1109/TSP.2007.896108
20. Mesin L, Merletti R, Vieira TM. Insights gained into the interpretation of surface electromyograms from the gastrocnemius muscles: a simulation study. *J Biomech*. (2011) 44:1096–103. doi: 10.1016/j.jbiomech.2011.01.031
21. Holobar A, Minetto MA, Farina D. Accurate identification of motor unit discharge patterns from high-density surface EMG and validation with a novel signal-based performance metric. *J Neural Eng*. (2014) 11:016008. doi: 10.1088/1741-2560/11/1/016008
22. Hodson-Tole EF, Loram ID, Vieira TM. Myoelectric activity along human gastrocnemius medialis: different spatial distributions of postural and electrically elicited surface potentials. *J Electromyogr Kinesiol*. (2013) 23:43–50. doi: 10.1016/j.jelekin.2012.08.003
23. Pernet CR, Wilcox R, Rousselet GA. Robust correlation analyses: false positive and power validation using a new open source matlab toolbox. *Front Psychol*. (2012) 3:606. doi: 10.3389/fpsyg.2012.00606
24. Héroux ME, Brown HJ, Inglis JT, Siegmund GP, Blouin J-S. Motor units in the human medial gastrocnemius muscle are not spatially localized or functionally grouped. *J Physiol*. (2015) 593:3711–26. doi: 10.1113/JP270307
25. Vieira TM, Wakeling JM, Hodson-Tole EF. Is there sufficient evidence to claim muscle units are not localised and functionally grouped within the human gastrocnemius? *J Physiol*. (2016) 594:1953–4. doi: 10.1113/JP271866
26. Merletti R, Lo Conte L, Avignone E, Guglielminotti P. Modeling of surface myoelectric signals. I. Model implementation. *IEEE Trans Biomed Eng*. (1999) 46:810–20. doi: 10.1109/10.771190
27. Ryan AS, Buscemi A, Forrester L, Hafer-Macko CE, Ivey FM. Atrophy and intramuscular fat in specific muscles of the thigh. *Neurorehabil Neural Repair*. (2011) 25:865–72. doi: 10.1177/1545968311408920
28. Lukács M, Vécsei L, Beniczky S. Large motor units are selectively affected following a stroke. *Clin Neurophysiol*. (2008) 119:2555–8. doi: 10.1016/j.clinph.2008.08.005
29. Vieira TM, Botter A, Muceli S, Farina D. Specificity of surface EMG recordings for gastrocnemius during upright standing. *Sci Rep*. (2017) 7:13300. doi: 10.1038/s41598-017-13369-1
30. Rafuse VF, Gordon T. Self-reinnervated cat medial gastrocnemius muscles. II. analysis of the mechanisms and significance of fiber type grouping in reinnervated muscles. *J Neurophysiol*. (1996) 75:282–97.
31. Genthon N, Gissot A-S, Froger J, Rougier P, Pérennou D. Posturography in patients with stroke: estimating the percentage of body weight on each foot from a single force platform. *Stroke*. (2008) 39:489. doi: 10.1161/STROKEAHA.107.493478
32. Roerdink M, Geurts ACH, de Haart M, Beek PJ. On the relative contribution of the paretic leg to the control of posture after stroke. *Neurorehabil Neural Repair*. (2009) 23:267–74. doi: 10.1177/1545968308323928
33. Garland SJ, Pollock CL, Ivanova TD. Could motor unit control strategies be partially preserved after stroke? *Front Hum Neurosci*. (2014) 8:864. doi: 10.3389/fnhum.2014.00864
34. Lee SSM, Piazza SJ. Inversion-eversion moment arms of gastrocnemius and tibialis anterior measured *in vivo*. *J Biomech*. (2008) 41:3366–70. doi: 10.1016/j.jbiomech.2008.09.029
35. Vieira TM, Minetto MA, Hodson-Tole EF, Botter A. How much does the human medial gastrocnemius muscle contribute to ankle torques outside the sagittal plane? *Hum Mov Sci*. (2013) 32:753–67. doi: 10.1016/j.humov.2013.03.003
36. Vieira TM, Merletti R, Mesin L. Automatic segmentation of surface EMG images: improving the estimation of neuromuscular activity. *J Biomech*. (2010) 43:2149–58. doi: 10.1016/j.jbiomech.2010.03.049
37. Van Leeuwen JL, Spoor CW. Modelling the pressure and force equilibrium in unipennate muscles with in-line tendons. *Philos Trans R Soc Lond B Biol Sci*. (1993) 342:321–33. doi: 10.1098/rstb.1993.0162
38. McNulty PA, Lin G, Doust CG. Single motor unit firing rate after stroke is higher on the less-affected side during stable low-level voluntary contractions. *Front Hum Neurosci*. (2014) 8:518. doi: 10.3389/fnhum.2014.00518
39. Bohannon RW, Walsh S. Nature, reliability, and predictive value of muscle performance measures in patients with hemiparesis following stroke. *Arch Phys Med Rehabil*. (1992) 73:721–5.
40. Fimland MS, Moen PMR, Hill T, Gjellesvik TI, Tørhaug T, Helgerud J, Hoff J. Neuromuscular performance of paretic versus non-paretic plantar flexors after stroke. *Eur J Appl Physiol*. (2011) 111:3041–9. doi: 10.1007/s00421-011-1934-z

Conflict of Interest Statement: The authors declare that the research was conducted in the absence of any commercial or financial relationships that could be construed as a potential conflict of interest.

frontiers in Neurology

ORIGINAL RESEARCH
published: 27 August 2019
doi: 10.3389/fneur.2019.00930

Repetitive Peripheral Magnetic Nerve Stimulation (rPMS) as Adjuvant Therapy Reduces Skeletal Muscle Reflex Activity

Volker R. Zschorlich[1,2]*, *Martin Hillebrecht*[3], *Tammam Tanjour*[1], *Fengxue Qi*[1,4,5], *Frank Behrendt*[6], *Timo Kirschstein*[7] and *Rüdiger Köhling*[2,7]

[1] Faculty of Philosophy, Institute of Sports Science, University of Rostock, Rostock, Germany, [2] Department of Ageing of Individuals and Society, Faculty of Interdisciplinary Research, University of Rostock, Rostock, Germany, [3] Department of Sport Science, University of Oldenburg, Oldenburg, Germany, [4] Department of Psychology and Neurosciences, Leibniz Research Centre for Working Environment and Human Factors, Technical University Dortmund, Dortmund, Germany, [5] Department of Sport Training, Sport Coaching College, Beijing Sport University, Bejing, China, [6] Reha Rheinfelden, Research Department, Rheinfelden, Switzerland, [7] Oscar-Langendorff-Institute of Physiology, University Medicine Rostock, Rostock, Germany

OPEN ACCESS

Edited by:
Xiaogang Hu,
University of North Carolina at Chapel Hill, United States

Reviewed by:
Domenico Antonio Restivo,
Ospedale Garibaldi, Italy
Cristiano De Marchis,
Roma Tre University, Italy

***Correspondence:**
Volker R. Zschorlich
volker.zschorlich@uni-rostock.de

Specialty section:
This article was submitted to Neurorehabilitation, a section of the journal Frontiers in Neurology

Received: *20 May 2019*
Accepted: *09 August 2019*
Published: *27 August 2019*

Citation:
Zschorlich VR, Hillebrecht M, Tanjour T, Qi F, Behrendt F, Kirschstein T and Köhling R (2019) Repetitive Peripheral Magnetic Nerve Stimulation (rPMS) as Adjuvant Therapy Reduces Skeletal Muscle Reflex Activity. Front. Neurol. 10:930. doi: 10.3389/fneur.2019.00930

Background: The reduction of muscle hypertonia and spasticity, as well as an increase in mobility, is an essential prerequisite for the amelioration of physiotherapeutical treatments. Repetitive peripheral magnetic nerve stimulation (rPMS) is a putative adjuvant therapy that improves the mobility of patients, but the underlying mechanism is not entirely clear.

Methods: Thirty-eight participants underwent either an rPMS treatment ($N = 19$) with a 5 Hz stimulation protocol in the posterior tibial nerve or sham stimulation ($N = 19$). The stimulation took place over 5 min. The study was conducted in a pre-test post-test design with matched groups. Outcome measures were taken at the baseline and after following intervention.

Results: The primary outcome was a significant reduction of the reflex activity of the soleus muscle, triggered by a computer-aided tendon-reflex impact. The pre-post differences of the tendon reflex response activity were −23.7% ($P < 0.001$) for the treatment group. No significant effects showed in the sham stimulation group.

Conclusion: Low-frequency magnetic stimulation (5 Hz rPMS) shows a substantial reduction of the tendon reflex amplitude. It seems to be an effective procedure to reduce muscular stiffness, increase mobility, and thus, makes the therapeutic effect of neuro-rehabilitation more effective. For this reason, the 5 Hz rPMS treatment might have the potential to be used as an adjuvant therapy in the rehabilitation of gait and posture control in patients suffering from limited mobility due to spasticity. The effect observed in this study should be investigated conjoined with the presented method in patients with impaired mobility due to spasticity.

Keywords: muscle spasticity, muscle hypertonia, pain, cerebral palsy, reflex, magnetic stimulation

INTRODUCTION

Reducing muscle hypertonia or spasticity in order to regain independent mobility is an essential goal of a physiotherapeutical treatment in neuro-rehabilitation. The rapid normalization of the muscle tone is a criterion that can crucially influence the outcome of future rehabilitation or in training programs. An increase of hypertonia and stiffness in skeletal muscles is a common phenomenon that is associated with considerable discomfort or pain and refers to both chronic and acute cases, e.g., in post-stroke rehabilitation (1), or might also occur after strength training (2–4). Some form of intervention is, therefore, required, in case of spasticity interferes with function, or where long-term complications are expected (5). Based on the knowledge of the mechanisms responsible for muscular hypertonia, one option for patients could be a targeted treatment with repetitive peripheral magnetic nerve stimulation (rPMS), as adjuvant therapy that could improve the mobility of patients or athletes.

Some studies have been conducted to describe the implications of rPMS (reducing hypertonia, spasticity, and so forth) on spinal neuromuscular structures [for review (6)]. By employing a pulsed magnetic stimulation of the peripheral nerve a twitch can be triggered in a specific skeletal muscle. This twitch contraction is achieved initially through the triggering of an action potential in the associated motor nerve (7). The axon of the α-motor neuron conducts the generated action potential to the neuromuscular junction, thus triggering a twitch contraction in the muscle. A rPMS caused muscle activation is induced by a nerve stimulation and not by direct muscle activation (8). Depending on the stimulation frequency, the repetitive stimulation of the nerve can lead to muscle contraction in such a way that the individual twitches merge on higher stimulation frequencies. In this experiment, the magnetic stimulation was performed at the branches of the posterior tibial nerve, which resulted in an unfused twitch contraction of the triceps surae muscle. The stimulation frequency was chosen to be low enough, at five pulses per second, so that no complete merging of the individual twitches was observed.

The effect of a magnetic stimulation, especially on the peripheral nerves, has been described by some authors (9–17). Transcutaneous electrical nerve stimulation (TENS) shows some efficacy in treating spasticity (18, 19), as measured by a modified clinical Ashworth-scale. A significant reduction of the muscle tone after a TENS treatment (decrease in resistive torque) was observed (20), but it was not always associated with a decrease in reflex activity. In contrast to TENS, magnetic pulses can be applied painlessly to the efferent motor nerves at higher intensities, since the cutaneous receptors and their nerves are not stimulated to the same extent. Furthermore, rPMS can stimulate deeper nerve structures that cannot be targeted with TENS. It is of particular importance, in terms of a painless use in therapeutic rPMS applications, that the activation of the afferent sensory nerves is significantly lower with a magnetic stimulation (21, 22). A painless treating of motor nerve structures with a magnetic stimulation is possible. Whereas, the treating of peripheral nerves with an electric stimulation gives rise to significant pain symptoms (23–25). Different rPMS protocols have been used to successfully treat skeletal muscle spasticity, which could be defined by an increase of phasic and tonic stretch reflex activity, depending on the velocity of the muscle stretch (26). In an earlier study, it was found that it was possible to improve electrophysiological measures of spasticity by using a biphasic 12 Hz rPMS protocol for 8 s, followed by a 22 s rest, for a total of 30 min stimulation (27). Stimulations with 15 Hz of 3 s duration and 30 trains, with an inter-train-interval of 2 s, with 1,350 impulses in total, and with an intensity of 60 A/μs (40% of maximal stimulator intensity), applied to the rectus femoris muscle (28), or the triceps surae muscle complex (29), results in different effects.

A magnetic stimulation, with a 20 Hz repetition rate, was used by Struppler et al. (30) and Marz-Loose and Siemes (31), but with a different amount of impulses (5,000 and 2,000, respectively), and with different stimulation sites. A 50 Hz rPMS protocol was used to decrease spasticity (32) in six sessions, with a continuous theta-burst of 200 ms, at an inter-stimulus interval of 5 sec^{-1}, with a repetition rate in a 60 s train, with 900 impulses and an intermittent theta-burst. The theta-mode consisted of 2 s trains, repeated every 10 s, with 900 impulses (300 s). The described intermittent theta-burst stimulation produced a cyclic activation-relaxation of the muscle (33).

A low-frequency stimulation with 3 Hz (34) was applied as an accompanying curative treatment to physiotherapy in post-stroke rehabilitation. This low- frequency rPMS was performed with 600 stimuli, in a series of 3 s, followed by 3 s rest, at a 60% intensity. All studies except one (29) reported positive clinical or physiological effects of the rPMS treatment. Despite these findings, the mechanisms of treating muscle tone, clonus, and spasticity, are still poorly understood (35, 36) and they are not ideally measurable, either mechanically (37), or by using clinical scales (38). A study of the reflex responses provides a quantitative representation of the effects of an rPMS treatment. One of the central questions in this context is: "under what conditions can the spinal motor circuits be influenced by means of targeted magnetic pulses?" Thus, the purpose of this study was to investigate the effect of 5 Hz rPMS on the regulatory spinal circuits. The underlying hypothesis was the following: the researchers presumed that the application of repetitive low-frequency pulsed magnetic fields to the peripheral nerves of the muscle would reduce the compound muscle action potential (CMAP) amplitudes of the tendon-reflex (T-reflex) activities of the soleus muscle. Since the measurement of muscle stiffness or spasticity, biomechanically encounters great difficulties, an investigation of the peripheral reflex processes serves as a quantifiable marker (31). A validation of the study's hypothesis, as given in the present paper, opens up the possibility of introducing rPMS, in order to treat the phenomenon of muscle hypertonia, in a wide range of applications in physiotherapy, and in the various forms of muscle training. To the best of the authors' knowledge, this study is the first, which addresses the effects of

Abbreviations: ANOVA, analysis of variance; $CMAP_{pp}$, compound muscle action potential (peak-to-peak); EMG, Electromyography; rPMS, repetitive peripheral magnetic stimulation; TENS, transcutaneous electrical stimulation; (T-reflex), tendon reflex.

rPMS on tendon reflex response behavior of the soleus muscle in quantitative detail, and it provides a quantifiable parameter of muscle relaxation.

METHODS

Ethics Statement

The study was approved by the local ethics committee of the medical faculty of the University Rostock, Germany (Identifier No. A20160052), as required by the international standards of the *Declaration of Helsinki* (39). All participants gave written informed consent prior participation.

Participants

The study involved 38 subjects (40). Of these, 19 volunteers participated in the treatment group (TG; 12 men/7 women), with a mean age of 25.4 (±3.0), a mean height of 177.3 cm (±8.9 cm), and a mean body weight of 73.3 kg (±13.5 kg). This was while 19 subjects (14 men/5 women) participated in the control group (CG; sham stimulation), with a mean age of 27.5 (±4.4), a mean height of 177.1 cm (±8.6 cm), and a mean body weight of 72.3 kg (±10.0 kg). Those cases with metallic implants were excluded from the study (41). All of the subjects were healthy students and staff members, with unremarkable lower extremities, both in orthopedic and neurological terms, from whom informed consent was obtained (42). The participants had ample opportunities to familiarize themselves with the experiment and with the treatment.

Study Design

The investigation was conducted in a pre-test post-test design with matched groups. To rule out every other influence on the study and a reflex modulation beside the rPMS treatment, for example, a response decrease in the course of the experiment (43), we chose a control group design. In the control group, the identical procedure was performed as in the treatment group except the stimulator did not generate a magnetic field. The experiment initially involved the measurement of the Achilles tendon-reflex responses of the soleus muscle, by means of a linear-actuator reflex hammer (fifteen measurement trials) in a sitting position. The subjects were asked to maintain a right angle, both at the hip and at the knee joint during the reflex measurements. The tendon taps were applied with a time interval of at least 10 s in between, followed by 5 Hz rPMS, based on the protocol as described below. The stimulation was applied in a standing position to the posterior tibial nerve in the popliteal fossa, resulting in contractions of the triceps surae muscle. The magnetic stimulation of peripheral nerves is somewhat unfocal. We have tried to exclude any cocontraction with palpation of the tibial anterior muscle simultaneously. The subjects maintained a slight tension in the stimulated muscle over the entire stimulation period. In the third part of the experiment, the subjects were re-investigated in the sitting position, in order to ensure an identical reflex triggering. The re-examination of the T-reflex responses of the soleus muscle was carried out as described. Care was taken for the exact repositioning of the participants for the post measurements. Throughout the entire reflex measurements, complete relaxation of the soleus muscle was carefully controlled via online electromyography (EMG). Trials with a muscular activity >50 μV in a period of 100 ms prior to the reflex triggering were discarded. In order to check the uniformity of the experimental conditions when triggering the reflex responses, the impact forces were tested likewise. All of the impact forces were evaluated according to the peak values of the reflex hammer's impact.

Tendon Reflex

The T-reflex excitability of the soleus muscle was probed by a brisk mechanical impact elicited by a linear-actuator (Copley Controls, Canton, MA 02021, USA) at the Achilles tendon, with a thrust rod being moved in the acceleration mode. The actuator showed perfect repeatability and produced an absolute position accuracy of 0.35 mm. The control parameters were chosen as follows: (i) the reflex hammer (head of the thrust rod) exactly covered a distance of 40 mm from the home position to the impact point on the Achilles tendon; (ii) the home position of the actuator was defined by a contact of the reflex hammer at the Achilles tendon; and (iii) the development of the maximum impact force occurred within <12 ms, triggering supra-maximal reflexes (44). A tendon vibration due to the impact, as described (45), could not be detected when using the brisk actuator impacts.

The T-reflex of the soleus muscle was triggered in the sitting position, via an impact at the Achilles tendon (**Figure 1**). The level of the impact force depended individually on the elasticity of the biological structures (tendon, muscle, subcutaneous fatty tissue), with a minimum of 40 N, up to a maximum of 100 N, between the subjects. While there was some inter-individual variability, it was possible to trigger fairly uniform impacts in any given subject. The machine-controlled tendon taps produced constant supra-maximal impacts and elicited constant reflex responses. Methodologically, there was an important advantage in investigating the muscular relaxation via the T-reflex activity, as a measure at an interval scale level, in comparison to the commonly used Ashworth Scale (38).

Force Measurement

The force was measured during the impact that triggered the entire measuring process. The triggering threshold was 7 N, as accurately defined by the home position of the linear actuator. The reflex hammer fixed at the head of the thrust rod of the programmable linear actuator was equipped with a piezoelectric force sensor (Type 9011A, Kistler Instruments, Winterthur, Switzerland) and it measured the impact force at the Achilles tendon. The force-sensor data was prepared for the online presentation by using a Kistler charge amplifier type 5037A. The constant and comparable triggering of the reflex responses required an exact repositioning of the impact point at the tendon.

Electromyography—Recording and Sampling

The reflex responses were recorded by using a bipolar montage (46) of the cup-electrodes (HELLIGE baby-electrodes; GE medical systems, Milwaukee, USA), with an electrode area of about 12 mm^2 (Ag/AgCl) and an inter-electrode distance of

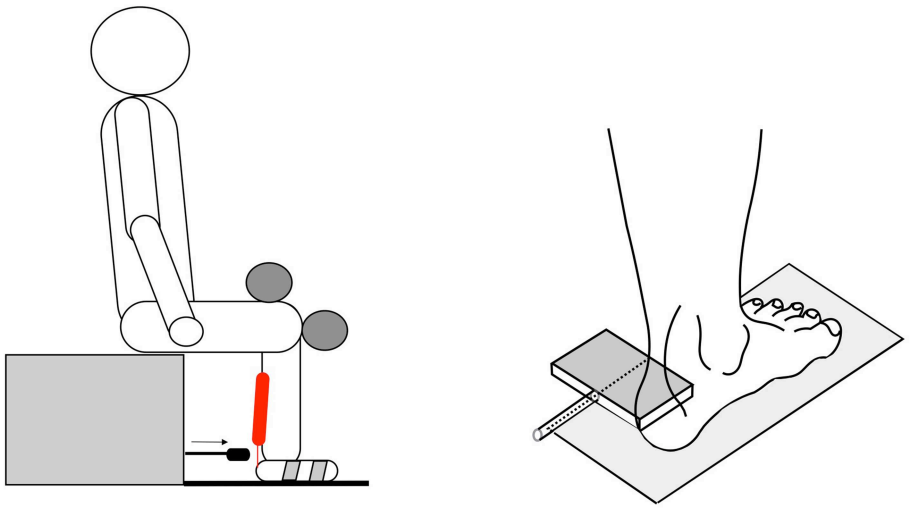

FIGURE 1 | The sketch shows the subject had a fixed sitting position. The subjects were seated comfortably upright, with a knee angle and a foot angle each of 90°. The left foot was fixed with two stirrups on a tempered (30°C) footplate. The upper leg was secured at the topside; the arm and head positions were kept constant during the whole experiment. The reflex-triggering hammer (right side) was equipped with a force sensor, in order to record the impact forces at the muscle-Achilles tendon-complex.

20 mm, placed longitudinally over the belly of the lateral soleus muscle. The skin preparation procedures were applied before the electrode application, i.e., cleaning the skin with alcohol and hair-removal before the positioning of the electrodes. An electrode gel (HELLIGE, GE medical systems, Milwaukee, USA) was used to ensure optimal skin-electrode contact. The electrodes and the twisted wires were fixed to the skin with adhesive tape. The surface electromyograms were recorded with a custom-made differential-amplifier (x1000 amplification, input resistance 16 GΩ). The signals were recorded with a DAQ-Card 6024 (National Instruments, Austin, Texas, USA) at a 12-bit resolution and at a sampling rate of 10,000/s, using the DIAdem 8.1 (National Instruments, Ireland) signal processing program. The movement artifacts in the EMG were filtered with a Butterworth 2nd-order high-pass filter with a cut-off frequency of 5 Hz (47).

Magnetic Stimulation

The pulsed magnetic stimulation was carried out with a Magpro 30+ stimulator with the Mag-Option (MagVenture, Skovlunde, Denmark—formerly Medtronic) and a parabolic coil type MMC-140, with the convex side being used. The stimulator generated biphasic symmetric pulses, with a duration of 280 μs, and a magnetic flux density of a maximal 4.5 Tesla. The stimulation protocol that was chosen from preliminary tests was performed with a stimulus intensity of 60% of the maximum stimulator output, corresponding to a current flux of 94 A/μs. The stimulation intensity was the same for each subject and was clearly visible above the motor threshold. The stimulation was carried out with bursts of 15 stimuli each, at 5 stimulations per second, and with 750 pulses in total. The interval between the trains was 3 s with 50 trains, and the stimulation lasted 5 min. The same procedure (coil positioning, stimulation, and the like) was conducted in the sham group, but without exposure to pulsed magnetic fields.

Data Analysis

The peak-to-peak compound muscle action potential ($CMAP_{pp}$) amplitude of the lateral site of the soleus muscle was recorded to characterize the reflex activity. The changes in $CMAP_{pp}$ were measured at the baseline condition and immediately after the magnetic stimulation or the sham stimulation. The $CMAP_{pp}$ amplitude measurements were made from the stationary EMG data (Butterworth high-pass filter). The algorithm added the absolute amplitude values from the lowest negative peak and the highest positive peak. In order to check the uniformity of the experimental conditions when triggering the reflex responses, the impact forces were observed online during each trial.

Statistics

The effects of the 5 Hz rPMS on the measurements of the spinal tendon reflex excitability were compared in the treatment group and the control group, using a mixed design analysis of variance (ANOVA) with between the group effects and the repeated-measure effects of time as the main factor. The data was analyzed by SPSS version 20.0 for Windows (SPSS Inc., Chicago, IL, USA). All of the values in the text, and figures, are expressed as mean ± SD. A $P < 0.05$ was considered significant.

RESULTS

The reflex response behavior of the skeletal musculature after the rPMS was measured in terms of the tendon tap triggered $CMAP_{pp}$ amplitude values. The $CMAP_{pp}$ amplitudes decreased after 5 Hz rPMS stimulation in the treatment group (**Figure 2**).

The ANOVA for repeated measures showed a significant interaction between the time and group [$F_{(1, 36)} = 16.789$; $P \leq 0.001$; $\eta_p^2 = 0.318$]. The *post-hoc* analysis with a Bonferroni adjustment demonstrated that the $CMAP_{pp}$ amplitude significantly decreased after the 5 Hz rPMS treatment

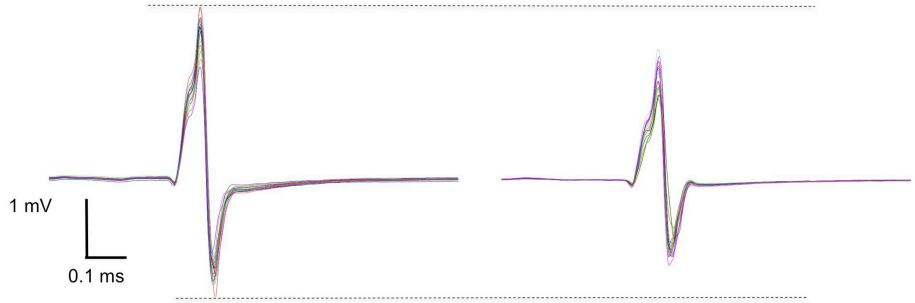

FIGURE 2 | A raw data set of one subject shows the effect of before (**left**) and after (**right**) the rPMS. Each graph shows 15 peak-to-peak superimposed compound muscle action potential ($CMAP_{pp}$) curves that were induced by a reflex hammer impact on the Achilles tendon. Mean $CMAP_{pp}$ amplitudes were ∼4.2 mV at baseline and ∼3.5 mV after the rPMS in this subject.

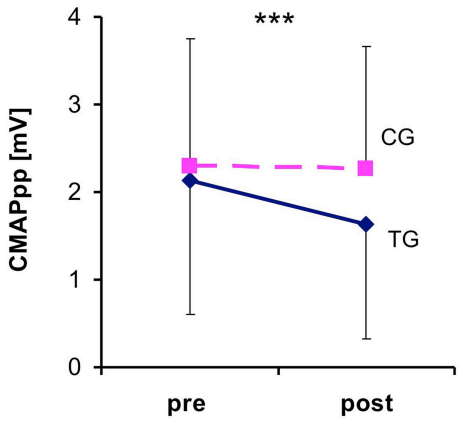

FIGURE 3 | Changes in the compound muscle action potential ($CMAP_{pp}$) size before the repetitive peripheral magnetic stimulation (rPMS) and post stimulation. The dashed line represents the control group (CG) and the continuous line indicates the treatment group (CG). Each bar corresponds to the SD value. Note that the reflex responses significantly decreased in size only after the rPMS in the treatment group. ***Denotes a significant difference between pre- and post-test (***$P \leq 0.001$) in CG.

when compared to the baseline measurements ($P \leq 0.001$). The $CMAP_{pp}$ amplitudes of the treatment group were 2.13 ± 1.54 mV in the pre-test and 1.63 ± 1.30 mV in the post-test, which meant a reduction of 23.7% (**Figure 3**). In contrast, the $CMAP_{pp}$ amplitudes of the control group revealed no significant differences ($P \leq 0.390$) from the pre-test (2.30 ± 1.45 mV) to the post-test (2.26 ± 1.40 mV) and the change rates were−1.74%.

DISCUSSION

The present paper demonstrates that a repetitive magnetic nerve stimulation (rPMS) with 750 stimuli at a stimulation frequency of 5 Hz reduces the T-reflex response of the soleus muscle. After the rPMS treatment, a substantial and significant reduction in the normalized $CMAP_{pp}$ amplitude after triggering the Achilles tendon reflex by −23.7% was found, in contrast to the control group (−1.74%). The pulsed magnetic stimulation of the muscles acted on the control state of the neuromuscular circuits; the reduction in the CMAP amplitude was apparently attributed to a significantly decreased excitation of the T-reflex triggered α-motor neurons. This means that the rPMS treatment of a muscle reduces a significant number of α-motor neurons from the triggering of an action potential. Presynaptic and/or postsynaptic processes may have influenced this.

The reason for the occurrence of such reflex inhibition after the treatment must remain unclear at this time since the functional processes of rPMS have not yet been fully explored. It is not known, for example, whether the effects of the magnetic stimulations take place via an orthodromic or an antidromic stimulation of the peripheral nerves. In the first case (orthodromic), the stimulation could directly act on the axons of the α-motor neurons and in the second case (antidromic), with a partial inactivation of the axon hillock. Alternatively, the stimulation could act on the axons of statically or dynamically oriented γ-motor neurons, or the muscle spindles, which would then induce secondary and indirect effects via spindle sensitivity changes. In the latter case (antidromic motor nerve stimulation), a reflex change via activation of a Renshaw inhibition is conceivable but not likely (48). Some investigations are hinting and speaking in favor of an effect being exerted on the γ-motor regulatory circuits by the magnetic stimulation, also influencing the tonus part of the γ-motor sensory system. This could, in part, explain the researchers' previous results (29), where no critical reduction of H-reflex activity was found after the rPMS, in accordance with the findings of Goulet et al. (19), who likewise found no substantial reduction of H-reflex activity after a TENS.

Thus, the sensory system's sensitivity appeared to decrease markedly. It is reasonable that this may be the explanation for the efficacy of an rPMS treatment. It is likely that the influence exerted by the magnetic stimulation of the tibial nerve caused a sensitivity reduction of the γ-motor regulatory circuit (see **Figure 4**). However, a conclusive differentiation among the possibilities as mentioned above would necessitate pharmacological interventions, which are impossible to obtain in healthy human subjects.

These findings might have a specific implication for clinical use, as there is varying evidence for the existing physiotherapeutic and pharmacological treatment approaches in the therapy of spastic syndrome. It is described in the literature, for instance,

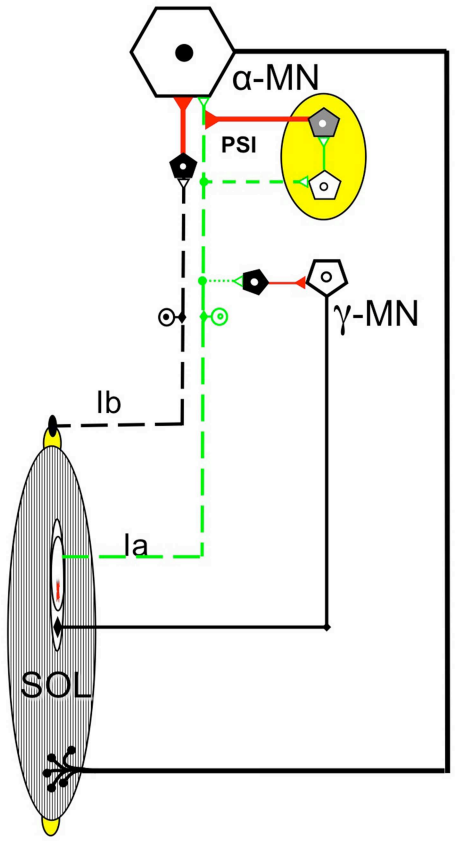

FIGURE 4 | The diagram shows the spinal circuitry that was possible involved γ-motor neurons (γ-MN), α-motor neurons (α-MN), Ia afferents (Ia), Ib afferents (Ib), or presynaptic mechanism (PSI), by near-muscle magnetic nerve stimulation. However, at this time, no conclusions can be reached about the mode of action of the magnetic stimulation on the spinal neuronal structures.

that there is a basically positive effect of a physiotherapeutical intervention (49), which is on the one hand, superior to a drug treatment alone, because of the side effects (50), but on the other hand, this still needs to be further investigated. Furthermore, anti-spastic drugs can improve spasticity on corresponding scales (e.g., on a modified Ashworth Scale), but the treatment is often not associated with an improvement in everyday activities. There was also no significant improvement in the gait parameters, as a result of the Botulinum toxin type A injection into the calf musculature (51, 52). In a combination with physiotherapy (53) or TENS (54, 55), positive effects were reported, which in turn, is still not sufficient for an unequivocal recommendation. However, in addition to controlled studies with a large number of subjects, systematic investigations of the dose-effect relationships of the various intervention combinations are lacking. Against this background, there is still room for new therapeutical methods. Based on this study's results, rPMS could indeed have a promising effect as an adjunct to other therapeutical methods. The duration of the outcome in healthy subjects and patients, the impact in a combination with other treatment approaches, and the usability and the feasibility in a clinical setting, should all be evaluated conjoined for a potential translation of rPMS into clinical practice with a quantitative tendon reflex measurement.

This study has some limitations. The stimulation of a peripheral nerve structure is not very focal. We used a large magnetic coil over the popliteal fossa, which limits specificity of stimulation in the posterior tibial nerve. It can not be ruled out that this peripheral stimulation causes further nerve structures to be excited. For this reason, we took care of the exact stimulation response and the fact that antagonistic muscles do not co-contract during the stimulation also. However, we cannot exclude subliminal influences on surrounding nerve structures (56). We only investigated healthy subjects, so it would be valuable to further verify whether the T-reflex is also altered in patient populations and whether that change is consistent with the positive effects found in the clinical assessments performed in earlier studies (34).

CONCLUSION

The results have demonstrated that the T-reflex was reduced after 5 Hz rPMS. This relaxing effect on the musculature was investigated in this experiment indirectly, by using the Achilles tendon reflex to represent the decrease in excitability of the α-motor neurons or the presynaptic effects. The artificial relaxation of the skeletal musculature has excellent practical benefits in a wide variety of fields. The use of rPMS in physiotherapy and neuro-rehabilitation is an important area where it can have significant effects; the therapeutical advances in spasticity and muscle hyperreflexia may also be achievable. In addition, the skeletal musculature tone can be reduced significantly after muscle training through an rPMS procedure.

DATA AVAILABILITY

The datasets analyzed in this manuscript are not publicly available. Requests to access the datasets should be directed to volker.zschorlich@uni-rostock.de.

AUTHOR CONTRIBUTIONS

The experiments were conducted in the Laboratory of the Department of Movement Science, Institute of Sport Science, University of Rostock, Germany. VZ and MH contributed to the conception and the design of the experiment. FQ, TT, and VZ collected the data. VZ, FB, FQ, and MH contributed to the analysis and the interpretation of the data. VZ, FB, FQ, MH, TK, and RK drafted the paper and revised it critically for important intellectual content.

FUNDING

FQ's funding was supported by the China Scholarship Council (201508080070).

ACKNOWLEDGMENTS

The researchers give thanks to Dipl. Eng. Andreas Mattke, and Dipl. Eng. Norbert Wolff, for their technical help in programming the reflex hammer.

REFERENCES

1. Turk R, Notley SV, Pickering RM, Simpson DM, Wright PA, Burridge JH. Reliability and sensitivity of a wrist rig to measure motor control and spasticity in poststroke hemiplegia. *Neurorehabil Neural Repair*. (2008) 22:684–96. doi: 10.1177/1545968308315599
2. Klinge K, Magnusson SP, Simonsen EB, Aagaard P, Klausen K, Kjaer M. The effect of strength and flexibility training on skeletal muscle electromyographic activity, stiffness, and viscoelastic stress relaxation response. *Am J Sports Med*. (1997) 25:710–6. doi: 10.1177/036354659702500522
3. Kubo K, Kanehisa H, Ito M, Fukunaga T. Effects of isometric training on the elasticity of human tendon structures *in vivo*. *J Appl Physiol*. (2001) 91:26–32. doi: 10.1152/jappl.2001.91.1.26
4. Grosset J-F, Piscione J, Lambertz D, Pérot C. Paired changes in electromechanical delay and musculo-tendinous stiffness after endurance or plyometric training. *Eur J Appl Physiol*. (2009) 105:131–9. doi: 10.1007/s00421-008-0882-8
5. Barnes MP. An overview of the clinical management of spasticity. In: Barnes MP, editors. *Upper Motor Neurone Syndrome and Spasticity: Clinical Management and Neurophysiology*. Newcastle upon Tyne: Cambridge University Press (2001). p. 1–8.
6. Beaulieu L, Schneider C. Effects of repetitive peripheral magnetic stimulation on normal or impaired motor control. A review. *Neurophysiol Clin*. (2013) 43:251–60. doi: 10.1016/j.neucli.2013.05.003
7. Zhu Y, Starr A, Haldeman S, Fu H, Liu J, Wu P. Magnetic stimulation of muscle evokes cerebral potentials by direct activation of nerve afferents: a study during muscle paralysis. *Muscle Nerve*. (1996) 19:1570–5.
8. Machetanz J, Bischoff C, Pichlmeier R, Riescher H, Meyer BU, Sader A, et al. Magnetically induced muscle contraction is caused by motor nerve stimulation and not by direct muscle activation. *Muscle Nerve*. (1994) 17:1170–5. doi: 10.1002/mus.880171007
9. Benecke R, Meyer B-U, Schönle P, Conrad B. Transcranial magnetic stimulation of the human brain: responses in muscles supplied by cranial nerves. *Exp Brain Res*. (1988) 71:623–32. doi: 10.1007/BF00248756
10. Maccabee P, Amassian V, Cracco R, Cadwell J. An analysis of peripheral motor nerve stimulation in humans using the magnetic coil. *Electroencephalogr Clin Neurophysiol*. (1988) 70:524–33. doi: 10.1016/0013-4694(88)90150-2
11. Chokroverty S. Magnetic stimulation of the human peripheral nerves. *Electromyogr Clin Neurophysiol*. (1988) 29:409–16.
12. Cros D, Day TJ, Shahani BT. Spatial dispersion of magnetic stimulation in peripheral nerves. *Muscle Nerve*. (1990) 13:1076–82. doi: 10.1002/mus.880131110
13. Amassian VE, Eberle L, Maccabee PJ, Cracco RQ. Modelling magnetic coil excitation of human cerebral cortex with a peripheral nerve immersed in a brain-shaped volume conductor: the significance of fiber bending in excitation. *Electroencephalogr Clin Neurophysiol*. (1992) 85:291–301. doi: 10.1016/0168-5597(92)90105-K
14. Polkey MI, Kyroussis D, Hamnegard CH, Mills GH, Green M, Moxham J. Quadriceps strength and fatigue assessed by magnetic stimulation of the femoral nerve in man. *Muscle Nerve*. (1996) 19:549–55.
15. Kobayashia M, Ueno S, Kurokawa T. Importance of soft tissue inhomogeneity in magnetic peripheral nerve stimulation. *Electroencephalogr Clin Neurophysiol*. (1997) 105:406–13. doi: 10.1016/S0924-980X(97)00035-0
16. Binkofski F, Classen J, Benecke R. Stimulation of peripheral nerves using a novel magnetic coil. *Muscle Nerve*. (1999) 22:751–7.
17. Harris ML, Luo YM, Watson AC, Rafferty GF, Polkey MI, Green M, et al. Adductor pollicis twitch tension assessed by magnetic stimulation of the ulnar nerve. *Am J Respir Crit Care Med*. (2000) 162:240–5. doi: 10.1164/ajrccm.162.1.9902073
18. Katz RT. Management of spastic hypertonia after stroke. *Neurorehabil Neural Repair*. (1991) 5:S5–12. doi: 10.1177/1361409691005 00502
19. Goulet C, Arsenault A, Bourbonnais D, Laramee M, Lepage Y. Effects of transcutaneous electrical nerve stimulation on H-reflex and spinal spasticity. *Scand J Rehabil Med*. (1996) 28:169–76.
20. Potisk K, Gregoric M, Vodovnik L. Effects of transcutaneous electrical nerve stimulation (TENS) on spasticity in patients with hemiplegia. *Scand J Rehabil Med*. (1995) 27:169–74.
21. Olney RK, So YT, Goodin DS, Aminoff MJ. A comparison of magnetic and electrical stimulation of peripheral nerves. *Muscle Nerve*. (1990) 13:957–63. doi: 10.1002/mus.880131012
22. Panizza M, Nilsson J, Roth BJ, Basser PJ, Hallett M. Relevance of stimulus duration for activation of motor and sensory fibers: implications for the study of H-reflexes and magnetic stimulation. *Electroencephalogr Clin Neurophysiol*. (1992) 85:22–9. doi: 10.1016/0168-5597(92)90097-U
23. Lotz BP, Dunne JW, Daube JR. Preferential activation of muscle fibers with peripheral magnetic stimulation of the limb. *Muscle Nerve*. (1989) 12:636–9. doi: 10.1002/mus.880120804
24. Han T-R, Shin H-I, Kim I-S. Magnetic stimulation of the quadriceps femoris muscle: comparison of pain with electrical stimulation. *Am J Phys Med Rehabil*. (2006) 85:593–9. doi: 10.1097/01.phm.0000223239. 93539.fe
25. Szecsi J, Götz S, Pöllmann W, Straube A. Force–pain relationship in functional magnetic and electrical stimulation of subjects with paresis and preserved sensation. *Clin Neurophysiol*. (2010) 121:1589–97. doi: 10.1016/j.clinph.2010.03.023
26. Lance J. What is spasticity? *Lancet*. (1990) 335:606. doi: 10.1016/0140-6736(90)90389-M
27. Nielsen JF, Klemar B, Hansen HJ, Sinkjær T. A new treatment of spasticity with repetitive magnetic stimulation in multiple sclerosis. *J Neurol Neurosurg Psychiatr*. (1995) 58:254. doi: 10.1136/jnnp.58.2.254-a
28. Zschorlich V, Baumgard L, Flack C. The influence of repetitive magnetic nerve stimulation (rMNS) on the spinal stretch reflex (in German: der Einfluss einer repetitiven magnetischen Nervenstimulation (rMNS) auf die Funktion des spinalen Dehnungsreflexes). In: Baumgärtner SD, Hänsel F, Wiemeyer JE, editors. *Dvs (German Society of Sportsscience) Conference - Section Sportmotorik*. Darmstadt: Verlag Universität Darmstadt (2009).
29. Behrens M, Mau-Möller A, Zschorlich V, Bruhn S. Repetitive peripheral magnetic stimulation (15 Hz RPMS) of the human soleus muscle did not affect spinal excitability. *J Sports Sci Med*. (2011) 10:39–44.
30. Struppler A, Angerer B, Gündisch C, Havel P. Modulatory effect of repetitive peripheral magnetic stimulation on skeletal muscle tone in healthy subjects: stabilization of the elbow joint. *Exp Brain Res*. (2004) 157:59–66. doi: 10.1007/s00221-003-1817-6
31. Marz-Loose H, Siemes H. Repetitive peripheral magnetic stimulation (in German: Repetitive periphere Magnetstimulation). *Der Nervenarzt*. (2009) 80:1489–95. doi: 10.1007/s00115-009-2835-9
32. Flamand VH, Beaulieu L-D, Nadeau L, Schneider C. Peripheral magnetic stimulation to decrease spasticity in cerebral palsy. *Pediatr Neurol*. (2012) 47:345–8. doi: 10.1016/j.pediatrneurol.2012.07.005
33. Flamand VH, Schneider C. Noninvasive and painless magnetic stimulation of nerves improved brain motor function and mobility in a cerebral palsy case. *Arch Phys Med Rehabil*. (2014) 95:1984–90. doi: 10.1016/j.apmr.2014. 05.014
34. Werner C, Zschorlich V, Hesse S. Repetitive peripheral magnetic stimulation as a muscle stiffness therapy after CNS-lesion (in German: repetitive periphere magnetstimulation als therapie der muskelstiffness nach ZNS-Läsion). In: *Jahrestagung der Deutschen Gesellschaft für Neurorehabilitation (DGNR)*. Fürth: German Neuroscience Society (GNS) (2012). p. 22.
35. Malhotra S, Pandyan A, Day C, Jones P, Hermens H. Spasticity, an impairment that is poorly defined and poorly measured. *Clin Rehabil*. (2009) 23:651–8. doi: 10.1177/0269215508101747
36. Voerman GE, Gregoric M, Hermens HJ. Neurophysiological methods for the assessment of spasticity: the Hoffmann reflex, the tendon reflex, and the stretch reflex. *Disabil Rehabil*. (2005) 27:33–68. doi: 10.1080/09638280400014600
37. Lindberg PG, Gäverth J, Islam M, Fagergren A, Borg J, Forssberg H. Validation of a new biomechanical model to measure muscle tone in spastic muscles. *Neurorehabil Neural Repair*. (2011) 25:617–25. doi: 10.1177/1545968311403494
38. Fleuren JF, Voerman GE, Erren-Wolters CV, Snoek GJ, Rietman JS, Hermens HJ, et al. Stop using the Ashworth scale for the assessment of spasticity. *J Neurol Neurosurg Psychiatry*. (2010) 81:46–52. doi: 10.1136/jnnp.2009.177071
39. Harriss D, Atkinson G. Ethical standards in sport and exercise science research: 2014 update·. *Int J Sports Med*. (2013) 34:1025–8. doi: 10.1055/s-0033-1358756

40. Lachin JM. Introduction to sample size determination and power analysis for clinical trials. *Control Clin Trials*. (1981) 2:93–113. doi: 10.1016/0197-2456(81)90001-5
41. Walsh V, Rushworth M. A primer of magnetic stimulation as a tool for neuropsychology. *Neuropsychologia*. (1999) 37:125–36.
42. Moher D, Hopewell S, Schulz KF, Montori V, Gøtzsche PC, Devereaux P, et al. CONSORT 2010 explanation and elaboration: updated guidelines for reporting parallel group randomised trials. *J Clin Epidemiol.* (2010) 63:e1–37. doi: 10.1016/j.jclinepi.2010.03.004
43. Crone C, Johnsen L, Hultborn H, Ørsnes G. Amplitude of the maximum motor response (Mmax) in human muscles typically decreases during the course of an experiment. *Exp Brain Res*. (1999) 124:265–70. doi: 10.1007/s002210050621
44. Stam J, Van Crevel H. Measurement of tendon reflexes by surface electromyography in normal subjects. *J Neurol.* (1989) 236:231–7. doi: 10.1007/BF00314505
45. Burke D, Mckeon B, Skuse NF. The irrelevance of fusimotor activity to the Achilles tendon jerk of relaxed humans. *Ann Neurol.* (1981) 10:547–50. doi: 10.1002/ana.410100609
46. Merletti R, Hermens H. Detection and conditioning of the surface EMG signal. In: Merletti R, Parker P, editors. *Electromyography: Physiology, Engineering, and Noninvasive Applications*. New York, NY: Wiley (2004). p. 107–32.
47. Zschorlich VR. Digital filtering of EMG-signals. *Electromyogr Clin Neurophysiol.* (1989) 29:81–6.
48. Nielsen J, Crone C, Hultborn H. The spinal pathophysiology of spasticity–from a basic science point of view. *Acta Physiol*. (2007) 189:171–80. doi: 10.1111/j.1748-1716.2006.01652.x
49. Ansari N, Naghdi S. The effect of Bobath approach on the excitability of the spinal alpha motor neurones in stroke patients with muscle spasticity. *Electromyogr Clin Neurophysiol.* (2007) 47:29–36.
50. Tariq M, Akhtar N, Ali M, Rao S, Badshah M, Irshad M. Eperisone compared to physiotherapy on muscular tone of stroke patients: a prospective randomized open study. *J Pak Med Assoc.* (2005) 5:202–4.
51. Pittock S, Moore A, Hardiman O, Ehler E, Kovac M, Bojakowski J, et al. A double-blind randomised placebo-controlled evaluation of three doses of botulinum toxin type A (Dysport®) in the treatment of spastic equinovarus deformity after stroke. *Cerebrovasc Dis*. (2003) 15:289–300. doi: 10.1159/000069495
52. Kaji R, Osako Y, Suyama K, Maeda T, Uechi Y, Iwasaki M. Botulinum toxin type A in post-stroke lower limb spasticity: a multicenter, double-blind, placebo-controlled trial. *J Neurol.* (2010) 257:1330–7. doi: 10.1007/s00415-010-5526-3
53. Giovannelli M, Borriello G, Castri P, Prosperini L, Pozzilli C. Early physiotherapy after injection of botulinum toxin increases the beneficial effects on spasticity in patients with multiple sclerosis. *Clin Rehabil.* (2007) 21:331–7. doi: 10.1177/0269215507072772
54. Sonde L, Fernaeus S, Nilsson C, Viitanen M. Stimulation with low frequency (1.7 Hz) transcutaneous electric nerve stimulation (Low-TENS) increases motor function of the post-stroke paretic arm. *Scand J Rehab Med.* (1998) 30:95–9. doi: 10.1080/00365509844192
55. Sonde L, Kalimo H, Fernaeus S, Viitanen M. Low TENS treatment on post-stroke paretic arm: a three-year follow-up. *Clin Rehabil.* (2000) 14:14–9. doi: 10.1191/026921500673534278
56. Nilsson J, Panizza M, Roth BJ, Basser PJ, Cohen LG, Caruso G, et al. Determining the site of stimulation during magnetic stimulation of a peripheral nerve. *Electroencephalogr Clin Neurophysiol*. (1992) 85:253–64. doi: 10.1016/0168-5597(92)90114-Q

Conflict of Interest Statement: The authors declare that the research was conducted in the absence of any commercial or financial relationships that could be construed as a potential conflict of interest.

frontiers in Neurology

BRIEF RESEARCH REPORT
published: 21 February 2020
doi: 10.3389/fneur.2020.00078

Are There Trigger Points in the Spastic Muscles? Electromyographical Evidence of Dry Needling Effects on Spastic Finger Flexors in Chronic Stroke

Zhiyuan Lu[1,2], *Amy Briley*[2], *Ping Zhou*[1,2] *and Sheng Li*[1,2]*

[1] Department of Physical Medicine and Rehabilitation, McGovern Medical School, University of Texas Health Science Center at Houston, Houston, TX, United States, [2] TIRR Memorial Hermann Hospital, Houston, TX, United States

The purpose was to examine the immediate effects of dry needling to spastic finger muscles in chronic stroke. Ten chronic stroke patients with spasticity in finger flexors participated in this experiment. Dry needling to the flexor digitorum superficialis (FDS) muscle was performed under ultrasound guidance for about 30 s (about 100 times). Clinical assessment and intramuscular needle EMG readings were made before and immediately after dry needling. Immediately after needling, the FDS muscle was felt less tight to palpation and the proximal phalangeal joint rested in a less flexed position ($p = 0.036$). The MAS score decreased for FDS ($p = 0.017$) and flexor digitorum profundus (FDP) ($p = 0.029$). Motor unit action potential (MUAP) spikes decreased from 41.6 ± 5.5 to 6.7 ± 2.2 spikes/s ($p = 0.002$), an 84% reduction after dry needling. However, the pre-needling spike frequency was not correlated to MAS or resting position of the FDS muscles. Dry needling to the spastic finger flexors leads to immediate spasticity reduction, increased active range of motion, and decreased frequency of motor unit spontaneous firing spikes. The results suggest that latent trigger points possibly exist in spastic muscles and they contribute partly to spastic hypertonia of finger flexors in chronic stroke.

Keywords: spasticity, stroke, trigger points, EMG, dry needling

OPEN ACCESS

Edited by:
Xiaogang Hu,
University of North Carolina at Chapel Hill, United States

Reviewed by:
Guang H. Yue,
Kessler Foundation, United States
Ales Holobar,
University of Maribor, Slovenia

***Correspondence:**
Sheng Li
sheng.li@uth.tmc.edu

Specialty section:
This article was submitted to Neurorehabilitation, a section of the journal Frontiers in Neurology

Received: *15 November 2019*
Accepted: *22 January 2020*
Published: *21 February 2020*

Citation:
Lu Z, Briley A, Zhou P and Li S (2020) Are There Trigger Points in the Spastic Muscles? Electromyographical Evidence of Dry Needling Effects on Spastic Finger Flexors in Chronic Stroke. Front. Neurol. 11:78. doi: 10.3389/fneur.2020.00078

INTRODUCTION

Spasticity is a common disabling motor impairment after stroke. Though not fully understood, spasticity is a result of disinhibited descending excitatory inputs to spinal reflex circuitry, adaptive changes in intraspinal network and peripheral changes in spastic muscles (1). These excitatory inputs at least in part lead to hyperexcitable or spontaneous firing of motor units of spastic muscles (2). Adaptive changes occur in parallel, such as muscle fiber shortening and stiffening (3). They interact with each other in a vicious cycle, thus contributing to muscle overactivity and spasticity (4). Spasticity amplifies other motor impairments, e.g., weakness, and imposes significant limitations in patient's mobility and activities of daily living (5).

A wide spectrum of treatment options is available, including physical modality, stretching, oral medications to botulinum toxin injection and surgery to target different factors. Recently, there are

clinical observational reports of dry needling for spasticity management after stroke. Dry needling is largely known to be effective for management of myofascial pain through breakdown of taut bands of trigger points (6). Unlike commonly used botulinum toxin therapy, dry needling causes immediate and short-term spasticity reduction, increased active range of motion, and improved gait (7). It remains unclear whether dry needling-induced spasticity reduction is mediated through the same mechanisms as for trigger points. The purpose of this study was to examine the immediate effects of dry needling to spastic finger muscles in chronic stroke and to explore the potential underlying mechanisms with intramuscular needle EMG recordings and analysis.

METHODS

Study Design and Participants

Ten chronic stroke survivors with spasticity in finger flexors participated in this experiment (6 males and 4 females; average: 61.1 ± 4.1 years of age; 5 right spastic hemiplegia, and 5 left spastic hemiplegia). Time since stroke ranged from 6 months to 8 years, with an average of 4.6 ± 0.7 years. These patients were scheduled to receive botulinum toxin injections, including to their finger flexors. They gave written consent prior to dry needling. The data were retrospectively analyzed with approval from local ethic committee.

Dry needling to the FDS muscle was performed prior to botulinum toxin injections. A 27 gauge botulinum toxin injection needle connected to the EMG machine (Nicolet Viasys Viking system, sampling rate at 48 k Hz with a band-pass filtering from 20–10 K Hz) was used. This type of needle is specifically designed and manufactured for intramuscular recording, stimulating and injection. The needle was inserted into the FDS muscle (typically 1.2–2.5 cm in depth) from the taut band found by palpation. The needle tip position was visualized under ultrasound imaging (M Turbo, SonoSite, Bothell, WA), and was further verified by stretching of the fingers at the proximal interphalangeal (PIP) joints that induced increase in EMG amplitude and frequency. Continuous dry needling was performed by the injecting physician under ultrasound guidance for about 30 s (about 100 pokes).

Measurements of modified Ashworth scale (MAS), passive and active range of motion (PROM/AROM), and resting position of finger flexors were taken in the 3rd metacarpal phalangeal (MCP), PIP and distal interphalangeal (DIP) joints before and immediately (between 5 and 10 min) after dry needling. Resting position was measured using a goniometer when the subject's hand was rested on a table. MAS for FDS was estimated by ranging the PIP joint, i.e., stretching the FDS muscle individually, while stabilizing the subject's wrist and MCP joints at the naturally resting positions. MAS for FDP was estimated by ranging the DIP joint, i.e., stretching FDP specifically, while stabilizing the shaft of the middle phalange. Firmness of taut band of FDS muscles was assessed as well. These clinical assessments were performed by an independent, experienced physical therapist. The body configuration, the wrist joint position in particular, was maintained the same before and after needling. Intramuscular needle EMG readings from FDS were taken before and immediately after dry needling to measure spikes of spontaneous motor unit action potentials (MUAPs). In order to reduce the shift of recording area before and after dry needling, the needle tip location was visually seen under ultrasound guidance, and the depth and location was verified by the markers on the screen.

Electromyogram Analysis

Intramuscular needle EMG readings were exported to a PC for further processing using Matlab (MathWorks Inc., Natick, USA). A custom program was developed in order to identify and locate MUAP spikes. An MUAP spike was defined as any spontaneous discharge with a magnitude >100 microvolt and a rise time < 4 microsecond (**Figure 1C**) (8). Frequency of spontaneous MUAP spikes (i.e., the average number of spikes per second) over a 10-s period was calculated.

Statistical Analysis

Paired *t*-test and Wilcoxon signed-rank test were performed to analyze the dry needling effects (PRE vs. POST) on interval measures (e.g., resting position) and ordinal measures (e.g., MAS score), respectively. A significance level of 0.05 was used.

RESULTS

Participants reported immediate relief of muscle tightness after dry needling (**Figure 1B**). The pain caused by dry needling was tolerated well by all participants. Immediately after needling, the PIP joints rested in a less flexed position (PRE vs. POST: 105.0 ± 5.8 vs. 112.1 ± 7.0 degrees, $p = 0.036$), while the resting positions for the DIP (113.6 vs. 125.3 degrees, $p = 0.115$) and MCP (120.5 vs. 120.3 degrees, $p = 0.971$) joints remained the same. The FDS muscle was felt less tight to palpation (3.4 ± 0.2 vs. 1.9 ± 0.2, $p < 0.001$) on a 1–5 taut band tightness scale. The MAS score decreased for FDS (2.3 ± 0.4 vs. 1.2 ± 0.4, $p = 0.017$) and FDP (2.2 ± 0.5 vs. 1.3 ± 0.5, $p = 0.029$), but no changes in MAS for the MCP joint (1.8 ± 0.5 vs. 1.3 ± 0.4, $p = 0.17$). There was no difference in PROM before and after dry needling. In majority of patients (7 out of 10), these joints could be passively ranged to the full extension, i.e., a ceiling effect. However, for those patients with residual voluntary finger extension ($n = 2$), active ROM increased by 23.5 degrees at the PIP joint, 10 degrees at the DIP joint and 10 degrees at the MCP joint. The needle EMG recordings showed that the spikes of spontaneous MUAPs decreased from 41.6 ± 5.5 spikes/s to 6.7 ± 2.2 spikes/s ($p = 0.002$), an 84% reduction after dry needling (**Figures 1A,D**). However, the pre-needling spike frequency was not correlated to MAS or resting position of the FDS muscles.

DISCUSSION

In our study, dry needling effectively and immediately reduced finger flexor spasticity, improved resting joint position and active range of motion in chronic stroke survivors with finger flexor spasticity. These effects were accompanied with a significant reduction of MUAP discharge rate of finger flexors by 84%.

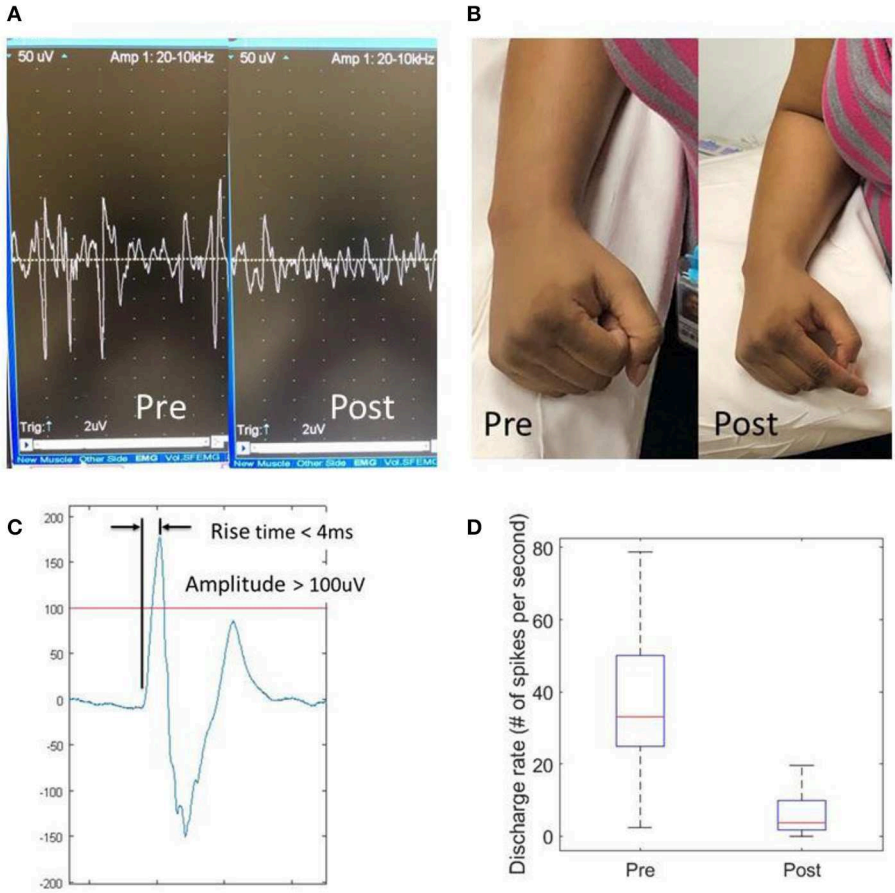

FIGURE 1 | Effects of dry needling on finger flexor spasticity after stroke. **(A)** Pre- and post-dry needling screen snapshots of resting spastic finger flexor EMG readings; **(B)** resting hand postures pre- and post-dry needling; **(C)** a representative motor unit action potential (MUAP). An MUAP must have a spike amplitude >100 uV with a rise time <4 ms; **(D)** Discharge rate of MUAPs pre- and post-dry needling.

Dry needling has been shown to break down muscle fibers and temporarily deplete acetylcholine neurotransmitters in animal studies (9), but EMG study in humans is rare. Our data show that dry needling is able to decrease MUAP spikes in humans. Spontaneous MUAP spikes are known to be reflective of motor units that are firing spontaneously or at subthreshold levels such that these motor units can easily be triggered by stretching or voluntary activation (2). Therefore, it is likely that concomitant reduction of finger flexor spasticity is resulted from temporary depletion of neurotransmitters. Though some muscle fibers were broken down by dry needling and such breakdown may contribute to MUAP reduction, the extent of MUAP reduction (84% reduction) and transit effects of spasticity reduction by dry needling (7) strongly argue against this relation.

On the other hand, it is known that trigger points develop as a result of excessive accumulation of acetylcholine at the motor endplate and intracellular Ca^{++} (10). Accumulated acetylcholine in the spastic muscles is likely to potentiate development of trigger points. Furthermore, muscle overactivity from sustained hyperexcitability and/or spontaneous firing of motor units could further facilitate and maintain trigger points in the spastic muscles. In turn, trigger points contribute to spastic hypertonia in a vicious cycle. The results of reduced muscle tightness and improved voluntary finger extension support the existence of trigger points in the spastic muscles and that breakdown of taut bands in trigger points contribute at least partly to the post-needling effects. The results also show that 30 s of dry needling has immediate effect on spasticity. Therefore, we believe that a combination of dry needling and botulinum toxin injection can enhance the outcome. The duration of the effect and the long-term cost/benefit of dry needling will be investigated in our future work by introducing a control group.

CONCLUSION

Dry needling to the spastic finger flexors leads to immediate spasticity reduction, increased active range of motion, and decreased frequency of spontaneous motor unit firing spikes. The results suggest that (latent) trigger points may exist in spastic

muscles and they contribute partly to spastic hypertonia of finger flexors in chronic stroke.

DATA AVAILABILITY STATEMENT

The datasets generated for this study are available on request to the corresponding author.

ETHICS STATEMENT

The studies involving human participants were reviewed and approved by the IRB committee, UTHealth. The ethics committee waived the requirement of written informed consent for participation.

AUTHOR CONTRIBUTIONS

SL was responsible for conceptualization. AB and SL were responsible for experiments and data collection. AB, ZL, PZ, and SL were responsible for data analysis and interpretation. ZL, PZ, and SL were responsible for manuscript draft and critical revision. All authors approved the final version.

REFERENCES

1. Li S, Francisco G. New insights into the pathophysiology of post-stroke spasticity. *Front Hum Neurosci.* (2015) 9:192. doi: 10.3389/fnhum.2015.00192
2. Mottram CJ, Wallace CL, Chikando CN, Rymer WZ. Origins of spontaneous firing of motor units in the spastic-paretic biceps brachii muscle of stroke survivors. *J Neurophysiol.* (2010) 104:3168–79. doi: 10.1152/jn.00463.2010
3. Lieber RL, Steinman S, Barash IA, Chambers H. Structural and functional changes in spastic skeletal muscle. *Muscle Nerve.* (2004) 29:615–27. doi: 10.1002/mus.20059
4. Gracies JM. Pathophysiology of spastic paresis. II: emergence of muscle overactivity. *Muscle Nerve.* (2005) 31:552–71. doi: 10.1002/mus.20285
5. Zorowitz RD, Gillard PJ, Brainin M. Poststroke spasticity: sequelae and burden on stroke survivors and caregivers. *Neurology.* (2013) 80:S45–52. doi: 10.1212/WNL.0b013e3182764c86
6. Cagnie B, Dewitte V, Barbe T, Timmermans F, Delrue N, Meeus M. Physiologic effects of dry needling topical collection on myofascial pain. *Curr Pain Headache Rep.* (2013) 17:348. doi: 10.1007/s11916-013-0348-5
7. Sánchez-Mila Z, Salom-Moreno J, Fernández-De-las-peñas C. Effects of dry needling on poststroke spasticity, motor function and stability limits: a randomised clinical trial. *Acupunct Med.* (2018) 36:358–66. doi: 10.1136/acupmed-2017-011568
8. Chang SH, Francisco GE, Zhou P, Rymer WZ, Li S. Spasticity, weakness, force variability, and sustained spontaneous motor unit discharges of resting spastic-paretic biceps brachii muscles in chronic stroke. *Muscle Nerve.* (2013) 48:85–92. doi: 10.1002/mus.23699
9. Liu QG, Liu L, Huang QM, Nguyen TT, Ma YT, Zhao JM. Decreased spontaneous electrical activity and acetylcholine at myofascial trigger spots after dry needling treatment: a pilot study. *Evid Based Complement Alternat Med.* (2017) 2017:3938191. doi: 10.1155/2017/3938191
10. Gerwin RD. The taut band and other mysteries of the trigger point: an examination of the mechanisms relevant to the development and maintenance of the trigger point. *J Musculoskelet Pain.* (2008) 16:115–21. doi: 10.1080/10582450801960081

Conflict of Interest: The authors declare that the research was conducted in the absence of any commercial or financial relationships that could be construed as a potential conflict of interest.

frontiers in Neurology

ORIGINAL RESEARCH
published: 28 February 2020
doi: 10.3389/fneur.2020.00101

Can the Large-Scale Decrement in Repetitive Nerve Stimulation Be Used as an Exclusion Criterion for Amyotrophic Lateral Sclerosis?

Li Shang†, *Hong Chu*† *and Zuneng Lu**

Department of Neurology, Renmin Hospital, Wuhan University, Wuhan, China

OPEN ACCESS

Edited by:
Francesco Negro, University of Brescia, Italy

Reviewed by:
David Abraham Gabriel, Brock University, Canada
Stefano Cotti Piccinelli, Civil Hospital of Brescia, Italy

****Correspondence:***
Zuneng Lu
lzn196480@126.com

†*These authors have contributed equally to this work*

Specialty section:
This article was submitted to Neuromuscular Diseases, a section of the journal Frontiers in Neurology

Received: *19 November 2019*
Accepted: *29 January 2020*
Published: *28 February 2020*

Citation:
Shang L, Chu H and Lu Z (2020) Can the Large-Scale Decrement in Repetitive Nerve Stimulation Be Used as an Exclusion Criterion for Amyotrophic Lateral Sclerosis? Front. Neurol. 11:101. doi: 10.3389/fneur.2020.00101

Objective: The objectives of this work were to identify the characteristics of repetitive nerve stimulation (RNS) in patients with amyotrophic lateral sclerosis (ALS) and further verify the electrophysiological exclusion criteria of ALS.

Methods: A total of 150 patients with ALS who were admitted to the Department of Neurology of Renmin Hospital of Wuhan University from January 2015 to December 2018 were enrolled. Clinical and electrophysiological data of the enrolled patients were collected. The differences in the amplitudes of the compound muscle action potential (CMAP) between the trapezius muscle (Trap) and the abductor digiti minimi (ADM) in low-frequency RNS were compared. Furthermore, we analyzed the associations between decremental responses and gender, onset age, duration of disease, onset site, Amyotrophic Lateral Sclerosis Functional Rating Scale—Revised (ALSFRS-R), disease progression rate, and CMAP amplitude.

Results: A significant decrement (≥20%) in at least one muscle was observed in 11.3% of the ALS patients, while decrements (≥10%) in at least one muscle were observed in 41.3%. The decremental percentage in the trapezius muscle was significantly higher than that in the abductor digiti minimi ($P < 0.001$). The onset age, duration of disease, onset site, and disease progression rate did not affect decremental responses. The decremental responses in RNS were more significant in ALS patients with low ALSFRS-R scores ($P = 0.01$). Moreover, there was a positive linear correlation between the CMAP amplitude and the decremental percentage of Trap and ADM in ALS patients.

Conclusions: CMAP decremental responses in RNS were common in ALS patients, suggesting abnormalities of neuromuscular junctions (NMJs). It is worthy of further discussion whether to consider a decrement >20% in RNS as a diagnostic exclusion criterion for ALS.

Keywords: amyotrophic lateral sclerosis, repetitive nerve stimulation, electrophysiological diagnostic criteria, compound muscle action potential, neuromuscular junctions

INTRODUCTION

Amyotrophic lateral sclerosis (ALS), the most quintessential motor neuron disease, affects both upper and lower motor neurons, and leads to progressive muscle atrophy and weakness (1). Mulder et al. (2) originally reported that decremental responses in low-frequency repetitive nerve stimulation (RNS) tests were observed in ALS patients. Subsequently, domestic and foreign studies have confirmed this phenomenon (3–5). The electrophysiological diagnostic criteria of ALS revised by the World Federation of Neurology Research Group on Motor Neuron Diseases pointed out that a significant compound muscle action potential (CMAP) decrement >20% in RNS was a diagnostic exclusion criterion for ALS (6). However, later studies demonstrated that a decrement >20% was observed in ALS patients (4, 7, 8). So far, none of the published studies has indicated the proportion of patients with a decrement of 20% or greater. And the exclusion criteria have not been extensively validated. In addition, the amplitude and incidence of decremental responses and the criteria for the positive decrement were inconsistent among previous research.

In this study, we described the amplitude and incidence of CMAP in low-frequency RNS of ALS patients and explored the correlations between decremental responses and clinical characteristics. We further validated the electrophysiological diagnostic exclusion criteria of ALS, which will enable a better understanding of the disease diagnosis.

METHODS

Patients

A total of 150 patients at the Department of Neurology of Renmin Hospital of Wuhan University were recruited from January 2015 to December 2018. According to the Awaji criteria (9), patients were classified into probable ALS (43 patients) and definite ALS (107 patients). All patients were subjected to rigorous neurological examinations, EMG examinations, blood tests, including serum acetylcholine (ACH) receptor antibodies, cerebrospinal fluid examinations, and imaging studies to exclude important ALS mimics. The exclusion criteria were as follows: (1) patients with a history of poliomyelitis; (2) patients with a positive response to ACH receptor antibodies; (3) patients with spinal cord tumor and with autoimmune disorders; (4) patients with other diseases affecting peripheral nerves, neuromuscular junction (NMJ), or muscles; and (5) patients without complete clinical records.

Method of RNS

All patients underwent routine electromyography performed on a Keypoint Workstation (31A06, Alpine BioMedApS, Denmark), including nerve conduction tests, needle electromyography, and RNS. The detection method followed the national guidelines (10). The surface electrode was stimulated and recorded, and the response to the stimulus was recorded 10 times each time. The accessory nerve was stimulated on the posterior border of the sternocleidomastoid. The ulnar nerve was stimulated on the wrist. The surface recording electrodes were used to record over the belly of the trapezius muscle (Trap) and the abductor digiti minimi (ADM), which respectively represented the proximal muscle and the distal muscle. The reference electrodes were placed on the tendon of the tested muscle. The skin temperature over the examined muscle was maintained at 33°C or above throughout the examination. Filters were set between 20 Hz and 3 kHz.

Study Design

The Amyotrophic Lateral Sclerosis Functional Rating Scale—Revised (ALSFRS-R) was used to calculate the monthly rate of change in ALSFRS-R, which represented the disease progression rate. The greater the value of progression obtained, the faster the disease progressed:

$$\begin{aligned} &\textit{Disease}\quad \textit{progression rate} \\ &\qquad = (48 - \textit{actual score})/\textit{duration}\ (\textit{months}) \end{aligned}$$

The decremental responses at a frequency of 3 Hz were mainly analyzed. The baseline-to-negative peak amplitudes of the first and fifth CMAPs at the supramaximal intensity (1.25-fold maximal intensity for the M-wave response) were measured. The CMAP decrement in the peak-to-peak amplitude was measured by the decremental percentage of the fifth CMAP as compared to the first CAMP amplitude. Decremental responses of ≥10% were defined as positive. Patients were divided into the positive decrement group and the negative decrement group based on whether the decrement was ≥10%. The data on the lower side of the CMAP amplitude was the standard. The correlations between the decremental responses and ALSFRS-R scores and CMAP amplitude were analyzed.

Statistical Analysis

Statistics calculations were performed on the SPSS 22.0 software. The Kolmogorov–Smirnov test was used to evaluate whether the data were normally distributed. Parameters with a normal distribution were described as the mean ± standard deviation (SD), and those with a non-normal distribution were expressed as the median values (M) and interquartile range (Q). Continuous variables that were normally distributed were compared using Student's t-test. Mann–Whitney U-tests were implemented to analyze values with a non-normal distribution. The categorical variables were expressed as the number of cases (n) and percentage (%), and the chi-squared test was used for comparison between groups. Correlation analysis was performed using Spearman's test. $P < 0.05$ was considered to be significant.

RESULTS

General Information

There were 85 males and 65 females, with ages from 28 to 80 years (mean age of 56.66 ± 11.29 years), in the included patients. The median duration from symptom onset was 14.34 ± 12.69 months. The ALSFRS-R scores were in the range 24–46, and the median was 40.5. There were 75 cases with upper limb onset and 41 cases with lower limb onset. The rest of the cases were with bulbar onset.

RNS Results

The distributions of decremental responses are summarized in **Table 1**. When the CMAP decrement of ≥10% was used as a criterion, the positive decrement in at least one muscle accounted for 41.3% (62/150), most of which were in the proximal muscle (**Figure 1**). The CMAP decremental percentage ranged from 10 to 29.57%, with an average of 16.63% in patients with a positive decrement.

Correlation Between Decremental Response and Clinical Features and CMAP Amplitude

Compared with the patients in the negative decrement group, the patients in the positive decrement group showed lower ALSFRS-R scores and CMAP amplitudes in both proximal and distal muscles (**Table 2**). There was a positive linear correlation between the CMAP amplitude and the decremental percentage in Trap and ADM of ALS patients ($r = 0.219$, $P = 0.007$; $r = 0.184$, $P = 0.024$, respectively; **Figure 2**).

DISCUSSION

A number of studies have demonstrated that decremental responses were frequently observed in ALS patients. Nevertheless, the positive rate of decremental responses varied due to the diverse sample sizes, muscles, and decremental positive criteria. When the CMAP decrement of ≥10% was defined as abnormal, the positive rate of decremental responses was 77% in one study with 48 ALS patients (5), while that in another study including 192 patients in total was only 29% (3). The positive rate of the present study was 41.3%. All of these indicated that decremental positive responses in RNS were common in ALS patients.

In light of the revised ALS diagnostic criteria by the World Federation of Neurology (6), it is noteworthy that a CMAP decrement >20% was a diagnostic exclusion criterion for ALS. However, our study investigated that

TABLE 1 | RNS decremental amplitude and frequency in ALS patients.

Decremental amplitude	Trap		ADM	
	n	%	*n*	%
≥20%	16	10.7	1	0.7
≥15%	15	10.0	0	0.0
≥10%	31	20.7	2	1.3
≥5%	27	18.0	15	10.0
<5%	61	40.6	132	88.0
Total	150	100.0	150	100.0

Trap, trapezius muscle; ADM, abductor digiti minimi; RNS, repetitive nerve stimulation; ALS, amyotrophic lateral sclerosis.

TABLE 2 | Comparison of positive and negative decrements in ALS patients.

	RNS+	RNS–	$t/z/\chi^2$	*P*
Sex, *n* (%)				
Male	32 (51.6)	54 (61.4)	1.414*	0.234
Female	30 (48.4)	34 (38.6)		
Onset age (years)	55.12 ± 11.95	55.71 ± 10.63	−0.316†	0.752
Disease duration (months) [*M*(*Q*)]	12.00 (11.5)	9.50 (11.5)	−1.695§	0.090
ALSFRS-R [*M*(*Q*)]	39.00 (6.0)	41.00 (5.0)	−2.588§	0.010
Disease progression rate [*M*(*Q*)]	0.75 (0.7)	0.70 (1.0)	−0.220§	0.826
Onset site, *n* (%)				
Bulbar	12 (19.4)	22 (25.0)	0.661*,ϕ	0.416
Upper limb	30 (48.4)	45 (51.1)	0.833*,&	0.316
Lower limb	20 (32.3)	21 (23.9)		
CMAP amplitude (mV)				
Trap	7.53 ± 3.59	9.10 ± 3.25	−2.788†	0.006
ADM	7.99 ± 3.74	9.94 ± 3.39	−3.319†	0.001

+, Positive decrement; –, Negative decrement.
ALS, amyotrophic lateral sclerosis; CMAP, compound muscle action potential; Trap, trapezius muscle; ADM, abductor digiti minimi.
χ^2-value.
z-value.
t-value.
Bulbar vs. limb onset.
Upper limb onset vs. lower limb onset.

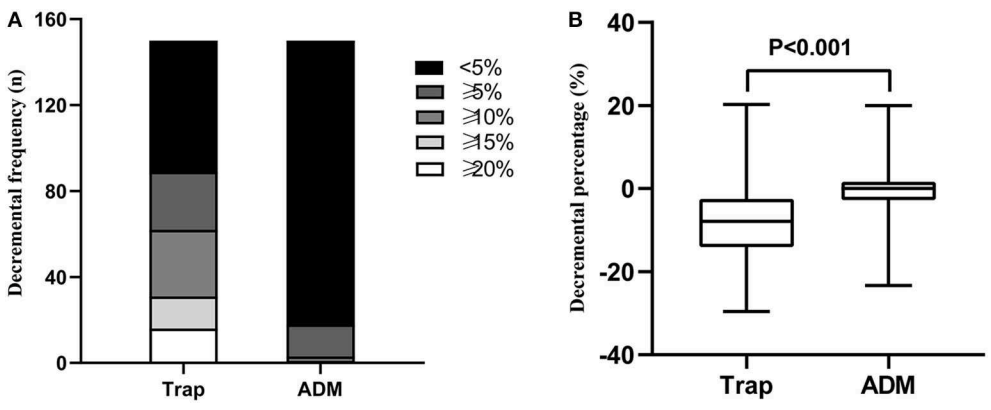

FIGURE 1 | (A) Decremental frequency in the Trap and ADM of ALS patients. **(B)** Decremental percentage in the Trap and ADM of ALS patients. Trap, trapezius muscle; ADM, abductor digiti minimi.

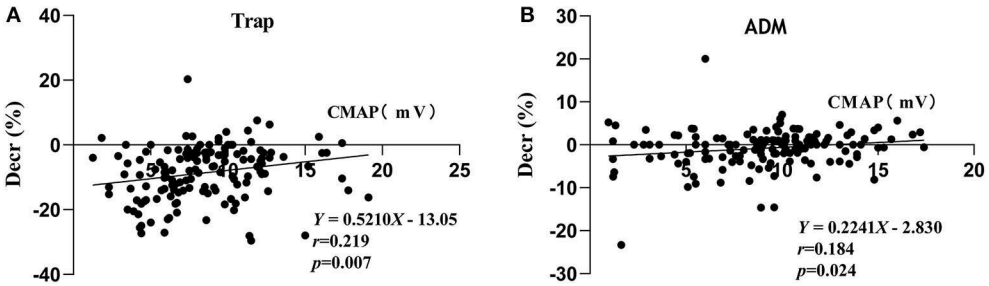

FIGURE 2 | Correlations between the CMAP amplitude and decremental percentages in TRAP **(A)** and ADM **(B)**. Decr(%), percentage of decremental response; CMAP, compound muscle action potential; Trap, trapezius muscle; ADM, abductor digiti minimi.

more than 20% of the patients had a decrement of ≥15%. Furthermore, more than 10% of the patients had a decrement of ≥20%. Although it has also been reported previously that the decremental percentage can reach 20% (4, 7, 8), the proportion of patients with such a characteristic was not mentioned. If the current electrophysiological diagnostic criteria were applied, more than 10% of ALS patients would be misdiagnosed. Consequently, it is worthy of further research whether a CMAP decrement >20% is an exclusion criterion for ALS.

The present study analyzed the distribution of the decremental responses in Trap and ADM. Consistent with previous research (3, 5), the investigation demonstrated that proximal muscles were more prone to show a positive decrement in RNS than do distal muscles, indicating a greater sensitivity of the proximal muscle to RNS. In severely atrophied muscles, the decremental responses of ALS patients were more pronounced (3, 11); however, it cannot be explained why more severely involved distal muscles, such as intrinsic hand muscles, in most ALS patients showed a less pronounced decremental positive response than did the proximal muscles. The lower safety factor of NMJ at the proximal muscle may be an interpretation (5). Besides, the study indicated that there was a positive linear correlation between the CMAP amplitude and the decremental percentage of Trap and ADM in ALS patients, which supported the decremental mechanisms of immature collateral sprouting and unstable NMJ transmission resulting from axonal degeneration. The Awaji diagnostic criteria indicated that electrophysiological and clinical evidence should be considered equally when judging the lower motor neuron (LMN) involvement in ALS patients (9). The decremental positive responses in RNS meant an impaired LMN (12). Accordingly, when the Awaji diagnostic criteria were applied, the decremental positive responses can be deemed as an additional evidence of the LMN involvement (12).

The ALSFRS-R score, as a significant predictor of prognosis, was extensively applied to assess the severity of the disease (7). The patients in the positive decrement group had lower ALSFRS-R scores compared with those in the decremental negative group, suggesting that the former were worse. Some studies have shown that the disease progressed more rapidly in ALS patients with a positive decrement (4, 8, 13, 14), but others contradicted this (5, 7, 15–17). If the RNS decrement responses were not related to the disease progression, the interpretation of the mechanism of decrement responses, the early neural reinnervation, may need to be corrected (5). It may be possible that the disease progression was too rapid to form the collateral sprouts in extreme cases. Therefore, the correlation between the RNS decremental responses and the disease progression rate in ALS patients is still confused. Consequently, advanced research is essential to clarify that the decremental positive responses are monitoring indicators of disease progression.

Moreover, this study showed that the onset of ALS did not affect the RNS decrement responses, which was consistent with previous research (8, 18). However, some studies have shown that patients with upper limb onset had higher decremental percentages compared with those with other sites of onset (7, 17). The underlying reason for these differences is unclear. It was speculated that the limited number of patients with lower limb and bulbar onset as well as the different types of muscles studied may be the underlying interpretations. In any case, more specifically designed research would be necessary to settle this issue. Besides, the patients' gender, onset age, and disease duration did not affect the RNS decremental percentages.

The decremental responses of ALS patients suggest the instability of NMJ transmission. The underlying mechanism of decremental responses remains controversial. One explanation is that, as the disease progresses, the anterior horn motor neurons of the spinal cord degenerate; then, the muscle fibers dominated by these neurons show denervation, leading to the corresponding NMJ structure changes. The remaining motor neurons around the degenerative neurons dominate the muscle fibers by the collateral sprouts, and new NMJ structures form. Before the new NMJ structures are fully mature, the motor neurons have degenerated and lost. Along with the repeated cycles, these highly immature reinnervations cause an intermittent conduction block in the newly formed nerve endings, eventually leading to a decremental response (4, 19). Another possible explanation is that the disease arises from distal axons or NMJs and proceeds to the cell body in reverse. This is the "dying back" hypothesis (17). Fischer et al. performed a good deal of pathological experimentation on the SOD1-G93A mice model and found that NMJ destruction and axon degeneration occurred before motor neurons degenerated. An autopsy on a single ALS patient showed

denervation and reinnervation changes in muscles, where the motor neurons remained structurally intact (20). The mechanism of "dying back" remains unclear. A possible explanation is energy deficiency resulting from the hypermetabolism and malnutrition of ALS, which could lead to NMJ dysfunction (17).

In conclusion, the decremental positive responses are common in ALS patients, but the pathophysiological mechanisms remain unclear. Advanced research is necessary to discuss whether the decremental percentage >20% is a diagnostic exclusion criterion for ALS patients. Patients with lower CMAP amplitudes were more prone to show decremental responses, both in the proximal and distal muscles. Besides, the onset age, duration of disease, and onset site of ALS do not affect RNS the decremental responses.

DATA AVAILABILITY STATEMENT

All datasets generated for this study are included in the article/supplementary material.

ETHICS STATEMENT

Ethics approval and written informed consent was not required as per local legislation and national guidelines, as repetitive nerve stimulation inspection is considered routine care.

AUTHOR CONTRIBUTIONS

LS drafted the paper. HC was responsible for data collection. ZL provided specialized expertise and critical appraisal of the article for submission.

ACKNOWLEDGMENTS

We are grateful to Drs. Wang Yan, Liu Shuping, and Fu Xiujuan (Department of Neurology, Renmin Hospital, Wuhan University).

REFERENCES

1. Kiernan MC, Vucic S, Cheah BC, Turner MR, Eisen A, Hardiman O, et al. Amyotrophic lateral sclerosis. *Lancet*. (2011) 377:942–55. doi: 10.1016/S0140-6736(10)61156-7
2. Mulder DW, Lambert EH, Eaton LM. Myasthenic syndrome in patients with amyotrophic lateral sclerosis. *Neurology*. (1959) 9:627–31. doi: 10.1212/WNL.9.10.627
3. Killian JM, Wilfong AA, Burnett L, Appel SH, Boland D. Decremental motor responses to repetitive nerve stimulation in ALS. *Muscle Nerve*. (1994) 17:747–54. doi: 10.1002/mus.880170708
4. Wang FC, De Pasqua V, Gerard P, Delwaide PJ. Prognostic value of decremental responses to repetitive nerve stimulation in ALS patients. *Neurology*. (2001) 57:897–9. doi: 10.1212/WNL.57.5.897
5. Iwanami T, Sonoo M, Hatanaka Y, Hokkoku K, Oishi C, Shimizu T. Decremental responses to repetitive nerve stimulation (RNS) in motor neuron disease. *Clin Neurophysiol*. (2011) 122:2530–6. doi: 10.1016/j.clinph.2011.05.019
6. Brooks BR, Miller RG, Swash M, Munsat TL. El Escorial revisited: revised criteria for the diagnosis of amyotrophic lateral sclerosis. *Amyotroph Lateral Scler Other Motor Neuron Disord*. (2000) 1:293–9. doi: 10.1080/146608200300079536
7. Hu F, Jin J, Kang L, Jia R, Qin X, Liu X, et al. Decremental responses to repetitive nerve stimulation in amyotrophic lateral sclerosis. *Eur Neurol*. (2018) 80:151–6. doi: 10.1159/000494670
8. Wang Y, Xiao Z, Chu H, Liang J, Wu X, Dong H, et al. Correlations between slow-rate repetitive nerve stimulation and characteristics associated with amyotrophic lateral sclerosis in Chinese patients. *J Phys Ther Sci*. (2017) 29:737–43. doi: 10.1589/jpts.29.737
9. de Carvalho M, Dengler R, Eisen A, England JD, Kaji R, Kimura J, et al. Electrodiagnostic criteria for diagnosis of ALS. *Clin Neurophysiol*. (2008) 119:497–503. doi: 10.1016/j.clinph.2007.09.143
10. Chinese Medical Association. Revised version of experts consensus for standardization for electromyography and clinical application. *Chin J Neurol*. (2015). 48:950–64. doi: 10.3760/cma.j.issn.1006-7876.2015.11.005
11. Henderson R, Baumann F, Hutchinson N, McCombe P. CMAP decrement in ALS. *Muscle Nerve*. (2009) 39:555–6. doi: 10.1002/mus.21105
12. Hatanaka Y, Higashihara M, Chiba T, Miyaji Y, Kawamura Y, Sonoo M. Utility of repetitive nerve stimulation test for ALS diagnosis. *Clin Neurophysiol*. (2017) 128:823–9. doi: 10.1016/j.clinph.2017.02.021
13. Mori A, Yamashita S, Nakajima M, Hori H, Tawara A, Matsuo Y, et al. CMAP decrement as a potential diagnostic marker for ALS. *Acta Neurol Scand*. (2016) 134:49–53. doi: 10.1111/ane.12510
14. Kaires PA. Prognostic value of decremental responses to repetitive nerve stimulation in ALS patients. *Neurology*. (2002) 58:836–7. doi: 10.1212/WNL.58.5.836
15. Yamashita S, Sakaguchi H, Mori A, Kimura E, Maeda Y, Hirano T, et al. Significant CMAP decrement by repetitive nerve stimulation is more frequent in median than ulnar nerves of patients with amyotrophic lateral sclerosis. *Muscle Nerve*. (2012) 45:426–8. doi: 10.1002/mus.22301
16. Zheng C, Jin X, Zhu Y, Lu F, Jiang J, Xia X. Repetitive nerve stimulation as a diagnostic aid for distinguishing cervical spondylotic amyotrophy from amyotrophic lateral sclerosis. *Eur Spine J*. (2017) 26:1929–36. doi: 10.1007/s00586-017-5060-4
17. Sun XS, Liu WX, Chen ZH, Ling L, Yang F, Wang HF, et al. Repetitive nerve stimulation in amyotrophic lateral sclerosis. *Chin Med J*. (2018) 131:2146–51. doi: 10.4103/0366-6999.240798
18. Alanazy MH, Hegedus J, White C, Korngut L. Decremental responses in patients with motor neuron disease. *Brain Behav*. (2017) 7:e846. doi: 10.1002/brb3.846
19. Fu LL, Yin HX, Liu MS, Cui LY. Study on variation trend of repetitive nerve stimulation waveform in amyotrophic lateral sclerosis. *Chin Med J*. (2019) 132:542–50. doi: 10.1097/CM9.0000000000000117
20. Fischer LR, Culver DG, Tennant P, Davis AA, Wang M, Castellano-Sanchez A, et al. Amyotrophic lateral sclerosis is a distal axonopathy: evidence in mice and man. *Exp Neurol*. (2004) 185:232–40. doi: 10.1016/j.expneurol.2003.10.004

Conflict of Interest: The authors declare that the research was conducted in the absence of any commercial or financial relationships that could be construed as a potential conflict of interest.

frontiers in Neurology

SYSTEMATIC REVIEW
published: 11 March 2020
doi: 10.3389/fneur.2020.00166

Disrupted Ankle Control and Spasticity in Persons With Spinal Cord Injury: The Association Between Neurophysiologic Measures and Function. A Scoping Review

Jasmine M. Hope[1,2], *Ryan Z. Koter*[1], *Stephen P. Estes*[1] *and Edelle C. Field-Fote*[1,2,3,4]*

[1] *Shepherd Center, Crawford Research Institute, Atlanta, GA, United States,* [2] *Graduate Division of Biological and Biomedical Sciences, Laney Graduate School, Emory University, Atlanta, GA, United States,* [3] *Division of Physical Therapy, School of Medicine, Emory University, Atlanta, GA, United States,* [4] *Georgia Institute of Technology, School of Biological Sciences, Program in Applied Physiology, Atlanta, GA, United States*

OPEN ACCESS

Edited by:
Francesco Negro, University of Brescia, Italy

Reviewed by:
Cristiano De Marchis, Roma Tre University, Italy
Luciano Bissolotti, Fondazione Teresa Camplani, Italy
Dirk Czesnik, University of Göttingen, Germany

***Correspondence:**
Edelle C. Field-Fote
edelle.field-fote@shepherd.org

Specialty section:
This article was submitted to Neurorehabilitation, a section of the journal Frontiers in Neurology

Received: *25 September 2019*
Accepted: *21 February 2020*
Published: *11 March 2020*

Citation:
Hope JM, Koter RZ, Estes SP and Field-Fote EC (2020) Disrupted Ankle Control and Spasticity in Persons With Spinal Cord Injury: The Association Between Neurophysiologic Measures and Function. A Scoping Review. Front. Neurol. 11:166. doi: 10.3389/fneur.2020.00166

Control of muscles about the ankle joint is an important component of locomotion and balance that is negatively impacted by spinal cord injury (SCI). Volitional control of the ankle dorsiflexors (DF) is impaired by damage to pathways descending from supraspinal centers. Concurrently, spasticity arising from disrupted organization of spinal reflex circuits, further erodes control. The association between neurophysiological changes (corticospinal and spinal) with volitional ankle control (VAC) and spasticity remains unclear. The goal of this scoping review was to synthesize what is known about how changes in corticospinal transmission and spinal reflex excitability contribute to disrupted ankle control after SCI. We followed published guidelines for conducting a scoping review, appraising studies that contained a measure of corticospinal transmission and/or spinal reflex excitability paired with a measure of VAC and/or spasticity. We examined studies for evidence of a relationship between neurophysiological measures (either corticospinal tract transmission or spinal reflex excitability) with VAC and/or spasticity. Of 1,538 records identified, 17 studies were included in the review. Ten of 17 studies investigated spinal reflex excitability, while 7/17 assessed corticospinal tract transmission. Four of the 10 spinal reflex studies examined VAC, while 9/10 examined ankle spasticity. The corticospinal tract transmission studies examined only VAC. While current evidence suggests there is a relationship between neurophysiological measures and ankle function after SCI, more studies are needed. Understanding the relationship between neurophysiology and ankle function is important for advancing therapeutic outcomes after SCI. Future studies to capture an array of corticospinal, spinal, and functional measures are warranted.

Keywords: corticospinal tract, spinal reflex circuit, Hoffman-reflex, transcranial magnetic stimulation (TMS), spastic gait, motor-evoked potentials (MEPs), clonus, stiffness

INTRODUCTION

Walking is a high-priority goal for most persons with spinal cord injury (SCI) (1). For walking to be the primary means of mobility, several conditions must be satisfied including low energy expenditure, good safety, and adequate speed for practical community-based walking (2). Each of these conditions is highly dependent on a number of factors, including the degree of control present at the ankle (3). Likewise, ankle control is influenced by a multitude of interrelated factors such as muscle strength, timing of activation, and spasticity, which collectively determine gait mechanics (4–6). Without adequate ankle dorsiflexion, foot drop during the swing phase of gait can impair foot clearance, contribute to decreased stride length, and increase likelihood of falls (7). Secondary gait deviations often develop to achieve foot clearance, including excessive hip and knee flexion, limb circumduction, or lateral trunk sway with pelvic hike. These deviations increase the energy cost of walking and decrease the likelihood that walking is a safe and feasible means of mobility (3).

Ankle-related impairments after SCI are attributed to neurophysiologic changes in both corticospinal tract (CST) transmission (8) and modulation of spinal reflex circuit (SRC) excitability (9) (**Figure 1**). To better understand the influences of CST transmission and SRC excitability, two commonly performed electrophysiological measures are utilized: cortical motor evoked potentials (MEPs) and Hoffman reflex (H-reflex). Both measures are commonly used as non-invasive probes of the underlying neurophysiology of CST transmission and SRC excitability, respectively. Decreased descending transmission impairs volitional control of the dorsiflexors (DF) and reduces the activation of inhibitory inputs to the plantar flexors (PF), further contributing to aberrant SRC activity. It is important to note that while the H-reflex is commonly used as a measure of excitability of the monosynaptic Ia SRCs, this reflex measure reflects oligosynaptic inputs (10).

Some study findings suggest that the reorganization of the cortical motor representation after SCI results in decreased volitional drive through the spared spinal pathways. Evidence indicates that training and neuromodulation approaches directed at increasing volitional drive can increase the amplitude of MEPs (11, 12), restore normal cortical organization (13, 14), and improve volitional muscle activation (15, 16). Altered activity of SRC, due to reorganization of spinal circuits and disruption of normal SRC modulation from descending corticospinal input, can result in several signs and symptoms commonly associated with spasticity after SCI. These symptoms include clonus or hyper-reflexive response to afferent input (i.e., stretch, touch, cold temperatures), muscle stiffness (hypertonia), and spontaneous involuntary muscle contractions (spasms) (17, 18). The maladaptive changes to the circuits controlling the DF and PF following SCI have been described (19–21); however, the relationship between decreased CST descending drive and disrupted SRC modulation with volitional ankle control (VAC) (dorsiflexion during gait, toe tapping, etc.) and/or spasticity remains unclear.

In order to improve functional outcomes after SCI, several recent advances have focused on neuromodulation of the corticospinal and spinal circuits. These advances have been summarized in a recent review (22), and include non-invasive stimulation of afferent inputs such as peripheral nerve somatosensory stimulation, whole body vibration, and transcutaneous spinal cord stimulation. These modalities directly modulate SRC excitability and indirectly activate corticomotor circuits (23). There are also techniques that directly target increased CST descending drive such as transcranial direct current stimulation and repetitive TMS (24). All of these neuromodulatory approaches have been shown to improve functional outcomes, including walking function, when used as an adjuvant to therapy (23). Although these advances show promise for improving walking, to truly optimize functional outcomes it is necessary to understand how neuromodulation of the CST and the SRCs impact variables that are elemental to walking function, such as ankle control and spasticity. As a precursor to exploring the impact of neuromodulation, a better understanding of how neurophysiological measures are related to VAC and spasticity is needed.

To elucidate the respective roles of CST transmission and SRC excitability in disrupted ankle control, we conducted a scoping review to summarize what is known and to identify existing gaps in the literature in order to frame more precise questions for future studies (25). The objectives were to (1) summarize the state of the literature (study designs, methods, evidence of an association), (2) identify existing gaps (variability, contradictions, lack of evidence), and (3) propose future directions (based on existing gaps). Addressing these objectives is important to understand the relationship between corticospinal and spinal neurophysiological measures in the DF and PF and their association with ankle-related function. A better understanding of this association will (1) facilitate the development of more targeted therapeutic strategies for improving ankle control, (2) refine spasticity management, and (3) enhance quality of life for persons with SCI.

MATERIALS AND METHODS

In the current review, we used the five stages of a scoping review outlined by Arksey and O'Malley (26): (1) identify the research question, (2) identify relevant studies, (3) select studies for inclusion, (4) [extract and] chart the data, and (5) collate, summarize, and report the results.

Inclusion/Exclusion Criteria

To determine the scope and extent of the literature, we used inclusion and exclusion criteria that focused on the association between neurophysiological measures and VAC and/or spasticity measures in persons with SCI. For inclusion, all studies had to include adults (mean age ≥18 years old) with SCI.

Abbreviations: SCI, spinal cord injury; DF, ankle dorsiflexors; VAC, volitional ankle control; SRC, spinal reflex circuitry; CST, corticospinal tract; H-reflex, Hoffman reflex; MEP, motor evoked potentials; PF, plantar flexors; TMS, transcranial magnetic stimulation.

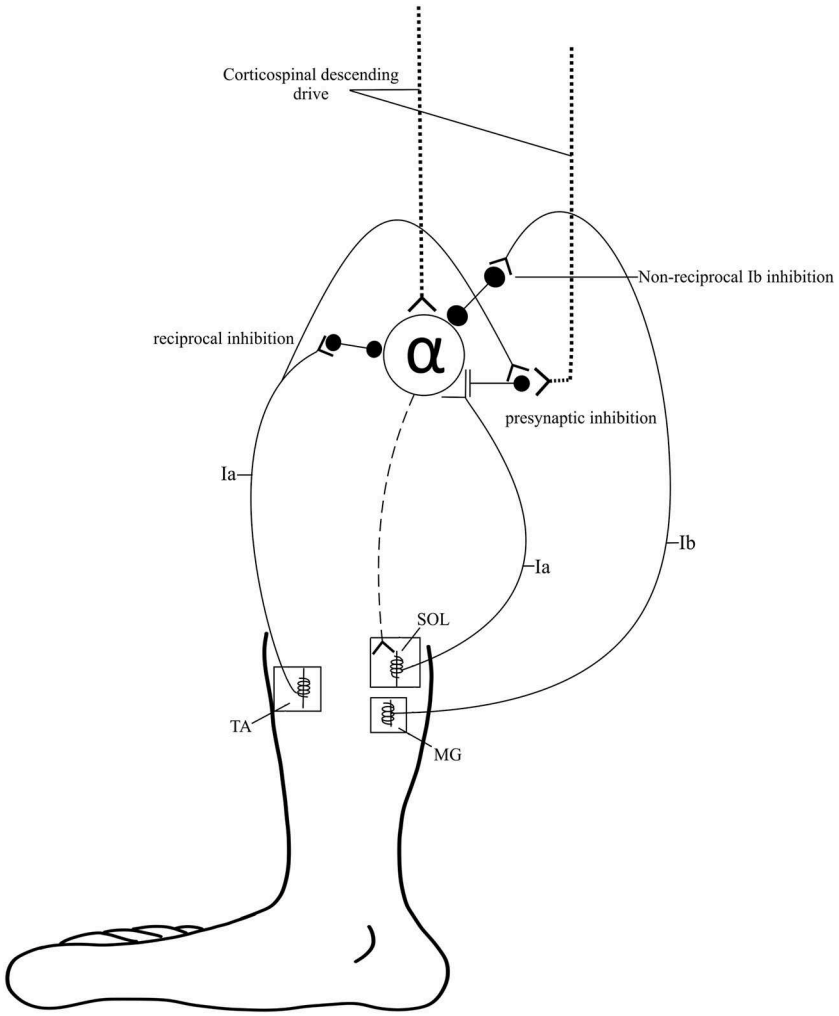

FIGURE 1 | Spinal pathways. Spinal pathways that likely contribute to ankle control and the development of spasticity including reciprocal inhibition, presynaptic inhibition, and non-reciprocal Ib inhibition.

Studies that compared measures obtained from persons with SCI to individuals with other neurological disorders or non-injured individuals were eligible for inclusion. Studies had to include the H-reflex and/or MEPs as measures of spinal and corticospinal neurophysiological changes, respectively. Peripheral nerve stimulation to evoke H-reflexes and transcranial magnetic stimulation (TMS) to evoke MEPs have been shown to be repeatable and consistent in both the DF and PF muscles (27, 28). Studies had to include at least one of these approaches to be eligible for inclusion in the review. To address the relationship between neurophysiological excitability and ankle functional measures, studies had to include at least one measure of VAC (e.g., ankle strength, ankle tapping, foot drop/toe drag during walking) and/or ankle spasticity (e.g., ankle clonus, ankle stiffness). Studies were excluded if subjects who lacked volitional ankle movement were enrolled or if ankle-specific results were not reported. Only studies published in English were included. Case studies, non-peer reviewed sources (e.g., dissertations, conference abstracts, unpublished data), theoretical simulations or models, and reviews were also excluded from the final review.

Sources and Search

In consultation with a medical librarian, the following databases were searched for articles published between the time of database inception to April 2018: PubMed (includes MEDLINE), Ovid-Medline, and EBSCO-CINAHL. The search terms were chosen to capture articles that included persons with SCI, spinal or corticospinal neurophysiological testing, and functional testing of the ankle DF or PF. The details of the terms and search combinations are described in **Table 1**. To restrict the population of interest to SCI, the following search terms were always used in combination with the other terms across all databases: (Spinal Cord Injury [Title/Abstract] OR SCI[Title/Abstract] OR spinal damage [Title/Abstract] OR spine damage [Title/Abstract] OR spine injury [Title/Abstract] OR spinal injury [Title/Abstract]). Syntax was adjusted accordingly for each database.

TABLE 1 | Detailed search terms.

Search category	Search terms
SCI	(Spinal Cord Injury [Title/Abstract] OR SCI [Title/Abstract] OR spinal damage [Title/Abstract] OR spine damage [Title/Abstract] OR spine injury [Title/Abstract] OR spinal injury [Title/Abstract])
CST	(Corticospinal Excitability OR CST OR Corticospinal OR corticospinal descending drive OR corticospinal OR TMS OR transcranial magnetic stimulation)
SPINAL	(Spinal reflex circuit OR reflex OR Hoffmann reflex OR H-reflex OR hyperreflexia OR hypertonia OR spinal reflex OR stretch reflex OR monosynaptic reflex)
DF	Control of ankle dorsiflexor OR ankle OR dorsiflexor OR tibialis anterior OR TA OR walking/physiology [MeSH Terms] OR Ankle joint/physiopathology [MeSH Terms] OR Ankle joint/innervation [MeSH Terms] OR Exercise therapy/methods [MeSH Terms] OR Gait Disorders [MeSH Terms] OR Gait [MeSH Terms])
PF	([Control of ankle plantar flexors OR ankle OR plantar flexors OR soleus OR walking/physiology [MeSH Terms] OR Ankle joint/physiopathology [MeSH Terms] OR Ankle joint/innervation [MeSH Terms] OR Exercise therapy/methods [MeSH Terms] OR Gait Disorders [MeSH Terms] OR Gait [MeSH Terms]])

The initial search term categories were combined in the following ways across 3 databases: 1. SCI + CST+ Spinal+ DF+PF, 2. SCI + CST + DF, 3. SCI + CST + PF, 4. SCI + Spinal + DF, and 5. SCI + Spinal + PF.

Screening/Extraction

Article screening was performed using an iterative approach, with 3 screeners (JMH, RZK, and SPE) participating in article selection and review. During the initial screen, the reviewers did not discuss the identity of the articles being considered for inclusion until the end of each screen. At least two of the screeners had to select each study for it to be included in the subsequent screen. There were three total screens: (1) title and abstract, (2) full-text, and (3) full-text with data extraction. For the title and abstract screen, authors only had access to the titles and abstracts to determine relevant studies. During the title and abstract screen, all authors were instructed to examine the text for population, neurophysiological tests of SRC excitability and/or CST transmission, and measures of VAC and/or spasticity. The neurophysiological tests of SRC excitability included measures of H-reflex modulation: reciprocal inhibition, presynaptic inhibition, low-frequency depression, Ib inhibition, ratio of the maximum H-reflex to maximum direct motor response (H/M ratio), and cutaneomuscular -conditioned soleus H-reflexes. Neurophysiologic tests of CST transmission included MEP amplitude and latency. The VAC studies included functional measures such as: DF and PF strength, foot clearance during walking, tapping task, active range of motion (the range of joint movement through which the subject is able to volitionally move the ankle), walking distance, and walking speed. Spasticity studies included biomechanical measures of stretch-induced spastic responses such as: clonus duration, number of oscillations during clonus, and PF reflex threshold angle. If the abstract met all the inclusion criteria, then it was included in the full-text screen. For the full-text screen, authors assessed whether each study met inclusion criteria by skimming through each article once. Finally, during data extraction, the authors determined the relevance of the articles in a more in-depth manner by carefully reading the selected text, while simultaneously extracting specific information from each article. The following information was extracted from each article: study design, study aims, population, participant injury severity, neurophysiological tests, VAC and/or spasticity assessments, and the relationship, if any, between the last two measures. A hand search was conducted on citations in relevant review articles to identify additional articles during the first two screens, and on the articles assessed during the data extraction screen. During the final screen, review articles were excluded.

All articles selected for the final inclusion were grouped based on whether SRC excitability or CST transmission was assessed. The articles were further grouped by whether contributing authors utilized measures of VAC or measures of spasticity. Some articles **directly** determined the relationship between neurophysiological measures and VAC and/or spasticity via correlation or linear regression analyses. In other articles there was no formal testing of the relationship between neurophysiological measures and VAC and/or spasticity. These latter articles were defined as having an **indirect** relationship.

RESULTS

Overview of Included Articles

In total, 1,538 records were identified in the database searches. After duplicates and dissertations were removed, 454 articles remained, which were subjected to a title and abstract screen. Fifty-five articles were read in full following the title and abstract screen and 18 additional articles were removed for not meeting all inclusion criteria. The remaining 37 articles were assessed for eligibility during the data extraction phase, 22 of which were eliminated for being reviews or not meeting criteria. In addition to the 15 remaining articles, two articles were identified for inclusion during the hand search, bringing the total included article count to 17. Of the 17 included articles, seven had interventional study designs, 10/17 contained measures to assess the relationship between SRC excitability and some aspect of VAC and/or spasticity, and 7/17 articles contained measures of the relationship between CST transmission and VAC. The screening process is illustrated in **Figure 2**.

The final 17 articles included in this review were published between 1994 and 2017. Neurophysiological data from 277 participants with SCI were captured across all studies. Some participants may be represented more than once, as some lead authors had multiple manuscripts included: Barthélemy (2 articles) (8, 30), Manella (3 articles) (6, 15, 31), and Wirth (4 articles) (32–35). The number of SCI subjects per study ranged from 7 to 40 (median = 15).

Demographics of Subjects Enrolled in Included Studies

The majority of subjects had chronic SCI with an initial onset ≥12 months prior to study enrollment. Two of the 17 studies included only subjects with acute or subacute SCI (34, 36). Three studies included subjects with subacute or chronic SCI (32, 33, 35). Of studies that reported subject sex, all had an equal

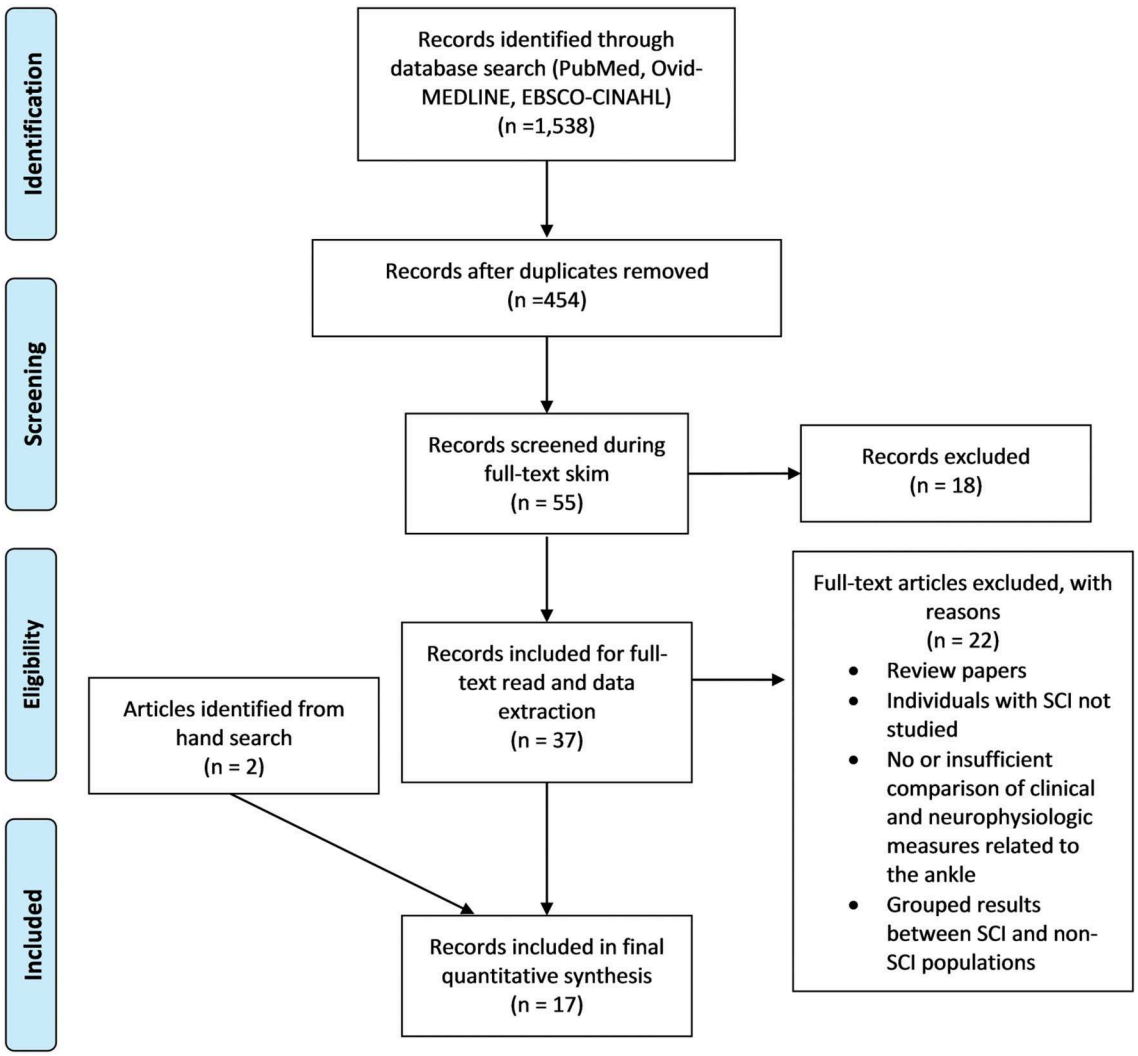

FIGURE 2 | PRISMA flow diagram. PRISMA flow diagram of the Screening process followed during the scoping review (29). For more information, visit www.prisma-statement.org.

or larger proportion of men to women. While all studies included subjects with motor-incomplete SCI, six also included subjects with motor-complete SCI (6, 37–41). Most studies included a control group of non-injured or "healthy" participants (12/17) (8, 30–32, 34–38, 40, 42, 43), while two studies also included subjects with hemiplegia (32, 37). Participant demographics for each included article are illustrated in **Table 2**.

SRC Excitability Articles

There were 10 studies that examined changes in SRCs. Four of 10 also included measures of VAC (15, 36, 38, 43); all four included correlation and/or association analyses to quantify the relationship between SRCs and VAC. Nine of 10 studies with SRC measures also had measures of ankle spasticity (6, 15, 31, 36–41); only six of these articles included correlation and/or association analyses to quantify the relationship between SRC excitability and spasticity (6, 15, 31, 36–38). There were 3/10 SRC articles that assessed both VAC and spasticity (15, 36, 38).

CST Transmission Articles

There were seven studies that examined changes in CST function, all of which included measures of VAC (8, 30, 32–35, 42). Six of seven performed correlation and/or association analyses to quantify the relationship between CST function and VAC (8, 30, 32–35). One study of CST transmission included subjects with stroke in addition to subjects with SCI without separating the data of those individuals prior to performing linear regression analysis, making it difficult to parse out SCI results from results of participants with stroke (32). None of the studies examining CST transmission included measures of ankle spasticity.

Relationship Between SRC Excitability and VAC

Disrupted modulation of SRC excitability after SCI has been associated with decreased VAC. This impaired ability to

TABLE 2 | Study characteristics and participant demographics.

SRC or CST	References	Study aims	ISNCSCI grades	Clinical description	Mean TPI	SCI subject sample size (sex distribution)	Mean Age of SCI subjects (y)	Non-SCI subject sample size (sex distribution)	Mean Age of Non-SCI subjects (y)
SRC									
	Manella et al. (6)	Examine reliability and construct validity of drop test to quantify ankle clonus in persons with SCI and compare results with the SCATS and H/M ratio	A–D	C2 to L1 LOI, Evidence of clonus	8.9 y	$n = 40$ (31 M, 9 F)	39.6 ± 13	N/A	N/A
	Piazza et al. (36)	Examine the effects of leg-cycling on conditioned H-reflex excitability and how it relates to lower extremity function after miSCI	C to D	C5-T10 LOI, capable of cycling	16 ± 3 weeks	$n = 9$ (6 M, 3 F)	44 ± 5	Non-injured: $n = 10$	34 ± 3
	Yamaguchi et al. (43)	Compare effect of anodal tDCS and PES on RI and ankle movement in miSCI	C to D	C1 to T11, 1+ PF spasticity (MAS)	4.5 ± 4.2 y	$n = 11$ (11 M)	51.8 ± 10.7	Non-injured: $n = 10$	50.7 ± 8.9
	Smith et al. (41)	Assess changes in H-reflex in different positions after locomotor training in persons with SCI	A to D	C1 to T10 LOI	4.3 y	$n = 15$ (10 M, 5 F)	37.53	N/A	N/A
	Manella and Field-Fote (31)	1. Investigate effects of LT on measures of spasticity and walking. 2. Assess association of change in walking speed with measures of reflex activity 3. Establish sensitivity to change and validity of PF RTA	C or D	C4 to L1 LOI, Evidence of clonus in some participants	8.9 y	Locomotor cohort: $n = 18$ (16 M, 2 F) Validity cohort: $n = 40$ (30 M, 10 F)	Locomotor cohort: 35.1 Validity cohort: 39.3	Non-injured: $n = 10$	27.3
	Manella et al. (15)	1. Examine effects of different operant conditioning interventions on ankle motor control, spasticity, and walking related measures in persons with miSCI. 2. Explore relationship between changes in neurophysiological and clinical outcome measures.	D	Positive ankle clonus, Median LL of TA group: C7; Median LL of SOL group: C5	TA group: 10.8 ± 10.0 y; SOL group: 10.8 ± 08.8 y	Total: $n = 12$; TA cohort: $n = 6$ (6 M); SOL cohort: $n = 6$ (4 M, 2 F)	TA cohort: 44.2; SOL cohort: 45.2	N/A	N/A
	Adams and Hicks (39)	Examine effects of BWSTT and TTS on spasticity and motor neuron excitability in chronic SCI	A to C	C5 to T10 LOI, stable spasticity, primary wheelchair user	5.0 ± 4.4 y	$n = 7$ (6 M, 1 F)	37.1 ± 7.7	N/A	N/A
	Murillo et al. (40)	Examine the effect of RF vibration on clinical and neurophysiological outcome measures of spasticity in SCI	A to D	C3 to T11 LOI; lower limb spasticity ≥ 1.5 (MAS)	5.6 y ± 1.9 months	$n = 19$ (16 M, 3 F)	36.0 ± 10.6	Non-injured: $n = 9$	33.8 ± 9.4
	Downes et al. (38)	Examine reflex actions of MG group Ib afferent stimulation on SOL H-reflex excitability and spasticity in persons with SCI	Both cSCI and iSCI	C4 to T10 LOI	16 mos	$n = 13$ (11 M, 2 F)	30	Non-injured: $n = 20$	25
	Faist et al. (37)	Assess effect of femoral nerve stimulation on SOL H-reflex activity in SCI. Examine association of spasticity and PI	Both cSCI and iSCI	LOI not reported	27.5 mos	$n = 17$	34.8	Non-injured: $n = 28$, Hemiplegic: $n = 18$	Non-injured age range: 21-59; Hemiplegic mean age: 49.6

(Continued)

TABLE 2 | Continued

SRC or CST	References	Study aims	ISNCSCI grades	Clinical description	Mean TPI	SCI subject sample size (sex distribution)	Mean Age of SCI subjects (y)	Non-SCI subject sample size (sex distribution)	Mean Age of Non-SCI subjects (y)
CST									
	Barthélemy et al. (30)	Examine the correlation of CST function and measures of gait and ankle function after SCI	D	C1 to L1 LOI	12 y	$n = 24$ (22 M, 2 F)	43.4	Non-injured: $n = 11$	45
	Labruyère et al. (42)	Assess deficits in quick and accurate movements in miSCI by combining TMS, EMG, and a response time task and comparing differences in clinical characteristics.	D	T2 to L4 LOI only	6.3 ± 5.5 y	n = 15 (10 M, 5 F)	50.2 ± 12.4	Non-injured: $n = 15$	50.1 ± 12.3
	Barthélemy et al. (8)	Examine the relationship between parameters that may reflect CST function and physical foot drop deficit observed after SCI	D[+]	C to L LOI; ability to walk 10m	12 ± 11 y	$n = 24$ (22 M, 2 F)	43 ± 14	Non-injured: $n = 15$	42 ± 16
	Wirth et al. (35)	Examine ankle DF timing during gait and in supine to CST conductivity and measures of strength and gait speed in persons with and without SCI.	C or D	C2 to T12	2.7 ± 3.5 y	$n = 12$ (9 M, 3 F)	58.3 ± 10.7	Non-injured: $n = 12$	59.2 ± 11.3
	Wirth et al. (32)	Examine the effects of CST damage on ankle dexterity and MMV in individuals with miSCI and stroke	miSCI	C3 to L5 LOI	13.3 ± 31.7 mos	$n = 12$ (6 M, 6 F)	62.3 ± 8.3	Stroke: $n = 12$; Non-injured: $n = 12$	Stroke 65.8 ± 10.5; Non-injured: 63.3 ± 10.7
	Wirth et al. (33)	Examine the relationship between ankle dorsiflexor strength, MVC, and MMV with CST integrity and with walking capacity in persons with miSCI	C or D	C3 to L1 LOI	Strength + MEP cohort: 2.4 ± 3.5 y; strength + gait cohort: 1.0 ± 2.2 y	$n = 26$; strength +MEP $n = 17$ (14 M, 3 F); strength + gait $n = 19$ (14 M, 5 F)	Strength + MEP cohort: 50.8 ± 16.5; strength + gait speed cohort: 54.3 ± 15.2	N/A	N/A
	Wirth et al. (34)	Examine recovery of ankle DF in miSCI via neurophysiological assessment of CST function and functional parameters	C or D	C3 to T12 LOI	All subjects tested at 1,3, and 6 mos post-injury	$n = 12$ (6 M, 6 F)	53.7 ± 18.5 months	Non-injured: n = 12	54.0 ± 18.0

[+]*One subject lacked sacral sparing and had an AIS A classification, but had motor function equivalent to AIS D.*

SRC, Spinal Reflex Circuitry; CST, corticospinal tract.

[a]*ISNCSCI, International Standards for Neurological Classification of Spinal Cord Injury; TPI, time post-injury; SCI, spinal cord injury; SCATS, Spinal Cord Assessment Tool for Spastic Reflexes; LOI, level of injury; N/A, not applicable; miSCI, motor incomplete spinal cord injury; tDCS, transcranial direct current electrical stimulation; PES, patterned electrical stimulation; RI, reciprocal inhibition; MAS, modified Ashworth scale; LT, locomotor training; PF, plantar flexor; RTA, reflex threshold angle; LL, lesion-level; TA, tibialis anterior; SOL, soleus; BWSTT, body-weight supported treadmill training; TTS, tilt table standing; RF, rectus femoris; cSCI, complete spinal cord injury; iSCI, incomplete spinal cord injury; MG, medial gastrocnemius; PI, presynaptic inhibition; TMS, transcranial magnetic stimulation; EMG, electromyography; MMV, maximal movement velocity; MVC, maximal voluntary contraction; MEP, motor evoked potential; DF, dorsiflexion; y, years.*

voluntarily activate ankle DF can negatively impact walking function (8). In the current review, 3/4 studies that included measures of SRC excitability and VAC (**Table 3**) provide evidence of a direct association between these measures (15, 36, 43). All three studies that support a direct relationship between SRC excitability and VAC had interventional study designs (15, 36, 43). Among the VAC measures included in these studies were foot clearance, foot tapping, DF strength, PF strength, active range of motion, and walking distance over time. Although evidence of an association between SRC excitability and VAC is clear, there was a wide range of SRC measures and interventions used across these studies (**Table 3**).

In contrast to the three interventional studies that provided evidence of a relationship between SRC excitability and VAC, the observational study captured during this review (38) assessed Ib inhibition from the medial gastrocnemius onto the soleus H-reflex. The authors concluded that Ib inhibition is not affected by SCI. This may suggest that the descending spinal circuits that modulate Ib SRCs differ from those that modulate Ia SRC excitability.

Relationship Between SRC Excitability and Ankle Spasticity

The development of spasticity in the ankle PFs is associated with poorer functional outcomes, interfering with ability to walk and perform daily tasks such as transfers (17). Of the nine studies with measures of ankle spasticity (**Table 4**), six provided evidence of an association with SRC excitability (6, 15, 31, 36, 40, 41). Only four of those six studies used statistical tests to quantify the relationship between SRC excitability and spasticity (6, 15, 31, 36). Five of the six studies that provided evidence of an association had an interventional design (15, 31, 36, 40, 41). Overall, these six studies had a large spectrum of interventions, assessments of spasticity, and measures of SRC excitability (**Table 4**).

Additionally, the two studies that did not support an association between measures of spasticity and measures of SRC excitability were observational (**Table 4**) (37, 38). One of these studies was described above in the section on VAC (38), wherein Ib inhibition from the medial gastrocnemius onto the soleus H-reflex was not found to be influenced by SCI. The authors likewise concluded that there was no relationship between excitability of this circuit and the Achilles tendon reflex testing. The other study (37) assessed the level of heteronomous Ia facilitation between the quadriceps and the soleus H-reflex amplitude as an index of presynaptic inhibition. The authors concluded that while there was less presynaptic inhibition in those with SCI, there was no relationship between the amount of presynaptic inhibition and the Ashworth scale scores. This conclusion directly conflicts with studies that have assessed presynaptic inhibition in other circuits and concluded that decreased presynaptic inhibition is associated with spasticity (44, 45).

Of the 6 interventional studies with assessments of SRC excitability and ankle spasticity, only one did not provide evidence of an association (39). In this study, clonus duration decreased more after body weight supported treadmill training compared to standing on a tilt table; however, there was no change in H/M ratio associated with either intervention. The lack of change in H/M ratio may be due to methodological issues, as prior studies have shown that the maximum H-reflex is less sensitive to modulatory influence than are submaximal reflex responses.

Relationship Between CST Transmission and VAC

Damage to the CSTs associated with SCI has been associated with deficits in walking ability and balance (46). There is evidence that CST transmission is also related to VAC in all seven of the articles in which the relationship between CST transmission and VAC was assessed (**Table 5**).

TABLE 3 | Is there a relationship between SRC excitability and volitional ankle control?

References	Study Design	Intervention	Electrophysiological measure	Relevant functional measure	Direct or indirect evaluation of association?	Evidence of association?
Piazza et al. (36)	Interventional	Leg-cycling	Plantar cutaneomuscular conditioned SOL[a] H-reflex	Strength (TA and Triceps Surae manual muscle score)	**Direct** (Multiple Stepwise Forward Regression and Spearman's Correlation)	Yes
Yamaguchi et al. (43)	Interventional	Anodal tDCS combined with PES	SOL H-reflexes in response to RI and PI	Ankle movement/tapping, Active ankle ROM	**Direct** (Pearson's correlation)	Yes
Manella et al. (15)	Interventional	Operant conditioning: TA EMG activation increase OR SOL H-reflex decrease	SOL H-reflexes in response to RI, PI, and LFD	Toe/foot clearance during walking, ankle movement/tapping, strength (DF and PF), active ROM (DF)	**Direct** (Spearman's correlation)	Yes
Downes et al. (38)	Observational	N/A	Ib conditioned-SOL H-reflex	Strength (DF and PF)	**Direct** Pearson's correlation	No

[a]*SOL, soleus; TA, tibialis anterior; tDCS, transcranial direct current stimulation; PES, patterned electrical stimulation ; RI, reciprocal inhibition; PI, presynaptic inhibition; ROM, active range of motion; EMG, electromyography; LFD, low frequency depression; DF, dorsiflexor; PF, plantar flexor.*

"Yes" indicates that there is evidence that at least one electrophysiological measure had an association with at least one relevant functional measure.

TABLE 4 | Is there a relationship between SRC excitability and ankle spasticity?

References	Study design	Intervention	Electrophysiological measure	Relevant functional measure	Direct or indirect evaluation of association?	Evidence of association?
Faist et al. (37)	Observational	N/A	PI (Quadriceps), SOL H/M ratio	Hypertonia (Achilles tendon reflex, Ashworth scale)	**Direct** (Pearson's correlation)	No
Downes et al. (38)	Observational	N/A	Ib conditioned-SOL H-reflex	Hypertonia (Achilles tendon reflex; tone of the ankle DF, PF)	**Direct** (Pearson's correlation)	No
Adams and Hicks (39)	Interventional	BWSTT v. TTS	SOL H/M ratio	Clonus duration (SCATS-Clonus)	**Indirect**	No
Murillo et al. (40)	Interventional	Focal vibration (RF)	SOL H/M ratio	Clonus duration and # of oscillations	**Indirect**	Yes
Manella and Field-Fote (31)	Interventional AND Observational	Locomotor training	SOL H/M ratio	Clonus duration, # of oscillations, PF RTA (Drop test), gait speed	**Direct** (Spearman's correlation)	Yes
Manella et al. (15)	Interventional	Operant conditioning: TA activation increase OR Soleus H-reflex suppression	SOL H-reflex: RI, PI, and LFD	Clonus duration, PF RTA	**Direct** (Spearman's correlation)	Yes
Manella et al. (6)	Observational	N/A	SOL H/M ratio	# of oscillations (Drop test)	**Direct** (Spearman's correlation)	Yes
Smith et al. (41)	Interventional	Locomotor training (Lokomat)	SOL H/M ratio	Clonus duration and # of oscillations (via soleus EMG analysis during walking)	**Indirect**	Yes
Piazza et al. (36)	Interventional	Leg-cycling	Plantar[a] cutaneomuscular conditioned SOL H-reflex	Hypertonia (MAS), clonus duration (SCATS clonus score)	**Direct** (Multiple Stepwise Forward Regression and Spearman's Correlation)	Yes

[a]*PI, presynaptic inhibition; SOL, soleus; DF, dorsiflexor; PF, plantar flexor; BWSTT, body-weight supported treadmill training; TTS, tilt table standing; SCATS, Spinal Cord Assessment Tool for Spastic Reflexes; RF, rectus femoris; RTA, reflex threshold angle; EMG, electromyography; RI reciprocal inhibition; LFD, low frequency depression.*
"Yes" indicates that there is evidence that at least one electrophysiological measure had an association with at least one relevant functional measure.

In contrast to the SRC studies, none of the CST transmission studies used an intervention; all had observational designs. Six of seven studies used direct measures of correlations or linear regressions to assess the relationship between CST transmission and volitional measures (8, 30, 32–35). Seven of 7 studies assessed MEP amplitude and latency in the TA. Functional measures including foot clearance, maximal movement velocity of the ankle, walking speed, walking distance over time, timing of dorsiflexion during walking, and ankle strength were all related to CST transmission. In one of these studies, a prospective cohort design was used to record longitudinal changes in the first six months after SCI. MEP amplitude, gait speed, DF muscle strength, and rate of activation increased significantly over time (34).

DISCUSSION

Summary—State of the Literature

While empirical evidence suggests there is an association between (1) measures of SRC excitability and VAC, (2) SRC excitability and spasticity, and (3) between CST transmission and VAC, the relationship between these measures in the literature is confounded by inherent variability in the neurophysiological measures and the wide range of functional measures utilized across the studies. To gain a better understanding of the evidence that does exist regarding the relationship between the underlying neurophysiological tests and ankle control, biomechanical, and functional outcomes were more closely examined and compared to specific neurological tests within and between studies (**Tables 3**–**5**).

Relationship Between SRC Excitability and VAC

After SCI, control of dorsiflexion depends on the extent to which hyperexcitability of the soleus SRCs degrades normal ankle kinematics. Ankle control can be examined using a variety of functional measures. It is important to determine the underlying mechanisms involved with each of these measures, as this knowledge could support the development of more effective rehabilitation strategies. The findings of this scoping review provide evidence that different components of ankle control may be associated with distinct measures of SRC excitability.

For the measure of ankle control during tapping tasks, 2 studies (15, 43) support the conclusion that the number of repetitions of ankle movements during a timed tapping task is associated with H-reflex excitability as measured by presynaptic and reciprocal inhibition. The relationship between

TABLE 5 | Is there a relationship between CST transmission and volitional ankle control?

References	Study design	Intervention	Electrophysiological measure	Relevant functional measure	Direct or indirect evaluation of association?	Evidence of association?
Barthélemy et al. (30)	Observational	N/A	TA MEP[a] amplitude, latency	Gait kinematics toe clearance, gait speed, walking distance	Direct (Spearman's and Pearson's correlation)	Yes
Labruyère et al. (42)	Observational	N/A	MEP amplitude, latency	Muscle strength (DF and PF), stepping task	Indirect	Yes
Barthélemy et al. (8)	Observational	N/A	TA MEP amplitude, latency	Gait kinematics – foot drop	Direct (Spearman's and Pearson's correlation)	Yes
Wirth et al. (35)	Observational	N/A	MEP amplitude, latency	Timing of ankle dorsiflexion during gait and in supine at 3 frequencies, DF MMV, TA muscle strength (MVC)	Direct and Indirect (Spearman's correlation)	Yes
Wirth et al. (32)	Observational	N/A	TA MEP amplitude, latency	Ankle dexterity, MMV	Simultaneous Direct (linear regression analyses-backward standardized regression GROUPED TOGETHER)	Yes
Wirth et al. (33)	Observational	N/A	MEP amplitude, latency	TA muscle strength (AIS motor score, MVC), DF MMV, gait speed, walking ability (WISCI)	Direct (linear, backwards multiple regression)	Yes
Wirth et al. (34)	Observational	N/A	MEP amplitude, latency	ankle dexterity, MMV, TA strength (AIS motor score, MVC), gait speed	Direct (linear regression and Spearman's correlation)	Yes

[a] *TA, tibialis anterior; MEP, motor evoked potential; DF, dorsiflexor; PF, plantar flexor; MMV, maximal movement velocity; MVC, maximal volitional contraction; AIS, ASIA impairment scale; WISCI, Walking Index for Spinal Cord Injury.*

"Yes" indicates that there is evidence that at least one electrophysiological measure had an association with at least one relevant functional measure.

ankle strength and reflex excitability is less clear, as two studies indicate there could be an association between strength and amplitude of the conditioned H-reflex responses (15, 36), while another did not (38). In addition to the divergence of findings, and perhaps the reason for the divergence, the type of H-reflex test used for each of these studies varied (see **Table 3**). For the two studies that measured active range of motion in the ankles, the first study demonstrated a possible association between this functional outcome with low frequency depression and presynaptic inhibition (15), while the other demonstrated a change in reciprocal and presynaptic inhibition, but not active range of motion (43). Lastly, in the study in which toe clearance during walking was measured, there was an association between change in toe clearance and reciprocal inhibition (15). Although most of these studies included correlations between SRC excitability and VAC measures, due to the variability of the tests, there is a strong need for additional studies to quantify the relationship between these two constructs.

Relationship Between SRC Excitability and Ankle Spasticity

The ability to achieve adequate dorsiflexion during functional tasks, such as walking and transfers, can be hindered by involuntary muscle contractions and stiffness associated with spasticity in the ankle plantar flexors. It is important to understand how commonly used tests of SRC excitability are associated with biomechanical measures of spasticity to develop more effective neuromodulatory strategies. In comparison to the number of studies that included measures of SRC excitability and VAC, there is a noticeably larger amount of studies dedicated to measuring SRC excitability and ankle spasticity. There are several biomechanical assessments to measure ankle spasticity, including: spinal cord assessment tool for spastic reflexes (SCATS), modified Ashworth scale, Achilles tendon reflex, and the ankle clonus drop test. These biomechanical tests can provide insight into properties such as ankle stiffness, clonus duration, and number of clonus oscillations. The large variety of biomechanical spasticity measures used across studies and the different types of SRC excitability measures utilized, make it difficult to quantify the relationship between the biomechanical measures of responsiveness to stretch and electrophysiologic SRC excitability measures. However, there is evidence that some biomechanical measures of spasticity may be associated with different components of SRC excitability (see **Table 4**).

One sensitive biomechanical measure of spasticity is the reflex threshold angle in the plantar flexors. One study provided evidence that reflex threshold angle appears to be related to reciprocal and presynaptic inhibition (15), while another showed it may be related to H-reflex excitability (31). Of the 6 studies that included measures of clonus duration, three provide evidence that there may be a relationship between clonus duration and cutaneomuscular conditioned-reflex (36), H-reflex excitability (40), and low frequency depression (15). The same number of articles demonstrated a potential association between number of oscillations during ankle clonus and H-reflex excitability (6, 40, 41). Only one study demonstrated evidence of a relationship

between ankle stiffness, measured using the modified Ashworth scale, and cutaneomuscular conditioned-reflex (36). Though there is some evidence of an association between measures of SRC excitability and functional outcomes related to spasticity, an increased amount of attention into the specifics of these measures and the underlying mechanisms that impact them is needed for a better understanding of this relationship.

Relationship Between CST Transmission and VAC

Spinal cord injury diminishes the capacity of the CST to transmit descending neural signals, thereby limiting both strength and speed of VAC in the dorsiflexors. Measures of VAC included: tapping tasks, ankle strength, toe clearance during walking, and gait measures. Both MEP amplitude and latency were shown to have some evidence of a relationship with each component of ankle control (see **Table 5**). It should be noted that although there were some differences in the methodologies used across studies, there was less variability between measures in the CST transmission studies than there were in the SRC excitability studies.

The coordination and timing of VAC can be assessed during tapping tasks to match a rhythmic tone. In the four studies that assessed VAC during tapping tasks, there was an association between maximal movement velocity and measures of CST transmission (32–35). Ankle strength is another important component of VAC. For the measure of ankle strength, two articles demonstrated an association between strength with MEP latency (33) and MEP amplitude (34), while two other articles did not support a relationship between those measures (35, 42). Foot drop/toe drag can be assessed by measuring toe clearance and ankle angle during swing phase. Toe clearance during walking was measured in two articles that assessed CST transmission (8, 30). Both articles demonstrated that maximum toe elevation was associated with MEP amplitude and latency. Lastly, 4/6 studies that contained some measure of gait parameters and stepping ability, presented evidence of an association with CST neurophysiology (8, 30, 35, 42). Additional work is warranted in this area to understand how measures of CST transmission relate to ankle spasticity, as none of these studies included any spasticity measures. There would be great value in future studies that include CST transmission and SRC excitability measures in conjunction with ankle-related functional and biomechanical outcomes.

Existing Gaps—Limitations

Limitations of Included Studies

The greatest limitation in the currently available literature related to the relationships among CST transmission, SRC excitability, spasticity, and function was the large variability in measures used in the studies. Overall, there was a wider range of neurophysiological measures in the studies that assessed SRC excitability than in the studies that assessed CST transmission. Although all of the reported neurophysiological measures assessed changes in SRC excitability, the studies tested different circuits at different timepoints, which may result in significant changes being observed in one study while non-significant results were observed in another. For example, although presynaptic inhibition and reciprocal inhibition both impact reflex excitability, the interneurons involved are not the same. Given that changes in the CST transmission can influence the SRC excitability, it is unfortunate that no articles included both corticospinal and spinal neurophysiological measures.

There was also variability in the types of measures used to assess spasticity and VAC in the studies which assessed SRC excitability and the articles that assessed CST transmission. In the articles that addressed SRC excitability, the studies included different biomechanical measures of ankle spasticity. None of the included CST transmission articles assessed spasticity. Both measures are important for assessing factors that influence changes in gait parameters after injury. Increases in voluntary control and decreases in spasticity are both beneficial for improving walking function in persons with SCI. Future studies should assess both volitional and spasticity related measures of the ankle.

Limitations of Review

The search strategy was potentially limited for two main reasons. The search included only studies of SRC excitability that used measures based on the H-reflex test and studies of CST transmission that used MEPs as neurophysiological measures. Studies which utilize other neurophysiological measures along with VAC and spasticity measures may have been excluded, potentially limiting the scope of this review. We chose to use H-reflex and MEPs as the primary measures of interest because they are both widely used, non-invasive neurophysiological tests with good reliability. However, despite being commonly used measures, H-reflexes and MEPs cannot isolate or provide information about the integrity of all pathways that may influence neuromotor control of the ankle (i.e., rubrospinal tract, reticulospinal tract, vestibulospinal tract, and group II afferent nerve pathways).

Conclusions and Future Directions

Based on the available literature there is evidence of an association between neurophysiological excitability with VAC and spasticity after SCI. Future studies assessing these relationships are important for the development of better targeted therapies such as whole body vibration, peripheral nerve somatosensory stimulation, transcutaneous spinal stimulation, and transcranial direct current stimulation to improve walking and balance in individuals affected by SCI. There is great potential for this knowledge to guide therapists in the use of non-invasive stimulation to increase descending drive or decrease spasticity. While it may be difficult to isolate interventions to either CST transmission or SRC excitability alone, it is important to understand neurophysiologic contributions to ankle control given its relevance to safe and efficient ambulation within clinical populations with central nervous system disorders. Studies that employ a battery of neurophysiologic and functional measures to assess both SRC excitability and CST transmission in persons with SCI are warranted.

AUTHOR CONTRIBUTIONS

JH was responsible for the development of the review question, conduction of the literature search, screening process, and wrote a substantial portion of each section. RK assisted with the screening process, created the tables and figures, and wrote portions of the background, results, and discussion. SE assisted in the screening process and developed sections of the results and discussion. EF-F assisted in the development of the review question, was a consultant during each stage of the review process, and played a role in the development and editing of the entire scoping review.

FUNDING

This work was supported by NIH Diversity Supplement: Shepherd Center (5R01HD079009-05 to EF-F) and the Hulse Spinal Cord Injury Research Fund.

ACKNOWLEDGMENTS

We would like to thank Christine Willis for her assistance with developing the search strategy and Jennifer Iddings, Ph.D. for helping with the design of our figures.

REFERENCES

1. Ditunno PL, Patrick M, Stineman M, Ditunno JF. Who wants to walk? Preferences for recovery after SCI: A longitudinal and cross-sectional study. *Spinal Cord.* (2008) 46:500–6. doi: 10.1038/sj.sc.3102172
2. van Hedel HJESG. Gait speed in relation to categories of functional ambulation after spinal cord injury. *Neurorehabil Neural Repair.* (2009) 23:1–8. doi: 10.1177/1545968308324224
3. Dubin A. Gait: the role of the ankle and foot in walking. *Med Clin North Am.* (2014) 98:205–11. doi: 10.1016/j.mcna.2013.10.002
4. Dobkin BH, Firestine A, West M, Saremi K, Woods R. Ankle dorsiflexion as an fMRI paradigm to assay motor control for walking during rehabilitation. *Neuroimage.* (2004) 23:370–81. doi: 10.1016/j.neuroimage.2004.06.008
5. Barbeau H, Nadeau S, Garneau C. Physical determinants, emerging concepts, and training approaches in gait of individuals with spinal cord injury. *J Neurotrauma.* (2006) 23:571–85. doi: 10.1089/neu.2006.23.571
6. Manella KJ, Roach KE, Field-Fote EC. Temporal indices of ankle clonus and relationship to electrophysiologic and clinical measures in persons with spinal cord injury. *J Neurol Phys Ther.* (2017) 41:229–38. doi: 10.1097/NPT.0000000000000197
7. Varoqui D, Niu X, Mirbagheri MM. Ankle voluntary movement enhancement following robotic-assisted locomotor training in spinal cord injury. *J Neuroeng Rehabil.* (2014) 11:46. doi: 10.1186/1743-0003-11-46
8. Barthélemy D, Willerslev-Olsen M, Lundell H, Conway BA, Knudsen H, Biering-Sorensen F, et al. Impaired transmission in the corticospinal tract and gait disability in spinal cord injured persons. *J Neurophysiol.* (2010) 104:1167–76. doi: 10.1152/jn.00382.2010
9. Knikou M. Neural control of locomotion and training-induced plasticity after spinal and cerebral lesions. *Clin Neurophysiol.* (2010) 121:1655–68. doi: 10.1016/j.clinph.2010.01.039
10. Burke D, Gandevia SC, McKeon B. The afferent volleys responsible for spinal proprioceptive reflexes in man. *J Physiol.* (1983) 339:535–52. doi: 10.1113/jphysiol.1983.sp014732
11. Thomas SL, Gorassini MA. Increases in corticospinal tract function by treadmill training after incomplete spinal cord injury. *J Neurophysiol.* (2005) 94:2844–55. doi: 10.1152/jn.00532.2005
12. Norton JA, Gorassini MA. Changes in cortically related intermuscular coherence accompanying improvements in locomotor skills in incomplete spinal cord injury. *J Neurophysiol.* (2006) 95:2580–9. doi: 10.1152/jn.01289.2005
13. Hoffman LR, Field-Fote EC. Cortical reorganization following bimanual training and somatosensory stimulation in cervical spinal cord injury: a case report. *Phys Ther.* (2007) 87:208–23. doi: 10.2522/ptj.20050365
14. Hoffman L, Field-Fote E. Effects of practice combined with somatosensory or motor stimulation on hand function in persons with spinal cord injury. *Top Spinal Cord Inj Rehabil.* (2013) 19:288–99. doi: 10.1310/sci1904-288
15. Manella KJ, Roach KE, Field-Fote EC. Operant conditioning to increase ankle control or decrease reflex excitability improves reflex modulation and walking function in chronic spinal cord injury. *J Neurophysiol.* (2013) 109:2666–79. doi: 10.1152/jn.01039.2011
16. Gomes-Osman J, Tibbett JA, Poe BP, Field-Fote EC. Priming for improved hand strength in persons with chronic tetraplegia: a comparison of priming-augmented functional task practice, priming alone, and conventional exercise training. *Front Neurol.* (2017) 17:242. doi: 10.3389/fneur.2016.00242
17. Adams MM, Hicks AL. Spasticity after spinal cord injury. *Spinal Cord.* (2005) 43:577–86. doi: 10.1038/sj.sc.3101757
18. McKay WB, Sweatman WM, Field-Fote EC. The experience of spasticity after spinal cord injury: Perceived characteristics and impact on daily life. *Spinal Cord.* (2018) 56:478–86. doi: 10.1038/s41393-017-0038-y
19. Gorassini MA, Knash ME, Harvey PJ, Bennett DJ, Yang JF. Role of motoneurons in the generation of muscle spasms after spinal cord injury. *Brain.* (2004) 127:2247–58. doi: 10.1093/brain/awh243
20. Boulenguez P, Liabeuf S, Bos R, Bras H, Jean-Xavier C, Brocard C, et al. Down-regulation of the potassium-chloride cotransporter KCC2 contributes to spasticity after spinal cord injury. *Nat Med.* (2010) 16:302–7. doi: 10.1038/nm.2107
21. Smith AC, Knikou M. A review on locomotor training after spinal cord injury: reorganization of spinal neuronal circuits and recovery of motor function. *Neural Plast.* (2016) 2016:1216258. doi: 10.1155/2016/1216258
22. James ND, McMahon SB, Field-Fote EC, Bradbury EJ. Neuromodulation in the restoration of function after spinal cord injury. *Lancet Neurol.* (2018) 17:905–17. doi: 10.1016/S1474-4422(18)30287-4
23. Field-Fote EC. Exciting recovery: Augmenting practice with stimulation to optimize outcomes after spinal cord injury. *Prog Brain Res.* (2015) 218:103–26. doi: 10.1016/bs.pbr.2014.12.006
24. Field-Fote EC, Yang JF, Basso DM, Gorassini MA. Supraspinal control predicts locomotor function and forecasts responsiveness to training after spinal cord injury. *J Neurotrauma.* (2017) 34:1813–25. doi: 10.1089/neu.2016.4565
25. Peters MDJ, Godfrey CM, Khalil H, McInerney P, Parker D, Soares CB. Guidance for conducting systematic scoping reviews. *Int J Evid Based Healthc.* (2015) 13:141–6. doi: 10.1097/XEB.0000000000000050
26. Arksey H, O'Malley L. Scoping studies: towards a methodological framework. *Int J Soc Res Methodol Theory Pract.* (2005) 8:19–32. doi: 10.1080/1364557032000119616
27. Tallent J, Goodall S, Hortobágyi T, St Clair Gibson A, French DN, Howatson G. Repeatability of corticospinal and spinal measures during lengthening and shortening contractions in the human tibialis anterior muscle. *PLoS ONE.* (2012) 7:1–8. doi: 10.1371/journal.pone.0035930
28. Leung H, Latella C, Lamon S, Hendy AM. The reliability of neurological measurement in the vastus medialis: Implications for research and practice. *Front Psychol.* (2018) 9:1–10. doi: 10.3389/fpsyg.2018.01857
29. Moher D, Liberati A, Tetzlaff J, Altman DG, The PRISMA Group. Preferred reporting items for systematic reviews and meta-analyses: the PRISMA statement. *PLoS Med.* (2009) 6:e1000097. doi: 10.1371/journal.pmed1000097
30. Barthélemy D, Knudsen H, Willerslev-Olsen M, Lundell H, Nielsen JB, Biering-Sørensen F. Functional implications of corticospinal tract impairment on gait after spinal cord injury. *Spinal Cord.* (2013) 51:852–6. doi: 10.1038/sc.2013.84
31. Manella KJ, Field-Fote EC. Modulatory effects of locomotor training on extensor spasticity in individuals with motor-incomplete spinal cord injury. *Restor Neurol Neurosci.* (2013) 31:633–46. doi: 10.3233/RNN-120255

32. Wirth B, Van Hedel HJA, Curt A. Ankle dexterity remains intact in patients with incomplete spinal cord injury in contrast to stroke patients. *Exp Brain Res.* (2008) 191:353–61. doi: 10.1007/s00221-008-1528-0
33. Wirth B, Van Hedel HJA, Curt A. Ankle paresis in incomplete spinal cord injury: Relation to corticospinal conductivity and ambulatory capacity. *J Clin Neurophysiol.* (2008) 25:210–7. doi: 10.1097/WNP.0b013e318183f4e3
34. Wirth B, Van Hedel HJA, Curt A. Changes in corticospinal function and ankle motor control during recovery from incomplete spinal cord injury. *J Neurotrauma.* (2008) 25:467–78. doi: 10.1089/neu.2007.0472
35. Wirth B, van Hedel HJA, Curt A. Ankle dexterity is less impaired than muscle strength in incomplete spinal cord lesion. *J Neurol.* (2008) 255:273–9. doi: 10.1007/s00415-008-0724-y
36. Piazza S, Gómez-Soriano J, Bravo-Esteban E, Torricelli D, Avila-Martin G, Galan-Arriero I, et al. Maintenance of cutaneomuscular neuronal excitability after leg-cycling predicts lower limb muscle strength after incomplete spinal cord injury. *Clin Neurophysiol.* (2016) 127:2402–9. doi: 10.1016/j.clinph.2016.03.007
37. Faist M, Mazevet D, Dietz V, Pierrot-deseilligny E. A quantitative assessment of presynaptic inhibition of la afferents in spastics: differences in hemiplegics and paraplegics. *Brain.* (1994) 117:1449–55. doi: 10.1093/brain/117.6.1449
38. Downes L, Ashby P, Bugaresti J. Reflex effects from golgi tendon organ. (ib) afferents are unchanged after spinal cord lesions in humans. *Neurology.* (1995) 45:1720–4. doi: 10.1212/WNL.45.9.1720
39. Adams MM, Hicks AL. Comparison of the effects of body-weight-supported treadmill training and tilt-table standing on spasticity in individuals with chronic spinal cord injury. *J Spinal Cord Med.* (2011) 34:488–94. doi: 10.1179/2045772311Y.0000000028
40. Murillo N, Kumru H, Vidal-Samso J, Benito J, Medina J, Navarro X, et al. Decrease of spasticity with muscle vibration in patients with spinal cord injury. *Clin Neurophysiol.* (2011) 122:1183–9. doi: 10.1016/j.clinph.2010.11.012
41. Smith AC, Rymer WZ, Knikou M. Locomotor training modifies soleus monosynaptic motoneuron responses in human spinal cord injury. *Exp Brain Res.* (2015) 233:89–103. doi: 10.1007/s00221-014-4094-7
42. Labruyère R, Zimmerli M, Van Hedel HJ. Slowed down: Response time deficits in well-recovered subjects with incomplete spinal cord injury. *Arch Phys Med Rehabil.* (2013) 94:2020–6. doi: 10.1016/j.apmr.2013.04.002
43. Yamaguchi T, Fujiwara T, Tsai Y-A, Tang S-C, Kawakami M, Mizuno K, et al. The effects of anodal transcranial direct current stimulation and patterned electrical stimulation on spinal inhibitory interneurons and motor function in patients with spinal cord injury. *Exp Brain Res.* (2016) 234:1469–78. doi: 10.1007/s00221-016-4561-4
44. Ashby P, Verrier M, Lightfoot E. Segmental reflex pathways in spinal shock and spinal spasticity in man. *J Neurol Neurosurg Psychiatry.* (1974) 37:1352–60. doi: 10.1136/jnnp.37.12.1352
45. Calancie B, Broton JG, John Klose K, Traad M, Difini J, Ram Ayyar D. Evidence that alterations in presynaptic inhibition contribute to segmental hypo- and hyperexcitability after spinal cord injury in man. *Electroencephalogr Clin Neurophysiol Evoked Potentials.* (1993) 89:177–86. doi: 10.1016/0168-5597(93)90131-8
46. Barthélemy D, Willerslev-Olsen M, Lundell H, Biering-Sørensen F, Nielsen JB. Assessment of transmission in specific descending pathways in relation to gait and balance following spinal cord injury. *Prog Brain Res.* (2015) 218:79–101. doi: 10.1016/bs.pbr.2014.12.012

Conflict of Interest: The authors declare that the research was conducted in the absence of any commercial or financial relationships that could be construed as a potential conflict of interest.

frontiers in Neurology

ORIGINAL RESEARCH
published: 17 March 2020
doi: 10.3389/fneur.2020.00191

A Preliminary Study of Effects of Channel Number and Location on the Repeatability of Motor Unit Number Index (MUNIX)

Farong Gao[1], *Yueying Cao*[1], *Chuan Zhang*[2] *and Yingchun Zhang*[2]*

[1] School of Automation, Artificial Intelligence Institute, Hangzhou Dianzi University, Hangzhou, China, [2] Department of Biomedical Engineering, University of Houston, Houston, TX, United States

Motor Unit Number Index (MUNIX) is a technique that provides a susceptive biomarker for monitoring innervation conditions in patients with neurodegenerative diseases. A satisfactory repeatability is essential for the interpretation of MUNIX results. This study aims to examine the effect of channel number and location on the repeatability of MUNIX. In this study, 128 channels of high-density surface electromyography (EMG) signals were recorded from the biceps brachii muscles of eight healthy participants, at 10, 20, 30, 40, 50, 60, 70, 80, and 100% of maximal voluntary contraction. The repeatability was defined by the coefficient of variation (CV) of MUNIX estimated from three experiment trials. Single-channel MUNIX (sMUNIX) was calculated on a channel-specific basis and a multi-channel MUNIX (mMUNIX) approach as the weighted average of multiple sMUNIX results. Results have shown (1) significantly improved repeatability with the proposed mMUNIX approach; (2) a higher variability of sMUNIX when the recording channel is positioned away from the innervation zone. Our results have demonstrated that (1) increasing the number of EMG channels and (2) placing recording channels close to the innervation zone (IZ) are effective methods to improve the repeatability of MUNIX. This study investigated two potential causes of MUNIX variations and provided novel perspectives to improve the repeatability, using high-density surface EMG. The mMUNIX technique proposed can serve as a promising tool for reliable neurodegeneration evaluation.

Keywords: channel number, high-density, motor unit number index, repeatability, surface electromyography, innervation zone

OPEN ACCESS

Edited by:
Xiaogang Hu,
University of North Carolina at Chapel Hill, United States

Reviewed by:
Le Li,
Sun Yat-Sen University, China
Zhiyuan Lu,
University of Texas Health Science Center at Houston, United States

***Correspondence:**
Yingchun Zhang
yzhang94@uh.edu

Specialty section:
This article was submitted to Neuromuscular Diseases, a section of the journal Frontiers in Neurology

Received: *15 December 2019*
Accepted: *28 February 2020*
Published: *17 March 2020*

Citation:
Gao F, Cao Y, Zhang C and Zhang Y (2020) A Preliminary Study of Effects of Channel Number and Location on the Repeatability of Motor Unit Number Index (MUNIX). Front. Neurol. 11:191. doi: 10.3389/fneur.2020.00191

INTRODUCTION

Motor Unit Number Index (MUNIX) has been accepted as a neurological tool for technically friendly indexing the number of functioning motor unit (MU) of target muscle (1). Being better tolerated, easier and quicker to perform than motor unit number estimation (MUNE), MUNIX has been proved an as reliable biomarker for assessing MU loss in different patient populations, including amyotrophic lateral sclerosis (ALS) (2), spinal cord injury (SCI) (3), multifocal motor neuropathy (MMN) (4), post-polio syndrome (5), stroke (6) and spinal muscular atrophy (SMA) (7). Specifically, studies have shown that MUNIX is capable of detecting motor neuron loss in early stages of ALS before the patient has obvious weakness (8).

A reproducible MUNIX is crucial to the acquisition of credible observations for interpretation. The repeatability of MUNIX can be affected by multiple factors, including the variation in electromyography (EMG) signals and electrode positioning. Variations in compound muscle action potential (CMAP) signals and surface EMG contraction signals, and randomness of surface interferential patterns (SIP) selection can affect MUNIX results. Furthermore, suboptimal electrode placement has been suggested as the most recurrent source of errors and systematic mistakes (9). The repeatability of MUNIX has been reported in both healthy and patient subjects, measured by coefficient of variation (CV), interclass correlation coefficients (ICC) and/or correlation coefficients (CC) (8–11). CV values up to 52.9% has been observed in healthy and ALS patients (10, 12–15). It is therefore necessary to find solutions to improve the repeatability of MUNIX; nonetheless limited effort has been made.

Recent advances of high-density surface EMG has enabled the non-invasive acquisition of abundant spatiotemporal information and consequently advanced analysis techniques (16–19). In this study, we aimed to employ high-density surface EMG measurements to examine the repeatability of MUNIX in relation to the number and location of recording channels. Specifically, a multi-channel MUNIX (mMUNIX) method was proposed to generate a more reproducible MU quantity index.

MATERIALS AND METHODS

Participants and Consent

Eight healthy subjects (two females, mean age 27 ± 4 years) without history of neurological diseases were recruited at the University of Houston. Subjects were well-informed of the experiment procedure, potential risks of the study and gave written informed consent. The experiment protocol was approved by the University of Houston and University of Texas Health Science Center-Houston institutional review board.

Experiment Protocol

The experiment procedure followed our previous study (20). Briefly, the biceps brachii muscle of the dominant arm was selected for MUNIX calculation. After skin preparation, two high-density surface EMG grids were placed adjacently to cover the muscle, as shown in **Figure 1A**. Each grid features an 8 by 8 surface electrode configuration, with an electrode diameter of 4.5 mm and an inter-electrode distance (IED) of 8.5 mm (TMSi, Enschede, the Netherlands). The reference electrode was placed on the medioepicondyle of the same arm and ground on the idle arm with a Velcro strap (TMSi, Enschede, the Netherlands). Subjects were seated in a mobile Biodex chair (Biodex, Shirley, NY) and instructed to perform three isometric elbow flexions at maximal voluntary contraction (MVC). Then three sets of experiment trials were performed. Each trial included contractions at 10, 20, 30, 40, 50, 60, 70, 80, and 100% MVC with visual feedback from a screen monitor and supramaximal compound muscle action potential (CMAP) elicited by electrical nerve stimulation. Rectangular stimulation with a pulse width of 0.2 ms was delivered to the proximal musculocutaneous nerve using a DS7 current stimulator (Digitimer Ltd, Welwyn Garden City, United Kingdom). The optimal stimulation site was determined by maximizing the CMAP response at a consistent stimulation intensity of 25 mA. Then stimulation intensity was increased in steps of 5 mA until no further increase in CMAP amplitude observed (21). Adequate interval was given between two consecutive contractions or stimulation to avoid muscle fatigue. All EMG signals were acquired via a 136 channel Refa amplifier (TMSi, Enschede, The Netherlands) at a sampling rate of 2,048 Hz, and stored for offline processing.

MUNIX Calculation

Data analysis was performed using Matlab R2015 (The Mathworks, Natick, MA). Contraction EMG signals were bandpass filtered at 10–500 Hz and notch filtered at 60 Hz using second order Butterworth filters, as shown in **Figure 1B**. CMAP recording was high pass filtered at 1 Hz and notch filtered at 60 Hz, exampled by **Figure 1D**. Stimulation artifact was identified and suppressed as described in a previous study (22). Very briefly, the artifact was identified using a Savitzky-Golay filter and Otsu thresholding. Then the contaminated data points were replaced by a spline interpolation. As the compound action potential propagates, morphological and temporal alterations of the CMAP recordings were observed from different surface channels. Therefore, the high-density CMAP profile was obtained on a channel-specific basis by identifying the onset and offset of each CMAP measurement. SIP epochs were extracted from EMG trials at each contraction levels, with a length of 300 ms (614 data samples). Ten randomly selected epochs were extracted from each contraction level; whereas only 5 from 100% MVC because of the shorter duration of stable contractions at maximal force, as shown in **Figure 1C**. The final SIP pool consists of 85 different SIPs (8 submaximal contraction levels * 10 epochs/level + 1 contraction level of 100% MVC * 5 epochs/level). The SIP pool was employed to construct 10 different combinations of SIP epochs for MUNIX calculation by randomly selected one epoch in each level (SIP epochs at 100% MVC were used twice).

Effect of Channel Number on MUNIX Repeatability

Single-channel MUNIX (sMUNIX) was calculated for each recording channel using the high-density SIP and CMAP profile. To evaluate the effect of channel number on the repeatability of MUNIX, a multi-channel MUNIX, denoted here as mMUNIX, was proposed. The method was inspired by a previous high-density MUNE approach (20, 23). Concretely, mMUNIX was calculated as the weighted average of multiple sMUNIX, with the weights defined as:

$$W(k) = \frac{A^2(k)}{\sum_{m=1}^{N} A^2(m)} \quad (1)$$

where $A(k)$ denotes the CMAP negative peak amplitude of the k-th channel, $W(k)$ denotes its corresponding weight. mMUNIX was calculated, respectively, based on the N channels ($N = 2$, 4, 8, 16, 32, 64, and 128) with the top N largest CMAP amplitude.

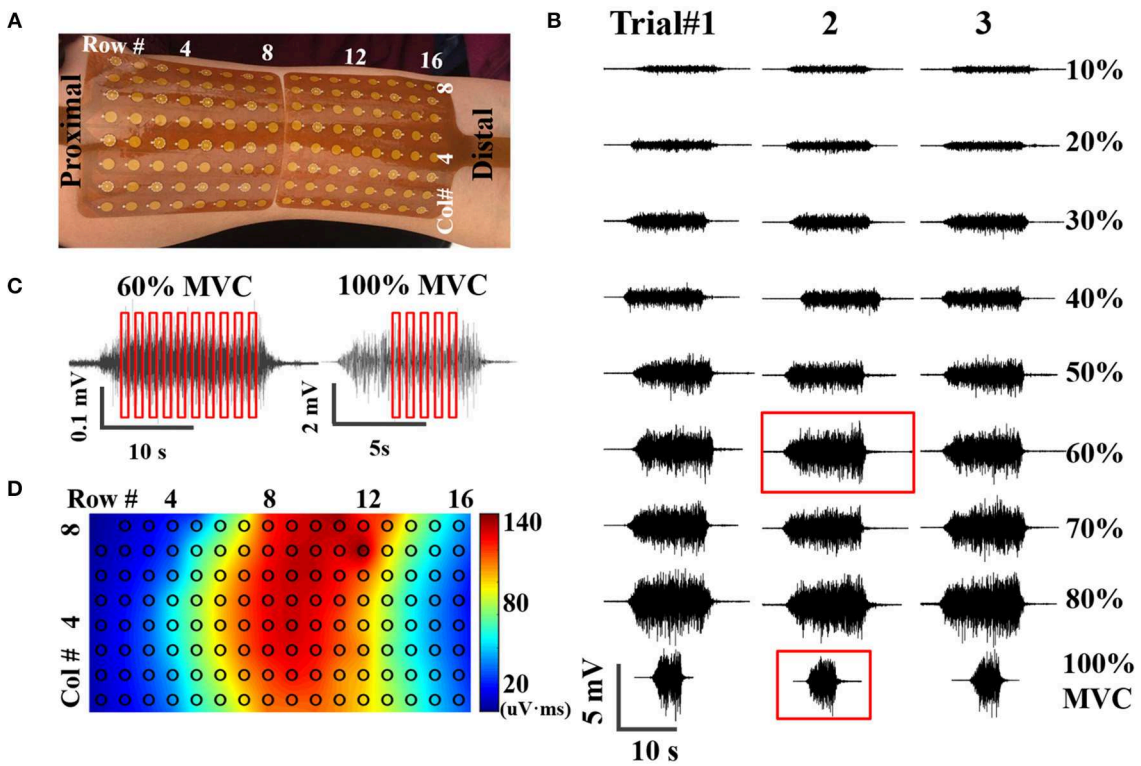

FIGURE 1 | (A) placement of high-density surface EMG grids, **(B)** An example of EMG signals acquired at nine contraction levels from three trials, **(C)** Examples of SIP epoch selection at submaximal (60% MVC) and maximal (100% MVC) contractions, **(D)** Potential mapping from one representative CMAP recording.

Effect of Channel Location on MUNIX Repeatability

As the CMAP area correlates with the MUNIX, the electrodes near IZ can often acquire larger CMAP response and consequently larger MUNIX (24). As innervation zone (IZ) closely related to the origin of EMG signals, the sMUNIX repeatability with respect to the IZ was also studied. The IZ was detected by treating each axial column as an evenly-spaced linear sensor array, and IZ was defined as the point of symmetry in the bipolar signals of each column, as shown in **Figure 2** (25). If phase reversal was observed in two neighboring bipolar channels, the IZ was identified as the monopolar channel in the middle that contributes to both bipolar channels. If a bipolar channel with near-zero signal amplitude separated the signal phase reversal; the midpoint of the two monopolar channels which contribute to the attenuated bipolar channel was identified as the IZ (16, 26–28). Therefore, a spatial resolution of 4.25 mm (half of the inter-electrode spacing) and 8.5 mm was achieved for IZ detection in the axial and mediolateral directions, respectively. IZ mapping was determined at 20, 50, and 100% MVCs, which are the commonly force levels used for IZ detection (29). The channel label was defined by its minimal distance to the IZ on a column-basis, as shown in **Figure 2**. In **Figure 2**, the three labeled columns are to show three representative cases of IZ distributions: (1) one IZ located between two neighboring channels, (2) one IZ located on one channel, and (3) two distinct IZs. Concretely, a channel was labeled as k ($k = 1, 2, \ldots, 13$) if the distance from the closest IZ was smaller than k IED but no less than $k - 1$ IED.

Statistical Analysis

The consistency between mMUNIX and conventional MUNIX was evaluated by Pearson correlation coefficient (PCC). The variability of MUNIX was evaluated by the CV of all three experiment trials. To assess the effect of channel number on MUNIX repeatability, CV of sMUNIX (single-channel MUNIX) and mMUNIX (multi-channel MUNIX) were compared. To assess the repeatability of sMUNIX with respect to the IZ, the sMUNIX values was grouped and compared based on the channel label.

RESULTS

mMUNX and sMUNIX were successfully calculated for all eight subjects. The conventional MUNIX can be represented by the sMUNIX of the channel with largest CMAP response, which is also equivalent to the mMUNIX when $N = 1$. **Table 1** summarizes the conventional MUNIX and mMUNIX results averaged across three trials and PCCs for all eight subjects. For conventional MUNIX, an average MUNIX of 103.8 $\pm$ 16.4 was obtained, ranging from 89.5 to 135.7. A very strong correlation (PCC $>$ 0.98) between the conventional MUNIX

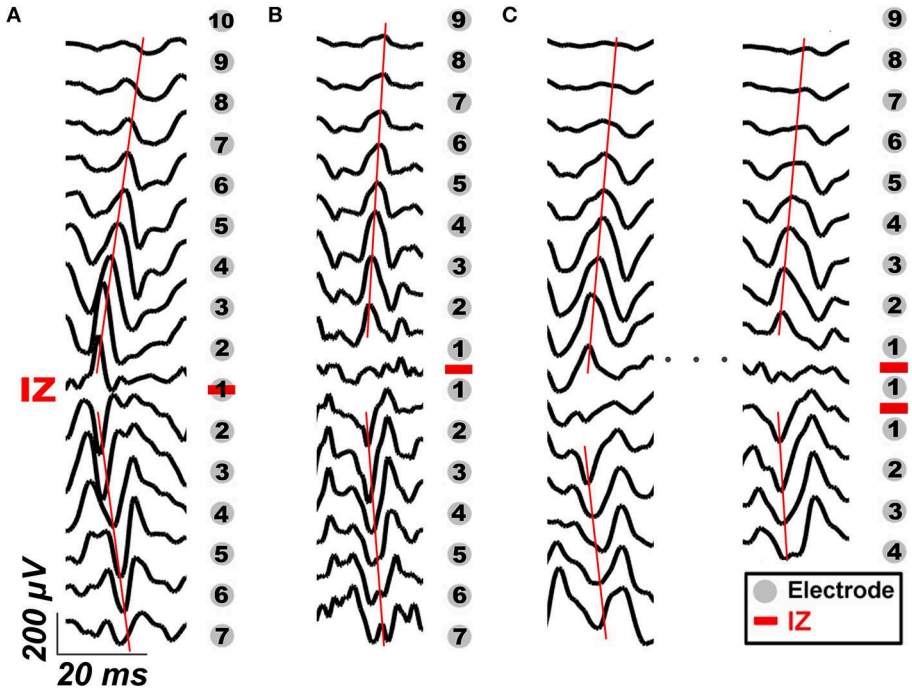

FIGURE 2 | IZ identification and examples of channel labeling based on its distance to IZ in three representative cases: **(A)** one IZ located between two neighboring bipolar channels, **(B)** one IZ located on one bipolar channel, and **(C)** two distinct IZs. The gray dots mark the location of EMG electrodes, the red bars mark the location of IZ detected. The black traces are representative bipolar signals during voluntary contraction. The red lines mark the propagation of IZ.

TABLE 1 | mMUNIX results (Mean and standard deviation) and PCCs of all subjects.

Sub #	$N = 1$	2	4	8	16	32	64	128
1	89.5 (2.5)	88.3 (2.0)	87.4 (2.0)	86.9 (2.2)	85.9 (2.0)	84.4 (2.0)	80.1 (2.3)	73.1 (2.4)
2	92.0 (2.0)	91.9 (1.9)	92.0 (1.9)	91.0 (1.9)	88.9 (2.2)	84.8 (2.0)	77.5 (1.7)	70.9 (0.9)
3	135.7 (4.5)	136.2 (4.7)	135.7 (3.9)	134.7 (4.0)	133.5 (3.3)	128.8 (3.0)	119.5 (2.6)	107.4 (2.2)
4	85.3 (3.1)	85.5 (3.0)	85.3 (2.7)	84.3 (2.3)	83.2 (2.5)	80.0 (2.3)	73.7 (2.0)	66.8 (1.6)
5	108.0 (10.1)	107.8 (9.9)	107.2 (9.7)	106.4 (9.4)	105.1 (9.4)	102.1 (9.2)	95.5 (8.8)	86.3 (7.6)
6	104.1 (2.7)	103.9 (3.2)	103.4 (3.5)	101.3 (3.4)	97.4 (2.9)	92.9 (2.4)	87.7 (2.1)	80.8 (1.8)
7	99.8 (2.6)	98.8 (2.4)	98.6 (2.1)	98.0 (1.9)	96.1 (1.5)	92.3 (1.1)	86.3 (0.8)	78.4 (1.3)
8	115.7 (4.4)	115.1 (3.6)	113.7 (3.4)	110.8 (3.4)	107.9 (3.3)	104.4 (3.5)	99.6 (3.7)	91.8 (3.6)
Mean	103.8 (16.4)	103.4 (16.6)	102.9 (16.5)	101.7 (16.2)	99.8 (16.2)	96.2 (15.7)	90.0 (14.8)	81.9 (13.1)
PCC	–	0.9995	0.9985	0.9967	0.9918	0.9893	0.9922	0.9948

Conventional MUNIX is reprensented by mMUNIX ($N = 1$).

and all mMUNIX results was observed. The mMUNIX value decreased when more channels were included for calculation.

The CVs of mMUNIX based on different channel number N were summarized in **Table 2**. Comparison between the repeatability of mMUNIX and conventional MUNIX was performed using a paired student's t-test, with p-values summarized. A significant lower CV of mMUNIX was observed. The overall CV decreased with the inclusion of more channels; yet in 3 of 8 subjects tested, the CV of mMUNIX increased when N was 64 or 128.

Figure 3 shows the sMUNIX, CMAP area and CV mapping in two representative subjects. The sMUNIX mapping tends to correlate well with the CMAP area. CV mapping suggested relatively stable sMUNIX near the IZ regions yet more variable observations away from the IZ. **Table 3** summarizes the results of CV of sMUNIX with respect to its distance to the IZ. Analysis showed higher sMUNIX CV in channels further from the IZ, yet no statistical signficant difference was observed after Benjamini-Hochberg correction. A larger CV variation was observed in sMUNIX of channels far away from the IZ.

DISCUSSION

In this study, MUNIX was evaluated in eight healthy subjects using high-density surface EMG, and results were consistent with previous studies (1, 8, 15, 30). A novel mMUNIX method

has been proposed, by including additional recording channels and taking into account spatiotemporal EMG information. Our results suggested a high consistency between mMUNIX and conventional MUNIX, whereas mMUNIX was significantly more repeatable. Furthermore, sMUNIX estimations showed a relatively stable MUNIX estimation in a wide range of recording site, albeit the repeatability decreased when moving the channel position away from IZ.

Limited effort has been made to improve the repeatability of MUNIX. Ahn et al. employed a digital instrument to improve the MUNIX reproducibility by reducing the variations in SIP signals (31). Peng et al. demonstrated that the inclusion of additional SIP epochs at lower contraction levels can significantly improve the repeatability (20). Bezerra et al. found that the averaging across multiple measurements could generate more repeatable MUNIX (32). To control for the experience-related variations and improve the automation of MUNIX calculation, in this study, the MUNIX repeatability was evaluated by taking into consideration all three previously proposed methods. This explains that the relatively low trial-to-trial CV compared to previously reported results (9, 33).

In this study, the performance of mMUNIX have been assessed by PCC and CV. The strong correlation (all >0.98) between mMUNIX and standard MUNIX, in addition to the significantly reduced variability, has evidenced the validity of proposed mMUNIX technique. The improved repeatability of mMUNIX may be attributed to the addition of more spatiotemporal EMG information from a broader muscle area, whereas conventional MUNIX is performed with only one EMG channel positioned at where the largest CMAP is obtained. Additive myoelectric information is expected to provide a more comprehensive sampling of the motor unit information and therefore benefit MUNIX repeatability. The mMUNIX can be clinically performed by searching for the *N* locations with the top *N* largest CMAP response, and calculating the weighted average of the *N* sMUNIX values. As MUNIX stands out due to its simplicity in implementation, using more channels can complicate the experiment protocol and system demands. This remains a trade-off between improving the repeatability and the inclusion of more channels. It is also interesting to note that in 3

TABLE 2 | CV of mMUNIX results with different channel number N.

Sub #	*N* = 1	2	4	8	16	32	64	128
1	3.79	3.12	2.99	3.03	3.08	3.37	3.69	3.88
2	3.62	3.45	3.16	2.76	3.01	2.88	2.69	2.35
3	2.84	2.32	2.31	2.52	2.37	2.42	2.82	3.22
4	2.41	2.22	2.14	2.12	2.52	2.37	2.23	1.20
5	9.39	9.21	9.01	8.85	8.92	8.99	9.26	8.83
6	2.60	2.44	2.13	1.89	1.54	1.21	0.97	1.68
7	4.75	4.24	3.74	3.95	3.82	3.61	3.44	3.11
8	3.12	3.18	2.98	2.92	2.54	1.87	1.46	1.30
Mean	4.06	3.77	3.56	3.50	3.48	3.33	3.32	3.20
p	N/A	0.0052	0.0004	0.0001	0.0007	0.0013	0.0106	0.0078

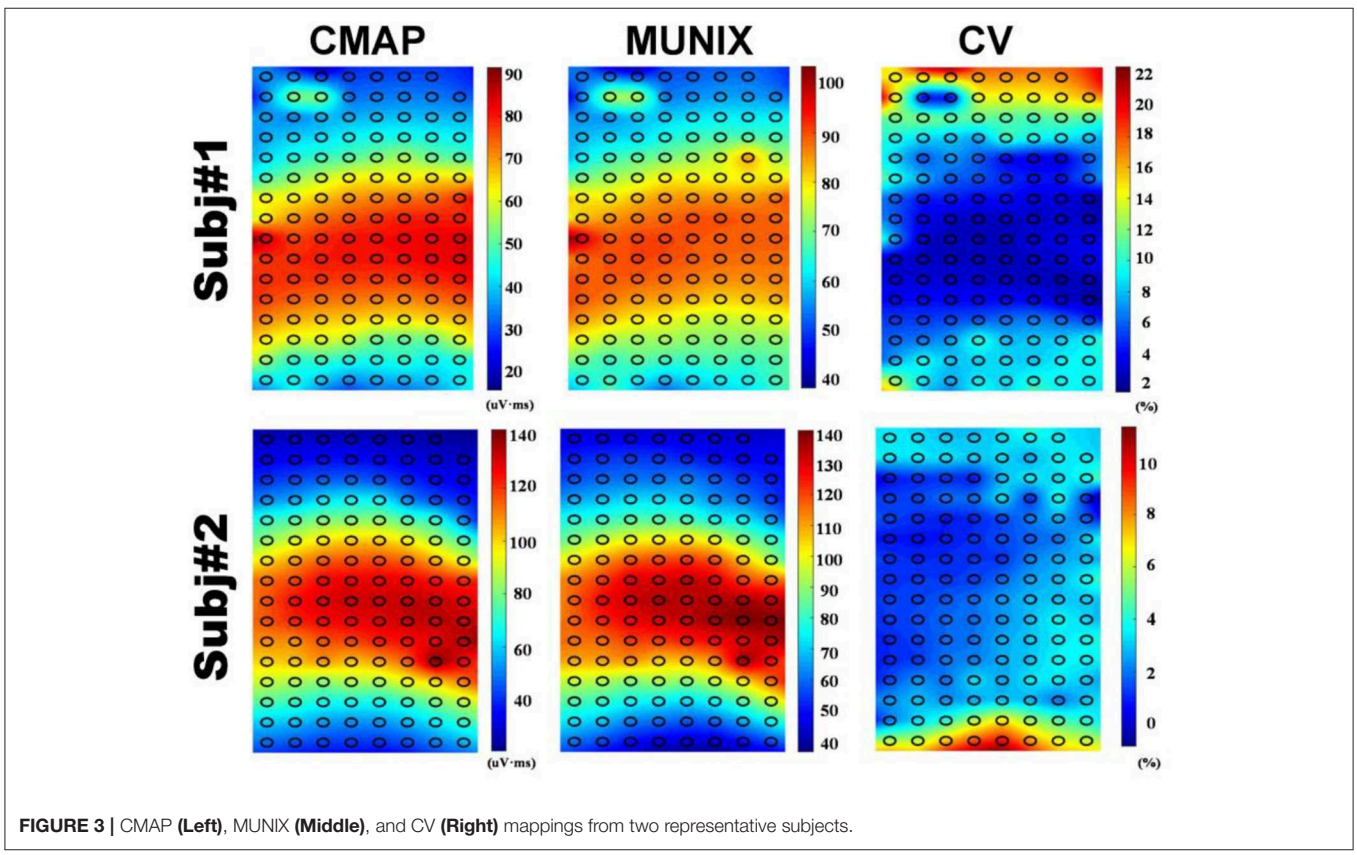

FIGURE 3 | CMAP **(Left)**, MUNIX **(Middle)**, and CV **(Right)** mappings from two representative subjects.

TABLE 3 | The CVs of mMUNIX results based on its distance from IZ.

MVC level	20%		50%		100%	
	Mean	Std	Mean	Std	Mean	Std
k = 1	3.53	2.49	3.56	2.46	3.57	2.49
2	3.59	2.74	3.57	2.78	3.6	2.69
3	4.13	3.01	4.06	3.15	4.06	3.1
4	4.7	3.14	4.57	3.31	4.65	3.3
5	5.94	3.61	5.89	3.82	5.69	3.77
6	7.1	4.31	7.57	4.85	7.35	4.57
7	8.43	5.62	8.62	5.13	8.37	5.18
8	10.26	7.37	10.37	7.04	10.44	7.08
9	9.79	8.45	9.25	7.35	9.17	7.49
10	7.78	7.52	7.75	6.82	7.86	6.76
11	9.59	8.4	11.21	8.06	10.4	8.7
12	11.32	8.04	12.96	10.19	13.54	9.37

k is the distance label.

of 8 subjects tested, the CV of mMUNIX increased when *N* was 64 or 128, i.e., a large number of EMG channels were included. This could be explained in part by the noise introduced by channels that were positioned outside the target muscle region.

Previous high-density surface EMG based MUNE methods defined the weight by the size of the single motor unit potential (SMUP) rather than the CMAP (20), as MUNE is often sensitive to the SMUP estimation (34). However, in MUNIX calculation, no direct estimation of SMUP size was provided. Therefore, assigning weight based on motor unit size is not feasible. We have found that weights determined by the CMAP and root-mean-square of SIPs were similar while CMAP often provide more stable weight estimations (Data not shown).

The repeatability of MUNIX at non-optimal locations was also evaluated. Conventional MUNIX requires the placement of recording electrode at the surface location where the maximal CMAP was observed, which correlates with the region where neuromuscular junctions, indicated by IZ, are densely distributed. As the CMAP area correlated with the MUNIX, the electrodes near IZ can often acquire larger CMAP response and consequently larger MUNIX. We have observed an increased variability of sMUNIX when moving further away from the IZ region, which may also explain the increased variations of mMUNIX when N is very large. However, the repeatability of sMUNIX is not very different unless the electrode is positioned very far from the IZ. As the sample size is relatively small, it is possible to achieve the level of significance by increasing the subject size. Our results suggest that rather than searching for the optimal site with maximal CMAP, suboptimal placement close to the IZ may also provide reasonable MUNIX estimation with similar level of repeatability, as shown in **Figure 3**. The consistency of electrode positioning can be ensured by anatomical landmarks. The similar mappings of CMAP amplitude and MUNIX estimation of these subjects suggested that MUNIX estimation relies largely on the size of the CMAP, which is consistent with previous findings (8). The mappings of CMAP amplitude and MUNIX CV have shown a very interesting negative correlation, which corresponds with our results that MUNIX variability increases with the electrode-IZ distance. However, it should be noted the study was only tested in healthy participants, whether similar observation holds under pathophysiological conditions requires further study. Moreover, the three trials in this study were performed without removal and re-attaching the electrode grids, which also in part explained the small trial-to-trial variability. The variations of mMUNIX across different visits require further studies.

A correlation between MUNIX value and with the size of CMAP area was observed (8, 35, 36). However, MUNIX can provide more information and is proved more sensitive than CMAP alone (1, 4, 36). It had to be underlined that MUNIX does not estimate the actual quantity of existent MUs, but more of an "index" that related to the number of motor neurons (30, 36). Although not carrying physiologically meaning, MUNIX provides a reliable biomarker to detect neurodegenerative diseases.

DATA AVAILABILITY STATEMENT

The datasets generated for this study are available on request to the corresponding author.

ETHICS STATEMENT

The studies involving human participants were reviewed and approved by University of Houston IRB. The patients/participants provided their written informed consent to participate in this study.

AUTHOR CONTRIBUTIONS

FG, YC, CZ, and YZ: experiment design and discussion and the final approval of the manuscript. YC and CZ: data collection. FG, YC, and CZ: data analysis. YC, CZ, and YZ: manuscript draft.

FUNDING

This work was supported in part by Zhejiang Provincial Natural Science Foundation of China (No. LY20E050011), Hangzhou Dianzi University and the University of Houston.

REFERENCES

1. Nandedkar SD, Nandedkar DS, Barkhaus PE, Stalberg EV. Motor unit number index (MUNIX). *IEEE T Bio-Med Eng.* (2004) 51:2209–11. doi: 10.1109/TBME.2004.834281

2. Neuwirth C, Nandedkar SE, Weber M. Motor unit number index (MUNIX): a novel neurophysiological technique to follow disease progression in amyotrophic lateral sclerosis. *Muscle Nerve.* (2010) 120:379–84. doi: 10.1002/mus.21707

3. Li X, Jahanmiri-Nezhad F, Rymer WZ, Zhou P. An examination of the Motor Unit Number Index (MUNIX) in muscles paralyzed by spinal cord injury. *IEEE Trans Inf Technol Biomed.* (2012) 16:1143–9. doi: 10.1109/TITB.2012.2193410
4. Philibert M, Grapperon AM, Delmont E, Attarian S. Monitoring the short-term effect of intravenous immunoglobulins in multifocal motor neuropathy using motor unit number index. *Clin Neurophysiol*. (2017) 128:235–40. doi: 10.1016/j.clinph.2016.11.012
5. Gawel M, Zalewska E, Szmidt-Salkowska E, Lipowska M, Lusakowska A, Kaminska AM, et al. Motor Unit Number Index (MUNIX) as a biomarker of motor unit loss in post-polio syndrome versus needle EMG. *J Electromyogr Kinesiol.* (2019) 46:35–40. doi: 10.1016/j.jelekin.2019.03.006
6. Li X, Wang YC, Suresh NL, Rymer WZ, Zhou P. Motor unit number reductions in paretic muscles of stroke survivors. *IEEE Trans Inf Technol Biomed*. (2011) 15:505–12. doi: 10.1109/TITB.2011.2140379
7. Günther R, Neuwirth C, Koch JC, Lingor P, Braun N, Untucht R, et al. Motor Unit Number Index (MUNIX) of hand muscles is a disease biomarker for adult spinal muscular atrophy. *Clin Neurophysiol.* (2019) 130:315–9. doi: 10.1016/j.clinph.2018.11.009
8. Neuwirth C, Nandedkar S, Stålberg E, Barkhaus PE, Carvalho Md, Furtula J, et al. Motor Unit Number Index (MUNIX): a novel neurophysiological marker for neuromuscular disorders; test-retest reliability in healthy volunteers. *Clin Neurophysiol*. (2011) 122:1867–72. doi: 10.1016/j.clinph.2011.02.017
9. Neuwirth C, Braun N, Claeys KG, Bucelli R, Fournier C, Bromberg M, et al. Implementing Motor Unit Number Index (MUNIX) in a large clinical trial: real world experience from 27 centres. *Clin Neurophysiol*. (2018) 129:1756–62. doi: 10.1016/j.clinph.2018.04.614
10. Ahn SW, Kim KW, Kim JE, Shin JY, Kim DG, Lee KW, et al. Motor unit number index (MUNIX) in the orbicularis oculi muscle of healthy subjects. *Muscle Nerve*. (2015) 51:197–200. doi: 10.1002/mus.24292
11. Neuwirth C, Burkhardt C, Weber M. Motor unit number index in the nasalis muscle in healthy subjects and patients with amyotrophic lateral sclerosis. *Muscle Nerve*. (2016) 54:733–7. doi: 10.1002/mus.25100
12. Nandedkar SD, Barkhaus PE, Stålberg EV. Reproducibility of MUNIX in patients with amyotrophic lateral sclerosis. *Muscle Nerve*. (2011) 44:919–22. doi: 10.1002/mus.22204
13. Escorcio-Bezerra ML, Abrahao A, de Castro I, Chieia MAT, de Azevedo LA, Pinheiro DS, et al. MUNIX: reproducibility and clinical correlations in amyotrophic lateral sclerosis. *Clin Neurophysiol*. (2016) 127:2979–84. doi: 10.1016/j.clinph.2016.06.011
14. Ahn SW, Kim SH, Kim JE, Kim SM, Kim SH, Park KS, et al. Reproducibility of the motor unit number index (MUNIX) in normal controls and amyotrophic lateral sclerosis patients. *Muscle Nerve*. (2010) 42:808–13. doi: 10.1002/mus.21765
15. Fathi D, Mohammadi B, Dengler R, Böselt S, Petri S, Kollewe K. Lower motor neuron involvement in ALS assessed by motor unit number index (MUNIX): long-term changes and reproducibility. *Clin Neurophysiol*. (2016) 127:1984–8. doi: 10.1016/j.clinph.2015.12.023
16. Dias N, Li X, Zhang C, Zhang Y. Innervation asymmetry of the external anal sphincter in aging characterized from high-density intra-rectal surface EMG recordings. *Neurourol Urodyn*. (2018) 37:2544–50. doi: 10.1002/nau.23809
17. Peng Y, Miller BD, Boone TB, Zhang Y. Modern theories of pelvic floor support. *Curr Urol Rep*. (2018) 19:9. doi: 10.1007/s11934-018-0752-9
18. Zhang C, Y.-Chen T, Liu Y, Zhou P, Li S, Zhang Y. *Three* dimensional innervation zone imaging in spastic muscles of stroke survivors. *J Neural Eng*. (2019) 16:034001. doi: 10.1088/1741-2552/ab0fe1
19. Zhang C, Peng Y, Liu Y, Li S, Zhou P, Rymer WZ, et al. Imaging three-dimensional innervation zone distribution in muscles from M-wave recordings. *J Neural Eng*. (2017) 14:036011. doi: 10.1088/1741-2552/aa65dd
20. Peng Y, He J, Yao B, Li S, Zhou P, Zhang Y. Motor unit number estimation based on high-density surface electromyography decomposition. *Clin Neurophysiol*. (2016) 127:3059–65. doi: 10.1016/j.clinph.2016.06.014
21. Li S, Liu J, Bhadane M, Zhou P, Rymer WZ. Activation deficit correlates with weakness in chronic stroke: evidence from evoked and voluntary EMG recordings. *Clin Neurophysiol*. (2014) 125:2413–7. doi: 10.1016/j.clinph.2014.03.019
22. Liu J, Li S, Li X, Klein C, Rymer WZ, Zhou P. Suppression of stimulus artifact contaminating electrically evoked electromyography. *NeuroRehabilitation*. (2014) 34:381–9. doi: 10.3233/NRE-131045
23. van Dijk JP, Blok JH, Lapatki BG, van Schaik IN, Zwarts MJ, Stegeman DF. Motor unit number estimation using high-density surface electromyography. *Clin Neurophysiol*. (2008) 119:33–42. doi: 10.1016/j.clinph.2007.09.133
24. Rodriguez-Falces J. A new method for the localization of the innervation zone based on monopolar surface-detected potentials. *J Electromyogr Kinesiol*. 35:47–60. doi: 10.1016/j.jelekin.2017.05.004
25. Masuda T, Miyano H, Sadoyama T. The position of innervation zones in the biceps brachii investigated by surface electromyography. *IEEE Trans Biomed Eng*. (1985) 1:36–42. doi: 10.1109/TBME.1985.325614
26. Liu Y, Ning Y, Li S, Zhou P, Rymer WZ, Zhang Y. Three-dimensional innervation zone imaging from multi-channel surface EMG recordings. *Int J Neural Syst*. (2015) 25:1550024. doi: 10.1142/S0129065715500240
27. Masuda T, Sadoyama T. Distribution of innervation zones in the human biceps brachii. *J Electromyogr Kinesiol.* (1991) 1:107–15. doi: 10.1016/1050-6411(91)90004-O
28. Zhang C, Dias N, He J, Zhou P, Li S, Zhang Y. Global innervation zone identification with high-density surface electromyography. *IEEE Trans Biomed Eng*. (2019) 67:718–25. doi: 10.1109/TBME.2019.2919906
29. Barbero M, Cescon C, Tettamanti A, Leggero V, Macmillan F, Coutts F, et al. Myofascial trigger points and innervation zone locations in upper trapezius muscles. *BMC Musculoskelet Disord*. (2013) 14:179. doi: 10.1186/1471-2474-14-179
30. Peng Y, Zhang Y. Improving the repeatability of Motor Unit Number Index (MUNIX) by introducing additional epochs at low contraction levels. *Clin Neurophysiol*. (2017) 128:1158–165. doi: 10.1016/j.clinph.2017.03.044
31. Ahn SW. Applicability of the digital instrument to improve the reproducibility of motor unit number index. *Ann Clin Neurophysiol.* (2018) 20:26–30. doi: 10.14253/acn.2018.20.1.26
32. Escorcio-Bezerra ML, Asb O, Ni DOB, Manzano GM. Improving the reproducibility of motor unit number index. *Muscle Nerve*. (2017) 55:635–8. doi: 10.1002/mus.25260
33. Higashihara M, Menon P, van den Bos M, Geevasinga N, Vucic S. Reproducibility of motor unit number index and multiple point stimulation motor unit number estimation in controls. *Muscle Nerve*. (2018) 58:660–4. doi: 10.1002/mus.26339
34. Blok JH, van Dijk JP, Drenthen J, Maathuis EM, Stegeman DF. Size does matter: the influence of motor unit potential size on statistical motor unit number estimates in healthy subjects. *Clin Neurophysiol*. (2010) 121:1772–80. doi: 10.1016/j.clinph.2010.03.048
35. Fatehi F, Grapperon MA, Fathi D, Delmont E, Attarian S. The utility of motor unit number index: a systematic review. *Neurophysiol Clin*. (2018) 48:251–9. doi: 10.1016/j.neucli.2018.09.001
36. Nandedkar SD, Barkhaus PE, Stålberg EV. Motor unit number index (MUNIX): principle, method, and findings in healthy subjects and in patients with motor neuron disease. *Muscle Nerve*. (2010) 42:798–807. doi: 10.1002/mus.21824

Conflict of Interest: The authors declare that the research was conducted in the absence of any commercial or financial relationships that could be construed as a potential conflict of interest.

frontiers in Neurology

ORIGINAL RESEARCH
published: 31 March 2020
doi: 10.3389/fneur.2020.00102

Muscular Activity Modulation During Post-operative Walking With Hybrid Assistive Limb (HAL) in a Patient With Thoracic Myelopathy Due to Ossification of Posterior Longitudinal Ligament: A Case Report

Hideki Kadone[1,2], Shigeki Kubota[3], Tetsuya Abe[3], Hiroshi Noguchi[3], Kousei Miura[3,4], Masao Koda[3], Yukiyo Shimizu[4], Yasushi Hada[4], Yoshiyuki Sankai[2], Kenji Suzuki[2] and Masashi Yamazaki[3]*

[1] Center for Innovative Medicine and Engineering, University of Tsukuba Hospital, Tsukuba, Japan, [2] Center for Cybernics Research, University of Tsukuba, Tsukuba, Japan, [3] Department of Orthopaedic Surgery, Faculty of Medicine, University of Tsukuba, Tsukuba, Japan, [4] Department of Rehabilitation Medicine, University of Tsukuba Hospital, Tsukuba, Japan

OPEN ACCESS

Edited by:
Jun Yao,
Northwestern University, United States

Reviewed by:
Antonino Naro,
Centro Neurolesi Bonino Pulejo (IRCCS), Italy
Le Li,
The First Affiliated Hospital, Sun Yat-sen University, China

***Correspondence:**
Hideki Kadone
kadone@md.tsukuba.ac.jp

Specialty section:
This article was submitted to Neurorehabilitation, a section of the journal Frontiers in Neurology

Received: 13 October 2019
Accepted: 29 January 2020
Published: 31 March 2020

Citation:
Kadone H, Kubota S, Abe T, Noguchi H, Miura K, Koda M, Shimizu Y, Hada Y, Sankai Y, Suzuki K and Yamazaki M (2020) Muscular Activity Modulation During Post-operative Walking With Hybrid Assistive Limb (HAL) in a Patient With Thoracic Myelopathy Due to Ossification of Posterior Longitudinal Ligament: A Case Report. Front. Neurol. 11:102. doi: 10.3389/fneur.2020.00102

Disorders of the central nervous system sometimes cause severe sensory motor paralysis accompanied by gait impairment. Recently, there are several reports on the effectiveness of robot-assisted gait training for patients experiencing these issues. The purpose of this case report was to assess the neuromechanical effect of a wearable robot suit HAL (Hybrid Assistive Limb) during post-operative gait training in a patient with gait impairment due to compressive myelopathy caused by ossification of the posterior longitudinal ligament (OPLL). For this purpose, we compared lower limb muscular activities while the patient was walking with and without the robot through a course of treatment sessions by (i) gait phase-dependent muscle usage analysis, (ii) muscle synergy analysis, and (iii) muscle network analysis. The results show (i) enhanced activity of the extensor muscles for weight-bearing in the initial sessions by using HAL and reduced knee extensor and increased hip extensor activations for achieving larger steps and faster gait in the later sessions; (ii) involvement of a greater number of synergies during walking with HAL than without HAL; and (iii) modulated muscle network property during walking with HAL remaining until the next HAL session. The patient's gait was improved after completing HAL sessions, acquiring close to normal joint profile with greater range of joint movement, faster walking speed, and larger step length. We discuss that the muscular activity modulation during walking with HAL suggests altered control of the muscles by the central nervous system during post-operative walking. Activity-dependent sensorimotor augmentation by HAL is discussed in the context of recovery of gait control by the central nervous system. The relationship between the altered control and the achieved gait recovery requires further investigation.

Keywords: myelopathy, gait recovery, Hybrid Assistive Limb (HAL), ossification of posterior longitudinal ligament (OPLL), muscle activity analysis, synergy analysis, muscle network analysis, exoskeleton robot

INTRODUCTION

Disorders of the central nervous system sometimes cause severe sensory motor paralysis accompanied by gait impairment. There are several recent reports on gait improvement after clinical intervention using wearable exoskeleton-type robots in patients with gait disturbance after central nervous system disorders; for example, ReWalk (1), Indego (2), Ekso (3), Lopes (4), Lokomat (5, 6), MindWalker (7), and HAL (8).

Robot suit HAL (Hybrid Assistive Limb; Cyberdyne, Tsukuba, Japan) assists motion of the bilateral hip and knee joints during walking in accordance with voluntary motion intension of the user (9). It actuates the electric motors embedded in the hips and knees of its exoskeleton in real time, amplifying bioelectric activation of the relevant muscles which are detected using surface electrodes attached on the hip and knee muscles. Previous studies using HAL for myelopathy (10–12), spinal cord injury (13–17), and post-surgery rehabilitation after total knee arthroplasty (18) reported improvement of walking ability after HAL training.

Ossification of the posterior longitudinal ligament (OPLL) is characterized by heterotopic ossification of the ligament usually at the cervical and thoracic spine (19, 20). Stenotic reduction of space for the spinal cord within the spinal canal due to the ossification induces spinal cord compression, resulting in severe myelopathy. The myelopathy is degenerative, categorized similarly to those caused by other reasons, including ossification of the ligamentum flavum, degenerative disc disease, and spondylotic myelopathy (21). Surgical treatment for spinal cord decompression is recommended when symptomatic neurological deterioration is observed, including gait disturbance, bladder disorder, and a myelopathic hand (22–24); otherwise, the risk of cervical spinal cord injury is suggested (25, 26). After decompression surgery, patients are prescribed with a rehabilitation program.

Analysis of myelopathic gait can be found for patients with cervical myelopathy due to cervical spondylosis and/or OPLL who were able to autonomously ambulate before and after decompression surgery (27). Compared with cervical myelopathy, neurological deterioration in thoracic myelopathy is rather concentrated in the lower limbs: lower limb numbness and weakness and an unsteady gait (28). Post-operative motor paralysis was observed in more than 30% of thoracic patients who underwent surgery for OPLL, more than 20% of whom underwent additional surgery to achieve recovery (29). Post-operative paralysis of thoracic OPLL patients tends to be severe, in accordance with the duration and severity of compression before surgery, even when enough decompression is obtained by surgery (30, 31). While the existing studies on gait of myelopathy patients deal with patients who could ambulate autonomously before and after surgery (27), here, we consider a case who had difficulty walking before and after surgery for thoracic OPLL.

The spinal cord has been considered to be housing the spinal locomotor network which coordinates the rhythmic limb motion during locomotion, based on evidences from non-human species and partly from humans (32, 33). For the recovery of spinal locomotor function after injury, the importance of sensory input of movement based on activity is suggested (34, 35). As well, the importance of task-specific active training is suggested to enhance plasticity of the supraspinal neural networks to adapt to the injured spinal cord in the generation of a closer to normal gait (36). Since HAL assists activity-based joint motion during locomotion and, hence, assists in providing coherent sensory input to the spinal cord through assistance of actual performance of the motion intended by the neural system, we think that HAL can provide an effective method for the recovery of gait after spinal cord disorder. Actually, gait improvement after training using HAL has been reported for patients after spinal cord injury (references cited above), among which, Shimizu et al. (17) reported reactivation in some of the paralyzed muscles of chronic spinal cord injury patients during walking with HAL. Compressive myelopathy and spinal cord injury are both spinal cord disorders leading to disturbance or impairment of gait, the difference being that the former is caused by chronic degeneration while the latter is caused by acute injury. Sensory input to the spinal cord achieved by HAL during walking is expected to be effective also for gait improvement of patients with severe thoracic myelopathy, bringing changes to the way the nervous system controls muscles during walking.

In previous studies on the application of HAL for post-operative gait rehabilitation of OPLL patients with thoracic myelopathy (10–12, 37–39), gait improvement is reported by comparing the state of the patient before starting and after finishing the entire robot-assisted intervention. However, this comparison hinders examination of the effect of the robot during the training *per se*, as well as how it differs from training without the robot. In this study, the gait and muscle activity during walking using the robot were recorded and analyzed in a patient with gait impairment due to thoracic myelopathy caused by OPLL. The purpose of this study was to examine the immediate effect of the robot on gait control and to discuss how it varies through intervention sessions. As far as we know, this is the first study showing the muscular activity changes during walking using HAL in a patient who had post-operative gait impairment after myelopathy. In this study, we analyze and compare the lower limb muscle activities during walking with and without HAL in each session of post-surgery rehabilitation. The analysis is made of three parts: gait phase-dependent amplitude analysis, muscle synergy analysis, and muscle signal network analysis.

Muscle synergy analysis is based on the idea that coordinated control of multiple muscles by the central nervous system is structured with the combination of a comparatively smaller number of basic synergy patterns (40) to simplify the control strategy by reducing the number of controlled variables (41–43). The neural basis of muscle synergies is reported as housed in the spinal cord (44) and the formation of spatiotemporal synergies by the brain (45) based on evidence from non-human species. Muscle synergy analysis is used to assess the efficacy of rehabilitation (46) as a physiological marker in patients suffering from stroke or trauma (47), an assessment tool of motor coordination in patients with cerebral palsy (48), and as a tool to evaluate recovery of bilateral control in stroke patients (49, 50).

While an altered muscle synergy of incomplete spinal cord injury patients during walking has been reported (36, 51), there are no reports so far concerning muscle synergies of myelopathy patients, as far as we searched.

Muscle network analysis (52) is a rather recently proposed method to investigate the structure of the signal network among muscles by analyzing the measured electromyography (EMG) in the frequency domain using methods of coherence analysis and complex graph analysis (52). It is based on the findings that the synchronous rhythm of neural firings coordinates the whole body signaling of the neural system, including the brain and reaching to the muscles (53, 54). Muscle network analysis and coherence analysis are utilized in several literatures to investigate the central nervous system's control of motion in a pathologic population (55, 56). This is the first study to apply muscle network analysis to gait of myelopathy patients.

CASE PRESENTATION

Patient

The case was a 64-year-old male patient (height, 165 cm; weight, 90 kg; body mass index, 33 kg/m^2) who had severely paralyzed lower limbs. The case, having had spent 10 years without subjective perception of symptoms after obtaining a diagnosis of cervical ossification of the posterior longitudinal ligament (OPLL) and lumbar spinal stenosis (LSS), was sent to a nearby hospital by emergency transportation after having difficulty standing. Frequent falls were experienced, about a month prior to this event. At the hospital, paralysis of the lower limbs was recognized by manual muscle test (MMT) as 0, 1, and 2 on the right and 2 and 3 on the left, together with sensory paralysis on the trunk and the lower limbs. The case was then transferred to our hospital for consideration of surgical treatment.

At the moment of transfer, MMT scores deteriorated on the right lower limb (**Table 1**, Before Surgery). Voluntary movement of the limb was not possible lying on a bed. The left lower limb maintained the MMT scores and showed voluntary movement slightly; however, standing was not possible. Sensory disorder included hypesthesia on the trunk and the bilateral lower limbs, and pain and dysesthesia around the trunk and bilateral groin regions. CT and MRI showed compression on the spinal cord due to cervico-thoracic OPLL ranging from C2 to L1 (**Figures 1A1,A2**). On these examinations, thoracic myelopathy due to compression by the OPLL and instability at Th6/7, Th7/8, and Th8/9 were considered as the principal causes of the pathology. Surgical treatment was performed, including C3-T1 laminoplasty and Th2-12 posterior decompression and fusion, following which gradual improvement of the lower limb motor functions was observed. Posture training was started in a seated posture 9 post-operative days (POD), in a standing posture using a tilt table 10 POD, and then using parallel bars at 28 POD. Lower limb MMT scores improved, but then stayed flat for 20 days, which led to the prescription of HAL gait training at 43 POD (**Table 1**). The patient was in our hospital for 83 days before being transferred to another hospital for continuing treatments.

TABLE 1 | Clinical assessment scores pre- and post-HAL.

		Before surgery	23 POD	PRE (43 POD)	POST (72 POD)
FIM-Motor		N/A	N/A	46	59
Barthel index		N/A	N/A	65	70
FAC		0	0	0	2
10–m walk test	Speed (m/min)	N/A	N/A	N/A	30.1
	Step length (m)	N/A	N/A	N/A	0.37
	Cadence (steps/min)	N/A	N/A	N/A	72.9
MMT (R/L)	Hip flexor	0/1	2/2	2/2	3/3
	Knee extensor	0/1	3/3	3/3	4/4
	Ankle dorsi-flexor	1/3	2/3	2/3	3/4
	Ankle plantar-flexor	0/2	3/3	3/3	3/3

POD, postoperative days; FAC, functional ambulation category; MMT (R/L), manual muscle test (right/left); N/A, not applicable.

Hybrid Assistive Limb

A double-legged HAL was used in this study. HAL has an exoskeleton structure corresponding to the pelvis, bilateral thighs, shanks, and feet of the patient, weighing 14 kg in total. Bracings, hinged plates, and shoes are used to tighten the exoskeleton structure to the user by belts. It has electric motors at the bilateral hip and knee joints of the exoskeleton to assist sagittal motions of the hip and knee joints of the user. The electric motors are actuated by amplifying the bioelectric neuromuscular activation of the relevant muscles to support voluntary joint motions. In mechanical sense, the interaction of HAL and the user is based on the force that they apply to each other through the bracings, supporting plates, and shoes. Disposable surface electrodes (Vitrode L, Nihon Kohden, Tokyo, Japan) were attached to the HAL's cables and pasted bilaterally on the surface of the hip flexor (tensor fasciae latae), hip extensor (gluteus maximus), knee extensor (vastus lateralis), and knee flexor (biceps femoris) muscles of the patient. The motor torques were generated in real time in accordance with the user's muscle activity: T_hip = G_hip_flex∗A_hip_flex-G_hip_ext∗A_hip_ext and T_knee = G_knee_flex∗A_knee_flex-G_knee_ext∗A_knee_ext are the hip and knee joint torques, where G_* are gain parameters, and A_* are the filtered activation of the muscles, respectively. The motors' force is transmitted to the user's limbs through the exoskeletal structure, the bracings, and shoes to realize intended limb motions. The gain parameters were manually adjusted for the patient's comfort during walking in each session.

HAL Sessions

Gait training using HAL (**Figure 1B**) was applied starting at 43 POD, followed by two or three sessions per week, 10 sessions in total, spanning a 28-day period. One session lasted about 1 h, including a 10-m walking test without using HAL (NoHAL), attachment of HAL, gait training using HAL (HAL), and detachment of HAL. HAL gait training included 20 min of overground walking activity at a comfortable pace on a 25-m oval course, with rest interval. All-in-One Walking Trainer (Ropox A/S, Naestved, Denmark) was used with a harness to provide weight-bearing support, in all walking (NoHAL and HAL) in all

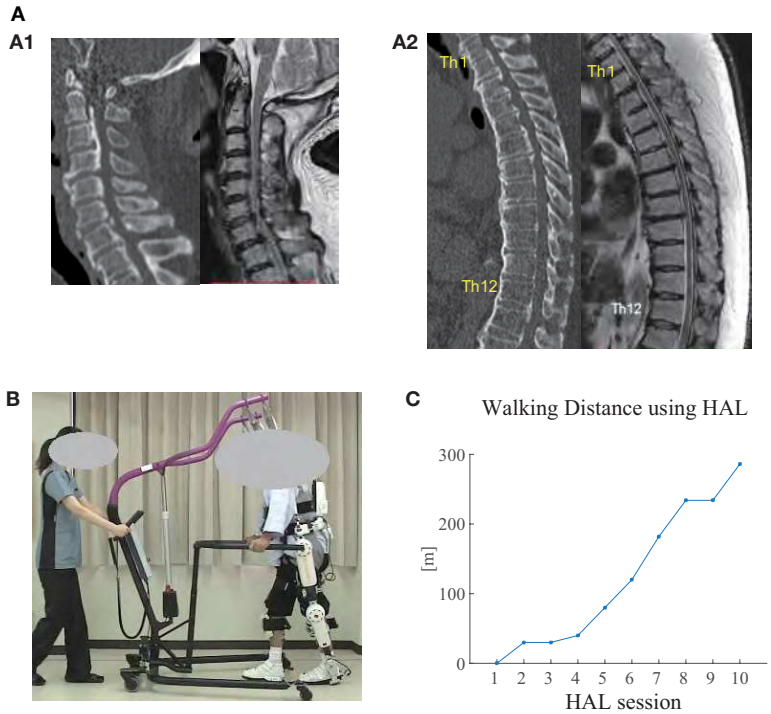

FIGURE 1 | (A) CT (left) and MRI (right) images of the cervical spine (A1) and thoracic spine (A2) before surgery. Ossification of posterior longitudinal ligament (OPLL) was observed in the cervical and thoracic spine (from *C2* to *L1*), where the spinal cord was being compressed. Diffuse idiopathic skeletal hyperostosis (DISH) was also observed from *C4* to *L2*. Herniated disc was observed at Th8/9. **(B)** The patient walking overground using Hybrid Assistive Limb (HAL) in the seventh HAL session. An All-in-One Walking Trainer device was also used to provide weight support and for safety. An assistant pulled the device in accordance with the patient's gait. **(C)** Walking distance using HAL in each session. The distance gradually increased through the sessions.

sessions. Weight support was manually adjusted in each session to provide minimum necessary weight support for the patient to keep walking in an appropriate posture. The All-in-One and HAL are completely separate and independent systems. There was no systematic interaction or shared control between them.

Measurement

Pre–post-evaluations before the first HAL session (PRE) and after the last HAL session (POST) included clinical assessment of MMT of the major lower limb muscles, Functional Independence Measure—Motor General (FIM-M), Barthel Index (BI), functional ambulation category (FAC), and the 10-m walking test. During the 10-m walk test, gait kinematics was recorded using a motion capture system (Vicon MX with 16 T20s cameras, Vicon, Oxford, UK) sampling at 100 Hz. Sixteen autoreflective markers were placed on the anatomical landmarks according to a Plug-in Gait marker set: anterior superior iliac spine, posterior superior iliac spine, lower lateral 1/3 surface of the thigh, flexion–extension axis of the knee, lower lateral 1/3 surface of shank, lateral malleolus for the ankle, posterior peak of the calcaneus for the heel, and the second metatarsal bone of the toe.

In all HAL sessions, lower limb muscle activity was recorded during walking without HAL (NoHAL) and during walking with HAL (HAL) using a wireless surface EMG measurement system (Trigno Lab, Delsys, Natick, MA, USA) sampling at 2 kHz. In both NoHAL and HAL, the patient walked with the All-in-One walking device. EMG sensors were placed bilaterally on the gluteus maximus, vastus medialis, medial hamstrings, tibialis anterior, and medial gastrocnemius muscles after cleaning the skin over the muscle bellies with alcohol swabs. Foot marker movements were recorded at the same time in synchronization with EMG using the motion capture system for the purpose of gait phase detection.

Data Processing

Marker positions of the motion capture data were converted to joint angles using the Plug-in Gait model of Vicon Nexus software (version 2.2.3). The rest of the processing was performed using custom scripts on MATLAB 8.4 R2014b (MathWorks, Natick, MA, USA). The flexion/extension angle of the hip and knee joints and the dorsi/plantar flexion angle of the ankle joint were extracted and divided into steps according to the height of the toe and heel markers. EMG data were first filtered with a band-pass filter (30–400 Hz), rectified and locally integrated using a 200-ms moving window to obtain an integrated EMG (iEMG) profile, which was then divided into steps according to the height of the toe and heel markers. The joint angle and iEMG profiles of each step were time-normalized to 101 points, with 0% representing a heel strike which initiates a cycle and 100% representing the subsequent heel strike which terminates the cycle. Data of multiple steps were averaged on the normalized

time domain to obtain an averaged joint angle and iEMG profile of an averaged step. The averaged angle profiles were used to compare gait between PRE and POST, and the averaged iEMG profiles were used to compare muscle activity between NoHAL and HAL of each session. Gait was also compared between NoHAL and HAL by the ratio of total iEMG during the stance phase of the measured muscles.

Muscle synergy analysis was also used to compare the muscle activities between HAL and NoHAL. iEMG of the measured 10 muscles was decomposed into muscle synergy patterns and temporal coefficients by the non-negative matrix factorization (NNMF) method (57) against each of the possible number of synergies ranging from 1 to 10. Supposing that there are m muscles, n data samples, and k synergies, the factorization algorithm gives a decomposition of the muscle activity matrix M $(m \times n)$ into $M = SC + E$, where S is an $m \times k$ matrix containing k muscle synergies, C is a matrix containing temporal coefficients, and E is residual. For each of the assumed number of synergies, the fitting of the synergy patterns to the original iEMG patterns was evaluated in terms of variances accounted for (VAF) to estimate the number of synergy patterns underlying in the measured EMG data (58). In equation, $VAF = 100\frac{(\sum_i \sum_j X_{ij} Y_{ij})^2}{(\sum_i \sum_j {X_{ij}}^2)(\sum_i \sum_j {Y_{ij}}^2)}$, where X_{ij} is the muscle activity and Y_{ij} is the reconstructed muscle activity of the ith muscle in the jth sample.

Muscle network analysis (52, 55) was also used to compare the muscle activities between HAL and NoHAL. Following the references, raw EMG data of each measured muscle was band-pass-filtered (20–70 Hz), resampled at 200 Hz, and rectified using Hilbert transform. The power spectral density (PSD) of each muscle was evaluated first to investigate the frequency range where the EMG signals have power. Welch's method was used here, with window length 1 s and overlap 0.75 s. Then, intermuscular coherence (IMCOH) was computed using Welch's method and the same window parameters for all pairs of the measured muscles. Coherence is commonly used to investigate coupling between neural activities (59, 60).

These data were then used to calculate the network measures clustering coefficient (CC) and global efficiency (GE) of a muscle network graph whose nodes are the measured muscles and whose arcs between the nodes are weighted by the IMCOH values. This gives a network representation of the measured muscles with their pairwise connectivity in the frequency domain. Supposing $w_{ij}(f)$ IMCOH of the ith and jth muscles after normalization in frequency domain, we calculated CC as the average of triplet multiplication of the connection weights $3w_{ij}(f)w_{jk}(f)w_{jk}(f)$, sufficing $i \neq j, \neq k, k \neq i$. GE was calculated as the average of the connection weights $w_{ij}(f)$, sufficing $i \neq j$. CC and GE were, respectively, averaged through a lower (2–22 Hz) and a higher (22–44 Hz) frequency range. CC is known to provide an indication of the extent of functional segregation of a network, while GE indicates the extent of functional integration of a network (61). We then, in order to investigate the causal relationship of CC and GE between HAL and NoHAL, CC and GE during HAL were tested against, respectively, CC and GE during NoHAL in the next session using a linear regression.

RESULTS

HAL Sessions

The patient completed 10 HAL sessions without any serious adverse events. The observed issues were redness on the skin due to attachment of the electrodes and minor scratches due to interference with belts and harnesses. All of these cutaneous issues disappeared promptly.

The patient did not manage to walk using HAL in the first session, in which stand-up training was provided in place. In the third session, gait data was not recorded because the patient reported perception of fatigue. Starting from the second session, the patient monotonically increased the walking distance using HAL (**Figure 1C**).

Pre- Post-comparison

Clinical assessments (**Table 1**) showed improvements after HAL in the FIM-M score, BI, and FAC. The 10-m walking test was not available in PRE because he could not manage to complete 10 m even with weight support. The 10-m walking test in POST was completed using the handrail of the walking device with a practical walking speed, step length, and cadence. MMT scores improved after the surgery in most of the muscles and improved after HAL in some of the muscles.

Pre–post-joint angle comparison demonstrated greater extension of the hip joint during stance and greater range of flexion motion during swing in POST than in PRE (**Figure 2**, left). In PRE, when the patient did not complete the 10-m walk, the joint angles and gait parameters were extracted from the several steps that he managed to perform. The knee joint showed greater extension during stance and greater range of flexion and extension during swing in POST than in PRE, and double knee action for shock absorption was observed in the earlier phase of stance in POST (**Figure 2**, middle). The ankle joint showed greater range of motion through the cycle, with greater planter flexion in the early phase of stance and greater dorsi-flexion at the end of stance and initial swing in POST than in PRE (**Figure 2**, right). Walking speed was faster and step length was greater in POST (**Figure 3**, left and middle). The swing-to-cycle duration ratio was comparable between PRE and POST (**Figure 3**, right).

Gait Changes in HAL Sessions

Comparing gait with HAL (HAL) and without HAL (NoHAL), the walking speed and step length were greater in HAL than NoHAL through the sessions (**Figure 4**, left and middle). The ratio of swing duration to cycle duration increased through the sessions in HAL and decreased in NoHAL; it was greater in HAL at the initial sessions and in NoHAL in the later sessions (**Figure 4**, right). Cadence was greater in NoHAL in most sessions (**Supplementary Figure 1**).

Muscular Activity Changes in HAL Sessions

Activation of the vastus medialis (VM) and gluteus maximus (GM) during stance was greater in HAL than in NoHAL in the second session (**Figures 5A,B**), but not in the fourth session

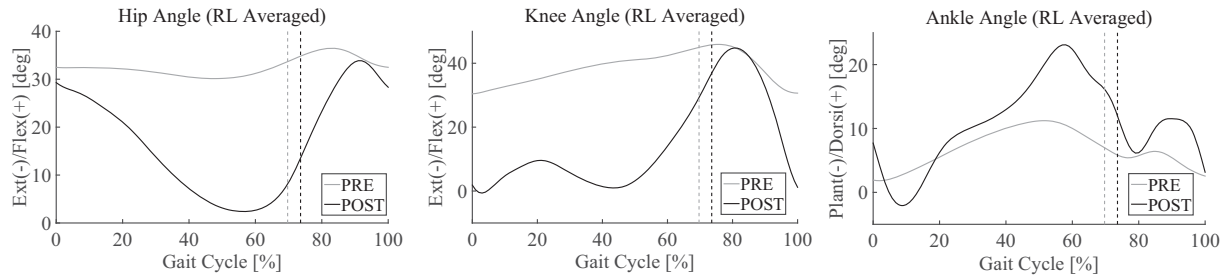

FIGURE 2 | Joint angle profiles in the sagittal plane PRE [before starting the first Hybrid Assistive Limb (HAL) session] and POST (after the last HAL session). Joint angles from the right and left sides are separated into steps and averaged. 0% corresponds to a heel contact and 100% corresponds to the subsequent heel contact on the same side. *Vertical lines* indicate the moment of toe lift.

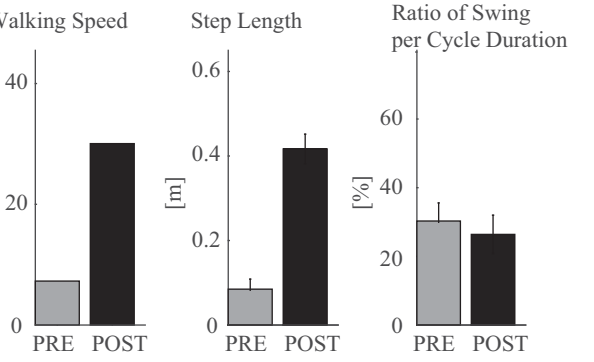

FIGURE 3 | Gait parameters during walking in PRE and POST.

(**Figure 5B**). Activation of VM was smaller and GM was greater in HAL than in NoHAL during stance in the seventh and 10th sessions (**Figures 5A,B**). The ratio of activation of VM in HAL per NoHAL during stance (**Figure 5C**, left) showed that the activation was initially increased with HAL (second session) and then decreased in the later sessions, typically in the 10th session. As for GM (**Figure 5C**, right), the activation was initially increased with HAL (second session), then slightly decreased (fourth and fifth sessions), and then increased through the later sessions.

Muscle synergy analysis showed smaller VAF in HAL than in NoHAL in each of the sessions in cases of one and two synergy patterns (**Figure 5D**, top left and right, respectively). Averaging through the sessions showed a significantly smaller VAF in HAL than in NoHAL in cases of one and two synergies ($p < 0.05$; **Figure 5D**, right bottom). Since VAF represents the percentage of reconstruction using the restricted number of synergy patterns, the smaller VAF in HAL meant involvement of a greater number of synergy patterns in HAL than in NoHAL.

Muscle network analysis showed the PSD residing mostly below 40 Hz (**Figure 6A**). IMCOH varied through the sessions for NoHAL and HAL (**Figure 6B**). CC and GE showed a statistically significant correlation in linear regression between CC during HAL and CC during NoHAL of the next session ($p = 0.0079178 < 0.01$, $R^2 = 0.785$; **Figure 6C**, top left), as well as in regression between GE during HAL and GE during NoHAL of the next session ($p = 0.0088224 < 0.01$, $R^2 = 0.776$; **Figure 6C**, top right). Conversely, no statistical significance was observed in the regression between CC during NoHAL and CC during HAL in the next session ($p = 0.68$, $R^2 = 0.039$). It was also the case for GE ($p = 0.66$, $R^2 = 0.041$; **Figure 6C**, bottom row).

DISCUSSION

In order to evaluate the effect of gait training using robot suit HAL, gait and lower limb muscle activity were recorded through HAL sessions and analyzed in a thoracic myelopathy patient who experienced a severe sensory motor paralysis and gait impairment before and after spine surgery. After the HAL sessions, the patient improved gait, with greater range of joint motion, faster walking speed, and greater step length (**Figure 3**). After transferring to another hospital, the patient was able to walk independently using a cane 2 months after HAL and achieved independent walking without a cane 11 months after HAL.

Disturbed gait of cervical myelopathy patients has been reported in the literature, characterized by a slower walking speed, shorter step length, longer step time, reduced range of joint motions (62–64), and altered timing and duration of muscle activities (65). After surgery for cervical decompression, improvement is observed in walking speed, step time, step length, and joint motions (66–68) and in knee kinetics (69). While the existing studies dealt with cervical myelopathy patients who could ambulate autonomously before and after surgery, in this study, we dealt with a thoracic myelopathy patient who had difficulty walking before and after surgery. When the patient became able to take a few steps, walking speed was slow, step length was short, and the range of joint motion was small (**Figures 2, 3**). These variables were improved after finishing the HAL training (**Figures 2**, **3**).

In the second HAL session, when the patient started to walk using the walking device, he needed a large amount of weight support and could barely move his legs. The step length was very small without HAL. The activity of the measured muscles was also minor without HAL (**Figure 5A**, top row). However, using HAL, the step length was greater (**Figure 4**, middle) and the extensor muscles (quadriceps and gluteus maximus) were

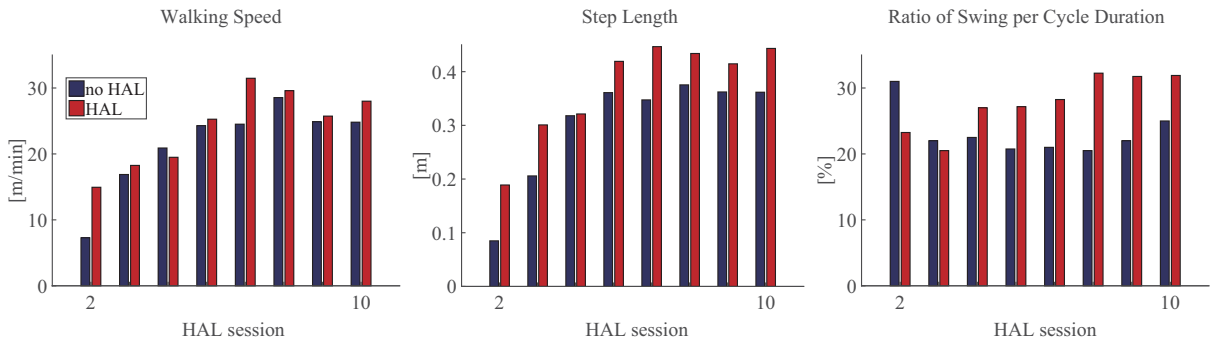

FIGURE 4 | Gait parameters during walking with HAL (*HAL*) and without HAL (*NoHAL*) in each of the Hybrid Assistive Limb (HAL) sessions.

activated more during the stance phase than without HAL (**Figure 5A**, second row and **Figure 5B**, left). The activation ratio of HAL against NoHAL of these muscles was >1 (**Figure 5C**). This is contrary to the idea that muscle activations might reduce with robotic assistance (70). We consider that it is because, due to HAL's assistance, the muscle activities were made functionally effective in the actual performance of gait generation and that it generated an activity-based sensory feedback to the neural system, possibly leading to plasticity in the sensorimotor activity of the spinal locomotor network (35) and supraspinal networks related to gait control (36). Gait parameters of walking speed, step length, and percentage of stance duration showed greater values in HAL than in NoHAL (**Figure 4**). The greater limb motions could have led to sensory signal-driven activation of the spinal cord by the proprioceptive feedback (71).

Ivanenko et al. (72) showed changes in the amplitude of EMG activation of the lower limb muscles along with increased body weight support in healthy participants, demonstrating the importance of sensory information of the plantar pressure on the sole of the foot for the generation of normal muscular activity. Coming back to our patient, the patient's weight-bearing was very weak without HAL, so the weight was mostly supported by the unweighing device. Contrarily with HAL, with the assistance of HAL which generates joint torques by amplifying the sensed muscle activity, the patient was able to better bear weight on his feet. HAL assists the patient's weight-bearing only when the patient's extensor muscles are active, and this assures consistent signaling of sensorimotor interactions in the patient's central nervous system. Passive weight support devices, for example long-leg brace (LLB), which completely locks the knee joint, can support the weight-bearing of patients with weak knee joint control. However, in this case, the patient does not need to activate the knee extensor muscles since the rigid frame of the LLB supports the weight irrespective of the muscle activity. Shimizu et al. (73) showed the effectiveness of HAL over LLB for the activation of lower limb muscles in spinal cord injury patients. The contribution of the step signal-dependent afferent information to the neural control of locomotion by the spinal cord is considered, based on observation of a loading and velocity-dependent increase of EMG activity in spinal cord injury patients with reduced supraspinal input (74).

In the following sessions, the iEMG ratios were slightly <1 in the fourth and fifth sessions (**Figure 5C**), but the gait assisted by HAL showed greater step length (fourth session; **Figure 4**, middle) or percentage of swing duration (fifth session; **Figure 4**, right), which are a necessary characteristic of larger gait, and it continued through the rest of the sessions. In the later sessions, the iEMG ratio was reduced in the quadriceps and increased in the gluteus maximus using HAL (**Figures 5A–C**). It was represented by gait, by its faster speed and greater step length and percentage of swing duration walking with HAL (**Figure 4**). The percentage of swing duration was comparative between the initial session without HAL and the later sessions with HAL. We consider that the increased activity of the hip extensor contributed to stance stability for better swing motion of a contralateral leg as well as to faster propulsion. The reduced activity of the knee extensor contributed to a smoother landing and shock absorption by double knee action. These were observed in the POST gait without HAL (**Figure 2**), having greater joint range of movement and closer to normal angular profiles, including a smooth double knee action during the initial to mid-stance phase. The activation ratio of HAL against NoHAL was closer to 1 in the later sessions in comparison to the initial session (**Figure 5C**). This is because the weight-bearing without HAL mentioned above was not an issue in the later sessions. Adjustment of muscle activity for achieving larger steps in the later sessions did not cause such a drastic change in the amplitude of muscle activity.

Muscle synergy analysis showed significantly smaller VAF in HAL when the number of synergies were restricted to one or two (**Figure 5D**, right bottom), suggesting that a greater number of basic synergy patterns was incorporated during walking with HAL. Reduced number of muscle synergies is known in locomotion of incomplete spinal cord injury patients (51) and of stroke patients (75). Lack of muscle synergies corresponding to posture control is known in spinalized cats (76). The neural implementation of muscle synergies is reported as being housed in the spinal cord (44, 77), and the brain is also considered as forming a spatiotemporal pattern of synergies (45). Considering these evidences, increased synergies during walking with HAL suggest, first, that the spinal control of gait is altered with HAL and, second, the myelopathic spinal cord of the patient is activated with HAL to deal with more degrees of control in view

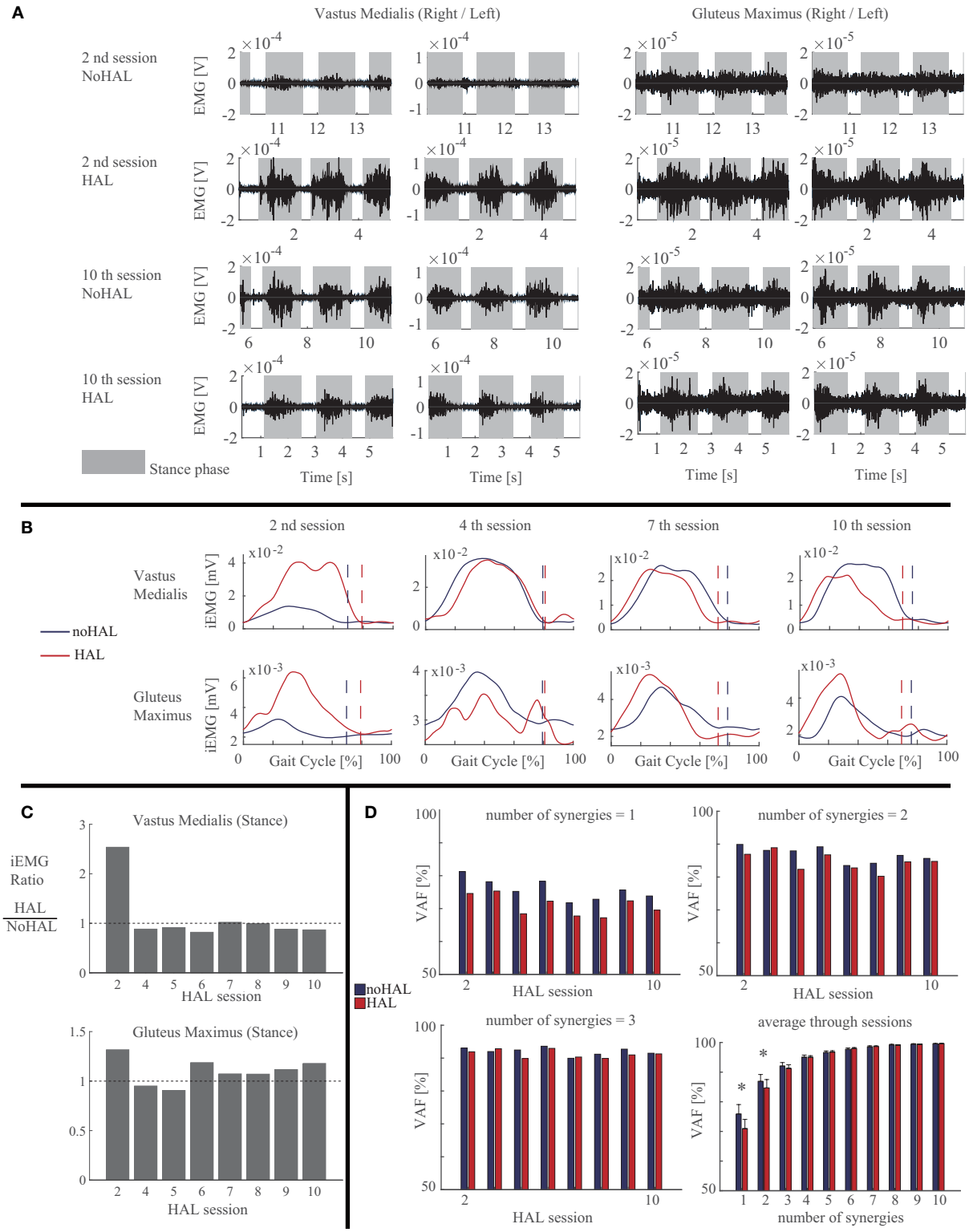

FIGURE 5 | Activity of the quadriceps and gluteus maximus muscles compared during walking with HAL (*HAL*) and without HAL (*NoHAL*), in each of the Hybrid Assistive Limb (HAL) sessions. **(A)** Band-pass-filtered EMG data of the right and left sides in the second and 10th HAL sessions. The *gray shaded areas* indicate the stance phase. **(B)** Muscle activity profile through a gait cycle, averaged from multiple steps, in the second, fourth, seventh, and 10th HAL sessions. **(C)** Ratio of muscular activities during walking with HAL with respect to without HAL in each of the HAL sessions. **(D)** Variances accounted for (*VAF*) ratios representing the ratio of the measured muscle activities that can be reconstructed using the computed muscle synergies, for the cases of the number of muscles synergies being 1 (top left), 2 (top right), and 3 (bottom left). Bottom right shows the mean VAF averaged among the sessions for each case of the number of muscle synergies varying from 1 to 10 (*$p < 0.05$, by a paired *t*-test).

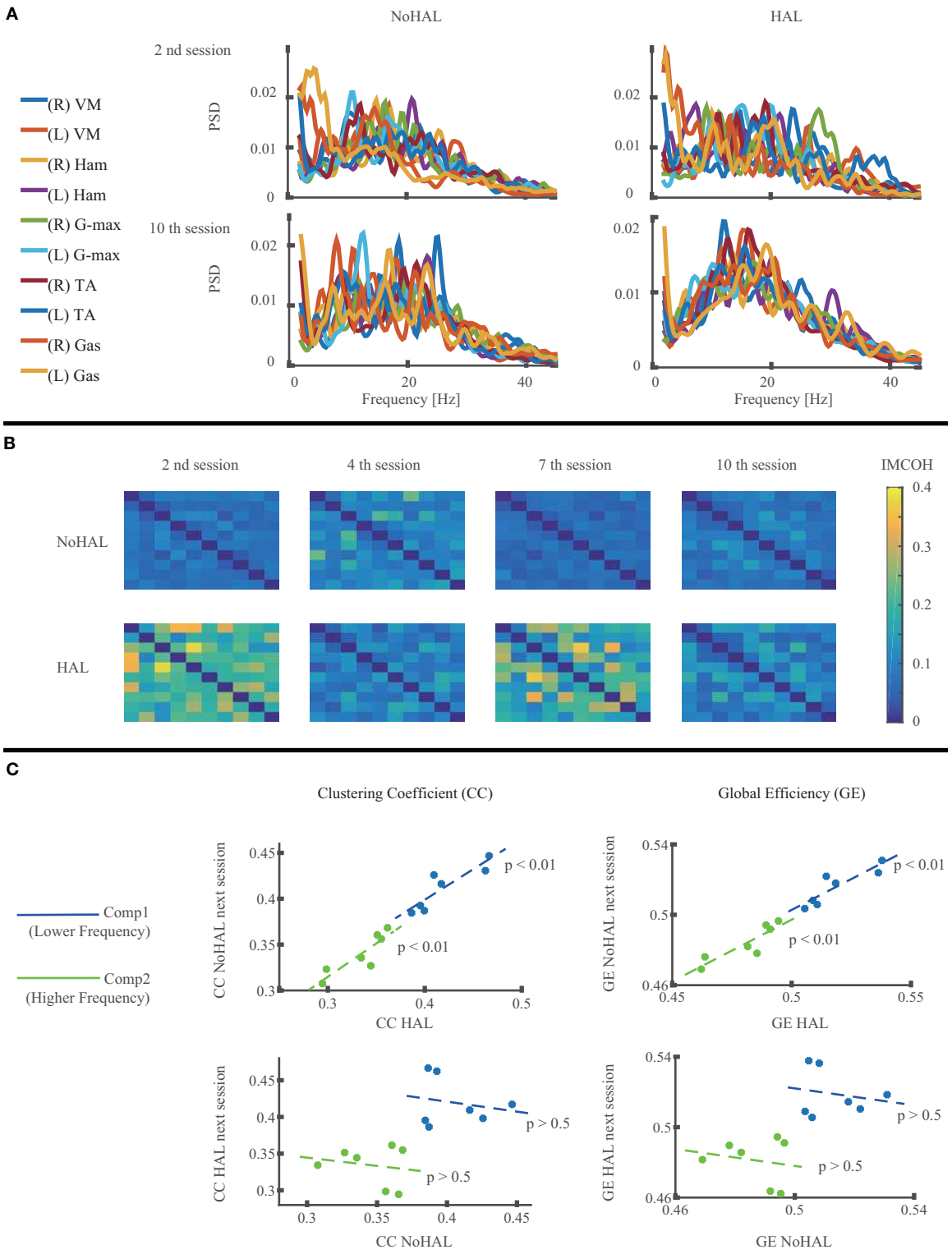

FIGURE 6 | Muscle network analysis of EMG during walking without Hybrid Assistive Limb (HAL) and with HAL in each session. **(A)** Power spectral density (PSD) of the measured muscles in the second and 10th HAL sessions. **(B)** Intermuscular coherence (IMCOH) between the measured muscles in the second, fourth, seventh, and 10th HAL sessions, averaged through frequency. The order of the muscles is the same as in the muscle list in **(A)**, from top to bottom and from left to right. Color scale is shown on the right. **(C)** Linear regression of the clustering coefficient (CC) during HAL and CC during NoHAL in the next session (top left), CC during NoHAL and CC during HAL in the next session (bottom left), global efficiency (GE) during HAL and GE during NoHAL in the next session (top right), and GE during NoHAL and GE during HAL in the next session (bottom right). The scatter plot is plotted and regressed for the averages on the lower frequency ranges (blue, 2–22 Hz) and higher frequency ranges (green, 22–44 Hz).

of the simplified synergies of neurological patients (47, 51, 75, 78), together with the adapted activity of the supraspinal networks utilizing the increased synergy of the spinal cord to control gait (36, 46).

Muscle network analysis showed a statistically significant correlation of CC and GE during HAL to those during NoHAL in the next session (**Figure 6C**, top row). But a similar analysis on the correlation of CC and GE during NoHAL and those during HAL in the next session did not show statistical significance (**Figure 6C**, bottom row). Considering that CC and GE respectively indicates the extent of functional segregation and integration of a network (61), the result suggests that the muscle network property is modulated during HAL, and the modulated gross structure is maintained until the next session. Naro et al. (55) showed that CC and GE during gait of patients with a type of muscular dystrophy are different from those of healthy people and discussed that their gait problem not only depends on the deterioration of the muscles but also on the deterioration of the signaling system of the muscle network utilized by the central nervous system. The modulation of CC and GE with HAL also suggests modulated control of muscles by the central nervous system during walking with HAL. Recent studies on the cortical control of muscle synergies discuss that beta-band frequency (13–30 Hz) and piper rhythm frequency (around 40 Hz) are used for communication between the cortical networks and the spinal cord for the purpose of formation, control, and maintenance of muscle synergies (79, 80). Our muscle network analysis used a frequency band of 22–44 Hz as the higher part of frequency band based on the PSD of each muscle. The modulation of the muscle network took place in this frequency band, suggesting a relationship between the modulation of muscle synergy and muscle network during walking with HAL, though further detailed investigation is necessary to clarify this relationship.

There are some reports on neural activity changes by HAL in recent literature: brain activity changes in the primary motor cortex of subacute stroke patients immediately after using HAL (81), cortical excitability changes in the primary somatosensory cortex of spinal cord injury patients after 3 months of training (16), muscle synergy changes in the lower limbs of stroke patients (50), segmental coordination changes in in the lower limbs of myelopathy patients after surgery for thoracic OPLL (11), and activation in some muscles of chronic spinal cord injury patients during and after HAL training (17).

Israel et al. (70) observed that, during walking with a robot which autonomously assists limb motion (hence, the legs were passively moved), activation of leg muscles was significantly reduced. They discussed that the reduction is not effective for activity-dependent plasticity of the spinal and supraspinal locomotor circuitry (34). In this study, we reported an increased muscular activity at the initial sessions and commitment of more synergy patterns during walking with HAL throughout the sessions. Instantaneous change of muscle activation and synergies by using HAL in each session suggested that the changes are in the neural control rather than musculature. Indeed, the muscle signaling network was modulated during walking with HAL and sustained until the next session, suggesting that a greater extent of plasticity may be taking part during HAL walking. It was considered that HAL's assistance based on bioelectric signals might have helped induce modulation in the control of the muscles by the central nervous system, non-invasively. Studies using invasive methods showed the importance of feeding proprioceptive sensory signal to the spinal cord for recovery of supraspinal control and locomotion (82, 83). Activity-based sensorimotor augmentation by HAL can be a non-invasive method to effectively alter central control of gait.

A limitation of the study is that, as a case report, the data are from only one subject. Generalization of the results is not reasonable, considering broad variations of gait impairment. As shown by our results, muscular activity modulation by the robot varies through the course of recovery. Future studies may include examination of muscular activity modulation in multiple subjects of various levels of gait impairment and recovery.

Another limitation of the study may be that mechanical parameters such as HAL's assistance level (gain parameters of the equations in section Hybrid Assistive Limb) were not recorded. On the other hand, from the view point of neuro-rehabilitation, neuromechanical observations from physiological data rather directly evaluate changes in neural control of gait. Advances in the analysis of muscle activity during assisted movements (84–86) may help further research in this direction.

In conclusion, the muscular activity modulation by HAL observed in a patient with gait impairment due to severe myelopathy suggested that HAL may be effective in modulating central control of gait of the patient by its activity-based sensorimotor augmentation. The relationship between the altered gait control during walking with HAL and achievement of gait improvement requires further investigation with more cases.

DATA AVAILABILITY STATEMENT

The datasets generated for this study are available on reasonable request to the corresponding author.

ETHICS STATEMENT

This study was approved by the University of Tsukuba Hospital Ethics Committee (approval number H26-22) and implemented according to the ethical principles of the Declaration of Helsinki and the University Guidelines for Clinical Trials. Before inclusion in the study, the patient received explanation of the research contents and data usage, for which written informed consent was obtained. At the time of submission of the manuscript, the patient was shown the manuscript and the images, and received explanation according to the Frontiers consent form, which meets the ICMJE guidelines. The patient gave a written agreement to a Japanese version of the Frontiers consent form (translation done by the authors).

AUTHOR CONTRIBUTIONS

HK collected, analyzed, and interpreted the data, and wrote and drafted the article. SK administered HAL treatment and collected the clinical scores. TA and HN diagnosed and operated the patient and prescribed HAL treatment. TA, KM, YSh, and MY reviewed and edited the article. KM, MK, YSh, and YH provided

important comments on the planning and implementation of HAL treatment. YSa originally developed the robot suit HAL and conceived the idea of HAL treatment. KS provided ideas on clinical gait analysis. MY organized the study. All authors made critical revisions of the manuscript and approved the final version.

FUNDING

This study was supported by the Industrial Disease Clinical Research Grant of the Ministry of Health, Labour and Welfare, Japan (14060101-01).

ACKNOWLEDGMENTS

We thank Mayuko Sakamaki and Yumiko Ito of the Center for Innovative Medicine and Engineering (CIME) of the University of Tsukuba Hospital for their excellent technical assistance.

SUPPLEMENTARY MATERIAL

The Supplementary Material for this article can be found online at: https://www.frontiersin.org/articles/10.3389/fneur.2020.00102/full#supplementary-material

REFERENCES

1. Zeilig G,Weingarden H, Zwecker M, Dudkiewicz I, Bloch A, Esquenazi A. Safety and tolerance of the rewalk^{TM} exoskeleton suit for ambulation by people with complete spinal cord injury: a pilot study. *J Spinal Cord Med*. (2012) 35:96–101. doi: 10.1179/2045772312Y.0000000003
2. Tefertiller C, Hays K, Jones J, Jayaraman A, Hartigan C, Bushnik T, et al. Initial outcomes from a multicenter study utilizing the indego powered exoskeleton in spinal cord injury. *Top Spinal Cord Inj Rehabil*. (2018) 24:78–85. doi: 10.1310/sci17-00014
3. Swank C, Sikka S, Driver S, Bennett M, Callender L. Feasibility of integrating robotic exoskeleton gait training in inpatient rehabilitation. *Disabil Rehabil Assist Technol*. (2019) 1–9. doi: 10.1080/17483107.2019.1587014
4. Veneman JF, Kruidhof R, Hekman EEG, Ekkelenkamp R, Asseldonk EHFV, van der Kooij H. Design and evaluation of the lopes exoskeleton robot for interactive gait rehabilitation. *IEEE Trans Neural Syst Rehabil Eng*. (2007) 15:379–86. doi: 10.1109/TNSRE.2007.903919
5. Jezernik S, Colombo G, Keller T, Frueh H, Morari M. Robotic orthosis lokomat: a rehabilitation and research tool. *Neuromodulation*. (2003) 6:108–15. doi: 10.1046/j.1525-1403.2003.03017.x
6. Mayr A, Kofler M, Quirbach E, Matzak H, Fröhlich K, Saltuari L. Prospective, blinded, randomized crossover study of gait rehabilitation in stroke patients using the Lokomat gait orthosis. *Neurorehabil Neural Repair*. (2007) 21:307–14. doi: 10.1177/1545968307300697
7. Wang S, Wang L, Meijneke C, van Asseldonk E, Hoellinger T, Cheron G, et al. Design and control of the MINDWALKER exoskeleton. *IEEE Trans Neural Syst Rehabil Eng*. (2015) 23:277–86. doi: 10.1109/TNSRE.2014.2365697
8. Kawamoto H, Kamibayashi K, Nakata Y, Yamawaki K, Ariyasu R, Sankai Y, et al. Pilot study of locomotion improvement using Hybrid Assistive Limb in chronic stroke patients. *BMC Neurol*. (2013) 13:141. doi: 10.1186/1471-2377-13-141
9. Sankai Y, Sakurai T. Exoskeletal cyborg-type robot. *Sci Robot*. (2018) 3:eaat3912. doi: 10.1126/scirobotics.aat3912
10. Kubota S, Abe T, Kadone H, Shimizu Y, Funayama T, Watanabe H, et al. Hybrid Assistive Limb (HAL) treatment for patients with severe thoracic myelopathy due to ossification of the posterior longitudinal ligament (OPLL) in the postoperative acute/subacute phase: a clinical trial. *J Spinal Cord Med*. (2019) 42:517–25. doi: 10.1080/10790268.2018.1525975
11. Puentes S, Kadone H, Kubota S, Abe T, Shimizu Y, Marushima A, et al. Reshaping of gait coordination by robotic intervention in myelopathy patients after surgery. *Front Neurosci*. (2018) 12:99. doi: 10.3389/fnins.2018.00099
12. Sakakima H, Ijiri K, Matsuda F, Tominaga H, Biwa T, Yone K, et al. A newly developed robot suit Hybrid Assistive Limb facilitated walking rehabilitation after spinal surgery for thoracic ossification of the posterior longitudinal ligament: a case report. *Case Rep Orthop*. (2013) 2013:621405. doi: 10.1155/2013/621405
13. Aach M, Cruciger O, Sczesny-Kaiser M, Hoffken O, Meindl R, Tegenthoff M, et al. Voluntary driven exoskeleton as a new tool for rehabilitation in chronic spinal cord injury: a pilot study. *Spine J*. (2014) 14:2847–53. doi: 10.1016/j.spinee.2014.03.042
14. Jansen O, Schildhauer T, Meindl R, Tegenthoff M, Schwenkreis P, Sczesny-Kaiser M, et al. Functional outcome of neurologic-controlled HAL-exoskeletal neurorehabilitation in chronic spinal cord injury: a pilot with one year treatment and variable treatment frequency. *Global Spine J*. (2017) 7:735–43. doi: 10.1177/2192568217713754
15. Jansen O, Grasmuecke D, Meindl R, Tegenthoff M, Schwenkreis P, Sczesny-Kaiser M, et al. Hybrid Assistive Limb exoskeleton HAL in the rehabilitation of chronic spinal cord injury: proof of concept; the results in 21 patients. *World Neurosurg*. (2018) 110:e73–8. doi: 10.1016/j.wneu.2017.10.080
16. Sczesny-Kaiser M, Höffken O, Aach M, Cruciger M, Grasmücke D, et al. HAL® exoskeleton training improves walking parameters and normalizes cortical excitability in primary somatosensory cortex in spinal cord injury patients. *J Neuroeng Rehabil*. (2015) 12:68. doi: 10.1186/s12984-015-0058-9
17. Shimizu Y, Kadone H, Kubota S, Suzuki K, Abe T, Ueno T, et al. Voluntary ambulation by upper-limb triggered HAL in patients with complete quadri/paraplegia due to chronic spinal cord injury. *Front Neurosci*. (2017) 11:649. doi: 10.3389/fnins.2017.00649
18. Yoshikawa K, Mutsuzaki H, Sano A, Koseki K, Fukaya T, Mizukami M, et al. Training with Hybrid Assistive Limb for walking function after total knee arthroplasty. *J Orthop Surg Res*. (2018) 13:163. doi: 10.1186/s13018-018-0875-1
19. Epstein N. Ossification of the cervical posterior longitudinal ligament: a review. *Neurosurg Focus*. (2002) 13:1–10. doi: 10.3171/foc.2002.13.2.16
20. Kalb S, Martirosyan NL, Perez-Orribo L, Kalani MYS, Theodore N. Analysis of demographics, risk factors, clinical presentation, and surgical treatment modalities for the ossified posterior longitudinal ligament. *Neurosurg Focus*. (2011) 30. doi: 10.3171/2010.12.FOCUS10265
21. Gibson J, Nouri A, Krueger B, Lakomkin N, Nasser R, Gimbel D, et al. Degenerative cervical myelopathy: a clinical review. *Yale J Biol Med*. (2018) 91:43–8.
22. Abiola R, Rubery P, Mesfin A. Ossification of the posterior longitudinal ligament: etiology, diagnosis, and outcomes of nonoperative and operative management. *Global Spine J*. (2016) 6:195–204. doi: 10.1055/s-0035-1556580
23. Yamazaki M, Okawa A, Fujiyoshi T, Furuya T, Koda M. Posterior decompression with instrumented fusion for thoracic myelopathy caused by ossification of the posterior longitudinal ligament. *Eur Spine J*. (2010) 19:691–8. doi: 10.1007/s00586-009-1266-4
24. Mehdi SK, Alentado VJ, Lee BS, Mroz TE, Benzel EC, Steinmetz MP. Comparison of clinical outcomes in decompression and fusion versus decompression only in patients with ossification of the posterior longitudinal ligament: a meta-analysis. *Neurosurg Focus*. (2016) 40:E9. doi: 10.3171/2016.3.FOCUS1630
25. Chen L, F, Tu T H, Chen YC, Wu JC, Chang PY, Liu L, et al. Risk of spinal cord injury in patients with cervical spondylotic myelopathy and ossification of posterior longitudinal ligament: a national cohort study. *Neurosurg Focus*. (2016) 40:E4. doi: 10.3171/2016.3.FOCUS1663
26. Wu JC, Ko CC, Yen YS, Huang WC, Chen YC, Liu L, et al. Epidemiology of cervical spondylotic myelopathy and its risk of causing spinal cord injury: a national cohort study. *Neurosurg Focus*. (2013) 35:E10. doi: 10.3171/2013.4.FOCUS13122

27. Siasios ID, Spanos SL, Kanellopoulos AK, Fotiadou A, Pollina J, Schneider D, et al. The role of gait analysis in the evaluation of patients with cervical myelopathy: a literature review study. *World Neurosurg*. (2017) 101:275–82. doi: 10.1016/j.wneu.2017.01.122
28. Takenaka S, Kaito T, Hosono N, Miwa T, Oda T, Okuda S, et al. Neurological manifestations of thoracic myelopathy. *Arch Orthop Trauma Surg*. (2014) 134:903–12. doi: 10.1007/s00402-014-2000-1
29. Imagama S, Ando K, Takeuchi K, Kato S, Murakami H, Aizawa T, et al. Perioperative complications after surgery for thoracic ossification of posterior longitudinal ligament: a nationwide multicenter prospective study. *Spine*. (2018) 43:E1389–97. doi: 10.1097/BRS.0000000000002703
30. Li Z, Ren D, Zhao Y, Hou S, Li L, Yu S, et al. Clinical characteristics and surgical outcome of thoracic myelopathy caused by ossification of the ligamentum flavum: a retrospective analysis of 85 cases. *Spinal Cord*. (2016) 54:188–96. doi: 10.1038/sc.2015.139
31. Yamazaki M, Okawa A, Mannoji C, Fujiyoshi T, Furuya T, Koda M. Postoperative paralysis following posterior decompression with instrumented fusion for thoracic myelopathy caused by ossification of the posterior longitudinal ligament. *J Clin Neurosci*. (2011) 18:294–6. doi: 10.1016/j.jocn.2010.04.030
32. Kiehn O. Decoding the organization of spinal circuits that control locomotion. *Nat Rev Neurosci*. (2016) 17:224–38. doi: 10.1038/nrn.2016.9
33. Klarner T, Zehr EP. Sherlock Holmes and the curious case of the human locomotor central pattern generator. *J Neurophysiol*. (2017) 120:53–77. doi: 10.1152/jn.00554.2017
34. Roy RR, Harkema SJ, Edgerton VR. Basic concepts of activity-based interventions for improved recovery of motor function after spinal cord injury. *Arch Phys Med Rehabil*. (2012) 93:1487–97. doi: 10.1016/j.apmr.2012.04.034
35. Rossignol S, Barrière G, Frigon A, Barthélemy D, Bouyer L, Provencher J, et al. Plasticity of locomotor sensorimotor interactions after peripheral and/or spinal lesions. *Brain Res Rev*. (2008) 57:228–40. doi: 10.1016/j.brainresrev.2007.06.019
36. Ivanenko YP, Poppele RE, Lacquaniti F. Distributed neural networks for controlling human locomotion: lessons from normal and SCI subjects. *Brain Res Bull*. (2009) 78:13–21. doi: 10.1016/j.brainresbull.2008.03.018
37. Fujii K, Abe T, Kubota S, Marushima A, Kawamoto H, Ueno T, et al. The voluntary driven exoskeleton Hybrid Assistive Limb (HAL) for postoperative training of thoracic ossification of the posterior longitudinal ligament: a case report. *J Spinal Cord Med*. (2017) 40:361–7. doi: 10.1080/10790268.2016.1142056
38. Kubota S, Abe T, Kadone H, Fujii K, Shimizu Y, Marushima A, et al. Walking ability following Hybrid Assistive Limb treatment for a patient with chronic myelopathy after surgery for cervical ossification of the posterior longitudinal ligament. *J Spinal Cord Med*. (2019) 42:128–36. doi: 10.1080/10790268.2017.1313932
39. Taketomi M, Shimizu Y, Kadone H, Kubota S, Abe T, Marushima A, et al. Hybrid Assistive Limb intervention in a patient with late neurological deterioration after thoracic myelopathy surgery due to ossification of the ligamentum flavum. *Case Rep Orthop*. (2018) 2018:6171760. doi: 10.1155/2018/6171760
40. Tresch MC, Jarc A. The case for and against muscle synergies. *Curr Opin Neurobiol*. (2009) 19:601–7. doi: 10.1016/j.conb.2009.09.002
41. Berniker M, Jarc A, Bizzi E, Tresch MC. Simplified and effective motor control based on muscle synergies to exploit musculoskeletal dynamics. *Proc Natl Acad Sci USA*. (2009) 106:7601–6. doi: 10.1073/pnas.0901512106
42. d'Avella A, Bizzi E. Shared and specific muscle synergies in natural motor behaviors. *Proc Natl Acad Sci USA*. (2005) 102:3076–81. doi: 10.1073/pnas.0500199102
43. Ivanenko YP, Poppele RE, Lacquaniti F. Five basic muscle activation patterns account for muscle activity during human locomotion. *J Physiol*. (2004) 556:267–82. doi: 10.1113/jphysiol.2003.057174
44. Takei T, Confais J, Tomatsu S, Oya T, Seki K. Neural basis for hand muscle synergies in the primate spinal cord. *Proc Natl Acad Sci USA*. (2017) 114:8643–8. doi: 10.1073/pnas.1704328114
45. Overduin SA, d'Avella A, Roh J, Carmena JM, Bizzi E. Representation of muscle synergies in the primate brain. *J Neurosci*. (2015) 35:12615–24. doi: 10.1523/JNEUROSCI.4302-14.2015
46. Ting LH, Chiel HJ, Trumbower RD, Allen JL, McKay JL, Hackney ME, et al. Neuromechanical principles underlying movement modularity and their implications for rehabilitation. *Neuron*. (2015) 86:38–54. doi: 10.1016/j.neuron.2015.02.042
47. Cheung VCK, Turolla A, Agostini M, Silvoni S, Bennis C, Kasi P, et al. Muscle synergy patterns as physiological markers of motor cortical damage. *Proc Natl Acad Sci USA*. (2012) 109:14652–6. doi: 10.1073/pnas.1212056109
48. Tang L, Chen X, Cao S, Wu G, Zhang X. Assessment of upper limb motor dysfunction for children with cerebral palsy based on muscle synergy analysis. *Front Hum Neurosci*. (2017) 11:130. doi: 10.3389/fnhum.2017.00130
49. Tropea P, Monaco V, Coscia M, Posteraro F, Micera S. Effects of early and intensive neuro-rehabilitative treatment on muscle synergies in acute post-stroke patients: a pilot study. *J Neuroeng Rehabil*. (2013) 10:103. doi: 10.1186/1743-0003-10-103
50. Tan CK, Kadone H, Watanabe H, Marushima A, Yamazaki M, Sankai Y, et al. Lateral symmetry of synergies in lower limb muscles of acute post-stroke patients after robotic intervention. *Front Neurosci*. (2018) 12:276. doi: 10.3389/fnins.2018.00276
51. Hayes HB, Chvatal SA, French MA, Ting LH, Trumbower RD. Neuromuscular constraints on muscle coordination during overground walking in persons with chronic incomplete spinal cord injury. *Clin Neurophysiol*. (2014) 125:2024–35. doi: 10.1016/j.clinph.2014.02.001
52. Boonstra TW, Danna-Dos-Santos A, Xie HB, Roerkink M, Stins JF, Breakspear M. Muscle networks: connectivity analysis of EMG activity during postural control. *Sci Rep*. (2015) 5:17830. doi: 10.1038/srep17830
53. Conway BA, Halliday DM, Farmer SF, Shahani U, Maas P, Weir AI, et al. Synchronization between motor cortex and spinal motoneuronal pool during the performance of a maintained motor task in man. *J Physiol*. (1995) 489:917–924. doi: 10.1113/jphysiol.1995.sp021104
54. Baker S. Oscillatory interactions between sensorimotor cortex and the periphery. *Curr Opin Neurobiol*. (2007) 17:649–55. doi: 10.1016/j.conb.2008.01.007
55. Naro A, Portaro S, Milardi D, Billeri L, Leo A, Militi D, et al. Paving the way for a better understanding of the pathophysiology of gait impairment in myotonic dystrophy: a pilot study focusing on muscle networks. *J Neuroeng Rehabil*. (2019) 16:116. doi: 10.1186/s12984-019-0590-0
56. Kitatani R, Koganemaru S, Maeda A, Mikami Y, Matsuhashi M, Mima T, et al. Gait-synchronized oscillatory brain stimulation modulates common neural drives to ankle muscles in patients after stroke: a pilot study. *Neurosci. Res*. (2019). doi: 10.1016/j.neures.2019.11.001. [Epub ahead of print].
57. Tresch MC, Cheung VCK, d'Avella A. Matrix factorization algorithms for the identification of muscle synergies: evaluation on simulated and experimental data sets. *J Neurophysiol*. (2006) 95:2199–2212. doi: 10.1152/jn.00222.2005
58. Torres-Oviedo G, Ting LH. Muscle synergies characterizing human postural responses. *J Neurophysiol*. (2007) 98:2144–56. doi: 10.1152/jn.01360.2006
59. Kerkman JN, Daffertshofer A, Gollo LL, Breakspear M, et al. Network structure of the human musculoskeletal system shapes neural interactions on multiple time scales. *Sci Adv*. (2018) 4:eaat0497. doi: 10.1126/sciadv.aat0497
60. Sporns O, Chialvo DR, Kaiser M, Hilgetag CC. Organization, development and function of complex brain networks. *Trends. Cogn. Sci*. (2004) 8:418–25. doi: 10.1016/j.tics.2004.07.008
61. Rubinov M, Sporns O. Complex network measures of brain connectivity: uses and interpretations. *Neuroimage*. (2010) 52:1059–69. doi: 10.1016/j.neuroimage.2009.10.003
62. Haddas R, Patel S, Arakal R, Boah A, Belanger T, Ju K, et al. Spine and lower extremity kinematics during gait in patients with cervical spondylotic myelopathy. *Spine J*. (2018) 18:1645–52. doi: 10.1016/j.spinee.2018.04.006
63. Kim CR, Yoo JY, Lee SH, Lee DH, Rhim SC. Gait analysis for evaluating the relationship between increased signal intensity on T2-weighted magnetic resonance imaging and gait function in cervical spondylotic myelopathy. *Arch Phys Med Rehabil*. (2010) 91:1587–92. doi: 10.1016/j.apmr.2010.07.008
64. Malone A, Meldrum D, Bolger C. Gait impairment in cervical spondylotic myelopathy: comparison with age- and gender-matched healthy controls. *Eur Spine J*. (2012) 21:2456–66. doi: 10.1007/s00586-012-2433-6
65. Malone A, Meldrum D, Gleeson J, Bolger C. Electromyographic characteristics of gait impairment in cervical spondylotic myelopathy. *Eur Spine J*. (2013) 22:2538–44. doi: 10.1007/s00586-013-2928-9

66. Haddas R, Lieberman I, Arakal R, Boah A, Belanger T, Ju K. Effect of cervical decompression surgery on gait in adult cervical spondylotic myelopathy patients. *Clin Spine Surg*. (2018) 31:435–40. doi: 10.1097/BSD.0000000000000719
67. Kuhtz-Buschbeck JP, Jöhnk K, Mäder S, Stolze H, Mehdorn M. Analysis of gait in cervical myelopathy. *Gait Posture*. (1999) 9:184–9. doi: 10.1016/S0966-6362(99)00015-6
68. Maezawa Y, Uchida K, Baba H. Gait analysis of spastic walking in patients with cervical compressive myelopathy. *J Orthop Sci*. (2001) 6:378–84. doi: 10.1007/s007760170002
69. Malone A, Meldrum D, Bolger C. Three-dimensional gait analysis outcomes at 1 year following decompressive surgery for cervical spondylotic myelopathy. *Eur Spine J*. (2015) 24:48–56. doi: 10.1007/s00586-014-3267-1
70. Israel JF, Campbell DD, Kahn JH, Hornby TG. Metabolic costs and muscle activity patterns during robotic- and therapist-assisted treadmill walking in individuals with incomplete spinal cord injury. *Phys Ther*. (2006) 86:1466–78. doi: 10.2522/ptj.20050266
71. Takeoka A, Arber S. Functional local proprioceptive feedback circuits initiate and maintain locomotor recovery after spinal cord injury. *Cell Rep*. (2019) 27:71–85.e3. doi: 10.1016/j.celrep.2019.03.010
72. Ivanenko YP, Grasso R, Macellari V, Lacquaniti F. Control of foot trajectory in human locomotion: role of ground contact forces in simulated reduced gravity. *J Neurophysiol*. (2002) 87:3070–89. doi: 10.1152/jn.2002.87.6.3070
73. Shimizu Y, Nakai K, Kadone H, Yamauchi S, Kubota S, Ueno T, et al. The Hybrid Assistive Limb® intervention for a postoperative patient with spinal dural arteriovenous fistula and chronic spinal cord injury: a case study. *J Spinal Cord Med*. (2018) 41:710–17. doi: 10.1080/10790268.2017.1329916
74. Beres-Jones JA, Harkema SJ. The human spinal cord interprets velocity-dependent afferent input during stepping. *Brain*. (2004) 127:2232–46. doi: 10.1093/brain/awh252
75. Clark DJ, Ting LH, Zajac FE, Neptune RR, Kautz SA. Merging of healthy motor modules predicts reduced locomotor performance and muscle coordination complexity post-stroke. *J Neurophysiol*. (2010) 103:844–57. doi: 10.1152/jn.00825.2009
76. Chvatal SA, Macpherson JM, Torres-Oviedo G, Ting L. Absence of postural muscle synergies for balance after spinal cord transection. *J Neurophysiol*. (2013) 110:1301–10. doi: 10.1152/jn.00038.2013
77. Desrochers E, Harnie J, Doelman A, Hurteau MF, Frigon A. Spinal control of muscle synergies for adult mammalian locomotion. *J Physiol*. (2019) 597:333–50. doi: 10.1113/JP277018
78. Giszter SF, Hart CB. Motor primitives and synergies in the spinal cord and after injury–the current state of play. *Ann N Y Acad Sci*. (2013) 1279:114–26. doi: 10.1111/nyas.12065
79. Aumann TD, Prut Y. Do sensorimotor β-oscillations maintain muscle synergy representations in primary motor cortex? *Trends Neurosci*. (2015) 38:77–85. doi: 10.1016/j.tins.2014.12.002
80. Zandvoort CS, van Dieën JH, Dominici N, Daffertshofer A. The human sensorimotor cortex fosters muscle synergies through cortico-synergy coherence. *Neuroimage*. (2019) 199:30–7. doi: 10.1016/j.neuroimage.2019.05.041
81. Saita K, Morishita T, Arima H, Hyakutake K, Ogata T, Yagi K, et al. Biofeedback effect of Hybrid Assistive Limb in stroke rehabilitation: a proof of concept study using functional near infrared spectroscopy. *PLoS ONE*. (2018) 13:e0191361. doi: 10.1371/journal.pone.0191361
82. Courtine G, Song B, Roy RR, Zhong H, Herrmann J, et al. Recovery of supraspinal control of stepping via indirect propriospinal relay connections after spinal cord injury. *Nat Med*. (2008) 14:69–74. doi: 10.1038/nm1682
83. Formento E, Minassian K, Wagner F, Mignardot JB, Le Goff-Mignardot C, et al. Electrical spinal cord stimulation must preserve proprioception to enable locomotion in humans with spinal cord injury. *Nat Neurosci*. (2018) 21:1728–41. doi: 10.1038/s41593-018-0262-6
84. Jacobs DA, Koller JR, Steele KM, Ferris DP. Motor modules during adaptation to walking in a powered ankle exoskeleton. *J. NeuroEng. Rehabil*. (2018) 15:2. doi: 10.1186/s12984-017-0343-x
85. Sylos-Labini F, La Scaleia F, d'Avella A, Pisotta I, Tamburella F, Scivoletto G, et al. EMG patterns during assisted walking in the exoskeleton. *Front Hum Neurosci*. (2014) 8:423. doi: 10.3389/fnhum.2014.00423
86. Tan CK, Kadone H, Miura K, Abe T, Koda M, Yamazaki M, et al. Muscle synergies during repetitive stoop lifting with a biologically-controlled lumbar support exoskeleton. *Front Hum Neurosci*. (2019) 13:142. doi: 10.3389/fnhum.2019.00142

Conflict of Interest: YSa is the C.E.O., shareholder, and director of CYBERDYNE Inc., which produces the robot suit HAL. CYBERDYNE was not involved in the study design, data collection, analysis, writing, or submission of this article.

The remaining authors declare that the research was conducted in the absence of any commercial or financial relationships that could be construed as a potential conflict of interest.

frontiers in Neurology

ORIGINAL RESEARCH
published: 03 April 2020
doi: 10.3389/fneur.2020.00204

Parkinson's Disease Exhibits Amplified Intermuscular Coherence During Dynamic Voluntary Action

Christopher M. Laine[1] *and Francisco J. Valero-Cuevas*[1,2]*

[1] *Division of Biokinesiology and Physical Therapy, University of Southern California, Los Angeles, CA, United States,*
[2] *Department of Biomedical Engineering, University of Southern California, Los Angeles, CA, United States*

Parkinson's disease (PD) is typically diagnosed and evaluated on the basis of overt motor dysfunction, however, subtle changes in the frequency spectrum of neural drive to muscles have been reported as well. During dynamic actions, coactive muscles of healthy adults often share a common source of 6–15 Hz (alpha-band) neural drive, creating synchronous alpha-band activity in their EMG signals. Individuals with PD commonly exhibit kinetic action tremor at similar frequencies, but the potential relationship between the intermuscular alpha-band neural drive seen in healthy adults and the action tremor associated with PD is not well-understood. A close relationship is most tenable during voluntary dynamic tasks where alpha-band neural drive is strongest in healthy adults, and where neural circuits affected by PD are most engaged. In this study, we characterized the frequency spectrum of EMG synchronization (intermuscular coherence) in 16 participants with PD and 15 age-matched controls during two dynamic motor tasks: (1) rotation of a dial between the thumb and index finger, and (2) dynamic scaling of isometric precision pinch force. These tasks produce different profiles of coherence between the first dorsal interosseous and abductor pollicis brevis muscles. We sought to determine if alpha-band intermuscular coherence would be amplified in participants with PD relative to controls, if such differences would be task-specific, and if they would correlate with symptom severity. We found that relative to controls, the PD group displayed amplified, but similarly task-dependent, coherence in the alpha-band. The magnitude of coherence during the rotation task correlated with overall symptom severity as per the UPDRS rating scale. Finally, we explored the potential for our coherence measures, with no additional information, to discriminate individuals with PD from controls. The area under the Receiver Operating Characteristic curve (AUC) indicated a clear separation between groups (AUC = 0.96), even though participants with PD were on their typical medication and displayed only mild-moderate symptoms. We conclude that a task-dependent, intermuscular neural drive within the alpha-band is amplified in PD. Its quantification via intermuscular coherence analysis may provide a useful tool for detecting the presence of PD, or assessing its progression.

Keywords: coherence, EMG, biomarker, manual tasks, alpha-band, kinetic tremor, action tremor

OPEN ACCESS

Edited by:
Francesco Negro, University of Brescia, Italy

Reviewed by:
Tjeerd W. Boonstra, Maastricht University, Netherlands
Jakob Dideriksen, Aalborg University, Denmark
Juan Álvaro Gallego, Northwestern University, United States

***Correspondence:**
Francisco J. Valero-Cuevas
valero@usc.edu

Specialty section:
This article was submitted to Neuromuscular Diseases, a section of the journal Frontiers in Neurology

Received: *05 September 2019*
Accepted: *09 March 2020*
Published: *03 April 2020*

Citation:
Laine CM and Valero-Cuevas FJ (2020) Parkinson's Disease Exhibits Amplified Intermuscular Coherence During Dynamic Voluntary Action. Front. Neurol. 11:204. doi: 10.3389/fneur.2020.00204

INTRODUCTION

The evaluation of Parkinson's disease (PD) is currently dominated by subjective clinical ratings of symptom severity, such as the Unified Parkinson's Disease Rating Scale (UPDRS). The coarse nature of this examination, along with the diversity of possible symptoms, has driven a search for more direct, quantitative measures of neural dysfunction which can objectively assess the early presence and progression of the disease.

The frequency spectrum of neural activity within the motor system is altered in PD. Neural oscillations are ubiquitous in the healthy motor system, but PD is characterized by a particularly large variety of abnormal oscillations. Tremor at rest (rest tremor) typically has a frequency of ∼3–6 Hz, while "action tremor" extends from ∼6–15 Hz and occurs during voluntary static (postural action tremor) or dynamic (kinetic action tremor) muscle activation (1–6). Further, PD is associated with increased corticomuscular drive in the range of 15–30 Hz during static contractions (7–11), as well as reduced neural drive to muscles in the 30–50 Hz range in unmedicated patients (12).

During motor behavior, coactive muscles often share a portion of their neural drive which synchronizes their activities at different frequencies. This entrainment of muscle activity by a common source of oscillatory neural drive can be quantified in the frequency domain by calculating the coherence between their EMG signals (13–20). Intermuscular coherence associated with postural action tremor (21) or rest tremor (22) in PD suggests that the distribution of tremulous neural drive across muscles could be an important feature of the disease, and one which cannot be assessed reliably within the context of typical clinical evaluations. Clinical evaluations, and indeed most scientific studies, have focused on the visible/overt forms of tremor, but it has been known for decades that in PD, dynamic voluntary activity consistently evokes kinetic action tremor in the alpha-band (∼6–15 Hz) which simultaneously affects multiple muscles and is observable in EMG even when no visible tremor is apparent (1).

In fact, this kinetic action tremor is the strongest and most consistently-evoked form of non-overt tremor in PD (1, 4, 23–25), and can be found in most individuals with PD. While kinetic action tremor is often described as an amplification of the ∼6–15 Hz physiological tremor seen in healthy adults due to its similarity in frequency and the fact that this frequency doesn't change with loading (4, 26), its underlying neurophysiology in PD is not well-understood, especially since ∼6–15 Hz neural drive to muscles can come from a variety of different sources (27–36). Also, compared with other manifestations of PD, kinetic action tremor has received relatively little attention.

Most previous studies of action tremor in PD have focused on forces, motions, or individual muscles rather than the coherence of tremor-generating drive across muscles. If the relevant descending drive is fundamentally intermuscular, then action tremor should not only depend on action, but also on the dynamic coordination among muscles required by a given task, as this is known to influence the strength of ∼6–15 Hz intermuscular neural drive (16, 19, 32, 37, 38). While elevated intermuscular coherence between anatomically-synergistic muscles has been found during static voluntary tasks in PD (7, 11), these findings may not extend to dynamic actions, or to functionally-different muscles whose coordination can change depending on task.

The aim of this study was therefore to characterize intermuscular coherence during voluntary dynamic tasks in participants with PD, compared to age-matched controls. Specifically, we tested two tasks: (1) rotation of a dial between the thumb and index finger, and (2) dynamic scaling of isometric precision pinch force. These tasks were chosen because they evoke different levels of coherence (especially between 6 and 15 Hz) between the first dorsal interosseous (FDI) and abductor pollicis brevis (APB) muscles (19), and because dynamic multifinger manipulation with the fingertips evokes strong functional coupling among the fingers (39).

Our primary hypotheses were that (1) intermuscular coherence would be larger in PD, especially at ∼10 Hz during both dynamic tasks, (2) the task-dependent modulation of intermuscular coherence seen in controls would be preserved in PD, and (3) the amplification of alpha-band coherence would correlate with clinical severity, since dynamic tasks should preferentially utilize neural pathways known to deliver alpha-band drive to muscles, and which are known to be disrupted in PD, such as the cerebello-thalamo-cortical circuit (30, 40–42). Given that intermuscular coherence analysis has been suggested as a potential avenue for biomarker development (11), and that we lack simple, cost-effective methods for detecting the presence of PD and the severity of neural damage, a secondary aim was to determine the ability of coherence measures to discriminate between PD and control groups, as this would justify future efforts to develop clinically-applicable metrics using EMG.

METHODS

Participants

We recruited 16 individuals with mild-moderate severity Parkinson's disease (age: 62.3 +/− 8.6, 8 male) and 15 control participants (age: 60.5 +/− 10.3, 9 male). The details of the patient population are shown in **Table 1**. All participants with PD were on their normal medication, and in the ON state at the time of testing. All were diagnosed with idiopathic Parkinson's disease, and all but one were on dopaminergic medication. All participants understood the task and scored >23 on the mini mental status exam. Our sample size is intended to be sufficient for detection of large differences and correlations, and is in line with similar recent literature [e.g., Flood et al., (11)] where such effects were found.

All participants gave written informed consent prior to participation and all procedures were approved by the University of Southern California Institutional Review Board.

Experimental Setup

We asked participants to pinch or rotate a custom-made dial (diameter: 3 cm) between the thumb and index finger, as described in Laine and Valero-Cuevas (19) (see **Figure 1**). Both tasks generate a physiological tremor in the muscles of the

TABLE 1 | Patient characteristics.

Patients	TSD	H&Y	UPDRS_total	UPDRS_II	UPDRS_III	LEDD
1	2	2	29	4	14	764
2	5.5	2	31	6	8	200
3	8	2	31	10	13	216
4	6	2	47	9	29	400
5	2.5	2	23	5	4	400
6	2	2	25	10	7	150
7	2.5	2	13	4	5	840
8	2	2	23	1	22	300
9	3.5	2	51	11	12	300
10	4	2	23	11	8	400
11	6	2	51	17	24	400
12	7	2	42	9	17	0
13	1.5	1	15	0	6	512.5
14	0.5	2	10	1	8	1305
15	1	2	52	15	22	287.5
16	1	2	25	7	10	100

TSD, Time Since Diagnosis (years); H&Y, Hoehn and Yahr; UPDRS_total, combined score on Unified Parkinson's Disease Rating Scale (UPDRS); UPDRS_II, Activities of daily living; UPDRS_III, Motor evaluation; LEDD, Levodopa Equivalent Daily Dose.

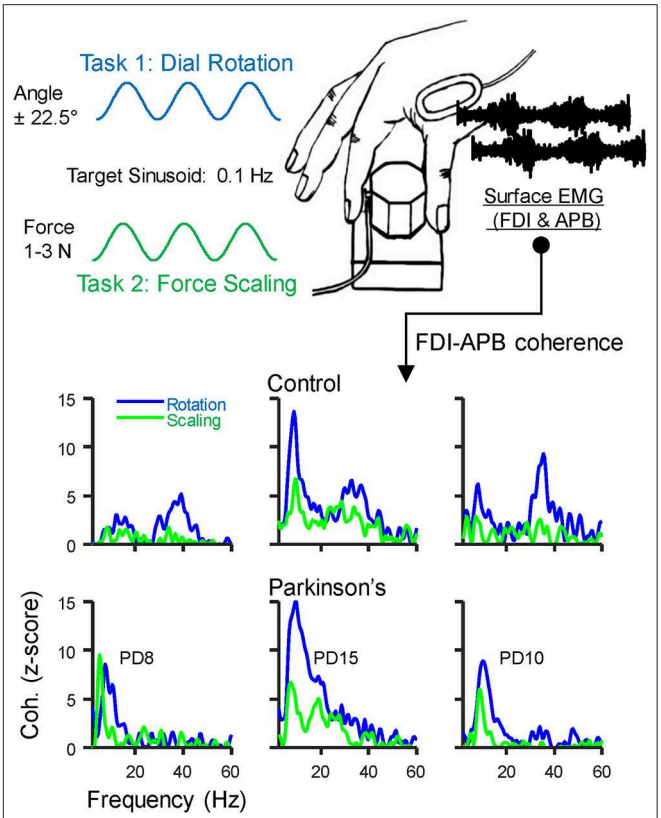

FIGURE 1 | Behavioral Task: Participants grasped a small dial between the thumb and index finger and either (1) slowly scaled their pinch force using visual feedback to track a 0.1 Hz sinusoid spanning 1–3 N, or (2) rotated the dial back and forth over 45 degrees at 0.1 Hz using visual feedback of dial rotation. A miniature load cell at the index finger pad measured pinch force, and surface EMG was recorded over the first dorsal interosseous (FDI) and abductor pollicis brevis (APB) muscles. The EMG signals were used to calculate intermuscular coherence. The bottom panels show coherence profiles for each task from three example individuals in the control group (top) and in those with Parkinson's disease (PD, bottom). The displayed identification numbers correspond to the participant descriptions in **Table 2**.

thumb and index finger, and coherence between their EMG signals varies across tasks even without related changes in the shape of their power spectra. Therefore, these tasks alter the extent to which alpha-band neural drive is shared among muscles rather than simply altering its amplitude. Briefly, the dial held a potentiometer to track rotation angle and a miniature load cell (ELB4-10, Measurement Specialties, Hampton, VA) under the index finger to measure pinch force. Surface EMG sensors (Biometrics, Newport, UK) were placed over the first dorsal interosseous (FDI) and abductor pollicis brevis (APB) muscles of each hand. All signals were acquired at 1,000 Hz using a Biometrics LTD DataLINK system (Biometrics, Newport, UK). Visual feedback of rotation or force was provided using custom software designed in MATLAB (The Math Works, Natick, MA). We instructed participants to prioritize the production of a smooth force or rotation effort, guided/paced by the target sinusoid. This instruction was intended to reduce the likelihood that participants with involuntary tremors would focus on counteracting them rather than executing the prescribed slow voluntary action. Each participant completed four, 3-min tasks with each hand, (2 trials for each of 2 tasks, described below). Practice trials were given prior to recordings, and breaks between each task were given to prevent fatigue. The order of tasks and hands was randomized for each participant, and subjects did not find these simple tasks fatiguing.

Task 1: Dynamic modulation of isometric pinch force. With each hand separately, participants pinched the dial and slowly varied their pinch force between 1 and 3 N by tracking a sinusoidal target displayed on screen. The vertical height of the cursor was controlled by pinch force and while the horizontal position moved left-to-right across the screen automatically as a function of time, taking 30 s before looping back to the left. The sinusoidal target had a peak-to-peak period of 10 s, such that the frequency of force modulation was 0.1 Hz. We chose this frequency for ease of tracking and used it for all participants to avoid potential effects of movement speed on our EMG measurements. Practice trials were given to familiarize each participant with the task prior to recordings.

Task 2: Dial rotation. In this task, subjects rotated the dial back and forth +/− 22.5 degrees with each hand separately. Visual feedback was provided as before, but with the vertical position of the cursor controlled by rotation angle. To ensure that pinch force remained similar across tasks, the cursor color changed to indicate if pinch force exited the 1–3 N range during the task. All participants were able to maintain pinch force within this range and made few errors after initial practice.

EMG signals were high-pass filtered using a zero-phase 4th order Butterworth filter with a cutoff at 250 Hz, then rectified and normalized to unit variance as in our previous study (19). This follows the general recommendations for accentuating the

timing and density of motor unit action potentials within the surface EMG signal (43–47). It should be noted that the extreme high-pass filtering may be a precaution more than a universal necessity, and that surface EMG signals can be expected to contain some degree of noise or amplitude cancellation which can distort coherence measures when assessing low frequency neural drive (e.g., <5 Hz) or using high contraction levels (48), neither of which are a concern in the present study. The two trials for each task for each hand were concatenated, yielding a total of 6 min of data per hand. The first few (∼5) seconds of each trial were trimmed manually to ensure that stable tracking had been obtained prior to analysis.

Coherence Analysis

Coherence between EMG signals describes the frequency content of their synchronized activity. Coherence between the EMG signals of the FDI and APB muscles was calculated using the "mscohere" function in MATLAB, specifying segment sizes of 2 s, tapered with a Hann window, and overlapped by 0.5 s. Prior to statistical comparisons, the raw coherence values (C) were first converted to Fisher's Z values using the formula $Fz = \text{atanh}[\text{sqrt}(C)]$. Then, for better comparison with previous work, and to provide a more standard index of statistical strength, we converted the *Fz* values to standard Z-scores using the formula $Z = \text{Fz} / \sqrt{(1/\ 2\text{L})}$—bias. In this formula, L is the degrees of freedom derived from the number of segments used in the coherence calculation (49–51), and the bias was calculated as the mean uncorrected Z-score between 100 and 500 Hz, since this frequency range contains no physiological coherence (19, 52). Coherence profiles for three individuals from each group are shown in the bottom panels of **Figure 1**.

Statistical Testing

Statistical evaluation of coherence is often simplified by binning the frequency spectrum into a few common bands of interest. The exact boundaries for each band can vary across studies, and such boundaries may change when evaluating pathology. Therefore, to address our main hypotheses, we allowed relevant frequency bands to be defined from the data itself, using a non-parametric version of statistical parametric mapping (SPM), as described previously (53, 54). This is a random-permutation test that assigns *p*-values to regions of interest (corrected for multiple comparisons) within a "map" of cross-group differences calculated over space, time, or (in our case) frequencies (55). To map group differences in coherence across frequencies, we used an effect size measure, Cohen's D, as our initial statistic. This was then smoothed over frequencies using a gaussian window spanning 4 Hz. We defined regions of interest, or "clusters," as any group of consecutive frequencies (min width = 3 Hz) exceeding a threshold. The threshold can be set arbitrarily but we automated this by using the 95% confidence interval for our Cohen's D values, calculated with respect to their mean and standard deviation from 100 to 500 Hz, where no true group level differences in coherence should exist. The above-threshold area of each cluster was tested for statistical significance based on a 10,000 iteration random permutation test, as described previously (55).

Using the above procedure, we identified differences in intermuscular coherence between controls and participants with PD for (1) the rotation task, (2) the scaling task, and (3) the difference between rotation and scaling (rotation-scaling, per hand). The latter addresses whether any effects of PD on intermuscular coherence are task-specific. For each, we also created box and whisker plots to visualize how the average coherence within each statistically significant frequency band varied across individuals. To better assess variability across individuals rather than hands, data from both hands were averaged per individual. A Cohen's D effect size as well as a *p*-value (derived from a random-permutation test) were also calculated for this binned/averaged data. Since it is possible that PD may have stronger effects on one hand, we confirmed the appropriateness of averaging across hands by calculated an absolute laterality index for each individual (the absolute difference in coherence between hands divided by their sum), and comparing across groups, again using a random-permutation test.

Correlation Analysis

The intermuscular coherence values above were tested for correlation with the total UPDRS score, as well as with its subsection II (activities of daily living) and subsection III (motor evaluation). To be conservative, this was conducted using a non-parametric Spearman's rank correlation. The correlation coefficients and associated *p*-values were obtained using the "corr" function in MATLAB. This analysis tested for a non-zero correlation between coherence and symptom measures. With so few participants, an exact magnitude of correlation cannot be determined with high precision. We therefore calculated a 95% confidence interval around each correlation measure using a 10,000 iteration bootstrap procedure.

Discriminability

We evaluated the extent to which the data above could classify a participant as being a member of the PD or control group. To do this, we constructed Receiver Operating Characteristic curves (ROC curves) for each task [for a brief overview, see Eng (56)]. Each point on an ROC curve describes the fraction of patients who could be correctly identified (true positive rate, y-axis) using a particular threshold value for discrimination, while at the same time misclassifying some proportion of the controls (false positive rate, x-axis). Defining these proportions for every possible threshold produces the ROC curve. The area under the curve (AUC) is 1 for perfect discrimination and 0.5 for random chance. Our SPM analysis identified that the greatest difference of coherence between PD and control groups occurred in the alpha-band for both tasks (5.8–16.6 Hz for the rotation task and 4.4–15.6 for the scaling task). Using this information, we extracted a single measurement from each coherence spectrum, herein referred to as the alpha-ratio, by calculating the fraction of total intermuscular coherence (between 2 and 80 Hz) falling within the alpha-band (defined per task, as described above). This ratio-based normalization strategy has been used previously for

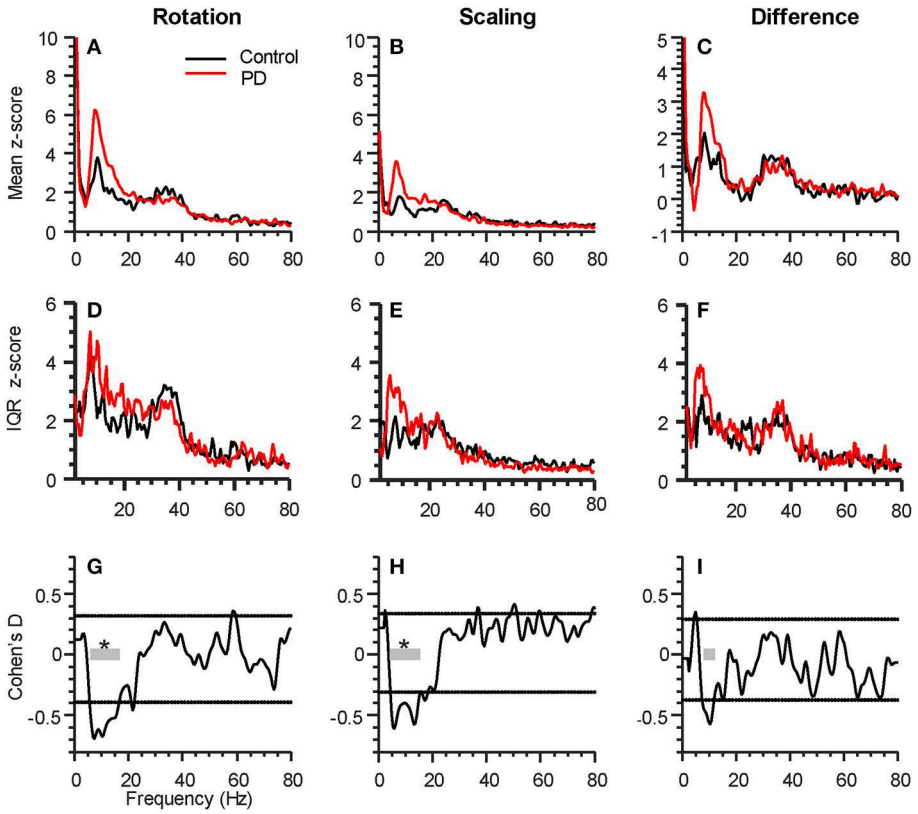

FIGURE 2 | Parkinson's disease (PD) affects intermuscular coherence in the alpha-band (6–15 Hz). The three columns represent analyses of group differences in intermuscular coherence (Control, black, 15 participants; Parkinson's, red, 16 participants) during the rotation task (left), the force scaling task (middle), as well as the difference between the two tasks (rotation minus scaling, right). All plots include data from both hands of each participant. **(A–C)** shows the grand average FDI:APB coherence in each task. **(D–F)** shows the interquartile range (IQR) of coherence z-scores across subjects at each individual frequency sample. **(G–I)** shows the statistical difference between groups (expressed as Cohen's D), calculated at every frequency. The horizontal dashed lines represent a statistical threshold for identifying frequency bands of interest for further statistical testing (see Methods). The gray bars show the bands of interest identified for each condition, with an * indicating that the band as a whole differed significantly between groups ($p < 0.05$, corrected for multiple comparisons).

reporting tremor measures (23, 57), and in our case, it reduces inter-subject variability from sources that could influence all frequencies at once (e.g., noise or cross-talk) while emphasizing the overall shape of the coherence spectrum. ROC curves were first constructed for each task. Then, for a final combined analysis, we created an ROC curve after averaging all 4 alpha-ratios obtained for each participant (2 hands × 2 tasks).

Task Performance

All participants could execute the task with both hands. Because systematic differences in the overall frequency/magnitude of error corrections could influence alpha-band drive to individual muscles (58, 59) we used a 10,000 iteration permutation test to determine if fluctuations in force/rotation about the target sinusoid differed significantly between groups. Here, performance was quantified as the standard deviation of pinch force or rotation angle after filtering out the 0.1 Hz modulation associated with the voluntary task of tracking the target sinusoid. Task performance was also tested for correlation with alpha-band drive using Spearman's rank correlation.

RESULTS

For both tasks, alpha-band coherence between the FDI and APB muscles differed between the PD and control group. For the rotation task, coherence differed within the frequency range of 5.8 to 16.6 Hz, with $p < 0.001$ (see **Figures 2A,G**). The scaling task showed significant difference between groups from 4.4 to 15.6 Hz, with $p < 0.001$ (**Figures 2B,H**). The difference between the two tasks (rotation—scaling) showed a range of interest between 7.8 and 12.2 Hz (**Figures 2C,I**), but was not statistically significant ($p = 0.58$). Intersubject variability was generally high (**Figures 2D–F**).

Figures 3A–C show the consistency of alpha-band differences in intermuscular coherence between controls and participants with PD, for each task separately, as well as and their difference. For these plots, the coherence values are averaged across both hands per individual, since we found that there were no group differences (PD vs. CT) in the laterality of coherence between right and left hands ($p = 0.55$, $p = 0.36$, and $p = 0.57$ for rotation, scaling, and their difference, respectively). For consistency, we defined the alpha-band per task according to the precise

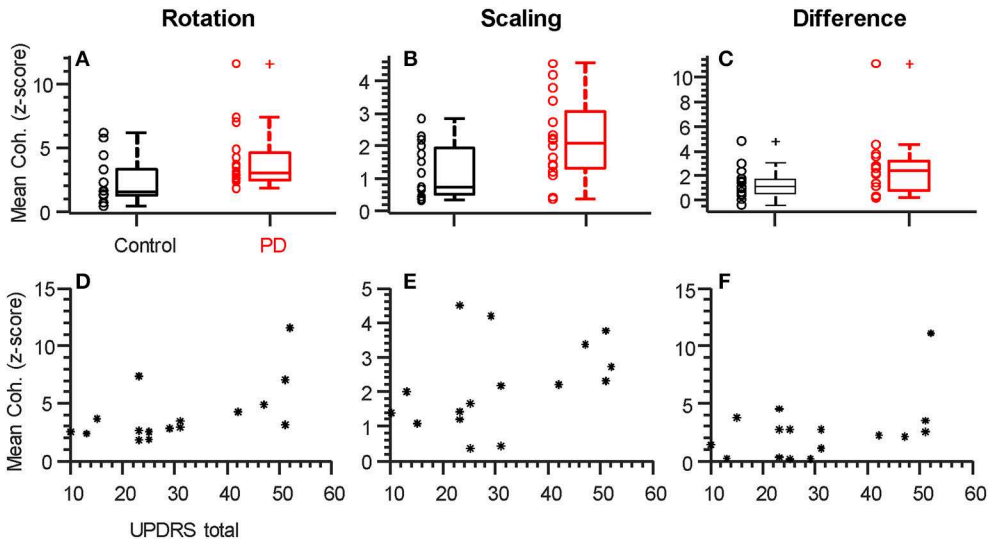

FIGURE 3 | Individual alpha-band coherence profiles differ between groups and correlate with UPDRS. **(A–C)** Box plots summarizing the mean coherence values for each participant calculated over the frequency range of significant difference (both alpha-band, see **Figure 2**). Both rotation **(A)** and scaling **(B)**, but not the difference between tasks **(C)**, showed significantly ($p < 0.05$) larger values in the Parkinson's Disease group relative to controls. **(D–F)** Total UPDRS scores vs. mean coherence (as plotted above). The correlation between UPDRS scores and alpha-band coherence was strongest for the rotation task and statistically significant (*D*, rho = 0.058, $p = 0.018$, see **Table 2**). + symbols indicate outliers. ○ symbols show the individual data from each participant, as summarized by the box plots. * symbols show individual data from each participant with PD.

frequency ranges identified in our SPM analysis. Using a generic 6–15 Hz frequency range for all tasks produced nearly identical results. Generally, a substantial degree of overlap between groups was apparent due to high inter-subject variability. Nonetheless, this binned/averaged alpha-band coherence measure showed significant differences between groups ($p = 0.04$, $p = 0.02$) for rotation and scaling tasks, respectively. Within each group, coherence in the alpha-band was task-dependent, differing significantly between scaling and rotation tasks ($p = 0.008$ and $p = 0.005$ for control and PD groups, respectively), but again, the magnitude of this difference did not differ between groups ($p = 0.95$). Coherence differences between groups had Cohen's D effect sizes of 0.75, 0.91, and 0.58, for the rotation task, the scaling task, and their difference, respectively.

Within the PD group, it is possible that coherence within the alpha-band covaries with symptom severity. We therefore tested the hypothesis of a non-zero correlation between coherence (as plotted in **Figures 3A–C**) and the total UPDRS score for each individual (**Figures 3D–F** and **Table 2**). **Table 2** shows the Spearman correlation coefficients between coherence in the alpha-band and the total UPDRS score, as well as the two main subsections of the UPDRS score: the motor symptoms score (Part III), and the self-evaluation of daily activities (part II). The 95% confidence interval around each correlation value is shown as well. Moderate correlations were found for coherence within the rotation task but not the force scaling task or their difference. Overall, the correlation between intermuscular coherence and symptom severity was not restricted to (or strongest for) the motor-only portion of the scale (UPDRS III), suggesting a more general relationship with disease state.

TABLE 2 | Spearman's correlation (rho) between mean coherence within the alpha-band, and patient symptom severities, as per the UPDRS, along with 95% confidence interval (CI) boundaries.

	UPDRS total	UPDRS II	UPDRS III
Rotation	**rho = 0.58**	rho = 0.48	**rho = 0.50**
	CI = [0.11 to 0.92]	CI = [−0.04 to 0.82]	**CI = [−0.03 to 0.84]**
	***p* = 0.018**	*P* = 0.058	***p* = 0.046**
Scaling	rho = 0.467	rho = 0.46	rho = 0.40
	CI = [−0.03 to 0.82]	CI = [−0.04 to 0.81]	CI = [−0.05 to 0.72]
	p =0.068	*p* = 0.073	*p* = 0.123
Difference	rho = 0.26	rho = 0.35	rho = 0.28
	CI = [−0.28 to 0.7]	CI = [−0.24 to 0.81]	CI = [−0.30 to 0.72]
	p = 0.327	*p* = 0.186	*p* = 0.293

Correlations were found to be significantly non-zero (bold, p < 0.05) between the rotation task and the total UPDRS score, and to a lesser extent, with the UPDRS motor-only score.

To determine if the accuracy with which controls and participants with PD performed the visuo-motor tracking related to coherence metrics, we compared the standard deviation of rotation angle or pinch force (after removing the 0.1 Hz target frequency), separately across groups. Task performance did not differ across groups ($p = 0.67$ and $p = 0.86$, respectively). This implies that any changes in alpha-band neural drive did not substantially contribute to tracking error, and indeed, neither group showed a significant correlation between tracking performance and alpha-band coherence in either task.

Finally, we sought to determine if a single coherence index calculated for each individual could be used to discriminate between groups. For this analysis, we calculated the proportion

of total coherence (2 to 80 Hz) falling within the alpha-band for each task/hand (the "alpha-ratio"). This is a simple way to reduce inter-subject sources of variability and focus on the contribution of alpha-band coherence to the overall shape of the coherence spectra. We confirmed that the alpha-ratio showed no group differences in laterality between hands ($p = 0.41$ and $p = 0.8$ for rotation and scaling tasks, respectively), and therefore averaged across hands to obtain a single ratio for each individual, per task. **Figures 4A,B** shows a clear separation between PD and control groups for the rotation ($p < 0.001$, Cohen's D = 1.96) and scaling task ($p = 0.001$, Cohen's D = 1.22). Since the purpose of this test was to determine the potential for coherence measures to discriminate between groups, we did not include an evaluation of the change in coherence between tasks, as there were no group differences in this measure. Instead, we averaged the alpha-ratio values obtained from the scaling and rotation tasks together (**Figure 4C**) to obtain a single, combined alpha-ratio per individual, which also differed significantly between groups ($p < 0.001$ Cohen's D = 1.84). We constructed Receiver Operating Characteristic Curves for the alpha-ratios derived for each task and their combination (**Figures 4D–F**). To quantify the overall discriminability, we calculated the area under the curve (AUC), which yielded values of 0.9, 0.84, and 0.96 for rotation, scaling, and their combination, respectively. These high values indicate that excellent separation between groups was possible in our study population, and that nearly all patients could be correctly classified, with practically no false positives (misclassified controls).

DISCUSSION

In this study, we describe a robust and consistent PD-related amplification of alpha-band (∼6–15 Hz) intermuscular coherence between finger muscles evoked during simple dynamic actions. Slow rotation of a dial between the thumb and index finger produced the strongest coherence, but the same effect was also observed during isometric modulation of precision pinch force. Clinical ratings of symptom severity (as per UPDRS) correlated significantly with the increased magnitude of intermuscular coherence during the rotation task only. The global alpha-ratio (proportion of total coherence within the alpha-band) provided an index which allowed excellent discrimination between controls and participants with PD within our study sample. This provides valuable information for future development of simple, practical measures of neural dysfunction in PD.

Kinetic Action Tremor in PD

The disruptions in neural drive that we have characterized in this study appear to be an intermuscular component of Parkinsonian kinetic action tremor (1, 4, 23, 60). In 1963, Lance et al. noted anecdotally that in PD a 5–15 Hz tremor was (i) always present at the beginning of a muscle contraction, (ii) was sometimes sustained during the static portion of a contraction, and (iii) was usually visible within EMG traces as a synchronous "grouping" of action potentials within and across contracting muscles—even when the tremor itself was not detectable by eye. Action tremor is distinct from rest tremor [or its re-emergence during steady contraction (2)] in that is higher in frequency (6–15 vs. 3–5 Hz), enhanced during dynamic action rather than reduced, and it is not attenuated by dopamine replacement in PD (4).

There is currently no standard clinical procedure for quantifying 6–15 Hz action tremor, perhaps because it is often invisible without special equipment and can be difficult to distinguish from "normal" physiological tremor (discussed further below). Most previous literature quantifies the magnitude of tremulous activity at a particular muscle or joint [e.g., (4, 60–63)]. However, if action tremor stems from an inherently common neural drive to multiple muscles, then it makes sense to use intermuscular coherence to quantify it and avoid reliance on limb/task/person-specific forces and motions.

Although the idea that tremor-generating neural drive in PD is inherently distributed to multiple muscles has received some support (21, 22), there has been less effort to identify the particular muscles/tasks in which an intermuscular action tremor is most reliably evoked and detected. So far, an amplified intermuscular coherence within the alpha-band has been reported only for static tasks such as isometric knee extension (11) or across two sides of a puckered upper lip (7). However, the alpha-band drive underlying action tremor in PD is best observed during dynamic actions (1, 4), where additional neural control circuitry may be required (64). Also, previous findings have described amplified coherence across anatomically synergistic muscles which naturally share a substantial amount of their neural drive (17). This makes it difficult to disambiguate changes in overall signal strength from an effect of PD on the process of "binding" of muscles into functional synergies through neural synchronization (65). Our results seem to suggest that a natural intermuscular alpha-band drive is amplified in PD. Further, the modification of this drive across different tasks is preserved, indicating that the amplification is not especially task-specific. This may indicate that the neural circuit which distributes alpha-band drive across muscles is still functional, even if overdriven.

Neural Origins of Parkinsonian Kinetic Action Tremor

Action tremor has been described as an amplification of naturally present physiological tremor rather than something that exclusively emerges in PD (4, 60); a notion that is well-aligned with our current data. Because the origins of physiological tremor are likely multifactorial (27–36), the effects of PD on each potential source of alpha-band neural drive to muscles must be considered. There are at least four potential sources for alpha-band neural drive in healthy individuals, and they are not mutually exclusive: (1) the stretch reflex system, (2) the motor cortex, (3) the brainstem (specifically reticulospinal output), and (4) the cerebellum (via the cerebello-thalamo-cortical circuit). We favor the latter, according to the following rationale.

If alpha-band drive is measured within the output of a single muscle, it may simply reflect cycles of excitation around the monosynaptic Ia afferent reflex loop of that muscle (27, 33, 34, 58, 66). However, this mechanism would not easily explain coherent ∼10 Hz activity across different muscles, which can be observed even between muscles in different hands in healthy adults (32,

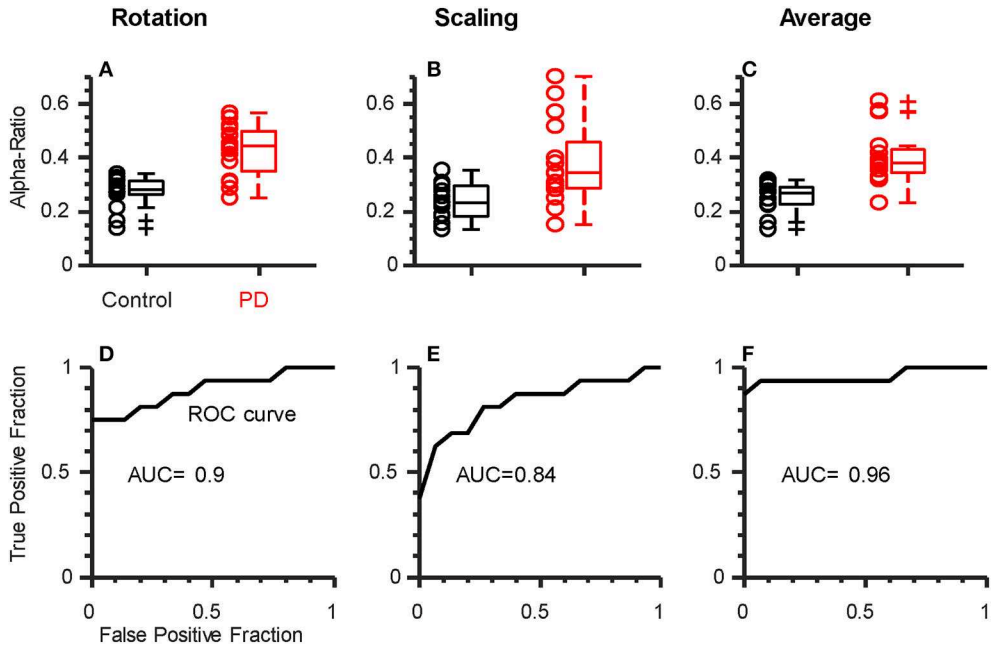

FIGURE 4 | Alpha-ratio (i.e., proportion of total intermuscular coherence within the alpha-band) can discriminate participants with PD from controls. Top row: Box plots showing the average alpha-ratio (across hands) for each individual. Results are shown for rotation **(A)**, scaling **(B)**, individually, as well as their combination **(C)**. Both rotation **(A)** and scaling **(B)** showed reasonable separation between groups, but the combination of both (average) per individual resulted in the least overlap **(C)**. **(D–F)** Receiver Operating Characteristic (ROC) curves for the metrics shown above. Area Under the Curve (AUC) values indicate strong-to-excellent discriminability in all cases.

38). Mechanical coupling among muscles may serve to link afferent feedback without need for monosynaptic connectivity, and a potential role for spinal interneuron pools in coordinating afferent activity across multiple muscles cannot be ruled out, but to our knowledge, there is no evidence that either mechanism could explain the generation of intermuscular coherence between the FDI and APB within the context of our task. Also, an origin in the peripheral reflex system would imply that stretch reflex or H-reflex amplitudes should be elevated in PD, which is not the case (67, 68). PD can, in some cases, disrupt task-dependent stretch reflex modulation (68), suggesting upstream mismanagement rather than pure peripheral dysfunction.

Studies of neural drive to individual muscles have indicated potential cortical involvement in alpha-band Parkinsonian tremor (12–18 Hz) during steady contraction of the wrist extensors (69, 70), although a subsequent delay analysis suggested that the cortical activity might not generate this drive, but instead, it may receive an efference copy from a subcortical source (69). Also, steady muscle contractions do not usually produce alpha-band corticomuscular coherence (EEG-EMG), even when intermuscular coherence (EMG-EMG) in this range is simultaneously observed (38, 71). For these reasons, it seems unlikely that our findings reflect an amplification of corticospinal output.

The reticulospinal pathway may also produce an alpha-band drive to muscles. Acoustic startle stimulates the reticulospinal pathway (72) and produces a brief wave of 12–16 Hz (73) coherent activity in bilateral pairs of muscles. However, involuntary reactions to acoustic startle may not directly predict reticulospinal contributions to intermuscular coherence during voluntary tasks. The potential association between acoustic startle responses and intermuscular coherence during voluntary tasks has never been fully explored, and current evidence is indirect. For example, spasticity in chronic stroke is thought to relate to overdriven reticulospinal drive to muscles (74, 75), and both alpha-band intermuscular coherence (76, 77) and responses to acoustic startle are increased in spastic muscles of stroke survivors (78, 79). However, if PD amplifies reticulospinal output, startle responses should be increased in magnitude or consistency relative to controls, but they are not (80). The preparation of brainstem output by upstream circuits may, however, be abnormal in PD since acoustic startle does not produce the usual acceleration of reaction times (the "StartReact" paradigm) in people with PD-associated freezing of gate (81). Therefore, the amplified alpha-band drive in PD may involve reticulospinal pathways, but probably not through an overall change in the excitability of the pontomedullary reticular formation.

Finally, the frequency spectrum of neural drive to muscles may be substantially influenced by the cerebellum via its actions within the cerebello-thalamo-cortical (CTC) circuit. The cerebellum oscillates in synchrony with the motor cortex at frequencies between 10 and 40 Hz (82), and slow movements of the finger produce coherent alpha-band oscillations between muscle activity and the cerebellum, thalamus, and motor cortex (30). In addition to a possible influence on the cortex and corticospinal output to muscles, the deep cerebellar nuclei may

also transmit a 10 Hz oscillation to muscles through modulation of the brainstem and reticulospinal tract output (82–84). In theory, output from the deep cerebellar nuclei to the cortex and brainstem could be amplified (disinhibited) in PD since Purkinje cell damage is associated with the disease (42, 85, 86). Regardless of the precise pathway to muscles, a wide variety of studies have implicated general CTC dysfunction in PD (40–42, 87–89). Further, dysfunction of the CTC is consistently associated with the generation of tremor in both PD (90–92) and the more common, but often-associated (93) condition known as essential tremor (94–99). In fact, medication in PD may reduce rest tremor by reconnecting cerebellar communication with the cortex through the ventrolateral thalamus (92), and a similar mechanism may explain the levodopa-reversible loss of 40 Hz corticomuscular drive in PD (12), since inactivation of the cerebellar cortex disrupts gamma-band cortical activity (100). In this view, basal ganglia dysfunction, as in PD, almost inevitably implies cerebellar network dysfunction. In fact, these structures have been described recently as nodes within a larger, tightly-interconnected network (101).

Taken together, it is clear that damage to this cerebellar circuit is not only plausible within our study population, but would very likely produce changes in alpha-band drive to muscles. Given the strong associations between cerebellar activity, cortical activity, and alpha-band spindle discharge during slow movements (102), it is likely that cerebellar-circuit dysfunction could both directly and indirectly influence the frequency spectrum of neuromuscular oscillations in PD. In addition to shaping neural oscillations, cerebellar circuit dysfunction can be expected to influence a variety of non-motor functions as well (86, 91, 103–106) and this might explain why correlations between coherence and UPDRS scores were not restricted to the direct motor evaluation in our study. That said, a specific or exclusive role for the CTC in the present study not possible to determine, and will require further research.

Intermuscular Coherence as a Potential Clinically-Practical Biomarker in PD

We found that the proportion of total coherence within the ∼6–15 Hz range was sufficient to statistically separate groups in either task. When all ratio values obtained from each individual were averaged together, it allowed for excellent discrimination between our two groups (AUC of 0.96). If this level of discriminability were to generalize to the larger population, it would meet or exceed the performance of the best MRI-based diagnostic biomarkers to date (107, 108) and yet not require expensive neuroimaging, invasive collection of cerebrospinal fluid, extensive patient history, etc. To be clear though, much larger studies would be needed to evaluate the readiness of any putative biomarker for clinical translation. Our intent in exploring discriminability between groups was not to establish an application-ready feature set or threshold for optimal real-world classification, but rather to provide evidence that EMG-based measures have clinical potential, since they have rarely been explored in this capacity. In fact, the only other EMG-derived measure which has achieved such strong discrimination between PD and controls was calculated from the cross-trial distribution of EMG burst durations in the biceps during fast elbow flexions in temporarily-off-medication patients (57). The neural mechanisms that contributed to that effect were not identified, and the measurement equipment and procedure itself was somewhat specialized and not well-suited for widespread clinical implementation. Our simpler method, with further refinements, seems more practical for common application and to complement other non-invasive biomarkers, such as those derived from olfaction (109, 110), or finger movements (111, 112).

Limitations

An important consideration in this study is that we recorded from participants who were on their normal medication, as this was a sample-of-convenience. To our knowledge, there is no evidence that medication could explain the increased alpha-band neural drive we observed, especially since tremor in this frequency range is not enhanced or attenuated by medication (4, 113). Of course, if it were attenuated, then presumably unmedicated participants would show even stronger differences from controls, strengthening our classification ability. Medication may have normalized 30–50 Hz intermuscular coherence in our study, as this frequency band is dopamine-dependent (12), but again, if our analysis were applied to unmedicated participants we would expect better discrimination between PD and controls, not worse. In PD, dopamine depletion in the basal ganglia is already extreme by the time of symptom onset (e.g., ∼80% loss in the putamen) making it difficult to detect or study the early stages of the disease (114). Thus, a method capable of detecting both low dopamine and amplified physiological tremor could contribute to such efforts, especially if combined with PD-sensitive metrics of finger movement speed/timing (111, 112). This would, in turn, enable the early initiation of neuroprotective strategies once they become available. Of course, any claims concerning translational/diagnostic capabilities at this point is speculative. Our sample size does not allow us to accurately characterize the strength and variability of effects across the total population of people with PD. Effect size estimates such as Cohen's D may be inflated in smaller studies, while skewed distributions or outliers may have the opposite effect. That said, our study is appropriately powered to detect the strong effects that are most likely to be of scientific and translational relevance, as well as to justify/enable their investigation in larger cohorts. Additionally, determining the optimal battery of task parameters will require future work. For example, it may be that features of visual feedback, the speed of the required dynamic action, the particular muscles measured, etc. may all be important variables. Also, this study focused on kinetic action tremor, however, the postural form of action tremor which emerges during static contractions may yield complementary information. A final limitation regarding intermuscular coherence analysis is that it measures the relative proportion of shared vs. total EMG

signal variance, and thus changes to both intramuscular (muscle-specific) and intermuscular (shared) neural drive can alter coherence. Separation of shared and muscle-specific neural drive can be accomplished using methods based on motor unit analysis [e.g., Laine et al., (17)], and may represent a valuable direction for future investigation. At present though, it is clear that tasks designed to evoke kinetic action tremor from functionally-coordinated muscles provide a clear window into the nervous system, which holds value for the assessment of PD and its progression.

DATA AVAILABILITY STATEMENT

The datasets generated for this study are available on request to the corresponding author.

ETHICS STATEMENT

The studies involving human participants were reviewed and approved by University of Southern California Internal Review Board. The patients/participants provided their written informed consent to participate in this study.

AUTHOR CONTRIBUTIONS

CL and FV-C contributed to the study design, interpretation of data, editing, and approval of the final manuscript. CL contributed to collection of experimental data, data analysis, and drafting of the manuscript.

FUNDING

This project was supported by NIH: NIAMS R01 AR-050520 and R01 AR-052345 to FV-C, and by: Department of Defense CDMRP Grant MR150091 and Award W911NF1820264 from the DARPA-L2M program to FV-C. The content of this endeavor is solely the responsibility of the authors and does not represent the official views of the National Institutes of Health, or the Department of Defense.

ACKNOWLEDGMENTS

The authors thank Catherine Parsekian, Lena Sulzenbacher, Shaohui Qian, Jamie Flores, and Kian Jalaleddini for assistance with subject recruitment and data collection, and Dr. Jun Yong Shin for creating the 3D-printed dial used in the study.

REFERENCES

1. Lance JW, Schwab RS, Peterson EA. Action tremor and the cogwheel phenomenon in Parkinson's disease. *Brain.* (1963) 86:95–110. doi: 10.1093/brain/86.1.95
2. Jankovic J, Schwartz KS, Ondo W. Re-emergent tremor of Parkinson's disease. *J Neurol Neurosurg Psychiatry.* (1999) 67:646–50. doi: 10.1136/jnnp.67.5.646
3. Timmermann L, Gross J, Dirks M, Volkmann J, Freund H-J, Schnitzler A. The cerebral oscillatory network of parkinsonian resting tremor. *Brain J Neurol.* (2003) 126:199–212. doi: 10.1093/brain/awg022
4. Raethjen J, Pohle S, Govindan RB, Morsnowski A, Wenzelburger R, Deuschl G. Parkinsonian action tremor: interference with object manipulation and lacking levodopa response. *Exp Neurol.* (2005) 194:151–60. doi: 10.1016/j.expneurol.2005.02.008
5. Jankovic J. Parkinson's disease: clinical features and diagnosis. *J Neurol Neurosurg Psychiatry.* (2008) 79:368–76. doi: 10.1136/jnnp.2007.131045
6. Rana AQ, Saleh M. Relationship between resting and action tremors in Parkinson's disease. *J Neurosci Rural Pract.* (2016) 7:232–7. doi: 10.4103/0976-3147.176192
7. Caviness JN, Liss JM, Adler C, Evidente V. Analysis of high-frequency electroencephalographic-electromyographic coherence elicited by speech and oral non-speech tasks in Parkinson's disease. *J Speech Lang Hear Res.* (2006) 49:424. doi: 10.1044/1092-4388(2006/033)
8. Hammond C, Bergman H, Brown P. Pathological synchronization in Parkinson's disease: networks, models and treatments. *Trends Neurosci.* (2007) 30:357–64. doi: 10.1016/j.tins.2007.05.004
9. Little S, Pogosyan A, Kuhn AA, Brown P. Beta band stability over time correlates with Parkinsonian rigidity and bradykinesia. *Exp Neurol.* (2012) 236:383–8. doi: 10.1016/j.expneurol.2012.04.024
10. Little S, Brown P. The functional role of beta oscillations in Parkinson's disease. *Parkinsonism Relat. Disord.* (2014) 20(Suppl.1):S44–8. doi: 10.1016/S1353-8020(13)70013-0
11. Flood MW, Jensen BR, Malling A-S, Lowery MM. Increased EMG intermuscular coherence and reduced signal complexity in Parkinson's disease. *Clin Neurophysiol.* (2019) 130:259–69. doi: 10.1016/j.clinph.2018.10.023
12. McAuley JH. Levodopa reversible loss of the Piper frequency oscillation component in Parkinson's disease. *J Neurol Neurosurg Psychiatry.* (2001) 70:471–5. doi: 10.1136/jnnp.70.4.471
13. Kilner JM, Baker SN, Salenius S, Jousmäki V, Hari R, Lemon RN. Task-dependent modulation of 15–30 Hz coherence between rectified EMGs from human hand and forearm muscles. *J Physiol.* (1999) 516:559. doi: 10.1111/j.1469-7793.1999.0559v.x
14. Boonstra TW, van Wijk B, Praamstra P, Daffertshofer A. Corticomuscular and bilateral EMG coherence reflect distinct aspects of neural synchronization. *Neurosci Lett.* (2009) 463:17–21. doi: 10.1016/j.neulet.2009.07.043
15. Boonstra TW. The potential of corticomuscular and intermuscular coherence for research on human motor control. *Front Hum Neurosci.* (2013) 7:855. doi: 10.3389/fnhum.2013.00855
16. DeMarchis C, Severini G, Castronovo AM, Schmid M, Conforto S. Intermuscular coherence contributions in synergistic muscles during pedaling. *Exp Brain Res.* (2015) 233:1907–19. doi: 10.1007/s00221-015-4262-4
17. Laine CM, Martinez-Valdes E, Falla D, Mayer F, Farina D. Motor neuron pools of synergistic thigh muscles share most of their synaptic input. *J Neurosci.* (2015) 35:12207–16. doi: 10.1523/JNEUROSCI.0240-15.2015
18. Farina D, Negro F, Muceli S, Enoka RM. Principles of motor unit physiology evolve with advances in technology. *Physiology.* (2016) 31:83–94. doi: 10.1152/physiol.00040.2015
19. Laine CM, Valero-Cuevas FJ. Intermuscular coherence reflects functional coordination. *J Neurophysiol.* (2017) 118:1775–83. doi: 10.1152/jn.00204.2017
20. Boonstra TW, Danna-Dos-Santos A, Xie, HB, Roerdink M, Stins JF, Breakspear M. Muscle networks: connectivity analysis of EMG activity during postural control. *Sci Rep.* (2015) 5:17830. doi: 10.1038/srep17830
21. van der Stouwe AMM, Conway BA, Elting JW, Tijssen MAJ, Maurits NM. Usefulness of intermuscular coherence and cumulant analysis in the diagnosis of postural tremor. *Clin Neurophysiol.* (2015) 126:1564–9. doi: 10.1016/j.clinph.2014.10.157
22. He X, Hao M-Z, Wei M, Xiao Q, Lan N. Contribution of inter-muscular synchronization in the modulation of tremor intensity in Parkinson's disease. *J NeuroEngineering Rehabil.* (2015) 12:108. doi: 10.1186/s12984-015-0101-x

23. Beuter A, Edwards R. Kinetic tremor during tracking movements in patients with Parkinson's disease. *Parkinsonism Relat Disord.* (2002) 8:361–8. doi: 10.1016/S1353-8020(01)00051-7
24. Kraus PH, Lemke MR, Reichmann H. Kinetic tremor in Parkinson's disease—an underrated symptom. *J Neural Transm.* (2006) 113:845–53. doi: 10.1007/s00702-005-0354-9
25. Gironell A, Pascual-Sedano B, Aracil I, Marín-Lahoz J, Pagonabarraga J, Kulisevsky J. Tremor types in Parkinson disease: a descriptive study using a new classification. *Park Dis.* (2018) 2018:5. doi: 10.1155/2018/4327597
26. Forssberg H, Ingvarsson PE, Iwasaki N, Johansson RS, Gordon AM. Action tremor during object manipulation in Parkinson's disease. *Mov Disord.* (2000) 15:244–54. doi: 10.1002/1531-8257(200003)15:2<244::AID-MDS1007>3.0.CO;2-H
27. Lippold OCJ. Oscillation in the stretch reflex arc and the origin of the rhythmical, 8–12 c/s component of physiological tremor. *J Physiol.* (1970) 206:359–82. doi: 10.1113/jphysiol.1970.sp009018
28. Elble RJ, Randall JE. Motor-unit activity responsible for 8- to 12-Hz component of human physiological finger tremor. *J Neurophysiol.* (1976) 39:370–83. doi: 10.1152/jn.1976.39.2.370
29. McAuley JH, Marsden CD. Physiological and pathological tremors and rhythmic central motor control. *Brain.* (2000) 123:1545–67. doi: 10.1093/brain/123.8.1545
30. Gross J, Timmermann L, Kujala J, Dirks M, Schmitz F, Salmelin R, et al. The neural basis of intermittent motor control in humans. *Proc Natl Acad Sci USA.* (2002) 99:2299–302. doi: 10.1073/pnas.032682099
31. Elble RJ. Characteristics of physiologic tremor in young and elderly adults. *Clin Neurophysiol.* (2003) 114:624–35. doi: 10.1016/S1388-2457(03)00006-3
32. Evans CMB, Baker SN. Task-dependent intermanual coupling of 8-Hz discontinuities during slow finger movements. *Eur J Neurosci.* (2003) 18:453–6. doi: 10.1046/j.1460-9568.2003.02751.x
33. Christakos CN, Papadimitriou NA, Erimaki S. Parallel neuronal mechanisms underlying physiological force tremor in steady muscle contractions of humans. *J Neurophysiol.* (2006) 95:53–66. doi: 10.1152/jn.00051.2005
34. Erimaki S, Christakos CN. Coherent motor unit rhythms in the 6–10 Hz range during time-varying voluntary muscle contractions: neural mechanism and relation to rhythmical motor control. *J Neurophysiol.* (2008) 99:473–83. doi: 10.1152/jn.00341.2007
35. Lakie M, Vernooij CA, Osborne TM, Reynolds RF. The resonant component of human physiological hand tremor is altered by slow voluntary movements. *J Physiol.* (2012) 590:2471–83. doi: 10.1113/jphysiol.2011.226449
36. Vernooij CA, Reynolds RF, Lakie M. A dominant role for mechanical resonance in physiological finger tremor revealed by selective minimization of voluntary drive and movement. *J Neurophysiol.* (2013) 109:2317–26. doi: 10.1152/jn.00926.2012
37. Nazarpour K, Barnard A, Jackson A. Flexible cortical control of task-specific muscle synergies. *J Neurosci.* (2012) 32:12349–60. doi: 10.1523/JNEUROSCI.5481-11.2012
38. de Vries IEJ, Daffertshofer A, Stegeman DF, Boonstra TW. Functional connectivity in the neuromuscular system underlying bimanual coordination. *J Neurophysiol.* (2016) 116:2576–85. doi: 10.1152/jn.00460.2016
39. Racz K, Brown D, Valero-Cuevas FJ. An involuntary stereotypical grasp tendency pervades voluntary dynamic multifinger manipulation. *J Neurophysiol.* (2012) 108:2896–911. doi: 10.1152/jn.00297.2012
40. Sen S, Kawaguchi A, Truong Y, Lewis MM, Huang X. Dynamic changes in cerebello-thalamo-cortical motor circuitry during progression of Parkinson's disease. *Neuroscience.* (2010) 166:712–9. doi: 10.1016/j.neuroscience.2009.12.036
41. Wu T, Hallett M. The cerebellum in Parkinson's disease. *Brain.* (2013) 136:696–709. doi: 10.1093/brain/aws360
42. Muthuraman M, Raethjen J, Koirala N, Anwar AR, Mideksa KG, Elble R, et al. Cerebello-cortical network fingerprints differ between essential, Parkinson's and mimicked tremors. *Brain.* (2018) 141:1770–81. doi: 10.1093/brain/awy098
43. Potvin JR, Brown SHM. Less is more: high pass filtering, to remove up to 99% of the surface EMG signal power, improves EMG-based biceps brachii muscle force estimates. *J Electromyogr Kinesiol Off J Int Soc Electrophysiol Kinesiol.* (2004) 14:389–99. doi: 10.1016/j.jelekin.2003.10.005
44. Riley ZA, Terry ME, Mendez-Villanueva A, Litsey JC, Enoka RM. Motor unit recruitment and bursts of activity in the surface electromyogram during a sustained contraction. *Muscle Nerve.* (2008) 37:745–53. doi: 10.1002/mus.20978
45. Brown SHM, Brookham RL, Dickerson CR. High-pass filtering surface EMG in an attempt to better represent the signals detected at the intramuscular level. *Muscle Nerve.* (2009). doi: 10.1002/mus.21470
46. Staudenmann D, Roeleveld K, Stegeman DF, van Dieën JH. Methodological aspects of SEMG recordings for force estimation—A tutorial and review. *J Electromyogr Kinesiol.* (2010) 20:375–87. doi: 10.1016/j.jelekin.2009.08.005
47. Boonstra TW, Breakspear M. Neural mechanisms of intermuscular coherence: implications for the rectification of surface electromyography. *J Neurophysiol.* (2012) 107:796–807. doi: 10.1152/jn.00066.2011
48. Dideriksen JL, Farina D. Amplitude cancellation influences the association between frequency components in the neural drive to muscle and the rectified EMG signal. *PLOS Comput Biol.* (2019) 15:e1006985. doi: 10.1371/journal.pcbi.1006985
49. Rosenberg JR, Amjad AM, Breeze P, Brillinger DR, Halliday DM. The Fourier approach to the identification of functional coupling between neuronal spike trains. *Prog Biophys Mol Biol.* (1989) 53:1–31. doi: 10.1016/0079-6107(89)90004-7
50. Terry K, Griffin L. How computational technique and spike train properties affect coherence detection. *J Neurosci Methods.* (2008) 168:212–23. doi: 10.1016/j.jneumeth.2007.09.014
51. Kattla S, Lowery MM. Fatigue related changes in electromyographic coherence between synergistic hand muscles. *Exp Brain Res Exp Hirnforsch Expérimentation Cérébrale.* (2010) 202:89–99. doi: 10.1007/s00221-009-2110-0
52. Baker SN, Pinches EM, Lemon RN. Synchronization in monkey motor cortex during a precision grip task. II effect of oscillatory activity on corticospinal output. *J Neurophysiol.* (2003) 89:1941–53. doi: 10.1152/jn.00832.2002
53. Holmes AP, Blair RC, Watson JDG, Ford I. Non-parametric analysis of statistic images from functional mapping experiments. *J Cereb Blood Flow Metab.* (1996) 16:7–22. doi: 10.1097/00004647-199601000-00002
54. Nichols TE, Holmes AP. Non-parametric permutation tests for functional neuroimaging: a primer with examples. *Hum Brain Mapp.* (2002) 15:1–25. doi: 10.1002/hbm.1058
55. Maris E, Oostenveld R. Non-parametric statistical testing of EEG- and MEG-data. *J Neurosci Methods.* (2007) 164:177–90. doi: 10.1016/j.jneumeth.2007.03.024
56. Eng J. Receiver operating characteristic analysis. *Acad Radiol.* (2005) 12:909–16. doi: 10.1016/j.acra.2005.04.005
57. Robichaud JA, Pfann KD, Leurgans S, Vaillancourt DE, Comella CL, Corcos DM. Variability of EMG patterns: a potential neurophysiological marker of Parkinson's disease? *Clin Neurophysiol.* (2009) 120:390–7. doi: 10.1016/j.clinph.2008.10.015
58. Laine CM, Yavuz SU, Farina D. Task-related changes in sensorimotor integration influence the common synaptic input to motor neurones. *Acta Physiol.* (2014) 211:229–39. doi: 10.1111/apha.12255
59. Laine CM, Nagamori A, Valero-Cuevas FJ. The dynamics of voluntary force production in afferented muscle influence involuntary tremor. *Front Comput Neurosci.* (2016) 10:86. doi: 10.3389/fncom.2016.00086
60. Christakos CN, Erimaki S, Anagnostou E, Anastasopoulos D. Tremor-related motor unit firing in Parkinson's disease: implications for tremor genesis. *J Physiol.* (2009) 587:4811–27. doi: 10.1113/jphysiol.2009.173989
61. Brown P, Corcos DM, Rothwell JC. Does parkinsonian action tremor contribute to muscle weakness in Parkinson's disease? *Brain.* (1997) 120:401–8. doi: 10.1093/brain/120.3.401
62. Teräväinen H, Calne DB. Action tremor in Parkinson's disease. *J Neurol Neurosurg Psychiatry.* (1980) 43:257–63. doi: 10.1136/jnnp.43.3.257
63. Brown P, Corcos DM, Rothwell JC. Action tremor and weakness in Parkinson's disease: a study of the elbow extensors. *Mov Disord.* (1998) 13:56–60. doi: 10.1002/mds.870130114
64. Oya T, Takei T, Seki K. Distinct sensorimotor feedback loops for dynamic and static control of primate precision grip. *bioRxiv.* (2019). doi: 10.1101/640201

65. Farmer SF. Rhythmicity, synchronization and binding in human and primate motor systems. *J Physiol.* (1998) 509:3. doi: 10.1111/j.1469-7793.1998.003bo.x
66. Nagamori A, Laine CM, Valero-Cuevas FJ. Cardinal features of involuntary force variability can arise from the closed-loop control of viscoelastic afferented muscles. *PLOS Comput Biol.* (2018) 14:e1005884. doi: 10.1371/journal.pcbi.1005884
67. Cody FWJ, Macdermott N, Matthews PBC, Richardson HC. Observations on the genesis of the stretch reflex in Parkinson's disease. *Brain.* (1986) 109:229–49. doi: 10.1093/brain/109.2.229
68. Hayashi R, Tokuda T, Tako K, Yanagisawa N. Impaired modulation of tonic muscle activities and H-reflexes in the soleus muscle during standing in patients with Parkinson's disease. *J Neurol Sci.* (1997) 153:61–7. doi: 10.1016/S0022-510X(97)00175-5
69. Salenius S, Avikainen S, Kaakkola S, Hari R, Brown P. Defective cortical drive to muscle in Parkinson's disease and its improvement with levodopa. *Brain.* (2002) 125:491–500. doi: 10.1093/brain/awf042
70. Caviness JN, Shill HA, Sabbagh MN, Evidente VGH, Hernandez JL, Adler CH. Corticomuscular coherence is increased in the small postural tremor of Parkinson's disease. *Mov Disord.* (2006) 21:492–9. doi: 10.1002/mds.20743
71. Reyes A, Laine CM, Kutch JJ, Valero-Cuevas FJ. Beta band corticomuscular drive reflects muscle coordination strategies. *Front Comput Neurosci.* (2017) 11:17. doi: 10.3389/fncom.2017.00017
72. Rothwell JC. The startle reflex, voluntary movement, and the reticulospinal tract. *Suppl Clin Neurophysiol.* (2006) 58:223–31. doi: 10.1016/S1567-424X(09)70071-6
73. Grosse P, Brown P. Acoustic startle evokes bilaterally synchronous oscillatory EMG activity in the healthy human. *J Neurophysiol.* (2003) 90:1654–61. doi: 10.1152/jn.00125.2003
74. Dewald JPA, Pope PS, Given JD, Buchanan TS, Rymer WZ. Abnormal muscle coactivation patterns during isometric torque generation at the elbow and shoulder in hemiparetic subjects. *Brain.* (1995) 118:495–510. doi: 10.1093/brain/118.2.495
75. Krakauer JW, Carmichael ST. *Broken Movement: The Neurobiology of Motor Recovery After Stroke.* Cambridge, MA: The MIT Press (2017). doi: 10.7551/mitpress/9310.001.0001
76. Lan Y, Yao J, Dewald JPA. Reducing the impact of shoulder abduction loading on the classification of hand opening and grasping in individuals with poststroke flexion synergy. *Front Bioeng Biotechnol.* (2017) 5:39. doi: 10.3389/fbioe.2017.00039
77. Chen Y-T, Li S, Magat E, Zhou P, Li S. Motor overflow and spasticity in chronic stroke share a common pathophysiological process: analysis of within-limb and between-limb EMG-EMG coherence. *Front Neurol.* (2018) 9:795. doi: 10.3389/fneur.2018.00795
78. Li S, Chang S-H, Francisco GE, Verduzco-Gutierrez M. Acoustic startle reflex in patients with chronic stroke at different stages of motor recovery: a pilot study. *Top Stroke Rehabil.* (2014) 21:358–70. doi: 10.1310/tsr2104-358
79. Li S, Bhadane M, Gao F, Zhou P. The reticulospinal pathway does not increase its contribution to the strength of contralesional muscles in stroke survivors as compared to ipsilesional side or healthy controls. *Front Neurol.* (2017) 8:627. doi: 10.3389/fneur.2017.00627
80. Kofler M, Müller J, Wenning GK, Reggiani L, Hollosi P, Bösch S, et al. The auditory startle reaction in parkinsonian disorders. *Mov Disord.* (2001) 16:62–71. doi: 10.1002/1531-8257(200101)16:1<62::AID-MDS1002>3.0.CO;2-V
81. Nonnekes J, Geurts ACH, Oude Nijhuis LB, van Geel K, Snijders AH, Bloem BR, et al. Reduced StartReact effect and freezing of gait in Parkinson's disease: two of a kind? *J Neurol.* (2014) 261:943–50. doi: 10.1007/s00415-014-7304-0
82. Soteropoulos DS. Cortico-cerebellar coherence during a precision grip task in the monkey. *J Neurophysiol.* (2005) 95:1194–206. doi: 10.1152/jn.00935.2005
83. Soteropoulos DS, Baker SN. Bilateral representation in the deep cerebellar nuclei. *J Physiol.* (2008) 586:1117–36. doi: 10.1113/jphysiol.2007.144220
84. Williams ER, Soteropoulos DS, Baker SN. Spinal interneuron circuits reduce approximately 10-Hz movement discontinuities by phase cancellation. *Proc Natl Acad Sci USA.* (2010) 107:11098–103. doi: 10.1073/pnas.0913373107
85. Kishore A, Meunier S, Popa T. Cerebellar influence on motor cortex plasticity: behavioral implications for Parkinson's disease. *Front Neurol.* (2014) 5:68. doi: 10.3389/fneur.2014.00068
86. O'Callaghan C, Hornberger M, Balsters JH, Halliday GM, Lewis SJG, Shine JM. Cerebellar atrophy in Parkinson's disease and its implication for network connectivity. *Brain.* (2016) 139:845–55. doi: 10.1093/brain/awv399
87. Lewis MM, Slagle CG, Smith DB, Truong Y, Bai P, McKeown M, et al. Task specific influences of Parkinson's disease on the striato-thalamo-cortical and cerebello-thalamo-cortical motor circuitries. *Neuroscience.* (2007) 147:224–35. doi: 10.1016/j.neuroscience.2007.04.006
88. Zhang J, Wei L, Hu X, Xie B, Zhang Y, Wu G-R, et al. Akinetic-rigid and tremor-dominant Parkinson's disease patients show different patterns of intrinsic brain activity. *Parkinsonism Relat Disord.* (2015) 21:23–30. doi: 10.1016/j.parkreldis.2014.10.017
89. Piccinin CC, Campos LS, Guimarães RP, Piovesana LG, Santos MCA, dos Azevedo PC, et al. Differential pattern of cerebellar atrophy in tremor-predominant and akinetic/rigidity-predominant Parkinson's disease. *Cerebellum.* (2017) 16:623–8. doi: 10.1007/s12311-016-0834-5
90. Dirkx MF, Ouden H, den, Aarts E, Timmer M, Bloem BR, Toni I, et al. The cerebral network of Parkinson's tremor: an effective connectivity fMRI study. *J Neurosci.* (2016) 36:5362–72. doi: 10.1523/JNEUROSCI.3634-15.2016
91. Caligiore D, Pezzulo G, Baldassarre G, Bostan AC, Strick PL, Doya K, et al. Consensus paper: towards a systems-level view of cerebellar function: the interplay between cerebellum, basal ganglia, and cortex. *Cerebellum.* (2017) 16:203–29. doi: 10.1007/s12311-016-0763-3
92. Dirkx MF, Ouden D, M HE, Aarts E, Timmer MHM, Bloem BR, et al. Dopamine controls Parkinson's tremor by inhibiting the cerebellar thalamus. *Brain.* (2017) 140:721–34. doi: 10.1093/brain/aww331
93. Tarakad A, Jankovic J. Essential tremor and Parkinson's disease: exploring the relationship. *Tremor Hyperkinetic Mov.* (2019) 8:589. doi: 10.7916/D8MD0GVR
94. Marsden JF, Ashby P, Limousin-Dowsey P, Rothwell JC, Brown P. Coherence between cerebellar thalamus, cortex and muscle in manCerebellar thalamus interactions. *Brain.* (2000) 123:1459–70. doi: 10.1093/brain/123.7.1459
95. Minks E, Mareček R, Pavlík T, Ovesná P, Bareš M. Is the cerebellum a potential target for stimulation in Parkinson's disease? results of 1-Hz rTMS on upper limb motor tasks. *Cerebellum.* (2011) 10:804–11. doi: 10.1007/s12311-011-0290-1
96. Bareš, M., Husárová I, Lungu OV. Essential tremor, the cerebellum, and motor timing: towards integrating them into one complex entity. *Tremor Hyperkinetic Mov.* (2012) 2.
97. Buijink AWG, Broersma M, van der Stouwe AMM, van Wingen GA, Groot PFC, Speelman JD, et al. Rhythmic finger tapping reveals cerebellar dysfunction in essential tremor. *Parkinsonism Relat Disord.* (2015) 21:383–8. doi: 10.1016/j.parkreldis.2015.02.003
98. Louis ED. Essential tremor: a common disorder of purkinje neurons? *Neurosci Rev J Bringing Neurobiol Neurol Psychiatry.* (2016) 22:108–18. doi: 10.1177/1073858415590351
99. Louis ED. Essential tremor then and now: how views of the most common tremor diathesis have changed over time. *Parkinsonism Relat Disord.* (2018) 46:S70–4. doi: 10.1016/j.parkreldis.2017.07.010
100. Popa D, Spolidoro M, Proville RD, Guyon N, Belliveau L, Léna C. Functional role of the cerebellum in gamma-band synchronization of the sensory and motor cortices. *J Neurosci.* (2013) 33:6552–6. doi: 10.1523/JNEUROSCI.5521-12.2013
101. Bostan AC, Strick PL. The basal ganglia and the cerebellum: nodes in an integrated network. *Nat Rev Neurosci.* (2018) 19:338–50. doi: 10.1038/s41583-018-0002-7
102. Schieber MH, Thach WT. Trained slow tracking. II. Bidirectional discharge patterns of cerebellar nuclear, motor cortex, and spindle afferent neurons. *J Neurophysiol.* (1985) 54:1228–70. doi: 10.1152/jn.1985.54.5.1228
103. Middleton FA, Strick PL. Basal ganglia and cerebellar loops: motor and cognitive circuits. *Brain Res Rev.* (2000) 31:236–50. doi: 10.1016/S0165-0173(99)00040-5
104. Tedesco AM, Chiricozzi FR, Clausi S, Lupo M, Molinari M, Leggio MG. The cerebellar cognitive profile. *Brain.* (2011) 134:3672–86. doi: 10.1093/brain/awr266

105. Gao L, Zhang J, Hou Y, Hallett M, Chan P, Wu T. The cerebellum in dual-task performance in Parkinson's disease. *Sci Rep.* (2017) 7:45662. doi: 10.1038/srep45662
106. Schmahmann JD. The cerebellum and cognition. *Neurosci Lett.* (2019) 688:62–75. doi: 10.1016/j.neulet.2018.07.005
107. Castellanos G, Fernández-Seara MA, Lorenzo-Betancor O, Ortega-Cubero S, Puigvert M, Uranga J, et al. Automated neuromelanin imaging as a diagnostic biomarker for Parkinson's disease. *Mov Disord Off J Mov Disord Soc.* (2015) 30:945–52. doi: 10.1002/mds.26201
108. Le W, Dong J, Li S, Korczyn AD. Can biomarkers help the early diagnosis of Parkinson's disease? *Neurosci Bull.* (2017) 33:535–42. doi: 10.1007/s12264-017-0174-6
109. Mesholam RI, Moberg PJ, Mahr RN, Doty RL. Olfaction in neurodegenerative disease: a meta-analysis of olfactory functioning in Alzheimer's and Parkinson's diseases. *Arch Neurol.* (1998) 55:84–90. doi: 10.1001/archneur.55.1.84
110. Haugen J, Müller MLTM, Kotagal V, Albin RL, Koeppe RA, Scott PJH, et al. Prevalence of impaired odor identification in Parkinson disease with imaging evidence of nigrostriatal denervation. *J Neural Transm.* (2016) 123:421–4. doi: 10.1007/s00702-016-1524-7
111. Arroyo-Gallego T, Ledesma-Carbayo MJ, Sánchez-Ferro Á, Butterworth I, Mendoza CS, Matarazzo M, et al. Detection of motor impairment in Parkinson's disease via mobile touchscreen typing. *IEEE Trans Biomed Eng.* (2017) 64:1994–2002. doi: 10.1109/TBME.2017.2664802
112. Shirani A, Newton BD, Okuda DT. Finger tapping impairments are highly sensitive for evaluating upper motor neuron lesions. *BMC Neurol.* (2017) 17:55. doi: 10.1186/s12883-017-0829-y
113. Kulisevsky J, Avila A, Barbanoj M, Antonijoan R, Torres J, Arcelus R. Levodopa does not aggravate postural tremor in Parkinson's disease. *Clin Neuropharmacol.* (1995) 18:435–42. doi: 10.1097/00002826-199510000-00006
114. Dauer W, Przedborski S. Parkinson's disease: mechanisms and models. *Neuron.* (2003) 39:889–909. doi: 10.1016/S0896-6273(03)00568-3

Conflict of Interest: The authors declare that the research was conducted in the absence of any commercial or financial relationships that could be construed as a potential conflict of interest.

frontiers in Neurology

ORIGINAL RESEARCH
published: 07 April 2020
doi: 10.3389/fneur.2020.00224

Effects of Changes in Ankle Joint Angle on the Relation Between Plantarflexion Torque and EMG Magnitude in Major Plantar Flexors of Male Chronic Stroke Survivors

Jongsang Son[1,2]* *and William Zev Rymer*[1,2]

[1] *Shirley Ryan AbilityLab (formerly the Rehabilitation Institute of Chicago), Chicago, IL, United States,* [2] *Department of Physical Medicine and Rehabilitation, Northwestern University, Chicago, IL, United States*

The slope of the EMG-torque relation is potentially useful as a parameter related to muscular contraction efficiency, as a greater EMG-torque slope has often been reported in stroke-impaired muscles, compared to intact muscles. One major barrier limiting the use of this parameter on a routine basis is that we do not know how the EMG-torque slope is affected by changing joint angles. Thus, the primary purpose of this study is to characterize the EMG-torque relations of triceps surae muscles at different ankle joint angles in both paretic and non-paretic limbs of chronic hemispheric stroke survivors. Nine male chronic stroke survivors were asked to perform isometric plantarflexion contractions at different contraction intensities and at five different ankle joint angles, ranging from maximum plantarflexion to maximum dorsiflexion. Our results showed that the greater slope of the EMG-torque relations was found on the paretic side compared to the non-paretic side at comparable ankle joint angles. The EMG-torque slope increased as the ankle became plantarflexed on both sides, but an increment of the EMG-torque slope (i.e., the coefficient *a*) was significantly greater on the paretic side. Moreover, the relative (non-paretic/paretic) coefficient *a* was also strongly correlated with the relative (paretic/non-paretic) maximum ankle plantarflexion torque and with shear wave speed in the medial gastrocnemius muscle. Conversely, the relative coefficient *a* was not well-correlated with the relative muscle thickness. Our findings suggest that muscular contraction efficiency is affected by hemispheric stroke, but in an angle-dependent and non-uniform manner. These findings may allow us to explore the relative contributions of neural factors and muscular changes to voluntary force generating-capacity after stroke.

Keywords: EMG-torque relation, stroke, muscular contraction efficiency, force-length relation, muscle weakness

OPEN ACCESS

Edited by:
Francesco Negro, University of Brescia, Italy

Reviewed by:
Kohei Watanabe, Chukyo University, Japan
Allison Hyngstrom, Marquette University, United States

***Correspondence:**
Jongsang Son
json@sralab.org

Specialty section:
This article was submitted to Neurorehabilitation, a section of the journal Frontiers in Neurology

Received: *15 November 2019*
Accepted: *10 March 2020*
Published: *07 April 2020*

Citation:
Son J and Rymer WZ (2020) Effects of Changes in Ankle Joint Angle on the Relation Between Plantarflexion Torque and EMG Magnitude in Major Plantar Flexors of Male Chronic Stroke Survivors. Front. Neurol. 11:224. doi: 10.3389/fneur.2020.00224

INTRODUCTION

Weakness of voluntary muscle contraction is a dominant clinical feature after hemispheric stroke, and the severity of such weakness is correlated with a stroke survivor's independence in performing many functional tasks (1). This reduction in voluntary muscle strength is typically the most obvious motor deficit (2), and many clinical phenomena observed in chronic stroke survivors could be attributed to a loss of strength rather than to a loss of control (3).

In addition to muscle weakness, muscular contractions in stroke-impaired muscles often appear less efficient than in contralateral muscles or in analogous muscles of intact subjects, potentially contributing to impaired voluntary force generation. To illustrate this assertion further (4), reported that in approximately half of the tested human stroke survivors, during sustained isometric voluntary contractions at different intensities, the slope of the biceps brachii (BB) electromyogram (EMG)-force relations was significantly greater on the paretic side than on the non-paretic side. A similar finding was also observed in paretic first dorsal interosseous (FDI) muscles of chronic stroke survivors (5), implying that paretic muscles may require the recruitment of more motor units to achieve a given muscle force, and thus, display inefficient muscular contractions.

It is evident then, that altered motor unit behavior may result in inefficient muscular contractions. For example, abnormally low mean motor unit firing rates were observed in paretic tibialis anterior (TA) muscles (6, 7) and in paretic BB muscles (8). There is also evidence for additional altered motor unit behavior, including compressed motor unit recruitment threshold ranges during isometric contractions of the paretic BB muscles (8), impairments in firing rate modulation in paretic BB muscles (9), disorganization in the rank order of recruitment in paretic FDI muscles (10), and a compressed range of motor unit firing rates in paretic FDI muscles (11). Moreover, a recent simulation study revealed that the recruitment compression and a compressed "onion-skin" firing pattern can potentially also contribute to voluntary muscle weakness (12). In addition, the slope of EMG-force relation was reported to increase in concert with compressed motor unit recruitment threshold ranges and reductions of mean motor unit firing rates (13). Although these earlier studies support the idea that altered neural factors can contribute, these neural factors may not be enough to explain a complicated EMG-force relation, because the EMG-force relation is an outcome of both neural and muscular factors.

In particular, muscular changes may also contribute to voluntary muscle weakness (14–17). Although our understanding of muscular changes after hemispheric stroke is still limited, it is relevant to note that decreased muscle thickness is often associated with reduced force output at a given level of muscle activation. In addition, the maximum isometric muscle force varies depending on the muscle length (18), and this force-length relation may also be substantially altered after stroke. For example, the width of the active force-length curve seems narrower in the paretic medial gastrocnemius (MG) muscles (19) than in the equivalent contralateral muscles. Such altered contractile properties may lead to modified torque-angle curves, showing a significant reduction in the magnitude of the torque at joint angles where muscle length is short (3, 20–22), potentially resulting in a higher slope of the EMG-torque relation at such a short length. This outcome is likely because the effective torque at shorter lengths is smaller at a given EMG. Furthermore, material properties of muscle tissues seem to contribute to muscle mechanics, revealing that a stiffer material surrounding contractile elements of muscle tissues can reduce fascicle strain as well as muscle force (23–26). Based on these observations, it is likely that muscular factors can also play a part in the abnormal EMG-torque relation observed in chronic stroke survivors.

In light of these uncertainties, the purpose of this study is to characterize the EMG-torque relations of calf muscles at different ankle joint angles on both paretic and non-paretic sides in chronic stroke survivors, and thus, to understand how the slope of such relations (i.e., muscle efficiency-related parameter) is altered by changing joint angles. We hypothesize that the slope becomes greater as calf muscle lengths shorten because the operating range of calf muscles is usually located in the ascending limb of active force-length curve, so that the maximum force gradually decreases with shortening muscle lengths (27–29). We also hypothesize that as the muscle length becomes shorter, a greater increase in the slope is more likely to be observed on the paretic side than on the non-paretic side. This is because the width of the active force-length curve may be narrower on the paretic side (19) and thus, the relative reduction in the magnitude of peak forces on the paretic side becomes greater at comparable muscle lengths.

As a secondary goal, we also seek to characterize the relation between the maximum joint torque at each joint angle and the EMG-torque slope at this joint angle. Our hypothesis here is that the greater the slope, the smaller the maximum joint torque. This is because the slope is a measure of muscular contraction efficiency.

In order to better understand the potential impact of intrinsic muscular changes of muscular contraction efficiency after, we propose to assess associations between the relative slope-related parameter and the relative shear wave speed (SWS) and between the relative slope-related parameter and the relative muscle thickness. SWS is a non-invasive measure of tissue stiffness (30), and it has been shown that shear waves travel faster in paretic MG muscles than in non-paretic muscles of chronic stroke survivors (31, 32).

METHODS

Participants

Nine male chronic stroke survivors participated in this study (age: 56.9 ± 7.8 yrs.; height: 174.8 ± 7.3 cm; weight: 81.1 ± 8.9 kg; time since stroke: 8.1 ± 4.1 yrs.). Inclusion criteria were: (1) chronic stroke survivors (more than 6 months after stroke); (2) age 18–75 years; and (3) medically stable with medical clearance to participate. Exclusion criteria were: (1) other physical impairments such as orthopedic injuries or recent surgeries in lower limbs; (2) knee or ankle contractures $>10°$; (3) unstable neurological or cardiovascular conditions that may affect the candidate's performance; (4) cognitive limitations, such that the subject cannot follow instructions; (5) anti-spasticity drug injections (such as botulinum toxin) in the 3 months prior to participation; and (6) musculoskeletal pain that interferes with participation in this study. All participants were ambulating independently and were not currently receiving physical therapy. They had no history of botulinum toxin treatments for at least 6 months before testing. Written informed consent was obtained from all participants prior to testing and Northwestern University's Institutional Review Board approved all procedures.

Experimental Setup

Participants were seated upright in a fully-adjustable chair with the trunk and thigh firmly strapped to the chair. The foot was secured to the footplate where a 6-axis force-measuring sensor (Omega160, ATI Industrial Automation, Apex, NC, USA) was installed. The knee joint was extended as much as possible to a comfortable position. The ankle center of rotation (defined as the mid-line between the malleoli) was aligned with the rotation axis of the dynamometer. A slight adjustment in the subject's posture was then allowed to make sure the subject was comfortable throughout the experiment (in most cases, the knee was flexed ∼10°).

Single differential surface EMG (sEMG) electrodes (GRASS, Asto-Med, Inc., West Warwick, Rhode, Island) were placed over the muscle belly of the MG, the lateral gastrocnemius (LG), the soleus (SOL), and the tibialis anterior (TA), in order to record activity in each muscle. A ground electrode was attached to the patella. The area for the electrodes was cleaned with alcohol pads before electrode placement.

A shear wave elastography ultrasound system (Aixplorer Supersonic Imagine, Aix-en-Provence, France) with a linear transducer array (4–15 MHz, SuperLinear SL15-4, Vermon, Tours, France) (30) was used to record the MG muscle thickness and SWS under passive conditions at each designated angle. The transducer was positioned directly adjacent to the EMG electrode of the MG muscle, avoiding interference between the transducer and the EMG electrode, and was then secured to the shank using a custom holder, in order to minimize translation, and pressure induced by the transducer.

During the experiment, voluntary isometric plantarflexion torque and EMG signals were recorded at a sampling rate of 2 kHz and synchronized through a data acquisition (DAQ) system (NI USB-6259 BNC, National Instrument, Austin, TX, USA).

Procedures

To investigate the effects of changing ankle joint angle on the slope of EMG-torque relations, five different ankle angles were chosen: maximum plantarflexion (PF), maximum dorsiflexion (DF), neutral, and two intermediate angles. The maximum PF and DF positions were determined while the ankle joint was passively moved by the experimenter. Then, two intermediate angles were set as angles between maximum DF and neutral or maximum PF and neutral. Positive angles indicate dorsiflexion and negative angles plantarflexion.

At each designated ankle angle, and in a randomized order, ultrasound images from the MG muscle were captured while the muscle was relaxed. The region of interest (RoI) for SWS measurements was manually located over the muscle belly. Subjects were then asked to perform maximum voluntary isometric contractions (MVICs) in ankle plantarflexion for 5 s each, with a 1 min break between each MVC trial. The average value of three maximum MG muscle activations for each MVC trial was used to calculate the level of the MG muscle contraction intensity for visual feedback. The subject was then asked to perform sustained isometric plantarflexion contractions at four different contraction levels (i.e., 0, 20, 40, and 60%MVIC) for 5 s. Three isometric plantarflexion contractions were elicited at each designated contraction level randomized. A 30 s rest period between repetitions was provided. Two sessions were separately conducted for both paretic and non-paretic sides.

Data Analysis

Torque signals were processed by applying a zero-phase second-order Butterworth low pass filter with a cut-off frequency of 6 Hz, followed by the root mean square (RMS) envelope with a moving window of 500 ms. The maximum isometric plantarflexion torque was determined using peak RMS envelope values corresponding to three MVC trials. EMG signals were processed by applying a zero-phase second-order Butterworth bandpass filter (bandwidth: 20–450 Hz), followed by the RMS envelope with the same moving window, in order to obtain RMS EMG values. The average value of the 1-s segment in each trial was estimated to represent the RMS EMG and ankle plantarflexion torque. This segment was determined by the minimum variability (i.e., standard deviation) of the 1-s window of each processed torque signal.

Afterward, the EMG-torque relations for MG, LG, and SOL muscles were derived, using the RMS EMG and the torque values. Considering the load-sharing among the calf muscles for the ankle joint, the arithmetic mean values of the calf muscles' RMS EMG (ALL) were calculated and then used to characterize the EMG-torque relation. A linear fitting was conducted to determine the slope of the EMG-torque relations (**Figures 1A–E**).

To determine how the EMG-torque slope would be affected by changes in joint angle and by the stroke, the relationship between the slope and the joint angle was determined as $S = aA^2 + b$, where S is the slope, A the joint angle, a the scaling factor, and b the intercept. As the slope was monotonically increased with increasing ankle plantarflexion, the maximum DF angle was subtracted by the joint angle (i.e., shift all the joint angle data to start from zero), so that the intercept b indicates the slope at the maximum DF angle. The greater coefficient a indicates the more increment in the slope, as the ankle joint becomes plantarflexed (**Figure 1F**).

The relation between the maximum joint torque (T) at each joint angle and the slope (S) at corresponding angles was characterized as $T = cS^{-1}$, where c is the shape coefficient. The smaller coefficient c, the quicker decay in the torque as the slope increases (**Figure 2**).

Image processing was performed to obtain the MG muscle thickness and SWS of the MG muscle. The MG muscle thickness was measured as the distance between superficial and deep aponeuroses (33). The RGB-colored map in RoI of each image was converted into SWS, and the average value of SWS over the largest muscular region was calculated for each image (34). All the data processing was performed, using custom-written software in MATLAB (Mathworks, Natick, USA).

Statistical Analysis

The RMS EMG and the maximum joint torque were compared between sides using repeated-measures ANOVA. Within-subject

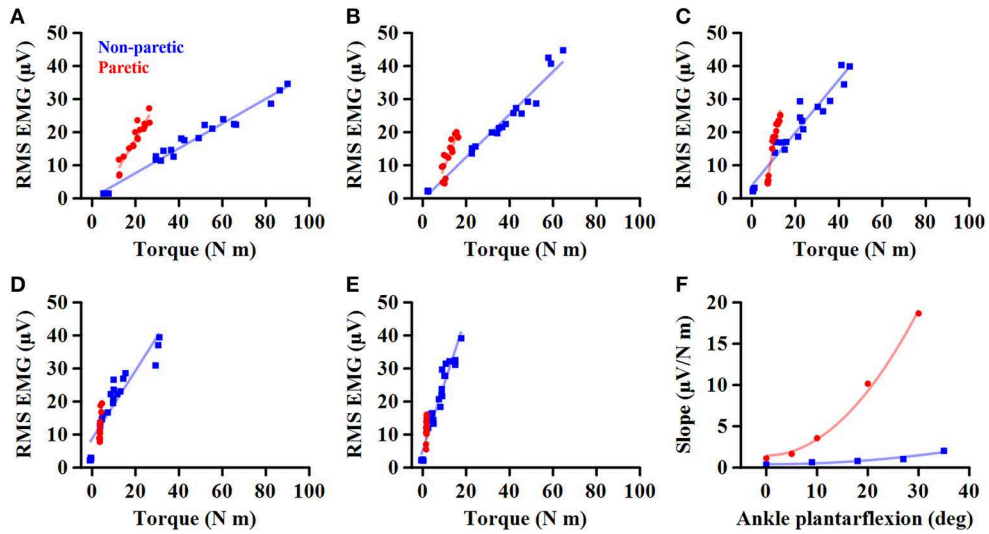

FIGURE 1 | Representative EMG-torque relations at different ankle joint angles from maximum dorsiflexion to maximum plantarflexion **(A–E)**. Overall, the EMG-torque slope on the paretic side (in blue) is greater than on the non-paretic side (in red). Moreover, the more the ankle plantarflexion, the greater the EMG-torque slope. **(F)** Greater changes in the EMG-torque slope on the paretic side with increasing ankle plantarflexion angle.

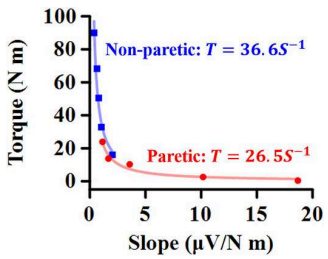

FIGURE 2 | Representative relationship between maximum torque (*T*) at each ankle angle and EMG-torque slope (*S*) at the corresponding angle. The smaller coefficient value, the quicker decay in *T* as *S* increases.

factors were the side (i.e., paretic or non-paretic) and the ankle joint angle. Multiple comparisons were done with Bonferroni adjustment. IBM SPSS Statistics (Version 21, IBM, New York, USA) with the significance level (α) of 0.05. The partial eta squared (η_p^2) was used to report the effect size for each comparison.

Further statistics were tested with a significance level $\alpha < 0.05$, using custom-written software in MATLAB (Mathworks, Natick, USA). The Kolmogorov-Smirnov test was performed to assess the assumption of the normal distribution for the fitting parameters (i.e., the coefficient *a*, *b*, and *c*) as well as ankle joint range of motion. As all the variables did not satisfy the assumption ($p < 0.05$), the Wilcoxon signed-rank test was conducted to evaluate the paired difference in the variables between the paretic and non-paretic sides. Cohen's d_z (35) was then calculated for the standardized mean difference effect size for within-subjects design (36). The data were described as the median value and the interquartile range (IQR).

The Spearman ranked correlation coefficient was calculated to determine the relationship between the relative (i.e., non-paretic/paretic) coefficient *a* and the relative (i.e., paretic/non-paretic) maximum plantarflexion torque, the relative SWS, or the relative muscle thickness. As the coefficient *a* value was greater on the paretic side, the relative coefficient *a* was calculated as the ratio of the non-paretic to the paretic values and thus, the smaller relative coefficient *a* indicates the less efficient muscular contraction on the paretic side compared to the non-paretic side.

RESULTS

The total number of subjects examined was 9 for MG and LG analyses and 8 for SOL and ALL analyses. This is because we excluded the subject when reporting SOL and ALL as the EMG recording from the SOL muscle was not successful in one of our subjects.

Passive Range of Motion at Ankle Joint

The passive range of motion at ankle joint on the paretic side (32.0°; IQR = 30.0–40.0) was significantly smaller by ∼25% than on the non-paretic side (42.0°, IQR = 37.3–45.0) ($p = 0.031$, $d_z = 0.992$). Although the median maximum PF (30.0°, IQR = 30.0–35.3) and DF (−3.0°, IQR = −6.3–1.5) on the paretic side was smaller than on the non-paretic side (PF: 34.0°, IQR = 30.0–37.8; DF: −5.0°, IQR = −11.3 to −3.8), there was no significant side-to-side difference in the maximum PF ($p = 0.156$, $d_z = 0.548$) or in the maximum DF ($p = 0.063$, $d_z = 0.816$).

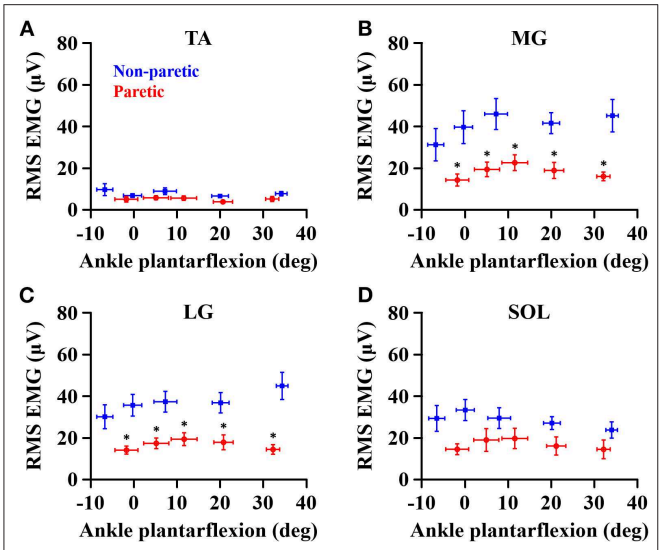

FIGURE 3 | Maximum RMS EMG in tibialis anterior **(A)**, medial gastrocnemius **(B)**, lateral gastrocnemius **(C)**, and soleus **(D)** muscles at each ankle angle. Negative angles indicate dorsiflexion. *a significant difference in pairwise comparisons between the side ($p < 0.05$).

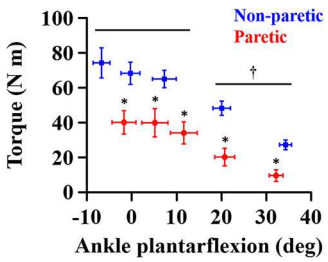

FIGURE 4 | Maximum joint torque at each ankle angle. Negative angles indicate dorsiflexion. *a significant difference in pairwise comparisons between the side ($p < 0.01$). †a significant difference in torque between dorsiflexed angles and plantarflexed angles ($p < 0.05$).

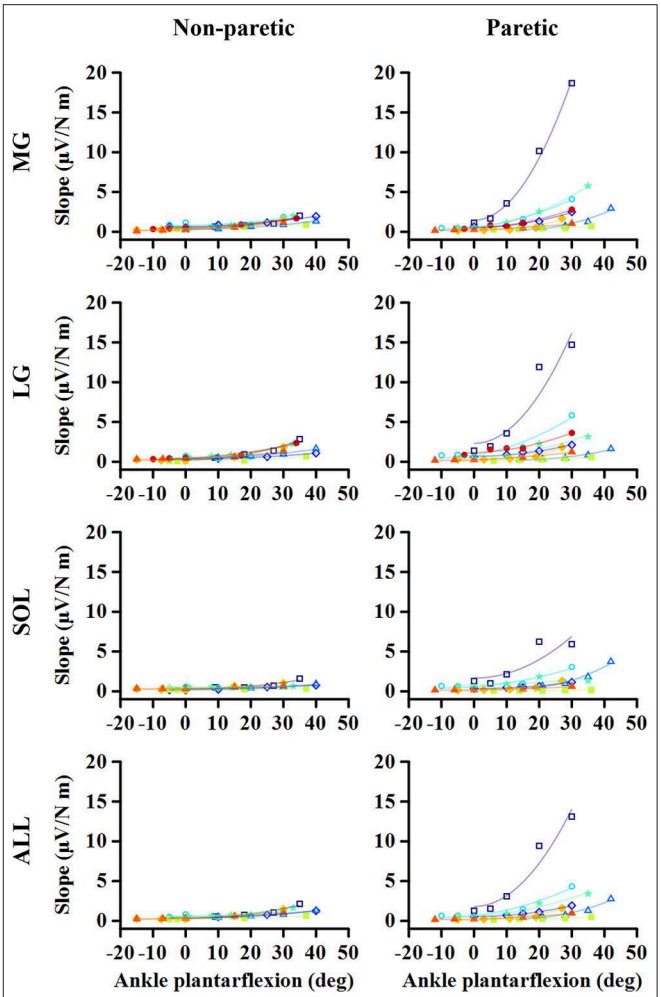

FIGURE 5 | Changes in EMG-torque slope as a function of ankle angle. Note that the effects of changing the ankle angle on the EMG-torque slope are more significant on the paretic side than on the non-paretic side. Markers and lines indicate raw data and fitted results from each individual (in different colors), respectively.

Effect of Joint Angles on Maximum RMS EMG and Joint Torque

When compared to the non-paretic side, the maximum RMS EMG on the paretic side was significantly smaller in the MG ($p = 0.003$, $\eta_p^2 = 0.683$) and LG ($p = 0.003$, $\eta_p^2 = 0.685$) muscles, but not in the TA ($p = 0.122$, $\eta_p^2 = 0.272$) and SOL ($p = 0.096$, $\eta_p^2 = 0.307$) muscles (**Figure 3**). However, the maximum RMS EMG was not a function of the ankle joint angles in all the muscles (TA: $p = 0.104$, $\eta_p^2 = 0.734$; MG: $p = 0.093$, $\eta_p^2 = 0.747$; LG: $p = 0.366$, $\eta_p^2 = 0.521$; SOL: $p = 0.172$, $\eta_p^2 = 0.666$). Moreover, there was no significant interaction between the side and the ankle joint angle in all the muscles (TA: $p = 0.387$, $\eta_p^2 = 0.507$; MG: $p = 0.271$, $\eta_p^2 = 0.586$; LG: $p = 0.247$, $\eta_p^2 = 0.604$; SOL: $p = 0.427$, $\eta_p^2 = 0.481$). Note that the magnitude of TA RMS EMG was considerably smaller than the other muscles, which indicates that the potential effects of muscle co-contraction would likely be negligible.

The overall magnitude of the maximum joint torque on the paretic side was significantly smaller than on the contralateral side ($p = 0.001$, $\eta_p^2 = 0.776$; **Figure 4**), showing significant differences at all the angles ($p < 0.01$). Furthermore, the maximum joint torque increased as the ankle joint became dorsiflexed ($p = 0.029$, $\eta_p^2 = 0.845$), showing that the maximum joint torque at the dorsiflexed angles beyond the neutral angles was significantly greater than at the plantarflexed positions ($p < 0.05$). There was a significant interaction between the side and the ankle joint angle ($p = 0.049$, $\eta_p^2 = 0.808$).

EMG-Torque Relations

As the ankle angle became more plantarflexed, the slope of the EMG-torque relations increased progressively (**Figure 5**). **Table 1** summarizes the coefficient *a* and *b* for each calf muscle and ALL. For the MG muscle, the coefficient *a* on the paretic side was significantly greater than on the non-paretic side ($p =$

TABLE 1 | The coefficient *a* and *b* values for the slope of EMG-torque relations (*S*) and ankle plantarflexion angle (*A*). $S = aA^2 + b$.

	$a^{\#}$		*b*	
	Non-paretic	**Paretic**	**Non-paretic**	**Paretic**
MG ($n = 9$)	0.655 (0.599–0.790)	2.133* (1.183–3.173)	0.41 (0.28–0.52)	0.35 (0.24–0.49)
LG ($n = 9$)	0.740 (0.465–1.063)	1.657* (1.257–2.505)	0.29 (0.23–0.42)	0.46 (0.19–0.80)
SOL ($n = 8$)	0.258 (0.140–0.376)	0.989* (0.383–2.774)	0.29 (0.22–0.36)	0.36 (0.11–0.61)
ALL ($n = 8$)	0.545 (0.419–0.701)	1.709* (0.886–2.633)	0.33 (0.23–0.42)	0.36 (0.18–0.56)

MG, medial gastrocnemius; LG, lateral gastrocnemius; SOL, soleus; ALL, average of MG, LG, and SOL.

#Actual values are x1,000 smaller than reported.

**Significant difference between non-paretic and paretic sides ($p < 0.05$).*

0.008, $d_z = 0.549$), indicating the greater increase in the slope as the ankle joint becomes plantarflexed. There was no significant difference in the coefficient *b* between sides ($p = 0.359$, $d_z = 0.089$), indicating that the slope was not significantly different at the maximum DF angles.

Similar results were found in the other muscles. The coefficient *a* on the paretic side was significantly greater than on the non-paretic side (LG: $p = 0.004$, $d_z = 0.548$; SOL: $p = 0.008$, $d_z = 0.802$; ALL: $p = 0.008$, $d_z = 0.601$), whereas there was no significant difference in the coefficient *b* between sides (LG: $p = 0.250$, $d_z = 0.501$; SOL: $p = 0.547$, $d_z = 0.357$; ALL: $p = 0.945$, $d_z = 0.315$).

Torque-Slope Relations

For all the cases, the maximum voluntary isometric plantarflexion torque was smaller as the slope of the EMG-torque relations was greater (**Figure 6**). **Table 2** summarizes the coefficient *c* for each calf muscle and ALL. The coefficient *c* was significantly smaller on the paretic side than on the non-paretic side (MG: $p = 0.020$, $d_z = 1.190$; SOL: $p = 0.016$, $d_z = 1.326$; ALL: $p = 0.016$, $d_z = 1.321$) except for LG ($p = 0.098$, $d_z = 0.627$). However, the coefficient *c* for pooled data from both sides was not significantly different with the coefficient *c* on the paretic side for all cases (MG: $p = 1.000$, $d_z = 0.053$; LG: $p = 0.074$, $d_z = 0.622$; SOL: $p = 0.109$, $d_z = 0.666$; ALL: $p = 0.742$, $d_z = 0.040$).

Correlation Analysis

A strong linear relationship was observed between the relative coefficient *a* and the relative maximum torque for MG ($r = 0.783$; $p = 0.017$; **Figure 7A**), SOL ($r = 0.762$; $p = 0.037$; **Figure 7C**), and ALL ($r = 0.881$; $p = 0.007$; **Figure 7D**). However, no significant relationship was found for LG ($r = 0.617$; $p = 0.086$; **Figure 7B**).

For the MG muscle, the relative coefficient *a* was smaller as the relative SWS measured at the neutral position was greater ($r = -0.733$; $p = 0.031$; **Figure 8A**). However, the relationship between the relative coefficient *a* and the relative muscle thickness was not significant ($r = 0.017$; $p = 0.982$; **Figure 8B**).

DISCUSSION

To summarize, the purpose of this study was to investigate: (1) the effect of changes in ankle joint angles on the muscular contraction efficiency of the calf muscles (i.e., the slope of EMG-torque relations); (2) the relation between the maximum joint torque at each joint angle and the EMG-torque slope at this angle; and (3) the association between the relative coefficient a and the relative muscle thickness or SWS. This is in order to understand the impact of intrinsic muscular changes on muscular contraction efficiency after stroke.

Our results show that the paretic side has a greater slope coefficient *a* (i.e., more increment in the slope as a function of ankle plantarflexion angle) and smaller *c* (i.e., steeper decay in the maximum torque as a function of the slope). There was also a strong linear relationship between the relative joint torque and the relative coefficient a, in the case of MG, SOL, or ALL. For the MG muscles, the relative coefficient *a* (i.e., muscular contraction efficiency) was negatively correlated with the relative SWS (i.e., muscle stiffness).

The Slope of EMG-Torque Relations Serves as a Measure of Muscular Contraction Efficiency

The greater coefficient *a* on the paretic side indicates that the slope of EMG-torque relations on the paretic side is greater than on the non-paretic side at comparable ankle angles, as also reported earlier (4, 5). Interestingly, the slope of EMG-torque relations has also been used in the field of sports exercise to understand the relative contribution of neural factors and muscle hypertrophy to muscle strength gain in response to muscle strengthening protocol (37). To illustrate, the slope of EMG-torque relations becomes lower as muscle strength increases (37, 38). Although the phenomena induced by training are different (i.e., one is the strength gain due to exercise and the other is strength loss due to injury), the common message may be that the slope of EMG-torque relations is a useful biomarker for muscular contraction efficiency.

Our results showed further that there is a strong relationship between the slope of EMG-torque relations at each joint angle and the normalized maximum joint torque at the corresponding joint angle (**Figure 6**), suggesting that the absolute slope of EMG-torque relations may be used to estimate the maximum joint torque-capacity. We also found that the relative coefficient *a* showed a strong positive relationship with the relative maximum joint torque (**Figure 7**), which further suggests that the relative coefficient *a* may be used as a measure of muscular contraction efficiency. This finding is also supported by earlier findings that a greater increase in the cross-sectional area resulted in a greater decrease in the slope of EMG-torque relations (37).

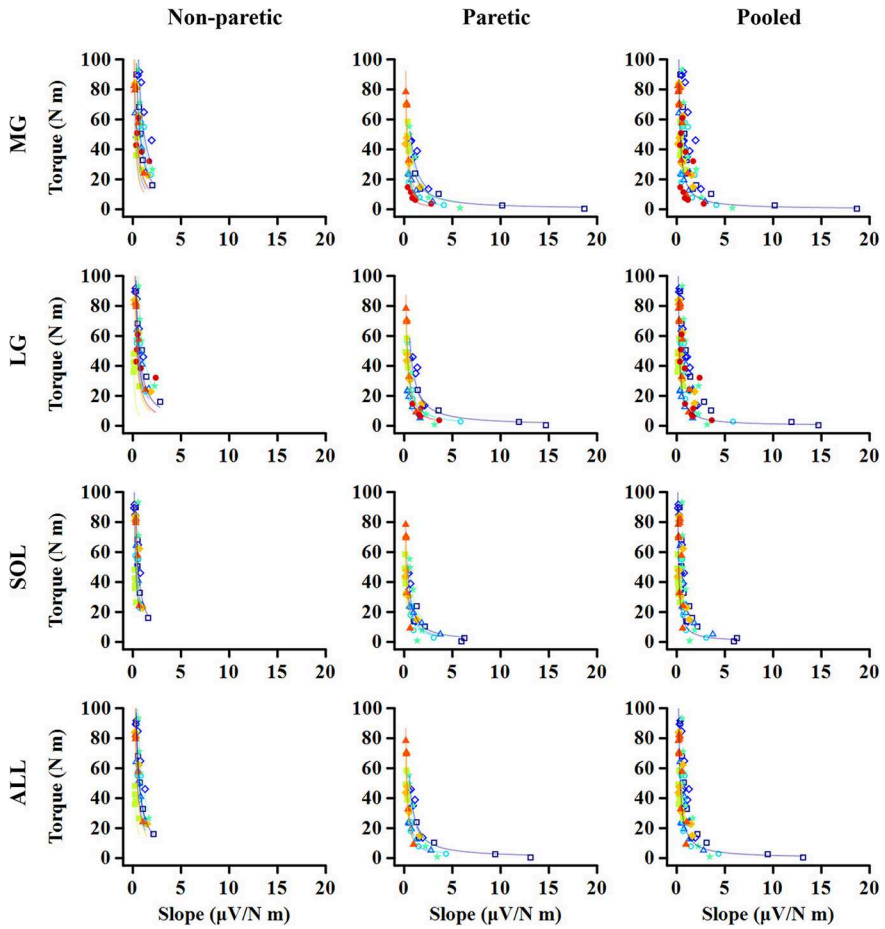

FIGURE 6 | Relationship between maximum torque at each ankle angle and EMG-torque slope at the corresponding angle. Note that the greater slope, the smaller torque. The quicker decay in the torque is shown on the paretic side than on the non-paretic side, whereas there is no significant difference between the paretic and pooled data. Markers and lines indicate raw data and fitted results from each individual (in different colors), respectively.

TABLE 2 | The coefficient *c* values for normalized maximum plantarflexion torque at each joint angle (*T*) and slope of EMG-torque relations (*S*). $T = cS^{-1}$.

	c		
	Non-paretic	**Paretic**	**Pooled**
MG ($n = 9$)	22.77 (17.51–43.63)	15.10* (11.18–27.00)	17.47
LG ($n = 9$)	26.60 (20.51–30.97)	16.38 (12.53–22.11)	13.33
SOL ($n = 8$)	20.82 (17.38–26.57)	13.99* (10.41–19.67)	10.07
ALL ($n = 8$)	26.99 (22.68–33.70)	14.63* (11.91–26.49)	18.02

MG, medial gastrocnemius; LG, lateral gastrocnemius; SOL, soleus; ALL, average of MG, LG, and SOL.

**Significant difference between non-paretic and paretic sides ($p < 0.05$).*

Effect of Joint Angle Changes on the Slope of EMG-Torque Relations

Based on our finding that the magnitude of RMS EMG at all the measured angles was significantly lower in the MG and LG muscles on the paretic side, the reduction in the magnitude of neural drive seems a primary factor contributing to the reduction in maximum joint torque on the paretic side. In addition, we also found that the effects of changes in joint angle on the slope were more significant on the paretic side than on the non-paretic side (i.e., greater coefficient *a*), although the magnitude of RMS EMG on both sides was not significantly different among the joint angles (i.e., relatively consistent magnitude of neural drive). These findings suggest that muscular changes after stroke, such as muscle atrophy, changes muscle architecture, or changes in material properties, can also contribute to the reduction in muscular contraction efficiency.

The slope increase with increasing ankle plantarflexion (i.e., the coefficient *a*) seems to be associated with active muscle force-length properties. As the practical operating range of calf muscles is usually located in the ascending limb of active force-length curve (27–29), the muscle length becomes shorter as the ankle joint becomes more plantarflexed. Given that the magnitude of force production is smaller at shorter muscle length in the ascending limb, the slope of EMG-torque relations will become greater at a shorter length, characterized here as the coefficient *a* in this study. The greater coefficient *a* on the paretic side can then

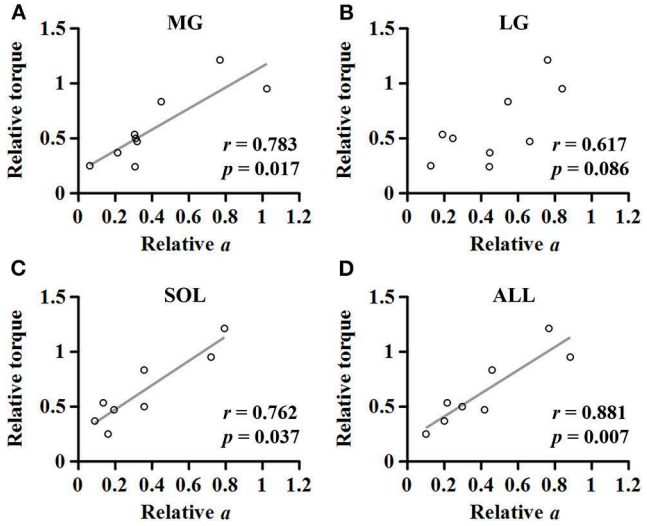

FIGURE 7 | Relationship between the relative maximum torque and the relative coefficient *a* in medial gastrocnemius **(A)**, lateral gastrocnemius **(B)**, soleus **(C)**, and the average of the muscles **(D)**.

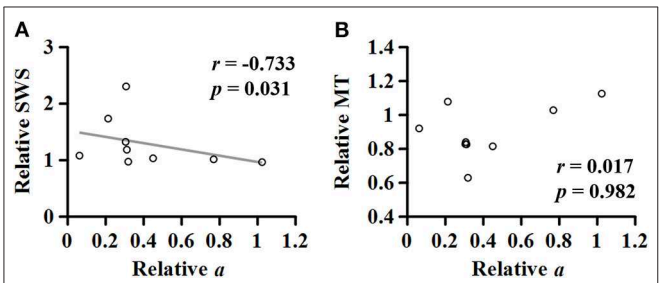

FIGURE 8 | Relationship of the relative (non-paretic/paretic) coefficient *a* with the relative (paretic/non-paretic) shear wave speed (SWS) **(A)** or muscle thickness (MT) **(B)** measured in medial gastrocnemius.

be explained by an altered active force-length curve after stroke such as narrower width of the curve (19) or by an altered torque-angle curve such as shortened range of the curve (3, 20–22). Since the reduction in the magnitude of peak forces at shorter muscle lengths becomes greater with a narrower curve width, the slope of EMG-torque relations is likely greater on the paretic side than on the non-paretic side.

Our correlation analysis revealed a strong negative relationship between the relative coefficient *a* and the relative SWS measured at the neutral ankle position (**Figure 8A**), potentially suggesting that the stiffer the muscle, the lower the muscular contraction efficiency. This result can be supported by an earlier simulation study showing that the increased intramuscular fat on the MG muscle resulted in lower force production for a given muscle activation (39). These observations indicate that altered material properties of muscle tissue can also affect muscular contraction efficiency and thus, further investigations are needed to understand how the connective tissues play a role in the voluntary force production.

We could not establish such a relationship between the relative coefficient *a* and the relative muscle thickness (**Figure 8B**). To better understand this, given a general agreement that the torque-generating capacity is positively correlated with the muscle thickness or cross-sectional area (40), further correlation analyses were conducted (**Figure 9**). Although no significant relationship was found between the relative torque and the relative muscle thickness (**Figure 9A**), there were three data points that seemed as outliers (circles filled with different colors). Interestingly, compared to the non-paretic side, those data points had a relatively well-preserved muscle thickness (**Figure 9B**) but a considerably affected torque-generating capacity (**Figure 9A**) as well as a significant effect of ankle joint angle on the slope of EMG-torque relations characterized by the coefficient *a* in this study (**Figure 9C**). Although it is uncertain, we speculate that those three participants might exhibit a more severe deficit in neural factors rather than in muscular changes. Collectively, it is likely that the relative contributions of neural factors and muscular changes can vary across the clinical spectrum in chronic stroke survivors. Further studies are required to define the relative contribution of both neural factors and muscular changes to voluntary force generating-capacity after stroke.

Limitations

A significant reduction in the RMS EMGs on the paretic side may sometimes be attributed to non-physiological factors. For example, the relative distance/orientation between the surface electrode location and the innervation zone may be different depending on the ankle angle as well as the contraction intensity (especially in a pennate muscle) (41), ultimately affecting our sEMG signals. This is likely because the pennation angle and fiber length of the MG, LG, and SOL each change with ankle plantarflexion as well as with contraction intensity (42).

Moreover, there have also been reports of altered muscle architecture in the calf muscles after stroke (16, 17, 43, 44), potentially leading to different magnitude of such influences across the participants and across the sides. However, such influences were not distinguishable in our results because the maximum RMS EMG at each ankle angle did not significantly differ on both sides and the magnitude in paretic calf muscles was systematically lower than in contralateral muscles at all measured ankle angle (**Figure 3**).

Increasing subcutaneous tissue thickness also tends to decrease the sEMG amplitude (45, 46). However, our ultrasound data showed no significant difference in subcutaneous tissue thickness between sides ($p = 0.055$, $d_z = 0.517$). Moreover, the muscle thickness between sides was not significantly different between sides ($p = 0.074$, $d_z = 0.691$). Based on these observations, it appears that the decreased RMS EMGs on the paretic side may be likely due to a reduction in neural drive rather than to changes in the subcutaneous tissue/muscle thickness.

It is also important to note that the muscle volume or cross-sectional area may not be a good measure of torque-generating capacity likely due to a loss of active muscle fibers and the substitution of non-contractile tissue (15, 47). Accordingly, more detailed characterization of muscular changes after stroke would

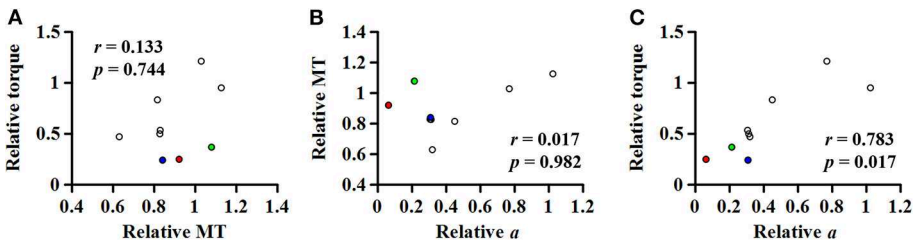

FIGURE 9 | (A) Relationship between the relative (paretic/non-paretic) muscle thickness (MT) and the relative maximum torque. Relationship of the relative (non-paretic/paretic) coefficient *a* with the relative MT **(B)** or the relative torque **(C)**. Note that three data points seem as outliers (circles filled with different colors), which had the relatively well-preserved MT but very low relative coefficient *a*, suggesting that chronic stroke survivors may potentially have the different relative contribution of both neural factors and muscular changes to voluntary force generating-capacity after stroke.

help us better understand underlying mechanisms of inefficient muscular voluntary contraction in chronic stroke survivors.

In addition, the magnitude of load-sharing is not readily estimated during voluntary contraction, and thus the average RMS EMG from the calf muscles was used to estimate the overall contribution to the joint torque. Considering that the calf muscle volume does not seem to be affected in a uniform manner after stroke (47), the average RMS EMG may not be accurate enough to represent the overall contribution.

Body mass normalization for torque data is widely accepted, particularly when strength-related outcomes are compared across individuals with varying body masses (48, 49), given a general agreement that muscle strength is positively related with body mass (50). Although we confirmed that our results were not affected by the normalization, there is an issue with such an approach. This is mainly due to non-uniform muscle atrophy across different muscles as well as changes in muscle composition after stroke (47). It is required to establish a reasonable way to compare strength-related outcomes between sides, accounting for muscular changes such as muscle quality (51, 52).

Lastly, our findings are potentially limited by relatively small sample size and by all male participants and thus, special care should be taken to generalize our findings especially due to gender difference in muscle architecture (53).

CONCLUSION

In summary, this study examined the EMG-torque relations of calf muscles at different ankle joint angles on both paretic and non-paretic sides in chronic hemispheric stroke survivors. The greater slope of the EMG-torque relations was found on the paretic side compared to the non-paretic side at comparable ankle joint angles (i.e., the greater coefficient *a* on the paretic side), indicating that muscular contraction efficiency may be affected after stroke but in a muscle length-dependent and non-uniform manner. Moreover, the relative coefficient *a* showed a strong relationship with the relative ankle plantarflexion torque or the relative SWS, but was not correlated with the relative muscle thickness. Based on such a discrepancy between the relative reduction in torque-generating capacity and in muscle thickness, our findings suggest that the relative contributions of neural factors and intrinsic muscular changes may vary substantially across the range of chronic stroke survivors. Further studies are needed to explore the relative contribution of both neural factors and muscular changes to voluntary force generating-capacity after stroke.

DATA AVAILABILITY STATEMENT

The datasets generated for this study are available on request to the corresponding author.

ETHICS STATEMENT

The studies involving human participants were reviewed and approved by Northwestern University's Institutional Review Board. The patients/participants provided their written informed consent for publication in this study.

AUTHOR CONTRIBUTIONS

This work was conceived, conducted, analyzed, and authored by JS and WR.

FUNDING

This study was supported by grants from the National Institute on Disability, Independent Living, and Rehabilitation Research (90SFGE0005) and the Davee Foundation Stroke Research Seed Grant initiative and the Northwestern University Department of Neurology, Division of Stroke and Neurocritical Care, and from the National Institutes of Health (R01HD089952).

ACKNOWLEDGMENTS

The authors thank all the participants. We are grateful to Andres Cardona for technical preparation for data collection.

REFERENCES

1. Andrews AW, Bohannon RW. Distribution of muscle strength impairments following stroke. *Clin Rehabil.* (2000) 14:79–87. doi: 10.1191/026921500673950113
2. Bohannon RW. Muscle strength and muscle training after stroke. *J Rehabil Med.* (2007) 39:14–20. doi: 10.2340/16501977-0018
3. Ada L, Canning C, Dwyer T. Effect of muscle length on strength and dexterity after stroke. *Clin Rehabil.* (2000) 14:55–61. doi: 10.1191/026921500671430626
4. Tang A, Rymer WZ. Abnormal force–EMG relations in paretic limbs of hemiparetic human subjects. *J Neurol Neurosurg Psychiatr.* (1981) 44:690–8. doi: 10.1136/jnnp.44.8.690
5. Suresh NL, Concepcion NS, Madoff J, Rymer WZ. Anomalous EMG–force relations during low-force isometric tasks in hemiparetic stroke survivors. *Exp Brain Res.* (2015) 233:15–25. doi: 10.1007/s00221-014-4061-3
6. Andreassen S, Rosenfalck A. Impaired regulation of the firing pattern of single motor units. *Muscle Nerve.* (1978) 1:416–8. doi: 10.1002/mus.880010514
7. Frontera WR, Grimby L, Larsson L. Firing rate of the lower motoneuron and contractile properties of its muscle fibers after upper motoneuron lesion in man. *Muscle Nerve.* (1997) 20:938–47. doi: 10.1002/(SICI)1097-4598(199708)20:8<;938::AID-MUS2>;3.0.CO;2-7
8. Gemperline JJ, Allen S, Walk D, Rymer WZ. Characteristics of motor unit discharge in subjects with hemiparesis. *Muscle Nerve.* (1995) 18:1101–14. doi: 10.1002/mus.880181006
9. Mottram CJ, Heckman CJ, Powers RK, Rymer WZ, Suresh NL. Disturbances of motor unit rate modulation are prevalent in muscles of spastic-paretic stroke survivors. *J Neurophysiol.* (2014) 111:2017–28. doi: 10.1152/jn.00389.2013
10. Hu X, Suresh AK, Rymer WZ, Suresh NL. Assessing altered motor unit recruitment patterns in paretic muscles of stroke survivors using surface electromyography. *J Neural Eng.* (2015) 12:066001. doi: 10.1088/1741-2560/12/6/066001
11. Hu X, Suresh AK, Rymer WZ, Suresh NL. Altered motor unit discharge patterns in paretic muscles of stroke survivors assessed using surface electromyography. *J Neural Eng.* (2016) 13:046025. doi: 10.1088/1741-2560/13/4/046025
12. Shin H, Suresh NL, Rymer WZ, Hu X. Relative contribution of different altered motor unit control to muscle weakness in stroke: a simulation study. *J Neural Eng.* (2018) 15:016014. doi: 10.1088/1741-2552/aa925d
13. Zhou P, Suresh NL, Rymer WZ. Model based sensitivity analysis of EMG–force relation with respect to motor unit properties: applications to muscle paresis in stroke. *Ann Biomed Eng.* (2007) 35:1521–31. doi: 10.1007/s10439-007-9329-3
14. Gray V, Rice CL, Garland SJ. Factors that influence muscle weakness following stroke and their clinical implications: a critical review. *Physiother Canada.* (2012) 64:415–26. doi: 10.3138/ptc.2011-03
15. Knarr BA, Ramsay JW, Buchanan TS, Higginson JS, Binder-Macleod SA. Muscle volume as a predictor of maximum force generating ability in the plantar flexors post-stroke. *Muscle Nerve.* (2013) 48:971–6. doi: 10.1002/mus.23835
16. Dias CP, Freire B, Goulart NBA, Onzi ES, Becker J, Gomes I, et al. Muscle architecture and torque production in stroke survivors: an observational study. *Top Stroke Rehabil.* (2017) 24:206–13. doi: 10.1080/10749357.2016.1210873
17. Son J, Rymer WZ, Lee SSM. Limited fascicle shortening and fascicle rotation may be associated with impaired voluntary force-generating capacity in pennate muscles of chronic stroke survivors. *Clin. Biomech*. (accepted).
18. Gordon AM, Huxley AF, Julian FJ. The variation in isometric tension with sarcomere length in vertebrate muscle fibres. *J Physiol.* (1966) 184:170–92. doi: 10.1113/jphysiol.1966.sp007909
19. Gao F, Zhang L-Q. Altered contractile properties of the gastrocnemius muscle poststroke. *J Appl Physiol.* (2008) 105:1802–8. doi: 10.1152/japplphysiol.90930.2008
20. Ada L, Canning CG, Low SL. Stroke patients have selective muscle weakness in shortened range. *Brain.* (2003) 126:724–31. doi: 10.1093/brain/awg066
21. Koo TK, Mak AF, Hung LK, Dewald JP. Joint position dependence of weakness during maximum isometric voluntary contractions in subjects with hemiparesis. *Arch Phys Med Rehabil.* (2003) 84:1380–6. doi: 10.1016/S0003-9993(03)00238-7
22. Lomaglio MJ, Eng JJ. Nonuniform weakness in the paretic knee and compensatory strength gains in the nonparetic knee occurs after stroke. *Cerebrovasc Dis.* (2008) 26:584–91. doi: 10.1159/000165111
23. Purslow PP. Strain-induced reorientation of an intramuscular connective tissue network: Implications for passive muscle elasticity. *J Biomech.* (1989) 22:21–31. doi: 10.1016/0021-9290(89)90181-4
24. Hodgson JA, Chi S-W, Yang JP, Chen J-S, Edgerton VR, Sinha S. Finite element modeling of passive material influence on the deformation and force output of skeletal muscle. *J Mech Behav Biomed Mater.* (2012) 9:163–83. doi: 10.1016/j.jmbbm.2012.01.010
25. Gindre J, Takaza M, Moerman KM, Simms CK. A structural model of passive skeletal muscle shows two reinforcement processes in resisting deformation. *J Mech Behav Biomed Mater.* (2013) 22:84–94. doi: 10.1016/j.jmbbm.2013.02.007
26. Azizi E, Deslauriers AR, Holt NC, Eaton CE. Resistance to radial expansion limits muscle strain and work. *Biomech Model Mechanobiol.* (2017) 16:1633–43. doi: 10.1007/s10237-017-0909-3
27. Ishikawa M, Pakaslahti J, Komi PV. Medial gastrocnemius muscle behavior during human running and walking. *Gait Posture.* (2007) 25:380–4. doi: 10.1016/j.gaitpost.2006.05.002
28. Arnold EM, Delp SL. Fibre operating lengths of human lower limb muscles during walking. *Philos Trans R Soc Lond B Biol Sci.* (2011) 366:1530–9. doi: 10.1098/rstb.2010.0345
29. Jonas R, Neville JP, Heok OL, Gavin JP, Damian GS. On the ascent: the soleus operating length is conserved to the ascending limb of the force–length curve across gait mechanics in humans. *J Exp Biol.* (2012) 215:3539–51. doi: 10.1242/jeb.070466
30. Bercoff J, Tanter M, Fink M. Supersonic shear imaging: A new technique for soft tissue elasticity mapping. *IEEE Trans Ultrason Ferroelectr Freq Control.* (2004) 51:396–409. doi: 10.1109/TUFFC.2004.1295425
31. Lee SSM, Spear S, Rymer WZ. Quantifying changes in material properties of stroke-impaired muscle. *Clin Biomech.* (2015) 30:269–75. doi: 10.1016/j.clinbiomech.2015.01.004
32. Jakubowski KL, Terman A, Santana RVC, Lee SSM. Passive material properties of stroke-impaired plantarflexor and dorsiflexor muscles. *Clin Biomech.* (2017) 49:48–55. doi: 10.1016/j.clinbiomech.2017.08.009
33. Franchi MV, Longo S, Mallinson J, Quinlan JI, Taylor T, Greenhaff PL, et al. Muscle thickness correlates to muscle cross-sectional area in the assessment of strength training-induced hypertrophy. *Scand J Med Sci Sports.* (2018) 28:846–53. doi: 10.1111/sms.12961
34. Lacourpaille L, Hug F, Nordez A. Influence of passive muscle tension on electromechanical delay in humans. *PLoS ONE.* (2013) 8:e53159. doi: 10.1371/journal.pone.0053159
35. Cohen J. *Statistical Power Analysis for the Behavioral Sciences*. New York, NY: Routledge Academic (1988).
36. Lakens D. Calculating and reporting effect sizes to facilitate cumulative science: a practical primer for t-tests and ANOVAs. *Front Psychol.* (2013) 4:863. doi: 10.3389/fpsyg.2013.00863
37. Moritani T, Devries HA. Neural factors versus hypertrophy in the time course of muscle strength gain. *Am J Phys Med Rehabil.* (1979) 58:115–30.
38. Devries HA. "Efficiency of electrical activity" as a physiological measure of the functional state of muscle tissue. *Am J Phys Med.* (1968) 47:10–22.
39. Rahemi H, Nigam N, Wakeling JM. The effect of intramuscular fat on skeletal muscle mechanics: Implications for the elderly and obese. *J R Soc Interface.* (2015) 12:20150365. doi: 10.1098/rsif.2015.0365
40. Bamman MM, Newcomer BR, Larson-Meyer DE, Weinsier RL, Hunter GR. Evaluation of the strength-size relationship *in vivo* using various muscle size indices. *Med Sci Sports Exerc.* (2000) 32:1307–13. doi: 10.1097/00005768-200007000-00019
41. De Luca CJ. The use of surface electromyography in biomechanics. *J Appl Biomech.* (1997) 13:135–63. doi: 10.1123/jab.13.2.135
42. Maganaris CN, Baltzopoulos V, Sargeant AJ. *In vivo* measurements of the triceps surae complex architecture in man: implications for muscle function. *J Physiol.* (1998) 512:603–14. doi: 10.1111/j.1469-7793.1998.603be.x

43. Gao F, Grant TH, Roth EJ, Zhang L-Q. Changes in passive mechanical properties of the gastrocnemius muscle at the muscle fascicle and joint levels in stroke survivors. *Arch Phys Med Rehabil.* (2009) 90:819–26. doi: 10.1016/j.apmr.2008.11.004
44. Zhao H, Ren Y, Roth EJ, Harvey RL, Zhang L-Q. Concurrent deficits of soleus and gastrocnemius muscle fascicles and Achilles tendon post stroke. *J Appl Physiol.* (2015) 118:863–71. doi: 10.1152/japplphysiol.00226.2014
45. Kuiken TA, Lowery MM, Stoykov NS. The effect of subcutaneous fat on myoelectric signal amplitude and cross-talk. *Prosthet Orthot Int.* (2003) 27:48–54. doi: 10.3109/03093640309167976
46. Nordander C, Willner J, Hansson GÅ, Larsson B, Unge J, Granquist L, et al. Influence of the subcutaneous fat layer, as measured by ultrasound, skinfold calipers and BMI, on the EMG amplitude. *Eur J Appl Physiol.* (2003) 89:514–9. doi: 10.1007/s00421-003-0819-1
47. Ramsay JW, Barrance PJ, Buchanan TS, Higginson JS. Paretic muscle atrophy and non-contractile tissue content in individual muscles of the post-stroke lower extremity. *J Biomech.* (2011) 44:2741–6. doi: 10.1016/j.jbiomech.2011.09.001
48. Aasa U, Jaric S, Barnekow-Bergkvist M, Johansson H. Muscle strength assessment from functional performance tests: role of body size. *J Strength Condition Res.* (2003) 17:664–70. doi: 10.1519/00124278-200311000-00007
49. Nuzzo JL, Mayer JM. Body mass normalization for isometric tests of muscle endurance. *J Strength Condition Res.* (2013) 27:2039–45. doi: 10.1519/JSC.0b013e3182736203
50. Frontera WR, Hughes VA, Lutz KJ, Evans WJ. A cross-sectional study of muscle strength and mass in 45- to 78-yr-old men and women. *J Appl Physiol.* (1991) 71:644–50. doi: 10.1152/jappl.1991.71.2.644
51. Ismail C, Zabal J, Hernandez HJ, Woletz P, Manning H, Teixeira C, et al. Diagnostic ultrasound estimates of muscle mass and muscle quality discriminate between women with and without sarcopenia. *Front Physiol.* (2015) 6:302. doi: 10.3389/fphys.2015.00302
52. Lees MJ, Wilson OJ, Hind K, Ispoglou T. Muscle quality as a complementary prognostic tool in conjunction with sarcopenia assessment in younger and older individuals. *Eur J Appl Physiol.* (2019) 119:1171–81. doi: 10.1007/s00421-019-04107-8
53. Chow RS, Medri MK, Martin DC, Leekam RN, Agur AM, Mckee NH. Sonographic studies of human soleus and gastrocnemius muscle architecture: gender variability. *Eur J Appl Physiol.* (2000) 82:236–44. doi: 10.1007/s004210050677

Conflict of Interest: The authors declare that the research was conducted in the absence of any commercial or financial relationships that could be construed as a potential conflict of interest.

frontiers in Neurology

ORIGINAL RESEARCH
published: 15 April 2020
doi: 10.3389/fneur.2020.00231

Characterization of Forearm Muscle Activation in Duchenne Muscular Dystrophy via High-Density Electromyography: A Case Study on the Implications for Myoelectric Control

Kostas Nizamis[1], Noortje H. M. Rijken[2], Robbert van Middelaar[1], João Neto[3], Bart F. J. M. Koopman[1] and Massimo Sartori[1]*

[1] Department of Biomechanical Engineering, Technical Medical Centre, University of Twente, Enschede, Netherlands, [2] Faculty Physical Activity and Health, Saxion University of Applied Sciences, Enschede, Netherlands, [3] Faculty of Sciences, University of Lisbon, Lisbon, Portugal

OPEN ACCESS

Edited by:
Xiaogang Hu, University of North Carolina at Chapel Hill, United States

Reviewed by:
Giacinto Luigi Cerone, Politecnico di Torino, Italy
Alberto Ranavolo, Istituto Nazionale per l'Assicurazione Contro gli Infortuni sul Lavoro (INAIL), Italy

***Correspondence:**
Kostas Nizamis
k.nizamis@utwente.nl

Specialty section:
This article was submitted to Neurorehabilitation, a section of the journal Frontiers in Neurology

Received: *18 December 2019*
Accepted: *11 March 2020*
Published: *15 April 2020*

Citation:
Nizamis K, Rijken NHM, van Middelaar R, Neto J, Koopman BFJM and Sartori M (2020) Characterization of Forearm Muscle Activation in Duchenne Muscular Dystrophy via High-Density Electromyography: A Case Study on the Implications for Myoelectric Control. Front. Neurol. 11:231. doi: 10.3389/fneur.2020.00231

Duchenne muscular dystrophy (DMD) is a genetic disorder that results in progressive muscular degeneration. Although medical advances increased their life expectancy, DMD individuals are still highly dependent on caregivers. Hand/wrist function is central for providing independence, and robotic exoskeletons are good candidates for effectively compensating for deteriorating functionality. Robotic hand exoskeletons require the accurate decoding of motor intention typically via surface electromyography (sEMG). Traditional low-density sEMG was used in the past to explore the muscular activations of individuals with DMD; however, it cannot provide high spatial resolution. This study characterized, for the first time, the forearm high-density (HD) electromyograms of three individuals with DMD while performing seven hand/wrist-related tasks and compared them to eight healthy individuals (all data available online). We looked into the spatial distribution of HD-sEMG patterns by using principal component analysis (PCA) and also assessed the repeatability and the amplitude distributions of muscle activity. Additionally, we used a machine learning approach to assess DMD individuals' potentials for myocontrol. Our analysis showed that although participants with DMD were able to repeat similar HD-sEMG patterns across gestures (similarly to healthy participants), a fewer number of electrodes was activated during their gestures compared to the healthy participants. Additionally, participants with DMD activated their muscles close to maximal contraction level (0.63 ± 0.23), whereas healthy participants had lower normalized activations (0.26 ± 0.2). Lastly, participants with DMD showed on average fewer PCs (3), explaining 90% of the complete gesture space than the healthy (5). However, the ability of the DMD participants to produce repeatable HD-sEMG patterns was unexpectedly comparable to that of healthy participants, and the same holds true for their offline myocontrol performance, disproving our hypothesis and suggesting a clear potential for the myocontrol of wearable exoskeletons. Our findings present evidence for the first

time on how DMD leads to progressive alterations in hand/wrist motor control in DMD individuals compared to healthy. The better understanding of these alterations can lead to further developments for the intuitive and robust myoelectric control of active hand exoskeletons for individuals with DMD.

Keywords: Duchenne muscular dystrophy, forearm, hand, high-density surface electromyography, motor control, myocontrol, principal component analysis (PCA), wrist

INTRODUCTION

Duchenne muscular dystrophy (DMD) is an X chromosome-linked recessive neuromuscular disease (1). The absence of dystrophin causes progressive weakness of skeletal, respiratory, and cardiac muscles and leads to severe physical disability and shortened life expectancy (2). Improved care standards and the recent introduction of assisted ventilation, in the later stages of the disease, contributed to the increase of their life span (3). This has led to increasing numbers of adults with DMD (4) who experience low quality of life and external aid dependency (5, 6).

In DMD individuals, the support of the upper extremity is central for ensuring daily life independence (7). Wearable devices such as hand/wrist exoskeletons can provide a functional solution by assisting individuals with DMD in performing activities of daily living (ADL) (7). However, dynamic active hand support currently remains a challenge (4), with passive hand orthoses (8) still representing the main clinical approach. Bushby et al. (9, 10) suggested that the treatment of individuals with DMD should become more multidisciplinary as well as promote further the use of technology. However, the effective use of active orthoses requires the accurate decoding of motor intention, which represents an important yet not well-addressed challenge (11).

The clinical golden standard for non-invasive motor intention decoding (12), control of robotic devices (13), and characterization of muscle activity (14) is low-density surface electromyography (sEMG). The most common approach involves bipolar sEMG, where muscle activation is measured with the placement of two closely placed electrodes above the muscle belly (15, 16). sEMG is currently biased by superposition of electrical potentials that compromise signal amplitude estimation, the need for identifying optimal electrode placement, skin–electrode impedance, power line interference, and physiological properties (intermuscular fat, skin humidity, etc.) (15). Despite the fact that sEMG is broadly used in amputee research (14, 17–19) to characterize forearm activity, in degenerative disorders such as DMD, there is a lack of understanding on how these individuals activate their forearm muscles to achieve functionally relevant tasks. A possible way to address this challenge is the use of high-density sEMG (HD-sEMG).

HD-sEMG is a non-invasive technique that collects high-resolution myoelectric signals from tens of monopolar electrodes, i.e., >60 electrodes simultaneously (20). With respect to conventional low-density approaches, HD-sEMG enables determining how large muscles, such as those in the human forearm, activate not only in the temporal domain but also in the spatial domain (14). This information can be used to create heatmaps encoding the spatial distribution of HD-sEMG amplitudes during different hand/wrist-related tasks (19). Such heatmaps can capture distinct HD-sEMG patterns associated to specific tasks, plus variations in amplitude, and repeatability over time. This is central for taking into account the manifestation of inhomogeneities in the control of the muscular fibers, something crucial to understand in pathological muscle activation (21). Moreover, this can be used to explore myocontrol in pathological populations when combined with currently used machine learning classification techniques (22). Currently, HD-sEMG is performed with a large number of cables and is biased by heavy and sizable amplifiers which limit its use in dynamic situations, such as the control of wearable exoskeletons (23).

HD-sEMG spatiotemporal analysis and pattern recognition were never applied to DMD individuals. The use of HD-sEMG can give insights in dimensionality and spatiotemporal similarity between healthy and DMD participant and additionally open a window to study hand/wrist motor control in DMD via a number of analyses and understand the hierarchical motor control in DMD and differences with respect to healthy people. Repeatability, spatial distribution, and distinguishability of HD-sEMG patterns together with HD-sEMG classification performance are important requirements for understanding the altered DMD motor control and use our findings in the context of robotic exoskeleton applications.

In this paper, we characterize HD-sEMGs of three individuals with DMD during seven hand/wrist-related tasks and compare with a baseline of eight healthy participants. This work is motivated by the near absence of a systematic and detailed spatiotemporal characterization of forearm muscle activations in individuals with DMD. First, we create HD-sEMG heatmaps and analyze them with principal component analysis (PCA) to identify the number of orthogonal muscle activation spatiotemporal patterns. Second, we characterize the ability of DMD individuals to produce repeatable and spatiotemporally distinguishable HD-sEMG patterns across tasks, as well as their amplitude distribution. Third, we employ pattern recognition to quantify the potential of each DMD individual to perform activities as those required for the control of assistive robotic exoskeletons. We hypothesize that participants with DMD will show lower activations, they will perform less repeatable patterns and show differences in dimensionality because DMD's central nervous system (CNS) acts on an impaired musculoskeletal apparatus, which may in turn lead to CNS adaptations. Finally, we hypothesize that myocontrol performance will be lower in DMD compared to the healthy participants.

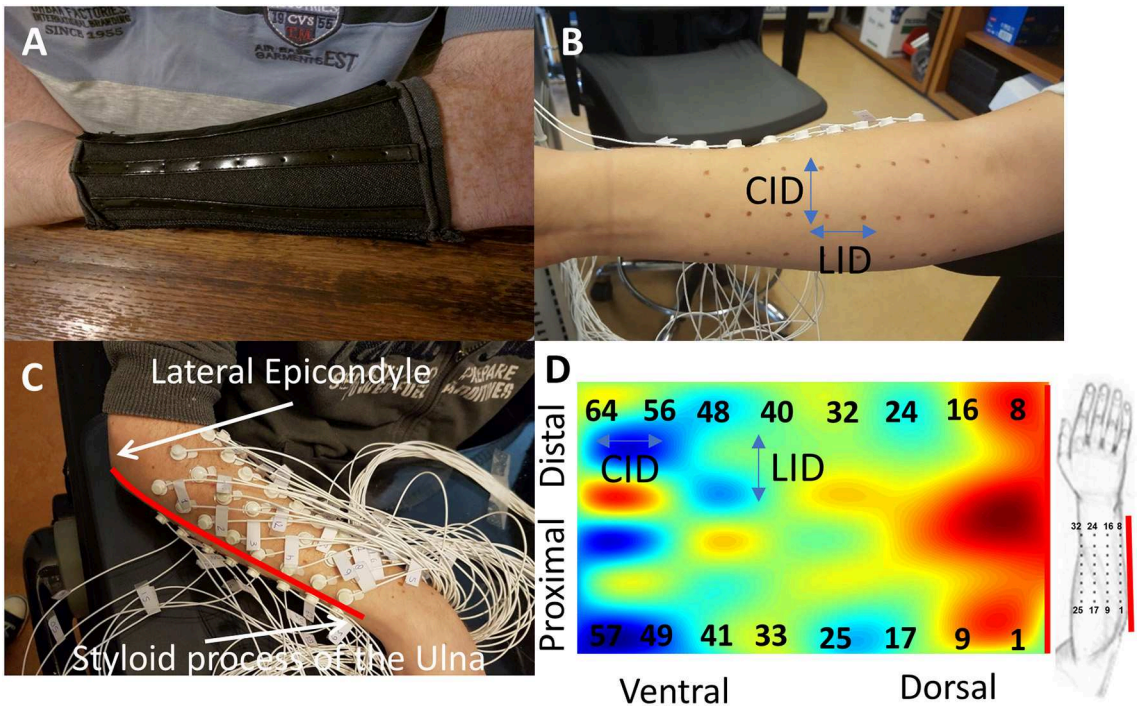

FIGURE 1 | The figure shows the process of the electrode placement. **(A)** The flexible custom-made sleeve that was used for marking the skin of the participant. The sleeve is flexible only around the circumferal direction and stiff along the longitudinal direction of the arm. **(B)** The marked skin of the participant. The longitudinal inter-electrode distance (LID) is fixed at 2 cm (L), while the circumferal inter-electrode distance (CID) depends on the forearm width of each participant. **(C)** The participant with all the 64 electrodes placed. The imaginary line (red line) that connects the lateral epicondyle and the styloid process of the ulna was used as the border between the dorsal and ventral side of the forearm. The placement of the electrodes starts right above this line, with electrode number one placed proximally (at 20% of forearm length from the elbow) and eight distally. The rest of the electrode rows are placed counterclockwise as someone is looking at his right arm. **(D)** This way, electrodes 1–32 were placed over the dorsal side (see sketch) and 33–64 over the ventral side of the forearm. The center of gravity (COG) is also shown for this gesture.

MATERIALS AND METHODS

Participants

The experiment was carried out by seven healthy female and one male adults (age: 21.4 ± 1.2 years, forearm length: 24.8 ± 1.8 cm, forearm circumference at 20% of length: 25.9 ± 1.8 cm), without any hand-related impairment, and three male adults with DMD (age: 22.3 ± 2.5 years, forearm length: 24.2 ± 2.9 cm, forearm circumference at 20% of length: 25.5 ± 3.9 cm).

The DMD participants had different levels of hand function. Participant one (DP1, 20 years old) was able to use his hands functionally, and no contractures relevant to hand/wrist movement were observed. Participant two (DP2, 22 years old) was able to functionally use his hand but experienced a decrease in strength and minimal contractures relevant to hand/wrist movement. Participant three (DP3, 25 years old) was not able to use his hands at all and was affected by immediate onset of fatigue during its use. Extensive contractures relevant to finger movement were observed, and only minimal movement of the fingers was possible (see **Supplementary Video**). All participants were able to perform the experimental protocol.

The Medical Ethics Committee of Twente approved the study design, the experimental protocol, and the procedures (Protocol number: NL59061.044.16). The study was conducted according to the ethical standards given in the Declaration of Helsinki in 1975, as revised in 2008.

Experimental Setup and Signal Acquisition

The experimental setup (**Figure 1**) included several components, and it was designed to record HD-sEMG signals from the forearm in a repeatable and systematic way. Muscular activity was measured with a 128-channel amplification system (REFA 128 model, TMS International, Oldenzaal, The Netherlands). We used 64 monopolar electrodes around the forearm to acquire the raw sEMG signals. The signals were recorded with a decimal gain of 26.55 before the analog-to-digital converter (ADC); however, this gain factor is compensated by the acquisition software (Polybench, TMS International, Oldenzaal, The Netherlands), after the ADC. Additionally, REFA includes a first-order analog low-pass filter placed before the ADC with a −3 db point at 6.8 kHz. The 6.8-kHz low pass helps to make the REFA immune to high-frequency electromagnetic interference such as mobile phone networks. The analog signals were sampled with a frequency of 2,048 Hz and digitally converted with a 24-bit conversion (a resolution of 0.018 μV per bit, 300 mV dynamic range). The ADC of the device has an anti-aliasing digital low-pass filter with a cutoff frequency of 0.2 * sample frequency. This

TABLE 1 | Participant information.

Participant	Dominant arm	Forearm length (20%) (cm)	LID (cm)	At 20% of forearm length from the elbow	
				Forearm circumference (cm)	CID (cm)
HP1	R	26 (5.2)	2	27	3.38
HP2	R	23 (4.6)	2	24	3
HP3	R	28 (5.6)	2	26	3.25
HP4	R	26 (5.2)	2	27	3.38
HP5	R	22.5 (4.5)	2	23.5	2.94
HP6	R	24 (4.8)	2	25	3.13
HP7	R	24 (4.8)	2	26	3.25
HP8	R	25 (5)	2	29	3.63
DP1	L	23 (4.6)	2	27.5	3.4
DP2	R	27.5 (5.5)	2	28	3.5
DP3	R	22 (4.4)	2	21	2.63

HP denotes the healthy participants and DP the participants with Duchenne muscular dystrophy (DMD). LID and CID denote the longitudinal and circumferal inter-electrode distance, respectively.

filter inside the ADC is used to convert the 1-bit signal with a high frequency into a 24-bit signal with a lower frequency. The acquisition software was executed in a host laptop (Lenovo Thinkpad T490, Lenovo, Beijing, China) with a Windows 10 operating system (Microsoft Corporation, Washington, USA). A computer screen was used to provide visual feedback of the task to the participants.

Electrode placement and configuration were based on previous work (19) that normalized the electrode locations to each participant's arm circumference in order to account for different forearm thicknesses (**Table 1**). The inter-electrode distance in the longitudinal direction of the forearm was kept constant at 2 cm for covering the entire forearm (24).

First, we cleaned the skin of the dominant forearm of the participant with alcohol. Then, we measured the forearm length from the lateral epicondyle until the styloid process of the ulna and the forearm circumference at 20% of the forearm length from the elbow (**Figure 1**). The participant had to wear a perforated sleeve (**Figure 1**) with equally placed holes and elastic only along the circumferal direction to ensure that the electrode placement was standardized for all participants. We used a non-permanent marker to mark the skin of the participant (**Figure 1**) and then visually inspect the markings before applying the electrodes.

Conductive gel was applied to each of the 64 electrodes with a syringe, and they were subsequently attached to the forearm. The first row of electrodes was placed above the imaginary line between the lateral epicondyle and the styloid process of the ulna and the last row below in such a way that the line lay in the middle between the two rows of electrodes (**Figure 1**). The first electrode was attached proximally starting at the 20% of the forearm length from the elbow. Electrodes were placed from proximal to distal and in counterclockwise direction (from the perspective of a right-handed participant). This way, electrodes 1–32 were placed over the dorsal side (mostly extensor muscles) and 33–64 over the ventral side (mostly flexor muscles) of the forearm. The reference electrode was placed at the distal end of the forearm, over the head of the ulna.

Participants performed seven different gestures involving hand and wrist motions (**Figure 2**). The chosen gestures included: hand open/close, thumb flexion/extension, wrist flexion/extension, and index extension. These were chosen as they are involved in the most frequent ADL (25). First, each participant was instructed to perform all gestures without constraints (dynamic) with maximal voluntary effort in a single recording. This way, we recorded the maximum voluntary contraction (MVC) for every electrode across all gestures. For every gesture, 10 repetitions of 3 s contractions were performed, together with 10 repetitions of 3-s resting periods between the contractions (**Figure 2**). The participants were instructed to perform all movements in a comfortable fashion in order to avoid forceful contractions that may elicit co-contractions of agonist–antagonist muscle groups.

The timing of the gestures was dictated with the use of visual feedback. The visual feedback illustrated via photographs of human hands which gesture had to be performed. The sequence of images served to instruct the participant as a metronome when to perform the gesture (image of gesture appearing for 3 s) and when to relax (image of relaxed hand appearing for 3 s). Additionally, the measurements were performed in the morning in order to avoid effects of the end-of-the-day fatigue, especially for the participants with DMD. Furthermore, the participants had short breaks between gestures in order to rest.

Signal Processing and Analysis

All signal processing and data analyses were performed in Matlab 2018b software (The MathWorks Inc., USA). The raw sEMG signals were processed offline in order to compute the envelopes for each of the 64 electrodes per gesture and per participant. First, the raw data were filtered with a band-pass filter (fourth-order Butterworth, 20–450 Hz). Additionally, a second-order digital infinite impulse response notch filter (cutoff frequency of 50 Hz, Q factor of 50) was used to remove the power line noise (50 Hz for the EU). Despite its main limitation (signal distortion around the attenuated frequency), notch filtering is the mainstream technique for powerline signal removal (26), and a narrow bandwidth with a high Q factor can already address this (27). For highly powerline-contaminated signals, spectral interpolation may be more appropriate (27). The signals were subsequently rectified and filtered with a low-pass filter (third-order Butterworth, 2 Hz). Our choice for the cutoff frequency was motivated by the low-frequency dynamic tasks involved in this study (28) and our previous study on real-time sEMG control of a hand exoskeleton (29). The resulting envelopes were visually inspected segmented, according to the acquisition protocol, to 10 contractions and periods (each lasting approximately 3 s) and normalized. A threshold was selected to define the onset of the activity, and the next 3 s after the onset were chosen as a contraction period. The threshold was defined as the time that the signal exceeded 10 standard deviations of the baseline (non-contraction) activity similar to Di Fabio (30), and the final segmentation was additionally assessed visually. The maximum

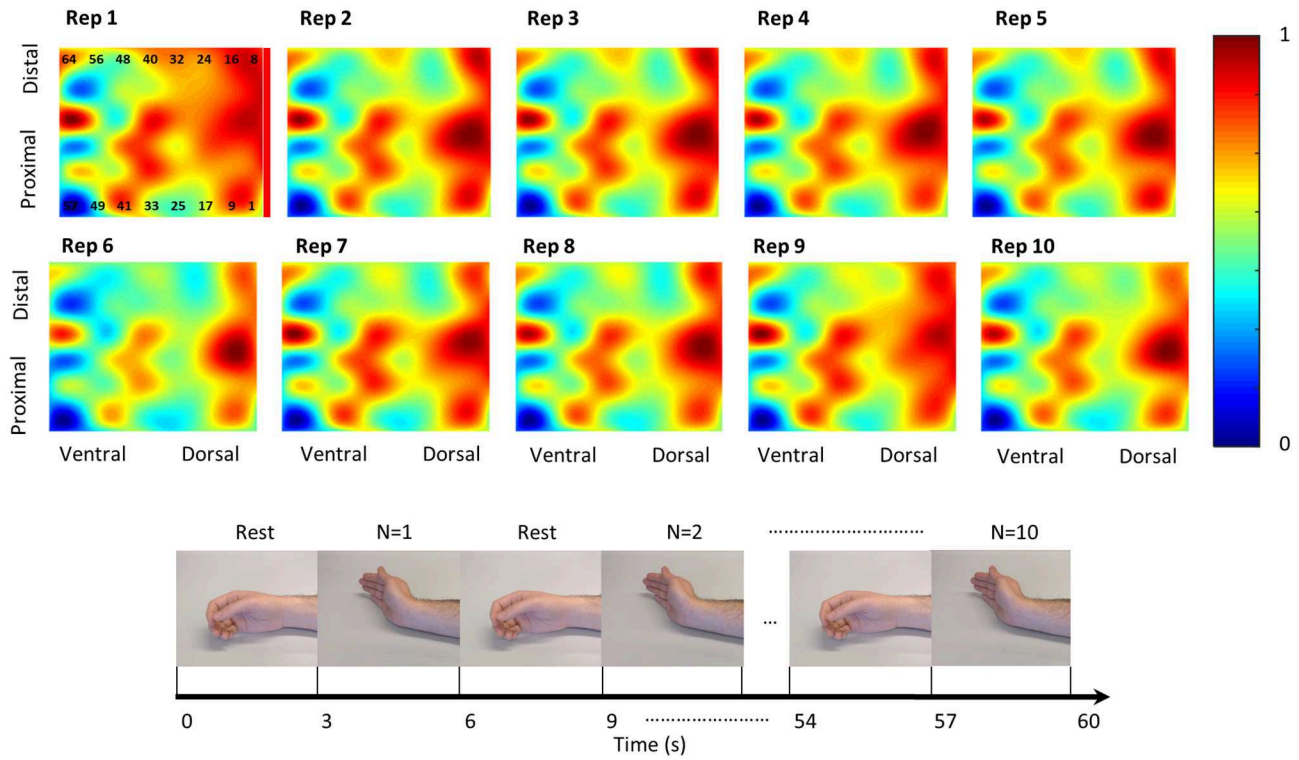

FIGURE 2 | The 10 repetitions of third Duchenne muscular dystrophy (DMD) participant (DP3) for wrist extension that were used to acquire the average normalized map. The lower part shows an example of the protocol followed to record the data. In this example, the participant was instructed to extend his wrist for 3 s and then rest for 3 s. This was repeated 10 times. The same procedure was followed for all the seven gestures.

value of the envelope of each electrode across the complete dataset was used as a normalization value for each electrode. This value was acquired using a moving average window of 1 s in order to account for signal artifacts. Signal quality was visually assessed both in the time and frequency domains, and faulty channels were replaced by linear interpolation of their surrounding neighboring channels (8-neighborhood) (14). Different local conditions were applied to faulty electrodes placed in the longitudinal extremes (<8 neighboring channels).

Every 3-s contraction was further segmented in 1-s segments by keeping only the middle second of the contraction (steady-state phase) and discarding the transient phase (31). For every electrode, the average of this 1-s contraction was calculated and used to construct 10 heatmaps per gesture (**Figure 2**). For the visual inspection of the forearm activity per gesture, we constructed activity heatmaps by averaging the 10 repetition heatmaps (**Figure 3**).

We analyzed the data to assess HD-sEMG pattern repeatability, peaks, and dimensionality, as well as individuals' potential to generate activation patterns suitable for myocontrol applications for both healthy and DMD participants. The raw data used for this analysis are available online (32). All signal processing and data analyses were performed in Matlab 2018b software (The Mathworks Inc., USA). In the remainder of this section, we describe a set of analyses aimed at investigating differences between DMD and healthy participants at the level of motor control properties (*Motor Control Properties* section) and myocontrol performance (*Myocontrol Performance* section).

Motor Control Properties

Activation Pattern Repeatability Tests

The degree of repeatability across repetitions per participant was calculated using squared Pearson correlation. Each heatmap (8 × 8) was reshaped into a vector (1 × 64) before the calculation of the squared Pearson correlation (33). The coefficient was extracted among the 10 repetitions per gesture and per participant. For every gesture, this resulted in 45 unique comparisons between the 10 repetitions and thus 45 coefficients per gesture (**Figure 4**).

Spatiotemporal Activation Pattern Tests

The temporal distribution of activations between healthy and DMD was calculated via normalized and absolute activations per repetition of each gesture (**Figure 5A**). A normalization factor was calculated across all gestures and repetitions. For each gesture, the maximum absolute and normalized value of the 64-electrode heatmap were calculated for every participant and each repetition and plotted.

Figure 5B shows the average spatial distribution of the healthy and DMD participants. The spatial distribution of the sEMG potentials over the 8 × 8 normalized heatmap was

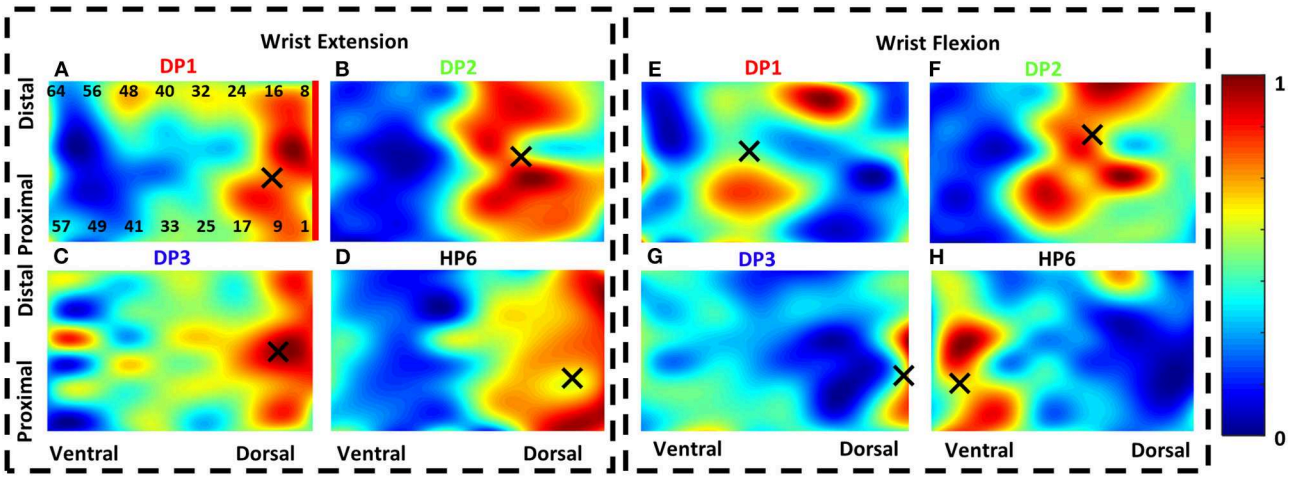

FIGURE 3 | The heatmaps of two representative gestures for the three participants with Duchenne muscular dystrophy (DMD) and one healthy participant. **(A–D)** show wrist extension heatmaps for DP1 **(A)**, DP2 **(B)**, DP3 **(C)**, and HP6 **(D)**. **(E–G)** show wrist flexion heatmaps for DP1 **(E)**, DP2 **(F)**, DP3 **(G)**, and HP6 **(H)**. Regarding wrist extension, all participants exhibit similar activation patterns. However, for wrist flexion, there is higher variability in the activation patterns within participants. X marks show the center of gravity (COG) for each heatmap. Only the activations that are higher than 80% are used to calculate the COG.

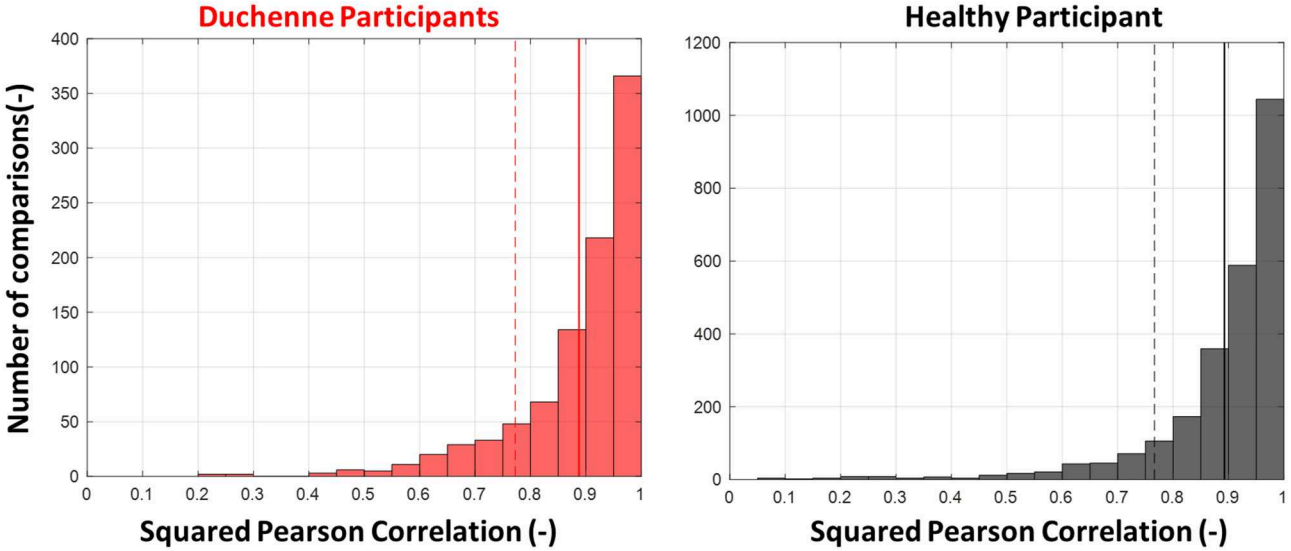

FIGURE 4 | The histogram of squared Pearson correlation between the 10 repetitions for all gestures and for all participants. High correlation shows similarity between the repetitions and thus high repeatability. Both healthy and Duchenne muscular dystrophy (DMD) participants achieved similarly high repeatability on the tasks. The full vertical lines represent the mean and the dashed the standard deviation. The number of unique comparisons between 10 repetitions is 45 multiplied by the seven gestures makes 315 unique comparisons per participant. That explains the total of 2,520 events in the healthy histogram compared to the 945 in the DMD.

calculated using the center of gravity (COG) by calculating the dorsal–ventral and the proximal–distal position of it as proposed by Elswijk et al. (34). The COG was calculated over electrodes presenting activations equal or larger than 80% of the maximal value of the heatmap (**Figure 3**). This way, only clusters of electrodes with a high peak amplitude were considered for the calculation of the COG in order to focus on the most relevant area of activation for each gesture.

Activation Pattern Dimensionality Tests

The 10 heatmaps, one per gesture repetition, were used to construct one single average heatmap per gesture per participant (**Figure 3**) that was used for the motor control analysis. We quantified differences in dimensionality of orthogonal and uncorrelated sEMG patterns between the healthy and DMD participants via a PCA (35) to the gesture-specific heatmaps per participant. For every participant, we performed a PCA to the concatenation (64×70) of the sEMG heatmaps of all gestures

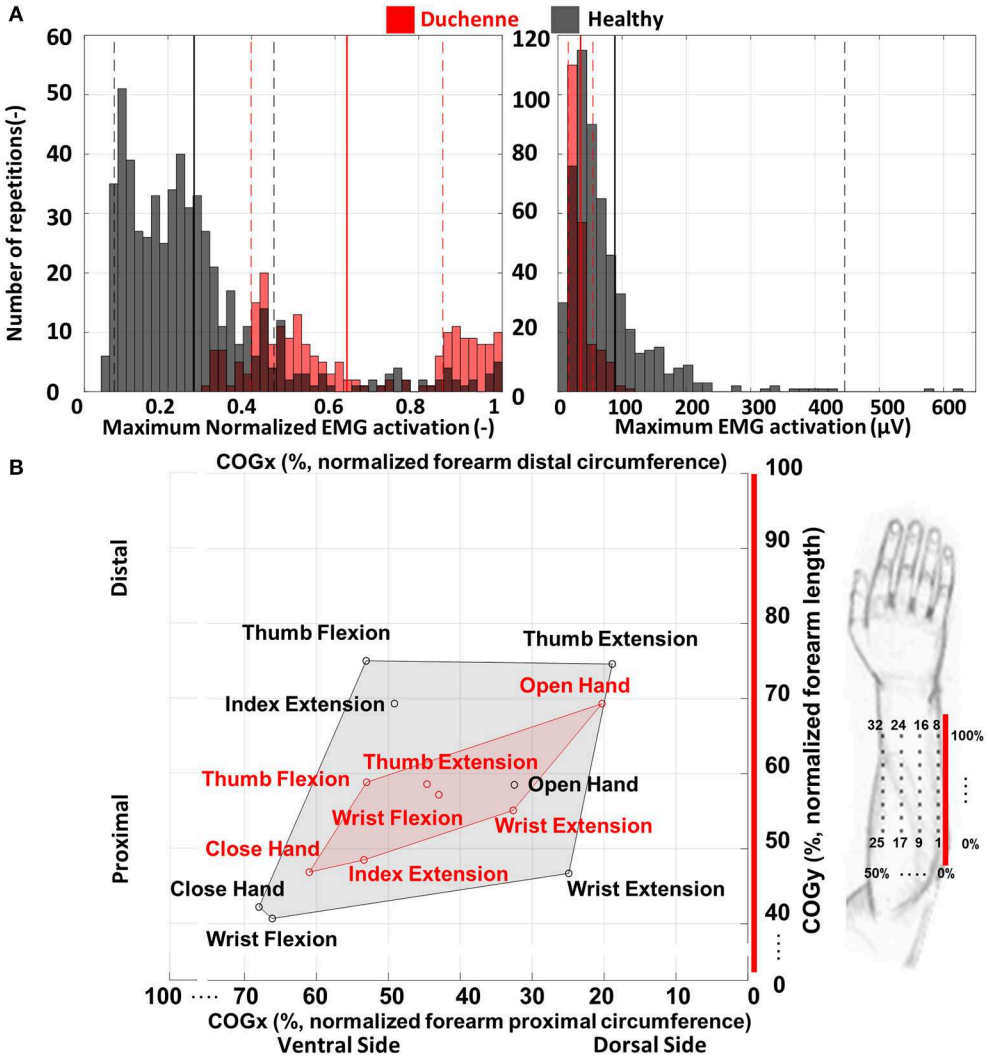

FIGURE 5 | (A) The maximum normalized (left) and absolute (right) activation for each of the 10 repetitions of each gesture for all participants. Healthy participants generally performed the tasks with low levels of maximum normalized activation, while participants with Duchenne muscular dystrophy (DMD) showed higher levels of maximum normalized activation during the tasks. However, the maximum absolute activations were higher for the healthy participants. The full vertical lines represent the mean and the dashed the standard deviation. **(B)** The average center of gravity (COG) for the seven gestures for the healthy participants (black) and the participants with DMD (red). Healthy participants (gray shaded area) show on average a broader spatial distribution of the seven gestures than the participants with DMD (red shaded area). The red line represents the imaginary line that connects the lateral epicondyle and the styloid process of the ulna and was used as the border between the dorsal and ventral side of the forearm (see also **Figure 1**). The COG coordinates are normalized over the forearm circumference (COGx) and length (COGy).

and repetitions per participant [64 electrodes × (7 gestures × 10 repetitions)]. The number of PCs needed to reconstruct the original seven gesture heatmaps was identified per participant by means of the variance explained (VE), and it was taken as the number of PCs that summed together explained more than 90% of the total variance. This number was used to explore the repertoire of orthogonal and uncorrelated sEMG patterns produced by the two groups of participants (**Figure 6A**).

Additionally, we calculated the squared Pearson correlation between all the gestures per participant (the same way as we did for the repeatability, *Activation Pattern Repeatability Tests* section). The coefficient was extracted from the average normalized heatmap of the 10 repetitions per gesture and per participant. For every participant, this resulted in 21 unique comparisons between the seven gestures and thus 21 coefficients per participant. We averaged the correlation values of the healthy participants and the participants with DMD separately to identify which gestures are mostly correlated per population, and we presented this in the form of a similarity matrix (**Figure 6B**).

Myocontrol Performance

We explored participants' gesture recognition performance via an offline pattern recognition algorithm applied to the band-pass filtered data (fourth-order Butterworth, 20–450 Hz) of each participant. We used a linear discriminant analysis (LDA) (36) to recognize each of the gestures performed.

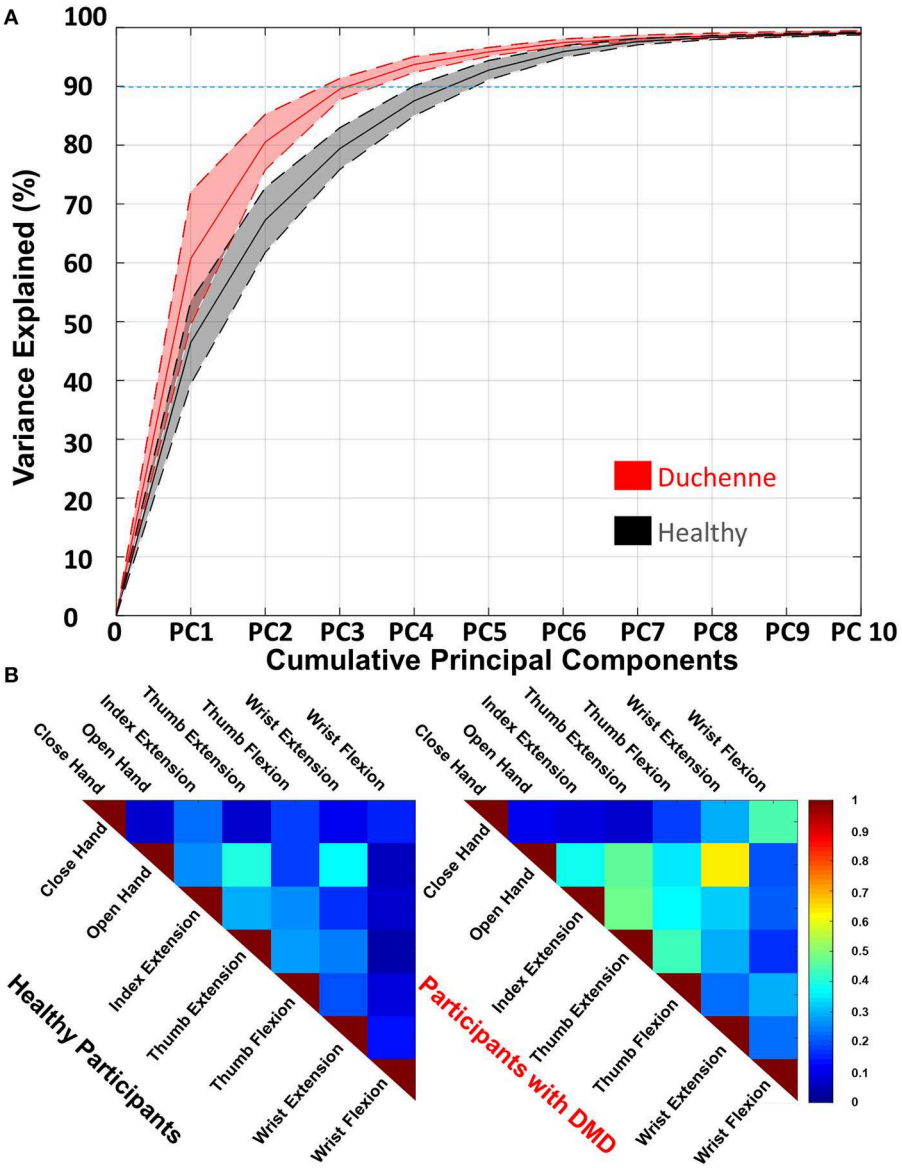

FIGURE 6 | (A) The percentage of variance explained as a function of the number of cumulative principal components (PCs). More than 90% of the variance (blue dashed line) of the data of the participants with Duchenne muscular dystrophy (DMD) is explained by three PCs, while for the healthy by five. The full lines represent the mean and the dashed the standard deviation. For clarity, we include only up to 10 of the 63 components, as those explain more than 99% of the variance explained. **(B)** The averaged squared Pearson correlation between the seven gestures of both groups of participants in the form of a similarity matrix. High correlation shows similarity between the gestures. Both healthy and DMD participants show correlated gestures; however, this phenomenon is more prominent in the DMD participants. A high value shows high correlation where one is the maximum (diagonal). The number of unique comparisons between the seven gestures is 21 per participant.

LDA is a commonly used pattern recognition algorithm for prosthetic control (37) and already commercialized by COAPT LLC (Chicago, USA) (38, 39). We chose it for the ease of implementation, classification speed, and high accuracy compared to other similar approaches (40). The 10 steady-state segments for every gesture were concatenated and created a 10-s vector. We trained the classifier by extracting four time-domain features from the raw segmented data including mean absolute value, zero crossing, slope sign change, and waveform length (41). We chose for a feature extraction window of 200 ms (with an overlap of 100 ms), which would be within acceptable range for real-time myoelectric applications (42). The classifier was validated with a three-split Monte Carlo cross-validation approach (43). Each time, a different part of the segmented data was used for training (always 70%) and testing (always 30%). The average off-line classification accuracy of these three trainings was used as performance metric per participant. Additionally, we tested how the offline classification accuracy per participant was affected by the number of gestures that had to be classified.

RESULTS

Motor Control Properties

Activation Pattern Repeatability

As illustrated in **Figure 4**, DMD individuals exhibited comparable correlation values to healthy individuals. The average R^2 coefficient was 0.89 ± 0.12 (mean ± SD) for DMD and 0.89 ± 0.13 for healthy participants between repetitions. An example of the 10 repetitions for a DMD participant can be seen in **Figure 2**.

Spatiotemporal Activation Patterns

Figure 5A shows the normalized and absolute activations of both participant groups. The normalized activation was on average higher for the DMD (0.63 ± 0.23) than for the healthy participants (0.26 ± 0.2). The maximum normalized value observed for participants with DMD was one (only DP3) and the minimum 0.3 (DP2), while for healthy were, respectively, one (only HP1) and 0.05 (HP8). The maximum absolute activation of the DMD participants was on average 35 ± 19 μV, while for healthy individuals, it was 89 ± 358 μV. The maximum value observed for participants with DMD was 108 μV (DP1) and the minimum 18.6 μV (DP3), while for healthy, were. Respectively. 628 μV (HP1) and 8.5 μV (HP8). Due to the difference in the number between the healthy and DMD participants, we have fewer repetitions for the DMD individuals, i.e., seven gestures multiplied by 10 repetitions per participant, which means 210 for the DMD vs. 560 for the healthy. **Figure 5B** shows the COG for the seven gestures in the electrode space for both participant groups. Healthy participants show a broader spatial distribution for the seven gestures. Wrist flexion and close hand appear to be spatially close. Along the dorsoventral direction, on average, thumb extension was at the dorsal limit (COGx = 18.9%), while close hand was at the ventral limit (COGx = 68%). In the proximodistal direction, wrist flexion was at the proximal limit (COGy = 41%), and thumb flexion was at the distal limit (COGy = 75%). Participants with DMD showed on average a close clustering of the seven gestures. Thumb extension and wrist flexion were the most spatially close gestures. In the dorsoventral direction, on average, open hand was at the dorsal limit (COGx = 20%), while close hand was at the ventral limit (COGx = 61%). In the proximodistal direction, the same gestures were again the limits, with close hand being the proximal (COGy = 47%) and open hand the distal (COGy = 69%).

Activation Pattern Dimensionality

The participants with DMD needed on average three PCs to explain >90% of the total variance of the seven gestures and 10 repetitions (**Figure 6A**). The same variance threshold was crossed on average by five PCs for the healthy participants. For the healthy group, PC1 explained 45%, while the same component explains 61% of the total variance for the DMD group.

Figure 6B shows which gestures were the most similar (by means of the squared Pearson correlation). The healthy participants exhibited correlations $R^2 > 0.3$ on average between two gestures. The highest correlations were found between hand open and thumb extension (0.39 ± 0.2) and wrist extension (0.36 ± 0.17). The participants with DMD exhibited $R^2 > 0.3$ on average across nine gestures. Those were found between close hand and wrist flexion (0.45 ± 0.23); between hand open and index extension (0.38 ± 0.23), thumb extension (0.46 ± 0.33), thumb flexion (0.34 ± 0.27), and wrist extension (0.62 ± 0.23); between index extension and thumb extension (0.47 ± 0.15) and thumb flexion (0.36 ± 0.04) and wrist extension (0.31 ± 0.16); and finally between thumb extension and thumb flexion (0.42 ± 0.21).

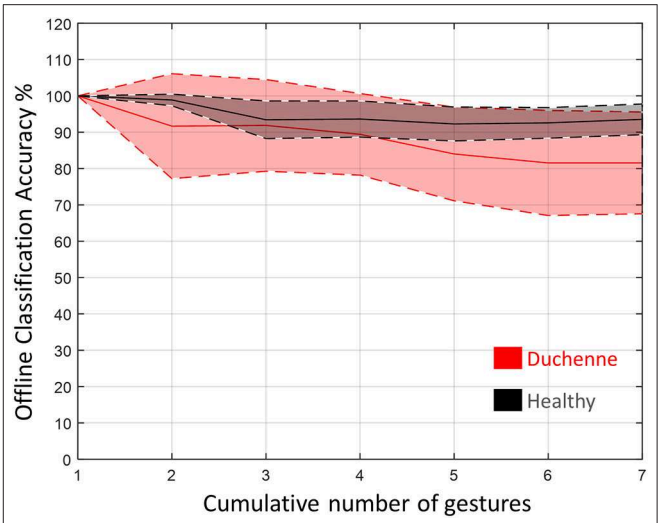

FIGURE 7 | The difference in average off-line classification accuracy for healthy and Duchenne muscular dystrophy (DMD) participants as a function of the gestures needed to be identified by the linear discriminant analysis (LDA) classifier. The full lines represent the mean and the dashed the standard deviation.

Gesture Recognition for Myocontrol

The LDA classifier was trained using the seven gestures. **Figure 7** shows the results of the off-line classification accuracy as a function of the gestures that had to be recognized. The average off-line classification accuracy of the DMD participants was always lower than the average of the healthy participants. When all the gestures were included, this accuracy reached 93.6 ± 4.2% for the healthy and 81.6 ± 14% for the DMD participants. The off-line accuracy stopped dropping at six gestures for the participants with DMD, while for the healthy participants, this happened at three (**Figure 7**).

DISCUSSION

In this study, we measured HD-sEMG activity from the forearm of eight healthy and three DMD participants during seven hand/wrist-related tasks. We performed analyses in order to characterize the differences in activation patterns shape, repeatability, and dimensionality, as well as gesture recognition between healthy and DMD individuals.

The three participants with DMD showed motor control alterations in terms of dimensionality and spatiotemporal

activations compared to the healthy population, supporting our hypothesis. These alterations were mainly expressed by the COGs across DMD gestures being more closely located than COGs across healthy gestures and comfortable muscle activations close to their maximal contraction level (0.63 ± 0.23). Also, participants with DMD showed a higher correlation between gestures, and when their gesture space was decomposed to its PCs, 90% of it was explained by fewer components (3) than for the healthy (5). Differences were also found between DMD participants likely due to different stages of the disease. However, in terms of repeatability per gesture, the two populations showed an unexpected clear similarity. Despite the consequences of muscular degeneration and minimal hand/wrist motion (especially for DP3, **Supplementary Video**), the myocontrol potential for the DMD participants is remarkably present and comparable to the healthy participants, disproving our hypothesis. However, the existing differences, due to the specificities of individuals with DMD, need to be addressed while developing myocontrol algorithms.

The results indicated that repeatability was intact for the participants with DMD and comparable to that of the healthy participants (**Figure 4**). This is an important requirement for robust and repeatable pattern recognition-based myocontrol (44) of assistive robotics.

Participants with DMD exhibited lower absolute activations and higher normalized activations compared to the healthy participants (**Figure 5**). This shows that participants with DMD operate closer to their maximum effort, as opposed to healthy participants, in order to perform simple hand/wrist-related tasks, and yet they produce lower absolute sEMG activity. This constant high effort can have detrimental consequences for the muscle integrity of people with DMD and even speed up disease progression or lead to disuse of the hand. Assistive wearable robotics may be able to decrease the mechanical load on the muscles and promote daily use (7, 45). This result, together with the fact that the most progressed participant (DP3) presented simultaneously the maximum normalized and the minimum absolute sEMG activity, agrees with previous studies stating that the disease progression results in lower absolute sEMG amplitude (46) and also in higher effort and fatigue (47). DP1 and DP3 exhibited comparable trends between each other. For DP1, we observed high absolute activations (around 100 μV, comparable to healthy participants) and on average medium absolute activations. DP2 showed lower absolute activations (around 60 μV), however also medium absolute activations. Regarding spatial distribution of the activation patterns, healthy participants showed lower spatial similarity than participants with DMD (**Figure 5B**). It appears that on average for the DMD participants, the seven gestures used in this study, engaged only a subset of the electrodes, closely clustered to each other compared to the healthy participants. Similarly, to lower spatial similarity, healthy participants (**Figure 6**) exhibited a higher degree of dimensionality, as expressed by the larger repertoire of orthogonal and uncorrelated sEMG patterns they can produce across the seven hand/wrist-related gestures and 10 repetitions. The healthy population needed five PCs to explain at least 90% of the variance in the original data, while DMD participants needed three, except DP1 that needed four. Additionally, the higher correlation between the gestures points toward the fact that, in terms of sEMG activation patterns, there is more similarity in DMD. This may provide another indication (together with variability in maximum activation) of how the progress of the disease affects motor control, since DP1 is the least affected participant. The decrease in dimensionality may be partially attributed to the increased level of co-contractions between agonist and/or antagonist muscle groups that we observed in the DMD participants when performing the tasks and further supported by a recent hand motor performance study in people with DMD (48). Co-contractions may be elicited by the effort of the participants to stabilize their wrist during the tasks, but further work is needed to explore this hypothesis.

According to the muscle synergies hypothesis, the CNS uses specific simplified commands (muscle synergies) in order to act efficiently upon the redundant musculoskeletal system and complete a motor task (49). In the case of DMD, the intact CNS and neural pathways are acting upon a progressively limited musculoskeletal system. This may lead to progressive adaptations in the CNS, similar to those observed in stroke survivors (50) expressed via compensatory movements (51), co-contractions, and lower dimensionality. Regarding gait analysis in DMD, it was shown that gait motor control complexity is minimally affected by the disease (in the early stages) (52); however, for the more complex hand and wrist control, there is no evidence. Considering the sEMG measurement for the participants with DMD as the neural output (53), it is not yet understood if the observed commonalities between different gestures can be attributed to the impaired musculoskeletal system (i.e., more similarities in how motor units process incoming axonal spike trains) or to adaptations in the CNS (i.e., increased common synaptic input to alpha motor neuron pools). Future work will employ HD-sEMG in combination with decomposition techniques (54) in people with DMD to provide further insights.

According to our results, there is potential for the robust decoding of hand/wrist motor intention in individuals with DMD. This can enable individuals with DMD to control a high-tech hand orthosis with multiple degrees of freedom. However, there was a noticeable decay of the LDA off-line classification performance when more gestures were added for the participants with DMD, which was larger than the one for the healthy participants (**Figure 7**). Despite the lower performance, the classification performance is on average larger than 80% for all the seven gestures and more or equal to 90% for up to four gestures. Together with the ability of the DMD participants to create repeatable HD-sEMG activation patterns, this result shows the potential of myocontrol for decoding of hand/wrist motor intention across a key selection of gestures. Currently, the implementation of HD-sEMG in dynamic control of wearable exoskeletons is limited by a number of factors, such as the number of cables between amplifiers and electrodes, as well as large amplifiers. This lack of portability restricts measurements in dynamic conditions (motion) and induces movement restrictions, user discomfort, and signal artifacts (23), therefore limiting control of wearables. However, recent developments show promising steps toward more portable amplifiers that reject movement artifacts and powerline interference, while at the same time do not obstruct

movements and ensure tight placement of the electrodes (23, 55). To this point, the main limitation of portable amplifiers is the relatively limited number of electrodes provided [32 (23) and 16 (55)]; however, they open new avenues for HD-sEMG control of exoskeletons.

The current performance of classification could be optimized with the development of DMD-tailored classification algorithms, which will take into account the specificities of the disease. Such specificities are the progression of the disease (co-contractions and fatigue), the low sEMG signal to noise ratio (46), and the differences in the motor control strategies (higher spatial similarity, lower dimensionality in terms of orthogonal and uncorrelated sEMG patterns, higher activation levels during low-intensity tasks). Further tailoring can be made by building numerical neuromusculoskeletal models of specific DMD individuals that can provide additional features for classification (56–58). The observed lower spatial dimensionality in the HD-sEMG may suggest that sEMG data compression before classification might be a strategy due to the lower variability that individuals with DMD present. This can be achieved by first lowering the dimensionality of the feature space of the raw data based on dimensionality reduction techniques such as PCA or partial least squares (PLS) (59) and use the resulting data as an input to an LDA classifier. Further, reduction of the number of electrodes can be achieved based on detection of heatmap areas carrying common and individual information (19). The higher spatial similarity is an important finding of this study that can be considered for guiding such decisions. More extensive research with individuals with DMD is necessary to identify the relevant feature space and test the performance of various classifiers and electrode numbers and configuration in order to inspire DMD customized classifiers.

We included in our case study three participants with DMD with large functional variability in order to explore a larger spectrum of the disease instead of a cluster of cases with similar characteristics. However, DMD is a disease with large functional heterogeneity due to different progression patterns (60) and our limited sample does not cover the complete spectrum. However, our study is limited by the low number of participants with DMD. This is an unavoidable limitation due to the low number of available participants. We also intended to comply with the ethical and legal standards while conducting our study by not recruiting participants who are already involved in other studies at the same time. Hence, our conclusions and results need to be taken as indicative until research is performed with more participants, which will allow for more general and strong conclusions.

Additionally, we did not monitor the level of contraction during the conduction of the measurements. We explicitly asked our participants to perform all movements comfortably, but we did not control this condition. It is known from the literature that different contraction levels elicit a small shift in the main activity area, however not significantly altering the spatial distribution of HD-sEMG in the forearm (14). Another limitation of this study is that the selection of the seven gestures used for acquiring and analyzing the data was based on gestures involved in common ADL (25), and each gesture was analyzed separately. However, in reality, ADL involves multiple combinations of the selected gestures in some case simultaneously, which would result in the activation of more than one muscle region when combined finger and wrist movements are occurring in order to allow for object grasping and manipulation. In such case, the spatial distribution of the sEMG activations will not be so clearly segmented. Therefore, before applying our findings for myocontrol targeting ADL, we need to take caution and further test the validity of our findings in situations demanding a higher degree of complexity (combination of gestures).

Future work will evaluate the application of our protocol to more participants with DMD in order to investigate further the characterization of forearm electromyograms for individuals with DMD and come to more general conclusions regarding this very diverse population. Moreover, we are interested in the exploration of online classification performance implemented outside of the lab in order to resemble daily-use conditions. An extended protocol in order to decode the neural drive (54) in DMD would offer further insights regarding the source of the differences in hand/wrist motor control observed in our analysis between participants with DMD and healthy participants. Next to that, the use of non-negative matrix factorization (NMF) may give further insights regarding muscle group synergies in hand movements in DMD (61). Lastly, an analysis of the homogeneity of activations needs to be carried out using HD-sEMG, as it is known that different joint positions and contraction strength and duration may cause muscles to activate in a non-homogeneous manner (21). The results of this study together with the future studies will be further used for the development of myocontrol algorithms for the robust control of an active hand exoskeleton (29, 62), developed within the Symbionics project (63) for individuals with DMD.

CONCLUSION

We characterized the forearm electromyograms spatiotemporally of three individuals with DMD and compared to eight healthy individuals. For the first time, we propose a systematic analysis on how the disease affects the distribution of HD-sEMG pattern in the forearm and the repeatability and activation distribution of these patterns. Additionally, we explored the potential for the myocontrol via decoding of motor intention from the forearm muscles of individuals with DMD. We performed this study in order to get a better understanding of DMD hand/wrist motor control with regard to exoskeleton applications. Future studies will focus on testing sEMG for the real-time decoding of hand/wrist motor intention with individuals with DMD. Moreover, we will implement and test the feasibility of sEMG control with a new active hand exoskeleton for individuals with DMD.

DATA AVAILABILITY STATEMENT

The datasets generated for this study can be found in the 4TU repository [https://data.4tu.nl/]. DOI: https://doi.org/10.4121/uuid:f252f933-90be-4543-9c13-3c4efe208052.

ETHICS STATEMENT

The studies involving human participants were reviewed and approved by Medical Ethics Committee (METC) of Twente, protocol number: NL59061.044.16. The patients/participants provided their written informed consent to participate in this study.

AUTHOR CONTRIBUTIONS

KN performed the main review of literature and research protocol development, data acquisition and analysis, creation of figures, and drafting of the manuscript. NR participated in the data acquisition, research protocol development, creation of figures, and made critical revision of the manuscript. RM participated in the measurements and partially in data analysis and proofread the document. JN participated in the PCA and performed the off-line LDA classification. MS oversaw the complete writing process and design of data analysis procedures. BK was actively involved in the writing process and made substantial revisions of the manuscript. All authors read and approved the final manuscript.

FUNDING

This work was supported by the Flextension Foundation through the Netherlands Organization for Scientific Research (NWO), the Duchenne Parent Project, Hankamp Rehab, Spieren voor Spieren, TMSi, Festo and Pontes Medical. Project Number: 13525. The work was also partly supported by the European Research Council *via* the ERC Starting Grant INTERACT (no. 803035).

ACKNOWLEDGMENTS

The authors would like to thank Dr. Mannes Poel and MSc. Wolfgang F. Rampeltshammer for their insightful comments regarding the PCA analysis and the LDA classification.

SUPPLEMENTARY MATERIAL

The Supplementary Material for this article can be found online at: https://www.frontiersin.org/articles/10.3389/fneur.2020.00231/full#supplementary-material

Video S1 | Characterization of muscle activation diversity in Duchenne muscular dystrophy via high-density electromyography: implications for myoelectric control.

REFERENCES

1. Van Opstal SLSH, Jansen M, Van Alfen N, De Groot IJM. Health-related quality of life and its relation to disease severity in boys with Duchenne muscular dystrophy: satisfied boys, worrying parents - a case-control study. *J Child Neurol.* (2014) 29:1486–95. doi: 10.1177/0883073813506490
2. Bartels B, Pangalila RF, Bergen MP, Cobben NAM, Stam HJ, Roebroeck ME. Upper limb function in adults with Duchenne muscular dystrophy. *J Rehabil Med.* (2011) 43:770–775. doi: 10.2340/16501977-0841
3. Eagle M, Baudouin SV, Chandler C, Giddings DR, Bullock R, Bushby K. Survival in Duchenne muscular dystrophy: Improvements in life expectancy since 1967 and the impact of home nocturnal ventilation. *Neuromuscul Disord.* (2002) 12:926–9. doi: 10.1016/S0960-8966(02)00140-2
4. Wagner KR, Lechtzin N, Judge DP. Current treatment of adult Duchenne muscular dystrophy. *Biochim Biophys Acta.* (2007) 1772:229–37. doi: 10.1016/j.bbadis.2006.06.009
5. Haley SM, Coster WI, Kao YC, Dumas HM, Fragala-Pinkham MA, Kramer JM, et al. Lessons from use of the pediatric evaluation of disability inventory: where do we go from here?. *Pediatric Phys Ther.* (2010) 22:69–75. doi: 10.1097/PEP.0b013e3181cbfbf6
6. Rahbek J, Werge B, Madsen A, Marquardt J, Steffensen BF, Jeppesen J. Adult life with Duchenne muscular dystrophy: observations among an emerging and unforeseen patient population. *Pediatric Rehabil.* (2005) 8:17–28. doi: 10.1080/13638490400010191
7. Bergsma A, Lobo-Prat J, Vroom E, Furlong P, Herder JL. 1st Workshop on Upper-Extremity Assistive Technology for People with Duchenne: state of the art, emerging avenues, and challenges. April 27th 2015, London, United Kingdom. *Neuromuscul Disord.* (2016) 26:386–93. doi: 10.1016/j.nmd.2016.04.005
8. Weichbrodt J, Eriksson BM, Kroksmark AK. Evaluation of hand orthoses in Duchenne muscular dystrophy. *Disabil Rehabil.* (2018) 40:2824–32. doi: 10.1080/09638288.2017.1347721
9. Bushby K, Finkel R, Birnkrant DJ, Case LE, Clemens PR, Cripe L, Kaul A, et al. Diagnosis and management of Duchenne muscular dystrophy, part 1: diagnosis, and pharmacological and psychosocial management. *Lancet Neurol.* (2010) 9:77–93. doi: 10.1016/S1474-4422(09)70271-6
10. Bushby K, Finkel R, Birnkrant DJ, Case LE, Clemens PR, Cripe L, Kaul A, et al. Diagnosis and management of Duchenne muscular dystrophy, part 2: implementation of multidisciplinary care. *Lancet Neurol.* (2010) 9:177–89. doi: 10.1016/S1474-4422(09)70272-8
11. Lenzi T, De Rossi SMM, Vitiello N, Carrozza MC. Intention-based EMG control for powered exoskeletons. *IEEE Trans Biomed Eng.* (2012) 59:2180–90. doi: 10.1109/TBME.2012.2198821
12. Farina D, Sartori M. Surface electromyography for MAN-machine interfacing in rehabilitation technologies. In: Merletti R, Farina D, editors. *Surface Electromyography: Physiology, Engineering and Applications*. Wiley (2016). p. 540–60. doi: 10.1002/9781119082934.ch20
13. Geethanjali P. Myoelectric control of prosthetic hands: State-of-the-art review. *Med Devices.* (2016) 9:247–55. doi: 10.2147/MDER.S91102
14. Gallina A, Botter A. Spatial localization of electromyographic amplitude distributions associated to the activation of dorsal forearm muscles. *Front Physiol.* (2013) 4:367. doi: 10.3389/fphys.2013.00367
15. Heo P, Gu GM, jin Lee S, Rhee K, Kim J. Current hand exoskeleton technologies for rehabilitation and assistive engineering. *Int J Precision Eng Manufact.* (2012) 13:807–24. doi: 10.1007/s12541-012-0107-2
16. Bos RA, Haarman CJW, Stortelder T, Nizamis K, Nizamis JL, Stienen AHA, et al. A structured overview of trends and technologies used in dynamic hand orthoses. *J Neuroeng Rehabil.* (2016) 13:62. doi: 10.1186/s12984-016-0168-z
17. Muceli S, Jiang N, Farina D, Ning Jiang, Farina D. Multichannel surface EMG based estimation of bilateral hand kinematics during movements at multiple degrees of freedom. *Conf Proc IEEE Eng Med Biol Soc.* (2010) 6066–9. doi: 10.1109/IEMBS.2010.5627622
18. Gazzoni M, Celadon N, Mastrapasqua D, Paleari M, Margaria V, Ariano P. Quantifying forearm muscle activity during wrist and finger movements by means of multi-channel surface electromyography. *PLoS ONE.* (2014) 9:e109943. doi: 10.1371/journal.pone.0109943
19. Daley H, Englehart K, Hargrove L, Kuruganti U. High density electromyography data of normally limbed and transradial amputee subjects for multifunction prosthetic control. *J Electromyogr Kinesiol.* (2012) 22:478–84. doi: 10.1016/j.jelekin.2011.12.012

20. Drost G, Stegeman DF, van Engelen BGM, Zwarts MJ. Clinical applications of high-density surface EMG: a systematic review. *J Electromyogr Kinesiol.* (2006) 16:586–602. doi: 10.1016/j.jelekin.2006.09.005
21. Rojas-Martínez M, Mañanas MA, Alonso JF. High-density surface EMG maps from upper-arm and forearm muscles. *J Neuroeng Rehabil.* (2012) 9:85. doi: 10.1186/1743-0003-9-85
22. Raez MBI, Hussain MSS, Mohd-Yasin F, Reaz MBI, Hussain MSS, Mohd-Yasin F. Techniques of EMG signal analysis: detection, processing, classification and applications. *Biol Proced Online.* (2006) 8:11–35. doi: 10.1251/bpo115
23. Cerone GL, Botter A, Gazzoni MA. Modular, smart, and wearable system for high density sEMG detection. *IEEE Trans Neural Syst Rehabil Eng.* (2019) 66:3371–80. doi: 10.1109/TBME.2019.2904398
24. Hermens HJ, Freriks B. SENIAM 5. recommendations for sensors and sensor placement procedures. *Roessingh Res Dev.* (1997) 10:361–74. doi: 10.1016/S1050-6411(00)00027-4
25. Saudabayev A, Rysbek Z, Khassenova R, Atakan Varol H. Data descriptor: human grasping database for activities of daily living with depth, color and kinematic data streams. *Sci Data.* (2018) 5:180101. doi: 10.1038/sdata.2018.143
26. Keshtkaran MR, Yang Z. A fast, robust algorithm for power line interference cancellation in neural recording. *J Neural Eng.* (2014) 11:026017. doi: 10.1088/1741-2560/11/2/026017
27. Soedirdjo SDH, Ullah K, Merletti R. Power line interference attenuation in multi-channel sEMG signals: algorithms and analysis. *Conf Proc IEEE Eng Med Biol Soc.* (2015) 2015:3823–6. doi: 10.1109/EMBC.2015.7319227
28. Winter DA. *Biomechanics and Motor Control of Human Movement: 4th Edn.* Wiley (2009). doi: 10.1002/9780470549148
29. Bos RA, Nizamis K, Koopman BFJM, Herder JL, Sartori M, Plettenburg DH. A case study with SymbiHand: an sEMG-controlled electrohydraulic hand orthosis for individuals with Duchenne muscular dystrophy. *IEEE Trans Neural Syst Rehabil Eng.* (2019) 28:258–66. doi: 10.1109/TNSRE.2019.2952470
30. Di Fabio RP. Reliability of computerized surface electromyography for determining the onset of muscle activity. *Phys Ther.* (1987) 67:43–8. doi: 10.1093/ptj/67.1.43
31. Martinez IJR, Mannini A, Clemente F, Sabatini AM, Cipriani C. Grasp force estimation from the transient EMG using high-density surface recordings. *J Neural Eng.* (2020) 17:016052. doi: 10.1088/1741-2552/ab673f
32. Nizamis, K. Raw data collected for the study of: characterization of forearm high-density electromyograms during wrist-hand tasks in individuals with Duchenne muscular dystrophy. (2019). doi: 10.4121/uuid:f252f933-90be-4543-9c13-3c4efe208052
33. Lury DA, Fisher RA. Statistical methods for research workers. *Stat.* (1972) 21:229. doi: 10.2307/2986695
34. van Elswijk G, Kleine BU, Overeem S, Eshuis B, Hekkert KD, Stegeman DF. Muscle imaging: mapping responses to transcranial magnetic stimulation with high-density surface electromyography. *Cortex.* (2008) 44:609–16. doi: 10.1016/j.cortex.2007.07.003
35. Jolliffe IT. *Principal Component Analysis. 2nd Edn.* Wiley (2002).
36. Young AJ, Smith LH, Rouse EJ, Hargrove LJ. Classification of simultaneous movements using surface EMG pattern recognition. *IEEE Trans Biomed Eng.* (2013) 60:1250–8. doi: 10.1109/TBME.2012.2232293
37. Parajuli N, Sreenivasan N, Bifulco P, Cesarelli M, Savino S, Niola V, et al. Real-time EMG based pattern recognition control for hand prostheses: A review on existing methods, challenges and future implementation. *Sensors.* (2019) 19:4596. doi: 10.3390/s19204596
38. Dellacasa Bellingegni A, Gruppioni E, Colazzo G, Davalli A, Sacchetti R, Guglielmelli E, et al. NLR, MLP, SVM, and LDA: a comparative analysis on EMG data from people with trans-radial amputation. *J Neuroeng Rehabil.* (2017) 14:82. doi: 10.1186/s12984-017-0290-6
39. COAPT. Available online at: https://www.coaptengineering.com/ (accessed 14 Feb, 2020).
40. Ortiz-Catalan M, Brånemark R, Håkansson B. BioPatRec: a modular research platform for the control of artificial limbs based on pattern recognition algorithms. *Source Code Biol Med.* (2013) 8:11. doi: 10.1186/1751-0473-8-11
41. Adewuyi AA, Hargrove LJ, Kuiken TA. Evaluating eMg feature and classifier selection for application to partial-hand prosthesis control. *Front Neurorobot.* (2016) 10:15. doi: 10.3389/fnbot.2016.00015
42. Smith LH, Hargrove LJ, Lock BA, Kuiken TA. Determining the optimal window length for pattern recognition-based myoelectric control: balancing the competing effects of classification error and controller delay. *IEEE Trans Neural Syst Rehabil Eng.* (2011) 19:186–92. doi: 10.1109/TNSRE.2010.2100828
43. Dubitzky W, Granzow M, Berrar D. *Fundamentals of Data Mining in Genomics and Proteomics*. Springer (2007). doi: 10.1007/978-0-387-47509-7
44. Daley H, Englehart K, Kuruganti U. Muscle activation patterns of the forearm: high-density electromyography data of normally limbed and transradial amputee subjects. *J Prosthetics Orthot.* (2010) 22:244–51. doi: 10.1097/JPO.0b013e3181f989c2
45. Nizamis K, Stienen AHA, Kamper D, Keller T, Farina D, Farina BFJM, et al. Transferrable expertise from bionic arms to robotic exoskeletons: perspectives for stroke and Duchenne muscular dystrophy. *IEEE Trans Med Robot Bionics.* (2019) 1:88–96. doi: 10.1109/TMRB.2019.2912453
46. Lobo-Prat J, Janssen MMH P, Koopman BFJM, Stienen AHA, de Groot IJM. Surface EMG signals in very late-stage of Duchenne muscular dystrophy: a case study. *J Neuroeng Rehabil.* (2017) 14:86. doi: 10.1186/s12984-017-0292-4
47. Janssen MMHP, Harlaar J, Koopman B, De Groot IJM. Dynamic arm study: quantitative description of upper extremity function and activity of boys and men with Duchenne muscular dystrophy. *J Neuroeng Rehabil.* (2017) 14:45. doi: 10.1186/s12984-017-0259-5
48. Nizamis K, Schutte W, Grutters JJ, Goseling J, Rijken NHM, Koopman BFJM. Evaluation of the cognitive-motor performance of adults with Duchenne muscular dystrophy in a hand-related task. *PLoS ONE.* (2020) 15:e0228128. doi: 10.1371/journal.pone.0228128
49. Singh RE, Iqbal K, White G, Hutchinson TE. A systematic review on muscle synergies: from building blocks of motor behavior to a neurorehabilitation tool. *Appl Bionics Biomech.* (2018). 2018:36153. doi: 10.1155/2018/3615368
50. Alnajjar FS, Moreno JC, Ozaki KI, Kondo I, Shimoda S. Motor control system for adaptation of healthy individuals and recovery of poststroke patients: a case study on muscle synergies. *Neural Plast.* (2019) 2019:8586. doi: 10.1155/2019/8586416
51. Martini J, Voos MC, Hukuda ME, de Resende MBD, Caromano FA. Movimentos compensatórios durante atividades funcionais em crianças deambuladoras com distrofia muscular de Duchenne. *Arq Neuropsiquiatr.* (2014) 72:5–11. doi: 10.1590/0004-282X20130196
52. Goudriaan M, Shuman BR, Steele KM, Van den Hauwe M, Goemans N, Molenaers G, et al. Non-neural muscle weakness has limited influence on complexity of motor control during gait. *Front Hum Neurosci.* (2018) 12:5. doi: 10.3389/fnhum.2018.00005
53. Negro F, Yavuz US, Farina D. The human motor neuron pools receive a dominant slow-varying common synaptic input. *J Physiol.* (2016) 594:5491–505. doi: 10.1113/JP271748
54. Farina D, Negro F. Accessing the neural drive to muscle and translation to neurorehabilitation technologies. *IEEE Rev Biomed Engg.* (2012) 5:3–14. doi: 10.1109/RBME.2012.2183586
55. Song W, Wang A, Chen Y, Bai S, Qingquan H, Lin Z, et al. Design of a flexible wearable smart sEMG recorder integrated gradient boosting decision tree based hand gesture recognition. *IEEE Trans Biomed Circuits Syst.* (2019) 13:1563–74. doi: 10.1109/TBCAS.2019.2953998
56. Sartori M, van de Riet J, Farina D. Estimation of phantom arm mechanics about four degrees of freedom after targeted muscle reinnervation. *IEEE Trans Med Robot Bionics.* (2019) 1:58–64. doi: 10.1109/TMRB.2019.2895791
57. Sartori M, Yavuz U, Farina D. *In vivo* neuromechanics: decoding causal motor neuron behavior with resulting musculoskeletal function. *Sci Rep.* (2017) 7:13465. doi: 10.1038/s41598-017-13766-6
58. Durandau G, Farina D, Asín-Prieto G, Dimbwadyo-Terrer I, Lerma-Lara S, Pons JL, et al. Voluntary control of wearable robotic exoskeletons by patients with paresis via neuromechanical modeling. *J Neuroeng Rehabil.* (2019) 16:91. doi: 10.1186/s12984-019-0559-z
59. Kemsley EK. Discriminant analysis of high-dimensional data: a comparison of principal components analysis and partial least squares

data reduction methods. *Chemom Intell Lab Syst.* (1996) 33:47–61. doi: 10.1016/0169-7439(95)00090-9

60. Desguerre I, Christov C, Mayer M, Zeller R, Becane HM, Bastuji-Garin S, et al. Clinical heterogeneity of Duchenne muscular dystrophy (DMD): definition of sub-phenotypes and predictive criteria by long-term follow-up. *PLoS ONE.* (2009) 4:e4347. doi: 10.1371/journal.pone.0004347
61. Israely S, Leisman G, Machluf CC, Carmeli E. Muscle synergies control during hand-reaching tasks in multiple directions post-stroke. *Front Comput Neurosci.* (2018) 12:10. doi: 10.3389/fncom.2018.00010
62. Bos RA, Nizamis K, Plettenburg DH, Herder JL. Design of an electrohydraulic hand orthosis for people with Duchenne muscular dystrophy using commercially available components. In: *2018 7th IEEE International Conference on Biomedical Robotics and Biomechatronics*. Enschede (2018). doi: 10.1109/BIOROB.2018.8487196
63. Symbionics-Hand Orthosis for DMD. Available online at: http://symbionics.info/project3/ (accessed April 7, 2020).

Conflict of Interest: The authors declare that the research was conducted in the absence of any commercial or financial relationships that could be construed as a potential conflict of interest.

frontiers in Neurology

ORIGINAL RESEARCH
published: 14 May 2020
doi: 10.3389/fneur.2020.00410

Altered Corticomuscular Coherence (CMCoh) Pattern in the Upper Limb During Finger Movements After Stroke

Ziqi Guo†, Qiuyang Qian†, Kiufung Wong, Hanlin Zhu, Yanhuan Huang, Xiaoling Hu and Yongping Zheng*

Department of Biomedical Engineering, The Hong Kong Polytechnic University, Kowloon, Hong Kong

Background: Proximal compensation to the distal movements is commonly observed in the affected upper extremity (UE) of patients with chronic stroke. However, the cortical origin of this compensation has not been well-understood. In this study, corticomuscular coherence (CMCoh) and electromyography (EMG) analysis were adopted to investigate the corticomuscular coordinating pattern of proximal UE compensatory activities when conducting distal UE movements in chronic stroke.

Method: Fourteen chronic stroke subjects and 10 age-matched unimpaired controls conducted isometric finger extensions and flexions at 20 and 40% of maximal voluntary contractions. Electroencephalogram (EEG) data were recorded from the sensorimotor area and EMG signals were captured from extensor digitorum (ED), flexor digitorum (FD), triceps brachii (TRI), and biceps brachii (BIC) to investigate the CMCoh peak values in the Beta band. EMG parameters, i.e., the EMG activation level and co-contraction index (CI), were analyzed to evaluate the compensatory muscular patterns in the upper limb.

Result: The peak CMCoh with statistical significance ($P < 0.05$) was found shifted from the ipsilesional side to the contralesional side in the proximal UE muscles, while to the central regions in the distal UE muscle in chronic strokes. Significant differences ($P < 0.05$) were observed in both peak ED and FD CMCohs during finger extensions between the two groups. The unimpaired controls exhibited significant intragroup differences between 20 and 40% levels in extensions for peak ED and FD CMCohs ($P < 0.05$). The stroke subjects showed significant differences in peak TRI and BIC CMCohs ($P < 0.01$). No significant inter- or intra-group difference was observed in peak CMCoh during finger flexions. EMG parameters showed higher EMG activation levels in TRI and BIC muscles ($P < 0.05$), and higher CI values in the muscle pairs involving TRI and BIC during all the extension and flexion tasks in the stroke group than those in the control group ($P < 0.05$).

Conclusion: The post-stroke proximal muscular compensations from the elbow to the finger movements were cortically originated, with the center mainly located in the contralesional hemisphere.

Keywords: stroke, compensatory contraction, upper limb, corticomuscular coherence (CMCoh), finger motion

OPEN ACCESS

Edited by:
Xiaogang Hu,
University of North Carolina at Chapel Hill, United States

Reviewed by:
Rong Song,
Sun Yat-sen University, China
Zhiyuan Lu,
University of Texas Health Science Center at Houston, United States

****Correspondence:***
Xiaoling Hu
xiaoling.hu@polyu.edu.hk

†These authors have contributed equally to this work

Specialty section:
This article was submitted to Neurorehabilitation, a section of the journal Frontiers in Neurology

Received: *18 December 2019*
Accepted: *20 April 2020*
Published: *14 May 2020*

Citation:
Guo Z, Qian Q, Wong K, Zhu H, Huang Y, Hu X and Zheng Y (2020) Altered Corticomuscular Coherence (CMCoh) Pattern in the Upper Limb During Finger Movements After Stroke. Front. Neurol. 11:410. doi: 10.3389/fneur.2020.00410

INTRODUCTION

Post-stroke motor recovery is usually associated with the cortical reorganization and adaptive learning experiences (1). Cerebral plasticity is the process by which the human body reorganizes neural networks and pathways after a stroke. Existing studies have found that the majority of motor recovery observed via cerebral plasticity reaches a plateau within the first 6 months after the onset (2, 3). Patients with chronic stroke (first onset over 6 months) regain the independence of the activities of daily living but always sustain upper extremity (UE) motor dysfunctions, e.g., muscle weakness, spasticity, and discoordination (4). Specifically, patients' distal UE segments, e.g., fingers and wrist, usually exhibit poorer functional recovery than the proximal elbow and shoulder parts (5). In our previous study (6, 7), we found that the dyscoordination observed following chronic stroke was particularly evident during distal UE joint motion tasks, and that stroke patients frequently relied on compensatory contractions from proximal UE muscles to substitute for a loss or reduction in hand function. However, Jones concluded that proximal compensations can be mistaken for recovery and constrain the potential motor restoration at the distal segments, leading to "learned non-use" or "learned dis-use" (8). Although such post-stroke behavioral deviation can further exacerbate motor impairments, the interaction between the cortical plasticity in chronic stroke and the dynamic muscular coordination in the upper limb has not yet been well-investigated.

Previous neuroimaging studies on motor restoration after stroke using positron emission tomography (PET), functional magnetic resonance (fMRI) imaging, and transcranial magnetic stimulation (TMS) have identified that post-stroke patients exhibit a reduction in brain activities at the lesioned side and a propensity to recruit the contralesional motor cortex when conducting tasks involving the arms (9–11). However, these methods were limited by the low temporal resolutions to reveal the transient relationship between the cortical and muscular dynamics in the investigation of the post-stroke compensatory mechanism to activate proximal muscle contractions in compensation for distal movements in the upper limb.

Electroencephalogram (EEG) and electromyogram (EMG) can capture faster dynamics in the cortex and peripheral muscles, respectively, comparing with the imaging techniques mentioned above. Furthermore, previous studies have found that the coherence between the two parameters can result in the demonstration of time-based functional connections in the neuromuscular pathways when subjects perform specific motion tasks (12, 13). This also makes it possible to identify the location of cortical sources and trace the neuroplasticity after stroke according to the coherence topography (14). The coherence between EEG and EMG was first described by Salenius et al. (15) and Gerloff et al. (16), who referred to it as corticomuscular coherence (CMCoh) to reflect voluntary descending control from the primary motor cortex to the effector muscles. Coherence can be calculated using both EEG and EMG signals, and it is typically observed within the frequency range of 13–30 Hz (Beta band) during the execution of steady-state isometric contraction and phasic movements (17). The maximum value (i.e., the peak CMCoh) denotes the most significant neuromuscular coupling of the coherent activities and location of the central generator over the whole motor cortex (18, 19). Mima et al. (20) first reported the topographical shift of CMCoh from the lesional side to the contralesional side observed among chronic stroke patients, which may be due to the contribution of lateral and/or medial premotor area control made to the muscles, as suggested by previous PET and electrocorticographic studies (21–23). Furthermore, the neuromuscular coupling between cortical commands and consequent muscle activities indicated by CMCoh values is usually not evident immediately after a stroke; rather, it seems to increase throughout the course of the recovery process gradually. Fang et al. (24) and Larsen et al. (25) reported that the CMCoh values in patients with acute and subacute stroke were weaker than those observed in unimpaired controls, while Chen and colleagues (26) found patients with chronic stroke demonstrated higher CMCoh values from the UE flexors than those in a control group. These studies have consistently indicated that data pertaining to the intensity and location of peak coherence could be employed to estimate the muscle representation areas after neural reorganization following stroke. However, most of the CMCoh studies on stroke patients to date investigating the cerebral-derived control on distal UE segments have been limited to EMG recording from distal muscles, e.g., the extensor carpi radialis muscle (19) or its antagonist muscle flexor carpi radialis (27) in wrist extension at the affected side. Rare studies have employed CMCoh to investigate the contractions of proximal muscles to compensate for distal motions, which could be traced back to a cortical-originated alteration in muscular discoordination at the peripheral.

The purpose of this study was to investigate the corticomuscular coordination pattern in the upper limb muscles during distal finger movements at the affected side of patients with chronic stroke, via a combination of EEG and EMG measurements.

MATERIALS AND METHODS

In the current study, we analyzed the CMCoh of both chronic stroke subjects and age-matched unimpaired subjects to make comparisons on their coherent activities between the motor cortex and effector muscles. The EMG parameters were also analyzed to evaluate the peripheral muscular coordination across the proximal and distal UE segments. For the stroke subjects, the experiment was performed on the affected hand, while the habitual hand was investigated in the case of the unimpaired subjects.

Experimental Setup

EEG and EMG Electrode Configuration

Figure 1A shows the experimental setup of this study. Each subject was comfortably seated in a chair in front of a 14-inch computer screen with his or her testing forearm placed in the neutral position on a horizontally fixed slab. A robotic hand orthosis consisting of a palm-wrist module and five individual finger assemblies (6, 7) was used to fix the wrist straight at a 0°

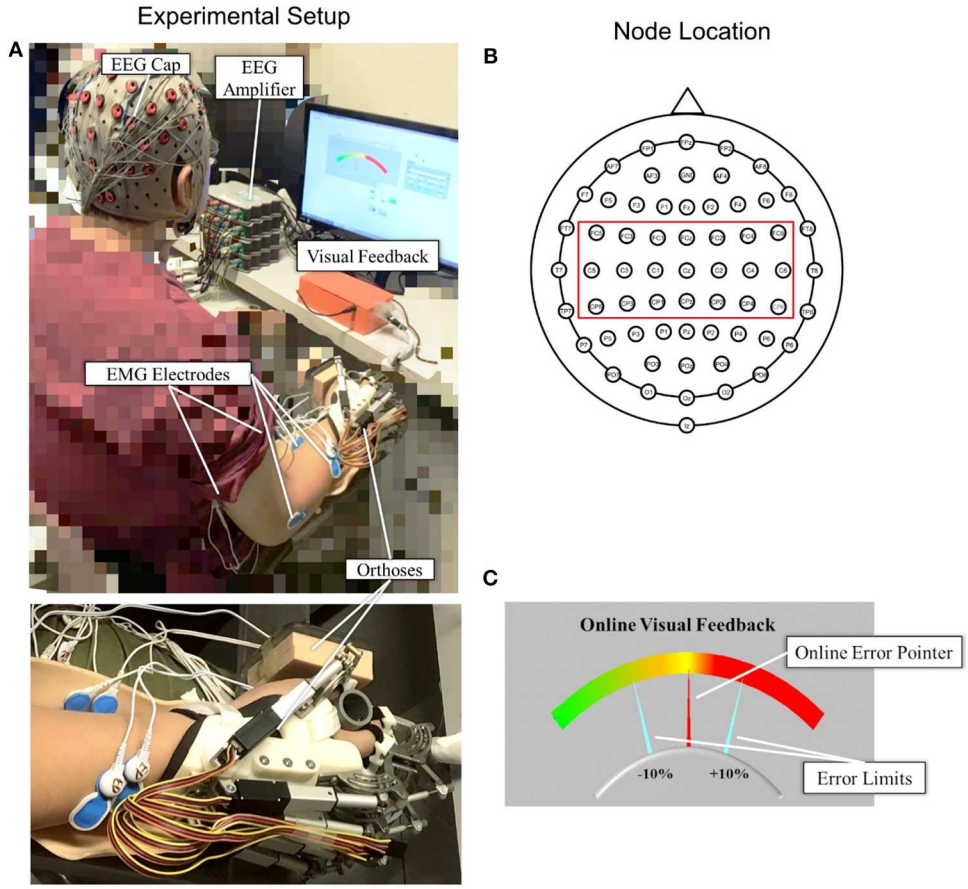

FIGURE 1 | (A) The experimental setup with an enlarged photo of the forearm and hand configuration; **(B)** top view of the 64-channel g.GAMMAsys cap with 21 channels selected for CMCoh analysis; **(C)** the interface of visual feedback for real-time contraction level control: The fixed yellow midline is the target contraction level, and the red pointer shows the real-time muscular contraction level.

angle. The index, middle, ring, and little fingers of the subjects were fixed at a position of 135° at the metacarpophalangeal (MCP) joint and 135° at the proximal interphalangeal (PIP) joints, which was at 50% open of the robotic hand orthosis, also with the thumb finger fixed at an angle of 180° at the MCP joint and 165° at the PIP joint. Then, the experimental upper limb of a subject was attached to the palm orthosis on the slab after wearing the robotic hand, as shown in **Figure 1A**. The weight of the robotic hand is 500 g. The patient arm after wearing the robotic hand was gravity compensated with this setting during the whole experiment. A 64-channel g.GAMMAsys active electrode EEG system referenced to left earlobe and ground at AF_z was mounted on the subject's scalp according to the 10-20 system. The EEG signals from the 21 channels (i.e., C_Z, C_1, C_2, C_3, C_4, C_5, C_6, CP_Z, CP_1, CP_2, CP_3, CP_4, CP_5, CP_6, FC_Z, FC_1, FC_2, FC_3, FC_4, FC_5, FC_6, as shown in **Figure 1B**) covering the sensorimotor area were adopted for the CMCoh analysis. All EEG signals were amplified 10,000 times (amplifier: g.USBamp, USA) before being band-pass filtered from 1 to 100 Hz with a 50 Hz Notch filter. EMG signals were collected from the antagonist muscle pair for finger extension/flexion, i.e., extensor digitorum (ED) and flexor digitorum (FD), and the antagonist muscle pair for elbow extension/flexion, i.e., triceps brachii (TRI) and biceps brachii (BIC), of subjects' UEs. Four pairs of EMG electrodes were attached to the skin surface of the four muscle bellies, with a 2-cm center separation. The reference electrode was attached to the surface of the olecranon. All EMG signals were amplified with a gain of 1000 (amplifier: INA 333, Texas Instruments Inc.) and filtered by a 10 to 500 Hz band-pass filter and the 50 Hz notch filter (7, 28). The impedances of all EEG and EMG electrodes were maintained below 5 kΩ. Both the EEG and EMG signals were synchronized with a sampling frequency of 1,200 Hz by a DAQ card (NI, USB-6009 14-Bit Multifunction DAQ USB) and stored for offline processing. Square wave markers (0.5 s in duration, 2 V for the start and 1 V for the end of the recording) were denoted onto the EEG and EMG trials for synchronized timing in the same recording. Furthermore, the EMG signals produced by the ED and FD were also used for later online processing in a visual feedback motion control evaluation of isometric finger contractions.

Visual Feedback Interface

A self-programmed operation interface based on LABVIEW 2015 was used for visual feedback motion control during the experiment, as shown in **Figure 1C**. The background panel of the screen exhibited a color gradient from left to right, which indicated the variation of contraction level calculated from the real-time EMG of a target muscle. Two fixed aquamarine pointers denoted the acceptable ±10% of the target contraction level with an indicated range in the visual feedback during the dynamic control, as per the work of Meng et al. (19). The real-time contraction level indicated by EMG was calculated as follows:

$$EMG_{c(ED\ orFD)} = \frac{EMG_{(ED\ or\ FD)} - EMG_{base}}{EMG_{\max(ED\ or\ FD)} - EMG_{base}} \times 100\% \quad (1)$$

where $EMG_{(EDorFD)}$ was the mean of the absolute real-time EMG envelope of the ED or FD muscle (i.e., rectified EMG with 10 Hz low-pass filtering) in a 100 ms windows under finger extension or flexion motion task; $EMG_{max(EDorFD)}$ represented the average of the absolute EMG envelope value of the ED muscle in an isometric maximum voluntary extension (iMVE) or FD muscle in an isometric maximum voluntary flexion (iMVF) contraction conducted at the beginning of each experiment; EMG_{base} was the average of the absolute EMG envelope of the muscle during resting state; $EMG_{c(EDorFD)}$ represented the contraction level performed in response to the real-time visual feedback in the user interface (**Figure 1C**) at values ranging from 0 to 100% (0% represented resting status while 100% represented the maximal value from iMVE or iMVF). The isometric maximum voluntary contraction (iMVC) test would be introduced in the protocol later.

Subject Recruitment

After obtaining approval from the Human Subjects Ethics Subcommittee of the Hong Kong Polytechnic University, chronic stroke survivors (stroke group) and age-matched unimpaired subjects (control group) were recruited and subsequently underwent EEG-EMG assessments in an electromagnetic shielded laboratory.

The inclusion criteria for subjects with chronic stroke were as follows: (1) aged between 35 and 70 years old; (2) had a diagnosed unilateral brain lesion due to stroke onset more than 1 year, without other neurological deficits or secondary onset (3, 7) had sufficient cognition (as measured by the Mini-Mental State Examination [MMSE>21]), to understand the content or purpose of the study and follow simple instructions during the assessment (4, 29) had a unilateral UE motor impairment that ranged from severe to moderate, as measured by the Fugl-Meyer Assessment for UE (15 < FMA-UE < 45, with a maximal score of 66) (5, 30) had ≤3 level muscle tension at the elbow, wrist, and fingers at the time of enrollment, as assessed by the Modified Ashworth Scale (MAS) (6, 31) had detectable voluntary EMG (i.e., three times SD above the baseline) from four UE muscles, i.e., ED, FD, TRI, and BIC, within the affected arm (32). The inclusion criteria for the unimpaired subjects were as follows: (1) aged between 35 and 70 years old; (2) no history of any neurological deficits; (3) no upper limb motor dysfunction due to any kind of osteoarticular or peripheral neuromuscular disease. Furthermore, subjects who were pregnant, had been previously diagnosed with severe dysphasia or hypertension, or participated in any intensive upper limb physical practice or botulinum toxin treatment within 1 year before the current experiment were excluded from participating in the research. According to the previous studies (26, 33, 34), the gender factor did not significantly affect the CMCoh parameters. Hence, we had no specific requirement on the gender in the recruitment process.

TABLE 1A | (A) Demographic data of the stroke and age-matched control groups.

Group	No. of Participants	Gender Female/ Male	Age	Stroke Type Hemorrhage/ Ischemic	Experiment Side Right/Left
Stroke	14	3/11	56.5 ± 9.5	7/7	7/7
Control	10	4/6	50.8 ± 15.8	/	7/3

TABLE 1B | Motor impairments of the stroke subjects measured by clinical scores.

Onset years	MAS			FMA		
	Finger	Wrist	Elbow	Full Score	Wrist/ Hand	Shoulder/ Elbow
8.1 ± 4.2	1.1 ± 0.8	1.4 ± 0.7	1.6 ± 0.6	33.6 ± 9.9	11.1 ± 3.2	22.5 ± 7.3

The final study population consisted of 14 chronic stroke patients and 10 unimpaired subjects. Written consent was secured from each participant after they were informed about the research purpose and content. **Table 1** shows the demographic data of all subjects in both groups and the clinical scores of the subjects in the chronic stroke group.

Experiment Protocol

iMVC Test

Each subject was instructed to conduct the iMVC test at the beginning of the experiment as follows: (1) Remain relaxed for 5 s to record the resting EMG levels over three repetitions; (2) execute distal UE joint iMVC movements, i.e., the fingers iMVE and iMVF, with the robotic hand orthosis at 50% open for 5 s over three repetitions; (3) execute proximal UE joint iMVCs, i.e., elbow iMVE and iMVF, for three times, respectively, with the arm fixed by an elbow orthosis with the shoulder abducted at 70° and the elbow flexed at 90°, as per our previous study (28, 35). The participants were provided with a 5 min rest period between two consecutive MVCs to prevent muscle fatigue. The mean values for the EMG envelopes of the three iMVCs of each agonist muscle (i.e., ED for finger iMVE, FD for finger iMVF, TRI for elbow iMVE, and BIC for elbow iMVF) were adopted as the maximum EMG amplitudes for the related muscles, denoted by $EMG_{max(i)}$. The average of the EMG envelopes of the three resting motions of each muscle was denoted by $EMG_{base(i)}$. All the raw EMG data obtained from the iMVC test were recorded and stored for further offline processing at a later stage. The elbow orthosis was

TABLE 2 | The target contraction levels for the CMCoh investigation.

Schemes	Description
20%Ex	Finger extension at 20% iMVE of ED
40%Ex	Finger extension at 40% iMVE of ED
20%Fx	Finger flexion at 20% iMVF of FD
40%Fx	Finger flexion at 40% iMVF of FD

removed after the iMVC test, while the palm and robotic hand orthoses continued to be used in the following finger motion tasks, as shown in **Figure 1A**.

Isometric Finger Extension/Flexion Tasks

After the iMVC test, each individual was instructed to conduct finger extension and flexion motions according to the same limb configuration presented in **Figure 1A** at different contraction levels. According to previous studies (19, 36, 37), constant and moderate (contraction level<50%) muscle contraction can demonstrate the most pronounced CMCoh in the Beta band range without the subject suffering from significant muscle fatigue, with less spontaneous discharges of muscles during the contraction compared with higher levels. The potential residual spontaneous discharges in the recorded EMG were further reduced by the baseline removal in Equation 1. In this work, four contraction schemes at 20 and 40% contraction levels for both finger extension (Ex) and flexion (Fx) were adopted as the motion target for CMCoh investigation, denoted as 20, 40% Ex, 20%, and 40% Fx. A summary of the schemes is provided in **Table 2**.

Each subject randomly performed the four motion schemes in the experiment (**Table 2**). The subjects were provided with a visual instruction on the screen showing the name of the target scheme and subsequently performed isometric extension or flexion contractions with the fixed 50% opened robotic hand orthosis at an appropriate strength to try and maintain the position of the red pointer at the midline of the plate (i.e., the target scheme). The ideal control corresponded to a 0% deviation from the midline over 35 s, and the fluctuation needed to be maintained within the ±10% error region, which was the achievable range for stroke subjects in the preliminary study (19). Each motion scheme was repeated five times with a 2 min rest after two consecutive contractions to minimize the effect of fatigue. The EMG mean power frequency (MPF) was calculated offline and any data with 10% reduction in the MPF was treated as fatigue (38). No fatigue was detected during the trials. All subjects were also instructed to minimize the possible bite, eye blinking and body movement during the contraction.

EEG EMG Processing

All subjects were instructed to conduct 35 s contraction in each trial, and we omitted the last 5 s during the offline processing, and each contraction repeated for 5 times. Then, we chopped the signal trial into epochs with a unit length of 1,024 point/epoch when the sampling frequency was 1,200 Hz (19, 39, 40). In the current study, non-rectified EMG signals were used for the CMCoh calculation to minimize frequency distortion as a result of the rectification (41). A total of 150 s of EEG and EMG signals were collected from each subject over the course of the five trials, following which 175 epochs were obtained, i.e. (1,200*30/1,024)*5, with respect to each scheme presented in **Table 2** and subsequently used for the coherence estimation as follows (42):

$$\boldsymbol{CMCoh}\ (\sigma) = \frac{\left| f_{xy}\ (\sigma) \right|^2}{f_{xx}\ (\sigma) \cdot f_{yy}\ (\sigma)} \tag{2}$$

where $f_{xx}(\sigma)$ and $f_{yy}(\sigma)$ represented the auto-spectrum of the selected EEG signal and EMG signal, respectively, and $f_{xy}(\sigma)$ represented the cross-spectrum of EEG and EMG. The confidence level was calculated according to the following equation:

$$\boldsymbol{CL}_{(\alpha\%)} = 1 - \left(1 - \frac{\alpha}{100}\right)^{\frac{1}{N-1}} \tag{3}$$

$$\boldsymbol{N} = \frac{\textit{Sampling Rate} \times \textit{Data Length} \times \textit{Trial Number}}{\textit{Epoch Length}} \tag{4}$$

where α was the significance level (α was 95 in this study, corresponding to a P value of 0.05); $\boldsymbol{N}$ was the number of data epochs ($\boldsymbol{N}$ =175 in this study); and $\boldsymbol{CL}_{(\alpha\%)}$ (0.0170 in this study) represented the coherence confidential limit, above which the coherence was considered to be significant.

The peak CMCoh of a target muscle (i.e., ED, FD, TRI, or BIC) was utilized to describe the highest significant coherence (19, 37, 40) among the 21 EEG channels and an EMG channel in the Beta band (13–30 Hz) during the finger extension and flexion movements. CMCoh topology was used to find the most related cortical activation area of the subjects in both groups.

In this study, EMG parameters were also adopted to investigate the muscle activation level and co-contraction pattern during the finger movements, (1) normalized EMG activation level (35) of ED, FD, TRI and BIC muscles; and (2) co-contraction index (CI)(35) between a pair of muscle (i.e., ED-FD, ED-TRI, ED-BIC, FD-TRI, FD-BIC, and TRI-BIC).

The EMG signals of a muscle $\boldsymbol{i}$ (i.e., ED, FD, TRI or BIC) were firstly normalized with the resting and iMVC EMG data expressed previously in iMVC Test as follows:

$$\boldsymbol{nEMG_i} = \frac{\boldsymbol{EMG_i} - \boldsymbol{EMG_{base(i)}}}{\boldsymbol{EMG_{max(i)}} - \boldsymbol{EMG_{base(i)}}} \tag{5}$$

Then the normalized EMG activation level was processed as follows:

$$\overline{\boldsymbol{EMG}} = \frac{1}{T} \int_0^T \boldsymbol{nEMG_i}\ (t)\ dt \tag{6}$$

where $\overline{\boldsymbol{EMG}}$ was the muscle activation level of muscle i, $\boldsymbol{nEMG_i}\ (t)$ was the normalized EMG linear envelope of the muscle over the duration of five isometric contractions, and $\boldsymbol{T}$ was the length of the signal.

The CI between a pair of muscles could be expressed as:

$$\boldsymbol{CI} = \frac{1}{T} \int_0^T \boldsymbol{A_{ij}}\ (t)\ dt \tag{7}$$

where $A_{ij}(t)$ represented the overlapping activity of the normalized EMG linear envelopes (as per Equation 6) of a pair of muscles (i and j). The CI value was between 0 (no overlapping) to 1 (fully overlapping) as adopted in previous robot-assisted post-stroke training studies (6, 7, 35). Higher CI values indicated a more significant co-contraction observed within the muscle pair, and lower CI values suggested a separation in the muscle activation across the muscle.

Statistical Analysis

The Lilliefors method was used to conduct normality tests on both the CMCoh values and the EMG parameters. The findings revealed that the data were normally distributed ($P > 0.05$). The demographic data of the stroke and unimpaired control groups were examined for baseline differences using the independent t-test and the Fisher exact test. Subjects in both groups did not differ significantly in terms of age, gender, and the side of the experimental hand ($P > 0.05$). The amplitudes of peak CMCoh and EMG parameters were first analyzed using the independent t-test to compare the intergroup differences under different motion schemes. Subsequently, a paired t-test was performed to investigate the intragroup variation of CMCoh and EMG parameters with respect to the factor of contraction level (i.e., 20 and 40%) for each muscle when conducting extension and flexion motions. The statistical significance was set at 0.05 in this study. All statistical calculations in the study were performed using SPSS 24.0 (2016). The levels of statistical significance were also indicated at 0.05, 0.01, and 0.001.

RESULTS

All the stroke and unimpaired subjects completed the four motion schemes at the finger joints.

Corticomuscular Coherence

Figure 2 illustrates the representative CMCoh spectra of the four muscles with corresponding frequencies to the peak value and representative topographic maps of coherence of a stroke subject and an unimpaired subject during right hand 20% Ex and 20% Fx schemes. When conducting 20% Ex, significant peak ED, FD, TRI, and BIC CMCohs were observed in the contralateral (left) hemisphere in the unimpaired subject. By contrast, the stroke subject presented peak TRI and BIC CMCohs on the contralesional (right) hemisphere and peak FD CMCohs on the central region showing the post-stroke shift of cortical activations during the 20% Ex scheme.When performing the 20% Fx movements, the pronouced shift of the peak CMCohs can be also observed in the stroke subject, i.e., ED and FD CMCohs shifted to the central region, and TRI and BIC CMCohs shifted to the contralesional (right) hemisphere. **Figure 2** represents the topography features of 64% stroke subjects (9/14) and 70% unimpaired subjects (7/10) in this work.

Figure 3 demonstrates the variations in peak CMCohs of both groups under the two contraction schemes when conducting finger extension (**Figure 3A**) and flexion (**Figure 3B**) movements. The following could be observed in **Figure 3A** during extension tasks: (1) Peak ED CMCohs were significantly lower in the stroke group than in the control group at 20% Ex ($P < 0.001$, effect size [EF]=1.645, independent t-test, **Table 3**); (2) peak FD CMCohs were significantly lower in the stroke group than in the control group at 40% Ex ($P < 0.001$, EF = 1.098, independent t-test, **Table 3**); (3) there was no significant intergroup difference between the stroke subjects and unimpaired controls in terms of peak TRI and BIC CMCohs observed during finger extension movements at both 20 and 40% Ex schemes. **Figure 3A** also demonstrates the following in terms of the intragroup comparison during extension tasks: (1) Peak ED CMCohs at 20% Ex were significantly higher ($P < 0.001$, EF = 1.969, paired t-test, **Table 3**) than those at 40% Ex for the unimpaired control subjects; (2) peak FD CMCohs at 20% Ex were significantly lower than those at 40% Ex ($P < 0.05$, EF = 1.057, paired t-test, **Table 3**) in the control group; (3) there was no significant change in the peak TRI or BIC CMCohs between the 20 and the 40% Ex schemes in the control group; (4) by contrast, the stroke group showed significantly higher peak TRI and BIC CMCohs at 20% Ex than those at 40% Ex (TRI: $P < 0.01$, EF = 1.324, paired t-test, **Table 3**; BIC: $P < 0.01$, EF = 1.366, paired t-test, **Table 3**); (5) there was no significant intragroup difference in peak ED or FD CMCohs between the two extension schemes for the stroke subjects. **Figure 3B** demonstrates that there was no significant intergroup difference between stroke and unimpaired control subject and no significant intragroup difference between 20 and 40% Fx schemes in the peak CMCohs as observed. All the statistical results pertaining to the values of peak CMCohs are summarized in **Table 3**, including the means and 95% confidence intervals, together with the paired t-test probabilities and EFs with respect to contraction levels, and independence t-test probabilities and EFs with respect to the group.

EMG Parameters

Figure 4 demonstrates the normalized EMG activation levels observed in the four muscles during different contraction schemes. In each motion scheme, the EMG activation level of the agonist muscle, i.e., ED or FD, was maintained at around 0.2 or 0.4 (i.e. the 20 and 40% target level), respectively, during the finger extensions and flexions.

Figures 4A–C shows the normalized EMG activation levels of FD, TRI, and BIC during finger extension. Significant intergroup differences were observed in the FD at 40% Ex ($P < 0.05$, EF = 0.915, independent t-test, **Table 4A**) and the TRI and BIC at both 20% Ex (TRI: $P < 0.01$, EF = 1.254, independent t-test; BIC: $P < 0.05$, EF = 0.964, independent t-test, **Table 4A**) and 40% Ex (TRI: $P < 0.05$, EF = 1.162, independent t-test; BIC: $P < 0.05$, EF = 1.085, independent t-test, **Table 4A**). Significantly lower FD but higher TRI and BIC activation levels were observed in the stroke group than those observed in the control group. Significant intragroup differences between the 20% Ex and 40% Ex contraction levels were observed only in the control group in the FD and TRI muscles (FD: $P < 0.05$, EF = 0.557, paired t-test; TRI: $P < 0.05$, EF = 0.955, paired t-test, **Table 4A**).

Figures 4D–F present the normalized EMG activation levels of ED, TRI, and BIC during flexion motion tasks. Significant intergroup differences were observed in the BIC at 40% Fx (P

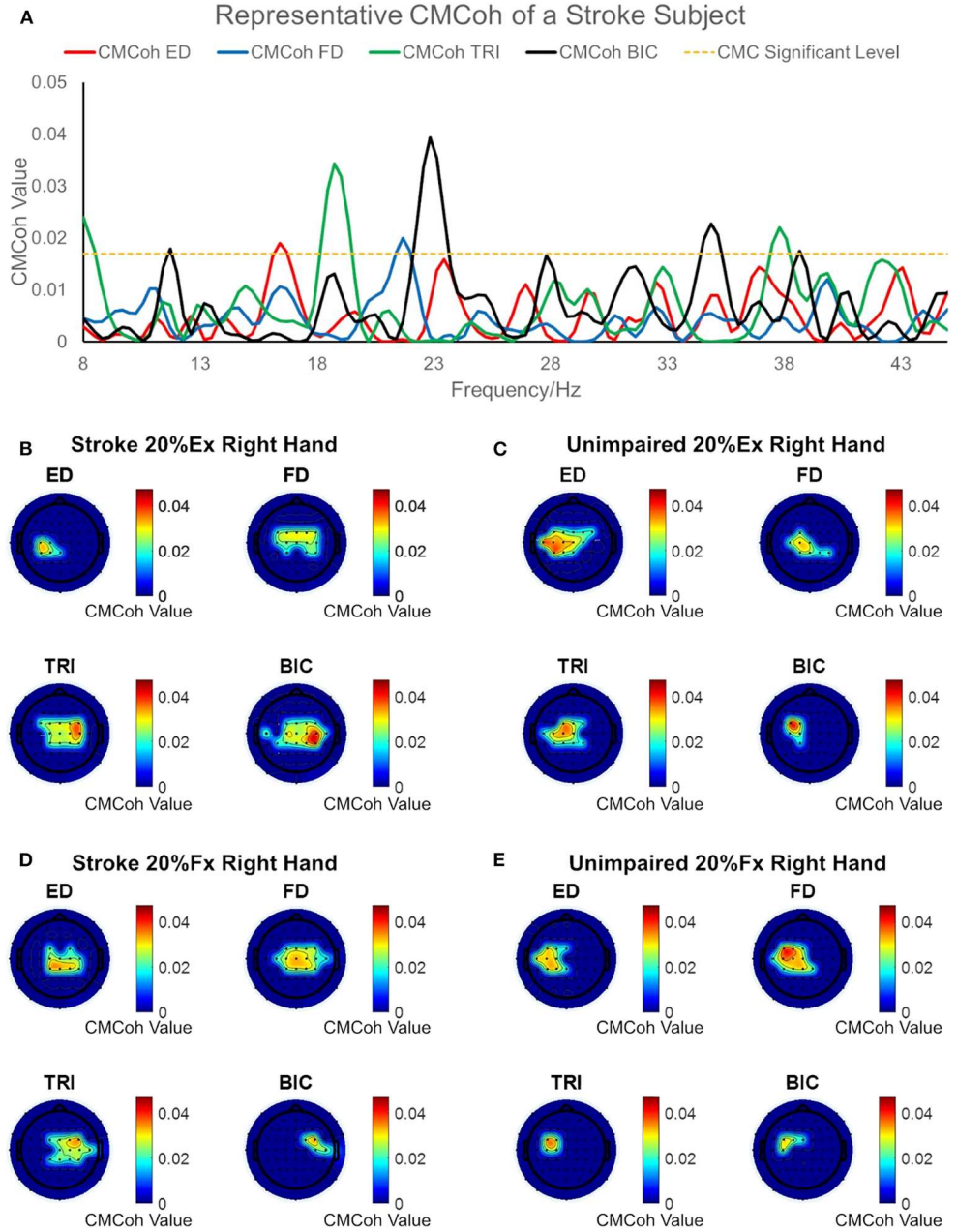

FIGURE 2 | (A) Representative CMCoh spectra with CL ($\alpha\% = 95\%$, $N = 175$) level from the peak CMCoh channels of a right hemiplegic subject in right hand 20% Ex; **(B–E)** representative topographical CMCoh map with peak CMCohs: **(B)** the stroke subject in right hand 20% Ex;**(C)** a right-handed unimpaired subject in right hand 20% Ex; **(D)** the stroke subject in right hand 20% Fx; **(E)** the unimpaired subject in right hand 20% Fx. The peak CMCoh values, corresponding frequency (Hz) and channels in **(B–E)** are shown in the table below.

Figures	Scheme		ED	FD	TRI	BIC
(B)	Stroke 20%Ex	Peak Value	0.0287	0.0276	0.0343	0.0394
		Frequency	27.54	27.54	18.75	22.85
		Channel	C_3	C_z	C_4	C_4
(C)	Control 20%Ex	Peak Value	0.0346	0.0309	0.0338	0.0391
		Frequency	17.87	21.68	21.09	22.56
		Channel	CP_3	C_1	C_1	FC_3
(D)	Stroke 20%Fx	Peak Value	0.0319	0.0325	0.0321	0.0297
		Frequency	15.23	20.51	18.46	13.80
		Channel	CP_z	C_z	FC_4	FC_4
(E)	Control 20%Fx	Peak Value	0.0307	0.0360	0.0323	0.0288
		Frequency	29.88	18.16	21.68	27.83
		Channel	C_3	FC_3	FC_3	FC_3

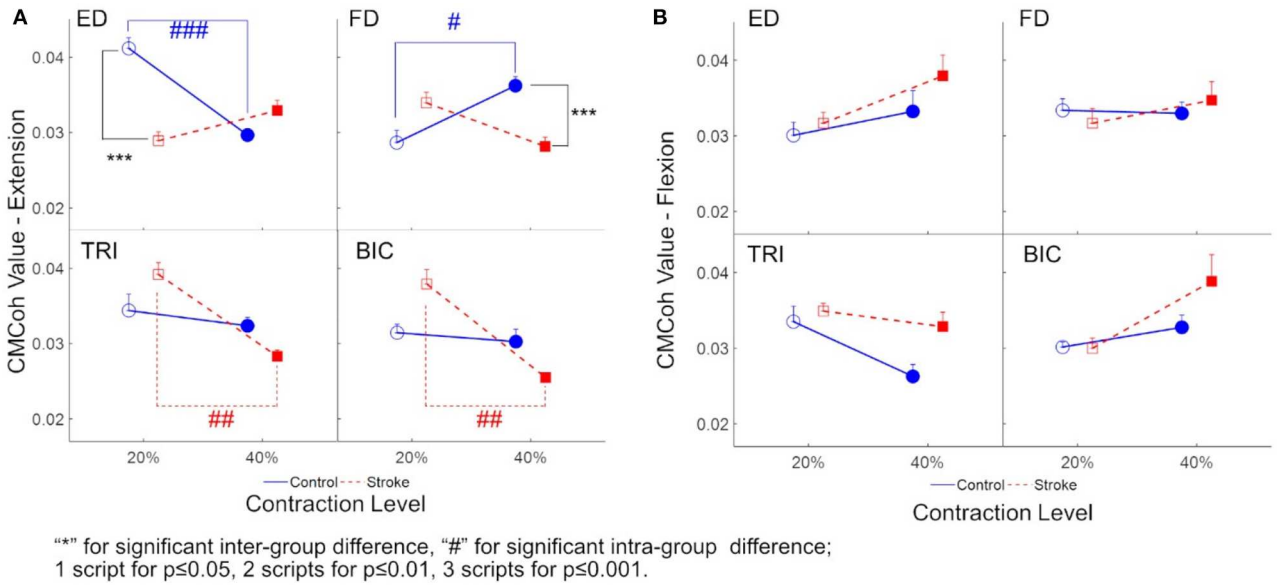

FIGURE 3 | (A) The peak CMCoh values of each muscle (i.e., ED, FD, TRI, and BIC) of both groups (the control group: circles; and the stroke group: squares) in 20 and 40% Exs; **(B)** The peak CMCoh values for the muscles of both groups in 20 and 40% Fxs. 1 superscript for $p \leq 0.05$, 2 superscripts for $p \leq 0.01$, 3 superscripts for $p \leq 0.001$. The significant inter-group difference is indicated by * (independent *t*-test), and # is used to indicate the significant intra-group difference (paired *t*-test).

< 0.05, EF $= 1.108$, independent *t*-test, **Table 4A**) and in the TRI at both 20% Fx ($P < 0.01$, EF $= 1.453$, independent *t*-test, **Table 4A**) and 40% Fx ($P < 0.05$, EF $= 1.166$, independent *t*-test, **Table 4A**). Higher TRI and BIC activation levels were also observed in the stroke group than those in the control group. Significant intragroup differences were observed only in the control group in the ED and TRI muscles between the 20 and 40% Ex contraction levels (ED: $P < 0.05$, EF $=$ 0.558, paired *t*-test; TRI: $P < 0.05$, EF $= 0.656$, paired *t*-test, **Table 4A**).

The varied patterns observed in the CI values between each pair of muscles are illustrated in **Figure 5**. During the extension schemes, significant intergroup differences in CIs between the stroke and unimpaired subjects could be observed in the ED-BIC, ED-TRI, TRI-BIC, FD-BIC and FD-TRI muscle pairs at both 20 and 40% Ex ($P < 0.05$, independent *t*-test, **Table 4B**). While ED-FD only demonstrated significant intergroup difference at 40% Ex ($P < 0.001$, EF $= 1.319$, independent *t*-test, **Table 4B**). Significant intragroup differences were observed only in the control group in the ED-FD ($P < 0.05$, EF $= 1.655$, paired *t*-test, **Table 4B**), ED-TRI ($P < 0.05$, EF $= 0.956$, paired *t*-test, **Table 4B**), and FD-TRI ($P < 0.05$, EF $= 0.958$, paired *t*-test, **Table 4B**) muscle pairs. During the flexion schemes, significant intergroup differences were observed in the ED-TRI at both 20% Fx ($P < 0.01$, EF $= 1.488$, independent *t*-test, **Table 4B**) and 40% Fx ($P < 0.05$, EF $= 1.012$, independent *t*-test, **Table 4B**), FD-BIC at 40% Fx ($P < 0.05$, EF $= 1.147$, independent *t*-test, **Table 4B**), FD-TRI at both 20% Fx ($P < 0.01$, EF $= 1.581$, independent *t*-test, **Table 4B**) and 40% Fx ($P <$ 0.01, EF $= 1.473$, independent *t*-test, **Table 4B**), and TRI-BIC at both 20% Fx ($P < 0.05$, EF $= 1.038$, independent *t*-test, **Table 4B**) and 40% Fx ($P < 0.05$, EF $= 1.113$, independent *t*-test, **Table 4B**). The intragroup differences between 20 and 40% Fx could be observed in the ED-FD ($P < 0.05$, EF $=$ 0.499, paired *t*-test, **Table 4B**), FD-BIC ($P < 0.05$, EF $= 0.371$, paired *t*-test, **Table 4B**) and FD-TRI ($P < 0.05$, EF $= 0.351$, paired *t*-test, **Table 4B**) muscle pairs in stroke subjects, while significant intragroup changes in unimpaired subjects were observed in the ED-FD ($P < 0.01$, EF $= 1.128$, paired *t*-test, **Table 4B**), ED-TRI ($P < 0.05$, EF $= 0.656$, paired *t*-test, **Table 4B**), FD-TRI ($P < 0.05$, EF $= 0.658$, paired *t*-test, **Table 4B**) muscle pairs.

Table 4 summarizes the statistical analysis of the EMG parameters, including the means and 95% confidence intervals, together with the paired *t*-test probabilities and EFs with respect to contraction levels, and independence *t*-test probabilities and EFs with respect to the group.

DISCUSSION

The participants in this study performed isometric finger extension and flexion movements at constant and moderate contraction levels. The values of ED, FD, TRI, and BIC CMCohs were significant ($CMCoh\ (\sigma) > 0.0170$) in both stroke and unimpaired control groups, which suggested the existence of corticomuscular functional coupling from the motor cortex to the muscles in the four distal UE motion schemes (i.e., 20, 40% Ex, 20, and 40% Fx). Although the CMCoh could represent a descending control from the motor cortex to the muscles, high-value CMCohs did not indicate increased muscular output; rather, an increase in cortical control of the movement precision, e.g., either excitatory or inhibitory (39, 43). Therefore, the

TABLE 3 | The means and 95% confidence intervals of the CMCohs in each muscle during different contraction schemes with paired *t*-test probabilities between the two contraction levels and the independent *t*-test probabilities between stroke and unimpaired control groups.

		Mean (95% Confidential Interval) $\times 10^{-2}$		*P*-value (Effect size)
CMCoh	**Group**	**20% Ex**	**40% Ex**	**Intra-group *T*-test**
ED	Stroke	2.89 (2.39–3.40)	3.29 (2.56–3.67)	0.410 (0.490)
	Control	4.12 (3.60–4.62)	2.96 (2.65–3.28)	$0.001^{\#\#\#}$ (1.969)
Inter-group *T*-test	*P*-value (Effect size)	0.001^{***} (1.645)	0.511 (0.482)	
FD	Stroke	3.04 (2.46–3.39)	2.77 (2.49–3.02)	0.113 (0.623)
	Control	2.86 (2.27–3.45)	3.62 (3.15–4.09)	$0.035^{\#}$ (1.057)
Inter-group *T*-test	*P*-value (Effect size)	0.564 (0.607)	0.001^{***} (1.098)	
TRI	Stroke	3.91 (3.23–4.52)	2.88 (2.52–3.24)	$0.010^{\#\#}$ (1.324)
	Control	3.44 (2.65–4.23)	3.24 (2.81–3.65)	0.666 (0.234)
Inter-group *T*-test	*P*-value (Effect size)	0.315 (0.454)	0.111 (0.725)	
BIC	Stroke	3.79 (2.78–4.72)	2.55 (2.30–2.80)	$0.009^{\#\#}$ (1.366)
	Control	3.14 (2.74–3.55)	3.03 (2.39–3.66)	0.784 (0.168)
Inter-group *T*-test	*P*-value (Effect size)	0.105 (0.674)	0.089 (0.755)	
CMCoh	**Group**	**20% Fx**	**40% Fx**	**Intra-Group *T*-test**
ED	Stroke	3.17 (2.58–3.76)	3.79 (2.65–4.92)	0.141 (0.442)
	Control	3.00 (2.40–3.62)	3.32 (2.34–4.30)	0.537 (0.277)
Inter-group *T*-test	*P*-value (Effect size)	0.687 (0.186)	0.514 (0.293)	
FD	Stroke	3.17 (2.37–3.96)	3.47 (2.64–4.47)	0.400 (0.196)
	Control	3.33 (2.61–4.07)	3.29 (2.73–3.86)	0.914 (0.054)
Inter-group *T*-test	*P*-value (Effect size)	0.737 (0.120)	0.764 (0.158)	
TRI	Stroke	3.49 (3.07–3.91)	3.29 (2.51–4.05)	0.475 (0.186)
	Control	3.33 (2.60–4.10)	2.62 (2.06–3.19)	0.094 (0.798)
Inter-group *T*-test	*P*-value (Effect size)	0.704 (0.169)	0.168 (0.668)	
BIC	Stroke	3.00 (2.45–3.55)	3.88 (2.44–5.32)	0.169 (0.472)
	Control	3.02 (2.54–3.49)	3.28 (2.69–3.86)	0.502 (0.422)
Inter-group *T*-test	*P*-value (Effect size)	0.962 (0.071)	0.450 (0.354)	

*1 superscript for $p \leq 0.05$, 2 superscripts for $p \leq 0.01$, 3 superscripts for $p \leq 0.001$. The significant inter-group difference is indicated by * (independent t-test), and # is used to indicate the significant intra-group difference (paired t-test).*

EMG parameters from the muscles were used to provide supplementary information to the significant CMCohs to support the identification of insights into the exact function of the coupling in the results. Distinct central rhythms and descending control of the UE muscles in both groups were observed in this study.

Finger Extension

The peak ED CMCohs of the unimpaired control group were significantly higher at 20% Ex than those observed at 40% Ex (**Figure 3A**). This was indicative of a higher assertion of cortical efforts in a more precise and agile motion control, which was consistent with the fact that most subjects exhibited more difficulties (higher degree of fluctuation of error) during the 30 s contraction tasks within the 20% scheme than they showed within the 40% scheme. We estimated the contraction accuracy for the two groups by evaluating the root-mean-square-error (RMSE) between the real-time contraction level of a target muscle (i.e., *EMGc* in Equation 1) in both extension and flexion and the target contraction level (i.e., 20 or 40% Ex and Fx). It was observed that during 20% Ex and Fx, the stroke (0.056 ± 0.033, mean $\pm$ standard deviation) demonstrated larger ($P = 0.012$, *t*-test) RMSE than the control (0.021 ± 0.022). However, there was no difference ($P = 0.319$, *t*-test) in RMSE between the two (the stroke: 0.051 ± 0.031; the control: 0.035 ± 0.037) during 40% Ex and Fx. The RMSEs showed no difference between the 20 and 40% contraction levels for the stroke group ($P = 0.614$, paired *t*-test). However, stroke participants reported verbally the experienced difficulties in controlling 20% contractions. Previous studies have found similar findings showing a correlation between motor cortical activation and the level of motion difficulties (44–47). The peak TRI and BIC CMCohs exhibited no significant changes between 20 and 40% Ex in the unimpaired subjects, implying uniform cortical effort over the two proximal muscles in the finger contractions.

The ED CMCoh patterns observed in the unimpaired group were not replicated in the ED of stroke subjects; however, they were observed across other UE muscles, especially the proximal UE muscles (i.e., TRI and BIC), which exhibited higher CMCohs than those of the FD during the 20% Ex. It demonstrated the cortical deviation of "learned-disuse" pattern after long-term loss of distal muscle functions and relevant proximal compensatory contractions (48, 49). The result was consistent with the EMG activation level results (**Figures 4A–C**) and the CI values (**Figure 5A**): **Figure 4A** demonstrated comparable FD EMG activation levels of both groups at 20% Ex and significant lower values in stroke group at 40% Ex, while **Figures 4B,C** illustrated significantly higher TRI and BIC activation levels at both 20 and 40% Ex in the stroke group than those in the control group. Besides, **Figure 5A** demonstrated that the co-contraction patterns between proximal and distal muscles of the chronic stroke patients, with significant higher CI values of ED-TRI, ED-BIC, FD-TRI, FD-BIC, and TRI-BIC at both 20 and 40% Ex, were different from those of the unimpaired controls. The EMG results illustrated that the proximal UE muscles were mainly activated by the brain during the finger extensions even at a lower contraction level and showed markable

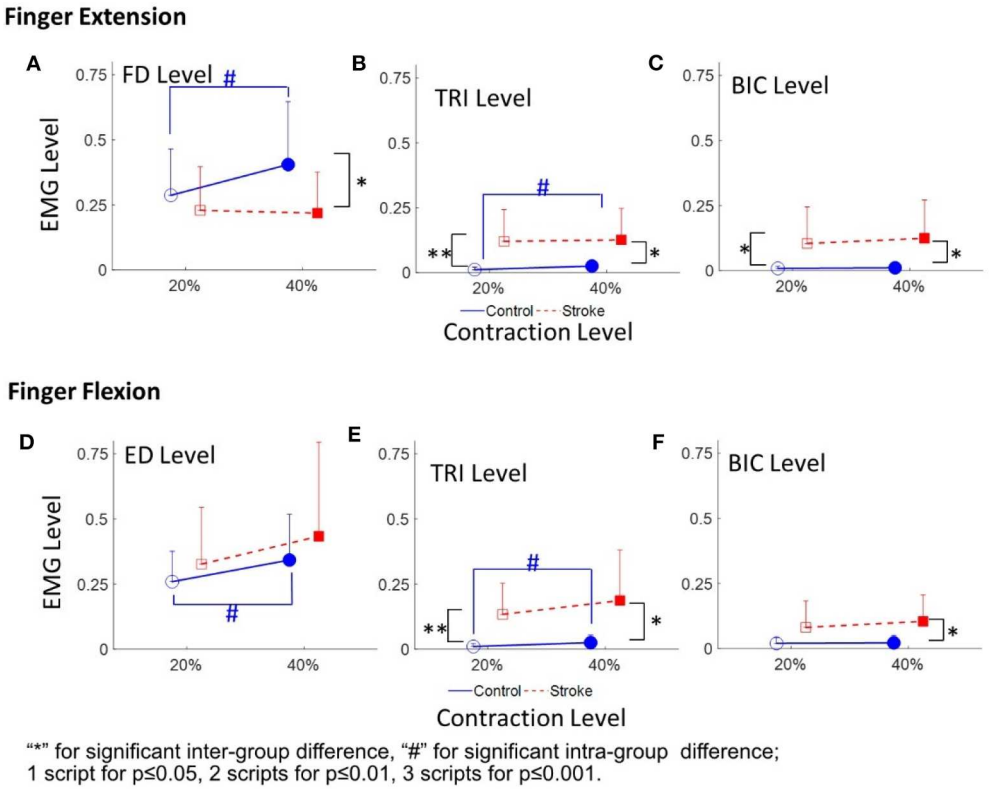

FIGURE 4 | The EMG activation levels of FD **(A)**, TRI **(B)**, and BIC **(C)** in 20 and 40% Exs, and the EMG activation levels of ED **(D)**, TRI **(E)**, and BIC **(F)** in 20 and 40% Fxs, for the two groups. 1 superscript for $p \leq 0.05$, 2 superscripts for $p \leq 0.01$, 3 superscripts for $p \leq 0.001$. The significant inter-group difference is indicated by * (independent *t*-test), and # is used to indicate the significant intra-group difference (paired *t*-test).

lower motion independence of the distal fingers in patients with chronic stroke. The shift of peak CMCoh values in **Figure 2** further indicated that the activation of contralesional sensorimotor cortex mainly contributed to such brain-induced compensatory pattern in a "learned-disuse" behavioral change'. The neurophysiological basis could be associated the capability of the neurons and neuron aggregates to adapt to the brain lesion (50): As a result of damage to the brain neuron axon, its stump is extended to the target issues or neuron cells to facilitate the creation of new synapses (51). At the same time, normal axons in the proximity of the injured region grow and extend to the target neurons (52). Previous studies involving fMRI have predominantly reported a shift in corticomotor activations from the ipsilesional side to the contralesional side in chronic stroke patients (53, 54). However, there is a lack of evidence relating to the impact that ipsilateral/contralesional corticospinal connections have on the distal muscle control during hand movements after stroke (55–57). The results of the current study (**Figure 2**) suggested that the similar cortical location shift was mainly related to the compensatory effects of the proximal UE muscles. The synaptic pruning and recreation (synaptogenesis) of neurons potentially stimulate the proximal muscles to perform a compensatory function.

The peak ED CMCohs of the stroke group increased from the low-level contraction to the high-level task. This could be due to the muscle weakness of ED (41) and the fact that stroke patients need to recruit more cortical effort when performing a higher-level contraction task. Unlike the ED muscle, the peak FD CMCohs of the unimpaired control group were lower at 20% Ex than that at 40% Ex. This was because FD is the antagonist muscle to the ED muscle; as such, to maintain joint stability within the wrist at a higher extension contraction level (58, 59), the subjects needed to increase the level of cortical effort to perform FD contractions correspondingly. By contrast, the peak FD CMCohs of the stroke group decreased from low-level to high-level finger extensions and the values were significantly lower than those of the unimpaired control group. It raised a possibility that the weakened antagonism of FD muscle after the stroke as shown in the EMG parameters, i.e., lower FD activation level and lower ED-FD CI than the control, was subsequent to the central functional loss of ED, rather than an initiative weakness in the flexor muscle.

Finger Flexion

Larsen et al. reported a reduction in CMCoh immediately following stroke and indicated that CMCoh did not appear significantly in the early recovery of hand function (25). In the current study, we found significant peak CMCoh ($CMCoh\ (\sigma) > 0.0170$) of all UE muscles in chronic stroke patients during both 20 and 40% Fx schemes. This suggested that the corticomuscular

TABLE 4 | The mean and 95% confidence intervals of EMG parameters during finger extension and flexion, with the intra-group paired *t*-test probabilities between the two contraction levels and the inter-group independent *t*-test probabilities.

		Mean (95% Confidential Interval) $\times 10^{-2}$		*P*-value (Effect size)
EMG Level	**Group**	**20% Ex**	**40% Ex**	**Intra-group *T*-test**
(A) THE EMG ACTIVATION LEVEL				
FD	Stroke	22.92 (12.33–33.50)	21.81 (11.88–31.74)	0.722 (0.068)
	Control	24.25 (15.28–33.21)	40.50 (21.89–59.10)	0.021# (0.557)
Inter-group *T*-test	*P*-value (Effect size)	0.447 (0.334)	0.043* (0.915)	
TRI	Stroke	12.01 (4.291–19.73)	12.58 (4.942–20.23)	0.777 (0.048)
	Control	1.110 (0.406–1.803)	2.508 (1.119–3.823)	0.012#(0.955)
Inter-group *T*-test	*P*-value (Effect size)	0.010** (1.254)	0.014* (1.162)	
BIC	Stroke	9.919 (0.960–18.87)	10.85 (1.704–20.01)	0.213 (0.138)
	Control	0.844 (0.212–1.476)	1.058 (0.210–1.904)	0.430 (0.208)
Inter-group *T*-test	*P*-value (Effect size)	0.048* (0.964)	0.038* (1.085)	
EMG Level	**Group**	**20% Fx**	**40% Fx**	**Intra-group *T*-test**
ED	Stroke	32.67 (18.94–46.39)	43.36 (17.93–68.78)	0.083 (0.359)
	Control	25.93 (17.46–34.40)	34.35 (21.65–46.84)	0.033# (0.558)
Inter-group *T*-test	*P*-value (Effect size)	0.369 (0.385)	0.484 (0.321)	
TRI	Stroke	13.39 (5.878–20.91)	18.68 (6.500–30.87)	0.096 (0.329)
	Control	1.059 (0.216–1.903)	2.522 (0.417–4.623)	0.039# (0.656)
Inter-group *T*-test	*P*-value (Effect size)	0.004** (1.453)	0.014* (1.166)	
BIC	Stroke	8.121 (1.771–14.46)	10.47 (4.077–16.85)	0.180 (0.232)
	Control	2.013 (0.419–3.607)	2.195 (0.900–4.297)	0.802 (0.071)
Inter-group *T*-test	*P*-value (Effect size)	0.062 (0.837)	0.017* (1.108)	
CI	**Group**	**20% Ex**	**40% Ex**	**Intra-group *T*-test**
(B) THE CI BETWEEN MUSCLES				
ED-FD	Stroke	14.76 (9.026–20.50)	16.37 (9.897–22.83)	0.291 (0.165)
	Control	16.93 (14.35–19.51)	30.32 (22.40–38.22)	0.001### (1.655)
Inter-group *T*-test	*P*-value (Effect size)	0.503 (0.312)	0.007** (1.319)	
ED-BIC	Stroke	7.858 (1.803–13.91)	9.714 (2.926–16.50)	0.082 (0.182)
	Control	0.844 (0.212–1.476)	1.058 (0.210–1.905)	0.430 (0.208)
Inter-group *T*-test	*P*-value (Effect size)	0.027* (1.026)	0.017* (1.128)	
ED-TRI	Stroke	9.645 (3.764–15.53)	11.20 (4.851–17.54)	0.394 (0.159)
	Control	1.110 (0.405–1.801)	2.509 (1.194–3.824)	0.012# (0.956)
Inter-group *T*-test	*P*-value (Effect size)	0.008** (1.285)	0.012* (1.198)	
FD-BIC	Stroke	8.110 (1.363–14.85)	9.682 (1.876–17.49)	0.143 (0.136)
	Control	0.799 (0.240–1.358)	1.058 (0.210–1.905)	0.322 (0.263)
Inter-group *T*-test	*P*-value (Effect size)	0.036* (0.962)	0.033* (0.978)	
FD-TRI	Stroke	8.970 (1.928–16.01)	9.886 (2.982–16.79)	0.414 (0.083)
	Control	1.100 (0.406–1.796)	2.508 (1.193–3.822)	0.012# (0.958)
Inter-group *T*-test	*P*-value (Effect size)	0.032* (0.99)	0.004** (0.938)	
BIC-TRI	Stroke	6.174 (0.366–11.98)	7.619 (1.126–14.11)	0.192 (0.147)
	Control	0.310 (0.101–0.519)	0.527 (0.274–0.780)	0.060 (0.693)
Inter-group *T*-test	*P*-value (Effect size)	0.048* (0.898)	0.035* (0.971)	
CI	**Group**	**20% Fx**	**40% Fx**	**Intra-Group *T*-test**
ED-FD	Stroke	18.54 (11.31–25.78)	25.09 (15.94–34.23)	0.006## (0.499)
	Control	18.34 (14.54–22.16)	26.69 (20.19–33.20)	0.004## (1.128)
Inter-group *T*-test	*P*-value (Effect size)	0.957 (0.023)	0.770 (0.133)	
ED-BIC	Stroke	5.246 (1.515–8.977)	7.949 (2.552–13.34)	0.095 (0.366)
	Control	2.005 (0.417–3.592)	2.185 (0.103–4.267)	0.803 (0.071)
Inter-group *T*-test	*P*-value (Effect size)	0.099 (0.725)	0.064 (0.902)	
ED-TRI	Stroke	8.664 (3.925–13.40)	11.55 (5.060–18.06)	0.165 (0.533)
	Control	1.059 (0.214–1.903)	2.519 (0.415–4.623)	0.039# (0.656)
Inter-group *T*-test	*P*-value (Effect size)	0.005** (1.488)	0.028* (1.012)	

(Continued)

TABLE 4 | Continued

CI	Group	Mean (95% Confidential Interval) $\times 10^{-2}$		*P*-value (Effect size)
		20% Ex	40% Ex	Intra-group *T*-test
FD-BIC	Stroke	6.260 (1.927–10.59)	9.015 (4.041–13.98)	0.010# (0.371)
	Control	2.001 (0.424–3.580)	2.193 (0.096–4.291)	0.790 (0.076)
Inter-group *T*-test	*P*-value (Effect size)	0.062 (0.834)	0.014* (1.147)	
FD-TRI	Stroke	10.80 (5.364–16.24)	14.25 (7.410–21.09)	0.016# (0.351)
	Control	1.056 (0.213–1.898)	2.520 (0.417–4.624)	0.039# (0.658)
Inter-group *T*-test	*P*-value (Effect size)	0.002** (1.581)	0.003** (1.473)	
BIC-TRI	Stroke	5.090 (1.277–8.903)	6.863 (2.920–10.81)	0.177 (0.288)
	Control	0.617 (0.164–1.071)	1.622 (0.025–3.270)	0.109 (0.609)
Inter-group *T*-test	*P*-value (Effect size)	0.026* (1.038)	0.016* (1.113)	

*1 superscript for $p \leq 0.05$, 2 superscripts for $p \leq 0.01$, 3 superscripts for $p \leq 0.001$. The significant inter-group difference is indicated by * (independent t-test), and # is used to indicate the significant intra-group difference (paired t-test).*

coupling has been reestablished during the chronic stage of stroke (19, 26). However, the reconstructed pattern could be different from that of the CMCohs observed among the movements of the unimpaired subjects. Even though the peak FD and ED CMCohs of the chronic stroke subjects during the flexion schemes have reached similar levels to those observed among the unimpaired subjects (**Figure 3**), the peak CMCohs of the distal muscles have shifted to the central region (**Figure 2**). This could be attributed to the activation of bilateral cortico-reticulospinal connections, as indicated in the study on primates performed by Soteropoulos et al. (60), which found that pontomedullary reticular formation contributed to the control of finger motions, especially those related to slow and fine movements.

In the unimpaired control group, the increment in peak BIC CMCohs and the reduction of peak TRI CMCohs observed from low-level to high-level contractions were associated with the stable EMG activation levels of both proximal UE muscles. The significant peak CMCohs of TRI and BIC could be related to the inhibition of the motions from the proximal muscles during the distal movements; i.e., the CMCoh of TRI was for the inhibition of the antagonist extensor and CMCoh of BIC was for the synergistic flexor during the finger flexion movements in the control (52, 61, 62).

Despite the fact that no significant intra-group and inter-group difference in peak TRI and BIC CMCohs was found, significant differences in the EMG parameters were observed between the stroke group and the unimpaired control groups as shown in **Figures 4D–F**, **5B**. **Figure 4D** demonstrated significant increase of ED activation level from 20 to 40% Fx in the unimpaired group, while no similar variation was found in the stroke group. It is reasonable that most stroke patients had the extensor weakness and was used to the "learned-disuse" pattern. **Figure 4E** demonstrated that the TRI activation levels were significantly higher in the stroke group than those in the control group during both 20 and 40% Fx, and **Figure 4F** demonstrated that BIC activation levels were significantly higher in the stroke group than those in the control group during 40% Fx. Furthermore, **Figure 5B** showed that the CI values of TRI-BIC, ED-TRI, FD-TRI at both 20 and 40% Fx as well as the FD-BIC at 20% Fx were also significantly higher in the stroke group. The results indicated that the proximal muscles were abnormally activated during the finger flexions in chronic stroke. Similar to our previous work (6, 7, 35), the results as shown in **Figures 4D–F** illustrated synchronic co-contractions of TRI and BIC during the finger flexions and suggested that the proximal muscles compensated for the distal flexors after stroke. Besides, in the finger flexion movements of the current study, we found that the peak TRI and BIC CMCohs shifted from the ipsilesional side to the contralesional side in chronic stroke patients, similar to the patterns observed in their finger extension exercise (**Figure 2**). Similar findings were reported by Chen et al. in chronic stroke patients with flexion synergy, while the increment of CMCohs of proximal flexors was expressed as a result of increased shared neural drive to both proximal and distal UE flexors (26). These may reflect a possibility that the original inhibition corticomuscular coupling has changed to a facilitation function to activate the proximal compensatory movements for the finger flexion. More investigations are required to confirm the mechanism of neuromuscular coupling after a proximal shift to the contralesional side.

In this study, the stroke participants were chronic strokes with moderate motor impairments measured by clinical behavioral assessments (**Table 1B**). In the chronic stage, behavioral compensation was usually developed. Previous fMRI studies on both animals and humans suggested that increased neural compensation at the cortical level could be interhemispheric for behavioral restorations after stroke (63–65). Carey and Wilkins also detected a shift of corticomotor activations from the ipsilesional to the contralesional in chronic stroke patients (53, 54). The mechanism for the cortical center shift after stroke as suggested by Christian et al. (50) and Chechik et al. (51) was related to the neural plastic strategies by recruiting resources from contralesional (i.e., interhemispheric) and additional intrahemispheric areas. Similar shifts of peak CMCohs were captured in the stroke participants in this study (**Figures 2B,D**). It suggested that the cortical compensation happened in chronic stroke with moderate motor impairments. Furthermore, the CMCohs shifts were mainly related to the proximal muscles in the stroke group, i.e., TRI and BIC shifted to the contralesional side with higher intensities (**Figures 2B,D**), compared to the shifts in the FD and ED (ipsilesional and center areas). It suggested that the post-stroke compensation facilitated more neuroplastic activities on the proximal muscles at the cortical level than the distal finger muscles. The behavioral changes in relation to this proximal compensation were represented by the significant increases in EMG levels (**Figure 4**) and CI values (**Figure 5**) related to the TRI and BIC detected peripherally.

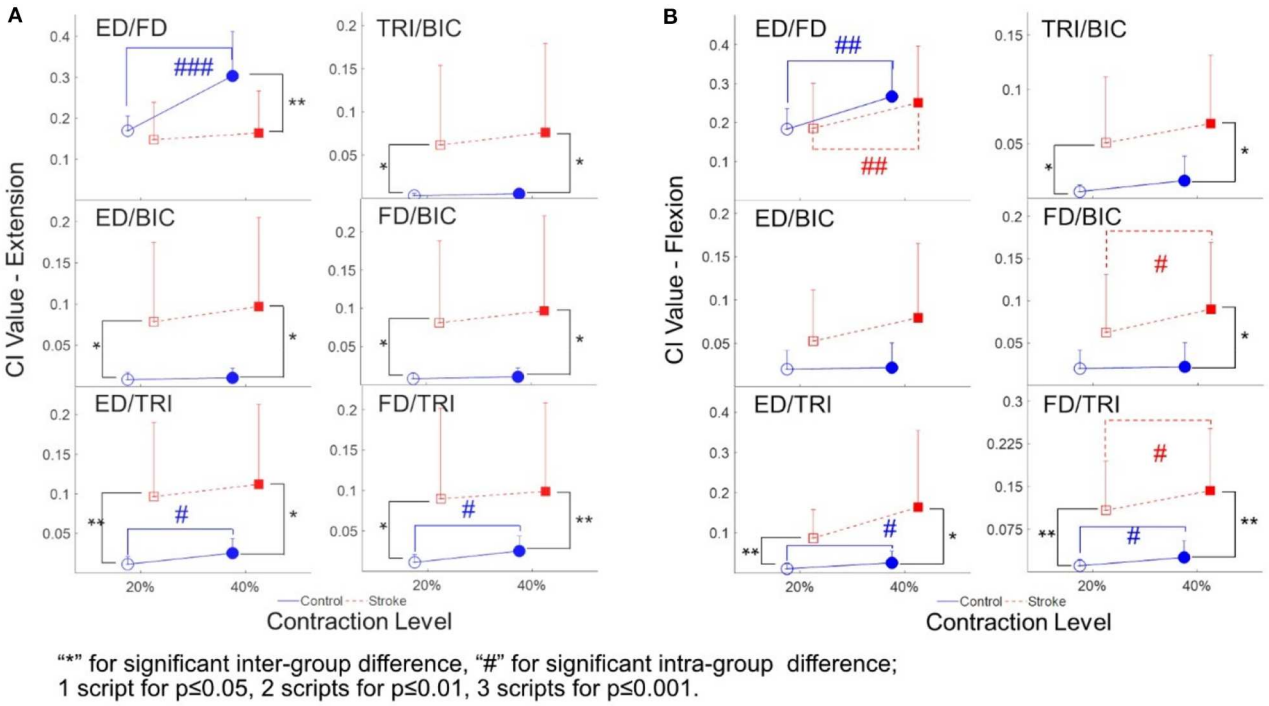

FIGURE 5 | The CI between the muscles of both stroke subjects (squares) and unimpaired subjects (circles): **(A)** The CI values of different muscle pairs during the extensions; **(B)** the CI values of different muscle pairs during the flexions. 1 superscript for $p \leq 0.05$, 2 superscripts for $p \leq 0.01$, 3 superscripts for $p \leq 0.001$. The significant inter-group difference is indicated by * (independent *t*-test), and # is used to indicate the significant intra-group difference (paired *t*-test).

LIMITATIONS

The main limitation of this study is the small sample size. Despite the relatively small populations recruited, we observed consistent results on the corticomuscular variation patterns demonstrated by the stroke patients by both CMCoh and EMG parameters. More investigations with larger scales will be conducted in the future to investigate the mechanism of neuromuscular coupling after a proximal shift to the contralesional side, and also to track the CMCoh variations from early/subacute stroke to the chronic period.

CONCLUSION

Neuromuscular coupling during dynamic muscular contraction as measured by CMCoh and EMG parameters were adopted in this study to investigate the corticomuscular coordinating pattern of post-stroke compensatory activities from the proximal UE when performing distal motions at the affected side. The results suggested that the proximal UE compensatory action of the distal finger in chronic stroke patients was cortically derived, and the TRI and BIC were mainly activated from the contralesional side. This study confirmed the cortical activation shift in chronic stroke reported by other functional neuroimaging studies and further demonstrated that the cortical shift was concentrated within the proximal UE muscles as opposed to the distal agonist muscles. Specifically, the stroke patients needed to recruit more cortical effort of ED to conduct higher-level contraction. In contrast, the corticomuscular coupling to the FD during finger flexion was comparable in terms of the intensity and pattern in the peak CMCoh of the stroke subjects and the unimpaired subjects. However, the CMCoh results showed that, similar to that of the ED, the neural drive to FD shifted to the central region in chronic stroke subjects.

DATA AVAILABILITY STATEMENT

The raw data supporting the conclusions of this article will be made available by the authors, without undue reservation, to any qualified researcher.

ETHICS STATEMENT

The study was carried out in accordance with the human ethic guidelines of the Human Subjects Ethics Subcommittee of the Hong Kong Polytechnic University. All participants recruited in the study gave written informed consent in accordance with the Declaration of Helsinki before the start of the measurements. The patients/participants provided their written informed consent to participate in this study.

AUTHOR CONTRIBUTIONS

ZG and QQ equally contributed in the experiment design, data collection and analysis, and manuscript drafting. KW and HZ contributed in the system design and maintenance. YH contributed in the subject recruitment

and data collection. YZ contributed in the data analysis. XH conceived the study and coordinated the whole project, including the experiment design, system design, and manuscript drafting.

FUNDING

This project was financially supported by PolyU Central Fund 1-ZE4R and NSFC 81771959.

REFERENCES

1. Langhorne P, Bernhardt J, Kwakkel G. Stroke rehabilitation. *Lancet*. (2011) 377:1693–702. doi: 10.1016/S0140-6736(11)60325-5
2. Dobkin BH. Rehabilitation after stroke. *N Engl J Med*. (2005) 352:1677–84. doi: 10.1056/NEJMcp043511
3. Kong K-H, Chua KS, Lee J. Recovery of upper limb dexterity in patients more than 1 year after stroke: frequency, clinical correlates and predictors. *NeuroRehabilitation*. (2011) 28:105–11. doi: 10.3233/NRE-2011-0639
4. Kwakkel G, Wagenaar RC, Kollen BJ, Lankhorst GJ. Predicting disability in stroke—a critical review of the literature. *Age Ageing*. (1996) 25:479–89. doi: 10.1093/ageing/25.6.479
5. Good DC, Bettermann K, Reichwein RK. Stroke rehabilitation. *Continuum*. (2011) 17:545–67. doi: 10.1212/01.CON.0000399072.61943.38
6. Nam C, Rong W, Li W, Xie Y, Hu X, Zheng, Y. The effects of upper-limb training assisted with an electromyography-driven neuromuscular electrical stimulation robotic hand on chronic stroke. *Front Neurol*. (2017) 8:679. doi: 10.3389/fneur.2017.00679
7. Qian Q, Nam C, Guo Z, Huang Y, Hu X, Ng SC, et al. Distal versus proximal - an investigation on different supportive strategies by robots for upper limb rehabilitation after stroke: a randomized controlled trial. *J Neuroeng Rehabil*. (2019) 16:64. doi: 10.1186/s12984-019-0537-5
8. Jones TA. Motor compensation and its effects on neural reorganization after stroke. *Nat Rev Neurosci*. (2017) 18:267–80. doi: 10.1038/nrn.2017.26
9. Pineiro R, Pendlebury S, Johansen-Berg H, Matthews P. Functional MRI detects posterior shifts in primary sensorimotor cortex activation after stroke: evidence of local adaptive reorganization? *Stroke*. (2001) 32:1134–9. doi: 10.1161/01.STR.32.5.1134
10. Calautti C, Leroy F, Guincestre J-Y, Baron J-C. Displacement of primary sensorimotor cortex activation after subcortical stroke: a longitudinal PET study with clinical correlation. *Neuroimage*. (2003) 19:1650–4. doi: 10.1016/S1053-8119(03)00205-2
11. Platz T, van Kaick S, Möller L, Freund S, Winter T, Kim IH. Impairment–oriented training and adaptive motor cortex reorganisation after stroke: a fTMS study. *J Neurol*. (2005) 252:1363–71. doi: 10.1007/s00415-005-0868-y
12. Mima T, Hallett M. Electroencephalographic analysis of cortico-muscular coherence: reference effect, volume conduction and generator mechanism. *Clin Neurophysiol*. (1999) 110:1892–9. doi: 10.1016/S1388-2457(99)00238-2
13. Mima T, Matsuoka T, Hallett M. Information flow from the sensorimotor cortex to muscle in humans. *Clin Neurophysiol*. (2001) 112:122–6. doi: 10.1016/S1388-2457(00)00515-0
14. Mima T, Steger J, Schulman AE, Gerloff C, Hallett M. Electroencephalographic measurement of motor cortex control of muscle activity in humans. *Clin Neurophysiol*. (2000) 111:326–37. doi: 10.1016/S1388-2457(99)00229-1
15. Salenius S, Portin K, Kajola M, Salmelin R, Hari R. Cortical control of human motoneuron firing during isometric contraction. *J Neurophysiol*. (1997) 77:3401–5. doi: 10.1152/jn.1997.77.6.3401
16. Gerloff C, Uenishi N, Nagamine T, Kunieda T, Hallett M, Shibasaki H. Cortical activation during fast repetitive finger movements in humans: steady-state movement-related magnetic fields and their cortical generators. *Electroencephalogr Clin Neurophysiol Electromyogr Motor Control*. (1998) 109:444–53. doi: 10.1016/S0924-980X(98)00045-9
17. Brown P, Salenius S, Rothwell JC, Hari R. Cortical correlate of the Piper rhythm in humans. *J Neurophysiol*. (1998) 80:2911–7. doi: 10.1152/jn.1998.80.6.2911
18. Govindan RB, Raethjen J, Kopper F, Claussen JC, Deuschl, G. Estimation of time delay by coherence analysis. *Phys A Stat Mech Appl*. (2005) 350:277–95. doi: 10.1016/j.physa.2004.11.043
19. Meng F, Tong K, Chan S, Wong W, Lui K, Tang K, et al. Cerebral plasticity after subcortical stroke as revealed by cortico-muscular coherence. *IEEE Transac Neural Syst Rehabil Eng*. (2009) 17:234–43. doi: 10.1109/TNSRE.2008.2006209
20. Mima T, Toma K, Koshy B, Hallett M. Coherence between cortical and muscular activities after subcortical stroke. *Stroke*. (2001) 32:2597–601. doi: 10.1161/hs1101.098764
21. Weiller C, Chollet F, Friston KJ, Wise RJS, Frackowiak RSJ. Functional reorganization of the brain in recovery from striatocapsular infarction in man. *Ann Neurol*. (1992) 31:463–72. doi: 10.1002/ana.410310502
22. Weder B, Knorr U, Herzog H, Nebeling B, Kleinschmidt A, Huang Y, et al. Tactile exploration of shape after subcortical ischaemic infarction studied with PET. *Brain*. (1994) 117:593–605. doi: 10.1093/brain/117.3.593
23. Seitz RJ, Huang Y, Knorr U, Tellmann L, Herzog H, Freund HJ. Large-scale plasticity of the human motor cortex. *Neuroreport*. (1995) 6:742–4. doi: 10.1097/00001756-199503270-00009
24. Fang Y, Daly JJ, Sun J, Hvorat K, Fredrickson E, Pundik S, et al. Functional corticomuscular connection during reaching is weakened following stroke. *Clin Neurophysiol*. (2009) 120:994–1002. doi: 10.1016/j.clinph.2009.02.173
25. Larsen LH, Zibrandtsen IC, Wienecke T, Kjaer TW, Christensen MS, Nielsen JB, et al. Corticomuscular coherence in the acute and subacute phase after stroke. *Clin Neurophysiol*. (2017) 128:2217–26. doi: 10.1016/j.clinph.2017.08.033
26. Chen X, Xie P, Zhang Y, Chen Y, Cheng S, Zhang L. Abnormal functional corticomuscular coupling after stroke. *NeuroImage Clin*. (2018) 19:147–59. doi: 10.1016/j.nicl.2018.04.004
27. Xu R, Wang Y, Wang K, Zhang S, He C, Ming, D. Increased corticomuscular coherence and brain activation immediately after short-term neuromuscular electrical stimulation. *Front Neurol*. (2018) 9:886. doi: 10.3389/fneur.2018.00886
28. Rong W, Li W, Pang M, Hu J, Wei X, Yang B, et al. A Neuromuscular Electrical Stimulation (NMES) and robot hybrid system for multi-joint coordinated upper limb rehabilitation after stroke. *J Neuroeng Rehabil*. (2017) 14:34. doi: 10.1186/s12984-017-0245-y
29. Folstein MF, Folstein SE, McHugh PR. "Mini-mental state": a practical method for grading the cognitive state of patients for the clinician. *J Psychiatr Res*. (1975) 12:189–98. doi: 10.1016/0022-3956(75)90026-6
30. Fugl-Meyer AR, Jääskö L, Leyman I, Olsson S, Steglind, S. The post-stroke hemiplegic patient. 1. a method for evaluation of physical performance. *Scand J Rehabil Med*. (1975) 7:13–31.
31. Bohannon RW, Smith MB. Interrater reliability of a modified ashworth scale of muscle spasticity. *Phys Ther*. (1987) 67:206–7. doi: 10.1093/ptj/67.2.206
32. Hu XL, Tong RKY, Ho NSK, Xue JJ, Rong W, Li LSW. Wrist rehabilitation assisted by an electromyography-driven neuromuscular electrical stimulation robot after stroke. *Neurorehabil Neural Repair*. (2015) 29:767–76. doi: 10.1177/1545968314565510
33. von Carlowitz-Ghori K, Bayraktaroglu Z, Hohlefeld FU, Losch F, Curio G, Nikulin VV. Corticomuscular coherence in acute and chronic stroke. *Clin Neurophysiol*. (2014) 125:1182–91. doi: 10.1055/s-0034-1371233
34. Sheng Y, Liu J, Liu H. Corticomuscular coherence and its applications: a review. *Front Hum Neurosci*. (2019) 13:100. doi: 10.3389/fnhum.2019.00100
35. Qian Q, Hu X, Lai Q, Ng SC, Zheng Y, Poon, W. Early stroke rehabilitation of the upper limb assisted with an electromyography-driven neuromuscular electrical stimulation-robotic arm. *Front Neurol*. (2017) 8:447. doi: 10.3389/fneur.2017.00447
36. Zheng Y, Gao L, Wang G, Wang Y, Yang Z, Wang X, et al. The influence of unilateral contraction of hand muscles on the contralateral corticomuscular coherence during bimanual motor tasks. *Neuropsychologia*. (2016) 85:199–207. doi: 10.1016/j.neuropsychologia.2016.03.028

37. Zheng Y, Peng Y, Xu G, Li L, Wang J. Using corticomuscular coherence to reflect function recovery of paretic upper limb after stroke: a case study. *Front Neurol.* (2018) 8:728. doi: 10.3389/fneur.2017.00728
38. Tecchio F, Porcaro C, Zappasodi F, Pesenti A, Ercolani M, Rossini PM. Cortical short-term fatigue effects assessed via rhythmic brain–muscle coherence. *Exp Brain Res*. (2006) 174:144–51. doi: 10.1007/s00221-006-0432-8
39. Divekar NV, John LR. Neurophysiological, behavioural and perceptual differences between wrist flexion and extension related to sensorimotor monitoring as shown by corticomuscular coherence. *Clin Neurophysiol*. (2013) 124:136–47. doi: 10.1016/j.clinph.2012.07.019
40. Lou X, Xiao S, Qi Y, Hu X, Wang Y, Zheng X. Corticomuscular coherence analysis on hand movement distinction for active rehabilitation. *Comput Math Methods Med*. (2013) 2013:10. doi: 10.1155/2013/908591
41. McClelland VM, Cvetkovic Z, Mills KR. Rectification of the EMG is an unnecessary and inappropriate step in the calculation of corticomuscular coherence. *J Neurosci Methods*. (2012) 205:190–201. doi: 10.1016/j.jneumeth.2011.11.001
42. Rosenberg JR, Amjad AM, Breeze P, Brillinger DR, Halliday DM. The Fourier approach to the identification of functional coupling between neuronal spike trains. *Prog Biophys Mol Biol.* (1989) 53:1–31. doi: 10.1016/0079-6107(89)90004-7
43. Schulz H, Übelacker T, Keil J, Müller N, Weisz N. Now i am ready—now i am not: the influence of Pre-TMS oscillations and corticomuscular coherence on motor-evoked potentials. *Cerebral Cortex*. (2013) 24:1708–19. doi: 10.1093/cercor/bht024
44. Boroojerdi B, Ziemann U, Chen R, Bütefisch CM, Cohen LG. Mechanisms underlying human motor system plasticity. *Muscle Nerve*. (2001) 24:602–13. doi: 10.1002/mus.1045
45. Calautti C, Leroy F, Guincestre J-Y, Baron J-C. Dynamics of motor network overactivation after striatocapsular stroke. *Stroke*. (2001) 32:2534–42. doi: 10.1161/hs1101.097401
46. Hallett M. Plasticity of the human motor cortex and recovery from stroke. *Brain Res Rev*. (2001) 36:169–74. doi: 10.1016/S0165-0173(01)00092-3
47. Wilcox T, Hawkins LB, Hirshkowitz A, Boas DA. Cortical activation to object shape and speed of motion during the first year. *Neuroimage*. (2014) 99:129–41. doi: 10.1016/j.neuroimage.2014.04.082
48. Bobath B. *Adult Hemiplegia: Evaluation and Treatment*. Oxford: Butterworth-Heinemann (1990).
49. Kwakkel G, Wagenaar RC. Effect of duration of upper- and lower-extremity rehabilitation sessions and walking speed on recovery of interlimb coordination in hemiplegic gait. *Phys Ther*. (2002) 82:432–48. doi: 10.1093/ptj/82.5.432
50. Christian KM, Poulos AM, Thompson RF. Learning andmemory: basic principles and model systems. In: Kwakkel G, Cohen L, Selzer M, Miller R, Clarke S, editors. *Textbook of Neural Repair and Rehabilitation: Volume 1: Neural Repair and Plasticity,* 2 ed. Cambridge: Cambridge University Press (2014). p. 22–35.
51. Chechik G, Meilijson I, Ruppin E. Synaptic pruning in development: a computational account. *Neural Comput.* (1998) 10:1759–77. doi: 10.1162/089976698300017124
52. Huttenlocher PR, Dabholkar AS. Regional differences in synaptogenesis in human cerebral cortex. *J Comp Neurol.* (1997) 387:167–78.
53. Carey JR, Kimberley TJ, Lewis SM, Auerbach EJ, Dorsey L, Rundquist P, et al. Analysis of fMRI and finger tracking training in subjects with chronic stroke. *Brain*. (2002) 125:773–88. doi: 10.1093/brain/awf091
54. Wilkins KB, Owen M, Ingo C, Carmona C, Dewald JPA, Yao J. Neural plasticity in moderate to severe chronic stroke following a device-assisted task-specific arm/hand intervention. *Front Neurol.* (2017) 8:284. doi: 10.1093/med/9780199689903.003.0010
55. Werhahn KJ, Conforto AB, Kadom N, Hallett M, Cohen LG. Contribution of the ipsilateral motor cortex to recovery after chronic stroke. *Ann Neurol.* (2003) 54:464–72. doi: 10.1002/ana.10686
56. Soteropoulos DS, Edgley SA, Baker SN. Lack of evidence for direct corticospinal contributions to control of the ipsilateral forelimb in monkey. *J Neurosci*. (2011) 31:11208–19. doi: 10.1523/JNEUROSCI.0257-11.2011
57. Zaaimi B, Edgley SA, Soteropoulos DS, Baker SN. Changes in descending motor pathway connectivity after corticospinal tract lesion in macaque monkey. *Brain*. (2012) 135:2277–89. doi: 10.1093/brain/aws115
58. Forner-Cordero A, Levin O, Li Y, Swinnen SP. Posture control and complex arm coordination: analysis of multijoint coordinative movements and stability of stance. *J Mot Behav*. (2007) 39:215–26. doi: 10.3200/JMBR.39.3.215-226
59. Raghavan P. Upper limb motor impairment after stroke. *Phys Med Rehabil Clin*. (2015) 26:599–610. doi: 10.1016/j.pmr.2015.06.008
60. Soteropoulos DS, Williams ER, Baker SN. Cells in the monkey ponto-medullary reticular formation modulate their activity with slow finger movements. *J Physiol.* (2012) 590:4011–27. doi: 10.1113/jphysiol.2011.225169
61. Kozlowski DA, James DC, Schallert T. Use-dependent exaggeration of neuronal injury after unilateral sensorimotor cortex lesions. *J Neurosci*. (1996) 16:4776–86. doi: 10.1523/JNEUROSCI.16-15-04776.1996
62. Frost SB, Barbay S, Friel KM, Plautz EJ, Nudo RJ. Reorganization of remote cortical regions after ischemic brain injury: a potential substrate for stroke recovery. *J Neurophysiol.* (2003) 89:3205–14. doi: 10.1152/jn.01143.2002
63. He BJ, Snyder AZ, Vincent JL, Epstein A, Shulman GL, Corbetta, M. Breakdown of functional connectivity in frontoparietal networks underlies behavioral deficits in spatial neglect. *Neuron.* (2007) 53:905–18. doi: 10.1016/j.neuron.2007.02.013
64. Carter AR, Astafiev SV, Lang CE, Connor LT, Rengachary J, Strube MJ, et al. Resting interhemispheric functional magnetic resonance imaging connectivity predicts performance after stroke. *Ann Neurol.* (2010) 67:365–75. doi: 10.1002/ana.21905
65. van Meer MPA, van der Marel K, Wang K, Otte WM, El Bouazati S, Roeling TAP, et al. Recovery of sensorimotor function after experimental stroke correlates with restoration of resting-state interhemispheric functional connectivity. *J Neurosci.* (2010) 30:3964. doi: 10.1523/JNEUROSCI.5709-09.2010

Conflict of Interest: The authors declare that the research was conducted in the absence of any commercial or financial relationships that could be construed as a potential conflict of interest.

frontiers in Neurology

ORIGINAL RESEARCH
published: 29 May 2020
doi: 10.3389/fneur.2020.00477

Motor Unit Discharge Variability Is Increased in Mild-To-Moderate Parkinson's Disease

*Jessica M. Wilson[1], Christopher K. Thompson[2], Laura Miller McPherson[3,4], Cindy Zadikoff[5], C.J. Heckman[1,6,7] and Colum D. MacKinnon[8]**

[1] Department of Physical Therapy and Human Movement Sciences, Northwestern University, Chicago, IL, United States, [2] Department of Health and Rehabilitation Sciences, Temple University, Philadelphia, PA, United States, [3] Program in Physical Therapy, Washington University School of Medicine, St. Louis, MO, United States, [4] Department of Neurology, Washington University School of Medicine, St. Louis, MO, United States, [5] Department of Neurology, Northwestern University, Chicago, IL, United States, [6] Department of Physiology, Northwestern University, Chicago, IL, United States, [7] Department of Physical Medicine and Rehabilitation, Northwestern University, Chicago, IL, United States, [8] Department of Neurology, University of Minnesota, Minneapolis, MN, United States

Individuals with Parkinson's disease (PD) demonstrate deficits in muscle activation such as decreased amplitude and inappropriate bursting. There is evidence that some of these disturbances are more pronounced in extensor vs. flexor muscles. Surface EMG has been used widely to quantify muscle activation deficits in PD, but analysis of discharge of the underlying motor units may provide greater insight and be more sensitive to changes early in the disease. Of the few studies that have examined motor unit discharge in PD, the majority were conducted in the first dorsal interosseous, and no studies have measured motor units from extensor and flexor muscles within the same cohort. The objective of this study was to characterize the firing behavior of single motor units in the elbow flexor and extensor muscles during isometric contractions in people with mild-to-moderate PD. Ten individuals with PD (off-medication) and nine healthy controls were tested. Motor unit spike times were recorded via intramuscular EMG from the biceps and triceps brachii muscles during 30-s isometric contractions at 10% maximum voluntary elbow flexion and elbow extension torque, respectively. We selected variables of mean motor unit discharge rate, discharge variability, and torque variability to evaluate motor abnormalities in the PD group. The effects of group, muscle, and group-by-muscle on each variable were determined using separate linear mixed models. Discharge rate and torque variability were not different between groups, but discharge variability was significantly higher in the PD group for both muscles combined ($p < 0.0001$). We also evaluated the asymmetry in these motor variables between the triceps and biceps for each individual participant with PD to evaluate whether there was an association with disease severity. The difference in torque variability between elbow flexion and extension was significantly correlated with both the Hoehn and Yahr scale (rho = 0.71) and UPDRS (rho = 0.62). Our findings demonstrate that variability in motor output, rather than decreased discharge rates, may contribute to motor dysfunction in people with mild-to-moderate PD. Our findings provide insight into altered neural control of movement in PD and demonstrate the importance of measuring from multiple muscles within the same cohort.

Keywords: motor unit, Parkinson's disease, EMG, biceps brachii, triceps brachii

OPEN ACCESS

Edited by:
Xiaogang Hu, University of North Carolina at Chapel Hill, United States

Reviewed by:
Ales Holobar, University of Maribor, Slovenia
Yingchun Zhang, University of Houston, United States

***Correspondence:**
Colum D. MacKinnon
cmackinn@umn.edu

Specialty section:
This article was submitted to Neurorehabilitation, a section of the journal Frontiers in Neurology

Received: *06 March 2020*
Accepted: *01 May 2020*
Published: *29 May 2020*

Citation:
Wilson JM, Thompson CK, McPherson LM, Zadikoff C, Heckman CJ and MacKinnon CD (2020) Motor Unit Discharge Variability Is Increased in Mild-To-Moderate Parkinson's Disease. Front. Neurol. 11:477. doi: 10.3389/fneur.2020.00477

INTRODUCTION

A hallmark of Parkinson's disease (PD) is the presence of an abnormal pattern of muscle activity when performing voluntary movements (1–4). This abnormal pattern is characterized by decreased EMG amplitude and the presence of multiple agonist bursts with highly variable duration rather than a single fused agonist burst. These changes in surface EMG patterns during voluntary movement are observed early in disease progression (4). Previous studies have provided evidence that abnormalities in muscle activation, and the accompanying deficits in motor output, are more pronounced in extensor muscles compared to flexor muscles. Ballistic elbow extension movements in people with PD are associated with increased slowing and more agonist bursts when compared with flexion movements (5, 6). Similarly, deficits in isometric force generation and movement velocity are greater in elbow extension than flexion, and these relative differences persist in both the off and on medication states (5–7). Greater deficits in extensor compared to flexor muscle function in PD have also been demonstrated in the lower extremity (5–10). These reductions in strength and movement speed have been ascribed to impairment in the ability to activate the agonist muscle rather than to co-contraction of agonist-antagonist muscles.

Surface EMG, which provides an interference signal of the electrical activity of its constituent motor units, has provided a substantial amount of information about abnormal muscle activation in PD. Yet, specific characteristics of the underlying motor unit discharge, such as discharge variability, cannot be extracted from the interference signal without its decomposition into individual motor unit spike trains (11). Further, individual motor unit discharge patterns may be more sensitive to disturbances of motor control and may thereby yield information that is not available with analysis of the interference EMG signal. Therefore, an investigation of motor unit discharge patterns may provide novel insight into the mechanisms of impaired muscle activation and asymmetry of extensor vs. flexor muscle function in PD. However, few studies have examined the activity of individual motor units in PD. The majority of those that have examined motor unit discharge were conducted in the first dorsal interosseous (FDI) muscle, and no studies have measured motor units from extensor and flexor muscles within the same cohort. Findings from these initial characterizations of motor unit firing abnormalities in PD include significantly lower firing rates in the finger extensors (12) and FDI (12–14), increases in firing rate variability in the FDI (12, 15, 16), alterations in recruitment order in the tibialis anterior (17), disturbances in rate modulation of the biceps brachii and FDI (18), and pauses in firing of the FDI, sometimes lasting up to 3 min in severe cases (14).

Given the differences in movement impairment between extensor and flexor muscles in PD and the paucity of studies with flexor and extensor recordings in the same person, the purpose of this study was to examine motor unit discharge rates and discharge variability in an elbow extensor (triceps brachii) and an elbow flexor (biceps brachii) in individuals with PD in the off-medication state compared with control individuals without PD. We chose to include individuals with mild-moderate motor impairment rather than more severe impairment due to the feasibility of testing them in the off-medication state. We hypothesized that discharge rates are decreased and that discharge variability is increased in individuals with PD compared to controls in the triceps but not the biceps. We also hypothesized that increases in discharge variability, if found, would be accompanied by increased torque variability, and decreases in discharge rates, if found, would be accompanied by decreases in maximal strength. Finally, we investigated in the PD group whether the postulated differences in discharge rate, discharge variability, and torque variability between muscle groups was associated with disease severity.

MATERIALS AND METHODS

Ten individuals with mild-to-moderate PD and nine age-matched control individuals without PD were included in the study. Participants with PD were included if they (8) had idiopathic PD with a tremor sub-score < 2 according to the motor subsection (part III) of the UPDRS, (1) had no cognitive impairments [defined as Montreal Cognitive Assessment (MoCA) score > 26], (5) had no other previously known neurological disorders, (15) had no known injuries or other diseases that might interfere with motor function of the tested upper limb, and (12) were not currently on medications that may influence motor unit output such as selective serotonin reuptake inhibitors (SSRIs) or calcium channel blockers. **Table 1** provides a summary of demographic information of the participants with PD. Nine of the 10 participants in this group were taking between one and three medications for PD-related symptoms (amantadine, ropinirole, levodopa/carbidopa, and/or pramipexole), and the remaining participant did not take any medication for PD. The control group consisted of seven men and two women with a mean $\pm$ SD age of 67.7 ± 6.2 years.

Participants with PD were tested in the practically defined "off" medication state that followed a 12-h period of withdrawal from their PD medications. The control participants had no known history of neurological disorders and no known injuries or diseases that might interfere with motor function of the tested upper limb. All participants were required to abstain from caffeine for 12-h before the experiment to remove any possible effects of caffeine on motoneuron function (19, 20). Motor testing as well as a clinical assessment of disease severity using the motor subsection (part III) of the UPDRS and classification according to the Hoehn and Yahr scale (21) was conducted in all participants (both PD and controls). Control

TABLE 1 | Demographic information for participants with Parkinson's disease.

	Age (years)	Sex	Disease duration (years)	Motor UPDRS (off-medication)	Hoehn and Yahr (off-medication)
Mean (SD)	64.4 (10.8)	8 M/2 F	6.9 (3.2)	19 (10)	2 (1)
Range	43–78		3–14	7–38	1–4

participants showed no abnormalities on the UPDRS (score = 0). The dominant limb was tested for all participants with the exception of one control participant (due to an injured shoulder muscle) and one participant with PD (due to excessive tremor in the dominant limb). All participants provided written informed consent to participate in the study, which was approved by the Institutional Review Board of Northwestern University in accordance with the ethical standards stipulated by the 1964 Declaration of Helsinki for research involving human participants.

Experimental Procedures

Participants were seated in a Biodex chair (Biodex Medical Systems, Shirley, NY) with their tested arm fixed in 75° shoulder abduction, 45° shoulder flexion (horizontal adduction from the frontal plane), 90° elbow flexion, 15° pronation, and a neutral wrist and finger posture (22, 23). The participant's shoulder and waist were secured to the chair with straps to minimize auxiliary movements of the trunk. The forearm and hand were encased in a fiberglass cast and coupled via a weight-bearing ring-mount interface to a six-degree-of-freedom load cell (Model 45E15A; JR3, Woodland, CA). Prior to the main experimental trials, participants were asked to generate maximal efforts in elbow flexion and in elbow extension. Maximum voluntary torque (MVT) was calculated as the average of three consecutive maximum torque values within 10% of one another without the last repetition being the greatest. Real-time visual feedback of elbow flexion/extension torque was given through a computer monitor in front of the apparatus, and participants were given vigorous verbal encouragement through the duration of the MVT measurements.

For experimental trials, participants completed isometric contractions in elbow flexion and in elbow extension at 10% MVT. A green circle on the computer screen represented real-time visual feedback of elbow flexion/extension torque, and a red circle target was displayed to represent 10% MVT. Participants completed the experimental task as follows. After 5-s of baseline measurements obtained while the participant was relaxed, each participant produced an isometric ramp-and-hold contraction at their own pace (typically ∼5-s to reach the target torque) so that the green circle on the computer screen reached the red circle target. They maintained 10% MVT by holding the circle in the target for 30-s and then decreased torque production back to zero at their own pace. Participants completed 1–2 practice trials before data collection to familiarize themselves with the task. Between each experimental trial, participants were given a 1-min break, and they were asked to produce small brief contractions of the agonist and antagonist muscles to ensure quiescence of muscle activity before the start of the next trial (22). Trials were visually inspected for quality of torque production and discarded and repeated if necessary. Eight out of 111 total trials across participants were discarded because of issues during the data collection (e.g., contraction of the wrong muscle, appeared to fall asleep during the trial) or with post-processing (e.g., no motor units could be detected).

Data Collection

Orthogonal forces and torques generated at the forearm-load cell interface were digitized at a sampling rate of 1,024 Hz and converted into elbow flexion and extension torques using custom MATLAB software employing a Jacobian-based algorithm (The Mathworks, Natick, MA). Torque measurements were smoothed using an acausal moving average filter with a 250 ms window.

Intramuscular EMG in the long head of the biceps and the lateral head of the triceps were recorded using custom bipolar fine-wire steel electrodes with 1 mm recording surfaces (221-28SS-730, Jari Electrode Supply, Gilroy, CA). Each bipolar unit had barb lengths for the two wires of 1 and 2.5 mm. Two electrodes were inserted into each muscle. The signals from each electrode were band-pass filtered (300–10,000 Hz) and amplified (x1-10k) (DAM50 Bio-Amplifier, World Precision Instruments, Sarasota, FL) before digitization at 10,240 Hz (EMG-USB2+, OT Bioelettronica, Inc., Torino, Italy). Because torque and intramuscular EMG signals were collected on separate computers, a brief synchronization pulse was generated at the beginning of each trial and recorded by both computers as a reference point for offline synchronization. Intramuscular EMG recordings were collected using OTBiolab software (version 1.7.4735.19, OT Bioelettronica, Inc., Torino, Italy).

Data and Statistical Analysis

Intramuscular EMG recordings were imported into EMGlab software (24) for decomposition into single motor unit spike trains. Briefly, EMGlab is a freely available software package that uses a template matching algorithm to extract the discharge times of individual motor units from intramuscular EMG. We analyzed our data using EMGlab as follows. Intramuscular EMG data were high-pass filtered at 1 kHz. Templates of motor unit action potentials were created for each identified motor unit and were used to automatically identify discharge times of that motor unit during a sliding window of 5–10-s. The resulting automatic decomposition was manually inspected and corrected as necessary based on the residual intramuscular EMG signal, which reaches zero when discharges for all motor units have been accurately identified and the motor unit action potential templates have been subtracted from the original EMG signal. Following decomposition of the current segment, the sliding window was moved ∼4-s ahead and the process was repeated until full decomposition of the entire trial was achieved. EMGlab is able to resolve superimpositions of multiple motor unit action potentials via this semi-automatic process. The discharge times for each motor unit were exported at 1 kHz for subsequent processing. A single trained operator decomposed the intramuscular EMG data. A second trained operator was consulted on difficult trials and reviewed the final decomposition.

Custom MATLAB software was used to analyze the torque data and motor unit spike trains for each trial. The first and last 10-s of torque and motor unit data corresponding to the initial and final baseline phases and ascending and descending phases of the contraction were removed to isolate 30-s of the steady contraction; this data was used for all subsequent analyses. Inter-spike intervals (ISIs) and the associated mean ISI were calculated for each motor unit spike train. Mean discharge rate (pps) for

each motor unit spike train was calculated as the reciprocal of the mean ISI. To quantify discharge variability, the coefficient of variation of the ISI (CoV_{ISI}) was calculated for each motor unit as the standard deviation of the ISI values divided by the mean of the ISI values, multiplied by 100. Torque variability was calculated similarly using torque data (CoV_{torque}).

A linear mixed model was used to determine main effects of group (PD, control) and muscle (biceps, triceps) as well as the interaction effect of muscle-by-group on the dependent variable of discharge rate. Discharge rate values from all recorded motor units were used. Group and muscle were included in the model as fixed factors, with muscle also included as a repeated factor. Participant was included in the model as a random factor with a random intercept. A scaled identity covariance structure was assumed for random and repeated factors. The same statistical analysis was used with the dependent variable of CoV_{ISI}.

For elbow flexion MVT, elbow extension MVT, elbow flexion CoV_{torque}, and elbow extension CoV_{torque}, the mean value was calculated for each participant across trials for use in group analyses. The Shapiro–Wilk test was used to assess whether these

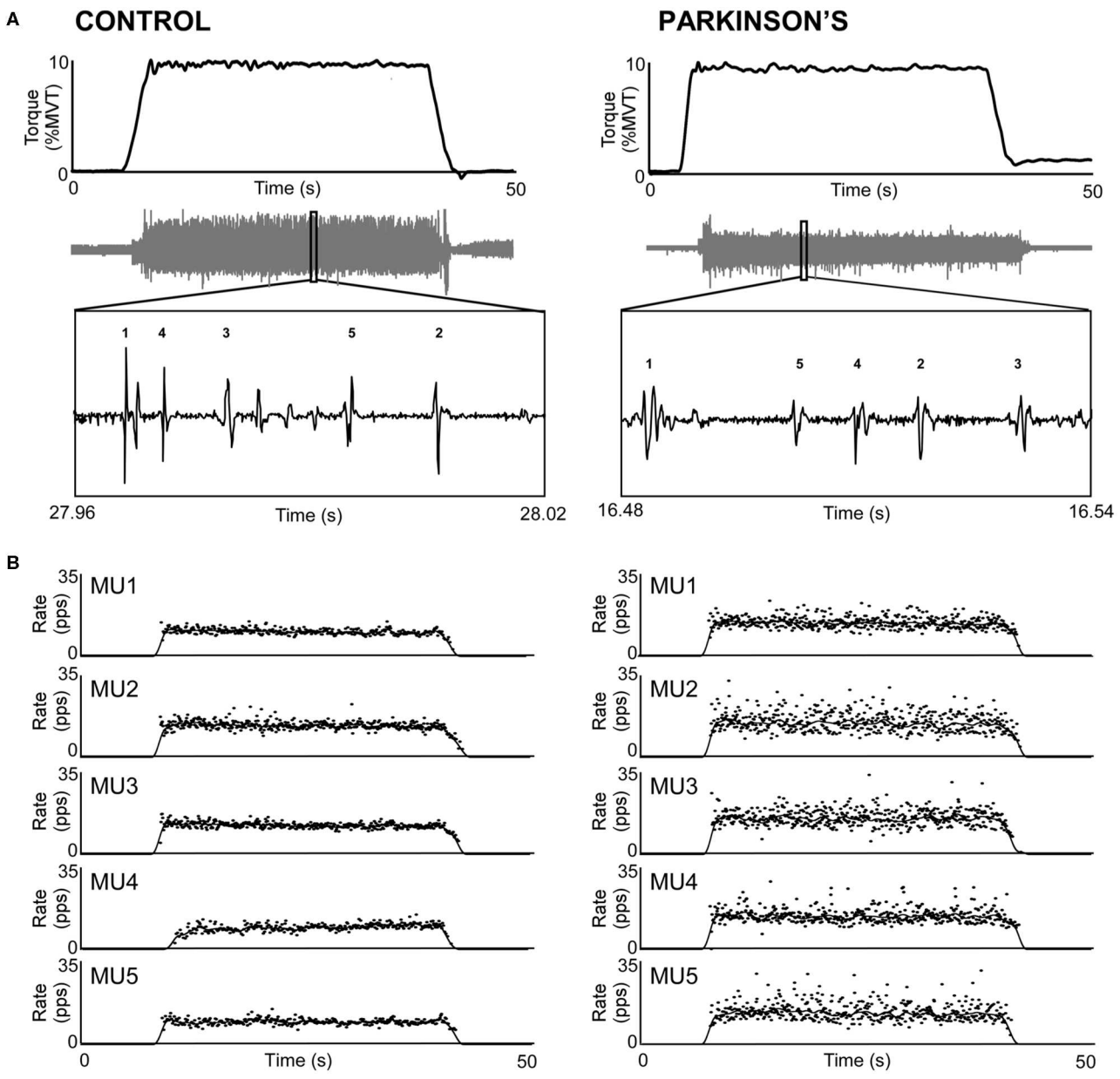

FIGURE 1 | Sample trials from the triceps brachii of a control participant (left) and a participant with PD (right). **(A)** Participants produced 30-s isometric contractions at 10% MVT, and intramuscular EMG (gray trace) was decomposed into its constituent motor units. **(B)** Instantaneous discharge rate (pps) is shown for each motor unit labeled in A. Motor unit discharge rates are also shown smoothed with a 2-s Hanning window.

TABLE 2 | Summary of motor unit discharge characteristics.

Muscle	Group	No. of MU per participant (mean ± SD)	Mean discharge rate (pps) (mean ± SE)	CoV_{ISI} (%) (mean ± SE)
Biceps brachii	Control	12 ± 7	11.75 ± 0.56	12.64 ± 1.16
	PD	13 ± 7	11.07 ± 0.53	18.8 ± 1.07
Triceps brachii	Control	14 ± 8	12.76 ± 0.56	12.75 ± 1.13
	PD	12 ± 4	11.98 ± 0.53	19.67 ± 1.09

Group mean ± SE values for discharge rate and CoV_{ISI} are displayed as estimates from the associated linear mixed model.

data were normally distributed. A 2 × 2 repeated measures ANOVA was used to determine main effects of group (PD, control) and torque direction (elbow flexion, elbow extension; repeated factor) as well as the torque direction-by-group interaction on the dependent variable of MVT. The same analysis was used for the dependent variable of CoV_{torque}.

We determined whether participants with higher disease severity demonstrated a greater difference in motor unit discharge rate, discharge variability, and torque variability between the triceps and the biceps. For each participant, we calculated the difference for each variable as the mean value for the biceps subtracted from the mean value for the triceps. Given our hypothesis that the triceps would exhibit increased motor unit discharge variability, we expected to find a positive correlation between disease severity (Hoehn and Yahr, UPDRS) and the difference in CoV_{ISI} and CoV_{torque} across muscles (the hypothesized direction of correlation is based on the assumption that there is no difference in discharge variability between muscles in the control group). Because we hypothesized that the triceps would exhibit decreased motor unit discharge rates, we expected to find a negative correlation between disease severity and the difference in discharge rate across muscles. We calculated the Spearman correlation coefficient for each comparison along with the associated 1-sided *p*-value.

Statistical analyses were conducted in SPSS. Statistical significance was determined as $p < 0.05$. Cases for which $0.05 < p < 0.10$ are presented.

RESULTS

Motor Unit Discharge Rates and Variability

Figure 1 shows representative torque and triceps motor unit instantaneous discharge rates during a 10% MVT elbow extension trial from one control participant (left panel) and one participant with PD (right panel). A summary of individual participant and group mean discharge characteristics for biceps and triceps motor units for control and PD groups are shown in **Table 2** and **Figure 2**. A total of 246 and 228 spike trains were analyzed in the PD and control groups, respectively.

Table 3 summarizes results of the linear mixed model used to determine the effects of group, muscle, and muscle-by-group on mean discharge rate and on CoV_{ISI}. For mean discharge rate,

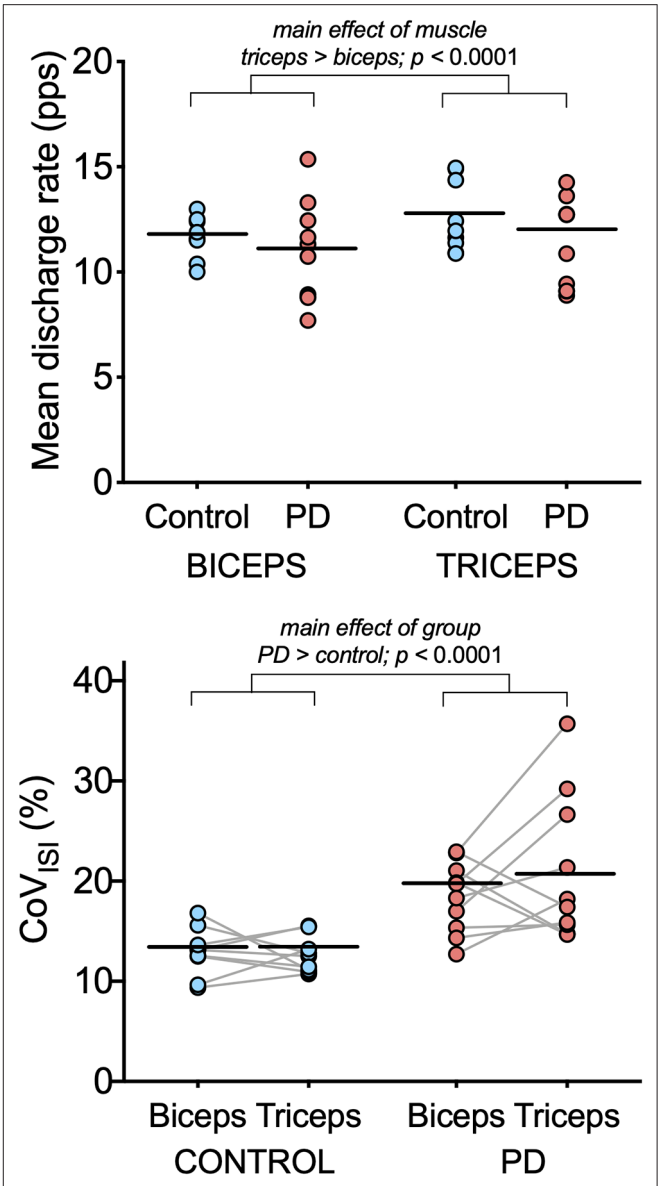

FIGURE 2 | Motor unit discharge characteristics in biceps brachii and triceps brachii for the PD and control groups. Individual participant means (light blue circles for the control group and light red circles for the PD group) and group means (black horizontal bars) are shown for mean discharge rate (top) and CoV_{ISI} (bottom). Note that while individual participant means are shown for illustrative purposes, the linear mixed model to assess effects of group and muscle were computed using data from all motor units.

the main effect of muscle was statistically significant, with higher mean discharge rates found in the triceps (mean ± SE: 11.41 ± 0.39 pps vs. 12.37 ± 0.39 for biceps and triceps, respectively; $p < 0.0001$). The main effect of group was not significant (11.53 ± 0.52 pps vs. 12.3 ± 0.55 pps for the PD and control groups, respectively; $p = 0.34$), nor was the muscle-by-group interaction ($p = 0.78$).

For CoV_{ISI}, the main effect of muscle was not statistically significant (mean ± SE: 15.74 ± 0.79% vs. 16.21 ± 7.8% for

TABLE 3 | Results from the linear mixed models testing the effects of muscle, group, and muscle-by-group on mean discharge rate and on CoV_{ISI}.

	Dependent variable	
	Mean discharge rate	**CoV_{ISI}**
Fixed effects		
Muscle	$p < 0.0001$	$p = 0.45$
	$F_{(1,458)} = 28.4$	$F_{(1,465)} = 0.58$
Group	$p = 0.34$	$p < 0.0001$
	$F_{(1,7)} = 0.95$	$F_{(1,16)} = 20.5$
Muscle by Group	$p = 0.78$	$p = 0.56$
	$F_{(1,458)} = 0.1$	$F_{(1,465)} = 0.35$

biceps and triceps, respectively; $p = 0.45$), nor was the muscle-by-group interaction ($p = 0.56$). The main effect of group indicated significantly higher CoV_{ISI} values in the PD group than in the control group (19.26 ± 1.0% vs. 12.70 ± 1.05% for PD and control groups, respectively; $p < 0.0001$).

Maximal Strength and Torque Variability

Maximum voluntary torque and CoV_{ISI} values were normally distributed for each group and torque direction (p-values ranging from 0.10 to 0.98). Maximum voluntary torque did not differ between the two groups [main effect of group: $F_{(1,7)} = 0.14$, $p = 0.71$; group × torque direction interaction: $F_{(1,7)} = 1.34$, $p = 0.26$]. In elbow flexion, the group mean ± SD MVT was 65.1 ± 25.7 N-m in the control group and 58.5 ± 14.4 N-m in the PD group. In elbow extension, the group mean ± SD MVT was 41.6 ± 16.7 N-m in the control group and 42.5 ±12.5 N-m in the PD group. MVT values were greater in elbow flexion than elbow extension for the groups combined [main effect of torque direction: $F_{(1,7)} = 36.6$, $p < 0.0001$].

Figure 3 shows representative torque data and individual and group means for CoV_{torque} for each torque direction. In elbow flexion, the group mean ± SD CoV_{torque} was 1.7 ± 0.7% in the control group and 1.9 ± 0.7% in the PD group. In elbow extension, the group mean ± SD CoV_{torque} was 1.9 ± 0.7% in the control group and 2.4 ± 1.4 N-m in the PD group. CoV_{torque} did not differ between the two groups [main effect of group: $F_{(1,7)} = 0.73$, $p = 0.40$; group × torque direction interaction: $F_{(1,7)} = 0.83$, $p = 0.38$] or between torque directions [main effect of torque direction: $F_{(1,7)} = 3.1$, $p = 0.098$]. Visual inspection of the individual mean values shown in **Figure 3** revealed that there were large increases in CoV_{torque} for elbow extension compared with elbow flexion for three of the 10 participants in the PD group compared with only one participant in the control group.

Motor Variables and Disease Severity

Table 4 presents the Spearman correlation coefficients and associated p-values for the comparisons between motor variables (CoV_{ISI}, CoV_{torque}, mean discharge rate) and disease severity (Hoehn and Yahr, UPDRS). CoV_{torque} was the only variable that was significantly correlated with disease severity, and it exhibited a moderate-strong correlation (Hoehn and Yahr: rho = 0.71, p = 0.01; UPDRS: rho = 0.62, $p = 0.03$). **Figure 4** presents these correlations graphically.

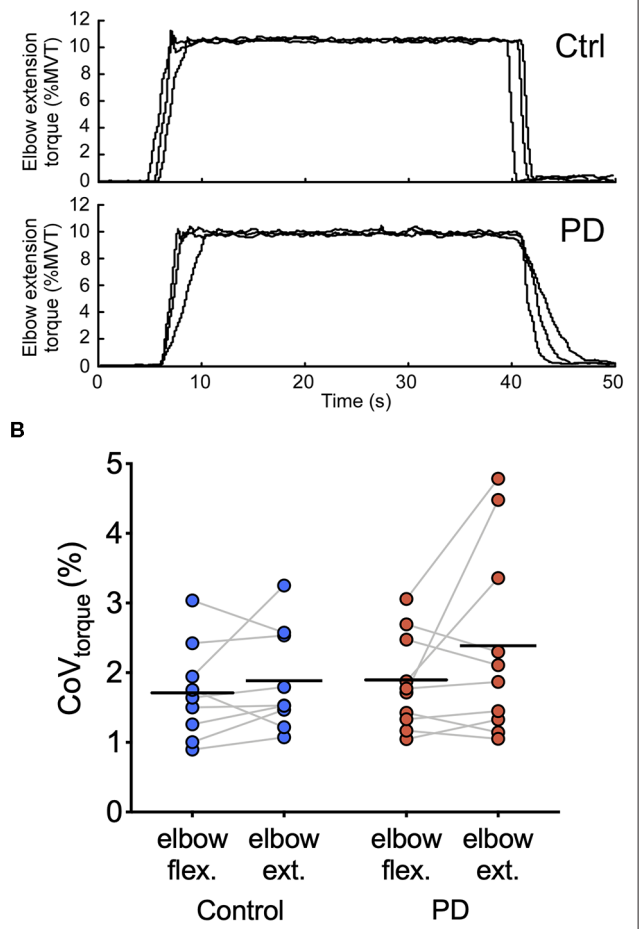

FIGURE 3 | Torque traces and torque variability during steady contractions. **(A)** Torque traces at 10% elbow extension MVT from a control participant (top) and a participant with PD (bottom) are shown. Data from three separate trials are superimposed. **(B)** Individual participant means (dark blue circles for the control group and dark red circles for the PD group) and group means (black horizontal bars) are shown for CoV_{torque} for elbow flexion and elbow extension torque directions.

DISCUSSION

The present study investigated differences in motor unit discharge rate and discharge variability of an elbow flexor (biceps brachii) and an elbow extensor (triceps brachii) among individuals with mild-to-moderate PD and control participants without PD.

Abnormalities in Motor Unit Behavior in Mild-to-Moderate Parkinson's Disease

Both Dietz et al. (12) and Milner-Brown et al. (14) observed significantly lower firing rates in individuals with severe motor

TABLE 4 | Correlations between triceps-biceps asymmetry of motor variables and disease severity.

	H&Y	UPDRS
Triceps-biceps difference in CoV_{ISI}	rho = 0.04	rho = 0.11
	$p = 0.46$	$p = 0.38$
Triceps-biceps difference in mean discharge rate	rho = −0.13	rho = −0.23
	$p = 0.36$	$p = 0.27$
Elbow extension-flexion difference in CoV_{torque}	rho = 0.71	rho = 0.62
	$p = 0.01$	$p = 0.03$

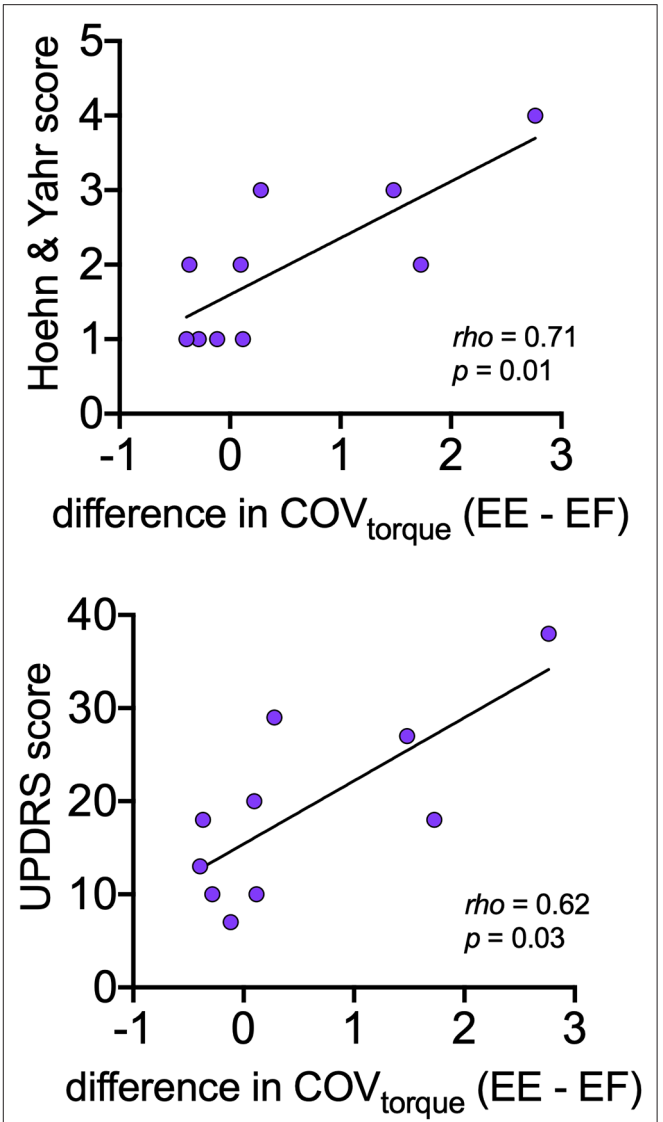

FIGURE 4 | Relationships between asymmetry of torque variability between elbow extension and elbow flexion with disease severity (Hoehn and Yahr, UPDRS) within the PD group. For each participant, asymmetry is expressed as the mean CoV_{torque} for elbow flexion subtracted from the mean CoV_{torque} for elbow extension.

symptoms of PD, with firing frequencies as low as 2–3 Hz and prolonged pauses in firing lasting from 10-s to 3-min (14). These significantly lower firing rates were present regardless of the presence of tremor. Dietz et al. (12) posited that these abnormally low discharge rates may be a common element of motoneuron function in PD. Such low discharge frequencies can contribute to variability in torque generation since muscle fiber twitches would remain unfused (13). However, in the present study, we did not observe any significant differences in mean discharge rate between our cohort with mild-to-moderate PD and control subjects in either muscle. This finding is consistent with the lack of strength differences observed between groups. A previous study showed differences in isometric strength between the elbow extensors and flexors in people with PD (5). This discrepancy might be explained by differences in the stage of disease between cohorts. It is possible that significant changes in slowing of motor unit discharge do not manifest in the earlier stages of PD but may be a source of increasing motor impairment with progression of the disease.

The main finding of this experiment was a significantly greater discharge variability in individuals with PD compared to controls in both the biceps and triceps muscles. Changes in discharge variability have also been reported in previous studies (12, 13). In particular, our results corroborate those of Dengler et al. (15), which showed that the first dorsal interosseous muscle of those with mild-to-moderate PD exhibited an increase in discharge rate variance without significant changes in mean discharge rates. In individuals without neurological disease, increased discharge variability is a known contributor to increased torque variability (25–28), but in the present study, torque variability was not significantly different between groups. A dissociation between discharge variability and torque variability has been documented in the literature before (29). The level of torque being used in this study may also be a contributing factor, as the presence of signal-dependent noise in the torque signal linearly increases with force output (30). It is possible that in the early stages of the disease, an insufficient part of the motoneuron pool is adversely affected enough for increased discharge variability to translate into a loss of force steadiness; the increased variance of CoV_{ISI} values within individuals with PD supports this possibility. The current results do suggest, however, that discharge variability may be a greater contributor to abnormal motor output than changes in discharge rates. Furthermore, results indicate that deficits in motor unit behavior may be observed in PD before the onset of deficits in torque generation.

Extensor vs. Flexor Deficits in PD

Other investigators have demonstrated that individuals with PD have greater deficits in extensor compared with flexor function in both the lower and upper limbs, suggesting differential impairment of neural activation of the flexor and extensor muscles (5–10). Thus, we also sought to explore potential differences in motor unit firing abnormalities in PD between the biceps and triceps. Interestingly, discharge variability was increased in both biceps and triceps of individuals

with PD compared to controls and further, the difference in torque variability between elbow extension and elbow flexion contractions was positively correlated with disease severity. In other words, for individuals with more severe PD, their elbow extension torque variability was greater than their elbow flexion torque variability and to a larger extent. These findings suggests that motor unit abnormalities in PD are not extensor-specific, at least in the case of discharge variability in a mild-moderate cohort; however, some asymmetry between muscle groups can be observed in terms of torque variability.

The participants with PD in the present study were studied in their OFF-medication state. Treatment with levodopa has been shown to significantly improve extensor force production more than the flexors in PD (5). This suggests that muscle asymmetry in PD is primarily mediated by the loss of dopamine in the striatum. Indeed, studies that have compared motor unit firing properties between the on and off medication states have shown that levodopa is associated with increased average firing rates and reduced discharge variability in the first dorsal interosseous (14, 18). Future work comparing motor unit discharge characteristics in the biceps and triceps of individuals with mild-to-moderate PD in the off-medication vs. the on-mediation state is warranted.

Limitations and Clinical Implications

Our results demonstrate that abnormalities in spinal motor output are observable in people with mild-to-moderate PD, characterized by an increase in discharge variability but not a difference in discharge rate. In addition, our data suggest that deficits in motor unit output can be detected before some deficits in force generation. These findings should be considered when comparing populations with mild-to-moderate and severe PD and for the development of longitudinal studies and rehabilitation therapies.

There are several limitations to the present work that should be considered. Our study was cross-sectional in nature and isolated to the off-medication PD population with mild-moderate disease. Additional work should be conducted to explore how our measurements would change longitudinally, in the on-medication status, and in individuals with more severe disease. Additionally, our sample size is relatively small due to the challenges inherent to taking invasive recordings from an older population with neurological injury; nonetheless, our findings provide important insight into alterations in neural control that underlie the movement dysfunction that presents with PD.

DATA AVAILABILITY STATEMENT

The datasets generated for this study are available on request to the corresponding author.

ETHICS STATEMENT

The presented study involving human participants was reviewed and approved by the Institutional Review Board of Northwestern University. The participants provided their written informed consent to participate in this study.

AUTHOR CONTRIBUTIONS

JW, CZ, CH, and CM conceived and designed research. JW and CZ recruited study participants. JW and CT performed experiments. JW, CT, and LM analyzed data. JW, CT, LM, CH, and CM interpreted results of experiments. JW, CT, and LM drafted the figures and manuscript, and all authors edited, revised, and approved final version of manuscript.

FUNDING

This work was funded by the National Institutes of Health [R01NS098509 (CH), R01NS085331 (CH), R01088679 (CM), T32HD07418 (CT), T32EB009406 (LM), and T32HD057845 (JW)], the Northwestern Memorial Foundation Parkinson's Disease and Movement Disorders Advisory Council (JW), the Craig H. Neilsen Foundation Postdoctoral Fellowship #260215 (CT), and a PODS II Scholarship from the Foundation for Physical Therapy Research, Inc. (LM).

REFERENCES

1. Berardelli A, Rothwell JC, Thompson PD, Hallett M. Pathophysiology of bradykinesia in Parkinson's disease. *Brain.* (2001) 124(Pt 11):2131–46. doi: 10.1093/brain/124.11.2131
2. Hallett M, Khoshbin S. A physiological mechanism of bradykinesia. *Brain.* (1980) 103:301–14. doi: 10.1093/brain/103.2.301
3. Pfann KD, Buchman AS, Comella CL, Corcos MD. Control of movement distance in Parkinson's disease. *Mov Disord.* (2001) 16:1048–1065. doi: 10.1002/mds.1220
4. Robichaud JA, Pfann KD, Leurgans S, Vaillancourt DE, Comella CL, Corcos MD. Variability of EMG patterns: a potential neurophysiological marker of Parkinson's disease? *Clin Neurophysiol.* (2009) 120:390–7. doi: 10.1016/j.clinph.2008.10.015
5. Corcos DM, Chen CM, Quinn NP, McAuley J, Rothwell CJ. Strength in Parkinson's disease: relationship to rate of force generation and clinical status. *Ann Neurol.* (1996) 39:79–88. doi: 10.1002/ana.4103 90112
6. Robichaud JA, Pfann KD, Comella CL, Brandabur M, Corcos MD. Greater impairment of extension movements as compared to flexion movements in Parkinson's disease. *Exp Brain Res.* (2004) 156:240–54. doi: 10.1007/s00221-003-1782-0
7. Folland JP, Haas B, Castle CP. Strength and activation of the knee musculature in Parkinson's disease: effect of medication. *NeuroRehabilitation.* (2011) 29:405–11. doi: 10.3233/NRE-2011-0719
8. Agostino R, Curra A, Giovannelli M, Modugno N, Manfredi M, Berardelli A. Impairment of individual finger movements in Parkinson's disease. *Mov Disord.* (2003) 18:560–5. doi: 10.1002/mds.10313
9. Dietz V, Zijlstra W, Prokop T, Berger W. Leg muscle activation during gait in Parkinson's disease: adaptation and interlimb coordination. *Electroencephalogr Clin Neurophysiol.* (1995) 97:408–15. doi: 10.1016/0924-980X(95)00109-X
10. Nogaki H, Kakinuma S, Morimatsu M. Muscle weakness in Parkinson's disease: a follow-up study. *Parkinsonism Relat Disord.* (2001) 8:57–62. doi: 10.1016/S1353-8020(01)00002-5

11. Farina D, Merletti R, Enoka MR. The extraction of neural strategies from the surface EMG. *J Appl Physiol (1985).* (2004) 96:1486–1495. doi: 10.1152/japplphysiol.01070.2003
12. Dietz V, Hillesheimer W, Freund JH. Correlation between tremor, voluntary contraction, and firing pattern of motor units in Parkinson's disease. *J Neurol Neurosurg Psychiatry.* (1974) 37:927–37. doi: 10.1136/jnnp.37.8.927
13. Freund HJ. Motor unit and muscle activity in voluntary motor control. *Physiol Rev.* (1983) 63:387–436. doi: 10.1152/physrev.1983.63.2.387
14. Milner-Brown HS, Fisher MA, Weiner JW. Electrical properties of motor units in Parkinsonism and a possible relationship with bradykinesia. *J Neurol Neurosurg Psychiatry.* (1979) 42:35–41. doi: 10.1136/jnnp.42.1.35
15. Dengler R, Wolf W, Schubert M, Struppler A. Discharge pattern of single motor units in basal ganglia disorders. *Neurology.* (1986) 36:1061–6. doi: 10.1212/WNL.36.8.1061
16. Freund HJ, Dietz V, Wita CW, Kapp H. Discharge characteristics of single motor units in normal subjects and patients with supraspinal motor disturbances. In: Desmedt JE, editor, Vol. 3. *New Developments in Electromyography Clinical Neurophysiology*. Basel: Karger (1973). p. 242–50.
17. Grimby L, Hannerz J. Disturbances in the voluntary recruitment order of anterior tibial motor units in bradykinesia of Parkinsonism. *J Neurol Neurosurg Psychiatry.* (1974) 37:47–54. doi: 10.1136/jnnp.37.1.47
18. Petajan JH, Jarcho LW. Motor unit control in Parkinsons-disease and influence of levodopa. *Neurology.* (1975) 25:866–9. doi: 10.1212/WNL.25.9.866
19. Walton C, Kalmar J, Cafarelli E. Caffeine increases spinal excitability in humans. *Muscle Nerve.* (2003) 28:359–64. doi: 10.1002/mus.10457
20. Walton C, Kalmar JM, Cafarelli E. Effect of caffeine on self-sustained firing in human motor units. *J Physiol.* (2002) 545(Pt 2):671–9. doi: 10.1113/jphysiol.2002.025064
21. Hoehn MM, Yahr MD. Parkinsonism: onset, progression and mortality. *Neurology.* (1967) 17:427–42. doi: 10.1212/WNL.17.5.427
22. McPherson JG, Ellis MD, Heckman CJ, Dewald PJ. Evidence for increased activation of persistent inward currents in individuals with chronic hemiparetic stroke. *J Neurophysiol.* (2008) 100:3236–43. doi: 10.1152/jn.90563.2008
23. Miller LC, Thompson CK, Negro F, Heckman CJ, Farina D, A Dewald JP. High-density surface EMG decomposition allows for recording of motor unit discharge from proximal and distal flexion synergy muscles simultaneously in individuals with stroke. *Conf Proc IEEE Eng Med Biol Soc.* (2014) 2014:5340–4. doi: 10.1109/EMBC.2014.6944832
24. McGill KC, Lateva ZC, Marateb RH. EMGLAB: an interactive EMG decomposition program. *J Neurosci Methods.* (2005) 149:121–33. doi: 10.1016/j.jneumeth.2005.05.015
25. Enoka RM, Christou EA, Hunter SK, Kornatz KW, Semmler JG, Taylor AM, et al. Mechanisms that contribute to differences in motor performance between young and old adults. *J Electromyogr Kinesiol.* (2003) 13:1–12. doi: 10.1016/S1050-6411(02)00084-6
26. Laidlaw DH, Bilodeau M, Enoka MR. Steadiness is reduced and motor unit discharge is more variable in old adults. *Muscle Nerve.* (2000) 23:600–12. doi: 10.1002/(SICI)1097-4598(200004)23:4<600::AID-MUS20>3.0.CO;2-D
27. Moritz CT, Barry BK, Pascoe MA, Enoka MR. Discharge rate variability influences the variation in force fluctuations across the working range of a hand muscle. *J Neurophysiol.* (2005) 93:2449–59. doi: 10.1152/jn.01122.2004
28. Tracy BL, Maluf KS, Stephenson JL, Hunter SK, Enoka MR. Variability of motor unit discharge and force fluctuations across a range of muscle forces in older adults. *Muscle Nerve.* (2005) 32:533–40. doi: 10.1002/mus.20392
29. Semmler JG, Steege JW, Kornatz KW, Enoka MR. Motor-unit synchronization is not responsible for larger motor-unit forces in old adults. *J Neurophysiol.* (2000) 84:358–66. doi: 10.1152/jn.2000.84.1.358
30. Jones KE, Hamilton AFC, Wolpert DM. Sources of signal-dependent noise during isometric force production. *J Neurophysiol.* (2002) 88:1533–44. doi: 10.1152/jn.2002.88.3.1533

Conflict of Interest: The authors declare that the research was conducted in the absence of any commercial or financial relationships that could be construed as a potential conflict of interest.

frontiers in Neurology

ORIGINAL RESEARCH
published: 09 June 2020
doi: 10.3389/fneur.2020.00493

Interfacing With Alpha Motor Neurons in Spinal Cord Injury Patients Receiving Trans-spinal Electrical Stimulation

Antonio Gogeascoechea[1], Alexander Kuck[1], Edwin van Asseldonk[1], Francesco Negro[2], Jan R. Buitenweg[3], Utku S. Yavuz[3†] and Massimo Sartori[1†]*

[1] Department of Biomechanical Engineering, University of Twente, Enschede, Netherlands, [2] Department of Clinical and Experimental Sciences, Università degli Studi di Brescia, Brescia, Italy, [3] Biomedical Signals and Systems Group, University of Twente, Enschede, Netherlands

OPEN ACCESS

Edited by:
Mariano Serrao, Sapienza University of Rome, Italy

Reviewed by:
Alberto Ranavolo, Istituto Nazionale per l'Assicurazione Contro gli Infortuni sul Lavoro (INAIL), Italy
Luca Sebastianelli, Hospital of Vipiteno, Italy

***Correspondence:**
Antonio Gogeascoechea
a.d.j.gogeascoecheahernandez@utwente.nl

† These authors have contributed equally to this work

Specialty section:
This article was submitted to Neurorehabilitation, a section of the journal Frontiers in Neurology

Received: *20 January 2020*
Accepted: *05 May 2020*
Published: *09 June 2020*

Citation:
Gogeascoechea A, Kuck A, van Asseldonk E, Negro F, Buitenweg JR, Yavuz US and Sartori M (2020) Interfacing With Alpha Motor Neurons in Spinal Cord Injury Patients Receiving Trans-spinal Electrical Stimulation. Front. Neurol. 11:493. doi: 10.3389/fneur.2020.00493

Trans-spinal direct current stimulation (tsDCS) provides a non-invasive, clinically viable approach to potentially restore physiological neuromuscular function after neurological impairment, e.g., spinal cord injury (SCI). Use of tsDCS has been hampered by the inability of delivering stimulation patterns based on the activity of neural targets responsible to motor function, i.e., α-motor neurons (α-MNs). State of the art modeling and experimental techniques do not provide information about how individual α-MNs respond to electrical fields. This is a major element hindering the development of neuro-modulative technologies highly tailored to an individual patient. For the first time, we propose the use of a signal-based approach to infer tsDCS effects on large α-MNs pools in four incomplete SCI individuals. We employ leg muscles spatial sampling and deconvolution of high-density fiber electrical activity to decode accurate α-MNs discharges across multiple lumbosacral segments during isometric plantar flexion sub-maximal contractions. This is done before, immediately after and 30 min after sub-threshold cathodal stimulation. We deliver sham tsDCS as a control measure. First, we propose a new algorithm for removing compromised information from decomposed α-MNs spike trains, thereby enabling robust decomposition and frequency-domain analysis. Second, we propose the analysis of α-MNs spike trains coherence (i.e., frequency-domain) as an indicator of spinal response to tsDCS. Results showed that α-MNs spike trains coherence analysis sensibly varied across stimulation phases. Coherence analyses results suggested that the common synaptic input to α-MNs pools decreased immediately after cathodal tsDCS with a persistent effect after 30 min. Our proposed non-invasive decoding of individual α-MNs behavior may open up new avenues for the design of real-time closed-loop control applications including both transcutaneous and epidural spinal electrical stimulation where stimulation parameters are adjusted on-the-fly.

Keywords: alpha motor neuron, coherence, common synaptic input, high-density EMG, spinal cord injury, trans-spinal direct current stimulation, tsDCS

1. INTRODUCTION

Spinal cord injury (SCI) disrupts synaptic inputs to below-injury motor, sensory and inter-neurons, thereby impairing physiological sensory-motor function (1). SCI is largely caused by physical trauma to spinal vertebrae, column disks or ligaments following accidents, falls, or sports injuries. Incomplete SCI is the most prevalent type of SCI (2), which causes limb paresis, muscle spasticity, or chronic pain, among other symptoms.

State of the art treatments aim at improving remaining neuromuscular function post-injury via pharmacological therapy (3), stem cell therapy (4), surgical intervention (5), or electrical stimulation. Over the past decade, growing interest has been directed to electrical spinal cord stimulation techniques. Supra-threshold electrical stimulation is used to establish functional neuroprostheses for restoring motor function, with epidural stimulation recently enabling activation of lumbar spinal circuits in rats (6), non-human primates (7) and paraplegic individuals (8). On the other hand, sub-threshold stimulation is used to modulate spinal excitability and induce spinal plastic changes (9–11), rather than establishing functional neuroprostheses. In SCI (12, 13) and stroke (14) patients, sub-threshold stimulation suppressed severe lower limb spasticity and enabled motor control. In this context, neuromodulation of the sub-threshold properties of the spinal neurons (resting potential, excitability) was key to recovery (12). However, while spinal cord stimulation became a standard for treating chronic pain, its use for motor dysfunctions, such as spasticity is still limited and often remains non-clinically accepted (15). With few exceptions (16, 17), spinal cord stimulation techniques operate in "open-loop," with parameters empirically hand-tuned and with no real-time corrective feedback at the level of α-motor neuron (α-MNs) cellular activity. This is a major element hampering applicability to clinical settings.

Sub-threshold transcutaneous spinal direct current stimulation (tsDCS) in particular, would have large potentials for clinical translation due to its non-invasive and unobstructive nature (18). However, due to the technique inherent non-selectivity as well as spinal cord complex bundle-like organization, it remains challenging to estimate how tsDCS alters spinal neuron function as well as resulting motor function. The ability of estimating how spinal neurons would respond to tsDCS in intact patients *in vivo* would enable a new class of closed-loop techniques, where stimulation parameters could be tuned online to optimally modulate the activity of selected neural targets.

Current approaches to estimate tsDCS neuromodulatory effects include perturbation-based experimental methodologies as well as numerical modeling. While modeling approaches are bound to assumptions as well as to parameter identification and validation challenges, current experimental strategies rely on delivering external stimuli to nerves or muscles to probe (indirectly) α-MN pools excitability (via stretch- or H-reflex, F-wave). Brain stimulation is also used to (indirectly) test corticospinal tract excitability, via transcranial magnetic stimulation (TMS)-induced motor evoked potentials (MEPs). Delivered electromechanical stimuli inherently perturb neuromuscular function, thereby altering physiological motor behavior and preventing translation to real-time closed-loop control applications. Additionally, these traditional experimental techniques cannot provide information on the behavior of individual α-MNs, but only on the global behavior of mixed populations. Therefore, a clinically viable, yet higher-resolution analysis of spinal neurophysiological changes after tsDCS is needed.

Here, we introduce an alternative methodology, with respect to current approaches, based on a direct analysis of α-MN behavior in incomplete SCI patients receiving tsDCS. We propose to use leg muscles as a biological interface to α-MNs. This is possible due to the one-to-one relationship between the action potentials produced in α-MNs and the ones generated in muscles. Thus, high-density surface electromyograms (HD-EMG) recorded from muscles contain neural information that can be derived by means of deconvolution-based blind source separation techniques, such as Convolution Kernel Compensation (CKC).

First, we describe an automated algorithm for assessing the quality of HD-EMG-decomposed α-MN spike trains and for selecting only those that contain physiological neural information, thereby addressing limits in current decomposition techniques. This is a central step as features extracted from α-MN spike trains (both in time and frequency domains) are sensitive to wrongly identified spike trains. Second, we employ coherence analysis to examine how the strength of common synaptic input to α-MN pools modulates in response to tsDCS (19–23).

By these means, our methodology provides an alternative approach to understand the effects of tsDCS on lower limb motor impairment after SCI, which may open up new directions for designing closed-loop neuromodulation techniques.

2. METHODS

2.1. Study Protocol

2.1.1. Participants

Four patients (P1–P4) with chronic incomplete SCI were recruited [age 34–70; walking index for SCI > 1; spinal cord independence measure > 30; and American Spinal Injury Association (ASIA) Impairment Scale (AIS) C or D]. **Table 1** shows an overview of each patient characteristics. All participants gave their written informed consent prior to the beginning of the study. The procedures and protocol were approved by the local Ethics Committee of Twente (METC Twente, reference number: NL49561.044.14 / P14-22).

2.1.2. Experimental Procedures

The experimental protocol was designed as a double-blinded, sham-controlled crossover study. The setup consisted of a medical chair in which the patients were seated throughout the experiment. Each patient was tightly strapped to the chair with build-in racing belts, limiting any forward movement of the trunk. The upper leg was fixed at a 90° hip angle by tightly attaching it to a solid frame using leg braces including velcro straps. A force platform (Advanced Mechanical Technology, Inc., Watertown, USA) was used to measure isometric ankle

joint plantar-flexion force. The platform was placed close to the chair ensuring that the ankle was positioned firmly with an ankle and knee angles of 90°. Maximum voluntary contractions (MVCs) were measured by asking the patients to generate as much plantarflexion force as possible by contracting only gastrocnemius and soleus muscles for at least 5 s. This was repeated three times with a resting period of 1–2 min between trials. The MVC was defined as the highest force within the three trials.

Patients underwent two types of stimulation in randomized order: cathodal (2.5 mA) and sham tsDCS. The electrode configuration was the same for both cathodal and sham stimulation: the cathode-electrode was centered between the 11th and the 12th thoracic vertebrae (∼L3–L5 segments of the spinal cord, **Figures 1A,C**) and the anode-electrode was located on the right shoulder (18). During sham, electrical stimulation profiles were ramped up to 2.5 mA and gradually turned off. Stimulation was administered using a custom-build direct-current stimulator (TMS International B.V., Oldenzaal, The Netherlands) while the patients performed the force tracking task for a total period of 15 min including: 8 min of reference force tracking with 3.5 min of rest before and after the tracking exercise. The task consisted of a mixture of sinusoidal waves with a mean of 5% MVC and a maximum of 10% MVC (**Figure 2A**).

The tsDCS effects were examined at three time conditions including: before (pre), immediately after (t0) and 30 min after (t30) stimulation was delivered. For each condition, patients performed ramp-and-hold tasks that consist of nine sub-maximal plantar flexion contractions at 8, 15, and 20% MVC (i.e., three tasks per level in random order, **Figure 2B**). Reference and subject-generated force profiles were fed back to the patient via a display. A single task (**Figure 2C**) consisted of a ramp up (2.5% MVC/s), hold (25 s) and ramp down (2.5% MVC/s).

During each phase, HD-EMGs were recorded using a TMSi Refa multi-channel amplifier (TMS International B.V.,

TABLE 1 | Overview of patients' characteristics.

Patient ID	Age	Sex	Weight (kg)	Height (m)	Injury level	AIS	Time since SCI (years)
P1	62	M	81.5	1.79	C4	D	2
P2	67	M	68	1.77	C4	C	3
P3	34	F	87	1.66	C8	C	4
P4	70	F	67	1.63	C7	D	11

ID, identification code used for each patient; AIS, American Spinal Injury Association (ASIA) Impairment Scale; SCI, spinal cord injury; M, male; F, female.

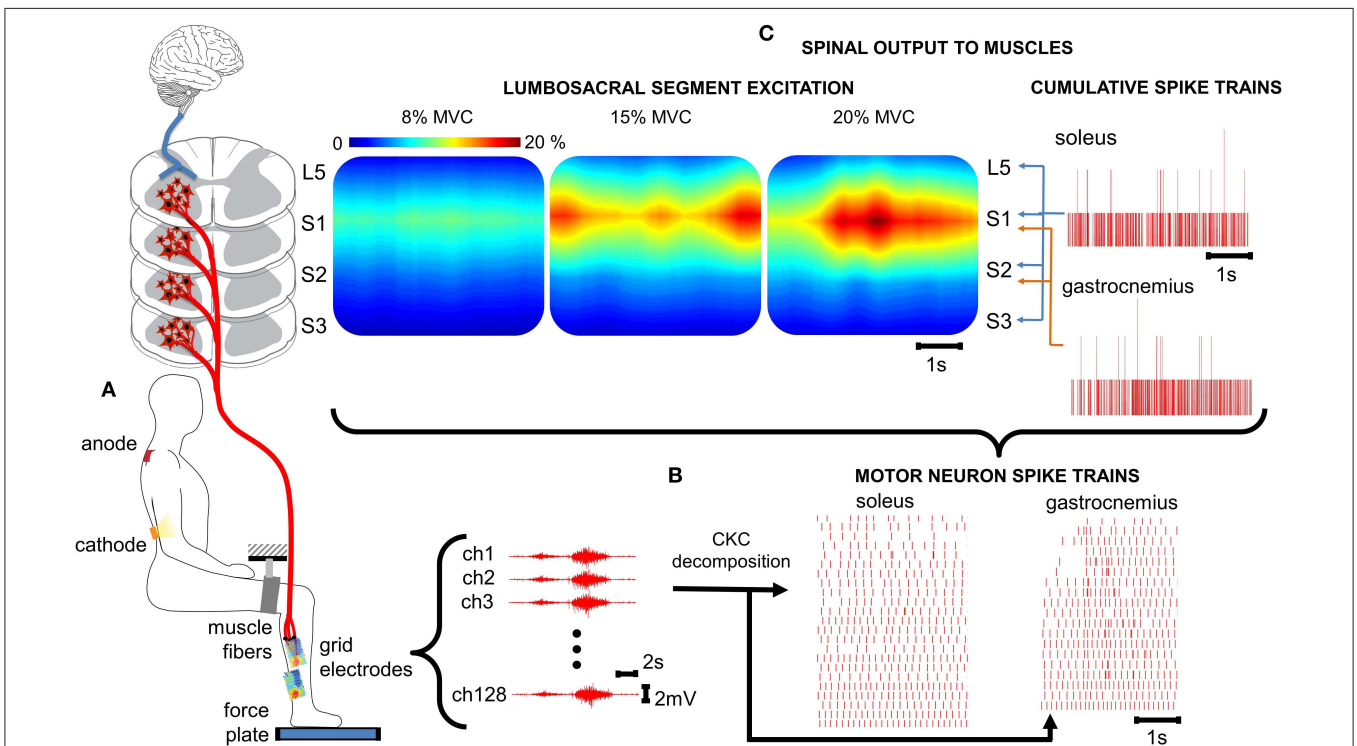

FIGURE 1 | Spatiotemporal spinal maps of ipsilateral α-MNs. **(A)** Experimental set-up for ankle plantar flexion. For the tsDCS, the cathode is placed between the 11th and 12th vertebrae (targeting the lumbosacral spinal segments) and the anode over the right shoulder. HD-EMGs are recorded from the triceps surae and the reference electrode is placed on the malleolus. A brace with velcro closure was attached to immobilize the upper leg and the force plate measures ankle plantar flexion force. **(B)** HD-EMG is decomposed into α-MN spike trains using a convolutive blind-source separation technique (24). **(C)** The spinal output to generate the neural drive to muscles is estimated from the α-MN spike trains. This reveals spatiotemporal information of α-MN activity in the spinal cord across different levels of force (% MVC). % MVC, percentage of maximum voluntary contraction; ch, channel; CKC, convolution kernel compensation.

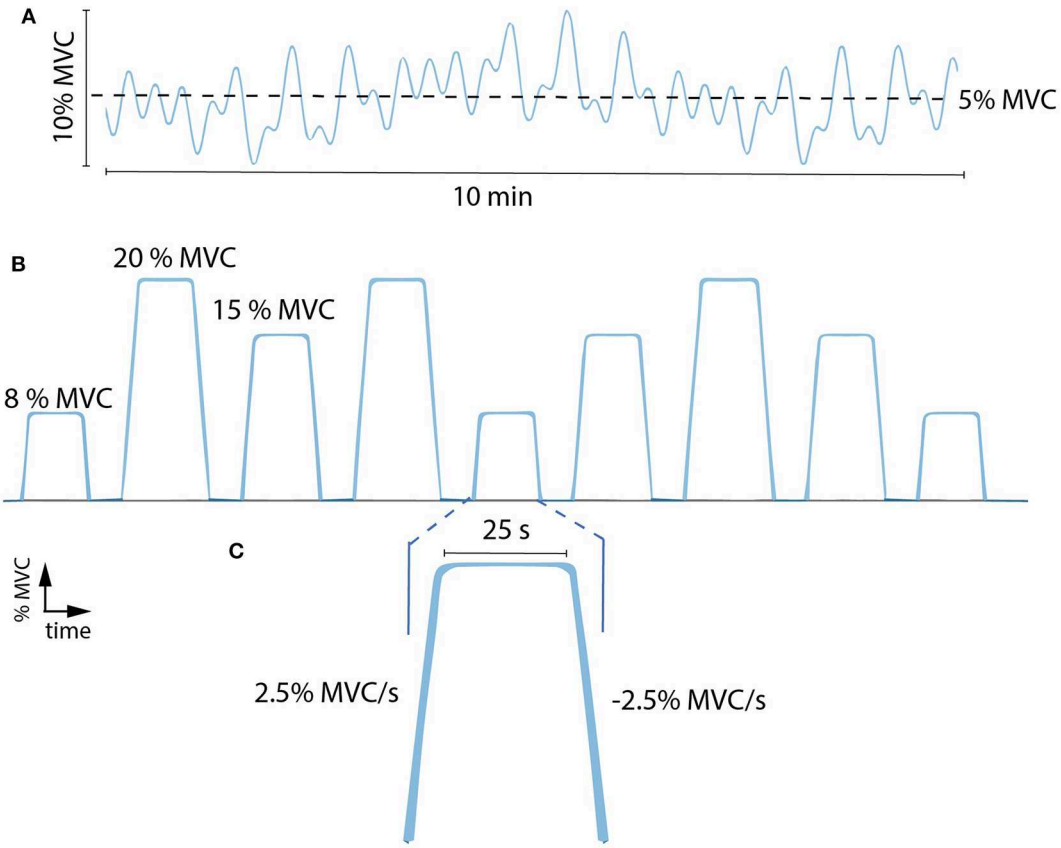

FIGURE 2 | (A) Example of a force tracking task during tsDCS. This consisted of following a force trajectory of low-intensity, low-frequency sinusoidal forces with a mean of 5% MVC and a maximum of 10% MVC for a duration of 10 min. **(B)** Example of force tracking tasks during each time condition (pre, t0, t30). These consisted of nine ramp-and-hold sub-maximal plantar flexion contractions at 8, 15, and 20% MVC (i.e., three tasks per level in random order). **(C)** Enlargement of a single force task: ramp up (2.5% MVC/s), hold (25 s) and ramp down (−2.5% MVC/s). % MVC, percentage of maximum voluntary contraction.

Oldenzaal, The Netherlands) with a sampling frequency of 2,048 Hz. A set of two 8x8-electrode grids with 8 and 3 mm inter-electrode distance were placed on the gastrocnemius medialis and soleus muscles, respectively. The grids were applied to the skin using 1-mm thick bi-adhesive foam layer filled with conductive paste to enhance skin-grid contact. The reference electrode is located on the fibula.

2.2. Data Analysis

HD-EMG and force data were offline analyzed with Matlab R2019a (The Mathworks Inc., Natick, MA,USA). The HD-EMG recordings were band-pass filtered (50–500 Hz) and decomposed into α-MN spike trains using CKC blind source separation algorithm (25) (**Figure 1B**). Each α-MN spike train consisted of a vector where the value of 1 indicated the time event at which the respective α-MN fired. The value 0 was used in all time frames where no discharge was detected. Subsequently, cumulative spike trains (CSTs) were defined as the sum of individual α-MN spike trains. CSTs provide the linearity that individual spike trains lack (21) and hence, allow a better estimate of coherence values. Smoothed CSTs were computed using a moving average zero-phase filter with a 400 ms window.

2.2.1. Quality Criteria

This analysis was conducted on soleus and gastrocnemius HD-EMGs recorded from all four patients. As CKC decomposition is a probabilistic iterative procedure to blindly estimate individual spike trains in presence of external noise, errors in the decomposition are inherently expected. Each spike train was inspected for quality control. For this purpose, two quality indices were evaluated in two subsequent steps (see **Algorithm 1**): first, the pulse-to-noise ratio (PNR) and second, the coefficient of variation (CoV) of the inter-spike intervals (ISI).

The PNR was defined as the logarithmic ratio (dB) between the means of the innervation pulse train at all time moments in which a α-MN is estimated to have discharged ($E(\hat{t}^2(n)|_{\hat{t}^2(n)\geq r}$) and not to have discharged ($E(\hat{t}^2(n)|_{\hat{t}^2(n)<r}$) (24), where $\hat{t}(n)$ denoted the innervation pulse train as a function of samples n and r the threshold to detect a pulse (1).

$$PNR(\hat{t}(n)) = 10 \cdot log\left(\frac{E(\hat{t}^2(n)|_{\hat{t}^2(n)\geq r}}{E(\hat{t}^2(n)|_{\hat{t}^2(n)<r}}\right), \quad (1)$$

The coefficient of variation of the ISI was calculated as the ratio between the standard deviation of the ISI and its mean

Algorithm 1: Quality control.

```
for all α-MNs in α-MN pool do
  STEP 1: PNR check
  if PNR < 20 dB then
    store MN
  else
    remove MN
  end if
  compute z1
  STEP 2: CoVISI {conditional check}
  if CoVISI < 0.3 then
    store MN
  else
    compute z2 without MN
    if z2 > z1 then
      remove MN
    else
      store MN
    end if
  end if
end for
```

MN, motor neuron; PNR, pulse-to-noise ratio; z_n, z-transformed correlation between force and estimate of neural drive (low-pass filtered cumulative spike train) of the n^{th} step (n=[1,2]); CoV_{ISI}, coefficient of variation of ISI (inter-spike intervals).

value (20, 25, 26). Only discharges with ISI > 33.3 ms (30 Hz) and ISI < 300 ms (3.3 Hz) were included for the CoV_{ISI}. Intervals outside this range did not represent physiological values for human leg muscles MNs, thus likely representing decomposition inconsistencies from the CKC algorithm (26–28).

The quality control algorithm computed PNR and CoV sequentially (see **Algorithm 1**). As PNR directly relates to the quality of the decomposition (i.e., ratio between pulse energy and noise level), it was computed as a first filter against low-quality, near-noise spike trains. The algorithm thus rejected all α-MNs with PNRs < 20 dB. The second step verified whether CoV_{ISI} < 0.3 was satisfied (20, 25, 26). Previous motor unit studies showed that motor unit discharge variability increases with SCI (29, 30). Therefore, we computed the Pearson correlation coefficient between reference force profiles and smoothed CSTs (for both soleus and gastrocnemius medialis) before and after the quality criteria were applied and we transformed them into z-scores ($z = \text{arctanh}\sqrt{CPeak}$). The algorithm applied this second condition only if it led to an increase in the correlation between smoothed CST and reference force profile. This was motivated by the fact that, in isometric condition there is direct proportionality between trends in α-MN pool spike trains and resulting muscle force (21).

Moreover, because the amount of α-MNs per CST influences the strength of the common synaptic input, α-MN pools with <4 α-MNs were not considered as eligible for quality control and subsequent analyses (section 3). **Algorithm 1** provides the iterative steps computed during the quality selection step. **Figure 3** depicts an example of how the quality criteria algorithm works.

2.2.2. Coherence Between CSTs

Because of the presence of pain while undergoing tsDCS, only half of the stimulation intensity (∼1.2 mA) was used with P4. For this reason, this analysis was conducted on the data of the soleus muscle only for P1, P2, and P3. For each trial and patient, spike trains decomposed from HD-EMGs were apportioned into three non-intersecting groups and used to create three CSTs. For instance, if the pool contained six α-MN spike trains, three groups with non-intersecting trains were extracted (e.g., α-MN1-α-MN2, α-MN3-α-MN4, and α-MN5-α-MN6).

The magnitude-squared coherence was computed between pairs of detrended CSTs using the Welch's periodogram with Hann windows of 1 s, 50% overlap. Only the steady state interval of both smoothed CSTs was considered. Moreover, the coherence values were transformed into standard Z-scores (31) as follows:

$$COH_{Zscore} = \frac{\text{arctanh}\sqrt{COH}}{\sqrt{1/(2N)}}, \quad (2)$$

where N is the number of segments used to calculate the coherence. The Fisher's z-transform was applied to the coherence values ($\alpha = 0.05$) in order to compare the normalized coherence values between the conditions (28). Because the low frequencies of common synaptic inputs are associated with force generation (21, 32, 33), significant peaks and areas were extracted in the delta band (<5 Hz). Lastly, we computed the average of the three coherence values between the three groups.

2.3. Statistical Analysis

2.3.1. Quality Criteria

In order to validate the quality control algorithm, the reference force signal and the smoothed CST (neural drive to the soleus and gastrocnemius muscles) were compared for each trial and patient. We assumed that if the correlation between force and CTS signals improved or remained the same after quality control, no relevant neuro-mechanical information was lost. **Figure 3C** shows how the smoothed CST still reflected the behavior of the reference force profile after some α-MNs with poor quality were removed. In order to compare the z-transformed cross-correlation coefficients at maximum likelihood before-and-after quality control, we computed histograms of the distributions (bin width = 0.02) normalized by the probability density function estimate and fitted into Epanechnikov kernel distributions (**Figure 4**).

2.3.2. Coherence Analysis

The statistical tests were run using IBM SPSS Statistics v.24 (IBM Corporation, New York, USA). As we recorded nine trials per time condition (three stages: pre, t0, and t30) across sham and cathodal stimulation conditions (i.e., 54 observations per patient), a linear mixed-effects model was performed to include and analyze all the repeated measures for the three patients that entirely followed the protocol.

The time (pre, t0, and t30) and stimulation (cathodal and sham) conditions were defined as fixed effects and the patients

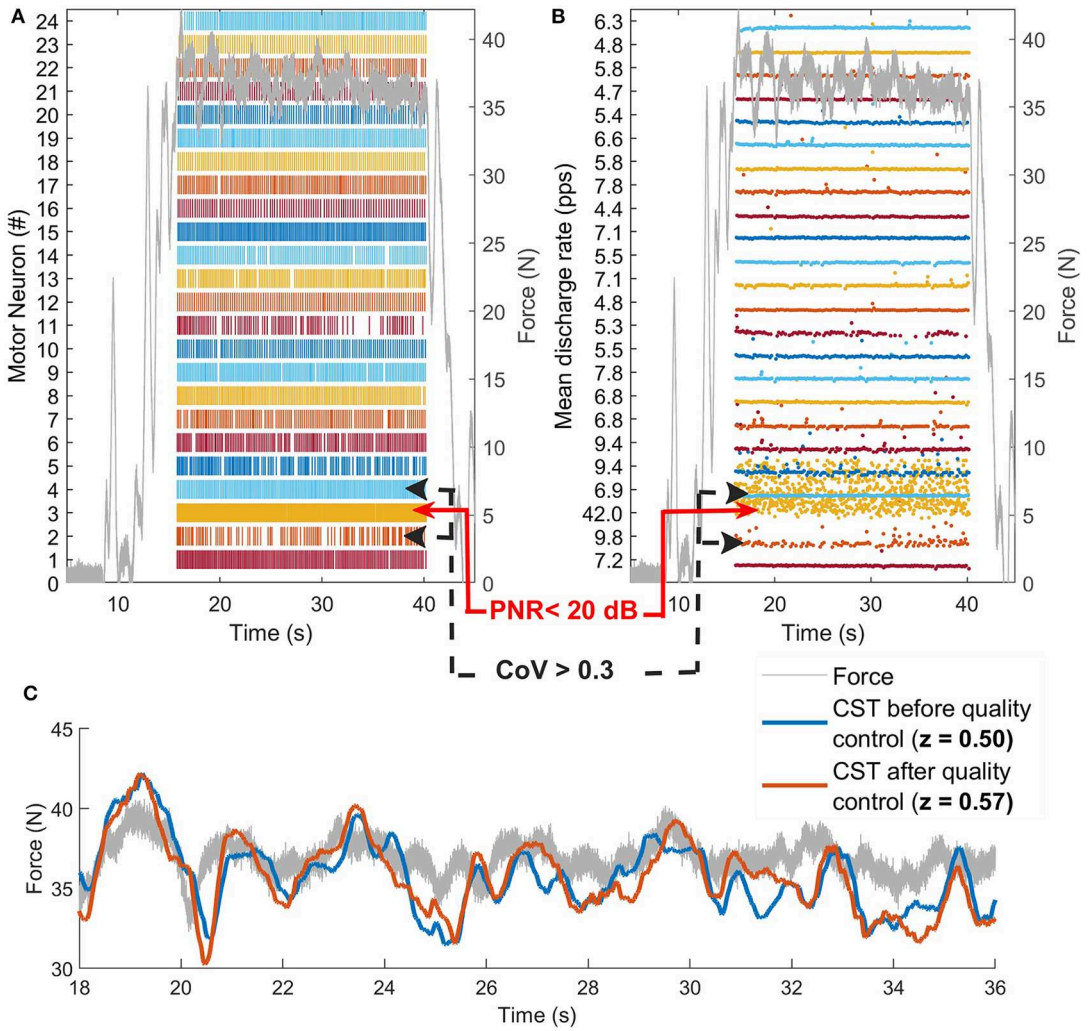

FIGURE 3 | Example of quality control procedure. **(A)** α-MN spike trains and **(B)** discharge rates of a α-MN pool before quality control. The algorithm rejects the α-MN with PNR <20 dB. In this case, as the cross-correlation improved by filtering the α-MNs with a coefficient of variation of the inter-spike intervals >0.3, the algorithm removes them as well. **(C)** Comparison between force (gray line) and the smoothed CST before (blue) and after (red) quality control. For illustrative purposes, the smoothed CST is scaled to the maximum value of the force and shifted to compensate for the neuro-mechanical delay (~0.6 s). Although some spike trains were removed after quality control, the correlation between force and smoothed CST improved. CST, cumulative spike train; pps, pulses per second.

were defined as a random effect (i.e., each patient is considered as a group of MN coherence measures). The auto-regressive model AR(1) was specified for the covariance structure of the repeated measures and the models were fitted and compared using the restricted maximum likelihood method. The normality of the residuals was checked with a Shapiro-Wilk test. The significance level was set to 0.05. Linear mixed models do not assume sphericity and are robust against violations of their own assumptions.

3. RESULTS

3.1. Quality Criteria

We performed a total of 216 HD-EMG recordings per muscle (i.e., soleus and gastrocnemius medialis) across all reference force tracking trials, stimulation conditions and patients. To corroborate the validity of the quality-check algorithm, we only included all cases where α-MN removal was required due to insufficient decomposition quality, i.e., $n = 157$ for the soleus and $n = 158$ for the gastrocnemius medialis, where n represents the total number of reference force tracking repetitions.

Figure 3C illustrates a visual example of improvement in correlation before ($z = 0.50$) and after quality control ($z = 0.57$). **Table 2** shows the total number of spike trains before and after quality control and the improvement in correlation per subject and muscle. **Figure 4** shows the distribution of the z-transformed correlation coefficients (see normalized histograms) as well as the associated kernel probability density functions (maximum likelihood correlation estimator).

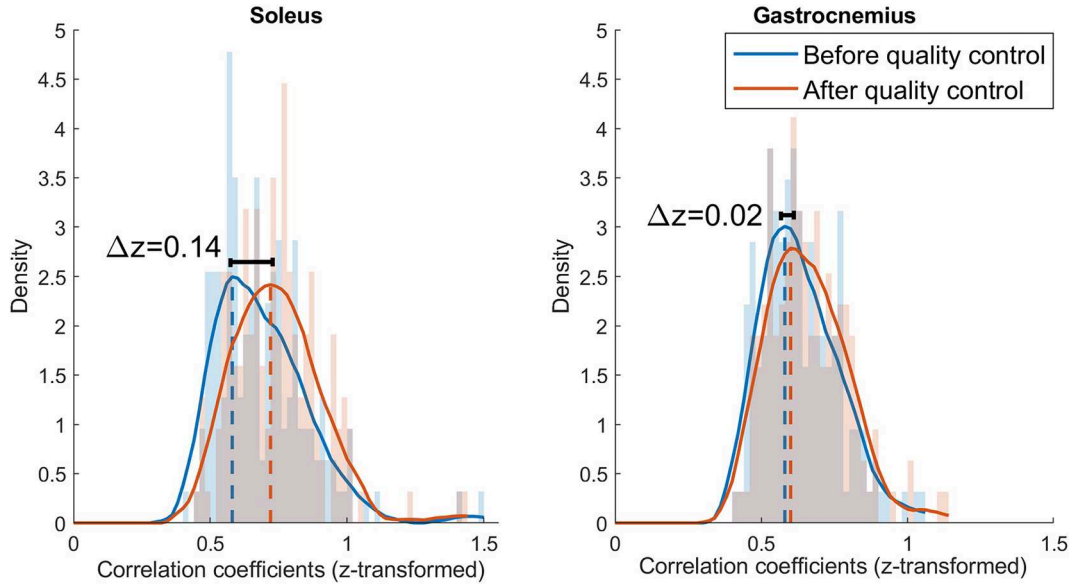

FIGURE 4 | Histograms and kernel density functions for the z-transformed correlation distribution of the soleus and gastrocnemius before and after quality control. The histograms are normalized by the power spectral density and the density function is estimated with a Epanechnikov kernel. The data before quality control is represented in blue and after quality control in orange.

TABLE 2 | Number of α-MNs before and after quality control and percentage of α-MNs removed for each patient and muscle.

Patient ID	Soleus			Gastrocnemius		
	Number of α-MN		% α-MNs removed	Number of α-MN		% α-MNs removed
	Before QC	Affter QC		Before QC	After QC	
P1	820	678	17%	809	705	13%
P2	361	291	19%	631	498	21%
P3	884	687	22%	300	220	27%
P4	1,573	801	49%	1,701	1,140	33%
Total	3,638	2,457	32%	3,441	2,563	26%

ID, identification code used for each patient; MN, Motor neuron; QC, Quality control.

Results showed that the z-transformed correlation coefficients were distributed toward higher values after quality control for both muscles, i.e., the maximum likelihood correlation coefficient improved from z = 0.58 to z = 0.72 (Δ z = 0.14) for soleus, and from z = 0.58 to z = 0.60 (Δ z = 0.02) for the gastrocnemius medialis.

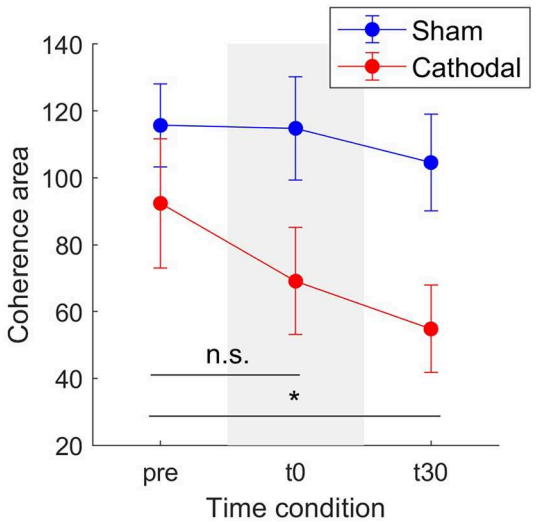

FIGURE 5 | Mean coherence area in the delta band for sham (blue) and cathodal (red) stimulation at pre, just after (t0) and 30 min after (t30) stimulation. (*) indicates significant differences between t30 and pre-stimulation ($p < 0.05$) and n.s. stands for no significance between pre and t0. Error bars represent standard error measure.

3.2. Coherence Between CSTs

Modulation of coherence between α-MN CSTs was analyzed in the delta band by extracting variations in coherence peak and area across stimulation type (sham, cathodal) and time-since stimulation (pre, t0, t30).

Concerning modulation of delta band coherence area, the mixed model analysis showed statistical significant variations for both stimulation type [$F_{(1,34.58)} = 23.77$, $p < 0.001$] and time-since-stimulation [$F_{(2,48.04)} = 4.66$, $p = 0.014$] conditions. **Figure 5** depicts the coherence area mean and standard errors (SE, 95% confidence interval) across pre, t0, and t30 condition in both sham and cathodal stimulation. In this, estimates of the fixed effects showed significant decrease between the pre- and t30 trials

$[t_{(44.92)} = -3.053, p = 0.004]$. Mean coherence area decreased from $z_{pre} = 92.36$ (SE = 19.35) to $z_{t30} = 69.09$ (SE = 16.01) and then to $z_{t30} = 54.8$ (SE = 13.05) across time conditions with cathodal stimulation; whereas for sham stimulation, it remained almost constant ($z_{pre} = 115.67$, SE = 12.45; $z_{t0} = 114.80$, SE = 15.42; $z_{t30} = 104.55$, SE = 14.44).

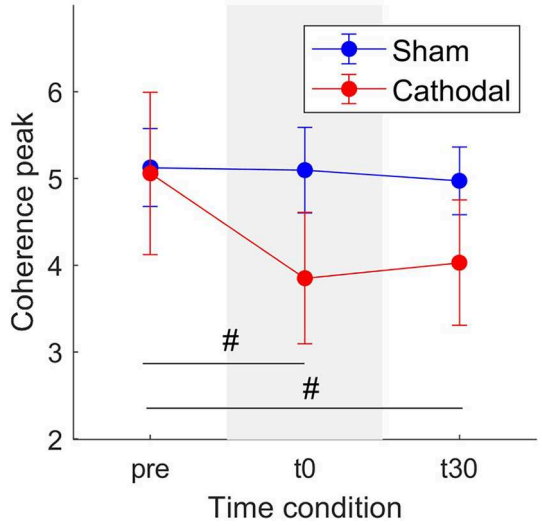

FIGURE 6 | Mean coherence peak in the delta band for sham (blue) and cathodal (red) stimulation at pre, just after (t0) and 30 min after (t30) stimulation. (#) indicates slight evidence of significant differences between pre and t0 and between pre and t30. Error bars represent standard error measure.

Similarly, **Figure 6** shows a decrease in coherence peaks from $z_{pre} = 5.06$ (SE = 0.93) to $z_{t30} = 3.85$ (SE = 0.75) followed by a minimal increase to $z_{t30} = 4.03$ (SE =0.72) with cathodal stimulation. For sham stimulation the coherence remained almost constant across all conditions ($z_{pre} = 5.12$, SE = 0.45; $z_{t0} = 5.09$, SE = 0.49; $z_{t30} = 4.97$, SE = 0.39). Nevertheless, in this case, the overall effects were weaker $[F_{(1,29.92)} = 3.03, p = 0.092]$ and time $[F_{(2,45.73)} = 2.82, p = 0.07]$.

Patient-specific analyses of both coherence areas and peaks showed pronounced decreasing trends primarily for P1 and P3 (areas: **Figure 7** and peaks: **Figure 7**) for cathodal stimulation. P1 presented a decrease from pre- to t0-stimulation and an slight increase from t0- to t30-stimulation in areas and peaks (areas: $z_{pre} = 106.17$, $z_{t0} = 81.29$ and $z_{t30} = 91.26$; peaks: $z_{pre} = 7.48$, $z_{t0} = 5.07$ and $z_{t30} = 6.18$). Similarly, P3 also presented a decrease in coherence peaks and areas, but with persistent effect across the three time conditions (areas: $z_{pre} = 123.79$, $z_{t0} = 86.39$ and $z_{t30} = 37.64$; peaks: $z_{pre} = 4.68$, $z_{t0} = 3.94$ and $z_{t30} = 3.05$). Contrarily, P2 presented a constant trend during cathodal stimulation (areas: $z_{pre} = 41.48$, $z_{t0} = 37.43$ and $z_{t30} = 33.08$; peaks: $z_{pre} = 2.75$, $z_{t0} = 2.53$ and $z_{t30} = 2.72$). **Tables 3**, **4** summarize the coherence mean area and peaks across individual patients and conditions.

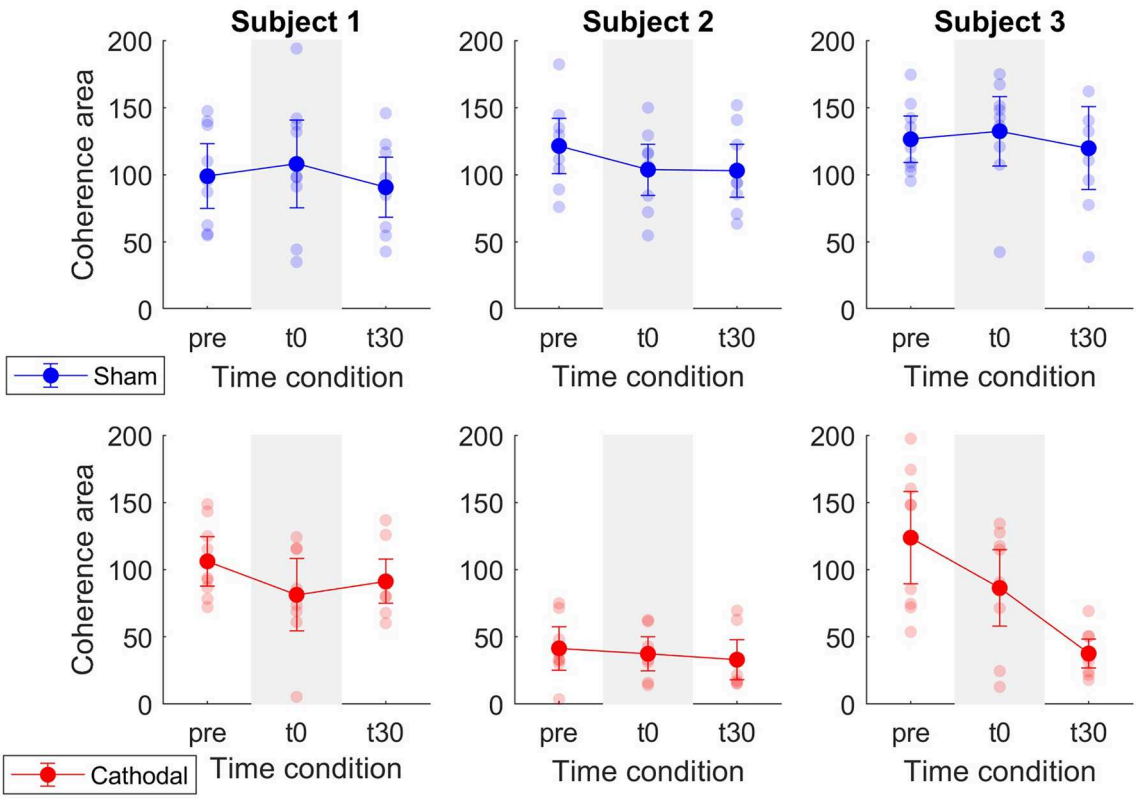

FIGURE 7 | Mean coherence area in the delta band for sham (blue) and cathodal (red) stimulation at pre, just after (t0) and 30 min after (t30) stimulation. Each column depicts the data for each patient.

TABLE 3 | Summary of coherence area means and standard errors across patients and experimental conditions.

Patient	Sham: Mean (SE)			Cathodal: Mean (SE)		
ID	pre	t0	t30	pre	t0	t30
P1	99.0 (24.1)	108.1 (32.5)	90.8 (22.3)	106.2 (18.3)	81.3 (26.9)	91.3 (16.4)
P2	121.5 (20.6)	103.9 (19.1)	103.1 (19.7)	41.5 (16.1)	37.4 (12.6)	33.1 (14.8)
P3	126.51 (17.34)	132.44 (25.89)	119.80 (30.8)	123.8 (34.3)	86.4 (28.5)	37.6 (10.8)

ID, identification code used for each patient; SE, Standard error; pre, before stimulation; t0, immediately after stimulation; t30, 30 min after stimulation.

TABLE 4 | Summary of coherence peak means and standard errors across patients and experimental conditions.

Patient	Sham: Mean (SE)			Cathodal: Mean (SE)		
ID	pre	t0	t30	pre	t0	t30
P1	4.70 (0.53)	5.66 (1.15)	4.69 (0.69)	7.48 (1.28)	5.07 (1.83)	6.18 (0.89)
P2	5.95 (0.75)	4.89 (0.74)	5.24 (0.64)	2.75 (0.58)	2.53 (0.70)	2.72 (0.69)
P3	4.72 (0.78)	4.74 (0.51)	4.98 (0.72)	4.68 (0.89)	3.94 (0.61)	3.05 (0.34)

ID, identification code used for each patient; SE, Standard error; pre, before stimulation; t0, immediately after stimulation; t30, 30 min after stimulation.

4. DISCUSSION

This study analyzed for the first time how large populations of α-MNs respond to tsDCS in incomplete SCI individuals performing isometric leg muscle contractions. In this context, we proposed to interface with α-MNs *in vivo*, using decomposition of HD-EMGs and subsequent analysis of α-MN spike trains in the frequency domain (via coherence analysis). Since inter-spike train coherence is sensitive to inaccuracies in the decomposition, we proposed a quality control algorithm for the automatic inspection of individual α-MNs spike trains. With this, we first removed spike trains with a PNR lower than 20 dB. Although a higher threshold for the PNR (30 dB) has been previously used (20, 25), this metric was relative to the quality of the acquired data. We considered that 20 dB (i.e., trains with identified spikes 10 times bigger in average than the baseline) was strict enough as a quality filter avoiding also the loss of relevant information. We then applied a second (conditional) filter using the CoV of the inter-spike intervals. However, as previous studies suggest that α-MN discharge variability increases with SCI (29, 30), this filter was only applied if it improved the correlation between the actual force and the estimate of neural drive (low-pass filtered CST).

We employed coherence analyses to estimate of the strength of the common synaptic input projected onto MS pools as previously proposed (21, 34) and showed that this frequency-dependent feature sensibly responded to stimulation conditions, unlike time-domain features (e.g., discharge rate). With independent synaptic inputs to α-MNs being attenuated by the α-MN pool population sampling, the remaining common synaptic input largely approximates to the neural drive to muscle in the delta band (21) (neural signal for force control). Therefore, coherence and common input analysis may serve as a robust indicator of tsDCS effect on motor function recovery (35). Our results showed consistent decrease in α-MN coherence in delta band immediately after trans-spinal electrical stimulation (i.e., t0-condition) as well as after 30 min from stimulation (i.e., t30-condition) with respect to the non-stimulation condition (i.e., pre-condition, **Figures 5**, **6**). From a neurophysiological point of view, the observed coherence decrease may underlie a decrease in the strength of common synaptic input to α-MN pools. Previous research (34) indicated that de-correlation between α-MN spike trains may be due to additional components of the common synaptic input to all α-MNs, but independent to the cortical drive. Thus, the reduction in delta band coherence may indicate demodulation (increased variability) in effective neural drive to the muscle, possibly due to higher frequency inputs.

Coherence peak and area modulations showed less pronounced trends in P2 with respect to P1 and P3 (**Figures 7**, **8**). That is, average coherence peaks and areas for P2 did not vary substantially across pre-, t0-, and t30-conditions. This may be due to the inability of personalizing the stimulation parameter for the individual patient (i.e., stimulation intensity) as well as the inability of accurately targeting the desired spinal segments (∼L5-S2). Moreover, it is worth stressing that tsDCS was prescribed blindly with no feedback on α-MN behavior. In this context, lesion and spinal cord anatomy differences across patients could explain the variability in the stimulation-effect (cathodal) results. Although, in this study, the lesion differences are rather small [all patients have injuries above C8 and their motor function is preserved below the injury (AIS-C and D)], larger differences can be found in the patients' physiological and anatomical factors including age, sex, height, and weight (**Table 1**). Future work will develop on-line HD-EMG recording and decomposition techniques to be used to adjust on the fly the location and stimulation parameters of multi-channel electrical stimulation.

We analyzed changes in α-MN coherence features with no direct observation of stimulation-effects on the neuromuscular system. Future work will employ electrically induced H-reflex to verify whether or not the administered stimulation induced facilitation of corticospinal output to muscles, thus providing further possibilities for interpreting coherence results at the α-MN level.

Moreover, the present study aimed at creating a methodology to analyze for the first time the response of multiple MNs to tsDCS in incomplete SCI individuals. However, further clinical validation is needed to test whether our methodology can be generalized to a larger population. Future work will extend this study to also include healthy individuals, multiple muscles and data modeling approaches.

The quality-check algorithm we proposed (**Algorithm 1**, **Figure 3**) may also be further improved in the future to enable detailed editing of α-MN spike trains. Our proposed methodology only enabled removing entire spike trains after

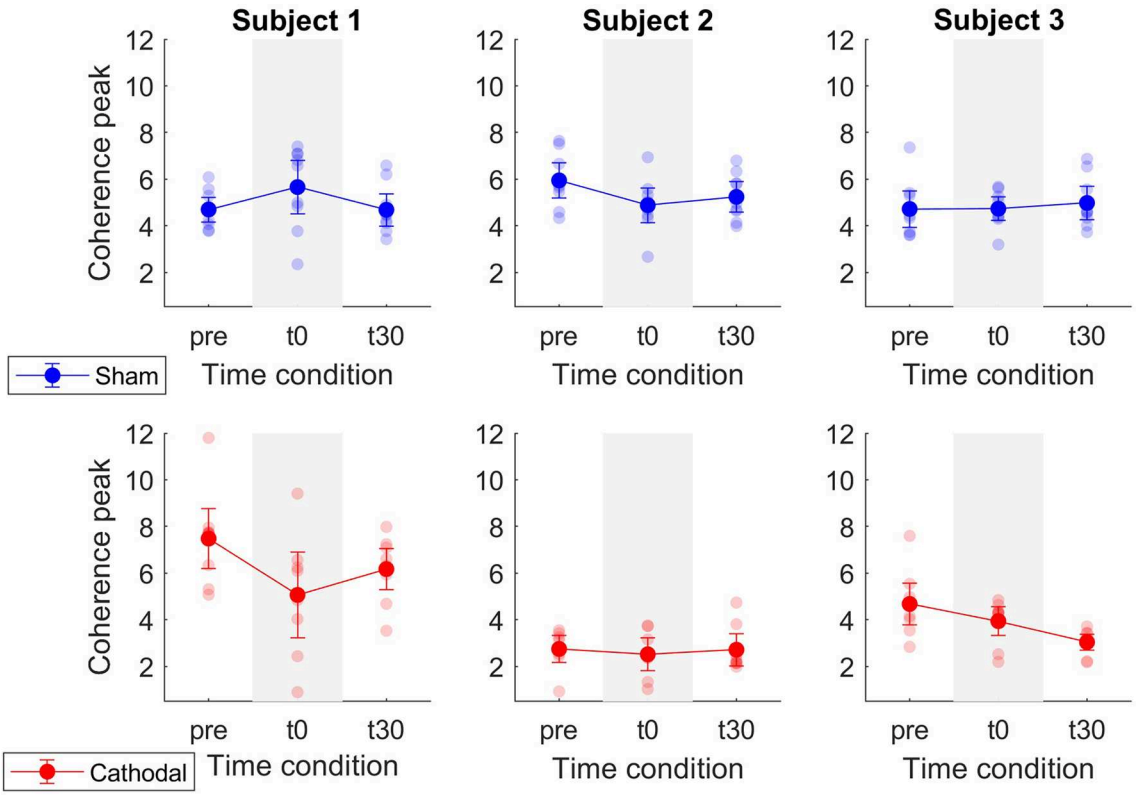

FIGURE 8 | Mean coherence peak in the delta band for sham (blue) and cathodal (red) stimulation at pre, just after (t0) and 30 min after (t30) stimulation. Each column depicts the data for each patient.

inconsistencies being detected. This may result in discarding potentially neurophysiologically-consistent information. The ability of identifying individual mismatched spikes (36) would avoid the need for eliminating entire spike trains in the quality control stage. As a result, less neural information would be compromised. However, this would make the experimental set-up more complicated as it requires not only surface EMG but also intramuscular EMG recordings.

This study demonstrated the ability of interfacing with α-MNs *in vivo* in SCI individuals receiving transcutaneous spinal cord electrical stimulation. First, we proposed a methodology that enabled removing compromised information from α-MN spike trains, central for analysing frequency domain features from bio-electrical data. Second, we reported how α-MN discharge coherence modulated in response to spinal cord electrical stimulation. Our study suggested that the common synaptic input to α-MN pools may decrease immediately after cathodal tsDCS, which was reflected in the decrease in coherence within the delta band.

The ability to non-invasively estimate how α-MNs respond to electrical stimuli is central to devise personalized rehabilitation therapies. To this aim, future work will first establish causal relations between common synaptic input to α-MNs and spinal cord excitability. In a rehabilitation scenario, knowing these relationships will enable building direct associations between electrical stimulation patterns and the resulting modulation in an individual patient's spinal cord excitability. This will permit using non-invasive electrical stimulation to restore physiological spinal excitability for treating a variety of related motor disorders associated with hyperexcitability of spinal neuronal structures, such as spasticity (37). Moreover, the ability to modulate spinal cord excitability may help understand how to best induce activity-dependent neuro-plasticity, thereby increasing the efficacy of rehabilitation programs (38).

In the context of neurorehabilitation technologies, our proposed methodology may open up new avenues for the design of real-time model-based closed-loop applications (39–41) including both transcutaneous and epidural spinal cord electrical stimulation methodologies. To this end, non-invasive estimates of individual spinal α-MN behavior may help optimize stimulation parameters on-the-fly (e.g., pulse width and amplitude of a multi-channel array of electrodes), thereby modulating spinal excitability in a closed-loop fashion.

DATA AVAILABILITY STATEMENT

The datasets generated for this study are available on request to the corresponding author.

ETHICS STATEMENT

The studies involving human participants were reviewed and approved by Ethics Committee of Twente (Enschede, The Netherlands). The patients/participants provided their written informed consent to participate in this study.

AUTHOR CONTRIBUTIONS

AG, AK, EA, FN, JB, UY, and MS contributed to the revision of the manuscript, approved it for submission, and agreed to be accountable for all aspects of the work in ensuring that questions related to the accuracy or integrity of any part of the work are appropriately investigated and resolved. AK and EA contributed to the data acquisition. AG, FN, JB, UY, and MS contributed to the data analysis and interpretation. AG, UY, and MS contributed to the conception of the work and writing of the manuscript.

FUNDING

This work was supported by the European Research Council Starting Grant INTERACT (grant no. 803035).

REFERENCES

1. Thomas CK, Bakels R, Klein CS, Zijdewind I. Human spinal cord injury: motor unit properties and behaviour. *Acta Physiol*. (2014) 210:5–19. doi: 10.1111/apha.12153
2. Jensen MP, Kuehn CM, Amtmann D, Cardenas DD. Symptom burden in persons with spinal cord injury. *Arch Phys Med Rehabil*. (2007) 88:638–45. doi: 10.1016/j.apmr.2007.02.002
3. Pointillart V, Wiart L, Vital JM, Lassieâ P, Thicoipeâ M, Dabadie P. Pharmacological therapy of spinal cord injury during the acute phase. *Spinal Cord*. (2000) 38:71–6. doi: 10.1038/sj.sc.3100962
4. Tsuji O, Miura K, Okada Y, Fujiyoshi K, Mukaino M, Nagoshi N, et al. Therapeutic potential of appropriately evaluated safe-induced pluripotent stem cells for spinal cord injury. *Proc Natl Acad Sci USA*. (2010) 107:12704–9. doi: 10.1073/pnas.0910106107
5. Duh MS, Shepard MJ, Wilberger JE, Bracken MB. The effectiveness of surgery on the treatment of acute spinal cord injury and its relation to pharmacological treatment. *Neurosurgery*. (1994) 35:240–9. doi: 10.1097/00006123-199408000-00009
6. van den Brand R, Heutschi J, Barraud Q, DiGiovanna J, Bartholdi K, Huerlimann M, et al. Restoring voluntary control of locomotion after paralyzing spinal cord injury. *Science*. (2012) 336:1182–5. doi: 10.1126/science.1217416
7. Capogrosso M, Milekovic T, Borton D, Wagner F, Moraud EM, Mignardot JB, et al. A brain-spine interface alleviating gait deficits after spinal cord injury in primates. *Nature*. (2016) 539:284–8. doi: 10.1038/nature20118
8. Harkema S, Gerasimenko Y, Hodes J, Burdick J, Angeli C, Chen Y, et al. Effect of epidural stimulation of the lumbosacral spinal cord on voluntary movement, standing, and assisted stepping after motor complete paraplegia: a case study. *Lancet*. (2011) 377:1938–47. doi: 10.1016/S0140-6736(11)60547-3
9. Winkler T, Hering P, Straube A. Spinal DC stimulation in humans modulates post-activation depression of the H-reflex depending on current polarity. *Clin Neurophysiol*. (2010) 121:957–61. doi: 10.1016/j.clinph.2010.01.014
10. Yamaguchi T, Fujimoto S, Otaka Y, Tanaka S. Effects of transcutaneous spinal DC stimulation on plasticity of the spinal circuits and corticospinal tracts in humans. In: *2013 6th International IEEE/EMBS Conference on Neural Engineering (NER)*. San Diego, CA (2013). p. 275–8. doi: 10.1109/NER.2013.6695925
11. Lamy JC, Boakye M. BDNF Val66Met polymorphism alters spinal DC stimulation-induced plasticity in humans. *J Neurophysiol*. (2013) 110:109–16. doi: 10.1152/jn.00116.2013
12. Gerasimenko Y, Gorodnichev R, Moshonkina T, Sayenko D, Gad P, Edgerton VR. Transcutaneous electrical spinal-cord stimulation in humans. *Ann Phys Rehabil Med*. (2015) 58:225–31. doi: 10.1016/j.rehab.2015.05.003
13. Hubli M, Dietz V, Schrafl-Altermatt M, Bolliger M. Modulation of spinal neuronal excitability by spinal direct currents and locomotion after spinal cord injury. *Clin Neurophysiol*. (2013) 124:1187–95. doi: 10.1016/j.clinph.2012.11.021
14. Picelli A, Chemello E, Castellazzi P, Roncari L, Waldner A, Saltuari L, et al. Combined effects of transcranial direct current stimulation (tDCS) and transcutaneous spinal direct current stimulation (tsDCS) on robot-assisted gait training in patients with chronic stroke: a pilot, double blind, randomized controlled trial. *Restor Neurol Neurosci*. (2015) 33:357–68. doi: 10.3233/RNN-140474
15. Nagel SJ, Wilson S, Johnson MD, Machado A, Frizon L, Chardon MK, et al. Spinal cord stimulation for spasticity: historical approaches, current status, and future directions. *Neuromodulation*. (2017) 20:307–21. doi: 10.1111/ner.12591
16. Zimmermann JB, Jackson A. Closed-loop control of spinal cord stimulation to restore hand function after paralysis. *Front Neurosci*. (2014) 8:87. doi: 10.3389/fnins.2014.00087
17. Wenger N, Moraud EM, Raspopovic S, Bonizzato M, DiGiovanna J, Musienko P, et al. Closed-loop neuromodulation of spinal sensorimotor circuits controls refined locomotion after complete spinal cord injury. *Sci Transl Med*. (2014) 6:255ra133. doi: 10.1126/scitranslmed.3008325
18. Bocci T, Marceglia S, Vergari M, Cognetto V, Cogiamanian F, Sartucci F, et al. Transcutaneous spinal direct current stimulation modulates human corticospinal system excitability. *J Neurophysiol*. (2015) 114:440–6. doi: 10.1152/jn.00490.2014
19. Dideriksen JL, Negro F, Falla D, Kristensen SR, Mrachacz-Kersting N, Farina D. Coherence of the surface EMG and common synaptic input to motor neurons. *Front Hum Neurosci*. (2018) 12:207. doi: 10.3389/fnhum.2018.00207
20. Laine CM, Martinez-Valdes E, Falla D, Mayer F, Farina D. Motor neuron pools of synergistic thigh muscles share most of their synaptic input. *J Neurosci*. (2015) 35:12207–16. doi: 10.1523/JNEUROSCI.0240-15.2015
21. Farina D, Negro F. Common synaptic input to motor neurons, motor unit synchronization, and force control. *Exerc Sport Sci Rev*. (2015) 43:23–33. doi: 10.1249/JES.0000000000000032
22. Negro F, Farina D. Factors influencing the estimates of correlation between motor unit activities in humans. *PLoS ONE*. (2012) 7:1–14. doi: 10.1371/journal.pone.0044894
23. Negro F, Holobar A, Farina D. Fluctuations in isometric muscle force can be described by one linear projection of low-frequency components of motor unit discharge rates. *J Physiol*. (2009) 587:5925–38. doi: 10.1113/jphysiol.2009.178509
24. Holobar A, Farina D, Gazzoni M, Merletti R, Zazula D. Estimating motor unit discharge patterns from high-density surface electromyogram. *Clin Neurophysiol*. (2009) 120:551–62. doi: 10.1016/j.clinph.2008.10.160
25. Holobar A, Minetto MA, Farina D. Accurate identification of motor unit discharge patterns from high-density surface EMG and validation with a novel signal-based performance metric. *J Neural Eng*. (2014) 11:016008. doi: 10.1088/1741-2560/11/1/016008
26. Martinez-Valdes E, Negro F, Laine CM, Falla D, Mayer F, Farina D. Tracking motor units longitudinally across experimental sessions with high-density surface electromyography. *J Physiol*. (2017) 595:1479–96. doi: 10.1113/JP273662
27. Pollock CL, Ivanova TD, Hunt MA, Garland SJ. Behavior of medial gastrocnemius motor units during postural reactions to external perturbations after stroke. *Clin Neurophysiol*. (2015) 126:1951–8. doi: 10.1016/j.clinph.2014.12.015
28. Yavuz UŞ, Negro F, Sebik O, Holobar A, Frömmel C, Türker KS, et al. Estimating reflex responses in large populations of motor units by

decomposition of the high-density surface electromyogram. *J Physiol*. (2015) 593:4305–18. doi: 10.1113/JP270635
29. Thomas CK, Butler JE, Zijdewind I. Patterns of pathological firing in human motor units. In: Gandevia SC, Proske U, Stuart DG, editors. *Sensorimotor Control of Movement and Posture*. Boston, MA: Springer US (2002). p. 237–44. doi: 10.1007/978-1-4615-0713-0_29
30. Wiegner AW, Wierzbicka MM, Davies L, Young RR. Discharge properties of single motor units in patients with spinal cord injuries. *Muscle Nerve*. (1993) 16:661–71. doi: 10.1002/mus.880160613
31. Rosenberg JR, Amjad AM, Breeze P, Brillinger DR, Halliday DM. The Fourier approach to the identification of functional coupling between neuronal spike trains. *Prog Biophys Mol Biol*. (1989) 53:1–31. doi: 10.1016/0079-6107(89)90004-7
32. De Luca C, Erim Z. Common drive of motor units in regulation of muscle force. *Trends Neurosci*. (1994) 17:299–305. doi: 10.1016/0166-2236(94)90064-7
33. Negro F, Yavuz U, Farina D. The human motor neuron pools receive a dominant slow-varying common synaptic input. *J Physiol*. (2016) 594:5491–505. doi: 10.1113/JP271748
34. Negro F, Farina D. Decorrelation of cortical inputs and motoneuron output. *J Neurophysiol*. (2011) 106:2688–97. doi: 10.1152/jn.00336.2011
35. Zheng Y, Peng Y, Xu G, Li L, Wang J. Using corticomuscular coherence to reflect function recovery of paretic upper limb after stroke: a case study. *Front Neurol*. (2018) 8:728. doi: 10.3389/fneur.2017.00728
36. Negro F, Muceli S, Castronovo AM, Holobar A, Farina D. Multi-channel intramuscular and surface EMG decomposition by convolutive blind source separation. *J Neural Eng*. (2016) 13:026027. doi: 10.1088/1741-2560/13/2/026027
37. Knikou M, Murray LM. Repeated transspinal stimulation decreases soleus H-reflex excitability and restores spinal inhibition in human spinal cord injury. *PLoS ONE*. (2019) 14:e0223135. doi: 10.1371/journal.pone.0223135
38. McPherson JG, Miller RR, Perlmutter SI, Poo MM. Targeted, activity-dependent spinal stimulation produces long-lasting motor recovery in chronic cervical spinal cord injury. *Proc Natl Acad Sci USA*. (2015) 112:12193–8. doi: 10.1073/pnas.1505383112
39. Sartori M, Yavuz U, Farina D. *In vivo* neuromechanics: decoding causal motor neuron behavior with resulting musculoskeletal function. *Sci Rep*. (2017) 7:13465. doi: 10.1038/s41598-017-13766-6
40. Durandau G, Farina D, Sartori M. Robust real-time musculoskeletal modeling driven by electromyograms. *IEEE Trans Biomed Eng*. (2018) 65:556–64. doi: 10.1109/TBME.2017.2704085
41. Lotti N, Xiloyannis M, Durandau G, Galofaro E, Sanguineti V, masia l, et al. Adaptive model-based myoelectric control for a soft wearable arm exosuit: a new generation of wearable robot control. *IEEE Robot Autom Mag*. (2020) 27:43–53. doi: 10.1109/MRA.2019.2955669

Conflict of Interest: The authors declare that the research was conducted in the absence of any commercial or financial relationships that could be construed as a potential conflict of interest.

frontiers in Neurology

ORIGINAL RESEARCH
published: 24 July 2020
doi: 10.3389/fneur.2020.00668

Improved Gait of Persons With Multiple Sclerosis After Rehabilitation: Effects on Lower Limb Muscle Synergies, Push-Off, and Toe-Clearance

Johanna Jonsdottir, Tiziana Lencioni, Elisa Gervasoni, Alessandro Crippa, Denise Anastasi, Ilaria Carpinella, Marco Rovaris, Davide Cattaneo and Maurizio Ferrarin*

IRCCS Fondazione Don Carlo Gnocchi, Milan, Italy

OPEN ACCESS

Edited by:
Jun Yao,
Northwestern University, United States

Reviewed by:
Vincent De Groot,
Amsterdam University Medical Center (UMC), Netherlands
Natalia Sanchez,
University of Southern California, Los Angeles, United States

****Correspondence:***
Tiziana Lencioni
tlencioni@dongnocchi.it

Specialty section:
This article was submitted to Neurorehabilitation, a section of the journal Frontiers in Neurology

Received: *15 December 2019*
Accepted: *03 June 2020*
Published: *24 July 2020*

Citation:
Jonsdottir J, Lencioni T, Gervasoni E, Crippa A, Anastasi D, Carpinella I, Rovaris M, Cattaneo D and Ferrarin M (2020) Improved Gait of Persons With Multiple Sclerosis After Rehabilitation: Effects on Lower Limb Muscle Synergies, Push-Off, and Toe-Clearance. Front. Neurol. 11:668. doi: 10.3389/fneur.2020.00668

Introduction: Persons with MS (PwMS) have markedly reduced push-off and toe-clearance during gait compared to healthy subjects (HS). These deficits may result from alterations in neuromotor control at the ankle. To optimize rehabilitation interventions for PwMS, a crucial step is to evaluate if and how altered neuromotor control, as represented by muscle synergies, improves with rehabilitation. In this study we investigated changes in ankle motor control and associated biomechanical parameters during gait in PwMS, occurring with increase in speed after gait rehabilitation.

Methods: 3D motion and EMG data were collected while 11 PwMS (age 50.3 + 11.1; EDSS 5.2 + 1.2) walked overground at self-selected speed before (T0) and after 20 sessions (T1) of intensive treadmill training. Muscle synergies were extracted using non-negative matrix factorization. Gait parameters were computed according to the LAMB protocol. Pearson's correlation coefficient was used to evaluate the similarity of motor modules between PwMS and HS. To assess differences in distal module activations representing neuromotor control at the ankle [Forward Propulsion (FPM) and Ground Clearance modules (GCM)], each module's activation timing was integrated over 100% of the gait cycle and the activation percentage index (API) was computed in six phases.

Ten age matched HS provided two separate speed-matched normative datasets for T0 and T1. For speed independent comparison for the PwMs Z scores were calculated for all their gait variables.

Results: In PwMS velocity increased significantly from T0 to T1 (0.74–0.90 m/s, $p < 0.05$). The activation profiles (API) of FPM and GCM of PwMS improved in pre-swing ($p < 0.05$): FPM (Mean [95% CI] [%]: T0: 12.5 [5.7–19.3] vs. T1: 9.0 [2.7–15.3]); GCM (T0: 26.7 [18.2–35.3] vs. T1: 24.5 [18.2–30.7]). This was associated with an increase in toe clearance (80.3 to 103.6 mm, $p < 0.05$) and a higher ankle power peak in pre-swing (1.53–1.93 W/kg, $p < 0.05$).

Conclusion: Increased gait speed of PwMS after intensive gait training was consistent with improvements in spatio-temporal gait parameters. The most important finding of this study was the re-organization of distal leg modules related to neurophysiological changes induced by rehabilitation. This was associated with an improved ankle performance.

Keywords: muscle synergies, multiple scleorsis (MS), rehabilitation, gait, EMG, push-off, toe-clearance

INTRODUCTION

Multiple sclerosis (MS) is a chronic inflammatory demyelinating disorder of the central nervous system (CNS) characterized by a progressive decline in various motor, sensory, and cognitive functions over the lifespan (1). Problems with mobility are evident in most persons with MS (PwMS), probably related to myelin damage which leads to adaptive changes in motor cortex and the spinal circuits (2, 3), as well as coordination problems, due to cerebellar circuit involvement (4). Resultant deficits in motor control and muscle weakness impact the gait function in PwMS and contribute to a reduction of participation in daily life activities (5, 6). Accordingly, regaining locomotor abilities is one of the primary goals of rehabilitation. Measuring the efficacy of rehabilitation on gait function at functional and neurophysiological levels is of utmost importance in this respect.

Clinical measures, frequently used to evaluate motor behavior and response to rehabilitation, are useful in describing the severity of mobility deficit, the functional walking status, and the amount of participation in daily life (5, 7). However, they do not inform on what may be the changes in neurophysiological or biomechanical mechanisms underlying an improvement in walking abilities following rehabilitation.

Spatiotemporal parameters and kinematic/kinetic variables derived through gait analysis have traditionally been used to objectively quantify walking abnormalities and biomechanical changes induced by rehabilitation (8). For example, it has been demonstrated (9–11) that PwMS walk slower and with a shorter stride length than healthy controls walking at matched speeds. Severini et al. (11) also found that PwMS showed decreased range of motion at hip, knee, and ankle while Filli et al. (10), in addition to the restrictions in joint excursion, found increased gait variability and asymmetry along with impaired dynamic stability. Such detailed information helps to describe the pathological gait patterns and to better understand the biomechanical contributions to possible recovery after rehabilitation but does not inform upon underlying changes in neuro-muscular control contributing to the improvement. Further, it would be important to verify whether observed post-treatment changes are related to a true physiological recovery rather than being a byproduct of the increased speed (10).

Modular organization of muscle coordination is thought to underlie motor control in both healthy individuals and individuals with neurological disorders (9, 12–14). Muscle synergies, derived from electromyographic signals during gait, are thought to reflect the underlying neural structures of muscle activation and local circuits (15, 16). Several studies have used muscle synergy analysis to model the complexity of motor control during gait, demonstrating that human gait can be described by a small set of robust synergies in healthy subjects (17–19) and in persons with neurological disorders (9, 20, 21).

Indeed, by using the muscle synergy approach as a framework, it was possible to study the neuromotor characteristics underlying walking in PwMS with moderate disability (9). The study of synergies in addition to gait biomechanics resulted in information not only on the biomechanical deficits present in gait of PwMS but also on corresponding deficits in neuromotor coordination. Main findings indicated that the walking deficits in PwMS were associated with muscle weakness and prolonged double support phases, corresponding to altered timing of the activation profiles of the distal motor modules (9). Importantly, PwMS had synergies number and module composition similar to healthy persons walking at the same speed, indicating a preserved organization of neuromotor control (9, 21).

Altogether, a combination of clinical scales, biomechanical, and muscle synergy analysis of gait allows understanding of deficits and limitations at the participation, activity, and impairment levels in persons with neurological disorders. This multivariate analysis can give information on functional performance as related to mobility, kinetics, kinematics, and neurological control of walking, all of which are essential for setting up effective customized treatments and for the evaluation of their efficacy. While muscle synergies and their relation to rehabilitation outcomes for persons post stroke (22) and with Parkinson's disorder (20) have been studied, to date no studies have yet been published that applied such a comprehensive approach in persons with MS.

In our recent work we described alterations in motor primitives of distal muscle synergies during walking of PwMS with respect to those of age and speed-matched healthy peers (9) in terms of important differences in timing activation across the gait cycle. In healthy individuals there are predominantly three to four modules that have been found to be related to walking (15, 23, 24). One or two modules are related to proximal muscle activity during gait. One usually consists mainly of activity from knee extensor, hip extensor, and abductor, which are primarily involved in early stance and late swing to prepare the leg for weight acceptance. The second proximal module consists mainly of hamstring activity from hip extensor and knee flexor, which are primarily involved in the early stance and late swing to extend the hip and decelerate leg swing (23). The two distal modules instead are related to propulsion and ground clearance and consist of the Forward Propulsion Module (FPM, mainly related to Soleus and Gastrocnemius) and Ground Clearance Module (GCM, mainly related to Tibialis Anterior and Rectus Femoris) (23). Using sEMG during overground gait, our prior investigation

of module composition across PwMS and healthy controls revealed that when only three modules are identified, there was a merging of the two proximal modules (9). When timing of motor primitives (activity percentage indexes) was compared between the two groups, these proximal modules (both when merged and separate) resulted similar between PwMS and healthy individuals. On the other hand, timing of the motor primitives of the distal modules (FPM and GCM) results were altered in PwMS, regardless of module number. In addition, biomechanical gait deficits (i.e., reduced push-off and toe clearance in swing) were found to be consistent with impairments in activation and coordination of these distal synergies. This corroborated findings of others that have identified the reduction of (i) propulsion and (ii) foot-ground clearance during swing to be among the most disabling deficits in gait of PwMS (25, 26).

To exploit the clinical application of this information and use it to optimize/tailor rehabilitation interventions for PwMS, a crucial step is to evaluate if and how altered distal muscle synergies and their associated biomechanical parameters can be improved by rehabilitation.

Therefore, the focus of this article is on neuromotor recovery in distal parameters occurring with successful gait rehabilitation. More specifically, we investigated changes in neuromodular organization of FPM and GCM, and in propulsion and foot-ground clearance, of PwMS following a gait rehabilitation that lead to clinically meaningful increase in gait speed. These changes were investigated relative to healthy individuals walking at matched pre and post intervention speeds. We hypothesized that greater natural speed of walking would be associated with improvement in ankle control and associated biomechanical parameters in line with changes of healthy individuals. Further, we also investigated whether changes in the various gait parameters were proportional to speed changes in the PwMS.

METHODS

Participants

Participants were 11 adults with relapsing-remitting or secondary progressive MS according to the 2005 McDonald criteria (27) who had volunteered for a larger controlled intervention trial carried out at IRCCS Don Gnocchi Foundation, Milan, Italy, in the period from October 2012 to April 2018 (see **Table 1** for demographic information). From the entire dataset only the PwMS who agreed to undergo a complete gait analysis (electromyography, kinematic, and kinetics of the lower limb) pre- and post-intervention on treadmill (28) were considered for the present study. Of those, we analyzed gait data of 11 participants that had increased their gait speed by more than 15%. Inclusion criteria for PwMS were: diagnosis of multiple sclerosis according to the criteria of McDonald, Expanded Disability Status Scale (EDSS) ≤ 7 (29), age between 18 and 75 years, capacity to stand 30 s and walk 10 m with or without an assistive device (but without assistance from another person), capacity to understand and follow instructions, and stable neurological condition. Exclusion criteria: presence of any musculoskeletal and/or other neurologic pathologies that could influence gait and balance functions, presence of severe cardiovascular disorders.

Additionally, we analyzed gait data from 10 age-matched healthy controls (HS) (age Mean 43.1 SD 14.6 years, 6 Female and 4 Males) to derive biomechanical and muscle synergies reference data. Inclusion criteria for these healthy controls were: exhibiting normal joint range of motion and muscle strength, without any neuromuscular and balance deficits that could interfere with their gait.

The experimental protocol was approved by the institutional Ethics Committee (Comitato Etico Fondazione Don Carlo Gnocchi) and was carried out according to ethical standards

TABLE 1 | Individual demographic and clinical characteristics of PwMS and number of synergies at baseline and post-intervention.

Subjects with MS	SEX	AGE [yrs]	ONSET [yrs]	EDSS	DGI	TUG [s]	2MWT [m]	N synergies (baseline)	N synergies (post)
S1	F	61	13	6	12	13.5	84	3	4
S2	M	40	11	7	11	21	41	3	4
S3	F	54	25	6	13	11.3	128	3	3
S4	M	39	2	3	12	10.5	135	4	4
S5	M	36	13	4	22	8.3	155	4	4
S6	F	42	21	5	17	9.9	98	3	3
S7	F	68	19.5	5	17	15.1	75	4	3
S8	F	53	19	5	18	9.9	99	4	4
S9	M	64	23	4	14	15.9	122	3	4
S10	F	42	22	6	8	14.7	82	4	4
S11	F	54	25	6	9	14.1	113	4	3
Mean		50.3	17.6	5.2	13.9	13.1	102.9	3.5	3.6
Standard deviation		7.1	11.1	1.2	2	4.2	32.1	0.5	0.5

PwMS, Persons with Multiple Sclerosis; MS, Multiple Sclerosis; EDSS, Expanded Disability Status Scale; DGI, Dynamic Gait Index; TUG, Timed Up and Go; 2MWT, Two Minute Walking Test; N, Number; F, female; M, male.

of the Declaration of Helsinki. All participants signed an informed consent.

Experimental Set Up and Procedures

We collected demographic and clinical variables according to study protocol [see Jonsdottir et al. (28)]. All participants with MS were evaluated with the following validated clinical scales: the 2 Minute Walking Test (2MWT) for gait endurance (30), the 10 meter timed walk (10MTW) for gait speed (31), and the Berg Balance scale for standing balance (32). The evaluation was carried out at baseline (T0) and after an intervention period (T1) by physical therapists blinded to the original study's group assignment (28).

Overground gait analysis of the PwMS participating in the present study and the HS was performed in a gait analysis lab. Kinematic, kinetic, and electromyography (EMG) data were thus collected both from healthy subjects (once) and from the participants affected by multiple sclerosis (twice, at T0 and T1). Kinematic data were collected using a 9-camera SMART-D motion capture system (BTS, Milano, Italy) sampling at 200 Hz, while a force plate (Kistler, Winterthur, Switzerland), with 960 Hz sampling frequency, provided ground reaction force (GRF).

We used an 8-channel EMG system (BTS, Milano, Italy) to record EMG data at 1,000 Hz from the following muscles: tibialis anterior (TA), soleus (SO), medial gastrocnemius (MG), lateral gastrocnemius (LG), vastus medialis (VM), rectus femoris (RF), semitendinosus (SE), gluteus medius (GM). Seniam recommendations for sEMG recording procedures were followed (33). The EMG sensors were placed on the most affected side for participants with MS [selected according to item 13 of the Berg Balance Scale, Standing unsupported one foot in front (32); the worse performance when right or left foot was in back during the pose] and on the dominant side (the leg that was used to kick a ball) for control subjects.

All participants (PwMS and HS) were asked to perform at least 5 gait trials barefoot at their natural self-selected speed, and the HS also performed trials at slower speeds (SW), to provide a reference dataset at gait speed matched with that of PwMS. In each trial only the central stride (the one on the platform) was analyzed. Since (i) PwMS significantly increased walking speed from T0 to T1 and (ii) there are speed-dependent effects on the timing patterns of muscle activity and on kinematic and kinetic parameters (34), we extracted two different speed-matched normative datasets across all trials at different speeds recorded from HS. This procedure provides two speed-matched datasets for comparison with trials of PwMS, one for baseline assessment and another dataset for post-treatment trials.

To create a speed matched dataset at baseline we included only trials from healthy subjects with normalized speed under the threshold of 62.2% BH/s. This threshold corresponded to 90% of the maximum normalized speed of PwMS at baseline. Analogously, for the post intervention database we included only trials of healthy subjects with normalized speed smaller than 66.0% BH/s corresponding to 90% of the maximum normalized speed of PwMS post-intervention. This is the same procedure for speed matching used in our previous study (9).

We adopted the total-body LAMB marker set, which includes 29 retro-reflective markers (12 mm diameter) positioned on the head, upper limbs, trunk, pelvis, and lower limbs (35).

Intervention

The intervention and the associated clinical results are described in detail in Jonsdottir et al. (28). Briefly, the participants with MS had received supervised treadmill training, 4–5 sessions per week, 20 sessions in total, and were part of a subgroup that had undergone gait analysis at baseline and post intervention. Each treadmill walking session lasted 30 min and was aimed at improving participants' resistance, walking velocity, balance, and cognitive functions during locomotion. The intervention was mostly focused on maximizing the amount and intensity of walking activities, both aerobically and with dual task motor and cognitive activities, with no specific focus on normalizing gait kinematics.

Gait Data Processing

After data acquisition, we low-pass filtered the markers' trajectories at a cut-off frequency of 6 Hz. We computed the anthropometric parameters of each subject from markers' positions recorded during the calibration trial according to the LAMB protocol (35), and used for estimation of internal joint centers. We also computed joint kinematics according to the LAMB protocol (35) and we used inverse dynamics to compute moments and powers at the ankle, knee, and hip joints of the selected leg with EMG probes. Each trial included the single gait cycle performed on the force plate. For each participant we computed the average value of selected parameters and the average pattern of kinematic/kinetic and EMG variables across trials.

Kinematic and Kinetic Variables

We calculated the following gait parameters:

- gait speed (m/s): ratio between the linear distance traveled by the hip joint centers' midpoint during a stride and the stride duration;
- stride length (m): linear distance traveled by ankle joint center, estimated as the midpoint between lateral and medial malleolus, during a stride;
- cadence (steps/min): was calculated as 60/(0.5*stride duration);
- step width (m): lateral distance between the ankle joint center of the right and the left leg at respective foot's heel strike;
- DS1 (%): percentage of double support during loading response phase, calculated as the ratio between the time from heel contact of the supporting foot to contralateral foot-off and the stride time;
- DS2 (%): percentage of double support during pre swing phase, calculated as the ratio between the time from heel contact of the contralateral foot to supporting foot-off and the stride time;
- Maximal foot clearance (mm): maximal height of toe marker during the second half of swing phase, mainly related to the GCM;

- peak of ankle power (W/kg): maximal values of ankle power in stance phases, mainly related to FPM.

Heel contact and toe off were defined from the presence or absence of GRF data, respectively (36).

EMG Processing

We high pass filtered the EMG signal with a cutoff frequency of 40 Hz, rectified and then low pass filtered with a cutoff frequency of 10 Hz, using a 4th order Butterworth filter. To focus on temporal dissimilarities in EMG, we normalized the signal of each muscle to its peak value across all recorded trials (14, 23). All data were time normalized to 100% of the gait cycle and subsequently averaged among trials of each subject.

We extracted muscle synergies using non-negative matrix factorization (NNMF) (37). For each participant the EMGs were combined into an $m \times t$ matrix, where m indicates the number of muscles and t is the time base (t = averaged stride $\times$ 101). We repeated the synergy extraction 50 times. The solution that accounted for >90% of the EMG variability for each muscle was selected, thus obtaining two matrices for each extracted muscle synergy: an $m \times 1$ array, which specifies the relative weighting of each muscle in the module (module composition) and an $1 \times t$ array, which specifies the activation timing profile of the module (9).

We calculated the following muscle synergies parameters:

- activation percentage index: for each gait phase [Early stance (P1), Mid stance (P2), Terminal stance (P3), Pre swing (P4), Early swing (P5), Late swing (P6)] each synergy's activation profile was integrated over 100% of the gait cycle and the percentage of such activation area was calculated within the specific phase;
- module similarity: Pearson's correlation coefficient of each module between each PwMS and the average module of the speed-matched control group. Higher correlations indicate more similarity in module compositions.

We calculated the activation percentage indexes for each participant, both for the PwMS and healthy subjects, while the module similarity parameter was calculated only in the multiple sclerosis group relative to the average of the speed matched control group.

We analyzed biomechanical and EMG measures with Matlab (The Mathworks Inc., Natick, MA).

Statistical Analysis

We used t-tests for independent samples to compare age, body mass, and body weight between PwMS and HS, and a Chi-square test to compare gender (female/male) between groups (PwMS and HS).

At each time point (baseline or post-intervention), we used independent samples t-tests to compare gait and muscle synergies parameters between PwMS and speed-matched healthy subjects.

For comparison within the group of PwMS (pre- vs. post-intervention), we transformed the values of spatio-temporal and muscle synergy parameters for each PwMS to z scores (see Equation 1) resulting in parameter values independent of speed changes. This was done in order to analyze the deviation from the reference speed-matched data to account for the change in gait speed from baseline to post-intervention. P is the parameter, $\mu_{speed-matchedHS}$ and $\sigma_{speed-matchedHS}$ are the mean value and the standard deviation, respectively, of that parameter for the reference control group at the matched speed.

$$Zscore_P = \frac{P - \mu_{speed-matched\ HS}}{\sigma_{speed-matched\ HS}} \quad (1)$$

Subsequently, we ran paired t-tests on the Z scores to evaluate the pre- to post-intervention changes induced by the rehabilitation treatment. A significant change in Z scores indicated a change of that specific parameter from T0 to T1 beyond the changes due merely to a gait speed increase, and thus attributable to a response to treatment that went beyond speed dependent improvement. We summarized and tabulated the values of analyzed parameters as means and with 95% of the confidence interval. We considered $P < 0.05$ as statistically significant and $0.05 \leq P < 0.1$ as near-significant trends (38).

We performed all statistical analyses using Matlab (The Mathworks Inc., Natick, MA).

RESULTS

General Demographics and Clinical Characteristics

Demographic characteristics of the participants and outcome of clinical scales are depicted in **Table 1** individually and as a group mean. The general picture indicates a sample of patients with moderate mobility difficulties. We did not observe any differences in sex ($P = 0.86$), body mass, or height (Mean [95 CI%] [kg] PwMS vs. HS, 59.2 [52.8–65.5] vs. 65.8 [54.9–76.7] $P = 0.24$; [cm] 165.0 [159.1–171.0] vs. 168.1 [161.0–175.2] $P = 0.46$) between PwMS and HS.

Spatio-Temporal Gait Parameters

All PwMS underwent gait analysis assessments autonomously without walking aids under the supervision of a physiotherapist.

See **Table 2** for all gait variables for healthy controls and PwMS. Regarding the PwMS, average gait speed was 0.74 m/s (95% CI, 0.56, 0.92) at baseline and then increased to 0.90 m/s (0.71, 1.08) after the intervention, showing a statistically and clinically significant increase of 33.1% ($P = 0.024$). Gait speed of healthy subjects was matched at pre- and post-rehabilitation, resulting in a matched gait speed of 0.71 m/s (0.67, 0.76) at baseline and 0.93 m/s (0.84, 1.01) at post-intervention ($P = 0.74$ and $P = 0.88$, respectively, at baseline and post-intervention).

Stride length of PwMS was 0.97 m (0.83, 1.11) at baseline and post-intervention it was 1.09 (0.97, 1.22), showing a statistically significant increase of about 13% ($p < 0.05$). Cadence of PwMS was 88.8 ([steps/min], 95% CI 75.3–102.4) at baseline and 94.6 (80.7–108.4) following intervention. There was no change in step width or double support phases with increased speed neither in PWMS nor in HS. Step width in PwMS at baseline was 149.4 mm (**Table 2**, 95% CI 127.4, 171.5), much larger than in the HS

TABLE 2 | Gait parameters and *Z*-scores of persons with Multiple Sclerosis (PwMS) at baseline (T0) and after treatment (T1).

		HS Mean (95% CI)		PwMS Mean (95% CI)		PwMS *Z*-score	
		Speed-Matched at T0	Speed-Matched at T1	T0	T1	T0	T1
Gait Speed	[ms^{-1}]	0.71 (0.67, 0.76)	0.93 (0.84, 1.01)*	0.74 (0.56, 0.92)	0.90 (0.71, 1.08)	0.35 (−2.40, 3.09)	−0.26 (−1.88, 1.37)[b]
Cadence	[steps min−1]	81.2 (71.1, 91.3)	93.2 (84.3, 102.0)*	88.8 (75.3, 102.4)	94.6 (80.7, 108.4)	0.54 (−0.42, 1.50)	0.11 (−1.01, 1.24)
Stride Length	[m]	1.10 (1.05, 1.16)	1.20 (1.14, 1.26)*	0.97 (0.83, 1.11)	1.09 (0.97, 1.22)*	−1.77 (−3.62, 0.08)	−1.24 (−2.66, 0.19)
Step Width	[mm]	88.2 (68.4, 107.9)	85.5 (70.1, 101.0)	149.4 (127.4, 171.5)+	147.5 (118.7, 176.3)+	2.22 (1.42, 3.02)	2.87 (1.54, 4.21)
Double Support early stance (DS1)	[%]	16.7 (15.4, 17.9)	13.9 (12.7, 15.2)	17.7 (13.4, 21.9)	15.3 (11.9, 18.7)	0.58 (−1.85, 3.02)	0.80 (−1.16, 2.75)
Double Support Pre Swing (DS2)	[%]	14.9 (13.5, 16.2)	13.2 (11.8, 14.6)	18.8 (12.9, 24.7)	15.9 (12.9, 18.9)	2.07 (−1.08, 5.21)	1.34 (−0.14, 2.83)
Peak Knee Flexion in swing	[deg]	60.3 (56.9, 63.6)	62.0 (59.2, 64.8)*	45.6 (32.4, 58.9)+	46.7 (32.6, 60.7)+	−3.12 (−5.95, −0.30)	−3.93 (−7.51, −0.35)
Foot Clearance	[mm]	123.6 (112.9, 134.4)	127.1 (118.0, 136.2)*	80.3 (56.2, 104.4)+	103.6 (81.7, 125.4)*	−2.89 (−4.50, −1.28)	−1.85 (−4.50, −1.28)[a]
Peak Ankle Plantarflexor Power	[W/Kg]	1.97 (1.58, 2.36)	2.55 (2.20, 2.91)*	1.53 (1.04, 2.03)	1.93 (1.50, 2.36)*+	−0.80 (−1.70, 0.11)	−1.26 (−2.13, −0.38)[b]

For comparison, the values of the two speed-matched groups of healthy subjects (HS) are reported.

+P < 0.05 at unpaired t-test between PwMS and HS before (pre) or after treatment (post) for the gait parameters.

**P < 0.05 at paired t-test within group before (pre) vs. after treatment (post) for the gait parameters.*

[a]P < 0.05 at paired t-test within group before (pre) vs. after treatment (post) for the z-score of gait parameters.

[b]0.05 ≤ P < 0.1 at paired t-test within group before (pre) vs. after treatment (post) for the z-score of gait parameters.

(88.2 mm, 95% CI 68.4, 107.9). *Z* scores were not significant for any of the above parameters.

Number of Modules and Module Composition

Among the healthy subjects ($N = 10$), 9 persons had 4 modules and one person had 3 modules when walking at the slower reference gait speed matching the pre-intervention gait speed of the PwMS, while at the higher reference gait speed, 6 persons (60%) had 4 modules and (40%) 4 persons had 3 modules (**Table 1**).

Of PwMS ($N = 11$), at baseline 6 persons (55%) had 4 modules and 5 persons (45%) had 3 modules. Post rehabilitation (**Table 1**) 7 PwMS had 4 modules (64%) and 4 persons had 3 modules (36%), indicating that the complexity of motor control was similar to that of healthy subjects at both reference speeds. There were no significant differences in demographic or clinical characteristics between subjects with 4 modules or 3 modules, except onset of MS where the persons with 3 synergies had an earlier onset of MS.

Module similarity of each module between each PwMS and the average module of the speed-matched control group was verified with the Pearson's correlation coefficient. At baseline module composition of the FPM in PwMS was similar to that of the HS, having a mean value >0.75 (Mean [95% CI], T0 0.79 [0.68–0.89]), while the overall composition of the GCM was less similar to that of the HS (T0 0.63 [0.43–0.83]). At T1 the module composition of muscle synergies of PwMS (Mean [95% CI] T1, FPM 0.85 [0.76–0.94]; GCM 0.76 [0.65–0.88]) increased in similarity to HS, although T0 to T1 difference on similarities were not statistically significant ($P = 0.34$ and $P = 0.25$, respectively, for FPM and GCM).

Module Activation Indexes and Profiles

Forward Propulsive Module (FPM)

Regarding the activation percentage index in FPM (**Table 3**, **Figures 1A–C**), at baseline PwMS was different from speed matched HS in early stance (P1) (HS vs. PwMS, 10.4 [8.0–12.8] vs. 15.6 [10.9–20.3], $p = 0.05$), mid stance (P2) (23.4 [19.5–27.4] vs. 18.1 [13.8–22.4] $p = 0.06$) terminal stance (P3) (51.8 [46.8–56.8] vs. 41.0 [33.8–48.2] $p = 0.01$) and late swing (P6) (3.9 [1.6–6.3] vs. 9.2 [6.3–12.2] $p = 0.01$), demonstrating difficulties in single and double support phases of gait. Regarding the comparison with HS, post intervention PwMS recovered mid stance where the activation index increased and become more similar to the physiological one (HS vs. PwMS 26.0 [22.1–29.8] vs. 22.7 [15.4–29.9], $P = 0.39$), while in the other gait phases the activation indexes remained different ($P < 0.05$) from HS. Looking at **Figure 1B**, it is noticed that in pre swing (P4) and early swing (P5) the morphology of activation profile of PwMS was more similar to the HS, recovering in early swing a second physiological activation peak as occurs in HS, even if anticipated in time.

On analysis of *z* scores of activation percentage indexes in PwMS (pre- vs. post-intervention) there was a statistically significant change in activation profiles following intervention in early stance where activation increased (worsening compared to HS), in terminal stance where there was a reduction of the activation (worsening), in pre swing (improvement) (**Table 3**, $P = 0.01$, $P < 0.01$ and $P = 0.03$, respectively), and a near significant increase in early swing ($P = 0.10$).

TABLE 3 | Activation percentage indexes (API) and *Z* scores of the Forward Propulsive Module activation profile during the gait phases for persons with Multiple Sclerosis (PwMS) at baseline (T0) and after treatment (T1).

Parameters		HS Mean (95% CI)		PwMS Mean (95% CI)		PwMS *Z*-score	
		Speed-Matched at T0	Speed-Matched at T1	T0	T1	T0	T1
P1 Early Stance	[%]	10.4 (8.0, 12.8)	7.3 (5.4, 9.2)*	15.6 (10.9, 20.3)	16.7 (12.4, 21.1)$^{+}$	1.57 (0.14, 3.00)	3.61 (1.94, 5.27)[a]
P2 Mid Stance	[%]	23.4 (19.5, 27.4)	26.0 (22.1, 29.8)	18.1 (13.8, 22.4)	22.7 (15.4, 29.9)	−0.96 (−1.72, −0.19)	−0.62 (−1.96, 0.72)
P3 Terminal Stance	[%]	51.8 (46.8, 56.8)	53.9 (50.3, 57.6)	41.0 (33.8, 48.2)$^{+}$	38.2 (32.1, 44.4)$^{+}$	−1.55 (−2.58, −0.52)	−3.06 (−4.26, −1.86)[a]
P4 Pre Swing	[%]	7.2 (4.4, 10.1)	7.0 (3.4, 10.5)	12.5 (5.7, 19.3)	9.0 (2.7, 15.3)*	1.32 (−0.37, 3.02)	0.40 (−0.87, 1.67)[a]
P5 Early Swing	[%]	3.2 (1.5, 4.9)	3.1 (1.6, 4.5)	3.6 (2.0, 5.2)	6.0 (2.5, 9.4)	0.16 (−0.49, 0.82)	1.40 (−0.28, 3.09)
P6 Late Swing	[%]	3.9 (1.6, 6.3)	2.8 (1.3, 4.3)	9.2 (6.3, 12.2)$^{+}$	7.4 (4.7, 10.2)$^{+}$	1.64 (0.74, 2.54)	2.22 (0.90, 3.53)

The same indexes are reported for the two speed-matched datasets of healthy subjects (HS).

$^{+}P < 0.05$ at unpaired t-test between PwMS and HS before (pre) or after treatment (post).

**$P < 0.05$ at paired t-test within group before (pre) vs. after treatment (post).*

[a]$P < 0.05$ at paired t-test within group before (pre) vs. after treatment (post) for the z-score of gait parameters.

Kinetic Parameter Regarding the Forward Propulsive Module (FPM)

Corresponding to changes in the activation percentage indexes, the peak ankle power (**Table 2**), related to the push off deficit, increased in PwMS from 1.53 W/kg (1.04–2.03) at baseline to 1.93 W/kg (1.50–2.36) post-intervention, a 21% difference ($P = 0.05$). As a reference, HS presented values of 1.97 W/kg (1.58–2.36) and 2.55 W/kg (2.20–2.91) at the correspondent pre and post gait speeds (**Table 2**). Only at post-intervention the peak ankle power was different between HS and PwMS ($P = 0.14$ and $P = 0.02$, respectively, at pre and post intervention).

Within group observation of *Z* scores of PwMS revealed that there was a statistical trend for an increase in peak ankle power from baseline to post-intervention (**Table 3** *P*-value of *Z*-score, $P = 0.07$) indicating an improvement in peak ankle power that went beyond the increase of speed. Since this is an important parameter to consider, we further investigated the changes within the individual PwMS. Of the 11 subjects, six PwMS improved from T0 to T1 by more than 15% of their baseline value, three PwMS improved between 10 and 15%, and two PwMS decreased their peak ankle power by 3 and 6%, respectively.

Ground Clearance Module (GCM)

Regarding the GCM activation percentage index (**Table 4** and **Figures 2A–C**) representing the synergy that controls clearance and loading response, at baseline the MS Group was different from speed matched HS in early stance (**Table 4**, HS vs. PwMS 26.4 [17.7–35.1] vs. 16.3 [9.8–22.9], $P = 0.03$), and pre swing (**Table 4**, 6.6 [2.9–10.2] vs. 26.7 [18.2–35.3], $P < 0.01$). The GCM, that in healthy subjects was mainly activated in early swing, in PwMS was activated in pre swing indicating an anticipated activation of tibialis anterior and rectus femoris muscles. With respect to the HS, at post intervention the MS Group recovered GCM activation index at early stance that became more similar to HS (HS vs. PwMS $P = 0.15$), while in pre swing ($P < 0.01$) and early swing ($P = 0.04$), it remained different from HS. Nonetheless, upon scrutiny of **Figure 2B** it is apparent that the activation profiles around pre swing and early swing (P4–P5) becomes sharper and more physiologically similar to that of the HS.

Regarding *Z* scores of PwMS, post-intervention there were significant changes in activation indexes in early stance (improvement), pre swing (improvement), and early swing (worsening) ($P = 0.01$, $P < 0.01$, and $P = 0.03$, respectively) with respect to baseline.

Kinematic Parameter Regarding the Ground Clearance Module (GCM)

Absolute foot-ground clearance (**Table 2**), defined as maximal height of toe marker during the second half of swing phase, increased with increased speed in both groups (T0–T1): in PwMS from 80.3 mm (95% CI 56.2–104.4) to 103.6 mm (81.7–125.4) ($P < 0.01$); and in HS from 123.6 mm (112.9–134.4) to 127.1 mm (118.0–136.2) ($P = 0.03$).

The *z*-score of absolute foot clearance in PwMS increased significantly from baseline to T1 ($P < 0.01$).

DISCUSSION

Objectives of this study were (i) to investigate the effect of rehabilitation induced improvement in preferred gait velocity on (1) leg distal modules composition and their timing activation profile, and (ii) on walking performance in PwMS with emphasis on gait parameters related to forward propulsion and ground clearance.

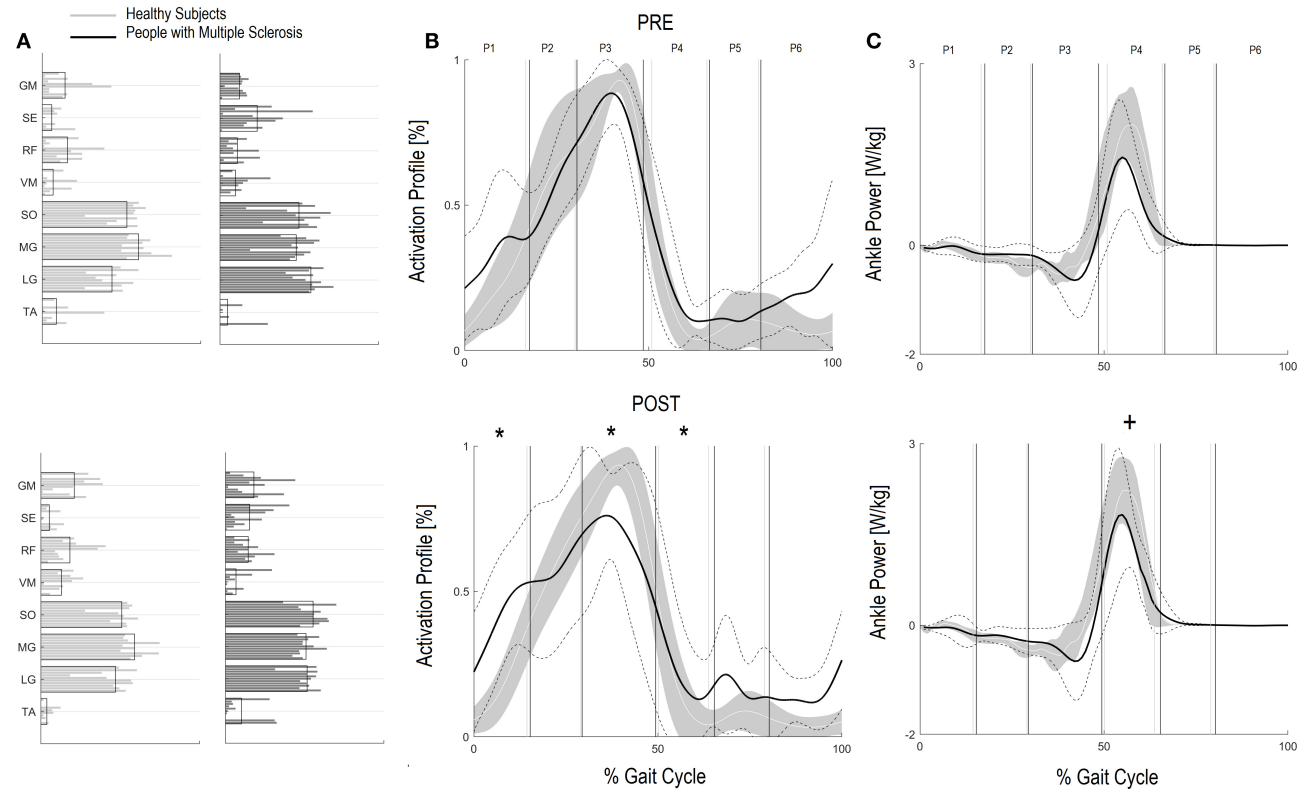

FIGURE 1 | Forward Propulsion Muscle Synergies (FPM) and Kinetics of Ankle joint. Weightings **(A)** and activation profile **(B)** of FPM and ankle power curve **(C)** for persons with multiple sclerosis (PwMS) pre (top panel) and post (bottom panel) treatment and speed-matched healthy subjects (HS). In **(B,C)** The solid black line represents the averaged profile of PwMS and the dashed black lines represent ± SD of PwMS curves. Vertical lines (solid gray line—healthy subjects and solid black line—PwMS) indicate the six phases of a normalized gait cycle (P1, early stance; P2, mid stance; P3, terminal stance; P4, pre swing; P5, early swing; P6, late swing). Range of HS normality is reported in gray. *$p < 0.05$ at paired *t*-test of *Z*-score, pre- vs. post-treatment, for activation percentage index of FPM **(B)** or peak ankle power parameter **(C)** in PwMS. +$0.05 < p < 0.1$ at paired *t*-test of *Z*-score, pre- vs. post-treatment, for activation percentage index of FPM **(B)** or peak ankle power parameter **(C)** in PwMS.

Resultant changes in spatiotemporal parameters were mostly proportionate to changes in speed, indicating the function was recovered through improvement in physiological strategies. Importantly, there were indications that distal muscle synergies and biomechanical parameters, e.g., peak ankle power and ground clearance, may be influenced by rehabilitation. In fact, when effects of training on peak ankle power and ground clearance were corrected for confounding by increases in walking speed, there was a response to rehabilitation that went beyond that being proportional to change in speed. Taken together these results indicate an improvement in distal neuromotor locomotion function and a recovery in response to treatment.

The PwMS in the present study were quite heterogeneous with moderate to severe gait disability. Baseline gait analysis confirmed findings from previous studies on gait performance in PwMS demonstrating reduced stride length, increased cadence and increased step width, with reduction of propulsive work at the ankle, decreased knee flexion during swing, and decreased foot clearance compared to speed matched healthy subjects (9, 39, 40). They did, however, all respond well to the intensive training on treadmill with an average increase in gait speed of 33% from baseline to post intervention. The change in gait speed was important at the participation level in that the group went from having a gait speed descriptive of a limited community ambulation to being in the unlimited category of community ambulation post intervention (>0.80 m/s) (41). These changes were corroborated with results from the gait analysis. Most spatiotemporal gait parameters improved in line with speed related changes in healthy subjects indicating PwMS can increase self-selected velocity without using compensatory strategies. Step width, instead, was a parameter independent from gait speed in both groups and remained much larger in PwMS also following intervention, consistent with known dynamic balance insecurities in that population (42, 43).

Regarding motor synergies, analysis of baseline neurophysiological parameters confirmed that PwMS tend to have a preserved number of modules in the lower leg during gait (three or four modules), and preserved modular composition within the distal leg modules related to propulsion and ground clearance (9, 21). On the contrary, timing of the modular muscle activations (motor primitives) differed from those of healthy controls walking at comparable speeds. Investigation of motor

TABLE 4 | Activation percentage index (API) and *Z* scores of the Ground Clearance Module activation profile during the gait phases for persons with Multiple Sclerosis (PwMS) at baseline (T0) and after treatment (T1).

Parameters		HS Mean (95% CI)		PwMS Mean (95% CI)		PwMS *Z*-score	
		Speed-Matched at T0	Speed-Matched at T1	T0	T1	T0	T1
P1 Early Stance	[%]	26.4 (17.7–35.1)	20.8 (12.1–29.6)*	16.3 (9.8–22.9)$^{+}$	14.3 (9.6–19.0)	−0.90 (−1.40, −0.41)	−0.53 (−0.92, −0.15)[a]
P2 Mid Stance	[%]	10.3 (6.2–14.4)	11.2 (7.7–14.8)	8.0 (4.0–11.9)	9.2 (5.9–12.5)	−0.67 (1.12, −0.22)	−0.41 (−1.07, 0.26)
P3 Terminal Stance	[%]	8.4 (6.0–10.8)	7.3 (5.1–9.4)	6.4 (4.9–8.0)	7.2 (4.0–10.4)	−0.26 (−0.68, 0.16)	−0.01 (−1.06, 1.04)
P4 Pre Swing	[%]	6.6 (2.9–10.2)	6.2 (3.7–8.7)	26.7 (18.2–35.3)$^{+}$	24.5 (18.2–30.7)$^{+}$	10.66 (7.17, 14.15)	5.18 (3.41, 6.96)[a]
P5 Early Swing	[%]	25.3 (18.6–32.1)	30.3 (23.0–37.5)*	23.0 (17.2–28.8)	22.4 (18.2–26.7)$^{+}$	−0.32 (−0.94, 0.30)	−0.77 (−1.19, −0.36)[a]
P6 Late Swing	[%]	23.0 (16.5–29.5)	24.2 (19.5–28.8)	19.5 (13.1–25.9)	22.3 (18.1–26.6)	−0.37 (−1.07, 0.32)	−0.29 (−0.94, 0.37)

The same indexes are reported for the two speed-matched groups of healthy subjects (HS).

$^{+}P < 0.05$ at unpaired t-test between PwMS and HS before (pre) or after treatment (post).

**P < 0.05 at paired t-test within group before (pre) vs. after treatment (post).*

[a]$P < 0.05$ at paired t-test within group before (pre) vs. after treatment (post) for the z-score of gait parameters.

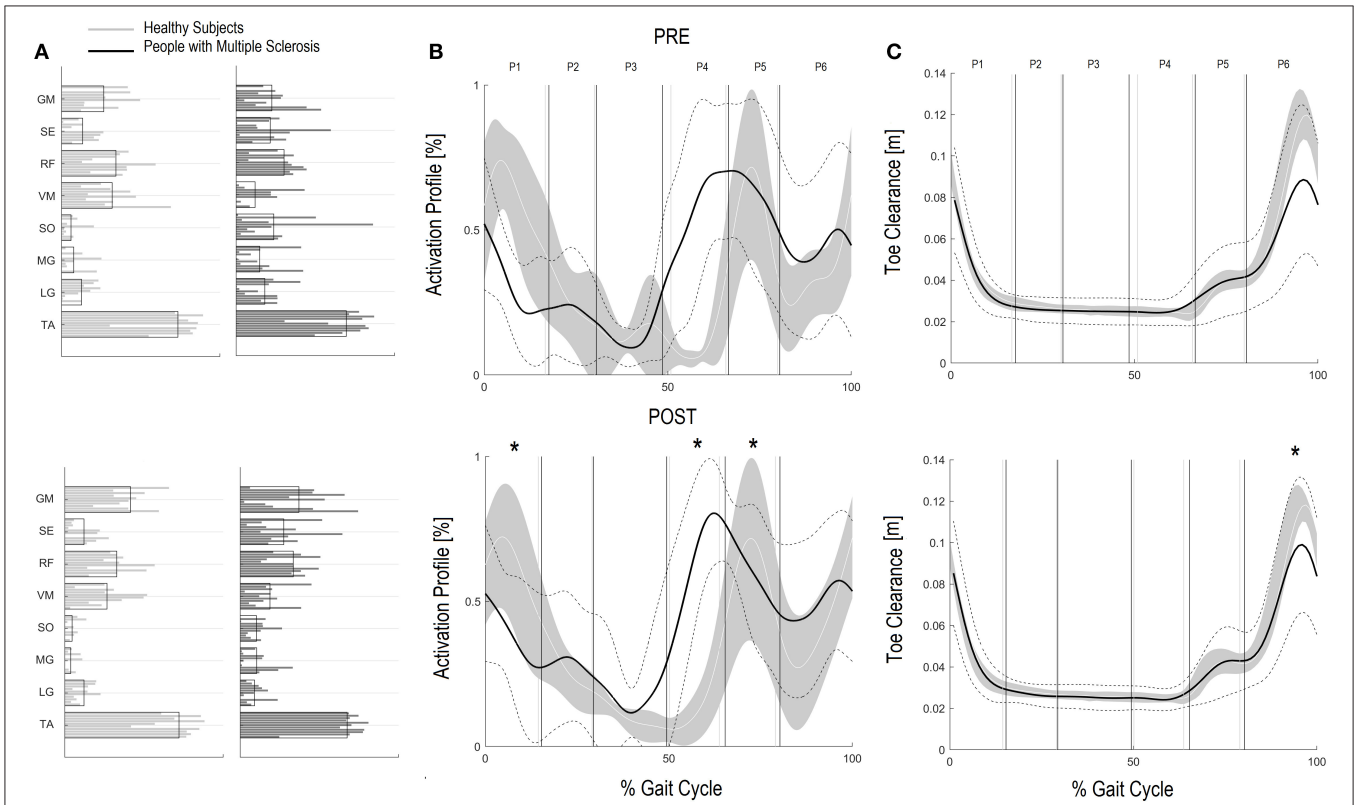

FIGURE 2 | Ground Clearance Muscle Synergies (GCM) and Foot clearance. Weightings **(A)** and activation profile **(B)** of GCM and toe marker trajectory curve **(C)** for persons with multiple sclerosis (PwMS) pre (top panel) and post (bottom panel) treatment and speed-matched healthy subjects (HS). In **(B,C)** the solid black line represents the averaged profile of PwMS and the dashed black lines represent ± SD of PwMS curves. Vertical lines (solid gray line—healthy subjects and solid black line—PwMS) indicate the six phases of a normalized gait cycle (P1, early stance; P2, mid stance; P3, terminal stance; P4, pre swing; P5, early swing; P6, late swing). *$p < 0.05$ at paired *t*-test of *Z*-score, pre- vs. post-treatment, for activation percentage index of GCM **(B)** or toe clearance **(C)** in PwMS. +0.05< $p < 0.1$ at paired *t*-test of *Z*-score, pre- vs. post-treatment, for activation percentage index of GCM **(B)** or toe clearance **(C)** in PwMS.

module number at baseline confirmed results from our previous work on PwMS (9) that demonstrated that PwMS recruit either 3 or 4 motor modules at preferred gait speed reflecting the preserved complexity of motor control (13). This is consistent with findings for persons with Parkinson's disorder that tend to have a preserved motor module number during gait (20), while on the contrary findings from persons post-stroke (22), persons with spinal injuries (44), and cerebral palsy (45) suggest an influence of the disorder on the motor module number during gait. This may be due to different central nervous system damages, since multiple sclerosis typically causes diffuse central and neuronal damage and atrophy that might allow preservation of neural control signals and synergy complexity (46).

Distal Modules and Gait Biomechanics

Efficacious gait rehabilitation (augmented preferred gait speed) led to a consolidation of the muscle weightings and improved consistency of the distal muscle synergies patterns, primarily with changes in motor primitives of the two distal modules. These changes were consistent with positive rehabilitation benefits in propulsion and absolute foot clearance, regardless of the change in speed.

Peak ankle power, the main kinetic parameter of the FPM (forward propulsive model) increased from baseline to post intervention with a positive trend of the treatment (**Table 2**, P-value of Z-score $= 0.07$). This is an important finding since it has been suggested that the ankle plantarflexion is the controlled variable in the gait cycle (47, 48). The intervention was quite intense, including both fast walking for aerobic training and dual motor tasks carried out with the treadmill in movement, that included walking on toes, doing long strides, high knee raises, etc. [see (28) for further details of the training protocol]. It is likely that these aspects of training facilitated an improved ankle plantarflexor neuromotor organization and peak ankle power during push off. Davies et al. (48) saw a similar effect on ankle plantarflexor control of PwMS after a neurorehabilitation protocol focusing on distal leg parameters with all of the outcome variables matching or trending toward those seen in healthy controls.

The results are also consistent with findings of Routson et al. (22) that saw treadmill training leading to better walking performance and modular organization in persons post stroke. An important finding of that study was that gait recovery was associated with improved motor primitives (activation profiles) in the distal modules, in particular in the FPM, likely contributing to improvement in biomechanical measures.

The suggestion is that gait specific training protocols have the potential to promote clinically relevant improvement in the ankle plantarflexor control as well as peak ankle power with beneficial effects on mobility parameters.

An increase in peak ankle power and improved distal modular activation are important for walking function in PwMS since plantarflexor weakness and ankle motor control are major deficits leading to difficulty in locomotion (9, 49). Improved ankle joint coordination during push off leads to more energy efficient gait, increased gait speed, and possibly easier participation in daily life community activities.

Additionally, since many falls in PwMS can be traced to tripping (50), the improved foot clearance points to safer locomotion and a potentially diminished risk of falling. Foot clearance occurs through coordinated movements of the leg joints and, in particular, with (i) a correct positioning of the foot and muscles recruitment in the terminal support phase, in order to prepare the leg for the swing phase and (ii) a coordinated recruitment of dorsiflexors during the swing phase (51). The foot clearance in the enrolled PwMS in this study was quite deficient. Their reduction in clearance during swing influences ankle joint position at the beginning of the stride, requiring greater ankle joint muscular coactivation (52). After the rehabilitation intervention foot clearance increased significantly by approximately 30% nearing values of healthy controls at matched speeds. In the PwMS it was the single most changed parameter when speed was accounted for (Z scores $P < 0.01$) indicating a strong therapeutic effect of the treatment. Upon scrutiny of the baseline GCM activation profile (see **Figure 2B**) it is evident that the modular impulse in healthy subjects occurs in the early swing phase of the gait cycle while in the PwMS the maximum value occurred earlier, in the pre swing phase, typical of inappropriate distal limb activation in persons with neurological disorders (53–55). This probably occurs due to the fact that, since the PwMS do not develop enough ankle power, they have to activate the dorsiflexors in early midstance and during late push off, preparing for lift off and elevation of foot during swing to reduce risk of tripping. Following the gait rehabilitation it was evident that they recovered a more physiological activation impulse in the GCM and had activation profiles that were more consistent with strategies observed in the HS (**Figure 2B**).

It has been suggested by many authors that the ankle plantarflexion is the controlled variable in the gait cycle, determining changes in speed (47, 48). In a recent work by Davies et al. (25) it was found that errors in the ankle plantarflexor force production were related to gait deficits of PwMS. They further suggested that the improvements seen in gait of PwMS following gait rehabilitation interventions were related to changes in the motor control of the ankle musculature. This is supported by our findings where gait rehabilitation resulted in improvement of dynamic motor control as evidenced by more appropriate activation profiles in FPM and GCM.

General Considerations

High intensity mobility training provided to persons with moderate to severe disability from multiple sclerosis resulted in substantial increase in gait velocity. The overall improvements seen, including the increase in preferred speed, are mainly due to the benefits produced by the rehabilitation in domains related to muscle coordination and walking performance. The methodologies adopted for data analyses in this study [i.e., (i) the choice to create two databases of healthy subjects matched with speed of PwMS, respectively, at pre- and at post-intervention, and (ii) consequently the statistical analysis on the Z-score values] allowed the evaluation of the underlying neurophysiological recovery following rehabilitation. The results highlighted that the two main gait parameters related to distal muscle synergies

control, the foot clearance and the peak ankle power, improved with reorganization at the modular level in PwMS. This was an effect of the treatment that went beyond preferred speed appropriate changes.

Those changes in preferred gait velocity were concurrent with improvements in distal neuromuscular and biomechanical aspects reflecting a recovery of motor control. Further investigation of modular organization in distal parameters demonstrated improved activation timing of plantarflexors in the push off and of dorsiflexors in mid/late stance corresponding to improved foot clearance. This was further confirmed by improvements in biomechanical walking parameters related to the distal modules indicating a potential reorganization at central and peripheral level. Modular reorganization in this context can be taken as a sign of neuroplasticity, a form of recovery in response to rehabilitation. To promote functional recovery and in order to stimulate neural plasticity and change modular organization, something (some activity or exercise) has to be done intensely, voluntarily, and for some time either by the person alone (starts exercising) or in collaboration with a therapist. Treadmill training might be a particularly appropriate approach to gait rehabilitation since it allows the PwMS to walk further and longer than might otherwise be possible. In this context it has been hypothesized that learning-dependent changes in Central Pattern Generator circuits occur primarily through rhythmic perceptual influences imposed by exercises, an example of which could be walking on treadmill during dual task activities [see gait protocol (28)]. The present analysis of distal leg muscle synergies during overground gait revealed an overall improvement in activation percentage indexes and correlated kinetic and kinematic parameters. In spite of this improvement altered early activation impulses were still evident in key activities of the gait cycle, in line with findings of Janshen et al. (21). Further research might consider adding an electrical stimulation or a biofeedback from plantarflexor muscles during gait activities on the treadmill to enhance even more timing of module activation. In this context, muscle synergies analysis as an adjunct to clinical and biomechanical analysis may become a useful tool for setting up increasingly efficacious rehabilitation protocols, and for evaluating and understanding changes due to rehabilitation at all levels of mobility.

Motor modules probably arise from neural plasticity in supraspinal and spinal structures and are shaped by regularities in biomechanical interactions with the environment (15). Effect of rehabilitation is interesting in this perspective. Task specific training should be intensive enough to harness use dependent neuroplasticity (56). The use of motor module analysis can help to highlight disease characteristic neuromotor deficits, as well as individuate individual specific neuromotor deficits. Further, the current results from PwMS indicate that motor module analysis can help in elucidating the effect of a therapeutic intervention. Most importantly, it can provide a framework for developing more efficacious therapies that enhance neural plasticity and promote motor recovery, both from a global perspective and an individual perspective.

Limitations

There are limitations to this exploratory study. The number of enrolled subjects is low given the heterogeneity of the subjects and so the results of the study can only be generalized to a PwMS with similar moderate mobility disabilities. In this study we analyzed data only from PwMS that had augmented their gait velocity after rehabilitation. This means we cannot know if the participants that do not respond to rehabilitation by increasing gait velocity adapt their biomechanical and neurophysiological gait parameters. A future study with a larger number of subjects should be planned to confirm the findings, including also PwMS that do not respond to the rehabilitation, in a comparison analysis.

Other limitations include the methodology; muscle synergy extraction depends on methodological factors that have to be considered, however, our synergy analyses are comparable to those of studies already published that have investigated changes in response to rehabilitation in stroke patients (22) similar to that of our population with MS.

DATA AVAILABILITY STATEMENT

The datasets generated for this study are available on request to the corresponding author.

ETHICS STATEMENT

The studies involving human participants were reviewed and approved by Fondazione Don Carlo Gnocchi. The patients/participants provided their written informed consent to participate in this study.

AUTHOR CONTRIBUTIONS

JJ, TL, MF, and DC: substantial contributions to the conception or design of the work or interpretation of data for the work. DA, EG, and AC: recruitment and treatment of participants and data acquisition. TL and IC: statistical analysis of the data. JJ, TL, and MF: drafting the work or revising it critically for important intellectual content. JJ, TL, MF, IC, DC, AC, DA, EG, and MR: final approval of the version to be published. TL, JJ, MF, DC, and MR: agreement to be accountable for all aspects of the work in ensuring that questions related to the accuracy or integrity of any part of the work are appropriately investigated and resolved. All authors: contributed to the article and approved the submitted version.

FUNDING

This work was partially supported by funding from the Italian Ministry of Health (Funding IRCCS Ricerca Corrente) and Fondazione Italiana Sclerosi Multipla (Grant # 2013/R/26), that had no role in this study design, analysis of results, writing the manuscript, or in the decision to submit for publication.

REFERENCES

1. Popescu BFG, Lucchinetti CF. Meningeal and cortical grey matter pathology in multiple sclerosis. *BMC Neurol.* (2012) 12:11. doi: 10.1186/1471-2377-12-11
2. Compston A, Coles A. Multiple sclerosis. *Lancet.* (2008) 372:1502–17. doi: 10.1016/S0140-6736(08)61620-7
3. Reich DS, Lucchinetti CF, Calabresi PA. Multiple sclerosis. *N Engl J Med.* (2018) 378:169–80. doi: 10.1056/NEJMra1401483
4. Wilkins A. Cerebellar dysfunction in multiple sclerosis. *Front Neurol.* (2017) 8:312 doi: 10.3389/fneur.2017.00312
5. Cattaneo D, Lamers I, Bertoni R, Feys P, Jonsdottir J. Participation restriction in people with multiple sclerosis: prevalence and correlations with cognitive, walking, balance, and upper limb impairments. *Arch Phys Med Rehabil.* (2017) 98:1308–15. doi: 10.1016/j.apmr.2017.02.015
6. Carpinella I, Gervasoni E, Anastasi D, Lencioni T, Cattaneo D, Ferrarin M. Instrumental assessment of stair ascent in people with multiple sclerosis, stroke, and parkinson's disease: a wearable-sensor-based approach. *IEEE Trans Neural Syst Rehabil Eng Publ IEEE Eng Med Biol Soc.* (2018) 26:2324–32. doi: 10.1109/TNSRE.2018.2881324
7. Bertoni R, Jonsdottir J, Feys P, Lamers I, Cattaneo D. Modified functional walking categories and participation in people with multiple sclerosis. *Mult Scler Relat Disord.* (2018) 26:11–8. doi: 10.1016/j.msard.2018.08.031
8. Jonsdottir J, Recalcati M, Rabuffetti M, Casiraghi A, Boccardi S, Ferrarin M. Functional resources to increase gait speed in people with stroke: strategies adopted compared to healthy controls. *Gait Posture.* (2009) 29:355–9. doi: 10.1016/j.gaitpost.2009.01.008
9. Lencioni T, Jonsdottir J, Cattaneo D, Crippa A, Gervasoni E, Rovaris M, et al. Are modular activations altered in lower limb muscles of persons with multiple sclerosis during walking? Evidence from muscle synergies and biomechanical analysis. *Front Hum Neurosci.* (2016) 10:620. doi: 10.3389/fnhum.2016.00620
10. Filli L, Sutter T, Easthope CS, Killeen T, Meyer C, Reuter K, et al. Profiling walking dysfunction in multiple sclerosis: characterisation, classification and progression over time. *Sci Rep.* (2018) 8:4984. doi: 10.1038/s41598-018-22676-0
11. Severini G, Manca M, Ferraresi G, Caniatti LM, Cosma M, Baldasso F, et al. Evaluation of clinical gait analysis parameters in patients affected by multiple sclerosis: analysis of kinematics. *Clin Biomech.* (2017) 45:1–8. doi: 10.1016/j.clinbiomech.2017.04.001
12. Scano A, Dardari L, Molteni F, Giberti H, Tosatti LM, d'Avella A. A comprehensive spatial mapping of muscle synergies in highly variable upper-limb movements of healthy subjects. *Front Physiol.* (2019) 10:1231. doi: 10.3389/fphys.2019.01231
13. Allen JL, Kesar TM, Ting LH. Motor module generalization across balance and walking is reduced after stroke. *J Neurophysiol.* (2019) 122:277–89. doi: 10.1152/jn.00561.2018
14. Routson RL, Kautz SA, Neptune RR. Modular organization across changing task demands in healthy and poststroke gait. *Physiol Rep.* (2014) 2:e12055–e55. doi: 10.14814/phy2.12055
15. Ting LH, Chiel HJ, Trumbower RD, Allen JL, McKay JL, Hackney ME, et al. Neuromechanical principles underlying movement modularity and their implications for rehabilitation. *Neuron.* (2015) 86:38–54. doi: 10.1016/j.neuron.2015.02.042
16. Safavynia S, Torres-Oviedo G, Ting L. Muscle synergies: implications for clinical evaluation and rehabilitation of movement. *Top Spinal Cord Inj Rehabil.* (2011) 17:16–24. doi: 10.1310/sci1701-16
17. Ivanenko YP, Poppele RE, Lacquaniti F. Five basic muscle activation patterns account for muscle activity during human locomotion. *J Physiol.* (2004) 556:267–82. doi: 10.1113/jphysiol.2003.057174
18. Monaco V, Ghionzoli A, Micera S. Age-related modifications of muscle synergies and spinal cord activity during locomotion. *J Neurophysiol.* (2010) 104:2092–102. doi: 10.1152/jn.00525.2009
19. Chvatal SA, Ting LH. Common muscle synergies for balance and walking. *Front Comput Neurosci.* (2013) 7:48. doi: 10.3389/fncom.2013.00048
20. Allen JL, McKay JL, Sawers A, Hackney ME, Ting LH. Increased neuromuscular consistency in gait and balance after partnered, dance-based rehabilitation in parkinson's disease. *J Neurophysiol.* (2017) 118:363–73. doi: 10.1152/jn.00813.2016
21. Janshen L, Santuz A, Ekizos A, Arampatzis A. Fuzziness of muscle synergies in patients with multiple sclerosis indicates increased robustness of motor control during walking. *Sci Rep.* (2020) 10:7249. doi: 10.1038/s41598-020-63788-w
22. Routson RL, Clark DJ, Bowden MG, Kautz SA, Neptune RR. The influence of locomotor rehabilitation on module quality and post-stroke hemiparetic walking performance. *Gait Posture.* (2013) 38:511–7. doi: 10.1016/j.gaitpost.2013.01.020
23. Clark DJ, Ting LH, Zajac FE, Neptune RR, Kautz SA. Merging of healthy motor modules predicts reduced locomotor performance and muscle coordination complexity post-stroke. *J Neurophysiol.* (2010) 103:844–57. doi: 10.1152/jn.00825.2009
24. Singh RE, Iqbal K, White G, Hutchinson TE. A systematic review on muscle synergies: from building blocks of motor behavior to a neurorehabilitation tool. *Appl bionics Biomech.* (2018) 2018:3615368. doi: 10.1155/2018/3615368
25. Davies BL, Hoffman RM, Healey K, Zabad R, Kurz MJ. Errors in the ankle plantarflexor force production are related to the gait deficits of individuals with multiple sclerosis. *Hum Mov Sci.* (2017) 51:91–98. doi: 10.1016/j.humov.2016.11.008
26. Artoni F, Fanciullacci C, Bertolucci F, Panarese A, Makeig S, Micera S, et al. Unidirectional brain to muscle connectivity reveals motor cortex control of leg muscles during stereotyped walking. *Neuroimage.* (2017) 159:403–16. doi: 10.1016/j.neuroimage.2017.07.013
27. Polman CH, Reingold SC, Edan G, Filippi M, Hartung HP, Kappos L, et al. Diagnostic criteria for multiple sclerosis: 2005 revisions to the "McDonald criteria." *Ann Neurol.* (2005) 58:840–6. doi: 10.1002/ana.20703
28. Jonsdottir J, Gervasoni E, Bowman T, Bertoni R, Tavazzi E, Rovaris M, et al. Intensive multimodal training to improve gait resistance, mobility, balance and cognitive function in persons with multiple sclerosis: a pilot randomized controlled trial. *Front Neurol.* (2018) 9:800. doi: 10.3389/fneur.2018.00800
29. Kurtzke JF. Rating neurologic impairment in multiple sclerosis: an expanded disability status scale (EDSS). *Neurology.* (1983) 33:1444–52. doi: 10.1212/WNL.33.11.1444
30. Gijbels D, Eijnde BO, Feys P. Comparison of the 2- and 6-minute walk test in multiple sclerosis. *Mult Scler J.* (2011) 17:1269–72. doi: 10.1177/1352458511408475
31. Kempen JCE, de Groot V, Knol DL, Polman CH, Lankhorst GJ, Beckerman H. Community walking can be assessed using a 10-metre timed walk test. *Mult Scler.* (2011) 17:980–90. doi: 10.1177/1352458511403641
32. Berg K, Wood-Dauphinee S, Williams JI, Gayton D. Measuring balance in the elderly: preliminary development of an instrument. *Physiother Canada.* (1989) 41:304–11. doi: 10.3138/ptc.41.6.304
33. Hermens HJ, Freriks B, Disselhorst-Klug C, Rau G. Development of recommendations for SEMG sensors and sensor placement procedures. *J Electromyogr Kinesiol.* (2000) 10:361–74. doi: 10.1016/S1050-6411(00)00027-4
34. Lencioni T, Carpinella I, Rabuffetti M, Marzegan A, Ferrarin M. Human kinematic, kinetic and EMG data during different walking and stair ascending and descending tasks. *Sci Data.* (2019) 6:309. doi: 10.1038/s41597-019-0323-z
35. Rabuffetti M, Marzegan A, Crippa A, Carpinella I, Lencioni T, Castagna A, et al. The LAMB gait analysis protocol: definition and experimental assessment of operator-related variability. *Proc Inst Mech Eng Part H J Eng Med.* (2019) 233:342–53. doi: 10.1177/0954411919827033
36. Mickelborough J, Van Der Linden ML, Richards J, Ennos AR. Validity and reliability of a kinematic protocol for determining foot contact events. *Gait Posture.* (2000) 11:32–7. doi: 10.1016/S0966-6362(99)00050-8
37. Lee DD, Seung HS. Learning the parts of objects by non-negative matrix factorization. *Nature.* (1999) 401:788–91. doi: 10.1038/44565
38. Gelman A. P values and statistical practice. *Epidemiology.* (2013) 24:69–72. doi: 10.1097/EDE.0b013e31827886f7
39. Kasser SL, Jacobs JV, Foley JT, Cardinal BJ, Maddalozzo GF. A prospective evaluation of balance, gait, and strength to predict falling in women with multiple sclerosis. *Arch Phys Med Rehabil.* (2011) 92:1840–6. doi: 10.1016/j.apmr.2011.06.004

40. Benedetti MG, Piperno R, Simoncini L, Bonato P, Tonini A, Giannini' S. Gait abnormalities in minimally impaired multiple sclerosis patients. *Mult Scler.* (1999) 5:363–8. doi: 10.1177/135245859900500510
41. Perry J, Garrett M, Gronley JK, Mulroy SJ. Classification of walking handicap in the stroke population. *Stroke.* (1995) 26:982–9. doi: 10.1161/01.STR.26.6.982
42. Peebles AT, Bruetsch AP, Lynch SG, Huisinga JM. Dynamic balance in persons with multiple sclerosis who have a falls history is altered compared to non-fallers and to healthy controls. *J Biomech.* (2017) 63:158–63. doi: 10.1016/j.jbiomech.2017.08.023
43. Lencioni T, Anastasi D, Carpinella I, Castagna A, Crippa A, Gervasoni E, et al. Dynamic balance during level walking in patients affected by multiple sclerosis, stroke and parkinson's disease. *Gait Posture.* (2018) 66:S23–S4. doi: 10.1016/j.gaitpost.2018.07.136
44. Hayes HB, Chvatal SA, French MA, Ting LH, Trumbower RD. Neuromuscular constraints on muscle coordination during overground walking in persons with chronic incomplete spinal cord injury. *Clin Neurophysiol.* (2014) 125:2024–35. doi: 10.1016/j.clinph.2014.02.001
45. Steele KM, Rozumalski A, Schwartz MH. Muscle synergies and complexity of neuromuscular control during gait in cerebral palsy. *Dev Med Child Neurol.* (2015) 57:1176–82. doi: 10.1111/dmcn.12826
46. Schlaeger R, Papinutto N, Panara V, Bevan C, Lobach IV, Bucci M, et al. Spinal cord gray matter atrophy correlates with multiple sclerosis disability. *Ann Neurol.* (2014) 76:568–80. doi: 10.1002/ana.24241
47. Honeine J-L, Schieppati M, Gagey O, Do M-C. By counteracting gravity, triceps surae sets both kinematics and kinetics of gait. *Physiol Rep.* (2014) 2:e00229. doi: 10.1002/phy2.229
48. Davies BL, Arpin DJ, Volkman KG, Corr B, Reelfs H, Harbourne RT, et al. Neurorehabilitation strategies focusing on ankle control improve mobility and posture in persons with multiple sclerosis. *J Neurol Phys Ther.* (2015) 39:225–32. doi: 10.1097/NPT.0000000000000100
49. Wagner JM, Kremer TR, Van Dillen LR, Naismith RT. Plantarflexor weakness negatively impacts walking in persons with multiple sclerosis more than plantarflexor spasticity. *Arch Phys Med Rehabil.* (2014) 95:1358–65. doi: 10.1016/j.apmr.2014.01.030
50. Carling A, Forsberg A, Nilsagård Y. Falls in people with multiple sclerosis: experiences of 115 fall situations. *Clin Rehabil.* (2018) 32:526–35. doi: 10.1177/0269215517730597
51. Little VL, McGuirk TE, Patten C. Impaired limb shortening following stroke: what's in a name? *PLoS ONE.* (2014) 9:e110140. doi: 10.1371/journal.pone.0110140
52. Lencioni T, Piscosquito G, Rabuffetti M, Sipio E Di, Diverio M, Moroni I, et al. Electromyographic and biomechanical analysis of step negotiation in charcot marie tooth subjects whose level walk is not impaired. *Gait Posture.* (2018) 62:497–504. doi: 10.1016/j.gaitpost.2018.04.014
53. Ardestani MM, Kinnaird CR, Henderson CE, Hornby TG. Compensation or recovery? Altered kinetics and neuromuscular synergies following high-intensity stepping training poststroke. *Neurorehabil Neural Repair.* (2019) 33:47–58. doi: 10.1177/1545968318817825
54. Fung J, Barbeau H. A dynamic EMG profile index to quantify muscular activation disorder in spastic paretic gait. *Electroencephalogr Clin Neurophysiol.* (1989) 73:233–44. doi: 10.1016/0013-4694(89)90124-7
55. Den Otter AR, Geurts ACH, Mulder T, Duysens J. Abnormalities in the temporal patterning of lower extremity muscle activity in hemiparetic gait. *Gait Posture.* (2007) 25:342–52. doi: 10.1016/j.gaitpost.2006.04.007
56. Dobkin BH. Strategies for stroke rehabilitation. *Lancet Neurol.* (2004) 3:528–36. doi: 10.1016/S1474-4422(04)00851-8

Conflict of Interest: The authors declare that the research was conducted in the absence of any commercial or financial relationships that could be construed as a potential conflict of interest.

frontiers in Neurology

BRIEF RESEARCH REPORT
published: 29 October 2020
doi: 10.3389/fneur.2020.540893

Impaired Firing Behavior of Individually Tracked Paretic Motor Units During Fatiguing Contractions of the Dorsiflexors and Functional Implications Post Stroke

*Francesco Negro[1], Kathleen E. Bathon[2], Jennifer N. Nguyen[3], Cassidy G. Bannon[2], Claudio Orizio[1], Sandra K. Hunter[4] and Allison S. Hyngstrom[4]**

[1] Department of Clinical and Experimental Sciences, Research Center for Neuromuscular Function and Adapted Physical Activity "Teresa Camplani", Università degli Studi di Brescia, Brescia, Italy, [2] Uniformed Services, University of Health Sciences, Bethesda, MD, United States, [3] Department of Physical Medicine and Rehabilitation, Medical College of Wisconsin, Milwaukee, WI, United States, [4] Department of Physical Therapy, Marquette University, Milwaukee, WI, United States

OPEN ACCESS

Edited by:
Ina M. Tarkka, University of Jyväskylä, Finland

Reviewed by:
Yingchun Zhang, University of Houston, United States
Jason M. DeFreitas, Oklahoma State University, United States

***Correspondence:**
Allison S. Hyngstrom
allison.hyngstrom@marquette.edu

Specialty section:
This article was submitted to Neurorehabilitation, a section of the journal Frontiers in Neurology

Received: *06 March 2020*
Accepted: *25 September 2020*
Published: *29 October 2020*

Citation:
Negro F, Bathon KE, Nguyen JN, Bannon CG, Orizio C, Hunter SK and Hyngstrom AS (2020) Impaired Firing Behavior of Individually Tracked Paretic Motor Units During Fatiguing Contractions of the Dorsiflexors and Functional Implications Post Stroke. Front. Neurol. 11:540893. doi: 10.3389/fneur.2020.540893

Introduction: This study quantified stroke-related changes in the following: (1) the averaged discharge rate of motor units (individually tracked and untracked) identified from high-density electromyography (HD-EMG) recordings, (2) global muscle EMG properties of the dorsiflexors during a fatiguing contraction, and the relationship between task endurance and measures of leg function.

Methods: Ten individuals with chronic stroke performed a sustained sub-maximal, isometric, fatiguing dorsiflexion contraction in paretic and non-paretic legs. Motor-unit firing behavior, task duration, maximal voluntary contraction strength (MVC), and clinical measures of leg function were obtained.

Results: Compared to the non-paretic leg, the paretic leg task duration was shorter, and there was a larger exercise-related reduction in motor unit global rates, individually tracked discharge rates, and overall magnitude of EMG. Task duration of the paretic leg was more predictive of walking speed and lower extremity Fugl-Meyer scores compared to the non-paretic leg.

Discussion: Paretic leg muscle fatigability is increased post stroke. It is characterized by impaired rate coding and recruitment and relates to measures of motor function.

Keywords: motor unit (MU), stroke, decomposition, fatigue, tracking, tibialis anterior, exercise, rehabilitation

INTRODUCTION

Impaired rate modulation and recruitment of motor units in chronic stroke survivors during sub-maximal fatiguing contractions of the leg muscles may limit functional endurance and interfere with mobility. Consistent with this notion, stroke survivors demonstrate altered kinematics after short bouts of walking (1–3) and decreased distance walked during the 6-min walk test compared with healthy controls (4). In addition, for a given level of muscle fatigue, there are greater detrimental effects on walking speed in chronic stroke survivors as compared to controls (5).

Neuromuscular fatigability can be quantified as the acute exercise-induced reduction in force or the time able to maintain a force during a contraction (6). Neuromuscular fatigue can be due to the nervous system's inability to excite the muscle (i.e., central factors) or impairments in muscle contractile properties (6–8). Likely due to damage to motor centers following stroke, evidence suggests that central factors contribute more toward neuromuscular fatigability post stroke vs. exercise-induced changes in contractile function of the muscle (9, 10). If the central nervous system is unable to excite motor neuron pools to meet the force demands of the task, this would present as impaired rate coding and recruitment of motor units.

Previous work has documented reduced rate coding and recruitment during brief sub-maximal contractions (11, 12), but little is known about motor unit firing behavior during fatiguing contractions. Mcmanus et al. have recently shown that the mean discharge rate from populations of motor units in the paretic and non-paretic FDI at the end of fatiguing contraction was decreased compared to baseline levels (10). However, population discharge rates could reflect the recruitment and identification of different motor units at the end of the fatiguing contraction than at baseline—leaving it difficult to interpret changes in rate coding within a specific unit. In fact, previous studies investigating motor unit behavior during neuromuscular fatigue in stroke individuals have quantified the global behavior of subpopulations of motor units decomposed using intramuscular or surface electromyography (EMG) signals before and after a fatiguing task. Due to the relative large variability in the interference EMG signals and the low stability of standard EMG recordings, there is no guarantee that the same populations of motor units can be identified before and after a fatiguing task, limiting our ability to compare motor unit behavior. On the other hand, the use of high-density surface EMG decomposition can provide the possibility to track the behavior of the same motor units comparing their two-dimensional spatial representation before and after different interventions, overcoming the limitations of standard population measures (13).

For these reasons, no studies have quantified the discharge rate behavior of individually tracked motor units or global muscle activation of functionally relevant leg muscles such as the ankle dorsiflexor muscles over the course of fatiguing task. The ankle dorsiflexor muscles are necessary for toe clearance during the swing phase of gait (14), and volitional dorsiflexion is often decreased following a stroke (15). Therefore, understanding the modifications in the neural control of the dorsiflexors during a fatiguing task is important to predict motor behavior and gait performance in people with stroke.

The purpose of this study was to quantify stroke-related changes in (1) individually tracked and untracked motor unit discharge rates, (2) global muscle EMG variables of the dorsiflexors during a fatiguing contraction, and (3) relate task endurance to measures of leg function.

Abbreviations: EMG, electromyography; MVC, maximal voluntary contractions; RMS, root mean square.

TABLE 1 | Characteristics of the study participants.

Subject ID	Age (years)	Years Post Stroke	LE-FM
101	80–85	8	32
102	55–60	33	21
103	60–65	24	13
104	35–40	10	26
105	40–45	10	28
106	70–75	8	19
107	65–70	28	23
108	55–60	6	21
109	70–75	6	32
110	60–70	25	32
Average ± SD	60.4 ± 13	15.8 ± 10	24.7 ± 6

METHODS

All protocols were approved by the Institutional Review Board at Marquette University (HR-2753).

Ten individuals with chronic stroke (>6 months) participated in this study, five males and five females (see **Table 1** for characteristics). Dorsiflexion force generated was measured by a load cell (SSM-AJ-150, Scottsdale, AZ) embedded in a custom-built ankle brace. Prior to acquisition, torque signals were low-pass filtered (500 Hz) and then sampled at 1 kHz using a data acquisition card (National Instruments Corp., Austin, TX) and PC. A constant current stimulator (Digitimer DS7AH, Welwyn Garden City, UK) delivered a rectangular pulse of 100-μs duration with a maximal amplitude of 400 V. The stimulation intensity (between 200 and 500 mA) was set to 10% above resting maximal twitch. Resting twitch measurements were performed by delivering electrical stimulation to the common peroneal nerve before and after the maximal voluntary contraction strength (MVC) trials during the baseline measures. Additionally, a resting twitch was elicited at the end of the fatigue task, after the MVC. The peak of the twitch torque was used as a measure of the contractile properties of the tibialis anterior muscle. Custom-written LabVIEW (National Instruments, Austin, TX) programs were used to generate stimulator and acquire all data. Peak and percent decline in MVC and resting twitch torque values in response to the fatigue protocol were calculated.

Surface EMG

One 64-channel surface matrix was positioned over the tibialis anterior muscle. The high-density surface EMG matrix was placed with the center at 1/3 on the line between the tip of the fibula and the tip of the medial malleolus. The monopolar surface EMG signals were amplified (EMG-USB2+, OT Bioelettronica, Italy), band-pass filtered (20–500 Hz), sampled at 2,048 Hz, and synchronized with the force signal. The EMG signals were decomposed into series of motor unit (MU) discharges using a convolutive blind source separation method (13, 16). This algorithm and similar blind source separation approaches have been previously validated and guarantee high accuracy

in the identification of MU discharge times (17–20). The decomposition accuracy was estimated with the silhouette measure (SIL), with an acceptable threshold of 0.87. The individual motor units were decomposed independently at the beginning and end of the fatiguing task and, in a subset of subjects, tracked across the two-time segments by two-dimensional cross-correlation (13, 21, 22). Matched motor units were identified by a normalized 2D cross-correlation >0.80. The threshold for the 2D cross-correlation was selected based on previous works that have shown a good reliability in matching motor units across different recording sessions using such level of similarity. From the decomposed discharge times, the average discharge rate and the coefficient of variation for inter-spike intervals of the individual motor units were computed. An example of motor unit matching is shown in **Figures 1B,C** for the paretic and non-paretic leg of one subject. The averaged root mean square (RMS) of EMG across the grid was calculated for 10 s at baseline and at the end of the fatigue protocol (at 5–10 s steady state prior to meeting task failure criteria). The percent change in RMS EMG from fatigue to baseline was calculated. Discharge statistics of the identified motor units was calculated in the same segments.

Protocol

Subjects were positioned in supine on a therapy table with their test leg positioned (ankle 35°s of plantarflexion, knee neutral, hip 10–15°s of flexion) in a custom-built ankle and lower leg brace that was secured to the table with Velcro straps. With visual feedback, 3–5 isometric dorsiflexor MVCs were made and immediately followed by a resting twitch measurement (**Figure 1A**). Resting twitch measurements were performed by delivering electrical stimulation to the tibialis anterior muscle at rest. Next, subjects were instructed to generate and sustain a target force of 30% of their MVC. The level of force was selected in order to understand the neuromechanical manifestations of fatigue during a task at moderate effort, similar to everyday life tasks. Tasks at higher force levels would lead to very short time-to-task failure with minimal influence of peripheral muscle properties. Criteria for task failure were as follows: failure to maintain target force for five consecutive seconds or five deviations below the target torque within a 10-s window. An error window of 10% of the target level was used. Upon meeting the task failure criteria, a final MVC and resting twitch measurement was performed. After a period of at least 15 min, the contralateral leg was tested (order counterbalanced). On a separate day, clinical measures of the LE-Fugl-Meyer and Ten Meter Walk Test were performed by a licensed physical therapist blinded to the fatigue testing.

Data are reported as mean ± standard deviation (±SD) and $\alpha = 0.05$. Normal distribution of the analyzed variables was verified using the Shapiro–Wilk test. Separate paired *t*-tests were performed on the following variables: MVC, task duration, percent decline in MVC, and percent increase in RMS of EMG. A student's *t*-test was performed to detect differences with the percent change in discharge rates for the matched units. A mixed-model ANOVA was used for the population discharge rate analysis.

RESULTS

Force and Task Duration Measurements

The paretic dorsiflexor isometric MVC force was less than that of the non-paretic MVC (106 ± 54 N vs. 177 ± 114 N, $P < 0.01$). Task duration was less for the paretic leg compared with the non-paretic leg (297.9 ± 217 s vs. 524.9 ± 262 s, $P = 0.04$). The relative decrease in MVC force due to the fatigue protocol was similar between the paretic and non-paretic legs (38 ± 15% vs. 36 ± 9%, $P = 0.59$). There was a trend for the relative decrease in resting twitch torque to be greater for the non-paretic than the paretic leg (55 ± 24% vs. 36 ± 33%, $P = 0.05$).

Motor Unit Rate Coding and Recruitment in Response to Fatiguing Exercise

The non-paretic leg had a larger relative increase in the global RMS magnitude of the EMG compared with the paretic leg (**Figure 2A**, $P = 0.02$). In total, 582 motor units were reliably decomposed (paretic leg: 162 pre fatigue and 138 post fatigue; non-paretic leg: 153 pre fatigue and 129 post fatigue), with an average of 16 ± 2 per subject in each leg/condition. A representative example of decomposition and matching is shown in **Figures 1B,C**. With respect to global measures of motor unit discharge rates (**Figure 2B**), there was a main effect of leg (p < np, $P < 0.01$) and time (post fatigue < pre fatigue, $P < 0.01$) and an interaction effect where there was a larger reduction in paretic leg discharge rates as compared to the non-paretic leg ($P = 0.023$). Similarly, in the subset of matched motor units identified in six subjects (90 motor units, 58 in paretic and 32 in the non-paretic leg), the paretic leg had a greater relative decrease in discharge rates compared with the non-paretic leg (**Figure 2C**, $P < 0.001$). Coefficient of variation for inter-spike intervals was greater post fatigue ($P = 0.01$), but no effect of legs was found ($P = 0.34$).

Relationship Between Task Duration and Leg Function

Task duration of the paretic leg was positively correlated with walking speed (**Figure 2D**, $P = 0.02$) and the lower extremity Fugl-Meyer score ($r^2 = 0.54$, $P = 0.01$). Task duration of the non-paretic leg was not significantly correlated with walking speed ($P = 0.11$).

DISCUSSION

As compared to the non-paretic leg, we show a decreased task endurance of the paretic dorsiflexors during a sub-maximal fatiguing contraction with greater reductions in the discharge rates of individually tracked and untracked motor units and global measures of whole muscle activation (**Figure 2**). These results are accompanied by, on average, a limited reduction in resting twitch response as compared to the non-paretic leg and comparably decreases in MVC. Finally, we are the first to establish a positive relationship between a measure of

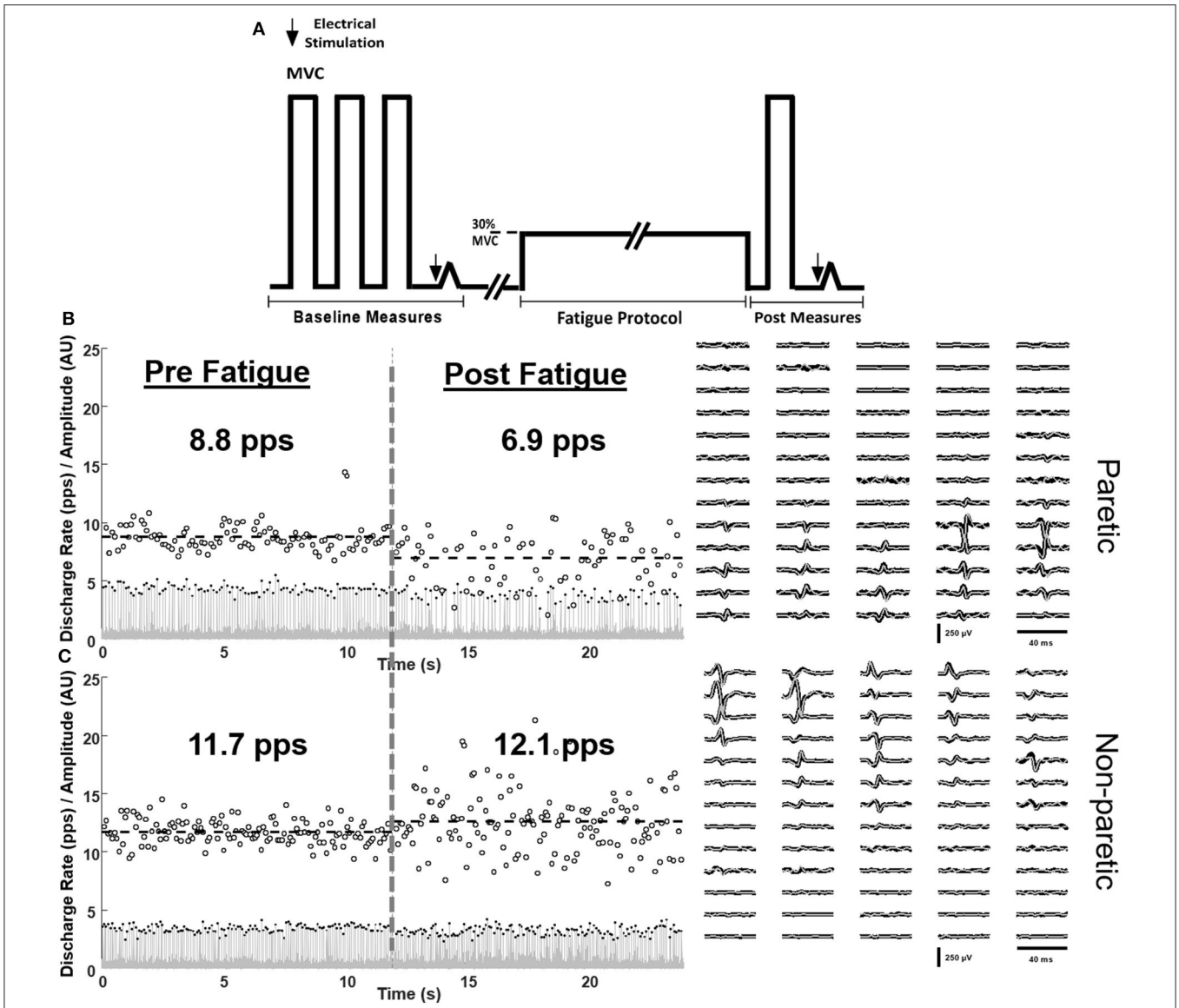

FIGURE 1 | Schematic of the protocol **(A)** and single-subject examples of matched motor unit discharge rates of the paretic **(B)** and non-paretic **(C)** tibialis anterior muscle at baseline (left) and in response to fatiguing contractions (right). Innervation pulse trains (gray lines), identified spikes (black dots), instantaneous discharge rates (empty circles), and the spike triggered averaged motor unit action potentials of the tracked motor units pre (black) and post (gray) fatigue are shown.

fatigability, task duration, and walking speed and the Fugl-Meyer score. Taken together, these results suggest that during fatiguing contractions of the paretic leg, the nervous system is unable to modulate rate coding or recruitment subsequently leading to the inability to maintain a sub-maximal force.

Here, we show deficiencies in the neural modulation of individual and populations of motor units during fatiguing contractions of the tibialis anterior, a muscle critical for walking function. Our evidence of a strong central (vs. peripheral) contribution to fatigue is consistent with previous investigations of mechanisms of neuromuscular fatigability post stroke. However, these studies focused on global measures of neural drive and excitability of the entire pathway from the cortex to muscle output (23–26) or, as with McManus et al., measures of discharge rates of populations of motor units in small hand muscles (10). Similar to the McManus study, during fatigue we showed a decrease in paretic motor unit discharge rates compared with the non-paretic muscle. However, in contrast, we showed a nearly 2-fold difference in task duration between the paretic and non-paretic muscles whereas the McManus study reported similar task durations. This study differences may be due to either (1) differences in fatigability of lower vs. upper limb muscle fatigability or (2) differences in the absolute force levels generated during the contractions. Neural drive to muscle (RMS of EMG and averaged discharge rate of motor units) typically increases during sub-maximal low- to

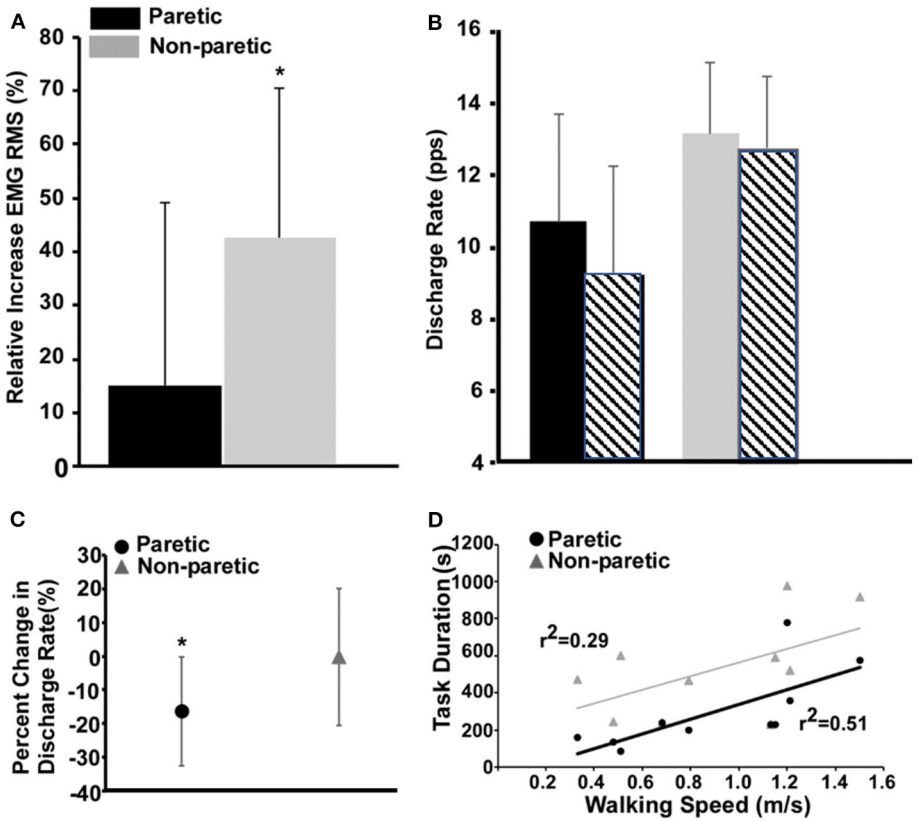

FIGURE 2 | Measures of fatigue-related differences in the paretic and non-paretic tibialis anterior RMS EMG **(A)**, population discharge rates **(B)**, individually tracked discharge rates **(C)**, and the relationship between task duration and walking speed **(D)**. **(A)** Values for the paretic leg are shown in black and the ones for the non-paretic in gray. **(B)** Same as **(A)**, and the striped bars show the corresponding values after the fatigue task. **(C)** The circle and the triangle depict the variations in discharge rates of the matched motor units for the paretic and non-paretic leg, respectively. **(D)** Comparison of the regressions between task duration (s) and walking speed (m/s) for paretic and non-paretic sides.

moderate-intensity fatiguing contractions in healthy individuals (27–35). Thus, our findings suggest that decreased rate coding and or the drop out of motor units likely contributed to the reduced magnitude of the paretic RMS EMG compared to the non-paretic leg and is consistent with findings from other studies showing impaired ability to modulate EMG post stroke and different load levels and during fatigue (36, 37). Our data demonstrate that the inability of the nervous system to activate individual units, populations of units, and the whole muscle at baseline is exacerbated with ongoing muscle contractions in the paretic leg of stroke individuals.

Additionally, in our study, we found a positive correlation between task duration of the paretic leg's tibialis anterior and walking speed and no significant correlation to walking speed with the non-paretic leg's task duration. Although not directly tested, these data suggest that impairments in the paretic leg are more predictive of walking function vs. the non-paretic leg. This is consistent with other studies which correlate strength of the paretic leg and walking speed (38–40). Previously, we have shown that fatigue-related reductions in maximal paretic hip flexor contraction strength were correlated with baseline walking speed (41) and dynamic fatiguing contractions of the paretic hip flexors caused a larger decrease in walking speed as compared to controls (5). To our knowledge, the present study is the first to show the relationship between neuromuscular fatigability of the ankle dorsiflexors and baseline walking performance in chronic stroke.

We should acknowledge some limitations of the study design of our study: (1) the enrolled chronic stroke patients had a relatively large difference in the years post stroke and LE-FMA scores and this may have increased the variability of the outcome measures. (2) The fatigue protocol was performed on both legs on the same day, including a recovery time between recordings based on the perceived fatigue of the subjects. For this reason, we cannot exclude the influence of a cross-over effect of fatigue between legs in our current results. Nevertheless, the variation in discharge rate pre and post fatigue in the non-paretic leg was similar to previous reports on healthy individuals (30), so the problem, even if not avoidable, was likely of moderate effect.

In conclusion, our data are clinically relevant as we demonstrate a relationship between task duration and leg function. Muscle fatigability is functionally relevant as many activities of daily living require the intermittent or sustained generation of sub-maximal forces. Taken together, our findings underscore the need to make clinical measures of fatigability

of functionally relevant muscles to fully assess motor capability post stroke.

DATA AVAILABILITY STATEMENT

The datasets generated for this study are available on request to the corresponding author.

ETHICS STATEMENT

The studies involving human participants were reviewed and approved by Institutional Review Board at Marquette University (HR-2753). The patients/participants provided their written informed consent to participate in this study.

AUTHOR CONTRIBUTIONS

AH, SH, and FN conceived and designed the research program. AH provided lab settings. KB, CB, JN, and AH conducted the experiments. FN and AH planned, carried out the signal analysis and the statistics, and wrote the first draft of the manuscript. All authors discussed the results and contributed to the final manuscript.

ACKNOWLEDGMENTS

The authors would like to thank NINDS, National Institutes of Health 1R15NS084130-01 and EU Horizon Marie Skłodowska-Curie IF N. 702491 (NeuralCon).

REFERENCES

1. Bayat R, Barbeau H, Lamontagne A. Speed and temporal-distance adaptations during treadmill and overground walking following stroke. *Neurorehabil Neural Repair*. (2005) 19:115–24. doi: 10.1177/1545968305275286
2. Dean CM, Richards CL, Malouin F. Walking speed over 10 metres overestimates locomotor capacity after stroke. *Clin Rehabil*. (2001) 15:415–21. doi: 10.1191/026921501678310216
3. Sibley E, Doroshow RW, Milliken JC, Anand SK. Subarachnoid hemorrhage and isolated atresia of the aortic arch. *J Emerg Med*. (2002) 22:179–83. doi: 10.1016/S0736-4679(01)00461-9
4. Pohl PS, Duncan PW, Perera S, Liu W, Lai SM, Studenski S, et al. Influence of stroke-related impairments on performance in 6-minute walk test. *J Rehabil Res Dev*. (2002) 39:439–44.
5. Rybar MM, Walker ER, Kuhnen HR, Ouellette DR, Berrios R, Hunter SK, et al. The stroke-related effects of hip flexion fatigue on over ground walking. *Gait Posture*. (2014) 39:1103–8. doi: 10.1016/j.gaitpost.2014.01.012
6. Enoka RM, Duchateau J. Muscle fatigue: what, why and how it influences muscle function. *J Physiol*. (2008) 586:11–23. doi: 10.1113/jphysiol.2007.139477
7. Gandevia SC. Spinal and supraspinal factors in human muscle fatigue. *Physiol Rev*. (2001) 81:1725–89. doi: 10.1152/physrev.2001.81.4.1725
8. Hunter SK. Performance fatigability: mechanisms and task specificity. *Cold Spring Harb Perspect Med*. (2018) 8:a029728. doi: 10.1101/cshperspect.a029728
9. Hyngstrom AS, Onushko T, Heitz RP, Rutkowski A, Hunter SK, Schmit BD. Stroke-related changes in neuromuscular fatigue of the hip flexors and functional implications. *Am J Phys Med Rehabil*. (2012) 91:33–42. doi: 10.1097/PHM.0b013e31823caac0
10. McManus L, Hu X, Rymer WZ, Suresh NL, Lowery MM. Motor unit activity during fatiguing isometric muscle contraction in hemispheric stroke survivors. *Front Hum Neurosci*. (2017) 11:569. doi: 10.3389/fnhum.2017.00569
11. Chou LW, Palmer JA, Binder-Macleod S, Knight CA. Motor unit rate coding is severely impaired during forceful and fast muscular contractions in individuals post stroke. *J Neurophysiol*. (2013) 109:2947–54. doi: 10.1152/jn.00615.2012
12. Gemperline JJ, Allen S, Walk D, Rymer WZ. Characteristics of motor unit discharge in subjects with hemiparesis. *Muscle Nerve*. (1995) 18:1101–14. doi: 10.1002/mus.880181006
13. Martinez-Valdes E, Negro F, Laine CM, Falla D, Mayer F, Farina D. Tracking motor units longitudinally across experimental sessions with high-density surface electromyography. *J Physiol*. (2017) 595:1479–96. doi: 10.1113/JP273662
14. Perry J. *Gait Analysis: Normal and Pathological Function*. First ed. Thorofare, NJ: SLACK, Incorporated (1992).
15. Sheffler LR, Chae J. Hemiparetic Gait. *Phys Med Rehabil Clin N Am*. (2015) 26:611–23. doi: 10.1016/j.pmr.2015.06.006
16. Negro F, Muceli S, Castronovo AM, Holobar A, Farina D. Multi-channel intramuscular and surface EMG decomposition by convolutive blind source separation. *J Neural Eng*. (2016) 13:026027. doi: 10.1088/1741-2560/13/2/026027
17. Boccia G, Martinez-Valdes E, Negro F, Rainoldi A, Falla D. Motor unit discharge rate and the estimated synaptic input to the vasti muscles is higher in open compared with closed kinetic chain exercise. *J Appl Physiol (1985)*. (2019) 127:950–8. doi: 10.1152/japplphysiol.00310.2019
18. Chen M, Zhang X, Lu Z, Li X, Zhou P. Two-source validation of progressive FastICA peel-off for automatic surface EMG decomposition in human first dorsal interosseous muscle. *Int J Neural Syst*. (2018) 28:1850019. doi: 10.1142/S0129065718500193
19. Dai C, Hu X. Independent component analysis based algorithms for high-density electromyogram decomposition: Experimental evaluation of upper extremity muscles. *Comput Biol Med*. (2019) 108:42–8. doi: 10.1016/j.compbiomed.2019.03.009
20. Del Vecchio A, Negro F, Holobar A, Casolo A, Folland JP, Felici F, et al. You are as fast as your motor neurons: speed of recruitment and maximal discharge of motor neurons determine the maximal rate of force development in humans. *J Physiol*. (2019) 597:2445–56. doi: 10.1113/JP277396
21. Del Vecchio A, Casolo A, Negro F, Scorcelletti M, Bazzucchi I, Enoka R, et al. The increase in muscle force after 4 weeks of strength training is mediated by adaptations in motor unit recruitment and rate coding. *J Physiol*. (2019) 597:1873–87. doi: 10.1113/JP277250
22. Martinez-Valdes E, Falla D, Negro F, Mayer F, Farina D. Differential motor unit changes after endurance or high-intensity interval training. *Med Sci Sports Exerc*. (2017) 49:1126–36. doi: 10.1249/MSS.0000000000001209
23. Gerrits KH, Beltman MJ, Koppe PA, Konijnenbelt H, Elich PD, de Haan A, et al. Isometric muscle function of knee extensors and the relation with functional performance in patients with stroke. *Arch Phys Med Rehabil*. (2009) 90:480–7. doi: 10.1016/j.apmr.2008.09.562
24. Horstman A, Gerrits K, Beltman M, Janssen T, Konijnenbelt M, de Haan A. Muscle function of knee extensors and flexors after stroke is selectively impaired at shorter muscle lengths. *J Rehabil Med*. (2009) 41:317–21. doi: 10.2340/16501977-0331
25. Horstman AM, Beltman MJ, Gerrits KH, Koppe P, Janssen TW, Elich P, et al. Intrinsic muscle strength and voluntary activation of both lower limbs and functional performance after stroke. *Clin Physiol Funct Imaging*. (2008) 28:251–61. doi: 10.1111/j.1475-097X.2008.00802.x
26. Riley NA, Bilodeau M. Changes in upper limb joint torque patterns and EMG signals with fatigue following a stroke. *Disabil Rehabil*. (2002) 24:961–9. doi: 10.1080/096382021000007932
27. Adam A, De Luca CJ. Firing rates of motor units in human vastus lateralis muscle during fatiguing isometric contractions. *J Appl Physiol (1985)*. (2005) 99:268–80. doi: 10.1152/japplphysiol.01344.2004
28. Bigland-Ritchie B, Cafarelli E, Vollestad NK. Fatigue of submaximal static contractions. *Acta Physiol Scand Suppl*. (1986) 556:137–48.

29. Bigland-Ritchie B, Furbush F, Woods JJ. Fatigue of intermittent submaximal voluntary contractions: central and peripheral factors. *J Appl Physiol (1985)*. (1986) 61:421–9. doi: 10.1152/jappl.1986.61.2.421
30. Castronovo AM, Negro F, Conforto S, Farina D. The proportion of common synaptic input to motor neurons increases with an increase in net excitatory input. *J Appl Physiol (1985)*. (2015) 119:1337–46. doi: 10.1152/japplphysiol.00255.2015
31. Dorfman LJ, Howard JE, McGill KC. Triphasic behavioral response of motor units to submaximal fatiguing exercise. *Muscle Nerve*. (1990) 13:621–8. doi: 10.1002/mus.880130711
32. Garland SJ, Griffin L, Ivanova T. Motor unit discharge rate is not associated with muscle relaxation time in sustained submaximal contractions in humans. *Neurosci Lett*. (1997) 239:25–8. doi: 10.1016/S0304-3940(97)00885-9
33. Griffin L, Ivanova T, Garland SJ. Role of limb movement in the modulation of motor unit discharge rate during fatiguing contractions. *Exp Brain Res*. (2000) 130:392–400. doi: 10.1007/s002219900253
34. Kuchinad RA, Ivanova TD, Garland SJ. Modulation of motor unit discharge rate and H-reflex amplitude during submaximal fatigue of the human soleus muscle. *Exp Brain Res*. (2004) 158:345–55. doi: 10.1007/s00221-004-1907-0
35. Mettler JA, Griffin L. Muscular endurance training and motor unit firing patterns during fatigue. *Exp Brain Res*. (2016) 234:267–76. doi: 10.1007/s00221-015-4455-x
36. Tang A, Rymer WZ. Abnormal force–EMG relations in paretic limbs of hemiparetic human subjects. *J Neurol Neurosurg Psychiatry*. (1981) 44:690–8. doi: 10.1136/jnnp.44.8.690
37. Zhou P, Li X, Rymer WZ. EMG-force relations during isometric contractions of the first dorsal interosseous muscle after stroke. *Top Stroke Rehabil*. (2013) 20:537–44. doi: 10.1310/tsr2006-537
38. Mentiplay BF, Adair B, Bower KJ, Williams G, Tole G, Clark RA. Associations between lower limb strength and gait velocity following stroke: a systematic review. *Brain Inj*. (2015) 29:409–22. doi: 10.3109/02699052.2014.995231
39. Nakamura R, Watanabe S, Handa T, Morohashi I. The relationship between walking speed and muscle strength for knee extension in hemiparetic stroke patients: a follow-up study. *Tohoku J Exp Med*. (1988) 154:111–3. doi: 10.1620/tjem.154.111
40. Ozgozen S, Guzel R, Basaran S, Coskun Benlidayi I. Residual deficits of knee flexors and plantar flexors predict normalized walking performance in patients with poststroke hemiplegia. *J Stroke Cerebrovasc Dis*. (2020) 29:104658. doi: 10.1016/j.jstrokecerebrovasdis.2020.104658
41. Kuhnen HR, Rybar MM, Onushko T, Doyel RE, Hunter SK, Schmit BD, et al. Stroke-related effects on maximal dynamic hip flexor fatigability and functional implications. *Muscle Nerve*. (2015) 51:446–8. doi: 10.1002/mus.24520

Conflict of Interest: The authors declare that the research was conducted in the absence of any commercial or financial relationships that could be construed as a potential conflict of interest.

Advantages of publishing in Frontiers

OPEN ACCESS
Articles are free to read for greatest visibility and readership

FAST PUBLICATION
Around 90 days from submission to decision

HIGH QUALITY PEER-REVIEW
Rigorous, collaborative, and constructive peer-review

TRANSPARENT PEER-REVIEW
Editors and reviewers acknowledged by name on published articles

Frontiers
Avenue du Tribunal-Fédéral 34
1005 Lausanne | Switzerland

Visit us: www.frontiersin.org
Contact us: frontiersin.org/about/contact

REPRODUCIBILITY OF RESEARCH
Support open data and methods to enhance research reproducibility

DIGITAL PUBLISHING
Articles designed for optimal readership across devices

FOLLOW US
@frontiersin

IMPACT METRICS
Advanced article metrics track visibility across digital media

EXTENSIVE PROMOTION
Marketing and promotion of impactful research

LOOP RESEARCH NETWORK
Our network increases your article's readership